THE ORIGINS OF NATURAL DIAMONDS

N. O. SOROKHTIN

Scrivener Publishing

WILEY

The Origins of Natural Diamonds

Scrivener Publishing
100 Cummings Center, Suite 541J
Beverly, MA 01915-6106

Publishers at Scrivener
Martin Scrivener (martin@scrivenerpublishing.com)
Phillip Carmical (pcarmical@scrivenerpublishing.com)

The Origins of Natural Diamonds

N. O. Sorokhtin

WILEY

This edition first published 2019 by John Wiley & Sons, Inc., 111 River Street, Hoboken, NJ 07030, USA and Scrivener Publishing LLC, 100 Cummings Center, Suite 541J, Beverly, MA 01915, USA

For more information about Scrivener publications please visit www.scrivenerpublishing.com.

Wiley Global Headquarters
111 River Street, Hoboken, NJ 07030, USA

For details of our global editorial offices, customer services, and more information about Wiley products visit us at www.wiley.com.

Library of Congress Cataloging-in-Publication Data

ISBN 978-1-119-59344-7

Cover image: Diamond/World - Alexlmx | Dreamstime.com,
Diamond Mine - Alicenerr | Dreamstime.com
Cover design by Kris Hackerott

Set in size of 11pt and Minion Pro by Manila Typesetting Company, Makati, Philippines

Printed in the USA

10 9 8 7 6 5 4 3 2 1

Dedicated to Professor Oleg G. Sorokhtin and to Academician of the Russian Academy of Sciences Felix P. Mitrofanov, my closest tutors and friends who elucidated the road in science for me.

Contents

Foreword

Before narrating an entertaining, interesting and scientifically important story of diamonds, I would like to devote a few lines to the people already gone but no less respected and loved by me. One of them was my father. Not only did he give me the instrument for learning the laws of the Universe but inculcated in me a love and an inquisitiveness toward natural sciences. Another one was looking after me for fully a half of my scientific life and directing my studies in the channel of the unknown. Both were great scientists of their time, both made a substantial contribution to the world of science. It is due to them that I eventually became a scientist and was able to write this book.

The origin of diamonds is closely tied to Earth's general planetary evolution. That is why the substantiation of the proposed diamond and diamond-bearing rocks' emergence mechanisms is conducted in the context of a modern concept of Earth's global evolution.

Based on this concept, the book describes the diamond formation exogenous mechanism, according to which diamond-bearing rock melts emerge due to remelting of pelagic oceanic deposits pulled in to great depths through ancient plate subduction zones under the continents. However, only heavy iron ore deposits whose density exceeded average density of continental lithospheric plates (around 3.2 g/cm^3) might have immersed to a great depth up to the base of these plates. It is known from the geological record that large volumes of such formations had been deposited only at the end Archean and in the second half of Early Proterozoic. In Archaean, due to high heat flows, the continental plate thickness (together with the continental crust) had not exceeded 60–80 km. In Proterozoic, Earth's tectonic activity had sharply declined and its further evolution had been proceeding under the lithospheric plate tectonics laws. At that time, plate subduction zones had emerged and the continental lithosphere (together with Earth's crust) thickness by the end Early Proterozoic had rapidly grown to 200–250 km. Exactly for this reason, melts of the depth diamond-bearing rocks (the kimberlites and lamproites) might have emerged only in

the second half of Early Proterozoic about 2.2–1.9 BYa. The fact of the kimberlites, lamproites and their affine rocks emergence from ancient iron rich oceanic deposits is evidenced by their chemical composition. The same is supported by the composition of eclogite xenoliths practically equivalent to the composition of oceanic tholeiite basalts melted out at shallow depths. At that, the kimberlites and carbonatites had formed most likely due to a submergence to great depths and remelting of Earth's tropical zone carbonate deposits and the lamproites, due to remelting at similar depths of boreal and circum-polar areas' clayey pelagic deposits. The origin of apatite-bearing sienites in the Khibin and similar massifs is explained by pulling oceanic upwelling zone phosphorites into subduction zones and of diamonds, by carbon reduction, at the expense of exothermal reactions between carbon dioxide gas released at thermal dissociation of the depositional carbonates and organic origin hydrocarbons. It follows thence that the entire carbon of the diamonds had only exogenous origin. The same is testified by isotopic data and by gas-liquid inclusions in this mysterious mineral.

Based on the described formation mechanism of diamond-bearing and their affine rocks, the structure is reviewed of the South African, Yakut and some other diamond-bearing provinces. A positive forecast is made of the diamond-bearing potential in the northeastern Baltic shield and northern Russia platform. The exploration criteria of these minerals in other world regions are formulated.

My special gratitude goes to Dr. Michael V. Gorfunkel who inspired me to write this book and was its guardian angel without whom its coming-into-being would not have been possible.

Introduction

Many scientists traditionally believe that the ore (and not only ore) matter of most endogenous economic minerals comes directly from the mantle or through the mantle matter differentiation and invasion of differentiated magmas in the crust together with water fluids rising from Earth's depth. However, this assumption is right only in part as the entire matter of the continental crust, including ore elements, had been indeed released in the past from the mantle along with the other rock-forming oxides. In substance, however, this assumption is the "path of least resistance" as it allows us to hide our lack of knowledge of the real mechanisms of local crust enrichment with trace elements in a "black box" of the mantle and to substitute one complex problem with another one, no less complex. Indeed, the entire complexity of the classical approach to explaining the formation causes of local ore and other trace element accumulations in Earth's crust is in that the concentration of most of them in the mantle is disappearingly low, whereas in commercial deposits it is relatively high and reaches sometimes top-cut grade value. For instance, gold and uranium concentration in the present-day mantle is on the order of 10^{-9}; mercury and thorium 10^{-8}; silver, tantalum, tungsten, platinum and lead 10^{-7}; lithium, niobium, molybdenum and tin 10^{-6}, etc., whereas in commercial deposits the concentration of these rare elements may rise to fractions and even whole percentages.

The current geodynamic concepts maintain that the entire matter in the mantle (both upper and lower) had been well stirred over 4 BY of Earth's tectonic activity by the convection flows and must have a uniform composition. That is why there is no hope today of existence in the mantle of local irregularities with elevated contents of both ore and volatile elements – strong mineralizers such as water, carbon dioxide gas, halogens, etc. Whereas the juvenile (chemically bonded) water content in the quenching glass of fresh oceanic basalts usually does not exceed 0.05%.

Water drastically decreases the melting temperature of silicates, thus, at basalt melt-out it should mostly concentrate exactly in basalt melts. It follows

thence that water concentration in the mantle at least does not exceed $5 \cdot 10^{-4}$. Therefore, the mantle is practically "dry". Any fluid flows in this geosphere (outside the plate subduction zones) capable of bringing in the crust noticeable amounts of ore, lithophilic and other trace elements are out of the question.

What, then, is an explanation of significant, sometimes outright top-cut grade contents of trace and rare elements in economic mineral deposits? Apparently, only the superposition of two processes, gradual accumulation of ore elements in Earth's crust and their subsequent concentration in the local volumes of deposits due to the secondary processing (recycling) of Earth's crust matter. The former process is totally dependent on Earth's tectonic activity, i.e., on the release rate in its subsurface of endogenous energy. The latter process is connected with the effect of exogenous causes of Earth's crust rocks destruction and weathering, with the deposition of crust rocks destruction products and often with their new remelting. The main factors controlling the exogenous processes on Earth, beside the Sun radiation, are the evolution of hydrosphere (including the oceans) and atmosphere, both substantially affecting Earth's climates. Only a simultaneous and total consideration of all these endogenous and exogenous factors may enable us to understand the nature of economic minerals' accumulation in Earth's crust.

Everything aforementioned is fully applied to the origins of diamond-bearing kimberlites, lamproites and their affine rocks of the carbonatite and alkali-ultramafic series. Indeed, on the one hand all these rocks are of a clearly depth origin; it is certain that their ancestral magmas had risen from the upper mantle levels. On the other hand, they all are sharply enriched in volatile and lithophilic elements and sometimes even contain notable amounts of complex hydrocarbons (for instance, the Khibin massif of apatite-bearing nephelinites on the Baltic shield). All of this forces us to reconsider long-held concepts of the origin of endogenous commercial minerals, in particular, diamonds. A detailed familiarization with traditional views of the origins of most endogenous commercial mineral deposits as well as of depth diamond-bearing rocks shows that within the framework of "classical" geological approach this problem is conceptually irresolvable. It is necessary to involve in its resolution new ideas based on the modern geological theory.

A theory of the planetary or global Earth's evolution created and developed by Professor O.G. Sorokhtin was selected as such a theoretical foundation. A component part of this theory is lithospheric plate tectonics; the theory describes general patterns of Earth's evolution as a planet. It is based on the energy approach, according to which its evolution occurs due to the

endogenous processes lowering to the greatest extent the potential energy of Earth itself and of the Earth – Moon system. As its development occurs with the loss of the endogenous heat, the evolution process is irreversible.

The Earth's evolution theory is based on two departure suppositions. First, it is assumed that Earth had emerged at the expense of a homogenous accretion of a cold proto-planetary gas-dust cloud, and second, that Earth's core is composed mostly of an alloy of iron and its oxide. At that, it is believed that we know the composition of Earth's crust and the mantle. Both these assumptions as of today are most substantiated and accepted by most geologists and geophysicists. It appears that these two assumptions are quite sufficient for the construction of a self-consistent Earth's evolution theory because they include the entire needed information about its primordial structure (a uniform and cold planet) and the reserve of its internal energy.

All these enabled the consideration of the diamond-bearing rock origin issue at a new angle and an attempt at a forecast of a potential diamond-bearing of some world regions. That is exactly why the description of the origin of diamond-bearing kimberlites, their affine rocks and diamonds themselves is accompanied by a more detailed review of major Earth's evolution theory positions.

The issues of diamonds and diamond-bearing kimberlites' origin are part of a greater natural phenomenon which is customary to call carbon global cycle. It needs to be noted that as carbon global cycle is traditionally understood its crustal-atmospheric interaction whereas the crustal-mantle carbon transfer is practically unstudied.

Earth's crust carbonates tie up about $3.91 \cdot 10^{23}$ g CO_2 and about $1.95 \cdot 10^{22}$ g of organic carbon (C_{org}). Its substantial fraction settles in the form of deposits on the seafloor and on continental slopes. Further on, the deposits are pulled in subduction zones and transferred by the mantle convection in Earth's divergent areas. For instance, in rift zones is observed a wide range of hydrocarbon gases' emanations, methane (CH_4) and ethane (C_2H_6) up to propane (C_3H_8) and butane (C_4H_{10}). In and of themselves, complex hydrocarbons in a free state are unstable under high PT conditions and tend to decompose into simpler ones, up to methane (CH_4). This is a proof that the generation of the listed compounds occurs in near-surface and low-temperature environments of the medium and not due to their release from the deep mantle. A question arises: how do they get there? A study of this issue showed that carbon transfer from the subduction zones into the rift systems might occur through the transformation of its phase states and the formation of specific compounds (metal carbides) in depth of the mantle. As a result of the crustal-mantle

cycle manifestation, carbon is subjected sequentially to a multistage transformation from chemogenous state into biogenic and back as well as to the submersion in the mantle on the levels of its convective stirring and to release on the surface through the rift zones. There, the metal carbide decomposition and the formation of a wide range of hydrocarbon gases occur. The process of carbon depth transfer process described in the book is closely tied with its crustal-atmospheric branch as the primary supplier of carbon is carbon dioxide gas and the organic matter. Together, these two branches form the global carbon cycle in nature. Geometrically, it may be imaged as the number 8, not 0 as is currently accepted.

This research was funded by the state assignment of IO RAS, theme 0149-2019-0005.

1

Major Parameters of Diamond-Bearing and Affine Rocks

The bed-rocks of diamond-bearing rocks are, as is well known, kimberlites and lamproites. Those are depth magmatic rocks usually encountered only on the ancient continental platforms and forming subvolcanic bodies – blowpipes (diatremes) or magma-bringing dykes. Affine but somewhat less depth rocks are carbonatites and alkali-ultramafic rocks of a quite wide composition range. However, their common feature is low silica contents and relatively elevated concentration of magnesium. This enables attributing all these formations with ultramafic rocks. As opposed to the classical ultramafic rocks of the peridotite series mantle origin, kimberlites, lamproites and alkali-ultramafic rocks are enriched in the titanium, alkalis (first of all, potassium), phosphorus, rare lithophilic and volatile elements including water and carbon dioxide (especially carbonatites).

The chemistry and geochemistry of diamond-bearing kimberlites and lamproites is described in many articles and monographs [1–4]. There are also numerous descriptions of the alkali-ultramafic rocks [5–7] and carbonatites [8–10]. For this reason, there is no need to analyze here in detail the chemical composition of these exotic rocks. Attention must be paid only to the geochemical specifics of kimberlites as most typical representatives of this rock class.

Analyzing specifics of kimberlites' chemical composition, I.P. Ilunin with colleagues [3] noted that the SiO_2/MgO and MgO/FeO ratios in kimberlites correspond with the dunite and peridotite values whereas the Al_2O_3 and Na_2O concentrations are notably lower than in basalts. On the other hand, in contents of some rare elements the kimberlites are close to alkaline basalts. Nevertheless, it is emphasized that no mixing of the peridotites with alkali-basaltoid matter allows to come with the kimberlitic composition. That is because any notable addition of a basaltoid matter to the peridotite will unavoidably result in an increase of the silica, aluminum

N. O. Sorokhtin (ed.) The Origins of Natural Diamonds, (1–5) © 2019 Scrivener Publishing LLC

and sodium concentrations, and at insignificant addition will not occur contents of rare elements typical for the kimberlites.

Also important is that compared to the mantle ultramafic rocks (peridotite and lherzolite), kimberlites are substantially enriched in titanium, potassium and phosphorus. At that, usually enrichment of the kimberlites with rare elements correlates with elevated phosphorus concentrations. To an even greater extent such correlation shows up in carbonatites [3].

The kimberlite geochemistry specifics could have been visually manifested at their comparison with samples of undepleted mantle matter. However, to our great regret, we are never dealing with fresh samples of the mantle rocks wherein the rare elements' contents would have been preserved undistorted. Instability of the dispersed elements' direct determinations in the mantle rocks brought in to Earth's surface is caused by the fact that in the process they practically always experienced a very strong influence from metamorphogenic factors which substantially distorts their primary composition in the rare element domain. Thus, if we use ultramafic rock samples from ophiolite nappes, we should take into account that their matter was at least twice subjected to hydrothermal actions. The first time, at the time of the oceanic crust formation due to its hydration by the oceanic water saturated with alkalis and other easily dissolvable elements. The second time, in the process of this crust obduction (the ophiolite nappe) on continental margins due to the action of overheated and mineralized water coming from plate subduction zones. No less distorted turns out the primary composition of dispersed elements in ultramafic xenoliths within the kimberlites themselves. It is caused by two reasons. First, it is quite likely that these xenoliths are fragments of the ancient oceanic crust pulled in the past geological epochs under the continent plates. Second, due to the fact that over the extended time of a close contact with kimberlite melts in these samples could have occurred (and have occurred) substantial metamorphic alterations [11–13]. In most cases, such alterations should have been boiled down to ultramafic rocks contamination with dispersed elements coming from mineralized hydrotherms or from the kimberlite magmas saturated with volatile components.

Nevertheless, comparisons of kimberlites and lherzolite xenoliths average chemical composition [14] are quite demonstrative. These comparisons show that kimberlites are somewhat impoverished in such major petrogenic elements as Si, Mg, Na, Cr, and Ni whereas their contents of Al, Fe, Mn and some ore elements (Co, Zn) almost correspond with their concentrations in lherzolites. But the most typical feature of kimberlite

rocks is their clear enrichment with dispersed elements. This is concerning especially of lithophilic and rare earth elements. Ya. Muramatsu's determinations showed that kimberlites are enriched with carbon 150-fold, phosphorus, 25-fold, alkali (K, Rb, Sc), 24–68-fold, light rare earth elements (La–Eu), 30 to 200-fold and radioactive elements Th and U, respectively, 80- and 60-fold.

It is difficult to verify these estimates for all trace elements by independent determinations but for some of them it was possible to accomplish. Accepting the quoted Muramatsu's concentrations of K, U and Th in the mantle as the genuine ones, it is easy to calculate that the total depth heat flow generated by them and coming from the mantle had to reach $4.8 \cdot 10^{20}$ erg/s. Added to this mantle flow must be heat generated by radioactive elements concentrated in the continental crust, which amounts approximately is $0.9 \cdot 10^{20}$ erg/s. In this case, total radiogenic heat generation in Earth must have reached $5.7 \cdot 10^{20}$ erg/s. However, another exceptionally powerful source of the heat energy is operating within the present-day Earth. This is the process of the mantle matter gravity differentiation resulting in separation within the planet's central parts of a high-density oxide-ferric core and in the initiation of convection currents in the mantle. Inclusion of this energy source (around $3 \cdot 10^{20}$ erg/s) would have made total Earth's heat loss in the considered case equal to $8.7 \cdot 10^{20}$ erg/s. However, actual heat loss by Earth is only half of this and is equal approximately to $4.2–4.3 \cdot 10^{20}$ erg/s [15–19].

The energy estimates quoted above indicate that accepted by Muramatsu [14] concentrations of a part of trace elements (K, U, and Th) in the mantle matter are clearly overvalued whereas the enrichment factor of kimberlite rocks with the same elements, substantially underestimated. More correct analysis of Earth's energy balance accounting for the energy of tidal interaction of Earth with Moon dispersed in mantle (close to $0.1 \cdot 10^{20}$ erg/s), for the potassium content and K/U and K/Th ratios in the continental crust and in lunar rocks enabled us to determine that Earth's mantle currently contains no greater than 0.012% K, $2.6 \cdot 10^{-7}$% U and $7 \cdot 10^{-7}$% Th [19]. Assuming these concentration values, we come up with the kimberlite enrichment with potassium reaches not 24 but 87-fold. For uranium and thorium, the values are even greater: respectively, 1,200 and 2,300-fold (instead of 62- and 80-fold).

The above example of independent radioactive elements' mantle concentrations estimates is begging for a general conclusion that for some other trace elements the extent of kimberlite rocks enrichment, compared with their Clarke contents in the mantle matter may turn out substantially greater than determined by Muramatsu [14].

Our estimates (see below) give the mantle content of about 110 g/t of carbon dioxide and no greater than 0.05% water. According to J. Dawson [1], the kimberlites contain around 3.3–7.1% CO_2 and 5.9–18.7% H_2O. Therefore, the kimberlites are enriched in these volatile compounds respectively 300–650 and 120–370-fold.

It is, however, noteworthy that in kimberlite minerals [1] and even within the diamond crystals [20, 21] are often encountered inclusions of gaseous and liquid hydrocarbons and even alcohols and more complex organic compounds.

Accounting for all these factors is making even more acute the problem of the kimberlites' origin and of determining the mechanism of so great enrichment of these rocks with lithophilic elements with simultaneously of the silica contents in them. At that, a question needs to be answered of where hydrocarbons in inclusions, with specific for them negative isotopic shifts for the carbon, are coming from.

By definition [4], lamproites are a community of high-magnesium potassium alkaline rocks saturated or slightly undersaturated with the silica and with low contents of aluminum and calcium. The lamproite composition, compared with the kimberlites, is distinct in much broader variability. However, always typical for them are the highest concentrations of potassium (up to 7–10% K_2O), rubidium (up to 300–500 g/t) and barium (up to 5,000–10,000 g/t), elevated content of strontium (up to 1,000–4,000 g/t) and light rare earth's elements (up to 300–600 g/t of La, up to 600–1,000 g/t of Ce, up to 250–500 g/t of Nd and up to 15–30 g/t of Sm). In the magnesium content (between 8 and 24% MgO), lamproites occupy an intermediate position between the mantle matter and basalts. On the other hand, they are enriched with the uranium (1 to 10 g/t) and thorium (12 to 150 g/t) respectively 400- to 4,000-fold and 1,700- to 20,000-fold compared with the mantle. The lamproites contain substantially smaller amounts of carbon dioxide and water than the kimberlites but compared with the mantle matter these rocks are enriched in carbon 20 to 600-fold and in water, 25- to 70-fold.

Carbonatites and alkaline-ultramafic formations, although not belonging with diamond-bearing rocks, are certainly affine formations of reasonably similar genesis. Their specifics, in brief, are as follows. Quite typical for the carbonatites are wide ranges in the composition of major petrogenic oxides [9]. The silica concentration in these rocks varies practically between 0% and 30–40%, ferrous oxides (in toto), 10–12% to 20–25%, magnesium oxide, 12% to 20%, etc. However, the main distinctive feature of the carbonatites is drastically elevated calcium oxide content, 12% to 50%, and carbon dioxide content, 3–8% to 30–40%. Commonly observed

in the carbonatites are elevated contents of sulfur (around 0.3–0.5%), fluorine (around 0.3%) and chlorine (up to 1–3%). Same as the kimberlites, the carbonatites are substantially enriched in light rare earth's elements but especially in strontium and rare earths: tantalum and niobium and also uranium and thorium.

The alkaline-ultramafic rocks are known for their undersaturation with the silica (its concentration usually does not exceed 40%) and saturation with alkali, especially sodium (up to 5–6% Na_2O and up to 1.5–2% K_2O). In the contents of the alumina, iron, magnesium and calcium, these rocks are close to the alkali series of basalts. However, the main distinction of the alkali-ultramafic rocks from alkali basalts is a typical set and elevated concentration in them of lithophilic elements and rare metals: phosphorus, niobium, tantalus, zirconium, rare earths, strontium, barium and radioactive elements. In some cases (for instance, in the Khibin massif apatite-bearing sienites) are encountered notable amounts (up to 150 cm^3 per a kilogram of rock) hydrocarbon gases and even heavy hydrocarbons, up to C_{19} [22].

Thus, with all variety and specifics of the rock association under review (kimberlites, lamproites, carbonatites and alkali-ultramafic rocks), they are brought close together by the depth (subcrustal) origins, low or moderate silica contents and a drastic enrichment with dispersed lithophilic elements, rare metals and volatile compounds (up to hydrocarbon inclusions). Besides, all these rocks are encountered only in the ancient, Early Pre-Cambrian continental crust.

It is important to include here also quite interesting data regarding the kimberlites' and carbonatites' isotopy. It is noted in the monograph by J. Dawson [1] that δD for serpentine and phlogopite (which contain a large mass of kimberlites' bonded water) varies within a range of 89 to 102‰ and $\delta^{18}O$ values vary between −1.08 and +12.2‰ by SMOW standard. Carbon $\delta^{13}C$ isotope composition in the kimberlites' carbonate phase for the rock as a whole as well as for the carbonatites varies within a range of +1 +2‰ to −8‰, and in some cases to −20 −25‰ by the PDB standard whereas variation of $\delta^{18}O$ oxygen ranges within +6 to +24 +25‰ SMOW [1]. The included data of $\delta^{13}C$ and $\delta^{18}O$ broad variations in a carbonate matter of kimberlites and carbonatites also indicate heterogeneity of the sources of matter involved in their formation.

2

Issues of the Diamond-Bearing Rocks' Origin

Great successes have been achieved in the studies of geology, petrology and geochemistry of diamond-bearing kimberlites, lamproites and affine rocks. An excellent summary is included, for instance, in the monograph by J. Dawson [1] and in publications [2–4, 10, 23–25]. Despite this, no commonly accepted concept of the origin of these enigmatic rocks has been so far formed. Nevertheless, today some features and even details of their formation are established with sufficient certainty.

For instance, it may be considered as firmly established that diamond-bearing kimberlites, and along with them, hard rock diamond deposits, are associated only with Archaean and sometimes Early Proterozoic ancient continental shields [1, 24–26]. Geologic studies in the oceans have shown that no kimberlites or lamproites and their affine depth rocks of the alkaline-ultramafic and carbonatite series were encountered anywhere on the ocean floor [27]. These very important results indicate that the kimberlite magmas might have formed only underneath most ancient Precambrian cratons and that their origin had possibly been closely associated with the very process of the continental lithosphere evolution.

The diamond formation conditions are usually studied from petrology and geochemistry of the eclogite and garnet peridotite depth inclusions often found in the kimberlite rocks [23, 28]. After the conduct of experimental studies in the mineral polymorphic transitions at high pressure and temperature occurring in samples of such composition [29–31] and especially after upgrading of barometric techniques [32, 33], it was possible to establish with certainty that the diamond-bearing kimberlites formed at depths exceeding 120-150 km. Exactly at such depths crystallize diamonds and emerge characteristic mineral associations in eclogites and garnet peridotites of the diamond -pyrope depth facies [23]. On the other hand, it has been known for a long time [34] that at depths of about 350 km the rhomboidal pyroxene must change into a denser cubic modification (spinel phase), i.e., ringwoodite. However, the ringwoodite has

N. O. Sorokhtin (ed.) The Origins of Natural Diamonds, (7–10) © 2019 Scrivener Publishing LLC

been nowhere found in the kimberlites or in diamond inclusions. This fact apparently restricts the maximum depth of diamond-bearing rock formation by 300 km [1].

Successes have been reached in the modern "petrologic" barothermometry based on studies of the correlation between mineral associations in eclogites and peridotites vs. pressure and temperature. These achievements enabled restoring positions of the ancient geotherms that had existed in the lithosphere mantle under the kimberlite diatremes at the time when the mineral composition of rocks corresponding with these xenoliths [1, 32, 33, 35–37] formed, based on xenoliths carried out by kimberlite magmas from various levels of the subcrustal lithosphere. Summarizing these data, it was possible with some certainty to outline the existence domain in the mantle of the diamond-bearing eclogites and garnet lherzolites [1, 23, 38]. This domain turned out sufficiently wide: at a pressure P around 50 kbar, the temperature range was 1,120-1,380°C, and at 70 kbar, 1,300-1,500°C. For the garnet lherzolites, this domain is no narrower and is restricted by temperatures 900-1,400°C (see Fig. 2.1). However, as J. Dawson emphasized, the actual temperature of the diamond-bearing eclogite formation range in each specific case may be much narrower. For instance, for Roberts-Victor diatreme in the Southern Africa it is within the range of 1,017 to 1,160°C. The finds of coesite inclusions in diamond crystals, according to N.V. Sobolev [39], also indicate a relatively low temperature of the upper mantle underneath continental platforms.

When studying genesis of kimberlite magmas and enclosing rocks' xenoliths they carry out, it is important to remember that at depths of the diamond formation (150 to 220 km), the mantle matter (garnet lherzolites) melting temperature, based on the experimental data [40], reaches respectively 1,600 and 1,700°C. An important conclusion follows from this, imposing rigid restrictions on a possible multitude of the diamond formation hypotheses. It turns out that the generation of much lower-temperature kimberlite magmas must have occurred without melting of the mantle matter. Moreover, at the present-day distribution of the mantle temperature, basalt melts at such depths cannot melt out at all, and therefore, the eclogite rocks also could not have formed *in situ*. This could have happened only at the time of the "peak" upper mantle overheating in Late Archaean but at that time the thickness of the lithosphere (together with the continental crust) had not yet exceeded 70-80 km (see Fig. 8.9).

Many eclogite and garnet peridotite xenoliths carry in themselves traces of substantial deformations often creating fluid and laminar flow structures [41]. This is an indication of complex ways of mantle rocks transformation underneath the continents. They often formed there in the environment

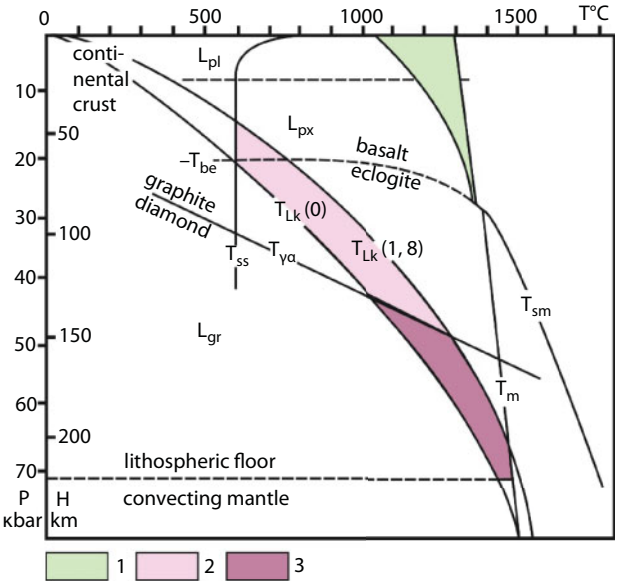

Fig. 2.1 Thermodynamic conditions of diamond formation: 1. Existence area of juvenile mantle (basalt) melts; 2. Existence area of alkali-ultramafic and alkali-carbonatite melts; 3. Existence area of diamond-bearing depth lamproite, kimberlite and calcium carbonatite melts; T_m is mantle temperature; T_{sm} is mantle matter solidus temperature; T_{be} is basalt – eclogite transition temperature; $T_{\gamma\alpha}$ is graphite – diamond transition temperature; $T_{Lk}(0)$ is the present-day continental geotherm; $T_{Lk}(1,8)$ is the ancient continental geotherm as of the time 1.8 BYa; L_{pl}, L_{px} and L_{gr} are stable existence areas of plagioclase, pyroxene and garnet lherzolites; T_{ss} is water-saturated deposit melting temperature.

of intense strike-slip deformations but not very high temperatures. Otherwise, all traces of the mantle matter flow structures would have been totally destroyed due to long rock annealing at sub-solidus temperature. Some diamond crystals also have suffered substantial plastic deformations. At that, in the process of crystal growth apparently occurred also notable alterations in chemical composition of the medium. This is indicated, in particular, by the changes in the nitrogen and other admixtures content within various crystal layers [42] as well as by variations of carbon isotope ratios in the individual diamonds [43]. In this connection it is hard to escape a conclusion that the kimberlite magma formation processes have been associated with the intense matter displacements in the upper mantle underneath the continents.

However, within the framework of classical diamond-bearing rocks genesis concepts many questions still remain unanswered. Among them, J. Dawson [1] includes the following: 1. What is the nature of carbon,

phosphorus and nitrogen sources in the upper mantle? 2. Why is the kimberlite carbonate phase represented by calcite, whereas in the stability environment of garnet peridotites, dolomite and magnesite should have been stable [44]? 3. Why do some kimberlites contain diamonds, and some others do not? 4. Are diamonds xenocrysts or inclusions? 5. Why are the kimberlites and their affine rocks encountered only on continents? 6. From where does water come into the kimberlite magma? 7. What causes carbon isotope shift in diamonds and kimberlite carbonatite matrix? 8. What is the mechanism of tectonic motions so substantially deforming rocks of depth inclusions in the kimberlites? 9. What is the nature of the energy that causes melting of the kimberlite magma, and what are cause and effect associations operating in the kimberlite formation process?

Within the framework of "classical" concepts of the diamond-bearing kimberlites' origins on the account of melting of the upper mantle matter enriched with volatile compounds, all these questions remain unanswered. In the model of the diamond-bearing kimberlites and their affine rocks origins we are describing in this book, to all these questions asked by J. Dawson are given relatively simple and, which is most important, natural responses (see Chapter 12).

3

Existing Concepts of the Diamond-Bearing Rocks Origin

The earliest kimberlite formation hypothesis is apparently an idea by P. Harris [45, 46] of a possible zonal melting of the mantle. It is suggested that due to this process a slowly rising layer of light melts must have gradually accumulated volatile and incoherent elements. However, for supporting the operating of such a mechanism powerful energy sources are needed, energy released in the process of its operation. In Early Archaean, the zonal melting of a mantle matter could have indeed occurred at the expense of the gravity energy of separating the metallic iron from silicates of the primary Earth's matter release [17, 18]. But at that time this process resulted in melting out only of the basalt or komatiite composition separation of the metallic iron from silicate of the primary Earth's matter, whereas more differentiated series of the tonalite-trondjhemite composition and primitive plagio-granitoids emerged only after their secondary remelting. Besides, in Early Archaean the lithospheric shell underneath the continents did not exceed in thickness several dozen kilometers (see below). In all other geological epochs, in the mantle energy sources capable of feeding the process of the mantle mater zonal melting simply did not exist.

In the mid-1960s, a hypothesis was popular of kimberlites' and their affine rocks formation due to partial melting of the garnet peridotite at depths around 80–100 km with the subsequent fractionation of picrite basalts [47]. At that, it was assumed that the fractional crystallization of picrite basalt at high pressure produced eclogite cumulates and residual silica-poor alkaline melts with kimberlite and its affine rocks composition.

J. Dawson [1] wrote that the origin of kimberlite magmas is indicated by limited volumes associated either with products of a lengthy fractioning of mantle melts or with products that are very insignificant in terms of the mass partial melt off of the mantle matter. At that, it is assumed that in the area of the source of partial mantle melting must have contained notable amounts of K, Ti, Ba as well as H_2O, CO_2 and other volatile components [48]. A rather peculiar spectrum of rare earth elements distribution in the

N. O. Sorokhtin (ed.) The Origins of Natural Diamonds, (11–17) © 2019 Scrivener Publishing LLC

kimberlites indicates a possibility of mica and diopside participation in the formation of this rock. This is also supported by the isotopy data of strontium and rare earths. J. Dowson believes that the ideal medium for such melt off of kimberlites is a garnet lherzolite enriched in phlogofite and carbonates.

Most current hypotheses also explain the origin of the kimberlite and their affine magmas by a partial melting of the mantle matter enriched in volatile elements or by the emergence of residual melts in the process of a long-term fractioning of the mantle matter. This approach until now remains most popular among many researchers of the diamond-bearing rocks and diamonds proper genesis. Thus, Yu.L. Orlov [49] wrote that the diamond was a magmatic mineral crystallizing at depth in an alkali-ultramafic magma from which kimberlite rocks form. The proponents of this concept believe that the carbon source of diamonds is a juvenile carbon contained in the magma itself, and the diamonds crystallize in this magma together with the olivine, garnet, pyroxene and other minerals found in the diamonds as syngenetic inclusions.

Despite a great popularity of the mantle-magmatic hypotheses of diamond-bearing rocks origins, they have a number of major and hardly surmountable drawbacks.

First, all present-day petrologic determinations of kimberlite magma formation conditions with certainty indicate their not so high temperature, about 1,000–1,250°C at the pressure of 45 to 65 kbar [1, 37]. This is approximately 500°C below the expected melting start temperature of the mantle matter. The melting occurs at a similar pressure within the temperature range of 1,570 to 1,720°C [40]. An unavoidable conclusion is that kimberlite magmas and their affine magmas simply could not have formed due to melting (even a partial melting) of the mantle matter as the temperature barrier separating the existence domains of kimberlite and mantle melts turns out too high.

Second, the kimberlite melts formation at the expense of a partial melting of the lherzolite composition mantle matter, even if it had occurred, could have resulted only in a moderate (equilibrial with lherzolites) enrichment of the emerging melts with lithophilic and volatile elements but without a sharp decrease of silica concentration so typical of kimberlites and especially carbonatites. Besides, such mechanism conceptually could not have resulted in "hurricane" concentration increase of many rare-earth and dispersed elements (for instance, radioactive ones).

Third, a suggestion that the source material for melting out of kimberlites could have been the garnet lherzolite containing admixtures of phlogopite and carbonates (often found in kimberlites and xenoliths) a priori

assumes the existence in the juvenile mantle of substantial heterogeneity, variability of its chemical composition. However, as we know now from a fact of the continuous drift of the lithospheric plates, Earth's mantle is subjected to an intense convection. During its lifetime its matter had numerous chances to intermix and homogenize. This is also supported, in particular, by tholeiite basalts melt outs in oceanic rift zones. That is why, according to the present-day understanding, the juvenile mantle on average is uniform in composition [50], maybe with its slight variations due to still continuing process of iron oxides transfer from the mantle to the Earth's core [17, 18]. This is the reason why it is difficult to perceive now numerous hypotheses deriving the origin of kimberlites and their affine rocks from melting of the anomalous mantle areas ostensibly drastically enriched in volatile compounds and lithophilic elements. Such anomalous areas downright do not exist in the juvenile mantle although within it may emerge narrow (local) inhomogeneities underneath the lithospheric plate subduction zones through pulling into them of the oceanic crust and deposits. However, these are already not primordial endogenous anomalies in the mantle composition but exogenous irregularities introduced in it together with the crust matter and deposits. These irregularities are totally homogenized again in the differentiation and disintegration process of the mantle matter on the surface of Earth's core (see Fig. 5.10). The participation of such exogenous factors in the diamond-bearing rocks and their affine rocks formation process is reviewed in a different group of hypotheses. In greater details, this approach is also elucidated in this book.

The abundant materials accumulated in recent years of the isotopy in the rock group under review and of inclusions in diamonds as well as materials of carbon isotopic shifts within the crystals proper forced a new approach to the entire issue of the origin of diamond and diamond-bearing rocks. Thus, V.S. and N.V. Sobolevs [51] came to a conclusion that, beside the mantle (juvenile) carbon, in diamond formation may take part also exogenous (carbonate) carbon pulled in together with the oceanic crust through the subduction zones to the great depths under the continents. Simultaneously, a natural explanation was given of eclogites' origin at the expense of altering basalts from the former oceanic crust. Analyzing carbon and oxygen isotopy in carbonatites and kimberlites, N.V. Kuleshov [10] came to a definite conclusion that in the formation of carbonate matter of kimberlites and carbonatites participates the crustal carbon dioxide of a primary-depositional origin. At that, it is emphasized that the mantle matter is sharply impoverished in volatile components including carbon dioxide. Thus, a conclusion is made of an impossibility to exist in the mantle in notable amounts of carbonate melts or significant CO_2 accumulations at

the expense of mobilizing the primary (juvenile) Earth's carbon. Therefore, the origin of high-temperature carbonates in the kimberlites and carbonatites must be associated with the remobilization of the crust matter, and first of all of the matter from Earth's sedimentary shell.

Studying an issue of the origins of kimberlites and their affine rocks from a perspective of lithospheric plate tectonics, we came to a conclusion that the entire matter of the kimberlite, carbonatite and alkali-ultramafic magmas emerged due to remelting of pelagic deposits pulled in through the subduction zones to great depths underneath the continents. Indeed, the isotopic composition of the diamond carbon is impossible to explain without involving the core matter [52]. A similar situation is observed in high-temperature depth rocks of the carbonatite and kimberlite association. Their carbon and oxygen isotope composition indicates that the core carbon dioxide of primary-depositional origin participated in the formation of carbonate matter in these rocks [10]. Analyzing sulfur isotope shifts and lead isotopic ratios from sulfide inclusions in diamonds, K. Eldridge with colleagues [54] came up with similar conclusions. Simultaneously, they confirmed an ancient age of diamond formation (about 2 BY) we predicted earlier based on lithospheric plate tectonics mechanism [55].

However, regular sediments of the present-day type, due to their low density, cannot be pulled in to great depths. For this to happen, density of the sediments in plate subduction zones should exceed average density of the continental plates [56]. Such iron-rich, therefore high-density (heavy) pelagic sediments have been deposited only in Early Precambrian. Only they could have been pulled in ("collapsed") to great depths through the ancient subduction zones underneath the continent shields. However, this mechanism of kimberlite formation might have been implemented only in Early Proterozoic when not only heavy ferruginous sediments have been deposited but also the continental plate thickness had increased to 200–250 km [11, 55, 57, 58]. Later, similar ideas (although without considering the role of the iron ore deposits in the kimberlite formation) have been embraced by the authors of a collective monograph "The Archangel diamond-bearing province" [59].

The issue of these exotic rocks' origin is reviewed in the monographs [55, 58]. According to the developed model, diamond-bearing kimberlites and their affine rocks have emerged due to pulling in of the oceanic crust and Early Proterozoic heavy (ferruginous) oceanic deposits to great depths (up to 200–250 km) through ancient subduction zones underneath the Archaean shield rocks (Fig. 3.1). Due to a high density of the ferruginous deposits they must have "collapsed" on their own in plate subduction zones and served within them a "lubricant" similar to the one that lubricates

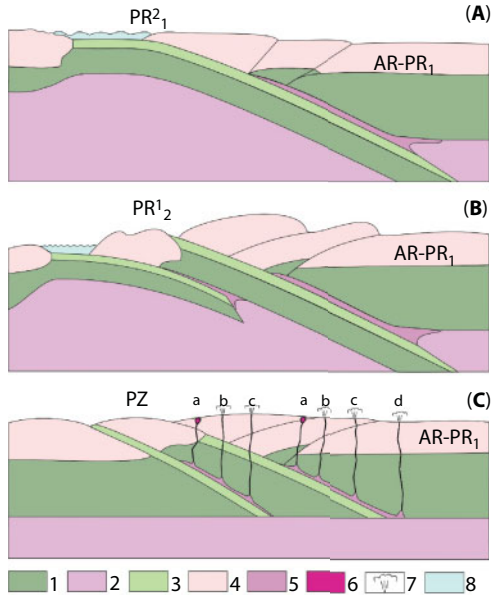

Fig. 3.1 The formation process of depth alkali-ultramafic, lamproite and kimberlite composition melts: (A) Geodynamic environment at the end Early Proterozoic; (B) At the boundary Early/Middle Proterozoic; (C) In Riphaean or Phanerozoic; a-d. Areas of a regular placement and structure of depth magmas' transport to the continental crust surface: a. alkali-ultramafic intrusions; b. Melilite and carbonatite diatremes; c. Nondiamond-bearing lamproite and kimberlite subvolcanic complexes; d. Diamond-bearing lamproite and kimberlite diatremes. 1. Subcrustal lithosphere; 2. Mantle astenosphere; 3. Early Proterozoic oceanic crust with overlying heavy ferruginous deposits; 4. Continental crust of Archaean (AR) and Early Proterozoic (PR_1) age, 5. Buried depth melts, 6. Central type alkali-ultramafic intrusions; 7. Explosive stuctures of various composition diatremes; 8. World ocean basins.

friction parts of any mechanism. Perhaps for this reason plate subduction zones at the end of Early Proterozoic (at the time of the Svecofennian orogeny) and in Middle Proterozoic have been mostly amagmatic, without the calcareous-alkali volcanism typical of the island arcs and active continental margins. This had been due to the fact that heavy and relatively cold deposits had been rapidly pulled in the subduction zone and had not have time to reach critical temperatures of melting their component matter.

Under the expounded idea (and contrary to the common view) it is not possible to consider the diamond-bearing kimberlites, lamproites and carbonatites as mantle rocks. This rock group should rather be called pseudomantle. As for the eclogite xenoliths found in them, practically all are metamorphosed fragments of the basalt layer from the former oceanic

crust. As opposed to them, the inclusions of garnet peridotites may have various nature. Most of them are fragments of the third (serpentinite) layer of the former oceanic crust, whereas the other part may be fragments of the subcrustal continental lithosphere torn off the eruption channel walls. Respectively, the first type of such ultramafic xenoliths may be diamond-bearing and the second, on the contrary, will always be "diamondless". A concept of the model expounded in this monograph of diamond-bearing kimberlites and their affine pseudo-mantle rocks formation is illustrated by Fig. 3.1.

In our model, formation moment of the depth melts is strictly restricted by the epoch of the second half of Early Proterozoic (1.8 to 2.2 BYa) or, on some rare occasions by the Middle Proterozoic epoch. The reason is that in Archaean, conditions had not yet existed for the generation of magmas belonging with the type under review because Earth's exceptionally high tectonic activity and very powerful heat flows had not then allowed the increase of the continental lithospheric plate thickness together with continental crust thickness to greater than 60–80 km. Subduction zones had not existed in Archaean at all and had been substituted with zones of heaping up and piling up of relatively thin oceanic lithospheric slabs of mostly basalt or komatiite composition. Only after Earth's core separation at the end of Archaean first subduction zones had emerged and Archaean continental lithospheric plate thickness had begun rapidly increasing. By the end of Early Proterozoic it reached maximum values of about 250 km. This created the conditions for a formation opportunity of depth (diamond-bearing) melts. However, the chance for the implementation of this opportunity had occurred only when about 2.2 BYa on the ocean floor had begun depositing heavy iron ore jaspilite type deposits. This epoch of a super massive deposition of iron ore deposits had lasted approximately until 1.8 BYa and exactly with this epoch (2.0–1.8 BYa) corresponded the birth in the depths of the continental lithosphere of maximum amounts of kimberlite and their affine magmas. The second, less significant impulse of depth melt generation, could have occurred during disintegration time of the second supercontinent, Stille's Megagea (around 1.6–1.4 BYa). At that time multiple relatively shallow-water intercontinental oceans have emerged from whose rift zones iron have been carried out. With this epoch had been associated the formation of unique anorogenic anorthosites and rapakivi granites that had usually formed due to "collapsing" of heavy ferruginous deposits, accumulated along passive continental margins, underneath the oceanic lithosphere [18]. If such deposits have been getting in plate subduction zones, they also may have given birth to depth pseudo-mantle alkali-ultramafic and even kimberlite melts.

Within the framework of the described model it was possible to describe from a unified position most of the specific features and sometimes even subtle details of the composition of diamond-bearing and their affine rocks, including diamonds proper and mineral inclusions in them. Thus, under this model kimberlites and lamproites are indeed depth rocks but they have emerged from pelagic deposits. A conclusion from this is that carbon, phosphorus, nitrogen, most lithophilic elements (Li, B, F, Cl, K, Ti, Rb, Sr, Y, Zr, Nb, Cs, Ba, Ta, Pb, Th, U), carbonates, water and other fluids in diamond-bearing rocks do not have mantle but primary depositional, i.e., purely exogenous origin. This is also indicated by high concentrations and spectrums of rare earth's elements, potassium/sodium, thorium/uranium ratios, by hydrogen, oxygen, sulfur and strontium isotopes in the kimberlites as well as gas-liquid inclusions in diamond of H_2O, H_2, CH_4, CO_2, CO, N_2, Ar, C_2H_4 and even ethyl alcohol C_2H_5OH [20, 21]. It is also supported by carbon isotope ratio shifts in diamond crystals clearly carrying biogenic marks. The diamond-bearing rock formations and other isotope data, for instance, neodymium/samarium, rubidium/strontium, strontium, uranium/lead, thorium/lead and lead/lead ratios neatly fit with the developed model.

Diamonds undoubtedly are the most exotic and mysterious mineral on Earth. They, as a microcosm, reflect the entire evolution of our planet. Within this context, to uncover the origin of this enigmatic mineral and to determine the natural conditions of its formation is possible only by preliminarily reviewing major patterns in the origins of Earth itself. That is why we will begin with a brief description of the modern theory of Earth's global evolution expounded in greater detail in the following monographs [17–19].

4

Earth's Origin, Composition and Structure

Under the modern cosmogonic concepts, the primordial proto-Sun – proto-planetary cloud formed from the interstellar gas and dust accumulations typical of our and other galaxies. Whereas the origin of the matter in these accumulations is associated with blowups of large stars (with the mass exceeding several times the Sun mass) that completely made their evolutionary path. Usually, the final blowups of such large stars are called flareups of "supernova" stars as for a short time their luminance increases by the factor of millions, they become the brightest objects in their galaxies and are perceived by us as the flareups of new stars against the customary background of the "old" firmament.

The origins of the Solar system planets, including Earth, have been numerously described in many special papers and monographs [60–67]; Levin, 1972, and also in popular books, for instance, by O. Yu. Schmidt [68]; W. Kaufman [69]; D. Fisher [70] and other authors. For this reason, we will not be dwelling on this issue in detail and will provide only a most general description of the process based on the foundational ideas of O. Yu. Schmidt [71] and aforementioned publications.

According to the modern cosmogonic concepts laid down by O. Yu. Schmidt already in the mid-1940s [68, 71], Earth's group's planets including Earth and Moon, formed by the accretion (adhesion and further growth) of solid particles from the gas-gust protoplanetary cloud. Usually, the original density of interstellar clouds is insufficient for the gravity compression and development within them of spontaneous star formation and planet formation processes. However, supernova explosions are accompanied by the emergence of shock waves in the interstellar medium. In cases when such waves cross a gas-dust cloud, the pressure and density of the mass on their front drastically increase. As a result, the concentrations may emerge capable of further compression already at the expense of self-gravity. That is why blowups of supernova stars not only deliver a new matter in the outer space but also serve the mechanism which in the final analysis is leading to the formation of new stellar generations and their surrounding planetary systems.

N. O. Sorokhtin (ed.) The Origins of Natural Diamonds, (19–40) © 2019 Scrivener Publishing LLC

It is likely that exactly such a situation had emerged about 4.7 BYa in the vicinity of the proto-solar gas-dust cloud. Having gotten an impulse of the initial compression and revolution, and having replenished with a new matter, this cloud subsequently began an irreversible compression already under the action of its own gravity field. In the course of the compression, the pressure and temperature in the central part of the cloud began rapidly increasing and gradually in this zone had formed a giant gas blob, the Protosun. However, initially, prior to the "flare-up" of nuclear reactions and the coming by the Protosun on the main sequence of the star evolution, its temperature was relatively low (no greater than 1,000 – 1,500°C) and the radiation was occurring mostly in the infrared and rad spectrum ranges.

The formation of the Sun as a normal not very large yellow star out of the compressing primordial clot of gases and dust had been occurring much faster than the planet formation (just in a few million years). At that, at the very beginning of "lighting up" in the bowels of a young Sun of the helium synthesis nuclear reactions but prior to reaching by him the regime of the star development's main succession, our Sun should have passed through a brief existence stage of τ-Taurus star type characterized by a rapid revolution, strong magnetic fields and very high intensity of the "stellar wind" radiation.

These particulars in the evolution of a young Sun unavoidably should have affected the matter accretion conditions in its surrounding protoplanetary cloud – disk. First, on the account of the exceptionally strong "solar wind" (a high-energy flow of charged particles) typical of the stars at the τ-Taurus stage, all gas and volatile components of the primordial protoplanetary cloud must have been wiped out from the circumsolar space into the remote periphery of the Solar system.

The reason for this was that the ionizing effect of the high-energy charged atomic particle's flow on a surrounding matter of the protoplanetary disk led to a strong interaction with it of the Sun's magnetic field. Perhaps, exactly as a result of such efficient "entanglement" of the rapidly revolving young Sun with its surrounding matter a redistribution occurred of the kinetic momentum from the central celestial body to the periphery of the protoplanetary disk. After that the Sun's axial revolution rate declined whereas the rates of orbital revolution around it of the matter in protoplanetary disk, on the contrary, increased. Perhaps, the same mechanism caused a notable matter separation in the protoplanetary cloud because all easily ionizing elements affected by the magnetic field's lines of force pressure have been as if wiped out of the near-solar space on the periphery of the protoplanetary disk.

Besides, a substantial influence on the matter's chemical differentiation in the protoplanetary cloud must have rendered also a great heating by the Sun of the disk's central areas already at a stage of its compression and especially after "lighting up" of nuclear reactions within the Sun. For this reason, many easily evaporating elements and compounds (for instance, sulfur and its volatile compounds, water, carbon dioxide, etc.) passed in the gaseous state after which the Sun radiation pressure removed them from these areas into a distant periphery of the Solar system.

The action of these mechanisms must have resulted in prevailing condensation within central areas of the protoplanetary disk of hard-melting elements and compounds with high ionizing potential (hard-melting metals including Fe and Ni, and oxides Al_2O_3, CaO, MgO, Ti_2O_3, SiO_2, Cr_2O_3, FeO, etc.) Whereas average concentrations of easily melting and easily ionizing elements (Li, Na, K, Rb, Cs, In, Ba, the elements of rare earth group, Hg, Pb, etc.). in this area of the protoplanetary cloud turned out substantially marked down. To a somewhat smaller extent, the planetary matter of Earth's group was impoverished in sulfur, zinc, tin and some other elements. Whereas gaseous components (H_2, He and other noble gases, H_2O, CO, CO_2, CH_4, NH_3, H_2S, SO_2 and SO_3, HCl, HF have been wiped out practically in toto from internal areas of the protoplanetary cloud and concentrated only on its periphery where subsequently formed giant planets with massive and dense gas shells. It is likely that the internal areas of the protoplanetary cloud have also been impoverished in hydro-silicates and carbonates that have dissociated affected by the solar radiation with a subsequent loss of volatile gases.

As a result, even before the beginning of the planet formation process the primordial protoplanetary gas-dust cloud had been substantially differentiated. This phenomenon perhaps may explain a clear correlation between the density of planets and their distance from the Sun (Mercury, 5.54 $g.cm^3$; Venus, 5.24; Earth together with Moon, 5.49; Mars, 3.94; Jupiter, 1.33; Saturn, 0.67; Uranus, 1.3; Neptune, 1.67 g/cm^3). This is also an explanation of the fact that only the outer planets have massive gas shells and their satellites are covered with thick shells of water ice, sulfur and other solidified or liquefied gases (CO_2, CH_4, NH_3, etc.).

A judgment may be made based on the composition and a relatively small mass of Earth's atmosphere and hydrosphere (not exceeding in total $2.4 \cdot 10^{-4}$ of the planet's mass), that Earth and other celestial bodies of Earth's group have been formed out of the matter which had almost completely lost all gas components. Indeed, Earth's atmosphere is practically devoid of primary heavy noble gases and Earth's matter is drastically impoverished in

hydrosilicates, carbonates, sulfur and its compounds, and notably impoverished in the alkaline and other low-melting metals.

Most likely, the aforementioned differentiation of the primordial matter in the protoplanetary cloud had been occurring quite rapidly, just in a few million or tens of million years (mostly as early during compression of the protoplanetary gas-dust disk and at the time of the young Son passing through the stage τ-Taurus star evolution). Whereas the planet formation had begun after the disk's planetesimals had already acquired circular orbits and continued for a relatively long time, on the order of 10^8 years [61]. A very important conclusion follows from this: the planets' accretion in their ring feeding zones (besides, having finite width) had been mostly homogenous (uniform). This means that average chemical composition of growing planets (in the absence in them of a differentiation processes) remained approximately constant along the entire radii of such planets.

The evaluation by V.S. Safronov [61], one of the creators of the modern planet-formation theory, indicate that the growth of Earth had continued for about 100 million years and in the beginning had been occurring under ever-accelerating accretion regime but then, due to exhaustion of the solid matter reserves in the near-Earth swarm of planetesimals of the protoplanet cloud, it had decelerated again. A giant amount of the gravity energy had been released at Earth's accretion, nearly $23.3 \cdot 10^{38}$ erg. This energy had been more than sufficient not only for melting of the entire Earth's matter but also for its total evaporation at the temperature of over 30,000°C. However, most of this accretion energy had been released within the most surficial portion of the growing Proto-Earth and lost again with its heat radiation. Naturally, the slower had been Earth's growth, the greater had been the heat loss.

This important result shows that Earth, in the process of its growth, not only had been heated by the strikes of planetesimals falling on its surface, but also had time to cool down radiating at that into the outer space most of the accretion heat energy. As a result, during the entire period of Earth growth (about 10^8 years) the temperature of its subsurface obviously remained everywhere below Earth's primordial matter melting temperature. Therefore, Earth itself at that time had been remaining a relatively cold, undifferentiated planet devoid of the core and Earth's crust. The same is indicated by plain geologic data. First, this is a total absence on Earth of any magmatic rocks within the age interval 4.6 – 4.0 BY. This is an indication of its originally cold state (first magmatic rocks appeared in Earth's crust only in about 600 – 800 MY after Earth's formation). Second, the strongest and practically irrefutable testimony of this are lead isotope ratios on the Moon and Earth. In lunar rocks certainly formed after the

planet's total melting and differentiation, the ratios of radiogenic lead isotopes with atomic weights 206, 207 and 208 formed on the account of uranium 238 and 235 decay, and thorium 232, to the stable (primary) isotope 204 are extremely high. These ratios reach in lunar rocks, respectively, values 207, 100, 226 and higher whereas for Earth's rocks averaged in the oceanic reservoir of pelagic deposits, the same ratios are 19.04, 15.68 and 39.07. And for the primary lead (judging by the isotopic composition of the Canyon Diablo iron meteorite, in Arizona, USA) they are even lower, 9.50, 10.36 and 29.45 [72]. The included lead isotope ratios are practically a unique indication of the total melting and differentiation of lunar matter; they equally convincingly show that Earth had never been totally melted and subjected to a differentiation so radical.

Therefore, Earth had been formed due to heterogenous accretion of cold protoplanetary gas-dust cloud under the influence of the sun wind, light pressure, short-term temperature rise and magnetic separation already at the pre-accretion stage. As a result of such protoplanetary matter differentiation, in the Earth and Moon formation zone, all primordial matter gas components have been practically completely removed from the primordial cloud. This matter had been impoverished in hydrosilicates, carbonates and sulfur as well as alkali and some other light-melting elements.

First proposed by O. Yu. Schmidt [71] and worked out in detail by V.S. Safronov [61], Earth and other Solar system planets' formation hypothesis turned out unusually fruitful not only for explaining planet formation mechanisms but also at considering Earth evolution already at the planetary stage of its evolution. We emphasize that for a study of Earth's geologic evolution the mentioned publications are starting and undoubtedly very important ones as they define initial conditions of our planet's existence. In particular, exceptionally significant for understanding of further Earth evolution paths are two major conclusions of the planet formation theory. First, the young Earth immediately upon its formation had been a relatively cold cosmic body, and the temperature anywhere in its bowels had not exceeded the Earth's matter melting temperature. Second, the primordial Earth had had a reasonably uniform composition; therefore, at that time Earth's core and chemical layering of its subsurface into the mantle and crust had not yet existed. As will be shown below, the young Earth had been also devoid of hydrosphere and had had only a low-density (around 10^{-3} atm) atmosphere composed at that time mostly of nitrogen with a small addition of noble gases.

If we accept these conditions as the initial conditions then the further Earth (its core, mantle, crust, hydrosphere and atmosphere) evolution must have been totally defined by Earth's matter initial composition, initial

thermal content of our planet and by the history of its interaction with the Moon. It is assumed at that, that endogenous energy sources (gravity differentiation of Earth's matter and radioactive elements' decay energy) actually controlling the entire course of Earth's global evolution have also been eventually defined by the initial composition of Earth. Hence it is expedient to begin with the composition of the initial Earth's matter.

The composition of primordial Earth. An estimate of average Earth's matter composition by main petrogenic oxides and elements may be performed by mentally mixing the matter of major Earth's geospheres: the mantle, Earth's crust and core. The results of such estimate are included in Table 4.1 as compared with the composition of the present-day crust, mantle, core and rock meteorites.

As Table 4.1 shows, Earth's primordial matter had been a clearly expressed ultramafic rock with low silica saturation factor (practically the same as for the olivine) and high relative content of bivalent iron oxide. Therefore, Earth's primordial matter had been characterized by a clearly expressed ortho-silicate composition and had been composed approximately of 75% olivine $(Mg_{0.62}Fe_{0.38})_2SiO_4$, 11% of other silicates and 13.6% of kamacite $Fe_{0.9}{\cdot}Ni_{0.1}$.

Judging by these estimates, it is possible to consider that relative the average Sun matter composition, therefore, average composition of the Solar system's planets and meteorites, Earth had been somewhat enriched in iron and its oxides (approximately by 50 – 60%), substantially impoverished in sulfur (approximately 10-fold), potassium (about 4 – 5-fold) and other mobile elements but had almost average for the Solar system oxygen abundance (relative to silicon).

It is much more difficult to estimate contents in the primordial Earth matter of volatile, mobile and rare (dispersed) elements. For that, unfortunately, often it is necessary to use only indirect methods always remembering that the encountered on the surface samples of Earth's depth rocks already in the invasion process or subsequent actions had been usually substantially contaminated by water and dispersed elements getting in these rocks from the outer geospheres (hydrosphere or Earth's crust). For instance, absolutely unfit for determining the mantle composition and the composition of its water and other volatile elements the depth rocks like kimberlites and lamproites as they themselves and their affine rocks emerged by pulling to great depths of Early Proterozoic oceanic deposits. In effect, these rocks are oceanic deposits remelted and highly metamorphosed at great pressure. Whereas contained in them ultramafic and eclogite xenoliths upon a closer view turn out to be fragments of the ancient oceanic crust (the eclogites are fragments of the basalt layer, the

Table 4.1 The composition of present-day Earth and of primordial Earth's matter.

Oxides	Continental crust composition[1)]	Model composition of Earth's mantle[2)]	Model composition of Earth core	Composition of primordial Earth's matter (estimate)	Chondrite average composition[3)]	Carbon chondrite average composition[4)]
SiO_2	59.3	45.4	–	30.71	38.04	33.0
TiO_2	0.7	0.6	–	0.41	0.11	0.11
Al_2O_3	15.0	3.7	–	2.54	2.50	2.53
Fe_2O_3	2.4	1.97	–	–	–	–
FeO	5.6	6.55	49.34	22.76	12.45	22.0
MnO	0.1	0.13	–	0.09	0.25	0.24
MgO	4.9	38.4	–	25.81	23.84	23.0
CaO	7.2	2.3	–	1.57	1.95	2.32
Na_2O	2.5	0.43	–	0.3	0.95	0.72
K_2O	2.1	0.012	–	0.016	0.17	–
Cr_2O_3	–	0.41	–	0.28	0.36	0.49
P_2O_5	0.2	–	–	–	–	0.38

(*Continued*)

Table 4.1 The composition of present-day Earth and of primordial Earth's matter. (*Continued*)

Oxides	Continental crust composition[1)]	Model composition of Earth's mantle[2)]	Model composition of Earth core	Composition of primordial Earth's matter (estimate)	Chondrite average composition[3)]	Carbon chondrite average composition[4)]
NiO	–	0.1	–	0.07	–	–
FeS	–	–	6.69	2.17	5.76	13.6
Fe	–	–	43.41	13.1	11.76	–
Ni	–	–	0.56	0.18	1.34	–
Total	100.0	100.0	100.0	100.0	99.48	98.39

[1)] A.B. Ronov, A.A. Yaroshevsky [73]
[2)] Our model using the data by L.V. Dmitriyev [74] and A. Ringwood [75]
[3)] H. Urey, H. Craig [76]
[4)] (Essays of a comparative planetology. Moscow, Nedra, 1981). p. 184–185.
Earth's mass: $M = 5.9772 \cdot 10^{27}$ g; core mass: $M_{я} = 1.9404 \cdot 10^{27}$ g; internal core mass: $M_{core1} = 0.1083 \cdot 10^{27}$ g; transition zone mass: $M_{core2} = 0.1299 \cdot 10^{27}$ g; outer core mass $M_{core3} = 1.8321 \cdot 10^{27}$ g; mantle mass: $M_{m} = 4.0143 \cdot 10^{27}$ g; continental crust mass: $M_{cc} = 2.25 \cdot 10^{25} = 0.0225 \cdot 10^{27}$.

ultramafics, of the serpentinite layer). Besides, it is necessary to screen out totally all data from depth rock xenoliths in volcanic lavas in view of the uncertainty of their formation history. Apparently, it is possible to use for this purpose only analyses of looked-for contents of the components in the tempering glass of fresh basalts from mid-oceanic ridge rift zones, and even that only after their thermal processing for the removal of sorbed H_2O *and* CO_2. Whereas for the determination of the potassium concentration in Earth the data of radiogenic argon contents in the atmosphere have to be utilized.

It was found that Earth's matter, compared with the carbonaceous chondrites close in their average composition to the primordial protoplanetary matter, in impoverished in water by the factor of 200 – 250; in potassium, by the factor of 5 – 7; in carbon approximately by the factor of 1,000, etc. Compounds like methane or ammonia have been apparently wiped out practically in toto from the Earth's group planet formation area and for this reason had not gotten on Earth at all. The noble gases (except the radiogenic argon) deficiency, from expert evaluations [77] reaches 10^{-6} – 10^{-14}. All these elements and compounds still might have gotten on Earth in small amounts but only in bonded state – water with hydro-silicates, carbon dioxide as carbonates, nitrogen in nitrides and nitrates, etc. Only the most minuscule amounts of primordial gases, including the noble ones, had been getting adsorbed on Earth on the surface of loose and porous particles of the primordial protoplanetary matter.

The structure of primordial Earth. Knowing the composition of the primordial Earth's matter and a fortiori assuming chemical uniformity of the young Earth, it is already possible to evaluate the density distribution inside it, for instance, from the data of iron and silicate shock compression. We performed such evaluation for most probable temperature distribution inside just formed Earth. The results of such evaluation of the density as well as of temperature, of gravity acceleration and pressure distribution are included in Table 4.2 and are displayed in Fig. 4.1. As the included evaluations show, primordial Earth did not have any separation boundaries except the phase transition zones at depths 400 to 700 km. In those faraway times, on Earth still had not existed either Earth's crust or mantle or even more so, Earth's core. All these geospheres had been isolated much later, only in Archaean, but before that (in Katarchaean) there had been only uniform in composition Earth subdivided into zones only by polymorph mineral associations depending on pressure dominating at certain depths. The matter density on the surface of young Earth reached 3.9 – 4.0 g/cm^3 and increased toward the center to 7.2 g/cm^3.

Table 4.2 Density, temperature, pressure and gravity acceleration distribution in young Earth*).

Depth (km)	Density (g/cm^3)	Temperature, (K)	Pressure (kbar)	Gravity acceleration, (cm/s^2)	Depth (km)	Density (g/cm^3)	Temperature, (K)	Pressure (kbar)	Gravity acceleration, (cm/s^2)
0	3.92	260	0	985	2200	6.15	1379	1042	764
200	4.15	1147	82	980	2400	6.25	1378	1133	734
400	4.38	1385	168	973	2600	6.35	1377	1223	703
400	4.50	–"–	–"–	–"–	2800	6.44	1376	1309	670
600	4.76	1457	261	986	3000	6.52	1375	1393	638
670	4.85	1294	285	955	3400	6.66	1373	1548	569
670	5.02	–"–	–"–	–"–	3800	6.78	1371	1688	498
800	5.16	1433	358	941	4200	6.90	1369	1810	425
1000	5.36	1411	456	921	4600	6.99	1367	1912	350

(*Continued*)

Table 4.2 Density, temperature, pressure and gravity acceleration distribution in young Earth*). (*Continued*)

Depth (km)	Density (g/cm^3)	Temperature, (K)	Pressure (kbar)	Gravity acceleration, (cm/s^2)	Depth (km)	Density (g/cm^3)	Temperature, (K)	Pressure (kbar)	Gravity acceleration, (cm/s^2)
1200	5.53	1400	556	898	5000	7.07	1365	1995	273
1400	5.68	1393	656	874	5400	7.11	1363	2057	196
1600	5.81	1387	754	848	5800	7.15	1361	2097	119
1800	5.93	1384	852	821	6200	7.18	1359	2116	52
2000	6.04	1381	948	793	6360	7.18	1358	2116	0

*) For the estimation of density, gravity acceleration and pressure distributions was utilized Earth mass value $M = 5.977 \cdot 10^{27}$ g, at that spherical Earth dimensionless momentum of inertia turned out equal to 0.374.

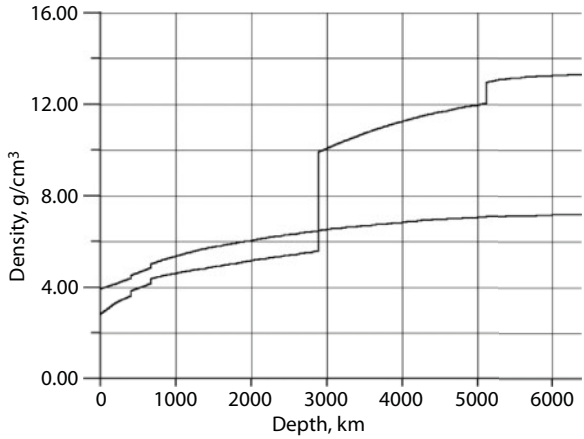

Fig. 4.1 Accepted density distribution in the present-day and primordial Earth.

Apparently, the young Earth's radius had not been much different from the current value. The reason was that in the process of Earth's evolution, two oppositely directed factors affected its size. On the one hand, the differentiation of Earth's matter accompanied by the release of a dense core, pressure increase in the central part of Earth and redistribution of the gravity acceleration inside it – all these must have resulted in a decrease of Earth's volume and its radius by 150 – 200 km. On the other hand, at Earth's differentiation, the density of its shallow layers must have noticeably decreased (from 3.9 – 4 g/cm^3 to 3.3 g/cm^3). This had decreased the pressure in the upper mantle and increased the contact depth of the main phase transitions in its underlying Golitsin's layer. This must have caused Earth's expansion. (In Table 4.2 the offset of phase transition boundaries is not shown). The same effect had occurred due to additional heating of Earth's subsurface by approximately 1,000°C so the summary expansion effect from these two actions had also been the same 150 – 200 km. Our estimate gives the primordial Earth radius at 6,360 km.

It is important that in the process of Earth's global evolution not only the temperature inside it had risen (see Fig. 5.2) but also had substantially increased the pressure in its central areas (see Fig. 4.2). The latter had been definitely associated with a dense core separation within Earth. The density distribution in young and present-day Earth is shown in Fig. 4.1.

Beside the density distribution in the young and present-day Earth, it is useful to know also heat storage capacity distribution within the same Earth's geospheres because this parameter is utilized for the evaluation of the planet's heat content. Estimates of such distributions for the young

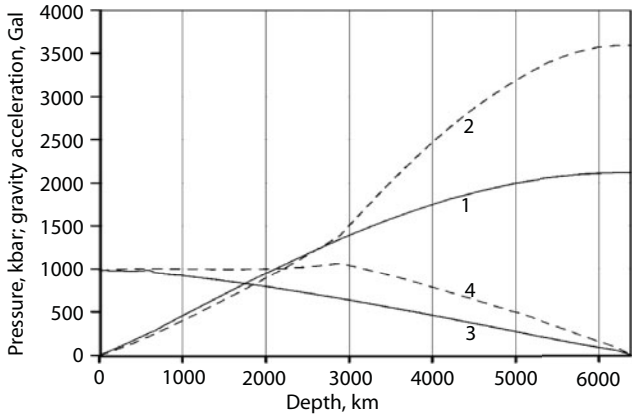

Fig. 4.2 Comparison of the pressure distribution: 1. In the young Earth; 2. In the present-day Earth; 3. Gravity acceleration in the young Earth; 4. Same in the present-day Earth.

and present-day Earth are presented in Fig. 4.3. For intermediate stages of Earth's evolution, we estimated approximate values of its average heat storage capacity $\overline{c}_p$ from the following equation:

$$\overline{c}_p \approx \frac{M_G}{\frac{m_c}{\overline{c}_{pc}} + \frac{m_m}{\overline{c}_{pm}}} \tag{4.1}$$

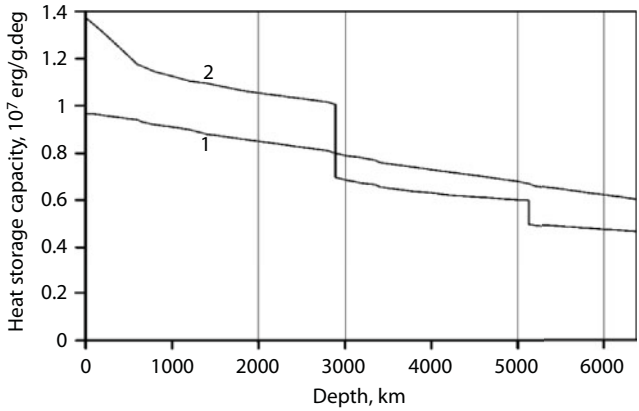

Fig. 4.3 Assumed heat storage capacity value distributions of Earth's subsurface matter: 1. Young Earth; 2. Present-day Earth.

where $M_G = 5.977 \cdot 10^{37}$ is Earth's mass; m_c is current Earth's core mass value: m_m is current mantle mass value; $\overline{c}_{pc} \approx 0.622\ 10^7$ erg/g deg is average heat storage capacity value of the core matter; $\overline{c}_{pm} \approx 1.12\ 10^7$ erg/g deg is average mantle heat storage capacity value; then $\overline{c}_p \approx 0.889\ 10^7$ erg/g deg.

Surface Earth's layers, practically during the entire period of its formation, were composed only of a low-porosity regolith that had been continuously forming through the deposition of finely dispersed dust and the condensation of planetesimals' matter dropping on Earth and evaporating at shock explosions. The sorption capacity of such ground had been exceptionally high. Undoubtedly, it had been actively absorbing all remains of volatiles released at heat explosions of planetesimals or had been captured by growing Earth out of the protoplanetary cloud (which of course had almost totally lost all its volatile components by the time of Earth's formation). This definitely includes also such volatiles currently common within the outer geospheres as water and carbon dioxide. In the process of Earth's formation both water and carbon dioxide partially released at evaporation of dropping on Earth planetesimals, had immediately strongly bonded with the ultramafic composition regolith, for instance, through serpentinization reaction

$$4Mg_2SiO_4 + 4H_2O + 2CO_2 \rightarrow Mg_6(Si_4O_{10})(OH)_8 + 2MgCO_3 \quad (4.2)$$

As the protoplanetary matter in Earth formation zone have already been earlier substantially impoverished in H_2O and CO_2 contents (as mentioned above), such serpentinization process and other similar regolith hydration reactions practically totally absorbed and buried under new buildups of Earth's matter almost the entire coming on Earth amounts of water and carbon dioxide. Out of all volatiles, only the heavy noble gases (Ne, Ar, Kr and Xe) that have gotten on Earth in minuscule amounts, perhaps with the Sun wind, and inert nitrogen in small amounts could have still been preserved in the gas phase in the proto-atmosphere of a young planet.

We would like to mention here that noble gases' isotope ratios are used sometimes to prove catastrophic events that had ostensibly occurred with young Earth that had led to its early heating and differentiation. Especially demonstrative in this respect are excessive contents in Earth's atmosphere of radiogenic xenon isotope ^{129}Xe. This fact, however, as will be shown in the next chapter, is not at all a testimony of early and catastrophic Earth differentiation.

The included theoretical considerations and estimates produce an important geologic conclusion: primordial Earth did not have a hydrosphere and its atmosphere could not have been high density and had been composed, most likely, of nitrogen with small additions of noble gases. The hydrosphere and dense atmosphere emerged much later, approximately 600 MY after Earth's formation.

4.1 Energy and Heat Regimes of Young Earth

Temperature distribution in primordial Earth for understandable reasons may be evaluated only theoretically based on the available concepts of the Solar system's planet formation. This, apparently most likely estimate for the earlier reviewed Earth formation model (through the accretion of a cold protoplanetary dust cloud) was performed by V.S. Safronov [61].

Under this model, the major part of growing Earth heat energy had been generated within its subsurface at the expense of the transition into heat of kinematic energy of planetesimals dropping on Earth's surface. Besides, as described above, a notable contribution in the energetics of growing young Earth must have introduced its tidal interaction with the Proto-Moon and Moon [19].

The total Earth accretion energy is tremendous (see below). It would have been quite sufficient not only for the total evaporation of Earth's matter but also for heating of the emerged plasma approximately to 30,000°C. However, the accretion energy had been being released mostly in the near-surface portions of the forming planet. For this reason, the heat generated in its upper layers had been easily lost with the heat radiation of the growing planet. At that, naturally, the fraction of the lost heat substantially depended on the planet accretion rate and the size of planetesimals dropping on it. The theory indicates that simultaneously with the growth of Proto-Earth, the size of planetesimals and the energy of their dropping on Earth's surface had been increasing. Due to this pattern, the temperature subsurface of young Earth had been increasing from the center to the periphery but then close to the surface it had been declining again through a faster cooling down of the near-surface portions. Under such a situation, the total young Earth's thermal content, and therefore the temperature distribution within its subsurface, had been totally determined by the planet growth rate.

Under all hypotheses with a short planet accretion (on the order of ten or a few dozen million years) and overestimated Earth's matter agitation depth when hit by planetesimals it so occurred that Earth must have been melted

even in the process of its formation. For this, of course, it was necessary to assume that Earth's overheating had been reaching then a few thousand degrees as Earth's matter melting temperature rapidly increases with depth and at Earth's core level much exceeds 6,000 – 7,000 K. However, should such an event have happened, in Earth as in Proto-Moon, a rapid matter differentiation would have occurred, adding its quite significant share to Earth's melting energy. As a result, in the very beginning of Earth life path about 4.6 BYa, a high-density iron core would have separated, a melted layer of a thick anorthosite crust would have formed and an early degassing of Earth's matter with the formation of a fluid water-carbon dioxide atmosphere would have occurred.

The theory reviewed here of the planet formation developed by V.S. Safronov [61] based on the ideas of O. Yu. Schmidt [71] leads to the conclusion of a relatively "cold" Earth's origin. His evaluation showed that Earth's formation had expanded for at least 100 MY and for this reason its subsurface had then remained everywhere colder than Earth's matter melting temperature. At the same time, the distribution of young Earth's temperature substantially depended on the mass of planetesimals that had been forming the planet in the accretion process. In consideration of this, V.S. Safronov proposed two extreme temperature distributions in young Earth (see Fig. 4.4). In accordance with one of these distributions derived based on an assumption of the planet growth due to the accretion of small bodies and particles, the temperature is smoothly growing from 300 K near

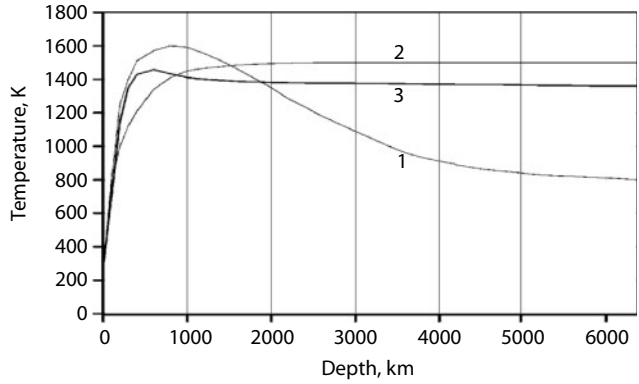

Fig. 4.4 Young Earth's temperature: 1 and 2 are extreme distributions of the initial Earth temperature: 1. After V.S. Safronov [61] in consideration of hits by various size bodies, first small and then larger; 2. After A.V. Vityazev *et al.* [67] in consideration of large bodies hits in the beginning of Earth's accretion process; 3. Assumed distribution of young Earth initial temperature derived in consideration of its energy balance.

the surface to 800 K in Earth's center. According to another distribution derived based on an assumption of a gradual growth of the size of planetesimals dropping on a growing Earth, the temperature of young Earth first increases with depth and then declines again toward Earth's center. Under this distribution, young Earth's temperature reached its maximum at a depth of about 800 km and rose there to 1,600 K, and declined again to the planet center approximately to 800 K (see Fig. 4.4). In the process of the Proto-Moon gravity capture, had been additionally released about $1.25 \cdot 10^{37}$ erg of the tidal energy having raised the temperature by 500 – 600°C [19].

Safronov's estimates did not account for the Proto-Moon tidal interaction energy with Proto-Earth. The role of Earth heating due to radioactive elements' decay was substantially overestimated. That was the reason for introducing appropriate corrections in his estimates. At that, it was assumed that tidal deformations are in proportion with tide-forming potential which, in its turn, is in proportion with squared radius of the deformed sphere. The total radiogenic heating of young Earth over the time of its formation, according to our estimates of Earth's matter radioactivity, did not exceed 30 – 50°C. As a result, the initial young Earth's temperature distribution is positioned somewhat below Vityazev's with colleagues distribution [67] but in its shape is intermediate between his two extreme distributions.

A verification of so derived temperature distribution may be performed based on Earth's energy balance by way of estimating the upper mantle temperature in Archaean and comparing it with experimentally determined temperatures of komatiite lavas melting. Such estimation included in the section 5.3 (see Fig. 5.5) showed not a bad match of theoretical temperatures with the empirical data. It follows herefrom that the derived initial temperature distribution of young Earth in general quite adequately corresponds with the actuality.

4.2 The Gadeyan Stage of Earth's Evolution

At the early stages of planetary Earth's evolution its structure, composition, thermal status and "tidal" tectonics were so drastically different from all subsequent regimes of the geologic evolution that this unique epoch that lasted about 600 MY, between the birth of our planet about 4.6 BYa and the beginning of Early Archaean should be identified as an independent subdivision in the history of our planet. However, in the geological nomenclature so far there is no commonly recognized term for its designation. Sometimes

this epoch between the moment of Earth formation and Archaean is called lunar. As we attempted to show above, such a term is totally inapplicable to Earth. In substance, this epoch could have been called pre-Archaean but long ago, in 1893, a Swedish geologist, J. Sederholm, introduced a term Katarchaean with about the same meaning, below the Archaean rocks, i.e., before Archaean. However, at the time of Sederholm the notion of Archaean had not yet become permanent and included at that time the age of the oldest granite-gneiss Scandinavian complexes. It was found out later that Archaean should reach the ages at least approximately 3.8 BY (including, for instance, the Isua Formation in the Western Greenland). After that the term Katarchaean has begun sometimes to be used as a synonym of the Lower (Early) Archaean, and that is semantically incorrect. For this reason, we believe it is legitimate to move the notion of Katarchaean in Earth history time scale to the epoch from its birth to the beginning of Archaean, i.e., to the time period approximately from 4.6 to 4.0 BYa.

We will show later that after the Archaean episode of the upper mantle melting in Earth's equatorial belt and the emergence in this geosphere of a "magmatic ocean", the entire primordial surface of Earth together with its primary and relatively high-density (around 3.9–4.0 g/cm^3) lithosphere very rapidly literally sank in the upper mantle melts, i.e., went down (in the mantle). That is why the translation of a Greek prefix κατα – down, may perhaps be understood as a reminder that all geological objects of pre-Archaean (i.e., Katarchaean) age dropped down, in Earth's melted upper mantle and completely vanished there from its historical chronicle.

Let us now review the outside environment dominating young Earth's surface and the specifics of the tidal tectonics in Katarchaean. This is even more useful because most arbitrary and speculative concepts are common about the initial conditions on Earth, about ostensibly tempestuous volcanic and hydrothermal activity on our planet occurring under the cover of a syrupy and dense atmosphere. We got such concepts as an inheritance mostly from the popular science literature of the epoch when geology was dominated by the contraction hypothesis based, of course, on the concept of Earth's "hot" origin.

The environment on young Earth's surface was indeed unusual but in an exactly opposite sense. In those faraway times, on our planet existed only landscapes of unfriendly, stern and cold desert with a dark and cloudless sky (as young Earth's atmosphere has been low density and devoid of moisture), yellow weakly warming Sun (its luminescence at that time had been approximately 25–30% lower that the present-day one) and exorbitantly large Moon disk which had been closer to Earth and on which had not existed yet so customary to us lunar "mares". Earth topography then

was similar to speckled with craters lunar surface. However, due to strong and practically continuous tidal earthquakes this topography had been substantially smoothed and composed only of monotonous dark-gray primordial matter overlain by equally dark and relatively thick regolith layer. No other, more differentiated rocks like basalts, peridotites, anorthosites or even more so granites have yet existed on Earth at all.

A desert landscape of primordial Earth from time to time had been disrupted by shakes and explosions from residual planetesimals falling on Earth. The frequency of their falls rapidly declined with time. Only in the equatorial zone of young Earth at that time did literally torrential flows of small stone and iron fragments still continue to drop from the satellite swarms of the recently destroyed Proto-Moon abundant. That is why Earth's surface in the equatorial zone for some time after the Moon formation remained hot (at least for hundreds or a few thousand years).

We would like once again to remind the reader that no volcanoes then existed that erupted on young Earth surface lava flows, gas and water steam jets and neither hydrosphere or dense atmosphere existed. Very small amounts of gases and water vapor released at heat explosions of dropping on Earth planetesimals and fragments of the Proto-Moon had been actively and rapidly sorbed by porous regolith of ultramafic composition that covered at that time with a thick layer the entire surface of young Earth.

The Sun movement at that time had been surprisingly fast. It was crossing the sky firmament in 3 hours and in 3 more hours appearing again in the east over the lifeless horizon of primordial Earth. The year duration was the same as now but there were almost 1,500 days in a year! The Moon motion was noticeably slower because it had been rapidly revolving around Earth in the same direction but the lunar phases changed literally in front of the eyes making all stages in just 6–8 hours. The astronomical month in the very beginning of the Earth – Moon system evolution had also been approximately equal to the satellite revolving period at the Roche limit, i.e., still the same 6 hours although it had been very rapidly increasing with time. Very surprising has been the apparent size of the Moon - 300–350 times greater than the visible surface of the present-day lunar disk.

In the very beginning of its existence, the Moon had been still a substantially hot planet radiating its heat energy in the red portion of the spectrum. So, day and night, beside a reflected Sun light, it shined its own dark-red light and due to its huge visible size noticeably heated Earth's surface (despite that, freezing then dominated Earth's surface). Once in a while, especially in the eastern part of the lunar disk flared up brightly luminating by the orange light spots of erupting on the lunar surface overheated magma from falling meteorite bodies at that time swept by the Moon out of the near-surface

satellite swarm. Besides, the entire huge lunar disk sometimes had been covered with zigzags of bright fractures emerging in a thin crust of lunar rocks at rapid changes of curvature radii of the Moon's tidal swells; the Moon at that time had been blisteringly distancing itself from Earth.

Astonishing also had been the presence near Earth of a disk of small particles revolving around it in the equatorial plain at close orbits. The trajectories of individual particles had been merging and creating an illusion of existing near Earth solid semi-transparent rings similar to the Saturn disks. At certain sight angles these disks had been reflecting the Sun light and then appeared rigid remaining in actuality ephemeral. Soon, their entire matter had been dropping on Earth.

Unusual has been the presence near Earth of a few satellites smaller than the Moon – "micro-Moons" distanced from Earth much farther that the "main" Moon but also well visible from Earth's surface and shining in the reflected Sun light as small disks or simply bright "starlets". There have been apparently at least 10 to 12 largest satellites of this series. (They all subsequently have fallen on the Moon engendering on its surface large craters flooded with basalts and called currently "lunar mares").

However, probably most impressive have been swarms of destructive earthquakes continuously following one after the other, caused by Earth's intense tidal deformations. Following the Moon and together with the tidal humps these earthquakes have been literally shook the primordial face of Earth. The periodicity of tidal earthquakes has been defined by the difference between the periods of Earth's axial revolutions and of the Moon's orbital revolutions so they have been continuously changing. In the beginning, when the Moon had been still on the Roche limit with Earth and Moon revolving and the angular velocities coinciding (a case of the stationary but metastable planet revolution), Earth's tidal humps have practically not been moving on its surface so that the earthquakes of this type must have been temporarily absent. But as soon as the Moon has left the Roche limit and begun distancing from Earth, the intense tidal earthquakes have returned and twice shaken Earth's surface at each visible Moon revolution around Earth.

As we know, the height of the tides is found from the equation of Earth's equipotential surface as follows (4.2).

$$V = V_g + V_t + \delta V_t + V_i \tag{4.3}$$

where V is the resulting potential on the satellite's surface; V_g is the potential of the satellite undistorted by tides; V_t is the tide-forming potential; δV_t

is additional tidal potential causing satellite deformations; V_i is the potential of centrifugal forces extending the satellite.

As the height of Earth's tides has always been much smaller than Earth radius, $\Delta R << R \approx R_0$, we find from (4.2):

$$\Delta R \approx \left(1 - k_2\right) \frac{m \cdot R_0^4}{M \cdot L^3} P_2\left(\varphi\right) \tag{4.4}$$

This expression shows that the height of tides on Earth is inversely proportionate with the cubed distance between the planets' centers of gravity. On the Roche limit, the Moon's center of gravity has been distanced from Earth's center by 17.2 thous. km (whereas the Moon surface at the time has been hanging over Earth's surface at a distance of only 8.2 thous. km). Thus, the lunar tides' height on Earth has been at that time very high, approximately 1.5 km. The tides that high, when moving on Earth's surface, have naturally been accompanied by swarms of numerous and strong earthquakes continuously shaking young Earth's surface. However, due to a rapid tidal Moon repulsion from Earth (inversely proportioned with 5.5^{th} power of a distance between the planets), already a million years after the planets' formation, the lunar tides on Earth have declined to 130 m. Another 10 MY, and their amplitude declined to 45 m and in 100 MY, to 15 m. By the end of Katarchaean about 4 BYa, the lunar tides have declined already to 7 m. For a comparison, the Moon currently is distanced 384.4 thous. km from Earth and the present-day solid Earth's tides near the sublunar point reach approximately 46 cm.

Blistering Moon retraction from Earth in Early Katarchaean and, as a result, a sharp decline of the tidal energy dispersed within young Earth subsurface has saved it from overheating but also has rapidly lowered the level of our planet's tidal seismicity. If we assume that only 1/1,000 of the tidal energy has been expended for the earthquake agitation and assume the total energy of the present-day earthquakes equal to 10^{25} erg/year, then the tidal earthquakes' energy in the very beginning of Katarchaean (around 4.6 BYa) had been approximately 17,000 times greater than the energy level of modern Earth's seismicity. However, already in a 100 MY, the total tidal earthquake energy has declined approximately to a level only 2.2 times above the present-day seismicity, and by the end of Katarchaean, 4 BYUa, it has further declined approximately by the factor of 6.

Discussing young Earth seismicity in Katarchaean, it is important to remember that its nature and the manifestation character at that time have been conceptually different from the seismic parameters of modern

earthquakes. First, the Katarchaean tidal earthquakes have been only exogenous in origin and not connected at all with some fixed tectonic zones (which simply did not exist then on Earth). Second, these earthquakes have consistently moved together with the running tidal wave in Earth's body and on the surface at a rate defined by a visible Moon revolution around Earth. As with usual tides, earthquake culminations have been occurring twice every Earth's revolution relative the Moon. Third, the tidal earthquakes have been of maximum intensity in Earth's equatorial-tropical belt and of minimum one in its circumpolar areas.

5

The Earth's Core Formation Process

After reviewing major positions of Earth's emergence and early stages of evolution, the issue of the time and regime of the Earth's core separation takes a most important position in the planetary geophysics. Whereas in a study of mechanisms and ways of Earth evolution, energy sources of its tectonic activity or major patterns of our planet geologic evolution, an issue of the time and mainly the regime of Earth's core separation is already taking the central position. This of course is understandable as currently nearly a third of the entire Earth mass is concentrated in the Earth's core and the process of so radical differentiation of its matter certainly could not but leave indelible traces in the geologic chronicle of our planet.

5.1 Delayed Earth's Core Separation Process

An important consequence follows from our planet formation theory reviewed in Chapter 4: the young Earth did not have a high-density core. It does exist currently, and with its formation is associated the release of a huge energy, nearly $17 \cdot 10^{37}$ erg. For this reason, it is very important to find out exactly when the dense core emerged in Earth and what way it had been forming, non-recurrently or gradually. This issue is closely associated with thermal formation regime of Earth proper. In many, sometimes quite serious publications, early heating of Earth accompanied by equally early separation of Earth's core is simply postulated or substantiated through solving not always well-formed problems of heating the growing Earth by falling on it planetesimals of various sizes [67, 78–80]. On the other hand, already in 1946, O. Yu. Schmidt [68] put forward a hypothesis of "cold" Earth formation. In 1962, S. Runcorn [81, 82] came up with a suggestion that Earth's core began growing much later than the Earth formation moment and that this process is still continuing. V. Elsasser [83] also supports hypotheses of a "cold" Earth's formation and late separation of Earth's core. However, "cold" Earth's formation, therefore, late Earth's core separation was developed in

N. O. Sorokhtin (ed.) The Origins of Natural Diamonds, (41–101) © 2019 Scrivener Publishing LLC

most detail and most substantiated, by V.S. Safronov [61]. As this issue is so important, we will review it in some more detail.

Based on all hypotheses with rapid planet accretion (on the order of a dozen or a few dozen million years) and overvalued Earth's matter agitation depth at planetesimal strikes, it was concluded that Earth must have molten already in the process of its formation. Should such have happened, in Earth, the same as in Proto-Moon would have happened a rapid and total matter differentiation, adding its no small fraction of the energy to Earth's melting. As a result, in the very beginning of Earth's life path nearly 4.6 BYa, it would have had a separated dense iron core, a formed molten layer of a thick anorthosite crust and the early degassing of Earth's matter with the formation of a very thick fluid water-carbon dioxide atmosphere. However, should the metallic core indeed have separated in young Earth nearly 4.6 BYa and a thick anorthosite crust formed, into this crust would have passed also a large part of radioactive elements depriving Earth of all endogenous energy sources and turning it into a tectonically dead planet.

If, as a result of such differentiation, thick (up to 80 km) and relatively light (density 2.7 g/cm^3) anorthosite Earth crust, 4.6 BY old, had indeed separated, it must have been preserved on Earth forever (as required by the Archimedes law). The same may be stated also about a thick originally basalt crust. However, despite all efforts by geologists, no traces of such primordial ancient crust as well as other indications of early catastrophic Earth's differentiation, have been found. At the same time, based on geologic data, as mentioned above, Earth's crust had begun forming much later than the formation moment of Earth proper. For instance, most ancient reliably identified continental crust rock ages are close to 3.8 BYa [84, 85].

It is true that in recent years appeared publications of Australian geologists about clastic zircon finds with the age of up to 4.2–4.3 and even almost up to 4.4 BY within Archaean age sandstones and conglomerates of an age apparently close to 3.5 BY [86]. It does not mean, however, that the continental crust had begun forming at the times so ancient, as some geologists believe. Indeed, as we will later show, almost during the entire Archaean, on the Earth surface had been exposed primordial Earth matter overlain by a layer of a finely porous lunar type regolith formed at the time of the planet itself formation and first 600 MY of its life (see Fig. 7.15). This matter should have included also zircons of most ancient ages ($t >$ 4 BY) formed in local melting of the near-surface layers of young Earth after the fall of planetesimals on them. Further on, after the emergence in Archaean of a dense atmosphere and hydrosphere these zircons could have been washed out of primordial Earth rocks and deposited in the Archaean sedimentary rock reminding us that Earth is much older than Earth crust.

Sometimes, for a proof of Earth's early heating and differentiation are used the data of noble gases isotope distribution in the atmosphere and mantle. Especially indicative in this respect are excessive contents in Earth's atmosphere of the radiogenic isotope of xenon ^{129}Xe (its concentrations are approximately 7% higher than is suggested for composition of the primordial xenon). But the isotope ^{129}Xe emerges at the decay of short-lived radioactive isotope of iodine ^{129}I with decay constant $\lambda_{129} = 4.41 \cdot 10^{-8}$ year^{-1}. A conclusion is made based on this that the presence of excessive ^{129}Xe in Earth atmosphere indicates early differentiation and degassing of Earth that had occurred even before the disappearance from Earth matter of the isotope ^{129}I [87–89]. At that certainly should be taken into consideration that in samples of Earth's rocks is also recorded excessive ^{129}Xe, sometimes in concentrations higher than the atmospheric values which rather indicates late Earth's degassing. Mentioning contradictory interpretations of xenon isotope ratios, M. Osima and F. Podosec, uncontested authorities in noble gases geochemistry, note: "An increase of radiogenic xenon isotopes' contents in the atmosphere as well as the existing excess of ^{129}Xe demand for the degassing to have been exceptionally rapid. This not only contradicts the models for argon and helium but also is internally contradictory. On the other hand, the closeness of isotope composition for a larger part of the mantle xenon with the atmospheric one and the absence of a substantial excess of ^{136}Xe associated with ^{129}Xe indicate a slow degassing" [88]. These authors see a way out in a two-step model: first, at a very early stage of Earth's evolution, its tempestuous and rapid degassing had been occurring, when the major portion of noble gases had been released into the atmosphere, and then, during the entire subsequent life of Earth, its gradual and more quiescent degassing had been operating.

It is difficult to disagree with the Osima-Podosec model except for a "small" detail: not Earth itself but falling on the planet planetesimals had been subjected to early degassing. Undoubtedly, this had been a quite tempestuous process as at striking Earth surface, in thermal explosions the planetesimals could have even evaporated. However, all chemically active gases (CO_2, H_2O and other volatiles) at that had been rapidly entering a reaction with a porous regolith of ultramafic composition covering then the growing Earth and had been rapidly removed from the atmosphere of primordial Earth [17, 19, 90, 91]. Whereas in the primordial atmosphere have been mostly preserved and accumulated only noble gases and partially nitrogen. Obviously, such tempestuous degassing of planetesimals could have by no means characterized the thermal regime of Earth itself and even more so, could have been an indicator of its early differentiation.

Besides, what is necessary to keep in mind is that Earth's early melting and Earth's core separation would have mandatorily been accompanied by

the total degassing of its insides. At that, in Earth atmosphere, in a relatively short time would have entered nearly $5 \cdot 10^{23}$ g of carbon dioxide currently bonded in carbonate rocks, and more than $2.5 \cdot 10^{24}$ g of water. A one-shot formation of so dense carbon dioxide atmosphere with the pressure of nearly 100 atm. would have led to the emergence of extremely strong greenhouse effect with the rise of near-Earth temperature above the critical temperature of water (+374°C). After that, the oceans would have boiled and the pressure of Earth atmosphere would have risen by approximately 500 more atm. As a result, on Earth, as on Venus, would have been established the irreversible (emphasizing, irreversible!) greenhouse effect with average temperatures in a sustained way exceeding 550 – 600°C. In this case, on Earth would not have been the liquid phase of water and not even allowing the most primitive life. Fortunately for us and all living on Earth, this did not happen.

There are, however, also direct evidences that young Earth had never molten and still has no dense metallic core. There are, for instance, numerous distinctions in lunar rocks' geochemistry from earthly ones which can be explained only by that the Moon parent body (i.e., the Proto-Moon), as opposed to Earth, had been totally molten soon after its formation. At that, the Proto-Moon had passed through a total differentiation with the separation of a metallic core and anorthosite crust [19]. This is indicated, for instance, by a thick anorthosite crust on the Moon as well as by a drastic impoverishment of lunar rocks (compared with Earth's ones) in all siderophile and chalcophile elements [92].

Contrary to the lunar matter, Earth matter had never been subjected to a rapid and radical differentiation. An explanation is that Earth's core had been forming gradually and without melting the silicates. It had been occurring due to the operation in the beginning of the zonal differentiation mechanism, with the separation of iron melts from silicate melts and then the barodiffusion mechanism of the mantle matter differentiation. The rate of their operating had always been restrained by extremely low thermal conductivity and diffusion of the mantle's silicates. Besides, both the primordial lead and its radiogenic isotopes accumulated by the time of running of the Earth matter differentiation process had been simultaneously passing into the Earth's core composition. Therefrom, intermediate and comparatively close to the initial (primordial) lead isotope ratios in Earth's rocks (compared with the same ration in the lunar matter).

Based on the quoted data and considerations, we suggested that Earth's core separation process had begun only 600 – 800 MY after the formation of Earth proper, i.e., nearly 4.0 – 3.8 BYa [93].

5.2 Earth's Core Separation

So, according to the most likely Earth's formation model under the O. Yu. Schmidt [68] hypothesis later developed in detail by V.S. Safronov [61], Earth and the other Solar system planets had formed due to accretion of the cold and homogenous matter of the protoplanetary cloud. In general terms, two scenarios of the dense core separation process' evolution within Earth may be suggested: 1) Earth core had formed simultaneously with the growth of the planet proper or immediately after its formation; 2) Earth's dense core separation had begun noticeably later, only after the precedential Earth's heating, and the very process of Earth matter differentiation had spread over billions of years and is currently continuing.

The former Earth's evolution way is least likely and might have been occurring only at "hot" origins of our planet if its accretion had been short (on the order of 10^7 years). For the substantiation of a rapid planet's differentiation with the separation within it of a dense core has been absolutely necessary practically global melting of the planet matter as it, for instance, had occurred with the Moon. For Earth, such suggestion is in a direct contradiction with the available geologic and geochemical data described in detail in section 6.1 in the publication [19, 94]. Repeating once again, under this scenario simultaneously with Earth's core separation must have been occurring Earth's crust formation. However, such ancient (Katarchaean) crust had been discovered nowhere on Earth. Besides, lead isotope ratios in Earth's rocks practically explicitly indicate that Earth had never molten totally and that its matter differentiation, therefore, Earth's core formation had been occurring gradually, spreading in time approximately from 4 BYa to the present. An analysis of Earth's energy balance indicates that this process is still continuing. The fact of young Earth, immediately after its formation, not passing through the stage of global differentiation is also supported by the absence on Earth of ancient (4.5 to 4 BY old) and thick lunar type anorthosite crust, a product of the planet's early melting. Moreover, the rocks more ancient than 3.8–3.85 BYa are absent from Earth's crust which convincingly supports Earth's tectonic passivity before that time.

The latter path of Earth's evolution appears to be much more likely if not to say the only possible one. Indeed, the current theory of the planet's origin briefly outlined in Chapter 4 is indicating homogenous and relatively lengthy (on the order of 10^8 years) accretion at which Earth's deep subsurface had remained relatively cold, with the temperature in the planet center not exceeding 800 – 1,500 K [61, 92, 95]. At that, initial stages of

our planet differentiation's evolution process had been completely defined by the primordial thermal content estimated in the section 6.5. With the insufficient thermal content of young Earth, the core separation, as already mentioned, could have started substantially later, only after a preliminary heating of Earth's subsurface at the expense of a release within it of the radiogenic and tidal energy. That is exactly what happened in actuality as the age of most ancient crustal rocks was found to be younger by 750–800 MY than the age of Earth itself.

Indeed, as shown above, the temperature distributions in the young Earth's subsurface are by many hundreds and even thousands of degrees below the expected Earth matter melting temperature values at great depths. This practically completely eliminates a possibility of our planet's global melting. Moreover, as it will be shown again in section 5.7, the radiogenic lead vs. primordial lead isotope ratios in Earth's rocks uniquely indicate that Earth, as opposed to the Moon, had never molten completely. However, for explaining the mechanisms of Earth's core separation there is no need at all to include the condition of Earth's matter melting. At that, Earth's differentiation in Archaean had been occurring under a mechanism of Earth's matter zonal melting, and after Archaean, under a mechanism of its barodiffuse differentiation [96, 97]. The Earth's core separation process scenario is shown in Fig. 5.1.

Indeed, both reviewed mechanisms of Earth matter zonal and barodiffusion differentiation allow for the evolution of this process in Earth's deep subsurface at temperatures much lower than the temperature of the silicate melting start. But both these mechanisms are slow-operating. For instance, the evolution of Earth's matter zonal differentiation is limited by a low heating rate of Earth's layers directly underlying the differentiation fronts (i.e., low values of Earth's matter heat conductivity, on the order of 10^{-7} erg/cm·s·deg), and the barodiffusion mechanism evolution rate is limited by exceptionally low diffusion factor values of silicate, ~ 10^{-20} – 10^{-22} cm^2/s. These features of most likely Earth's matter differentiation mechanisms totally exclude the possibility of a rapid separation of the entire mass of the present-day core. This is the reason why the Earth's dense core formation process stretched out for billions of years and is still continuing.

It is important that the process of Earth matter early differentiation could have started only on Earth's equator because it had been exactly on the equator that the tidal energy of the Moon/Earth interaction had been at its maximum (see Chapter 6). For this reason, the initial tectono-magmatic

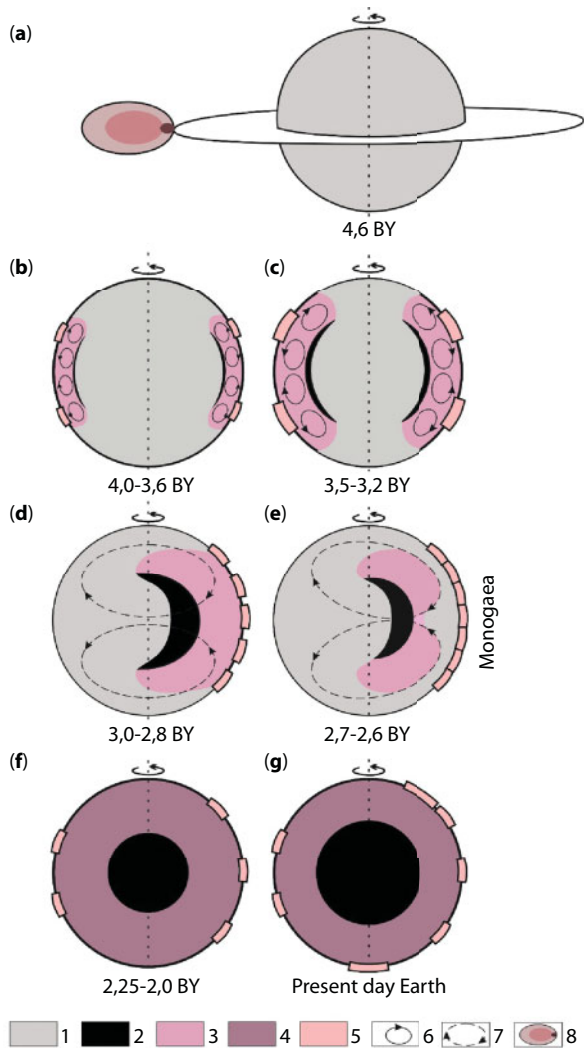

Fig. 5.1 Earth structure evolution: a. Young Earth and Moon formation; *b-f.* Sequential stages of Earth's core separation and formation; g.–Present-day Earth. 1. Earth's primordial mattert; 2. Iron and iron oxides' melts; 3. Archaean depleted mantle impoverished in iron, iron oxodes and siderophillic elements; 4. Present-day type mantle; 5. Continental massifs, shields and platforms; 6. Fine-meshed Archaean age convection; 7. Present-day type global chemical-dencity convection; 8. Proto-Moon.

activity on Earth had been occurring only within its relatively narrow low-latitude belt [98]. Somewhat later with a similar concept of Early Archaean continental crust formation within the equatorial "early Earth's hot belt" came M.Z. Glukhovsky, V.M. Moralev and M.I. Kuzmin [99].

Having begun on the equator, the Earth's matter zonal differentiation process had subsequently gradually widened up to high latitudes. However, Earth matter zonal differentiation evolution process had resulted in Archaean in the emergence of a drastic gravity instability of the planet. Indeed, formed due to the zonal melting dense (heavy) ring layer of molten iron and its oxides had been positioned then above the lighter matter of the primordial Earth's "heart" (see Fig. 5.1-*b*-*c*).

How had the above-mentioned situation of Earth's gravity instability been resolved at that time? Only one way, by buoying of rigid Earth's "heart" in the equatorial belt of one of Earth's hemispheres and by immersing heavy melts to Earth's center on the side of the opposite hemisphere, as is shown in Fig. 5.1-*d* and *e*. This event, undoubtedly, had created a strong asymmetry in the structure of our planet at the end of Archaean epoch. This asymmetry had led to a drastic increase in Earth's precession angle but simultaneously with this had provided for a stable orientation of the main Earth's axis of inertia along the axis of its own revolution, therefore, stable planet's revolution.

This process had to be developing under the accruing catastrophic scenario with the eventual formation of Earth's dense core. The reason for this had been a substantial nonuniformity of young Earth heating. Indeed, after the capture of Proto-Moon by Earth, Moon formation and further evolution of its orbit, major portion of the tidal energy – and it had been huge, nearly $(4\div5)\cdot10^{37}$ erg - had been being released mostly in Earth's upper parts and in its equatorial ring sector. As a result, Earth had turned out noticeably more heated in lower latitudes than in the polar sectors. For this reason, the first asthenosphere and the associated zone of iron separation had to emerge in the upper mantle exactly under the equatorial belt of our planet. In Middle Archaean, the differentiation zone had expanded in the midlatitudes and included the middle mantle. In the end of Archaean, the differentiation zone had already covered most of Earth after which, at the very end of Archaean, the differentiation zone had involved the entire Earth (see Fig. 5.1-*e* and 5.3). In the Early Archaean equatorial belt had also emerged all ancient Archaean continental shields and platforms.

Simultaneously with this, the upper and middle mantle temperature underneath both Earth's poles had been remaining relatively lower. For this reason, the asthenosphere layers for a long time had not been emerging there. It follows from this that in Early and Middle Archaean, a ring layer of the "core"

matter high-density melts might have existed, broadened and surrounded a cold and rigid $\eta > 10^{30}$ poises) heart of the young Earth only from the side of its low latitude belt. At the same time, this heart, through high-latitude and polar planet areas, had been as earlier rigidly tied with Earth's middle and upper mantle and for this reason had been maintaining its stable position.

Later, a gradual heating had occurred of high-latitude areas due to the energy of then proceeding Earth's matter gravity differentiation and in adjoining Earth's zones due to radioactive elements' decay and Earth's tidal agitation. As a consequence of that, their matter viscosity had declined below the level of $10^{24} - 10^{23}$ poises, and the rigid tie between the cold Earth's heart and the upper mantle had been disrupted. Since that moment, earlier emerged Earth's gravity instability might have been resolved by way of subsiding of "core" matter heavy melts in central areas of the planet and compensatory squeezing out its rigid but lighter heart to Earth's surface (see Fig. 5.1-*d*).

Due to large masses of "core" matter accumulated by the middle of Late Archaean in the ring differentiation zones (up to 12 – 13% of Earth mass) and a high density of this matter compared with the primordial Earth's matter ($\Delta\rho \approx 4$ g/cm^3), the ejecting process of the young Earth's heart from its central areas must have been developing at an accelerated regime and bearing a catastrophic nature. However, the evolution rate of Earth's core separation process had been restrained by a high viscosity of the cold primordial matter of the former Earth's heart spreading at that time in the active belt of upper mantle forced by huge excessive pressure acting on it from the side of Earth's forming core and large uncompensated Earth's surface protrusion above the depth matter rising area (see Fig. 5.1-*d*).

Earth's core formation process had been accompanied by the release of huge energy, on the order of $5{\cdot}10^{37}$ erg. It had been mostly expended for additional heating of the mantle and Earth's matter from the former Earth's heart. This, in turn, had caused acceleration of the core separation process. As a result, the entire process of Earth's core formation had lasted overall, apparently, nearly 200 MY. It had been evolving in an accelerated regime and had been completed only at the very end of Archaean nearly 2.6 BYa by a catastrophic event of a dense core formation in Earth's center.

Earth's core separation had been accompanied by the emergence of exceptionally strong convection flows in Earth's mantle. These flows had totally rebuilt the entire earlier existing tectonic plan of Earth's lithospheric shell. Based on the considered process scenario, at the very end of Archaean, a single-cell convection structure must have emerged with a single ascending flow above the surfacing place of the former Earth's heart and one descending flow above the runoff area of the "core" matter. This gives reason to believe that exactly above this descending mantle flow at the Archaean/Proterozoic boundary

nearly $2.6 \cdot 10^9$ years ago had formed the first supercontinent in Earth's history, which we called Monogea [17, 96, 100, 101]. A suggestion of the existence of Early Proterozoic supercontinent was also made based on independent geologic data by V.E. Khain and N.A. Bozhko [102] who called it "Pangea 0".

Based on the aforementioned, it appears quite enticing to tie the described geodynamic catastrophe with most outstanding epoch of Kenoran tectono-magmatic diastrophism which had completed Archaean stage of Earth's evolution (as a result of it had emerged the first supercontinent in Earth's history, Monogea). The first and most tempestuous stage in Earth's core formation had ended up filling the central areas of our planet with the "core matter" and in an offset of the primordial Earth's heart to Earth's periphery. At that very time the first stage of Earth's differentiation under the mechanism of iron and its oxides' zonal separation from Earth's matter had ended also. The further separation of the "core" matter and growth of the core itself had already been occurring under the barodiffusion mechanism described in section 5.4.

In connection with the emergence in the process of Earth's core separation of a strong asymmetry in Earth's mass distribution, Earth's precession angle might have substantially increased, perhaps to 40°.

However, at that the positions of the exciting mass of the ascending and descending mantle flows had to be positions in Earth's equatorial plain although it had been substantially inclined relative to the ecliptics' plain.

However, with this position of the agitating masses in the ascending and descending mantle flows must have been positioned in Earth's equatorial plain although it had been substantially inclined to the ecliptic plain. It follows from this that Monogea, the first supercontinent in Earth's history, had also been positioned on the equator.

5.3 Mechanism of Earth's Matter Zonal Differentiation

Due to low temperatures in the young Earth subsurface (see Figs. 4.4 and 5.2), the barodiffusion mechanism could not have operated in those faraway epochs. For this reason, the process of separation of a dense "core matter" (Fe and Fe_2O or Fe·FeO) from the silicate Earth's matrix matter might have begun only after Earth's temperature, as affected by the decay of radioactive elements and its tidal interaction with the Moon, had risen to the level of iron and its oxides melting start in the local maximum area of young Earth geotherm in the upper mantle.

Most likely, the iron separation process from silicates in Earth matter had begun approximately at depths 200 – 400 km and pressure nearly

80 – 170 kbar commensurate with the pressure of the first electron-phase transfer in iron between the phases of α–Fe and ε-Fe on the order of 130 kbar [19], i.e., in the area of the beginning of a stable Fe_2O oxide existence. However, judging by the correlation of C*, the concentration maximum silicates' saturation with FeO solution (see Fig. 5.8), at these depths is $C^* > 50\%$ whereas the iron oxide concentration in the primordial matter had been approximately half of it, $C(FeO)_0 \approx 24\%$. Therefore, in young Earth at depths of nearly 400 km, the separation of a low-melt iron oxide component in the "core" matter from mantle silicates might not have occurred because the critical depth of starting operation of the barodiffusion separation mechanism of Fe_2O from silicates at that time had been positioned at depths approximately equal to 1,200 – 1,400 km (in the present-day Earth this depth descended approximately to 1,900 – 2,000 km). For this reason, the first asthenosphere on Earth might have emerged in the lower portion of the upper mantle only at the expense of partial silicate melting. But then existing intense tidal agitation (see section 6.3) by the closely positioned Moon must have been mostly concentrated in the upper mantle layers of the equatorial belt. This had resulted in additional temperature rise in this layer up to a level of the free iron melting (see Fig. 5.2) and had caused thereby in the primordial asthenosphere the process of Earth matter density differentiation.

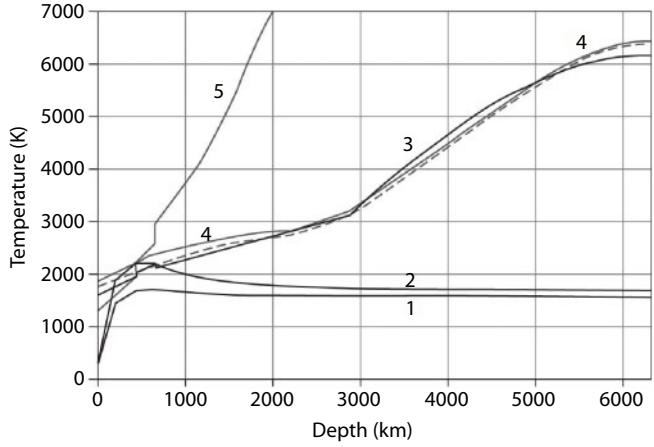

Fig. 5.2 Temperature distributions in the young and present-day Earth: 1. At Earth's formation nearly 4.6 BYa; 2. In the beginning of Archaean, nearly 4.0 BYa; 3. Temperature distribution in present-day Earth; 4. Iron melting temperature; 5. Silicates' melting temperature; dashed line is melting temperature of eutectic Fe·FeO melt.

We will recall that the free iron initial concentration in the primordial Earth matter had reached 13 – 14% (see Table 4.1). For this reason, as soon as free iron contained in young Earth matter had begun melting, the further differentiation process of its matter could have already spread both up and in the depth of Earth independently, only due to the release of the gravity energy. This process had been stable and had supported itself at unfading action regime. The silicates' melting temperature in the upper mantle is known to be always lower than iron and its oxides' melting temperature and low-melt Fe_2O composition had not been emerging yet at pressures reigning in this geosphere. For this reason, the initial Earth matter differentiation at these levels might have been operating only under the zonal melting mechanism described in the publications by A.P. Vinogradov and A.A. Yaroshenko [103, 104].

In the present-day Earth the energy sources capable of supporting the zonal melting process at the nonfading regime do not exist [105]. The contents of radioactive elements in the mantle are insufficient for this (see section 6.2). The mantle melting liquation and flotation gravity energy only is also insufficient for supporting of such processes. This covers also the energy of the modern-time lunar tides. Whereas in the young Earth such energy sources capable of supporting the matter zonal melting process in the upper mantle under the unfading regime had certainly existed. First, in the beginning of this there had been energy of the lunar tides and in Early Archaean the Moon had been positioned much closer to Earth and its tidal action on the heating of the asthenosphere layers had been very strong. Second, after melting of some areas of the upper mantle such energy had begun to be generated by the very process of gravity differentiation of Earth matter due to the separation of the metallic iron and its oxides (not bonded in the silicate phase) from lighter silicates.

A thermodynamic estimate of the upper mantle zonal melting process in young Earth shows that this process had been accompanied by a release of substantial gravity energy [106, 107]. The so released gravity energy provided total self-support of this process evolution within the entire upper and middle mantle. Whereas the tidal energy dispersed then in the matter melting zones accelerated and strengthened the zonal melting process. For this reason, in Early Archaean this process in the upper mantle and in Earth's equatorial zone had indeed been developing quite tempestuously and resulted in melting of the most ancient areas of anorthosite and basalt composition continental crust. Simultaneously a substantial overheating of the matter in the upper mantle had already been occurring in the first half of Early Archaean.

In deeper parts of the mantle, where melting temperature of silicates substantially exceeded the iron melting temperature, Earth matter

differentiation could have occurred only due to a simple separation of molten iron from solid, not molten silicates. This had been facilitated by that at the metallic iron concentrations of about 13% it must have remained as a separate phase and contained in intergranular spaces of the silicate crystals similarly as observed in mesosiderite meteorites.

The advance of the differentiation zone in the mantle depth had been occurring due to the flotation of lighter silicate crystals from the base of asthenosphere layers of molten iron to their top. In this situation the layer of a heavy melt itself, descending, must have been gradually increasing in mass and thickening at the expense of the arrival of ever new portions of molten iron from the underlying melting zone primordial Earth matter. It follows from the nature of the zonal differentiation of Earth matter process under review that the temperature at the base of the molten iron descending layer had always been equal to the melting temperature of iron at a given depth. However, due to the separation of iron from silicates and silicates flotation through the liquid iron layer, this layer must have been significantly heated in the direction up. As a result, the temperature distribution in such layer of molten iron might have been substantially lower than adiabatic and become even negative (i.e., growing up). This resulted in two important consequences. First, the overlying mantle must have been experiencing a substantial overheating because in the process of differentiation the "current" mantle temperature had been set by the temperature at the top of the overheated layer of the zonal differentiation (of molten iron). Second, the zonal differentiation process of Earth matter must have been accompanied by the emergence in the overlying part of the mantle that had already undergone the primordial differentiation, by intense thermal convection.

Despite the release of a substantial energy, the zonal separation process of molten iron from the silicate matrix of Earth matter might not have spread deeper than some limiting level. It had been associated with a fact that with depth the temperature of young Earth matter had been decreasing and the temperature of iron melting, on the contrary, had been increasing. Therefore, their difference had been substantially increasing in the same direction (see Fig. 5.4). Thus, it is obvious that the fraction of energy used for a preliminary heating of Earth matter must have been substantially increasing with depth. This was exactly the reason why beginning at some level the released gravity energy might not have been sufficient for supporting the continuous regime of the process. Obviously, for the process evolution it had been necessary for the energy released at differentiation to have been sufficient for heating the matter of the underlying medium to the level of melting of metallic iron contained in it.

The amount of energy released at floating of unit volume ΔV, that had undergone the differentiation of the silicate matter, through a layer of molten iron with the thickness *h,* is equal:

$$\Delta E=[1-C(Fe)]\cdot\Delta\rho\cdot h\cdot g\cdot\Delta V, \tag{5.1}$$

where *C(Fe)* = 0.131 is the metallic iron and its oxiudes concentration in the free phase of Earth primordial matter; $\Delta\rho=\rho_{Fe}-\rho_{Si}$; ρ_{Fe} is molten iron and its compounds density; ρ_{Si} is silicate fraction density; *g* is gravity acceleration. This energy is spent for heating relatively cold primordial matter $\rho_0\cdot c_p\cdot\Delta T\cdot\Delta V$, for melting and overheating new portions of iron and its compounds. I this case, energy balance of the differentiation process is

$$[1-C(Fe)]\cdot\Delta\rho\cdot h\cdot g\approx\rho_0\cdot c\cdot\Delta T+C\,(Fe)\cdot\rho_{Fe}\cdot q+\delta T_H\cdot\rho_{Fe}\cdot c_p(Fe) \tag{5.2}$$

where ρ_0 is the primordial Earth matter density; $c_p\approx 10^7$ erg'g · dfeg is heat capacity of this matter; $\Delta T=T(Fe)_m-T_0$; $T(Fe)_m$ is iron melting temperature at depth *H;* T_0 is initial temperature of Earthых subsurface at the same depth (see Fig. 5.2); $q\approx 2.77\cdot10^9$ erg/g is iron melting heat; δT_H is molten iron and its oxides' overheating value compared to their melting temperature at depth *H*; $c_p(Fe)\approx 0.5\cdot10^7$ erg/g·deg is molten iron heat capacity.

Form equation (5.2) is easily found the value δT_H of melt overheat emerging at differentiation of Earth matter at a given level *H*

$$\delta T_H\approx\frac{\left[1-C(Fe)\right]\cdot\Delta\rho\cdot h\cdot g-\Delta T\cdot\rho_0\cdot c_p-C(Fe)\cdot\rho_{Fe}\cdot q}{\rho_{Fe}\cdot c_p(Fe)} \tag{5.3}$$

At that, as usual,

$$\frac{1}{\rho_0}=\frac{C(Fe)}{\rho_{Fe}}+\frac{1-C(Fe)}{\rho_{Si}}\text{ and }g=\gamma\frac{m(r)}{r^2} \tag{5.4}$$

where $\gamma=6.67\cdot10^{-8}$ cm^3/g·s^2 is gravity constant; *m(r)* mass of Earth subsurface withing a sphere with the radius *r.*

Re-evaluation of δT_H values for the surface conditions in Archaean is done as follows:

$$\delta T_0 = \delta T_H \cdot \frac{T(Fe)_0}{T(Fe)_H} \tag{5.5}$$

where $T(Fe)_H$ is iron melting temperature at depth H (found from excperimental data [19]); $T(Fe)_0 \approx 1{,}803$ K = 1,530 °C is iron melting temperature on Earth's surface, degrees of Kelvin or Celsius. Adjusted mantle surface temperature Tm_0, degrees of Celsius, is estimated using a simple equation

$$Tm_0 = 1530°C + \delta T_0 \tag{5.5'}$$

where 1530 °C is iron melting temperature at normal pressure $p \approx 1$ atm.

The thickness of molten iron layer h at depth H within Earth subsurface is easily determined from mass balance of the occurred Earth matter differentiation

$$h = \frac{H + \left[[R^3 - (R-H)^3] \cdot \frac{\rho}{\rho_{Fe}} \cdot C(Fe) + (R-H)^3 \right]^{1/3} - R}{S_{AR}} \tag{5.6}$$

where H is front depth of the zonal differentiation; R = 6,370 km is Earth radius; it is suggested that the width of iron melts' ring of zone of separation from mantle silicates is proportionate with the thermal energy of the mantle, for this reason, the factor

$$S_{AR} = \frac{E_m T}{E_m T_{2.6}} \tag{5.7}$$

takes into account a gradual widening of Earth matter differentiation in the equatorial zone in Archaean after the beginning of Earth matter partial melting nearly 4 BYa at depth of 200 to 400 km, up to involving the entire Earth surface at the end Archaean: here $E_m T$ is the current value of mantle endogenous thermal energy, $E_m T_{2.6}$ is mantle's endogenous energy at the end Archaean nearly 2.6 BYa (see Fig. 6.13, curve 3). At that, the width of a tectono-magmatic zone on и Earth's surface turns out equal to (see Fig. 5.3)

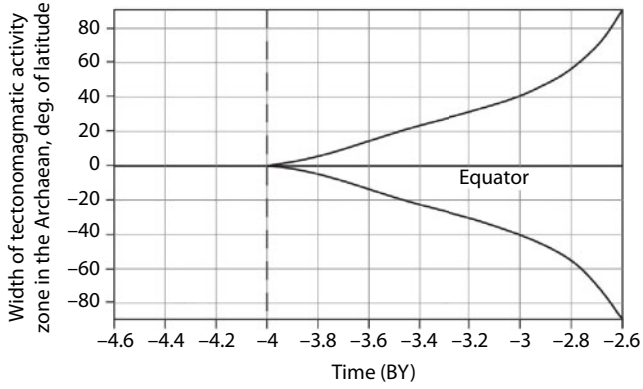

Fig. 5.3 Tectono-magmatic activity zone width on Earth's surface in Archaean, in degrees of latitude (the dashed line is a moment of the beginning of Earth's core separation process). The rest of Earth surface outside the zone of tectono-magmatic activity in Katarchaean and Archaean is primordial Earth's matter overlain by ultramafic regolith.

$$S_{Tm} = \frac{E_m T - T_m T_{4.0}}{E_m T_{2.6} - E_m T_{4.0}} \qquad (5.7')$$

At qualitative evaluation of the process parameters, we assume as the first approximation that Earth matter, silicates and iron compressibility are approximately equal. But $\rho_0 \approx 3.98$; $\rho_{Fe} \approx 7.8$; $\rho_{Si} \approx 3.71$ g/cm^3, in this case we may assume $\Delta\rho/\rho_0 \approx 1.043$; $\rho_{Fe}/\rho_0 \approx 1.96$ and $\rho_{Fe}/\rho_{Si} \approx 2.1$, where $\Delta\rho = \rho_{Fe} - \rho_{Si}$. Then, from equation (5.6) we determine that, for instance, at depth 200 km the molten iron layer thickness is approximately approximate 212 km. Similarly, at the intersection by differentiation front of the depth of 1,000 km, the melt thickness increase approximately to 305 km and at the intersection of depths 1,600 and 3,200 km, the thickness of such molten iron and oxides layers increased respectively to 337 and 400 km (see Fig. 5.6). We will note for comparison that the radius of young Earth's core formed at the very end of Archaean had been equal to 3,010 km whereas the radius of the present-day core is equal to 3,485 km.

The mantle heating δT in Archaean had substantially depended on the original temperature distribution in young Earth as shown in Fig. 4.4. Selecting the original temperature distribution, as already noted in section 4.2, we used the estimates by V.S. Safronov [61] and V.S. Safronov, A.V. Vityazev (1990) who evaluated temperature values in primordial Earth based on a model of "cold" accretion of our planet. However, these calculations did not take into account the tidal interaction energy of Earth with the

Proto-Moon and did not take into account the energy balance of young Earth. As a result, we had to introduce appropriate corrections in these distributions as shown in Fig. 4.4.

The additional heating of the convecting Earth's mantle in Archaean due to radioactive elements' decay, tidal interaction with the Moon, Earth matter differentiation and Earth's core formation is equal ΔT_W. At that:

$$\Delta T_W = \frac{\Delta E_{R+T}}{M_m \cdot c_p} \tag{5.8}$$

where ΔE_{R+T} is the total of radiogenic and tidfqal energy released in Archaean in the convecting mantle; M_m is the convecting mantle mass:

$$M_m = \frac{4\pi}{3} \cdot \left[R^3 - \left(R - H \right)^3 \right] \cdot \overline{\rho} \cdot S_{AR} \tag{5.9}$$

where S_{AR} is the equatorial zone width of Earth matter differentiation (see Fig. 5.3).

Judging by the temperature distribution in Earth's subsurface at the border of Katarchaean and Archaean and iron melting temperature under high pressure (see Fig. 5.2), their difference ΔT rapidly increases with depth. The estimates based on equation (5.2) indicate that the metallic iron zonal differentiation in a pure form might have occurred in young Earth only up to the depths of nearly 2,400 km. In this case, at the average rate of the process evolution of 0.2 to 0.15 cm/g, Earth's gravity differentiation must have stopped sometime in Late Archaean. However, due to the disintegration of solid silicate solutions under high pressure (see section 5.4), approximately at depths of 1,400 – 1,600 km from iron silicates had begun releasing in the free phase iron oxides, forming at that "core matter's" Fe_2O eutectic melts Fe·FeO with iron. Starting at this moment, i.e., approximately 3.2 BYa, the total concentration of such melts had begun rapidly growing. That had significantly increased the rate of Earth matter zonal differentiation front advance (to 0.4 cm/year) and the energy efficiency of the differentiation process. As a result, temperature distribution in Archaean mantle had been substantially changing with time as is shown in Fig. 5.4.

Estimates show that the upper mantle overheating had occurred rather rapidly approximately 200 MY after the action start of Earth matter zonal differentiation process. First, it had been rapidly increasing but then began gradually weakening. The mantle temperature decrease in the first

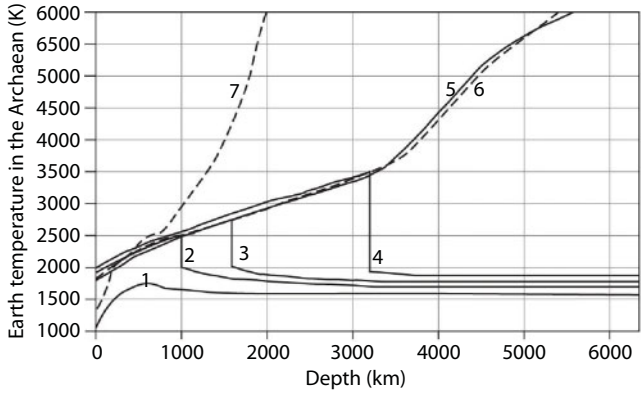

Fig. 5.4 Temperature of young Earth in Archaean: 1. temperature distribution in Earth after its formation nearly 4.6 BYa; 2. Earth's temperature in Archaean nearly 3.6 BYa; 3. Nearly 3.2 BYa; 4. Nearly 2.8 BYa; 5. Earth's temperature after the separation of Earth's core nearly 2.6 BYa; 6. Iron melting temperature; 7. Silicates' melting temperature.

overheating maximum had been due to a gradual increase with depth of the temperature diffenence between iron melting and Earth's subsurface on the zonal differentiation front. The second mantle overheating maximum had been associated first of all with the involvement in the process of melting out from the "core" matter of iron oxides, and begun at the end Archaean process of Earth's core formation (see Fig. 5.1-*d* and *g*). Our estimate is that at that time, approximately in 200 MY, within Earth must have been released nearly $4.2 \cdot 10^{37}$ erg of thermal energy (see section 6.5). In this time interval, Earth had lost with the thermal radiation nearly $1.8 \cdot 10^{37}$ erg. Therefore, in Late Archaean for Earth's heating had been expended nearly $2.4 \cdot 10^{37}$ erg more of gravity energy. This had resulted in its additional heating by approximately 330°C. Besides, in Archaean had been released nearly $1.35 \cdot 10^{37}$ erg more of radiogenic energy. This had added 190°C. As a result, despite a decrease of the temperature difference ΔT at the end Archaean of nearly 2.7 – 2.6 BYa, normalized to the surface temperature of the mantle, based on our estimates, still had to exceed 1,700°C, and its overheating, compared to the present-day temperature (≈ 1,320 –1,330 °C) had been at that time equal to 460°C (see Fig. 5.5).

The reviewed mechanism of Earth zonal differentiation provides a decent explanation not only of overheating of the Archaean mantle but also the presence in time of the two temperature maxima. The first one had appeared in Early Archaean, approximately 3.8 – 3.2 BYa. The second overheating impulse had occurred in Late Archaean, between 3.2 and 2.6 BYa whereas nearly 3.2 BYa had occurred a relative minimum of these temperatures.

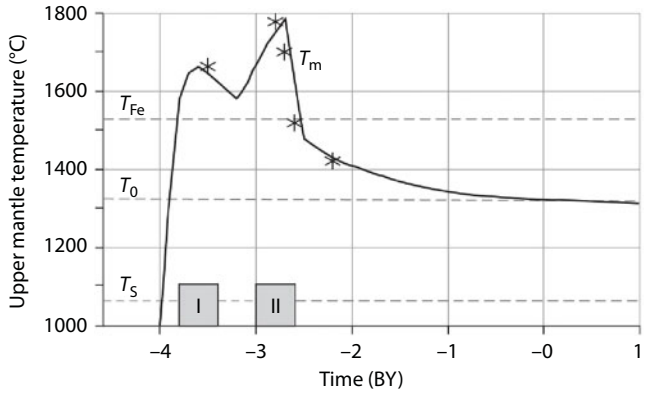

Fig. 5.5 The upper mantle temperature in Archaean normalized for the surface (°C): T_s = 1,060 is mantle matter solidus temperature; T_0 = 1,320 is normalized for the surface temperature of the present-day mantle; T_{Fe} = 1,530 is iron melting temperature under normal conditions. Starred are temperatures of the basalts and comatiites based on petrologic data (determined by us using the L.L. Perchuk program); I–II are eruption epochs of overheated comatiite lavas after V.I. Kovalenko *et al.* [108].

This process also provides a good explanation of an extremely important and very interesting feature of the mantle magmatism evolution in Archaean. This is the existence of two melting out impulses from the mantle of overheated high-temperature comatiite lavas [108] exactly coinciding in time with the defined above maxima of the mantle temperature (see Fig. 5.5).

In connection with the identification in Archaean of iron and its oxides in relatively narrow differentiation layers, the density diustribution in Earth of those faraway epochs had been characterized by sharp contrasts as shown in Fig. 5.6. However, the main distinction of the Archaean Earth from the present-day one had been, as was already numerously mentioned, the absence to the very and of Archaean of Earth's core. Estimates show that by the moment 2.8 BYa had been released nearly $1.01 \cdot 10^{27}$ g of the "core matter" which is approximately 52.8% of the mass of the present-day Earth's core equal to $1.942 \cdot 10^{27}$ g. In 200 MY, i.e., by the end Archaean had been released nearly $2 \cdot 10^{26}$ g (or 10.7%) more "core matter". As a result, the mass of Earth's core formed by the very end of Archaean had already reached $1.21 \cdot 10^{27}$ g or approximately 62.3% of the present-day core mass. Thus, during the Archaean era (duration 1.4 BY) had been released nearly 62.3% of the "core matter," whereas in Proterozoic and Phanerozoic (the total duration nearly 2.6 BY), only 37.7%. This shows that Earth matter differentiation processes have been going in Archaean at least 3 times more intensely than in subsequent epochs.

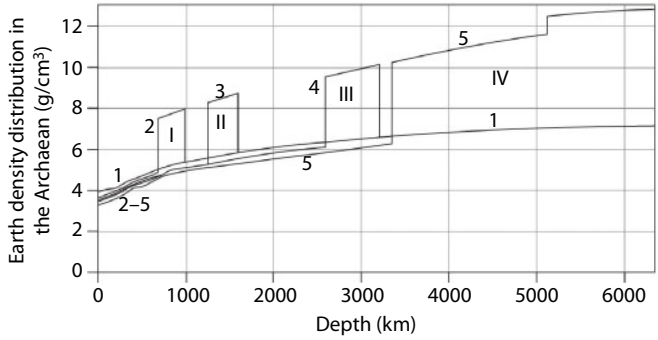

Fig. 5.6 Density distribution in Earth in Archaean: 1. Primordial Earth matter density before the differentiation; 2–5. Density of the mantle matter after Earth matter differentiation: **I** and **II.** Density of ferrugineus melts separated at zonal differentiation of Earth matter respectively nearly 3.6 and 3.2 BYa; **III.** Density of oxide- ferrugineus melts nearly 2.8 BYa; **IV.** Density of Earth's core separated at the end of Archaean.

We will now review young Earth's matter viscosity using a known correlation of the density vs. temperature

$$\eta = \eta_0 \exp\left\{\frac{W}{RT}\right\} \tag{5.10}$$

where $\eta_0 \approx 10^{-5}$ poise is maximuim density of molten matter at indefinitely high temperature T; W is viscous flow activation energy; R = 1.987 cal/mole·deg is the gas constant. The activation energy is substantially depends on the pressure p [109]

$$W = W_0 + V \cdot p \tag{5.11}$$

where W_0 is activqation energy at p = 0, and V is a factor depending on the value of the activated volum ΔV. Having now accepted most likely values of the temperature and viscosity in the mantle of present-day Earth, it is possible to determine the likely values $W(p)$ in the present-day Earth. For the depth interval 200 to 2,000 km (i.e., to the depth of beginning separation in the intergranular spaces of a single valence phase iron melts), the coincidence with the distribution of mantle viscosity is reached at the following parameter values in the equation (5.11): W_0 = 210 kcal/mole and activation volume ΔV = 6.91 cm^3/mole. Then, as 1 calory is equal $4.187 \cdot 10^7$ erg/s and p is measured in kilobars, we find $V = 6.91 \cdot 10^6 / 4.187 \cdot 10^7 = 0.165$.

The quoted equation (5.11) is quite approximate but it may be used at the pressure $p << K$, where K is isothermal modulus of rock compression [109]. For the rocks of Earth's mantle $K \approx (1.5 \div 2)$ Mbar. For this reason, the equation (5.11) may be used only for characterizing the convecting mantle in the upper parts of young Earth sections. This is even more justified that in Archaean from the convecting mantle had been practically totally removed the entire metallic iron and for this reason its composition, except for the concentration of iron oxides, was close to the composition of the present-day mantle with already determined parameters of equation (5.11). As the young Earth's matter (and the matter of convecting mantle in Archaean) included nearly 22–23% of iron oxides, and an increase of FeO content in silicates, as is well known, lowers their melting temperature, it may be expected that matter's activation energy in the convecting mantle in Archaean had been substantially lower than its determined above value for the present-day mantle. We assumed twice as small activation energy value W_0 in equation (5.11), for the convecting mantle in Archaean:

$$W \approx 100 + 0.165 \cdot p, \tag{5.11'}$$

For the iron melt viscosity in Earth matter differentiation zones we assumed even a smaller W_0 value:

$$W = 0.45 \cdot 10^5 + 0.165 \cdot p. \tag{5.11"}$$

At higher pressures approaching the compression modulus K, it is better to use a different equation [109]

$$W = W_0 \cdot \left(\frac{\rho}{\rho_0} \right)^L \tag{5.12}$$

where ρ is the matter density under pressures $p >> 0$; ρ_0 is the matter density at $p = 0$; parameter L is determined from the equation:

$$L = \frac{V}{W_0} \cdot K \tag{5.12'}$$

(usually $L \approx 2$). For describing the viscosity in the primordial Earth's matter and in consideration of a greater metallic iron concentration in it, we assumed in our estimates the W_0 value approximately 2.5 times lower than in the present-day mantle ($W_0 = 84$ kcal/mole) and value $L \approx 2$.

In connection with a low temperature of young Earth, its subsurface had had a very high viscosity reaching in the planet's center values on the order of 10^{30} poise (Fig. 5.7). This practically completely eliminates any probability of convection. The explanation is that the evolution rate of convective processes is always in the inverse proportion with the matter viscosity in the medium and therefore is negligibly small. Exactly for this reason had been impossible a rapid formation of Earth's core at early stages of Earth existence, including by way of the mechanism of lowing through such medium of dense ferruginous melts to Earth's center as this was suggested by V. Elsasser [83]. Only due to the emergence of the Earth matter zonal differentiation process in Earth's layers greater heated by the tidal interaction with the Moon but reasonably near-surface Earth layers (at depths nearly 200–400 km and viscosity on the order of 10^{16} poise), this process could have developed further and gradually moved in depth of Earth. But heating itself of a relatively cold matter within young Earth had been quite slow, at a rate on the order of 0.2 – 0.15 cm/year in Early and Middle Archaean and nearly 0.4 cm/ryear in LateArchaean (after the beginning of eutectic alloy Fe·FeO melting beginning). For this very reason Earth's core formation process, according to our estimates, had been lasting approximately 1.4 BY (from 4 to 2.6 BYa).

Emphasizing again that due to exceptionally high viscosity of the primordial matter in central areas of Earth, the only mechanism of the core formation in Earth's center could have been squeezing to the surface of Earth's primordial matter the heart of considerably heavier melts of iron

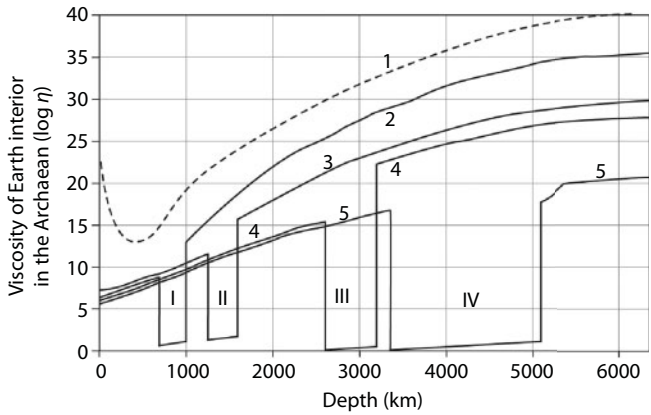

Fig. 5.7 Logarithm of young Earth subsurface viscosity: 1. Earth viscosity after formation nearly 4.6 BYa; 2–5. Earth viscosity in Archaean, respectively nearly 3.7, 3.2, 2.9 and 2.8 BYa; **I** and **II** molten iron viscosity in Earth's matter differentiation zones**; III** and **IV**. Viscosity of the "core matter" (monovalent phase of Fe_2O iron) In Earth's differentiation zone nearly 2.9 and 2.8 Bya.

and its oxides, as shown in Fig. 5.1. After the formation of Earth's core at the border of Archaean and Proterozoic and transition to a quieter barodiffusion mantle matter differentiation regime, the mantle temperature had begun gradually declining. When estimating the mantle cooling rate we assumed the current normalized to the surface mantle temperature close to 1,330–1,320°C.

As a result of the transition of the primordial Earth matter differentiation process from the mechanism of the metallic iron and its oxides zonal separation to the barodiffusion mechanism of separation of the eutectic Fe·FeO melts, in the entire mantle had to emerge the chemic-density convection. At that, leveling had also occurred of the mantle temperature under the adiabatic law according to the temperature of "core" matter Fe_2O melting at Earth's core surface. We may note here as well that this theoretical conclusion nicely fits with the empiric data of a rather rapid disappearance of high-temperature comatiites at the border between Archaean and Proterozoic [108].

5.4 Earth's Matter Barodiffusion Differentiation

The development of a theoretical model of the currently operating process of Earth matter differentiation resulting in the separation in Earth's center of a dense core involves the solution of a number of very difficult problems. Indeed, the differentiation process is not directly observable and must be judged only based on its indirect manifestations on Earth's surface using analysis of the data of the experimental and theoretical physics. One of such complex moments in the studies of this process emerges due to a substantial excess of the silicates' melting temperature at great depths over the adiabatic mantle temperature. Indeed, according to most likely estimates of mantle silicates' melting temperature under high pressure at the mantle base exceeds 8,000 K whereas the mantle temperature at these depths is close to adiabatic temperature, approximately 3,200 K [19]. Obviously, the existence of such a significant temperature barrier (more than 5,000°C) totally eliminates a suggestion of a possible Earth's core separation at the expense of melting it out from the mantle matter.

Exactly this difficulty forces the suggestion that currently the separation of iron oxides from the mantle silicates occurs due to the decomposition of solid solutions, affected by high pressures and iron oxide diffusion from the silicate crystals and oxides' crystallites into intergranular spaces of the mantle matter [110]. This suggestion is based on the Le Chatelier principle and experimentally established phenomenon of solid solutions'

decomposition when affected by a high pressure in those cases when the molar volume of these solutions V_s exceeds the sum of molar volumes V_i of its components

$$V_s > \sum_i^n V_i \tag{5.13}$$

The decomposition of such solutions occurs due to a decline of maximum concentrations C_i^* of the solution components under the pressure p

$$\left(\frac{\partial \ln C_i^*}{\partial p} \right)_T = \frac{\Delta V_i}{R \cdot T} \tag{5.14}$$

where DV_i is a variation in the total volume of the solution at dissolving of one mole of component i in its saturated solution; R is the gas constant; T is the absolute temperature.

Experiments with real solid solutions [111] showed that their decomposition is well described by equation (5.14). This enables us to use it for describing the process of iron oxides' separation from the mantle silicates. Unfortunately, we don't know from the experiment the value of the volume offset effect of iron oxide with silicates under the super-high pressures. However, it is expected that after the first electron-phase transition in the iron, the stereometry of its oxide Fe_2O will be drastically different from the structure of other silicates forming oxides. Based on experimental data, miscibility of components with different crystalline structure sharply declined at pressure increase. This enables a suggestion that the solid silicate solutions containing iron oxide under a pressure exceeding the level of the first electron-phase transition in the iron ($p \approx 130$ kbar) may decompose [112].

However, for the separation of iron oxides from the mantle matter is insufficient the only process of silicate decomposition because it is still necessary to carry these iron oxides out of the silicate crystalline grid into the intergranular spaces. A mechanism of such removal of iron oxides from silicate crystals and grains obviously may be associated only with diffusion. However, usually thermal diffusion results in homogenization of the matter, whereas here a directly opposite concentration of iron oxides in the intergranular spaces and films should occur. Such situation may emerge only in a case if on the way of diffusing atoms exist energy barriers allowing them to move in one direction and making return motions difficult.

When the condition (5.13) is fulfilled, such natural energy barriers emerge on facets of the crystals and individual grains. Indeed, at diffusion from a crystal of come volume V of iron oxides the energy δE is released proportionate to the emerging decrease of the total amount of matter δV and pressure p

$$\delta E = p \cdot \delta V \tag{5.15}$$

It is also obvious that for a return diffusion of the iron oxides in the crystal, an additional energy would have to be expended directed for overcoming pressure and for expanding the volume of the matter by the same value δV. At this,

$$\delta A = \delta E \tag{5.15'}$$

Due to this phenomenon, iron oxides diffusing from silicate crystals and grains at high pressure reining in the lower mantle cannot return back and must gradually accumulate in the intergranular spaces and films.

When dealing with a diffusion processes, it is necessary to remember that in actuality only atoms and not their compounds move through the vacancies and defects of crystalline grids. For this reason, it would be more correct to speak separately about diffusion of the iron and oxygen with their partial diffusion coefficients D(Fe) and D(O). Mismatch of these coefficient values results in different rates of the atom motions and, as a consequence, in a disruption of the stoichiometric compositions in equilibrium compounds of diffusing elements. However, the disruption of stoichiometric ratios in its turn causes the appearance and increase of chemical potentials in boundary layers separating the drifting apart atoms. As a result, the addition of a new energy to the diffusion rate of the iron and oxygen must level correspondingly to the composition of a compound stable at given P–T conditions or eutectic melt. Taking these considerations into account, here and thereafter we will be talking about the diffusion of oxides tentatively, for simplicity, having actually in mind their effective diffusion and remembering that physically in solid media only atoms may diffuse.

Under the influence of a high pressure exceeding pressure of the first electron-phase transition the iron drastically changes its physical and chemical properties. Indeed, after such transition in the atoms of iron as well as of copper on the external s-shell only one electron remains. But no endogenous copper silicates exist, and for this reason it is possible to expect that iron silicates in the lower mantle will also become unstable and must decompose. Under these conditions a stable form of iron compound,

apparently, is a eutectic melt Fe·FeO equivalent to the oxide of a univalent iron phase Fe_2O [113]. It is also possible to suggest that the decomposition reaction of bivalent iron oxide $2FeO \rightarrow Fe_2O + O$ will be occurring on crystal facets due to diffusion of iron and oxygen atoms from ferruginous silicates. On the other hand, the same reaction will be controlling the values of diffusion coefficients $D(Fe)$ and $D(O)$ in such a way that beyond the crystal facets (in the intergranular spaces) would emerge a stable compound Fe_2O.

From the point of view of physics this may be explained so that at high pressures average diffusion rate of iron atoms from crystals u_- and back u_+ to a greater extent change in iron because after an electron-phase transition exactly this metal sharply changes its physical and chemical properties. If at that iron diffusion is indeed accompanied by a release of energy (5.15) the mandatorily will be $u(Fe)_- > u(Fe)_+$. Whereas the diffusion rate of oxygen atoms from crystals $u(O)_-$ and back $u(O)_+$ on their own, without considering the effect of chemical interactions with iron, most likely, will remain at equilibrium, i.e. $u(O)_- \approx u(O)_+$. But inasmuch as part of the oxygen atoms diffused from crystals now enters a chemical reaction with iron forming outside of the crystals a new stable compound Fe_2O, a balanced diffusion is disrupted as in this case already $u(O)_- > u(O)_+$, therefore, the value of effective coefficient of oxygen diffusion $D(O)$ also changes [112]. Due to such reaction mechanism it may be expected that the eutectic melt Fe·FeO (or iron protoxide Fe_2O) will be forming and accumulating only in the intergranular spaces outside of the silicate crystalline grids whereas the iron oxide FeO and the oxygen released in the reaction will be preserved in the defects of crystals themselves forming in the excess of the oxygen molecules of the magnetite.

$$3FeO + O \rightarrow Fe_3O_4. \tag{5.16}$$

The magnetite has spinel crystalline structure with a very dense atomic packing. For this reason, magnetite is a very stable mineral at при high pressure. It is also not impossible that often observed magnetite ionclusions are fringes of olivines (fayalites) of mantle origin and are consequences of the (5.16) reaction.

It follows from equation (5.14) that at positive volume effect of the solution $\Delta V > 0$, i.e. if a condition of (5.13) is observed, the maximum concentration of C_i^* component in the solution will only decline with the pressure increase

$$C_i^* = C_{0i}^* \cdot \exp\left\{-\frac{\Delta V \cdot (p_H - p_0)}{R \cdot T}\right\} \tag{5.17}$$

where C^*_{0i} is concentration of the component i in a saturated solution at $p = p_0$; $p_0 \approx 130$ kbar $= 0.13 \cdot 10^{12}$ dynes/cm is pressure of the first electron-phase transition in iron of the mantle at depth of approximately 400 km (the pressure if the beginning of the iron oxides decomposition). It follows from equation (5.14) that the fraction separation process may develop only if the original concentration of component C_i exceeda the maximumk concentration C^*_i for given values of pressure and temperature (see Fig. 4.8) only at

$$C_i > C^*_i \tag{5.17'}$$

For iron oxide in the composition, for instance, of olivine, up to the pressure $p \leq 130$ кбар in the presence of MgO is observed tota miscibility of oxides with silica, up to stoichiometric ratio if fayalite (Fe_2SiO_4). For this reason, it may be accepted that for olivive C_0*(FeO) = 0.706 or recalculated for the "core" matter, C_0*(Fe_2O) ≈ 0.628. The present-day average concentration in the mantle of iron oxides (in conversion to FeO) is equal to $\overline{C}$ (FeO) = 0.083 (see Table 4.1) and in conversion to Fe_2O: $\overline{c}$ (Fe_2O) = 0.074. For this reason, at low pressures no differentiation of iron oxides may occur.

Taking into account that he maximum concentration of saturatioin of silicates by iron oxides C*(FeO) with pressure rapidly declines under (5.14) law, it may be expected that in the lower mantle exists a level deeper of which begins to work the condition of solid solutions decomposition $\overline{C}$ (Fe_2O) > C_0*(Fe_2O). We suggested that this level coincides with the depth of inflexion of the mechanical Q-factor curve for the mantle Q_μ at depth nearly 2,000 km [112] which corrtesponds with pressure $p = 0.89 \cdot 10^{12}$ dyne/cm^2 and temperature of nearly 2,730 K. Let us now assume that in the lower mantle the ratio of molar volumes $\Delta V/V$ weakly changes with pressure. Then volume effect ΔV_j at any j^{st} level in the mantle may be expressed through a change of molar volume ΔV and density ρ at the critical level 2,000 km: $\Delta V_j = \Delta V \cdot \rho / r_j$ (the ρ and ρ_j values are included in Table 4.2). From the equation (5.14) composed for depths of the beginning of iron oxides decomposition nearly 400 km ($p \approx 0.13 \cdot 10^{12}$ dyne/cm^2) follows that C^*_0 = 0.628. From the same equation but only composed for a critical depth of the beginning of iron oxides separation from mantle silicates nearly 2,000 km, we find $\Delta V_{2000} \approx 0.655$ cm^3/mole. In this case, at the base of the mantle $\Delta V_{mc} \approx 0.655 \times 5.16/5{,}6 \approx 0.604$ cm^3/mole. Pressure at the surface of Earth's core reaches approximately $1.4 \cdot 10^{12}$ dyne/cm^2, then from equation (5.14) we find the searched for value of maximum concentration of the saturation

by iron oxides of the mantle silicates at its base $C^*_{mc} \approx 0.027$. The curve of (5.14) correlation for conditions of Earth mantle is shown in Fig. 5.8.

The barodiffusion separation of "core" matter from the silicates is accompanied by the release of a notable energy. According to equation (5.15), at depth 2,000 km this energy is equal to $5.5 \cdot 10^{11}$ erg/mole or 102 cal per each gram of the released Fe_2O oxide. At the base of lower mantle this energy increases to $8.15 \cdot 10^{11}$ erg/mole or 151.6 cal/g. On the whole, duting the time of Earth life, approximately $1.3 \cdot 10^{37}$ erg or nearly 9% of the total Earth's gravity differentiation energy had been released this way. We may mark in passing that most of this energy had been used for elastic compression of the matter.

Estimates included here of the medium compaction effect at barodiffusion mantle matter differentiation were published already in 1981 [110]. Somewhat later appeared an experimental work by W. Ohtani, A. Ringwood and W. Habberson [114] showing that under influence of high pressures, the formation of eutectic alloys $Fe_x \cdot FeO_{1-x}$ is also accompanied by the emergence of exceptionally strong compaction effects. The obtained results show that the formation of "core" matter composition with large negative volume effects, emerging under influence of high pressures, must go along the line of formation of the eutectic alloy $Fe_x \cdot FeO_{1-x}$ withj minimal molar volume.

The suggestion that the differentiation of the mantle matter had been developing only in the lower mantle is indirectly aupported also by some

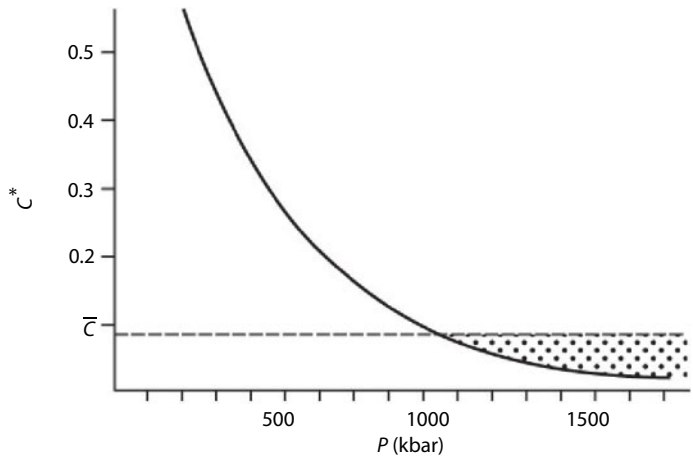

Fig. 5.8 Correlation of maximum concentration of iron oxides' solid solutions saturation in the mantle silicates vs. pressure. The evolution area of iron oxides barodiffusion from mantle silicates is shown in speckles.

geophysical data. Thus, at depths 1,800 – 2,000 to 2,900 km noticeably increases fading of seismic vibrations, and the Q-factor Q_μ for compression waves in this depth interval declines approximately from 500 to 115 near the core surface [115]. Also, the lower mantle layer D" is identified from fading Earth's natural vibrations and the Q-factor in it declines almost 10-fold [116]. The mentioned anomaly is so clear that the authors of the mentioned publications even suggested to call layer D" of the lower mantle the second Earth's asthenosphere. In the context of the mechanism under consideration of Earth's matter differentiation, a comparison of the lower layer of the mantle with the asthenosphere is quite justified as within a zone of Fe_2O liquid phase (or the eutectic Fe·FeO melt) release it is natural to expect also a drastic decline of matter's effective viscosity. Moreover, based on dynamic features of seiqmic waves reflected by the core surface [117, 118] was identified a relatively thin boundary layer, only about 20 km thick we called the Berzon layer [112] in which the lower mantle matter's mechanical rigidity quite continuously declines with depth practically to zero. The quoted fact indicates that due to fill-up of the intergranular space in polycrystalline mantle matter by Fe_2O melts, this layer gradually acquires the properties of a low-viscosity liquid, at that without melting of silicates.

Let us now review a change in time due to the diffusion of the heavy fraction's (iron oxides) concentration in silicate crystals. For this purpose, we will watch one of the silicate crystals going together with the descending convective flow from the upper mantle to the lower one toward the core surface. We will assume that the mantle matter differentiation develops only in the lower mantle, i.e., approximately in a depth interval of 2,000 – 2,900 km, and that the very separation of the heavy fraction from the mantle matter and the transition of the iron oxides in the core occurs only in a very thin layer at the base of the mantle. We will also assume that prior to the intersection of 2,000 km level, the heavy fraction was uniformly distributed in the entire volume of the crystal at concentration $C_0 < C^*$. Until the crystal intersects the level of critical pressure $0.89 \cdot 10^{12}$ dyne/cm^2, the diffusion of iron and oxygen atoms from the crystal will be obstructed by chemical binds of these elements with the silica.

After the intersection of critical level $C_0 = C^*$ at a depth about 2,000 km, the unequality $C_0 > C^*$ begins to implement, and the diffusion displacements of the iron and oxygen atoms through the silicate crystal facets stop being balanced as the diffusion of these atoms from crystals is already accompanied by energy release (5.21). As a result, the concentration of iron oxide C(FeO) on the internal side of crystal facets begins to decline. At each moment in time it will be defined, according to equation (5.14), by the value of maximum concentration C^*(FeO) in the saturated solution of

the iron oxide in the silicates at the existing in the lower mantle pressures and temperatures.

With the mantle matter descent to the base of the lower mantle, the iron oxide concentration along the silicate crystala and grains periphery will be ever more declining not overcoming at that the C^*(FeO) values on the crystal facets. However, in the process of the crystal descent through the lower mantle, i.e., at the time on the order of 10^7 years, concentration changes C(FeO) may spread in the depth of the crystalline grid by a very small distance. It happens because the diffusion coefficients in silicates at pressures exceeding 10^{12} dyne/cm^2 and temperatures much lower than silicate melting temperaturesmust be very small, perhaps on the order of $D \approx 10^{-21} - 10^{-22}$ cm^2/s.

For finding out major patterns in the process of the fraction separation, find a solution of the diffusion equation with some suggestions simplifying the problem. For instance, we will assume that the diffusion coefficient is isotropic and constant in value in the entire subsidence depth interval from 2,000 km to the core surface at the depth of 2,900 km. In this case, the problem may be boiled down to the solution of a unidimentional diffusion equation

$$\frac{\partial C}{\partial t} = D\frac{\partial^2 C}{\partial \xi^2}\,. \tag{5.18}$$

where ξ is the co-ordinate exis perpendicular to the crystal facet. The solution of this equation (4.18) is included in our publications [17, 110, 101].

Let us assume that the penetration depth of the change in concentrations (FeO) in depth of the crystal over the time interval under consideration ($\sim 10^7$ years) is small compared with the dimensions of the crystal itself. Let us assume that the time coordinate origin t = 0 is the moment of the intersection by the crystal of the critical pressure level at depth 2,000 km. The iron oxide C*(FeO) concentration on facets of the crystal is determined from equation (5.14). Inasmuch as in the differentiation layer, according to Table 4.2, the pressure changes relatively insignificantly compared with its average value (0.891 to 1.384 Mbar), we will use as the first approximation the linear term of this function resolution and assume $C^* = C_0 - ap$. Taking now into account a linear pressure buildup with depth at these levels and assuming a permanent descent rate of the matter in a convective flow, it is possible to approximate concentration changes on crystal facets by a linear time function

$$C^* = C_0 - at \tag{5.19}$$

As is known, the diffusion and thermal conductivity equations are totally similar to one another. This enables us, at the set limitations, to use a solution of the thermal conductivity equation for a linear flow in a semibounded solid body included in a monograph by G. Carlslow and D. Yeger [119]. In this solution, the body under consideration at the initial moment in time has zero temperature and on its surface is operating a heat source with temperature linearly varying in time. Then, in consideration of the equivalency of the thermal conductivity and diffusion equations:

$$C = C_0 - a \cdot t\{(1 + \frac{\xi^2}{2D \cdot t}) \cdot \left[1 - \Phi\left(\frac{\xi}{2\sqrt{D \cdot t}}\right)\right] - \frac{\xi}{\sqrt{\pi \cdot D \cdot t}} e^{\xi^2/4D \cdot t}\} \tag{5.20}$$

where $\Phi(z) = \frac{2}{\pi}\int_0^z e^{-\xi^2} d\zeta$; C_0 is the initial FeO concentration in the crystal at t = 0 (C_0 = const).

Equation (5.20) determines the iron oxide concentration only in crystals of the ferruginous silicates. Outside their limits, in the intergranular spaces, is accumulated a pure iron protoxid Fe_2O. For this reason, it may be assumed that in-between the silicate crystals $C(Fe_2O) = 1$.

In Fig. 5.9 is shown concentration distribution nature of the iron oxide in crystals of silicates derived from equation (5.20), and of the "core" matter (Fe_2O) in the intergranular space based on an assumption that these crystals, together with the convective flow, have been descending to the surface of the core during the time on the order of 10^7 years. As the mantle matter in the descending convective flow neared Earth's core surface, the fraction of iron oxides diffusing from silicate crystals and grains into intergranular spaces was ever increasing. At that, the liquid state of the external core is saying that within the intergranular spaces the "core" matter, i.e., Fe_2O, had also to be in melted state. Therefore, rigid bonds operating between the crystals in the lower mantle, with approach to the core gradually weaken. Exactly this phenomenon is the reason for a sharp decrease in the seismic Q-factor of the mantle matter in layer D" and especially in Berzon layer. As soon as near Earth's core individual inclusions of molten iron oxide Fe_2O merge in a single system of tied with one another liquid films and discharges enveloping individual crystals, its disintegration begins.

It is obvious that under the descending convective flows, i.e., under heavier areas of the mantle, must have mandatorily emerged mantle

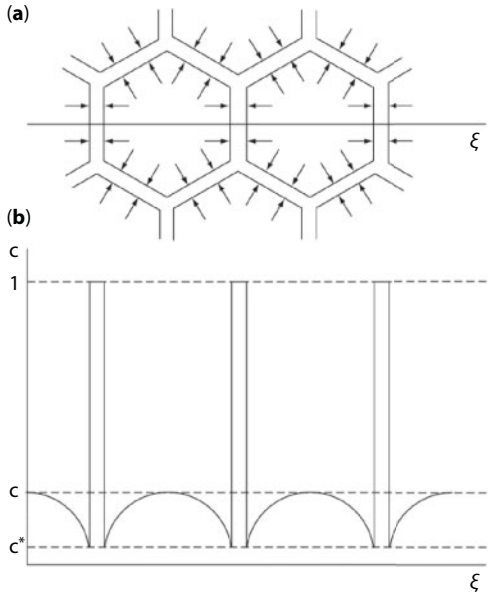

Fig. 5.9 Barodiffusion distribution of Fe_2O concentration in silicate crystals of the lower mantle layer D": *a*. Directioins of iron oxides diffusion in silicate crystals; *b.* Distribution of iron oxide concentration in the same crystals and intercrystalline spaces ax after the diffusion.

protrusions squeezed into the core matter, whereas under the ascending convective flows, on the contrary, must have been observed highs of the core surface as shown in Fig. 5.10 [15, 17, 120]. In mid-1980s [121], by means of the core's seismic tomography, a reliable proof of reality of this conclusion has been obtained: such ups and downs of the mantle-core boundary really exist and topographic vatiations in them reach ± 6 km.

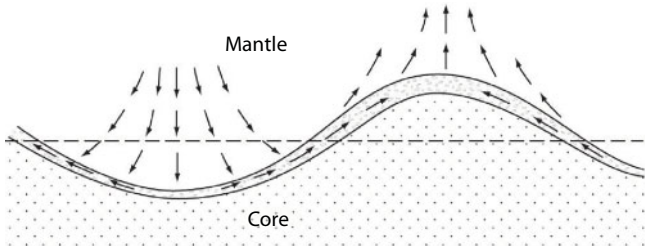

Fig. 5.10 Schematics of convective flows near the mantle–core boundary and formation of the ascending flows in the mantle [112].

Large hills-and-hollows at the base of the lower mantle and large density variations between the "core" and mantle matter ($\Delta\rho_{mc} \approx 4$ g/cm^3), naturally, had to result in the appearance in the roots of descending mantle flows of substantial tensile stresses reaching, in our estimates, on the order of 10 kbar [112]. Exactly due to such stresses at the mantle base under the descending flows is occurring final decomposition of polycrystalline mantle matter into individual crystals and granules suspended in molten Fe_2O with the formation of an aggregate state reminding a "magmatic gruel". At that, the univalent iron oxide ("core matter") earlier released from crystals of the mantle matter transits in Earth core providing for a gradual growth of its mass. Perhaps this phenomenon might explain occurring in the boundary of Berzon layer gradual loss of the mantle matter rigidity as it transits on the surface of Earth's core in substantially liquid state [117, 118]. It is important to stress once again that the processes of the "core matter" release from the mantle, as described here, are developing without melting of silicates.

Spreading of the decomposed mantle matter from under the roots of the descending flows toward the ascending convective flows, it would appear, had to result in leveling Earth's core topography. However, such topography leveling, in conditions of the convecting mantle, is continuously compensated by descending on these levels ever and ever newer portions of a fresh mantle matter and rising of the already differentiated matter in the development areas of the ascending flows. As a result, at the boundary between the mantle and core establishes itself some balanced motion of a disintegrated mantle matter tying up the mantle convective flows into united closed cells.

Within the ascending mantle matter convective flows are evolving the processes opposite to those described above. Affected by the confined pressure, from the buoying matter's mass is gradually squeezed in the core most of the molten iron oxide. At that, silicate crystals and grains, due to emerging in them plastic deformations and processes of intergranular diffusion, again are gradually welded between themselves into a "compact" medium. However, in the composition of silicates that made it through differentiation is contained smaller iron oxides than in the source mantle matter. For this reason, the mantle matter average density in the ascending mantle flows is always notably lower than in the descending flows. The lifting (Archimedes) force emerging due to this in Earth's gravity field ultimately is putting in motion convective mass exchange in the mantle.

The iron oxides diffusion in the ascending flow matter will now be going in the opposite direction, from intergranular spaces into silicate crystals.

Simultaneously with this, in the crystals increases the Fe_2O_3/FeO ratio with the formation of magnetite Fe_3O_4 molecules and zonal distribution of iron oxides in crystals.

The described qualitative interpretation of undations (wavelike irregularities) of Earth's core surface enables us to determine average density difference between the original and made it through the differentiation mantle matter in its descending and ascending flows. Indeed, the pressure of the mantle on the surface of Earth's core under the ascending mantle flow turns out somewhat lower than under its descending flow. Thus, $\Delta p = \Delta\rho \cdot \Delta h \cdot g$, where Δp is the difference of average mantle pressures on Earth core under ascending and descending mantle flows; $\Delta\rho$ is density difference between the mantle and "core" matter; Δh is amplitude of Earth's core surface gradient under the ascending and descending mantle flows; g is gravity acceleration on the core surface. After [112], $\Delta\rho = 9.92 - 5.6 = 4.32$ g/cm^3 and $g = 1{,}067$ cm/s^2, and $\Delta h = 12$ km. In this cse, $\Delta p = -5.53 \cdot 10^9$ dyne/cm^2 = –5.53 kbar. On the other hand, from pressure gradients between the ascending and descending flows is possible to determine parameters of the flows themselves: $\Delta p = \delta\rho \cdot H_m \cdot \overline{g}_m$ where $\delta\rho$ is difference of average denseity values the original matter of the descending mantle flow and the matter gone throught the differentiation in the ascending flow; H_m = 2,886 km is average thickness of Earth mantle; $\overline{g} \approx 1{,}000$ cm/s^2 is average value of the gravity acceleration it the mantle. Then we are finding

$$\delta\rho = \frac{\Delta p}{H_m \cdot \overline{g}_m} = 0{,}019 \text{g/cm}^3 \tag{5.21}$$

As we see, the density difference turned out not very significant but over a long time of Earth's tectonic activity the mantle density managed to decline noticeably. Thus, estimates show that after Earth's core formation at the very end of Archaean and to our days average mantle density decreased by approximately 0.38 g/cm^3. This means that during the last 2.6 BY its entire volume managed to go through the differentiation on Earth's core surface nearly 20 times. This enables an estimation of average convective motions' rate in the viscous medium matter of the lower and middle mantle (it turned out equal to approximately 4.6 cm/year which appears to be a quite reasonable value). Indeed, within a relatively thin and low-viscosity asthenospheric layer in which the mantle matter flow rates may be much higher, based on the motion rates of the oceanic plates in the Pacific, they reached only a few dozen cm/year.

5.5 Earth's Core Growth

The quantitative side of Earth's core separation process, same as the Earth differentiation process, is more convenient to review starting with the present-day situation when the core growth is occurring due to operation of the Earth matter barodiffusion differentiation mechanism. The rate of this process running under the barodiffusion mechanism of "core" matter (Fe_2O) separation from mantle silicates obviously turns out to be proportionate to the difference between iron oxides' concentration (converted to Fe_2O) in the mantle C and value of maximum saturation concentration C^* with these very oxides of solid silicate solutions at the base of mantle $C - C^*$ (see section 5.4). On the other hand, the rate of iron oxides' runoff from the boundary layer at the base of lower mantle (Berzon layer) into the core, i.e., the rate of "core" matter separation from the mantle's one, must be proportionate to gravity acceleration g_c on the core surface, to the size of this surface and to some constant K defined by the rate of barodiffusion itself. Therefore, the total separation rate of core mass is

$$\dot{M}_c = K \cdot (C - C^*) \cdot 4\pi \cdot r_c^2 \cdot g_c \tag{5.22}$$

where r_c is the radius of growing Earth's core. The gravity acceleration on the core surface is defined by the following equation:

$$g_c = \gamma \cdot \frac{M_c}{r_c^2} \tag{5.22'}$$

where $\gamma = 6.67 \cdot 10^{-8}$ cm^3/g·s^2 is the gravity constant. At $M_c \approx 1.942 \cdot 10^{27}$ g and $r \approx 3.47 \cdot 10^8$ cm, we find the present-day value of $g_c \approx 1{,}075$ cm/s^2. K is a proportionality coefficient.

For finding a correlation between the "core" matter concentration in the mantle C and the core mass M_c it is convenient to utilize the concept introduced by V.P. Keondzhean and A.S. Monin [122, 123] of the evolution parameter or core's relative mass

$$x = \frac{M_c}{C_0 \cdot M} \tag{5.23}$$

where $M = 5.977 \cdot 10^{27}$ g is Earth's mass, $C_0 = 0.376$ is the total concentration of the "core" matter in Earth (iron, its oxides and other heavy sidepophilic

elements passing into Earth's core). The present-day value of parameter x may be determined from the chemical composition of present-day Earth. Currently, in Earth's core is contained $1.942 \cdot 10^{27}$ g of the "core" matter, in the present-day mantle (the mass is $4.012 \cdot 10^{27}$ g) still remains nearly 4.15% of Fe_2O_3 and 4.37% of FeO which, converted to eutectic component Fe·FeO gives 7.646%, or $2.249 \cdot 10^{27}$ g of the "core" matter. On the whole, Earth contains, including iron oxides in the continental crust, $2.251 \cdot 10^{27}$ g of this matter. Therefore, the total concentration of potentially "core" matter in Earth $C_0 = 0.376$, and the present-day value of Earth's evolution parameter which in fact determines the relative value dimentionless mass of Earth's core is $x_0 = 0.864$.

Concentration of the "core matter", i.e., iron oxides remaining in the mantle and continental crust converted to Fe_2O is determined from a simple equation

$$C = C_0 \frac{1-x}{1-C_0 x}, \tag{5.24}$$

according to which currently in the mantle and crust must be contained nearly 7.57% of the potential "core matter".

Average density of Earth's core, apparently, changed little with time as simultaneously with its growth the pressure on the core surface had been gradually decreasing and in its center, on the contrary, increasing. Indeed, based on our estimates initial core density had been 10.7 g/cm^3 whereas average density of the present-day core is 10.6 g/cm^3. Taking this into account, it follows from eq. (5.23):

$$\dot{M}_c = C_0 \cdot M \cdot \dot{x} \tag{5.25}$$

Now, using eqs. (5.23) – (5.25), we will determine the correlation between the growth rate of Earth's core relative mass and parameter x

$$\dot{x} = \frac{1}{\tau} \cdot \left(C_0 \cdot \frac{1-x}{1-C_0 \cdot x} - C^* \right) \cdot x \tag{5.26}$$

where $\tau = K_c / 4\pi \cdot \gamma$ is a constant with the dimension of time; K_c is a coefficient describing the rate of the core matter passing from the mantle into the core under barodiffusion mechanism of Earth matter differentiation.

For the determination of function $x(t)$, the equation (5.26) must be integrated over time and parameter x. As in Earth center the gravity acceleration is equal to zero, then according to equation (5.22) the evolution of Earth matter barodiffusion differentiation process must not have started in Earth center but might have occurred only after the formation of Earth's core embryo. We reviewed a possible evolution scenario of such process in the section 5.2. Based on geologic data and theoretical arrangements reviewed above, the formation process of Earth's core embryo with relative mass x_e expanded almost over 1.4 BY but by the Archaean/Proterozoic boundary, nearly at $t_e \approx 2.6$ BYa such core embryo had been already completely formed (see Fig. 5.1). After this time, the further growth of the core had been proceeding only due to the operation of Earth matter differentiation barodiffusion mechanism described in section 5.4. This view is supported, in particular, by the fact of a quite sharp and radical change in Earth's crust evolution tectonic regimes in Archaean dominated by domal-fluidal structures of granite-green stone Archaean belts, by the lineaments of geosynclinals and riftogenic belts of Proterozoic and Phanerozoic.

Integrating equation (5.26) between t_e and t, and x_e and x, we arrive at [93]:

$$t - t_e = \frac{\tau}{1 - C^*}\left[\ln\frac{a - x}{a - x_e} - \frac{1}{aC_0}\cdot\ln\frac{x_e\cdot(a - x)}{x\cdot(a - x_e)}\right] \qquad (5.27)$$

where $a = (C_0 - C^*)/C_0(1 - C^*)$; t_e is the time of Earth's core embryo formation completion; x_e is relative mass of the core embryo at the moment in time t_e.

The total value of Earth "core" matter concentration C_0 was determined above: $C_0 = 0.376$; the present-day evolution parameter value, from equation (5.23), is $x_0 = 0.864$.

The time constant τ in equations (5.26) and (5.27) may be determined based on energy considerations. In the analysis of Earth energy balance in section 6.5 will be shown that currently the process of Earth matter gravity differentiation is generating nearly $3.07\cdot10^{20}$ erg/s or $9.67\cdot10^{27}$ erg/year of thermal energy. As a first approximation, we will assume that the total energy of Earth gravity differentiation is approximately proportionate to the mass of "core" matter released by the present moment of time, i.e.

$$E_g \approx E_\infty \cdot x \qquad (5.28)$$

$$\dot{E}_g \approx E_\infty \cdot \dot{x} \qquad (5.28')$$

where $\dot{E}_g$ is thermal component of the total energy of Earth gravity energy. Over the entire Earth evolution history, in its subsurface had been released nearly $E_g \approx 1.26 \cdot 10^{38}$ erg of thermal energy associated with Earth's matter gravity differentiation. From that, $E_g \approx 1.458 \cdot 10^{38}$ erg. Knowing the present-day value of $\dot{E}_g \approx 3.065 \cdot 10^{20}$ erg/s, it is easy to determine from (5.28') the value $\dot{x}_0 \approx 0.664 \cdot 10^{-10}$ years^{-1}.

Now, knowing that $C^* = 0.027$ (see section 5.4) and determined here parameter values $x_0 = 0.864$ and $C_0 = 0.376$, it is possible to determine that $a = 0.954$, and from equation (5.26) $\tau \approx 0.635 \cdot 10^9$ years. Substituting now the determined parameter values in equation (5.27) and assuming $t_0 - t_e = 2.6 \cdot 10^9$ years, we may find a relative mass of Earth's core embryo at the moment of its final formation at the Archaean/Proterozoic boundary nearly 2.6 BYa $x_e = 0.543$.

Equations (5.26) and (5.27) define Earth's core growth only on the main evolution sequence of the planets of Earth group under the barodiffusion separation mechanism of iron oxides from the mantle silicates at $t > t_e = -2.6 \cdot 10^9$ years. For Earth's core embryo formation time interval $-4 \cdot 10^9 < t < t_e = -2.6 \cdot 10^9$ years, i.e., in Archaean, the analytical correlation $x(t)$ may be determined from the convecting mantle mass (5.9), and therefore, also the mass of a released "core" matter, from equation (5.29):

$$x = \frac{\frac{4}{3} \cdot \left[(R_g - H + h)^3 - (R_g - H)^3 \right] \cdot S_{AR} \cdot \rho_{Fe}}{M \cdot C_0} \qquad (5.29)$$

where R_g is Earth radius; H is depth to the base of Earth's matter zonal differentiation layer in Archaean; h is thickness of ferruginous melts layer determined from equation (5.6); ρ_{Fe} is the ferruginous melts' density; S_{AR} is, as previously, the factor taking into account a gradual expansion of the equatorial zone of Earth's tectonic activity in Archaean mantle (5.7); Δt is current time from the beginning of Archaean (4 BYa); $1.4 \cdot 10^9$ years is the Archaean duration.

Value of the evolution parameter x in equation (5.29) depends on the concentration of the "core" matter *C(Fe)*, arriving into the melt (through the thickness of ferrugineus melts h as determined from equation (5.6))

$$C(Fe) = 0.136 + 0.239 \cdot \left[1 - \exp\left\{ \frac{-\Delta V \cdot (p - p_{\kappa p})}{R \cdot T} \right\} \right] \qquad (5.30)$$

where ΔV is the change in the total volume of iron oxide in silicates' saturated solid solution at solution in it of one mole of iron oxide; p is pressure at depth H; p_{cr} is pressure at critical depth of oxides' separation beginning (in our case, $H_{cr} \approx 1{,}400$ km and $p_{cr} = 656$ kbar); R is, as earlier, the gas constant; T is Earth's temperature at depth H. Selecting now the ΔV value such that the values of parameters x determined from eqs. (5.27) and (5.29) for the Archaean/Proterozoic boundary coincide with one another ($x_{2.6} = 0.543$), we find that $\Delta V \approx 0.026$ cm^3/mole.

From the determined Earth evolution parameter vs. time correlation it is possible to determine Earth's core growth curve. As the present-day mass of Earth's core equals approximately to $1.94 \cdot 10^{27}$ g and the present-day value of the parameter $x = 0.864$, for this determination taken from the curve value Fig. 5.11 need to be multiplied by $2.212 \cdot 10^{27}$ g. Now, from eq. (5.26) may be determined the rate of change of the evolution parameter $\dot{x}(t)$ shown in Fig. 5.12, and also Earth's core separation rate from the mantle matter (see Fig. 5.13). Similarly, from the evolution parameter curve may be determined Earth's core mass growth (see Fig. 5.14).

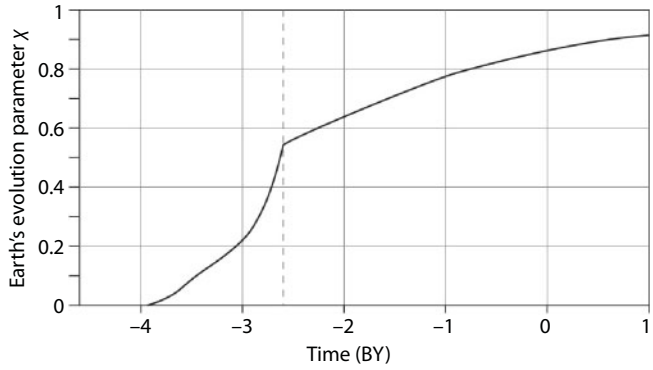

Fig. 5.11 Earth's evolution parameter describing a relative growth of Earth's core (in Archaean, a relative mass of the separated "core matter"). The vertical dashed line marks the moment when Earth's core separation process ended.

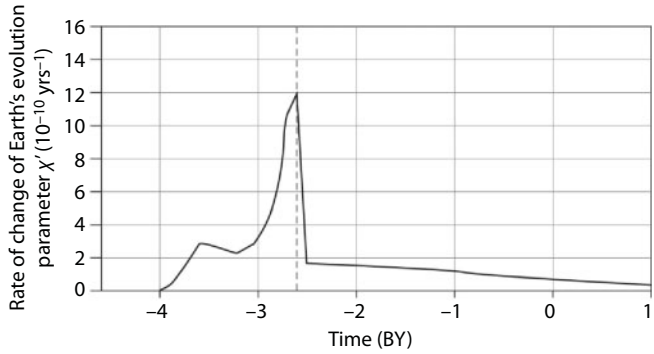

Fig. 5.12 Rate of Earth's evolution parameter change. The parameter describes a relative separation rate of the "core matter" and of Earth's core growth.

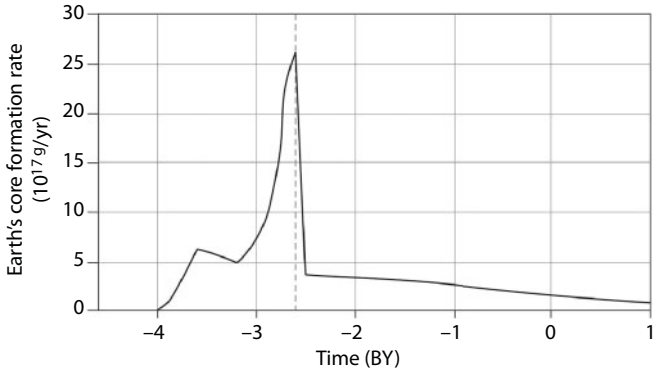

Fig. 5.13 Earth's core growth rate.

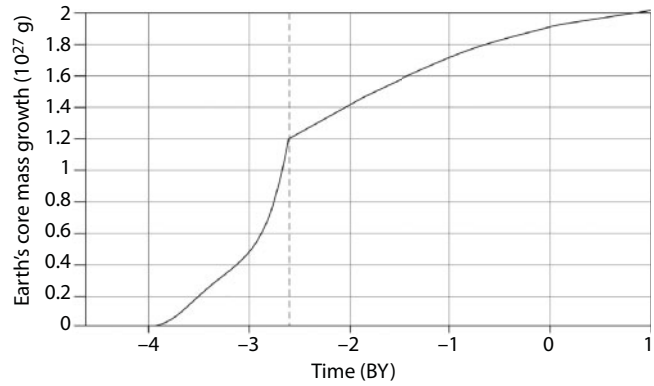

Fig. 5.14 Accumulation of Earth's core matter mass (the growth of Earth's core).

Emerged in Archaean Earth's gravity instability associated with functioning of Earth's matter zonal differentiation mechanism, as noted in the previous section, most likely had resulted at the end Archaean in catastrophic events which had quite rapidly moved all separated before this "core matter" to Earth's center (Fig. 5.1). For this reason, it is reasonable to assume that at the boundary Archaean/Proterozoic nearly 2.6 BYa had already been completed the formation in Earth of a young core and a further Earth's matter differentiation had sharply switched to a more quiescent mechanism of the barodiffusion separation of the univalent iron phase oxide Fe_2O. The moment of Earth's transition to a new evolution regime, which might be called the main sequence of the planet evolution, is clearly seen in Fig. 5.13 at the time about 2.6 BYa. As Fig. 5.14 shows, by this time, i.e., during the first 1.4 BY of Earth's geologic evolution, approximately 63% of the present-day core mass had time to form. The remaining 37% had separated during Proterozoic and Phanerozoic, i.e., over the time duration of 2.6 BY.

Thus, In Earth's evolution model under consideration in Archaean had not yet existed Earth's core in its present-day form. Instead, most likely, had existed a ring belt of eutectic composit heavy melts of iron its oxides. This liquid iron-iron oxide asthenosphere had been slowly moving in Archaean in the depth of Earth (Fig. 5.1). At this, its gradual broadening and thickness increase had been occurring. Appropriately, the geomagnetic field at that time had to have been substantially different from the present-day one and had to have a toroidal configuration. In Archaean, Earth's core had had somewhat smaller size and mass ($M_{2.6} \approx 1.22 \cdot 10^{27}$ g) than the present-day one ($M_{0.0} \approx 1.94 \cdot 10^{27}$ g) and had formed only on Archaean/Proterozoic boundary. For this reason, it may be assumed that in Archaean mantle had been going on the accumulation of Earth's core matter and starting in Proterozoic, after its separation, the growth of the core proper had already been occurring (see Fig. 5.1 and equation 5.14).

After the formation of Earth's real iron oxide core, obviously also emerged a dipole magnetic field of the present-day type. Field paleomagnetic data [124] indicate that this theoretical conclusion is fairly supported by experimental materials included in Fig. 5.17.

Based on eqs. (5.25) and (5.26) and the present-day value of parameter $\dot{x} \approx 0.664 \cdot 10^{-10}$ year^{-1}, it is reasonable to suggest that at present time from the mantle in the core is transiting nearly $1.45 \cdot 10^{17}$ g/year, or 145 billion tons a year of the "core matter" (Fe_2O), i.e., approximately 127 billion tons/year of the metallic iron. Whereas in Late Archaean, nearly 2.8 BYa, had been melting out approximately 1.9 trillion/year of the metallic iron.

5.6 Evolution of the Mantle Chemical Composition

The above-quoted description of Earth's core separation process enables us to determine theoretically the evolution of Earth's mantle chemical composition. Reviewing this issue, we will first of all be interested in the composition of convecting mantle. In Proterozoic and Phanerozoic, after the end of young Earth's core formation process the concepts of a convecting mantle and simply Earth's mantle had been totally coincident. However, it had been different in Archaean. As the convecting mantle in Archaean should be understood only the areas of Earth shell that had undergone zonal differentiation of Earth's matter and had been involved in convective flows. In Early Archaean the convecting mantle had been relatively thin and most likely existed as a ring geosphere underneath the equatorial belt of Earth (Fig. 5.1). Only by the very end of Archaean had the convecting mantle expanded almost to a size of Earth's spherical shell. Also, it should be remembered that at the moment of Earth's core formation nearly 2.6 BYa, to the convecting mantle had been added the matter of the former Earth "heart" with primordial concentrations of iron, its oxides (nearly 13% and 23%), siderophile elements, sulfides of chalcophile metals and other ore elements including platinoides. Direct witnesses of this are unique differentiated intrusions of basic and ultramafic rocks of Early Proterozoic age that had invaded in Early Proterozoic numerous ancient shields. Most salient and classical complexes of this type are rich in platinum, cobalt, nickel, copper and other ore elements stratified intrusive massif Bushweld in SAR; the Great Dyke intrusion in Zimbabwe; Sudbury norite intrusion in Canada, gabbro-norite Pechenga complex and Pan intrusion on the Kola Peninsula of Russia. We emphasize that intrusive formations of such types with so high concentrations of ore elements had never again emerged, before or after Early Proterozoic.

It is obvious that the removal of iron, its compounds and other siderophile elements from the primordial Earth matter into the separation zones of heavy fractions, with their further transition into the formed Earth core, and of highly mobile and lithophilic elements into Earth's crust, hydrosphere and atmosphere must have been accompanied by substantial alterations in the chemical composition of the convecting mantle. At that, the removal from the mantle matter of the heavy fraction ("core matter") must have unavoidably resulted in a relative concentration increase of the remaining elements and compounds.

Thus, in Early Archaean, after the operation start of the zonal differentiation process and removal from the convecting mantle of the entire

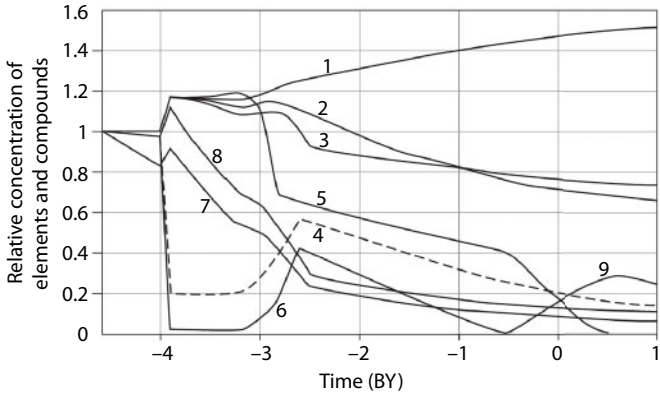

Fig. 5.15 Evolution of the chemical compositionof convecting mantle in relative concentrations (as the unit is taken the concentration of a given element in the primordial Earth's matter): 1. SiO_2; TiO_2; MgO; CaO; Al_2O_3; 2. H_2O; 3. K_2O; 4. Ni and other siderophile and chalcophile elements and compounds; 5. FeO; 6. Fe; 7. U; 8. Th; 9. Fe_3O_4.

iron (C_0(Fe) = 0.131) contained in the primordial Earth matter, the concentrations of the other elements and compounds ($C(i)$) in the residual mantle had sharply increased by approximately 15% (see Fig. 5.15) to a level defined by the equation

$$C(i) = \frac{C_0(i)}{1 - C_0(Fe)}. \tag{5.31}$$

where $C_0(i)$ is the initial concentration of a given element (compound) in the primordial Earth's matter. In Proterozoic and Phanerozoic, i.e., after the functioning start of the barodiffusion Earth matter differentiation mechanism, the residual concentration of elements and compounds in the mantle as a result of iron and its oxides transition in the core had begun increasing under the following pattern:

$$C(i) = \frac{C_0(i)}{1 - C_0 \cdot x}, \tag{5.32}$$

here $C_0 = 0.376$ is, as previously, the initial concentration of the "core" matter (Fe + FeO + FeS + Ni) in Earth's matter as converted in Fe_2O. Whereas the total concentration of the "core" matter (converted in Fe_2O) in the

mantle in Proterozoic and Phanerozoic with time had been declining according to the following pattern:

$$C = C_0 \frac{1-x}{1-C_0 \cdot x}. \tag{5.33}$$

According to a similar pattern in the after-Archaean mantle had been changing also the concentrations of nickel, gold, platinoids, iron, lead, copper and some other siderophile element sulfides which had been also gradually passing in Earth's core:

$$C(i) = C(i)_0 \cdot \left[\frac{1-\alpha \cdot x}{1-C_0 \cdot x} \right] \tag{5.33'}$$

where α is the mobility factor of an element or compound defining its fraction passing from the mantle into the core: at $\alpha = 0$ the equation (5.33') becomes equation (5.32) and at $\alpha = 1$ it becomes equation (5.33). In Fig. 5.15 is shown the relative concentration of main petrogenic elements estimated from equations (5.31)–(5.33').

Substituting now the values of relative contents of elements and compounds in Fig. 5.15 with values of their initial concentrations in primordial Earth [112], it is possible to determine the contents of these elements and compounds in percentages (Fig. 5.16).

After the zonal differentiation process of Earth's matter had begun at the boundary of Katarchaean and Archaean nearly 4 BYa, the metallic iron content

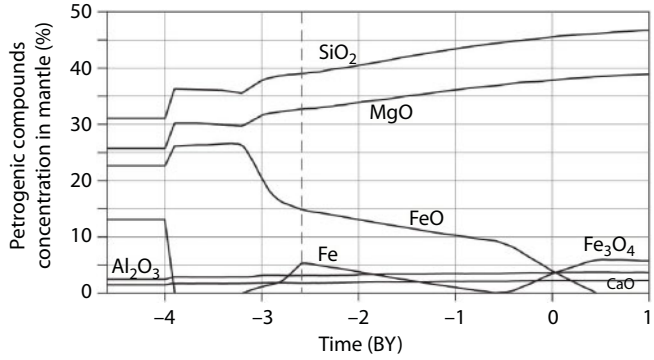

Fig. 5.16 Evolution of the convecting mantle chemical composition for the major petrogenic elements and compounds.

in the convecting mantle (above the zones of iron separation), the concentration of this metal in silicate melts of the overheated upper mantle must have rapidly declined to an equilibrium concentration. Because of a poor miscibility of such melts and a large difference in their densities, it may be assumed that during the most of Archaean the concentration of the metallic iron in the convecting mantle of that time had been close to zero: $C(\mathrm{Fe}) \approx 0$. In Late Archaean, nearly 2.8 BYa, the metallic iron concentration in the convecting mantle had begun growing and by the end Archaean had already reached the level of 5.5%. This had been associated with that at the end Archaean in the convecting mantle had entered a large amount of primordial Earth matter with the initial iron concentration in it of 13.1%; it had floated then up in the upper stages of the mantle from the former Earth's "heart" (see Fig. 5.1).

However, in Proterozoic, the metallic iron concentration in the mantle had begun declining again due to its transition in the formed Earth's core (see Fig. 5.15 and 5.16). The correlation of iron and its oxides concentration changes in the mantle at post-Archaean stages of Earth's evolution may be determined from major reactions of the "core matter" formation. Thus, in Proterozoic (same as at the very end Archaean, in the age interval 2.8 to 2.6 BY) the formation of this matter had been proceeding according to the reaction

$$\mathrm{FeO} + \mathrm{Fe} \rightarrow \mathrm{Fe_2O} \tag{5.34}$$

At that, for each 56 parts by weight of the metallic iron and 72 parts by weight of its bivalent oxide had been emerging 128 parts by weight of the "core matter". In this case, from the mantle into the core had been removed a mass of iron:

$$m(Fe) = \frac{56}{128} \cdot \tilde{C}_0 \cdot M \cdot x \tag{5.35}$$

where $\tilde{C}_0 = 0.363$ is the total concentration in Earth of Fe and FeO converted to $\mathrm{Fe_2O}$ (disregarding the other heavy components of the "core" matter such as, for instance, FeS and Ni); M is Earth' mass. At that, some iron had remained in the post-Archaean mantle.

$$C(Fe) \cdot M_m = C(Fe)_0 \cdot M - \frac{56}{128} \cdot \tilde{C}_0 \cdot x \cdot M \tag{5.36}$$

Taking now into consideration that the mass of mantle M_m after Archaean with time had been dereasing according to:

$$M_m = M \cdot (1 - C_0 \cdot x), \tag{5.37}$$

we are finding finally

$$C(Fe) = \left[C(Fe)_0 - \frac{56}{128} \cdot \tilde{C}_0 \cdot x \right] \cdot \frac{1}{1 - C_0 \cdot x} \tag{5.38}$$

Similarly, we are determining that the bivalent iron oxide in the post-Archaean mantle had been changing as follows

$$C(FeO) = \left[C(FeO)_0 - \frac{72}{128} \cdot \tilde{C}_0 \cdot x \right] \cdot \frac{1}{1 - C_0 \cdot x} \tag{5.39}$$

An extremely important and very interesting conclusion follows from equation (5.38): the free (metallic) iron might have been preserved in the mantle only to a certain critical moment in time t_{cr1} to which correspond C(Fe) = 0 and the critical value of the evolution parameter $x = x_{cr1}$. Taking into account, that $C(\mathrm{Fe})_0 = 0.131$, from equation (5.38) we determine $x_{cr1} \approx 0.825$, and from equation (5.27) we find the time of total metallic iron disappearance from the mantle: it turned out equal to approximately 500 MYa. Despite a highly approximate nature of the estimate, the determined time surprisingly closely matches the age of a major biological boundary in the evolution of highly organized life on Earth, the boundary between Proterozoic and Phanerozoic (nearly 570 MYa). This coincidence is quite remarkable and may not be considered accidental. Indeed, this event of the metallic iron disappearance from the mantle and rift zones of Earth where it prior to that had been in contact with oceanic water, had predetermined a radical change in the reduction potential in Earth's external shells. Because the metallic iron had been the main chemical reagent actively absorbing oxygen from the hydrosphere (and atmosphere) during the entire Precambrian evolution of Earth. Only after almost total disappearance of the metallic iron from the convecting mantle, in Earth's atmosphere might have accumulated oxygen produced by plants (and by the photodissociation of water vapor) in the amounts sufficient for the emergence and normal functioning of animal forms on Earth surface [112] (Sorokhtin *et al.*, 2011). The mechanisms of iron transition from the mantle into the hydrosphere with subsequent absorption of oxygen from the atmosphere will be discussed in more detail in section 11.5.

Equations (5.38) and (5.39) may be used only in the interval of the evolution parameter values $x_{2.6} \le x \le x_{0.5}$ (a reminder: here, as before, subscripts correspond with age in BY), i.e., in Proterozoic when the "core" matter formation had been going on according to reaction (5.34). For the moments in time corresponding to $x \ge x_{cr1} = x_{0.5}$ it is necessary to remember that after the disappearance of metallic iron from the mantle, the formation of the "core" matter in the lower mantle have already been occurring under a different reaction:

$$2FeO \rightarrow Fe_2O + O \tag{5.40}$$

At that, oxygen released under this reaction in excess of the existence level of stable iron oxides' solutions with silicates (see section 5.4) is bonded again with iron oxides forming the magnetite component of the mantle

$$3FeO + O \rightarrow Fe_3O_4. \tag{5.41}$$

For this reason, until the total oxidizing of the bivalent iron at $x = x_{cr2}$ the "core" matter formation had to be occurring under the following net reaction:

$$5FeO \rightarrow Fe_2O + Fe_3O_4, \tag{5.41'}$$

under which per every 360 weight units of the bivalent iron oxide emerges 128 units of the "core" matter and 232 units of magnetite.

Using the reaction (5.41'), we may record the total balance of the mass participating in the iron oxides' differentiation

$$C\left(FeO\right)\cdot M_m = C(FeO)_1 \cdot M_{m1} - \tilde{C}_0 \cdot M \cdot \left(x - x_{cr1}\right) - \\ - \frac{232}{128} \cdot \tilde{C}_0 \cdot M \cdot \left(x - x_{cr1}\right), \tag{5.42}$$

where $C(FeO)_1$ and M_{m1} are, respectively, FeO concentrations and the mass of mantle at $x = x_{cr1}$. Based on this, for the interval of the evolution parameter values $x_{cr1} \le x \le x_{cr2}$ is possible to determine:

$$C\left(FeO\right) = C(FeO)_1 \cdot \frac{1 - C_0 \cdot x_{cr1}}{1 - C_0 \cdot x} - \frac{360}{128} \cdot \tilde{C}_0 \cdot \frac{x - x_{cr1}}{1 - C_0 \cdot x} \tag{5.43}$$

and

$$C\left(Fe_3O_4\right) = \frac{232}{128} \cdot \tilde{C}_0 \cdot \frac{x - x_{\kappa cr1}}{1 - C_0 \cdot x} \tag{5.44}$$

The second critical value of the parameter x_{cr2} is easily found from a condition $C(FeO) = 0$ at $x = x_{cr2}$ in consideration of that at $x_{cr1} = 0.825$, the $C(FeO) = 0.102$. In this case $x_{cr2} = 0.894$, and from equation (5.27) we find $t_{cr2} \approx +0.6 \cdot 10^9$ years. The oxide of trivalent iron, unstable at high pressure, changes into a denser modification of the magnetite $3Fe_2O_3 \rightarrow 2Fe_3O_4 + O$. Therefore, in the future, approximately in 600 MY, all iron preserved in the mantle will be oxidized to a stable under the high pressure conditions magnetite phase of Fe_3O_4. For this reason, at the third stage of operating the barodiffusion Earth's differentiation mechanism at $x \geq x_{cr2}$, the "core" matter formation must proceed under the reaction of magnetite decomposition with oxygen release

$$2Fe_3O_4 \rightarrow 3Fe_2O + 5O \tag{5.45}$$

At that, the magnetite composite content in the mantle is determined from a simple equation

$$C(Fe_3O_4) = \frac{464}{384} \cdot \tilde{C}_0 \cdot \frac{1 - x}{1 - C_0 \cdot x} \tag{5.46}$$

We will now note one more very interesting and important conclusion defining the understanding of the ways of further evolution of life on Earth. After the total oxidation of the entire mantle iron to the magnetite, approximately in 600 MY in the future, the oxygen released at formation of the "core" matter under reaction (5.45) will no longer be retained in the convecting mantle and will begin entering Earth's hydrosphere and atmosphere. Starting at that moment in time, oxygen partial pressure will begin significantly growing [112]. This will undoubtedly be ruinous for the entire land life, and only limited oxygen solution in water will allow the life to be preserved for a short time in the depths of the world ocean. However, an increase in the total pressure of Earth's atmosphere caused by this phenomenon must result in a drastic increase of the greenhouse effect and emerging on Earth of the irreversible condition of a hot climate, Venus-kind.

Obviously, a direct filtration of dispersed in the mantle matter volatile and mobile elements and compounds through a dense mantle matter with viscosity on the order of $\eta \approx 10^{20} - 10^{23}$ poise is practically totally impossible due to the extremely low diffusion factor in such matter ($D \approx 10^{-21} - 10^{-25}$ cm^2/s). Therefore, a transition from the mantle in the external geospheres (the continental crust, hydrosphere and atmosphere) of lithophilic and volatile components may occur only due to melting of the mantle matter. This, however, is possible only in the near-surface parts of the mantle and even that not everywhere but only wherever the rigid Earth's shell (the lithosphere) is broken by depth faults through which effusions of basalt magmas occur. For this reason, for estimating the changes in volatile and easily mobile elements and compounds concentrations passing in the process of Earth evolution from the mantle into Earth's crust, hydrosphere or atmosphere, it is necessary to introduce an additional parameter β characterizing the mobility of the mentioned components.

Mobility β of elements and compounds depends not only on their chemical properties but also on the extent and depth of melting the mantle matter under Earth's rift zones which are major avenues of the delivery on Earth's surface of juvenile basalt magmas and dissolved in them volatile and mobile elements. If we are talking about mobile elements concentrated predominantly in the continental crust, then their mobility parameters also depend on the regime of oceanic crust rocks' and deposits' processing within the subduction zones. There, occurs the secondary mobilization of mobile elements and their transition from the oceanic crust in the continental. Besides, some elements and chemical compounds, for instance, H_2O, CO_2, K_2O, etc., which earlier got in the external geospheres (Earth's crust, hydrosphere and atmosphere), may again be pulled through the plate subduction zones into the mantle and be again involved in the mantle matter turnover. For this reason, the mobility of such elements and compounds should be understood as their effective value.

It is worth mentioning here that the very processes of degassing volatile compounds become possible only due to the existence in the mantle of convective mass exchange. It is continuously delivering to Earth's surface through rift zones ever new and new volumes of the mantle matter capable of separation and release of mobile elements. A conclusion is that the transition rate of mobile components from the mantle in the Earth's external geospheres must be proportionate to the rate of convective mass exchange in the mantle. In this case, the removal rate of such component from the mantle will be

$$\dot{m}_i = -\left(m_i\right)_m \cdot \beta_i \cdot \dot{z}\,, \tag{5.47}$$

where $(m_i)_m$ is the mass of i-th component in convecting mantle; β_i is its mobility parameter; $\dot{z}$ is parameter of Earth's tectonic activity (and of convective mass-exchange in the mantle). In general, Earth's tectonic activity is proportionate with coming from the mantle depth heat flow $\dot{z} \propto \dot{Q}_m$ (see section 6.6)

$$z = (Q_m - Q_{4.0})/(Q_{m0} - Q_{4,0}), \tag{5.48}$$

where $Q_{4.0} \approx 1.6 \cdot 10^{37}$ erg is Earth's heat loss by the beginning of its tectonic activity nearly 4 BYa; $Q_m \approx 10.77 \cdot 10^{37}$ erg is total heat loss by Earth's mantle by the present time. In this case, Earth's tectonic activity is characterized by by time derivative of parameter z

$$\dot{z} = (\dot{Q}_m - \dot{Q}_{m0}), \tag{5.48'}$$

where $\dot{Q}_m$ is current value of the depth heat flow: $\dot{Q}_{m0} = 3.39 \cdot 10^{20}$ erg/s is present-day value of this flow.

Let us now switch to concentrations of elements and their compounds

$$C(i) = \frac{(m_i)_m}{M_m} \tag{5.49}$$

for Archaean we get

$$C(i) = \frac{C(i)_0}{1 - C(Fe)_0} \cdot e^{-\beta_i \cdot z}, \tag{5.50}$$

similarly, for Proterozoic and Phanerozoic

$$C(i) = \frac{C(i)_0}{1 - C_0 \cdot x} \cdot e^{-\beta_i \cdot z} \tag{5.50'}$$

In general case, due to different mechanisms of the mantle matter differentiation and different formation conditions of the continental crust,

hydrosphere and atmosphere in Archaean and after Archaean, mobility parameters β_i in those epochs may have differed from one another. This certainly makes the solution of equations (5.50) and (5.50') more difficult and forces to involve additional data of the distribution of components under consideration in Archaean and Proterozoic. In some cases, this condition is doable. For instance, if we assume after S. Tailor and S. Mac-Lennan [85] that up to 70% of the continental crust mass had formed in Archaean (which is close to our theoretical estimates) and it contained nearly 1.8% K_2O, and if we assume for the present-day crust $C(K_2O) \approx 2.1\%$, then the potassium mobility parameter in Archaean had been approximately: $\beta(K_2O)_{AR} \approx 0.56$ and in subsequent epochs ≈ 1.07.

A similar estimate for water performed using a technique described in Chapter 10 shows that in Archaean $\beta(H_2O)_{AR} \approx 0.123$ and for post-Archaean time $\beta(H_2O)_{PAR} \approx 1.45$, i.e., after Archaean the effective value of water mobility parameter increased approximately by the factor of 12. The derived significant differences in effective values of water mobility parameter at its degassing from the mantle in Archaean and in subsequent epochs are apparently associated with that in our estimates we were taking water thermally dissociated in layers of molten metallic iron in the overheated Archaean age mantle (see Fig. 5.1). Besides, some contribution might have come from water decomposition already after its degassing from the mantle, for instance, by oxidizing of contained in Early Precambrian oceanic crust metallic iron or due to the photodissociation of water vapors by hard radiation of the Son in conditions of the oxygen-free atmosphere of Early Precambrian.

Average values of the mobility parameters for the uranium (^{238}U) and thorium turned out significantly higher: $\beta(U) \approx 2.26$ and $\beta(Th) \approx 2.65$. Because of this and due to radioactive decay of the uranium and thorium, concentrations of these elements in the mantle had declined most of all.

Estimate results of evolution changes in the chemical composition of a convecting mantle (without accounting for the mass of water dissociated on iron melts) in relative and absolute concentrations are shown in Figs. 5.15 and 5.16.

The included diagrams show that after the beginning of evolution in Earth of the zonal separation process of the metallic iron on the boundary Katarchaean/Archaean nearly 4 BYa, the chemical composition of convecting mantle had drastically changed due to a removal from its matter of nearly 13% of metallic iron. Since that time the concentration in the mantle of most common and least mobile oxides SiO_2; MgO; Al_2O_3; CaO in general had been regularly increasing. At present their concentration in the mantle is approximately 1.4 – 1.5 times higher than in Earth's primordial matter (see Table 4.1). The concentration of such low-mobility components as Na_2O

also somewhat increased but much weaker than for the previous compound group (Na_2O concentration increase is not shown in Fig. 5.16). H_2O, K_2O and Rb_2O compounds had been carried out of the mantle in a much higher degree. For this reason, their concentration had decreased with time by 1.4 – 1.3 times. A few times greater decreased the concentration in the mantle of radioactive elements U and Th. This had happened, as already noted, for two reasons, due to decay of the radioactive elements and due to their greater lithophility and dominating transition in the continental crust. Beginning in mid-Archaean nearly $(3.0–2.9)\cdot10^9$ years ago, after the transition of Earth matter zonal differentiation process to the separation of eutectic Fe·FeO melts (see section 5.3), had begun a decrease with time also of the FeO concentration. The total content of the "core" matter in the mantle beginning 4 BYa had been regularly declining and by the present time no more than 7.5% remains of its initial concentration of nearly 37%.

At first sight, the behavior of free (metallic) iron in the convecting mantle appears unusual. As soon as in Early Archaean had occurred melting of involved in convection areas of the upper mantle and the density differentiation of these melts had happened, the concentration of metallic iron in them immediately sharply declined from 13% to almost zero equilibrium level of iron solution in the silicate melts. At the end Archaean primordial Earth matter of the former Earth "heart" had begun to enter the convecting mantle (see Fig. 5.1) and the metallic iron concentration in the mantle had increased again. This perhaps is an explanation why in some Late Archaean and Early Proterozoic basalts are found inclusions of native iron as, for instance, is observed on Disco Island in the West Greenland (Levinson-Lessing, 1940). By the moment of Earth's core separation approximately 2.6 BYa, average iron concentration in the mantle had already risen to 5.5%. However, thereafter the iron content in the mantle had again begun smoothly declining and totally vanished from this geosphere, as estimates show, only about 500 MYa. Reminding again that this time found by estimating the differentiation rate of Earth at the set composition of its core (the external core is composed of Fe_2O, the internal core, of the alloy $Fe_{0,9}\cdot Ni_{0,1}$) closely coincides with most radical boundaries in the life evolution on our planet, the boundary between Proterozoic and Phanerozoic.

After the total disappearance from the mantle of metallic iron, oxygen released at the formation of the "core" matter had begun bonding under reaction (5.41) in the magnetite phase. Appropriately, had begun increasing the concentration of magnetite in the mantle matter having risen by the present time to the value nearly 3.7%. The increase of Fe_3O_4 concentration in the mantle will continue for approximately 600 MY in the future, until the total disappearance from this geosphere of the entire silicate (bivalent) iron. After

this moment the entire mantle iron will be associated only with the magnetite phase. As a result, the endogenous oxygen released under reaction (5.45) will be able to reach Earth surface. In this case, at balanced mantle degassing, each million years partial pressure of oxygen in the atmosphere will be increasing approximately by 1 bar destroying at that all life on the surface of Earth.

5.7 Geologic Data About Earth's Core Separation Time

A theory of Earth's core formation reviewed above, together with general data about Earth's evolution in Early Precambrian, indicate that Earth's core matter had begun forming at the boundary of Katarchaean and Archaean nearly 4 BYa and had finally formed only at the end Archaean nearly 2.6 BYa. However, for resolving the issue of the beginning time of its separation is insufficient only theory. It is already necessary to involve additional geologic and geophysical data as well as age determinations of lunar and most ancient Earth's rocks. Indeed, Earth's crust rock formation might have begun only in a case when in Earth's subsurface had begun evolving powerful energy processes resulting in exciting of our planet's tectono-magmatic activity.

We have already discussed the late separation of Earth's core in section 4.7 when we referred to the beginning time of Earth's crust formation and ages of the oldest crust rocks approximate equal to 3.8 BY. Indeed, Earth's crust could have begun separating only after melting in the upper mantle but with this very event should have corresponded also the beginning of Earth's gravity differentiation, i.e., the start of Earth's core separation. Exactly for this reason the beginning of Earth's crust separation marked by the age of the oldest crust rocks is a convincing indication of the beginning of the Earth's core separation process. Reliably determined ages of most ancient Earth's crust rocks as a rule do not exceed 3.75 – 3.8 BY [84, 85].

In recent years publications substantiating a more ancient age of Earth's crust rocks began appearing with increasing frequency. For instance, in greenstone belt schists discovered near Nuvvuagittuq settlement in Quebec have been identified amphiboles whose age was determined by Sm/Nd method at 4.28 BY [125]. The schists discovered by Canadian scientists are surrounded by a massif of tonalite gneisses whose age was determined in zircons at 3.66 BY by the U/Pb method. The schists are metamorphosed sedimentary rocks, and minerals contained in them might have gotten in them from the matter of the pre-geologic stage of Earth's evolution (see section 5.1). Alarming is only the fact that in the conclusions of the Canadian geologists the kummingtonite is a secondary metamorphic mineral formed

at diaphtoresis (retrograde metamorphism) of magmatic pyroxenes. The ages derived by Sm/Nd method in kummingtonite are most likely bearing an imprint of the secondary recrystallization of sedimentary-volcanogenic sequences which formed later discovered schists. As the age of magmatically encasing tonalites is 3.66 BY and of kummingtonite grains, 4.28 BY, a xenogeneic nature of amphibole (kummingtonite) which got in the schists from rocks of the pre-geologic stage of Earth's evolution, is possible.

As already noted above, colossal efforts of geologists the world over to find more ancient Earth's rocks have so far been unsuccessful. What happened with more ancient rocks? What is an explanation of practically total "memory loss" in Earth's geological chronicle between the moment of its formation approximately $4.6 \cdot 10^9$ years ago and the time about $3.8 \cdot 10^9$ years ago? An explanation of this fact may be only that initially young Earth, within approximately the first 600–800 MY of its life had indeed been a cold and tectonically passive planet. Exactly for this reason in Earth's subsurface at that time differentiation processes leading to melt-out of light crust rocks (basalts, anorthosites or plagio-granites) had not developed and that all carrier minerals have at closer view a xenogeneic nature.

Analyzing causes of primordial tectono-magmatic activation of Earth, V.E. Khain [126, 127] justly noted that an intense granitization on the boundary nearly 4 BYa, possibly, had been stimulated by causes external toward Earth because major tectonic events on a similar scale had been happening at that very time on the Moon. An explanation of this is that exactly at that epoch in Earth, apparently, had for the first time been formed the asthenosphere and decreased tidal Q-quality of Earth that accelerated distancing of the Moon from Earth, as a result of which on Moon have begun dropping still remaining at that time large bodies from the near-Earth planetesimal swarm. The formed asthenosphere, as is known, further on also played an exceptionally important role in the tectonic life of our planet. The very fact of emerging of the first in Earth's history granitization epoch V.E. Khain tied with melting and differentiation of the primordial basalt crust or with its metasomatic reformation at differentiation of the juvenile mantle.

In Chapters 4 and 6 is shown that as such decisive external action exciting tectono-magmatic activity on Earth, which V.E. Khain mentioned, could have served "pumping in" of the tidal energy in the asthenosphere first emerging nearly 4 BYa. Exactly for this reason its formation and rapid expansion with the subsequent reheating of the asthenospheric matter had served the real push for beginning of the evolution of a major energy process on Earth, chemical-density differentiation of Earth's matter. The overheating of emerging asthenosphere must have been accompanied not

only by the separation start of ferruginous melts (i.e., the matter of a future Earth's core) but also by degassing of the mantle with the formation on Earth surface of first, still shallow-water sea basins where most of the tidal energy dissipated. For this reason, it is legitimate to tie the beginning of Earth's core separation process with the moment of a sharp strengthening in the process of the tidal interaction between Earth and Moon and with the beginning of the second stage in an accelerated moving the Moon away from Earth at the Katarchaean/Archaean boundary. Exactly with this stage corresponded the second intense bombardment of the lunar surface by large cosmic bodies – satellites and micro-moons "swept out" at that time by the accelerated Moon moving away from Earth from still preserved at that time near-Earth satellite swarm [19, 112]. The beginning of those catastrophic events on the Moon, based on the determination of lunar basalts absolute age [128–131], belongs to the time approximately 4.0 BYa. For this reason, it would be legitimate for us to believe that Earth's core separation process had begun at approximately the same time, nearly $4.0 \cdot 10^9$ years ago.

After the start of Earth's core separation, when Earth had been already heated to the extent that first melts appeared in its subsurface and emerging convective flows had broken primordial lithospheric shell, first crustal igneous rocks appeared on Earth's surface. At that, the entire primordial lithosphere which in effect had been an analog of primitive but heavier oceanic lithospheric plates, must have been rapidly subsiding in the mantle at the edges of broadening Archaean belt of Earth's tectono-magmatic activity. Total destruction of its traces on the surface of young Earth had been also facilitated by that the primordial lithosphere was composed of rich in iron, therefore quite heavy (nearly 4 g/cm^3) primordial matter, whereas the density of the melted upper mantle after the beginning of zonal differentiation had begun rapidly to decline to 3.2 – 3.3 g/cm^3. At the same time, igneous rocks which presented then extreme differentiates, must have been much lighter, with density nearly 2.9 – 3.0 g/cm^3. That is exactly why they had been preserved to our days having formed on Earth's surface most ancient areas of Earth crust with the age nearly of 3.8 BY. However, after "pumping in" tidal energy in Earth's equatorial belt, for the separation of Earth's crust rock was required some time during which had been occurring melting and differentiation of Earth's matter at the upper mantle level. If we suggest that iron zonal melting process had begun in the upper mantle at depths about 400 km (see Fig. 5.1) and could have spread up and down at a rate nearly 0.2 cm/year, then in approximately 200 MY it must have reached Earth's surface, thus engendering melt-out of the oldest Earth's crust rocks. It follows from this that the separation of Earth's core

had begun approximately 200 MY earlier than the oldest rocks of the continental crust had formed.

Therefore, the multitude of all arguments quoted here, in Chapter 4 and the following Chapter 6, enables us to maintain with high probability that Earth's core separation process had indeed begun nearly 4 BYa, and the tectono-magmatic activity of Earth clearly manifested after this on its surface only 200 MY later (nearly $3.8 \cdot 10^9$ years ago). Exactly at that time had appeared the oldest igneous rocks, had begun forming the hydrosphere and dense atmosphere. To the same period, with a small delay, had most likely belonged also the emergence of the first and most primitive forms of life.

However, beside an indirect connection of the beginning of Earth's core separation process with the formation time of the oldest areas of continental crust, there is also a direct indication of later Earth's core separation recorded by paleomagnetic data. Indeed, magnetic fields of the revolving planets, including Earth, are most likely associated with flows in liquid layers of the core of their electrically conductive "core matter" (see section 5.5). It follows from this that Earth's magnetic field must have appeared only after Earth's core formation process had begun, and the dipole magnetic field of the present-day type had appeared only after its formation. Judging by paleomagnetic data (see Fig. 5.17), the beginning of Earth's core formation had occurred in Early Archaean nearly 4 BYa, whereas its formation had happened only at the end Archaean approximately $2.6 \cdot 10^9$ years ago [124].

Beside the geomagnetic data, there are also weighty lead isotope indications of a late Earth's core separation. Thus, when scientists began

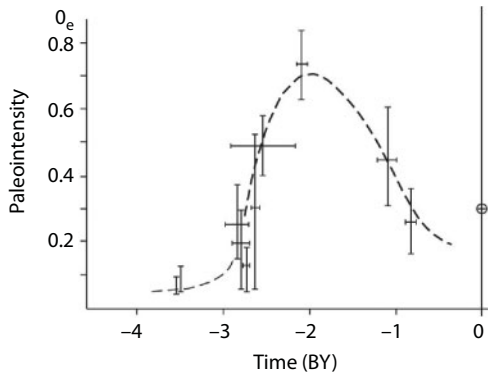

Fig. 5.17 Variations in Earth' magnetic field intemsity based on palromagneric data [124]. Horizontal and vertical lines are variations' confidence intervals; the circle with cross is intensity of the present-day geomagnetic field.

checking lead-isotope age determinations of Earth's lead deposits with standard methodology (based on the assumption of a single and unchangeable mantle-crust reservoir for lead, uranium and thorium under the Holmes-Hautermans [132] model, it turned out that all such determinations resulted in age underestimation of Earth's rocks approximately by 400 – 500 MY [133]. Systematic mismatches of single-stage Pb-dating with ages of the same rocks determined from other isotope or geologic data demanded upgrading the Earth lead evolution model. Considering this, J. Stacey and J. Kramers [134] proposed a two-stage model of the isotope ratios change in leads of different ages. The model parameters have been selected so that it approximated the best way empirical age data from most lead deposits of the world whose age has been reliably determined by other methods (for instance, from rubidium-strontium, potassium-argon or samarium-neodymium ratios and also from geologic data based on uranium-lead ratios in zircons). According to the Stacey-Kramers model, the evolution of lead isotope ratios had begun 4.57 BYa in a closed reservoir but then, approximately 3.7 BYa, U/Pb and Th/Pb isotope ratios had sharply changed as a result of geochemical differentiation of Earth's matter. Notably, in this model the beginning of accumulation of excessive radiogenic lead approximately coincides with the beginning of Earth's crust formation (indeed, caused by geochemical differentiation of Earth matter), therefore, with the beginning of Earth's core formation process.

Under our model, within the age interval 4.6 – 4.0 BY U/Pb and Th/Pb ratios, same as in Stacey-Kramers model have been forming within a closed reservoir of young Earth without leakage of lead. After the moment 4.0 BYa (Stacey-Kramers, 3.7 BYa) the ratio of radiogenic lead to primordial ^{204}Pb in the mantle is already affected by a gradual transition of lead in Earth's core matter. The dominating movement of radioactive elements into the continental crust had been going on under the law similar to the expression for degassing of the mantle (10.1). According to this equation, the transition rate of the mantle matter i^{th} component in Earth's crust $\dot{m}_i$ is proportionate to the content of this component in the mantle $(m_i)_{\text{m}}$, to its mobility parameter χ_i and convective mass exchange rate in the mantle $\dot{z}$

$$\dot{m}_i = -(m_i)_m \cdot \chi_i \cdot \dot{z} \tag{5.51}$$

To simplify further recording of the equations, we will introduce the following symbols:

$$\frac{^{206}Pb}{^{204}Pb} = a; \frac{^{207}Pb}{^{204}Pb} = b; \frac{^{208}Pb}{^{204}Pb} = c \tag{5.52}$$

and will be using the subscript for indicating the age in BY of the moment to which the parameter under consideration belongs. In this case, for the initial (Katarchaean) stage of Earth evolution we may record usual expressions for the correlation of lead isotope ratios with its age according to the single-stage model of Holmes-Hautermans [133]

$$\begin{aligned} a_i &= a_{4,6} + \mu \cdot (e^{\lambda_1 \cdot t_{4,6}} - e^{\lambda_1 \cdot t_i}), \\ b_i &= b_{4,6} + \mu \cdot \frac{(e^{\lambda_2 \cdot t_{4,6}} - e^{\lambda_2 \cdot t_i})}{137,88}, \\ c_i &= c_{4,6} + \omega \cdot (e^{\lambda_3 \cdot t_{4,6}} - e^{\lambda_3 \cdot t_i}), \end{aligned} \tag{5.53}$$

where $\lambda_1 = 0.15513 \cdot 10^{-9}$; $\lambda_2 = 0.98485 \cdot 10^{-9}$ and $\lambda_3 = 0.049475 \cdot 10^{-9}$ years^{-1} are decay constants of ^{238}U, ^{235}U and ^{232}Th; $\mu = \frac{^{238}U}{^{204}Pb}$ and $\omega = \frac{^{232}Th}{^{204}Pb}$, coefficient 137.88 defines isotope ratios ^{238}U/^{235}U in Earth's matter. In the two-stage model of Stacey – Kramers, at the initial stage, before the geochemical differentiation, $\mu_1 = 7.192$ and $\omega_1 = 32.208$. At the second stage, after the beginning of Earth matter differentiation, $\mu_2 = 9.735$ and $\omega_2 = 36.837$.

In our model we changed somewhat the initial values of coefficients $\mu = 7.767$ and $\omega = 33.593$ but introduced in them corrections X_i for the transition of lead in Earth core. These corrections may be determined assuming that the transition of lead into the core is also determined by the equation (5.51), only with a different mobility parameter q. In this case the residual concentrations of lead isotopes in the mantle are determined from equations

$$\begin{aligned} a_i &= a_{4,6} + \mu \cdot \frac{(e^{\lambda_1 \cdot t_{4,6}} - e^{\lambda_1 \cdot t_i})}{X_i}, \\ b_i &= b_{4,6} + \mu \cdot \frac{(e^{\lambda_2 t_{4,6}} - e^{\lambda_2 t_i})}{137,88 \cdot X_i}, \\ c_i &= c_{4,6} + \omega \cdot \frac{(e^{\lambda_3 \cdot t_{4,6}} - e^{\lambda_3 \cdot t_i})}{X_i}, \end{aligned} \tag{5.53'}$$

in which:

$$X_i = 1 - q \cdot \left[1 - \frac{(1 - x_i)}{1 - C_0 \cdot x_i} \right], \tag{5.54}$$

where x is relative mass of Earth's core matter withdrawn from the mantle, and in Proterozoic and Phanerozoic, the mass of the core itself (see equation 5.23). Let us now assume for our model primordial and present-day lead isotopes ratios (i.e. boundary conditions of the problem) same as in the Stacey-Kramers model: $a_{4.6}$ = 9.307; $b_{4.6}$ = 10.294; $c_{4.6}$ = 29.476; $a_{0.0}$ = 18.700; $b_{0.0}$ = 15.628; $c_{0.0}$ = 38.630. In this case, for Archaean and the subsequent epochs equations (5.53') will be defining lead isotope ratios in the mantle. It must be remembered that the mobility coefficient q in equation (5.54) defines already not lead transition into the core but only associated with such transitions changes of the isotope ratios formed during the time of Earth's core formation, i.e., during the last 4 BY. However, the formation rate of radiogenic lead isotopes also turns out different. For instance, over the time of Earth's geologic evolution, i.e., over the same last 4 BY, isotope ratio $^{206}Pb/^{204}Pb$ increased by 42% whereas the isotope ratios $^{207}Pb/^{204}Pb$ and $^{208}Pb/^{204}Pb$, only by 19% and 21%. Appropriately, for different lead isotopes their effective values of mobility coefficients q also turn out to be different changing from 0.184 for isotope ^{206}Pb to 0.074 and 0.087 for isotopes ^{207}Pb and ^{208}Pb.

Now we may estimate correlations of coefficients b_i vs. a_i; and all parameters a_i, b_i and c_i vs. time t_i. The results of such estimates in comparison with the Stacey-Kramers model are shown in Figs. 5.18 and 5.19. As we see, both double-stage models very nicely match each other. But the Stacey-Kramers model was coordinated with different independent age determinations of actual lead deposits, and for this reason, considered here our model also must nicely correspond with the same empirical data. Therefore, it may be maintained that the reviewed here transition model of the lead into Earth core indeed corresponds with the available empirical data on Earth's lead isotopy.

In connection with a gradual lead transition in the growing Earth core, the fraction of its radiogenic isotopes in the total mass of the mantle (and crustal) lead, naturally, should be gradually increasing. It is easy to estimate that if the lead did not transition into Earth core, then under the model by Stacey-Kramers the isotope ratios at present time would be (a_0)'=16.8; (b_0)'=15.04 and (c_0)'=37.71, and under our model, respectively, 17.32; 15.3 and 38.0 instead of customary values for the present-day crustal isotope

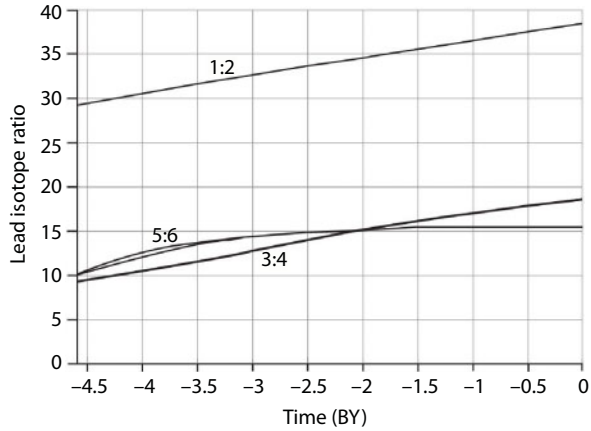

Fig. 5.18 Comparison of evolution of the lead isotope ratios under the double-stage model of Stacey–Kramers coordinated with the empirical data, and under a theoretical model accounting for a partial lead transition into Earth core: 1 and 2. Curves of ratios $^{208}Pb/^{204}Pb$; 3 and 4. $^{206}Pb/^{204}Pb$; 5 and 6. $^{207}Pb/^{204}Pb$ in models under consideration.

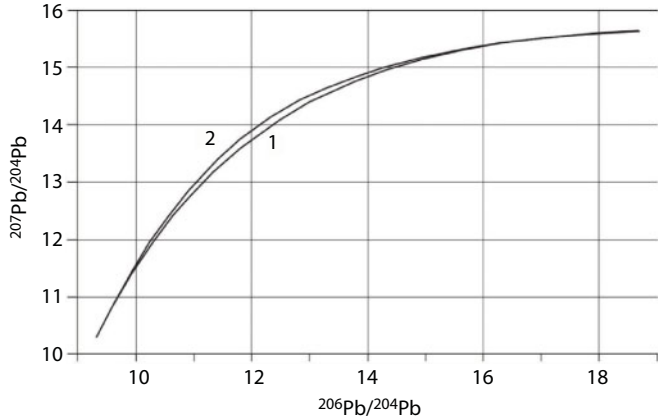

Fig. 5.19 Evolution of lead isotopes: 1. Under the two-stage model by Stacey-Kramers; 2. Under the two-stage model accounting for the transition of some lead into Earth core.

ratios: 18.7; 15.63 and 38.63. Taking into account the included values of lead isotope ratios, it is possible to estimate that into Earth core have already submerged approximately nearly 30% of this metal. Complementing these data with the determinations of radioactive elements' distribution in Earth included in Table 6.1 [17], it turns out possible to determine the mass of lead that had passed during the time of Earth's geologic evolution into its

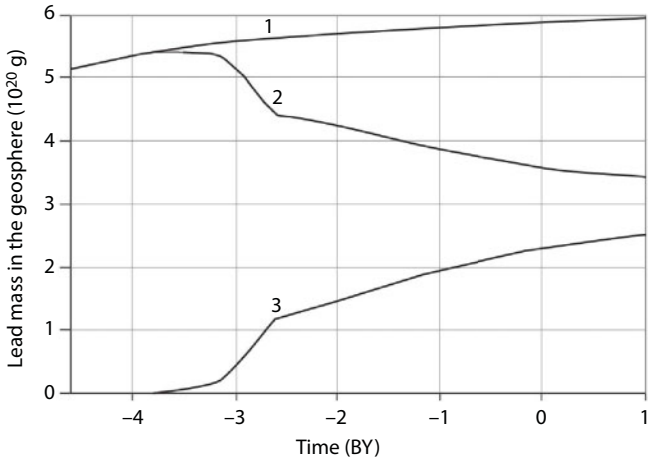

Fig. 5.20 Evolution of lead mass in Earth accounting for the formation of its isotopes at radioactive decay of uranium and thorium: 1. Total lead mass in Earth; 2. Total lead mass in the mantle and continental crust; 3. The mass of lead transited in Earth core.

core: the total is nearly $2.29 \cdot 10^{20}$ g (see Fig. 5.20). This example presents the expected evolution of lead relative concentration in the convecting mantle and estimated by equation (5.33') at $\alpha = 0.15$.

The lead belongs with the dispersed elements, it does not form the free phase in the mantle matter and enters crystalline grids of silicates or sulfides. For this reason, the lead separation from the mantle matter and its transition into Earth's, most likely, occurs under the same barodiffusion mechanism (although with different diffusion coefficients) under which are separated iron oxides forming Earth core, i.e., without melting of the mantle matter [110]. Besides, it must be taken into consideration that in Earth's conditions together with the primordial lead, its radiogenic isotopes pass in the core.

Therefore, the evolution of lead isotope ratios as well as many other geologic data support the model reviewed here of a late and gradual separation of Earth's core. The stratification of the originally uniform and relatively cold Earth into a dense core and residual silicate shell (its mantle) shows that at Earth's planetary evolution stage, an efficient mechanism of chemical-density differentiation of Earth matter had been operating. A detailed study of Earth's energy balance forces a conclusion that today as well this process not only is continuing to operate but also is most powerful among the other endogenic energy processes. Exactly due to the operation of this process, in Earth's mantle emerges and develops an intense convection causing the movement of its matter and drift of the lithospheric plates on Earth's surface.

6

Earth's Energy Balance

The issue of energy sources defining Earth's heat regime and tectonic activity is among the most fundamental in planetary geophysics. It should be resolved only in the closest tie with the present-day data about Earth's composition, structure and evolution.

As has already been numerously noted [15, 18, 19, 91, 112], major processes controlling tectonic activity of Earth may be only those depth energy processes which to the greatest extent lower potential (internal) energy of our planet and of the system Earth–Moon. At that, lowering of the potential energy occurs at the expense of its transit in heat and in kinetic energy of the movement of Earth's mass – convection, movement of lithospheric plates, continental drift, orogeny, etc. In turn, any displacements of Earth masses is also accompanied by the dissipation of the kinetic energy and release of heat which results in partial melting of the matter of upper mantle or continental crust rocks, thereby feeding Earth's magmatism with its energy. However, eventually all this heat is gradually lost with Earth's heat radiation and through Earth surface is dissipated in the outer space. Thus, an important theoretical conclusion: the natural and quantitative measure of Earth's tectonic activity is heat coming from its subsurface, which further on is radiated in the outer space**.** Therefore, if we manage, based on an analysis of Earth's energy balance, to estimate its depth heat loss in past geological epochs, we thereby will determine also the evolution of our planet's tectonic activity.

With the most powerful energy processes developing subsurface of our planet should be included three global processes. First, this is the process of Earth's matter gravity differentiation by density causing Earth stratification into high density iron oxide core, residual silicate mantle, low density aluminum silicate crust and hydrosphere with atmosphere. Second, this is radioactive element's decay resulting in heat energy release. The third notable energy process is the tidal interaction between Earth and Moon. All other endogenous energy sources are either incommensurably lower than the aforementioned or totally reversible due to convective mass exchange within the mantle. For instance, energy transits of mineral associations as affected by the pressure in ascending and descending convective flows are

N. O. Sorokhtin (ed.) The Origins of Natural Diamonds, (103–143) © 2019 Scrivener Publishing LLC

sign-opposite. For this reason, the effect of such reactions on Earth's summary endogenous energy balance may be disregarded although they also may affect the convective flow configuration in the mantle.

6.1 The Accretion and Differentiation Earth's Energy

With the basic Earth's energy sources, the energy it had accumulated already in the process of its formation, may be included part of the energy of gravity accretion of Earth's matter and the compression energy of Earth's subsurface. As previously noted, the Earth formation process by means of accretion from the protoplanetary gas-dust cloud had been evolving over the course of about 100 MY and had ended about 4.6 BYa in the formation of a young and on average compositionally uniform Earth.

At the geologic stage of our planet evolution, starting approximately 4.0 BYa, another powerful process of gravity energy release associated with the density differentiation of Earth's subsurface had begun evolving. This process eventually had resulted in the separation in Earth's center of a high-density iron-oxide core and in the emergence in the residual silicate shell, i.e., in its mantle, of intense convective movements – a direct cause of our planet's tectonic activity.

Accretion of the planet had occurred through the transit of a dispersed protoplanetary matter from no matter how remote orbits in the local space where it had condensed in a single cosmic body. That is why the accretion energy of any planet, including Earth, is equal to the work which must be expended for collecting from the "infinity" dispersed there protoplanetary matter and its concentration in a planet body. Numerically, the planet's accretion energy E_a is equal to its potential (gravity) energy U with the opposite sign (because the potential energy by definition is always negative). However, the potential energy of any system depends on its configuration, in our case on density and matter distribution in the planet subsurface.

$$U = -4\pi\gamma \int_0^R r \cdot m(r) \cdot \rho(r)\, dr \tag{6.1}$$

where

$$m(r) = 4\pi \int_0^r \rho(r) \cdot r^2\, dr \tag{6.1'}$$

here $m(r)$ is the mass of Earth's subsurface contained within a sphere with the radius r; $\rho(r)$ is density of Earth's matter within the radius r; $\gamma = 6.67 \cdot 10^{-8}$ cm^3/g·s^2 is gravity constant; $R = 6.371 \cdot 10^8$ cm is average radius of Earth. The heat store (heat content) of Earth may be determined from a simple equation

$$W = 4\pi \int_0^R \rho(r) \cdot T(r) \cdot c_p(r) \cdot r^2 \, dr \tag{6.2}$$

where the density and temperature distributions in the present-day and young Earth are borrowed from [19] and in Fig. 4.3. Assumed heat capacity distributions in the present-day and young Earth are imaged in Fig. 4.2.

For the determination of accretion energy of young Earth, naturally, is necessary to know the density distribution in its subsurface. Such density distribution in young Earth, as mentioned above, was completed based on average composition of Earth's matter (see Table 4.1) and on the data of silicates and metals impact compression [135, 136]. We will remark in passing that the present-day technique of estimating the rock density at high pressure based on impact compression of rock-forming oxides (not the rocks themselves) reaches 2 – 4%.

Using the density distribution in young Earth, we will find from Eqs. (6.1) and (6.1') that in the process of Earth formation about 4.6 BYa had been released a tremendous amount of accretion energy approximately equal to its primeval potential energy $U_{(4.6)} \approx -23.255\ 10^{38}$ erg. Already in Earth formation process, part of this energy, about $E_{com(4.6)} \approx 3.25 \cdot 10^{38}$ erg, had been spent for Earth subsurface elastic compression and primary heating of Earth whose heat store turned out equal to $W_{(4.6)} \approx 0.838 \cdot 10^{38}$ erg. However, overwhelmingly large fraction of accretion energy, about $E_{T(4.6)} \approx 19.17 \cdot 10^{38}$ erg, turned out lost with heat radiation. This energy would have been quite sufficient for raising the average temperature of our planet to 30,000°C, and as a result Earth matter would have completely evaporated. In actuality, as we know, such intense heating of Earth subsurface did not occur. The reason for this is that the formation of our planet had been occurring during a rather long time interval, on the order of 100 MA, and the energy of planetesimal impacts had been released only in the near-surface layers of growing Earth and for this reason had been rapidly lost with the planet's heat radiation. Moreover, estimates coordinated with geological data, as mentioned above show that the primary heating of Earth at that time in general had not been too significant (see Fig. 4.3).

The accretion energy had been released only at the time of Earth growth. Whereas at the geological stage of its evolution, the major source of endogenous energy had become the gravity differentiation process of Earth matter into a high-density core and a lighter silicate shell – Earth mantle. Numerically, the gravity differentiation energy is equal to the difference between the potential energy of a uniform Earth, which it had possessed directly before beginning of the differentiation process (i.e., about 4 BYa), and the potential energy of the present-day stratified Earth

$$E_g = U_{4,0} - U_{0,0} \tag{6.3}$$

The potential energy of present-day Earth is equal to minus $24.952 \cdot 10^{38}$ erg. Therefore, by definition, the total energy of Earth gravity differentiation is equal to $-23.255 - (-24.952) = 1.698 \cdot 10^{38}$ erg. Part of this energy had been expended for the additional elastic compression of Earth ($0.4355 \cdot 10^{38}$ erg). But most of it, $1.2625 \cdot 10^{38}$ erg, had passed first in the kinetic energy of the mantle matter convective movements and then in heat. Exactly this energy had been the main component of total energy feeding tectonic activity of Earth. The determined value of Earth gravity differentiation energy is huge and substantially exceeds the summary release in its subsurface of all other kinds of energy. Indeed, during this very time, i.e., from Earth formation and to the present, in the mantle had been released about $0.3106 \cdot 10^{38}$ erg of radiogenic and $0.2238 \cdot 10^{38}$ erg of tidal energy. The total energy release in Earth mantle had been $(1.698+0.3106+0.2238-0.4355) \cdot 10^{38} = 1.7969 \cdot 10^{38}$ erg. Taking now into consideration that in Earth's crust during the same time had been released about $0.1223 \cdot 10^{38}$ erg of radiation energy, we find that overall in Earth, in consideration of the elastic energy and its additional compression, had been released about $2.3547 \cdot 10^{38}$ erg.

The present-day heat store of Earth is equal $W_{(0)} \approx 1.592 \cdot 10^{38}$ erg. Therefore, over the time of Earth geological evolution its heat energy had increased by $\Delta W_{(0)} = W_{(0)} - W_{(4.6)} \approx 1.592 \cdot 10^{38} - 0.838 \cdot 10^{38} = 0.754 \cdot 10^{38}$ erg. The energy released in the mantle had been expended for additional heating of Earth $\Delta W_{(0)} \approx 0.754 \cdot 10^{38}$, heat radiation $\Delta Q_{m(0)} \approx 1.077 \cdot 10^{38}$ erg and additional Earth compression during its differentiation $\Delta E_{com(0)} \approx 0.436 \cdot 10^{38}$ erg to the total of: $E_{m(0)} \approx 0.754 \cdot 10^{38} + 1.077 \cdot 10^{38} + 0.436 \cdot 10^{38} = 2.267 \cdot 10^{38}$ erg.

One of most important issues in the determination of major patterns of Earth gravity differentiation and energy release is the determination of the formation timing of Earth core in the central areas of our planet. Many hypotheses of Earth origin and evolution, as already mentioned in the previous chapter, postulate an early separation of Earth core (for instance, [80]). However, we included there a number of geological and geochemical

data convincingly showing that such process had not occurred in Earth before 4.0 BYa. Moreover, analyzing joint evolution of the system Earth – Moon [19], we succeeded in showing that 4.0 BYa the process of Earth core separation had only begun. Most convincing arguments on this issue, as noted above, are paleomagnetic data (see Fig. 5.17) and lead isotopic ratios (see section 5.7 and Figs. 5.18–5.20). In this connection, in the previous chapter and in a publication [19] were used lead isotopic ratios in the lunar and Earth rocks to prove that the Moon had experienced total melting and early differentiation whereas the Earth, on the contrary, had never melted and gone through the early differentiation. Therefore, the evolution of lead isotopic ratios and numerous other geological data also support the model of Earth core gradual separation considered here.

We have already mentioned the absence of proved finds of Earth crust magmatic rocks older than 3.8 – 4.0 BY despite active searches. Should the hypothesis of early Earth differentiation been fair, such ancient and light derivatives of Earth matter, similar to the rocks of Moon light anorthosite crust, would be not only preserved forever but even currently would be dominant in Earth crust, which does not occur in actuality. The conclusion is that this process had begun without total melting of Earth matter approximately 600 MY after the formation of Earth itself. The same is supported by the paleomagnetic data included, for instance, in Fig. 5.17.

For a description of Earth tectonic activity, the definitive value has only the heat portion of Earth's subsurface gravity differentiation energy (without the energy expended for the additional Earth compression). The release of this energy had not remained constant during Earth geologic history but changed with time. At first approximation, the gravity energy generation rate turns out proportionate to the separation rate from Earth matter of the heavy fraction mass, i.e., the "core matter" which had descended later (nearly 2.6 BYa) in Earth core. For more convenient description of this process may be useful the evolution parameter x defined by Eq. (5.23) and quantitatively estimated in section 5.5. The present-day value of the parameter $x = 0.864$. In this case, heat fraction of Earth gravity differentiation energy is

$$E_{gT} \approx 1.458 \cdot 10^{38} \cdot x \text{ erg}, \tag{6.4}$$

Then the rate of this energy release is

$$\dot{E}_{gT} \approx 1.468 \cdot 10^{38} \cdot \dot{x} \text{ erg / year} \tag{6.4'}$$

(for Archaean, the coefficient in front of x and x is equal to $1.25 \cdot 10^{38}$ erg).

Major patterns of Earth tectonic activity will be reviewed in the next chapter (7). Here, based on these patterns, we include only diagrams of gravity differentiation energy rate of Earth (see Fig. 6.1) and a diagram of the gravity energy vs. time (increase in time) (see Fig. 6.2).

The gravity differentiation energy release in Earth had begun rather drastically about four billion years ago and already approximately 3.8 BYa its release in a form of heat had been almost 3 times the current (the current is about $3 \cdot 10^{20}$ erg/s). If, however, we take into consideration that this energy in Early Archaean had been being released only in a relatively narrow equatorial belt (see Fig. 5.3) where in actuality had begun Earth tectonic activity, then per-unit heat flows at that time exceeded by many times their present-day values. In Late Archaean, a substantial increase in the gravity energy release rate had occurred. The reason for this had been a transition of Earth matter differentiation process from the separation of metallic iron to the release of eutectic Fe·FeO melts. This time, gravity energy release rate had exceeded its present-day level approximately by the factor of 14 and about 2.8 BYa had reached approximately $43 \cdot 10^{20}$ erg/s. However, the release rate of gravity energy only at the very end of Archaean had been reached about 2.6 BYa at the time of catastrophic formation in Earth a real high-density core (see section 5.2). At that time, the rate of gravity energy release had reached $70 \cdot 10^{20}$ erg/s. At that, the amplitude of gravity energy

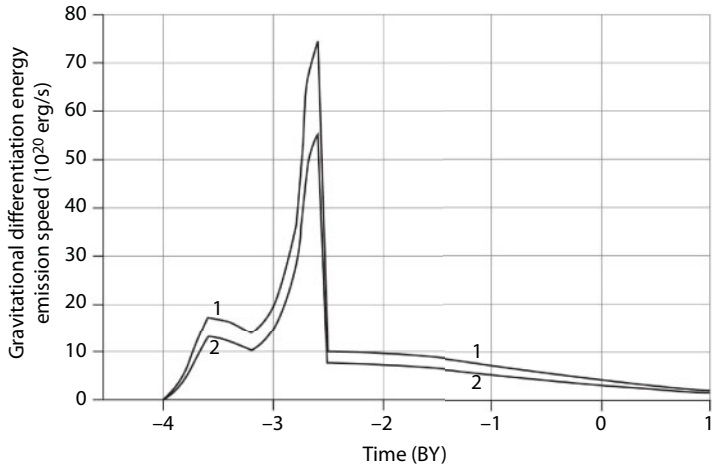

Fig. 6.1 Earth gravity differentiation energy release rate: 1. The entire gravity energy (including the energy of additional elastic Earth compression at Earth core separation); 2. Heat component of the gravity energy. A sharp flash-up in energy release rate at the time of about 2.6 BYa is due to Earth core formation process at this time.

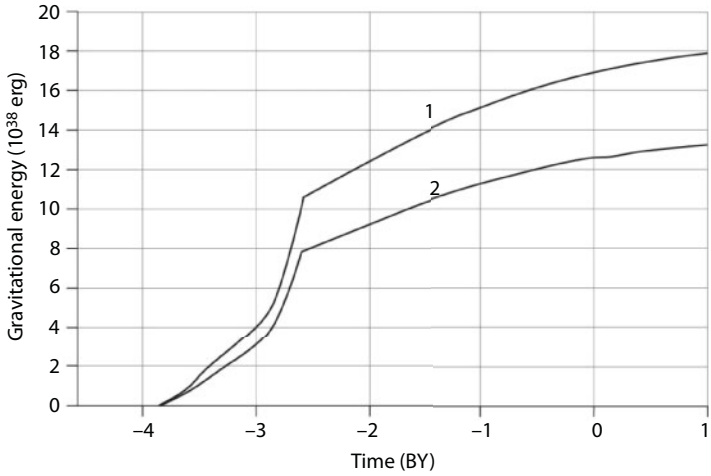

Fig. 6.2 Earth's released energy and gravity differentiation vs. time: 1. Full energy including additional heat release at adiabatic Earth compression; 2. Earth's differentiation kinetic (heat) energy.

heat component had reached almost $53 \cdot 10^{20}$ erg/s, i.e., had exceeded the present-day rate of its release approximately by the factor 18. Conspicuous is the fact that Earth matter gravity differentiation energy release rate maximum had occurred in a unique epoch of Late Archaean Kenoranian diastrophism when, judging by the geological data, Earth tectonic activity indeed had been the greatest.

Obviously, Earth gravity differentiation energy might have been released only after the upper mantle matter melting had begun. As we already mentioned, such an event had happened most likely about 4.0 BYa, when in the equatorial zone of Earth, the upper mantle at depths about 200–400 km, affected by the tidal interactions with Moon, had for the first time formed a molten layer of Earth matter – the asthenosphere. This moment in Earth history had been clearly marked by the start of basalt magmatism on Moon and with some delay, by melting out of Earth crust most ancient rocks. That is why in the described Earth evolution model is assumed that the gravity energy release subsurface our planet had begun approximately 600 MY after its formation (i.e., at the moment of the asthenosphere emergence in the upper mantle) and initially had been associated with the separation of metallic iron melts from Earth matter silicates.

After Earth core separation at the end Archaean, generation rate of the gravity energy heat component in Early Proterozoic had substantially declined to $7 \cdot 10^{20}$ erg/s. The further process of Earth gravity differentiation

had been going on much quieter, gradually declining to the present-day level of the heat energy release approximately equal to $3 \cdot 10^{20}$ erg/s. Fading of this process will continuing in the future.

The gravity energy accumulation had been occurring much quieter. As the diagram in Fig. 6.2 shows, total gravity energy released in Earth until the present is about $16.85 \cdot 10^{37}$ erg. Out of this, $4.36 \cdot 10^{37}$ erg had been expended for additional Earth compression, and the heat component of the gravity differentiation energy converted to the kinetic energy of convective flows equals approximately to $12.63 \cdot 10^{37}$ erg.

Another notice is that the diagrams in Figs. 6.1 and 6.2 are only averaged energy release parameters. In real life, due to the transience of gravity convection in Earth mantle, therefore, of Earth gravity differentiation processes, the energy release diagram of Fig. 6.1 is somewhat more complex, as if the oscillatory process of cycling restructurings corresponding with tectonic cycles is overlaid on it (see Fig. 7.8). However, a possible amplitude of such complicating modulations of the curve, compared with its average background is, most likely, not too great.

6.2 Radioactive Elements and their Decay Energy

The history of establishing the idea of radiogenic heat sources in Earth is very demonstrative and didactic. First, it played an important role in the criticism and departure of geologists from the once very popular contraction hypothesis of Elie de Beaumont that dominated the Earth sciences for almost an entire century and even survived to the 1930s. A reminder: under the concepts of this hypothesis based on the ideas of Kant and Laplace about a "hot" origin of the Solar system planets, our Earth had been formed out of the primordial gaseous cloud and then, after its condensation, out of the overheated liquid-molten magma. While cooling down, Earth had been covered with ever thicker crust and squeezed, reducing in diameter (i.e., it had been contracting). In the conceptions of proponents of this hypothesis, such compression (similar to a desiccating apple) had resulted in the emergence of the wrinkles on the surface of Earth crust which would explain the formation of Earth's folded (mountainous) belts and the emergence of earthquakes. Breakthroughs of under-crustal magma outside has created volcanoes, and its invasions in Earth crust had been forming granite plutons.

However, the discovery by Becquerel in 1896 of the phenomenon of radioactivity and the finding that in Earth crust was concentrated so much radioactive elements that, it would appear, there was more than enough

of them for melting the entire Earth without involving the Kant—Laplace hypothesis, the idea of a primordially hot origin of the planet began falling into oblivion. This discovery and its application to Earth, apparently first spoken by Rayleigh as early as 1906, ultimately knocked the bottom out of the old concepts of Earth origin and the nature of geological processes operating in it. Somewhat later, radiogenic-isotopic methods of determining the age of rocks overturned the old concepts of a relatively young age of Earth. It became clear that the lifespan of our planet amounted not to millions, as the thinking was at the end of the 19th century, but to billions of years. This finally undercut the prestige of the Kant-Laplace cosmogonic hypothesis as from its positions and earlier determined heat flows through Earth's surface, the age of Earth did not exceed 100 MY.

All this actively stimulated the development of new ideas in planetology, geophysics, geology, tectonics and other contiguous areas of Earth sciences. In particular, this happened also with the development of the present-day hypothesis by O.Yu. Schmidt of a "cold" origin of Earth and other Solar system's planets which we have already discussed in Chapter 4. At that, among the causes of its coming into being was undoubtedly the discovery of a new and powerful source of radiogenic energy capable of providing the entire energy needed for Earth's tectonic activity.

All these positive moments of the radiogenic hypothesis undoubtedly played an important role in the progress and evolution of present-day geology. However, it had its own difficulties and even major drawbacks. In particular, when estimating the capability of a radiogenic energy source in Earth, always total ambiguity remained regarding the concentration of radioactive elements in Earth mantle. This problem has been decided according to the geological world view of scientists. But as most geologists and geophysicists totally adhered to the radiogenic hypothesis of heating Earth subsurface, the concentration of radioactive elements in Earth mantle was usually determined on condition of equality of the subsurface generated heat with average heat flow value through Earth surface. However, using such research methodology automatically and completely eliminated from consideration all different possible sources of endogenous energy in Earth, and they could have been enormous and, combined, could have substantially exceed a real contribution from the radiogenic heat in the energy balance of our planet. That is what eventually happened. Detailed studies showed that in the entire Earth lifetime the other energy sources in Earth subsurface had released approximately 4 to 4.5 times more energy than radiogenic heat. Such oblivion of all other and much more powerful sources of endogenous energy undoubtedly played a negative role in the evolution of the present-day geological theory by impeding its evolution by

many years. This is undoubtedly the main pitfall of excessive enthusiasm about the "conspicuity" of the radiogenic hypothesis.

Thus, the weakest spot of the radiogenic hypothesis and at the same time methodologically most difficult issue is the determination of radioactive element contents at mantle depths inaccessible for direct observation. At that, the major attention is paid only to most energy-intensive and long-lived isotopes of radioactive elements with half-life periods commensurate with the age of Earth itself. Such isotopes are uranium isotopes with atomic weights 235 and 238, thorium 232 and potassium 40 (^{235}U, ^{238}U, ^{232}Th and ^{40}K).

At estimating the radioactive elements' contents in Earth usually is taken into consideration that the subject isotopes belong with the lithophilic chemical elements mostly concentrated in light aluminosilicates. This property of radioactive elements at Earth matter differentiation defines the direction of their migration in those places where occur the largest concentrations of aluminosilicates with elevated contents of silica (SiO_2), alumina (Al_2O_3) and alkalis (Li, Na, K, Rb, etc.), i.e., in the continental crust. Much lower contents of these elements must be associated with aluminum-poor but magnesium rich high-density ultramafic mantle rocks, and they should be totally absent from Earth core (a testimony of this is, in particular, the composition of iron meteorites and their sulfide phase, troilite).

The radioactive element concentrations in Earth crust are usually estimated by their contents in most common crust rocks and in the mantle, by analogy with their concentration in chondritic meteorites [137, 447], or in ultramafic rocks [138, 139]. However, this approach does not result in firm solutions. The reason for this is that meteorites taken for a paragon may have formed in portions of the Solar system different from Earth with totally different features of the protoplanetary matter differentiation. Empirically, this was convincingly demonstrated by P. Gast [140]. The second way to determine the mantle radioactivity by direct measurements of radioactive elements' concentrations in Earth ultramafic rocks is also uncertain due to a wide scattering of experimental data, especially for uranium and thorium.

Instability of direct determinations of radioactive element contents in the mantle rocks reaching Earth surface is due to the fact that they practically always experience the strongest influence of metamorphogenic factors significantly distorting the primary composition in the area of rare and trace elements. Usually the "infection" of ultramafic rocks by alkali occurs simultaneously with the processes of their hydration. This concerns even more such trace elements as uranium and thorium. Indeed, as was demonstrated by A.V. Peive [141] and his colleagues [142] and also by R. Coleman [143, 144], J. Dewey, J. Bird [145, 146] and other experts, all ophiolite nappes in whose composition are present the subject mantle origin

ultramafic rocks are in fact fragments of an ancient oceanic crust thrown over the continental margins. The oceanic crust formation usually occurs under a thickness of the oceanic water saturated with alkali and other dissolved elements including potassium, uranium and thorium.

For similar reasons, for the determination of radioactive element contents in the mantle cannot be used data on the composition of mantle rock xenoliths from kimberlite diatremes or from products of volcanic eruptions in island arcs. This is associated with the fact that ultramafic and eclogite xenoliths of diatremes in fact are fragments of the Early Proterozoic oceanic crust pulled in through subduction zones of Svecofennian age deep underneath of lithospheric plates of Archaean continents [55, 58]. Whereas volcanoes of island arcs and active continental margins are functioning only by means of remelting and deep alteration of the oceanic crust subducted underneath them. Great caution should be applied also to the selection for analyses of ultramafic xenoliths from the Hawaiian type oceanic volcanoes as many such samples have a cumulative origin and emerge at existence levels of intermediate magmatic foci. Besides, magmatic melts in such volcanoes are often contaminated with sea water penetrating in hot zones through the lamination of stratovolcanic lava covers.

In such a situation, it is simply impossible to conduct *a determination* of "most likely" radioactive elements' concentrations in Earth only from the empirical data, and it becomes necessary to resort to indirect methods. For instance, it would be possible first to determine the content in Earth of its most common radioactive elements, potassium and then, from ratios K/U and K/Th, to determine the concentrations of uranium and thorium. This path, however, is also insufficiently reliable as the determination of these ratios in mantle rocks results in a very large data scatter.

To reduce the estimate uncertainty in the determination of radioactive element contents in the continental crust the limitation could be utilized imposed on a possible concentration of these elements in the crust by the value of average heat flow through continents $q_{cr} \approx 1.41 \cdot 10^{-6}$ cal/cm^2·[16]. The total heat flow through continents is made of two parts, of the radiogenic and mantle (depth) flows. The mantle flow on Precambrian platforms of the age $t > 1.8 \cdot 10^9$ years (responsible, in terms of the area, for about 75% of all continents, is currently stationary for all practical purposes and may be estimated from a simple equation

$$\overline{q}_m \approx \lambda_l \frac{\Delta T}{\Delta H_l} \tag{6.5}$$

where $\lambda_l \approx 6.21 \cdot 10^{-3}$ cal/cm·s·deg (2.6 wt/m·K at 1,300 K по in a reference book *Physical properties…*", [147]) is heat conductivity of the subcrustal lithosphere; $\Delta T \approx 1{,}100$ °C is temperature gradients in the subcrustal lithosphere; $\Delta H \approx 250 - 40 = 210$ km is the thickness of the subcrustal lithosphere on the ancient platforms. In this case, average depth heat flow through ancient platforms is equal $\overline{q}_m \approx 0.33 \cdot 10^{-6}$ cal / cm^2 · s. On young platforms ($t < 1.8 \cdot 10^9$ years), the mantle heat flow must depend on their age

$$\overline{q}_m \approx 2\lambda_l \frac{\Delta T}{\sqrt{\pi \cdot a \cdot \tau}} \tag{6.6}$$

where $\tau = 1.8 \cdot 10^9$ years is the maximum are of platforms yet unsettled heat regime; $a = 5.7 \cdot 10^{-3}$ см^2/s is coefficient of the lithosphere thermal conductivity. From Eq. (6.6) we find that average depth heat flow through platforms younger than 1.8 BY is equal approximately $0.43 \cdot 10^{-6}$ cal/cm^2·s and average depth heat flow on all continents is equal $0.35 \cdot 10^{-6}$ cal/cm^2·s. In this case, for average radiogenic heat flow remains $(q_R)_{kk} \approx 1.41 \cdot 10^{-6} - 0.35 \cdot 10^{-6} = 1.06 \cdot 10^{-6}$ cal/cm^2·s, and total radiogenic heat flow through the entire continental crust, area $2.04 \cdot 10^{18}$ cm^2, is then equal $\left(\dot{Q}_R\right)_{kk} \approx 0.9 \cdot 10^{20}$ erg/s, which is about 21% of total heat loss by Earth $\dot{Q} \approx 4.3 \cdot 10^{20}$ erg/s. A similar estimate in the publication by J. Sclater with colleagues [148] shows that the decay of radioactive elements in the crust releases somewhat less energy $0.71 \cdot 10^{20}$ erg/s, which is approximately 17% of the total Earth radiation (according to their determinations, $\dot{Q} \approx 4.2 \cdot 10^{20}$ erg/s).

Judging by the publications of S. Taylor [149], P. Gast [140], A.B. Ronov and A.A. Yaroshevsky [73], it is reasonable to accept that average potassium concentration in the continent crust is equal to 2%. We will also accept that $^{40}K/(^{39}K + ^{41}K) = 1.167 \cdot 10^{-4}$ [133]. Then, at the total mass of the crust of $2.25 \cdot 10^{25}$ g, it contains $4.5 \cdot 10^{23}$ g of potassium and $5.24 \cdot 10^{19}$ g of radioactive isotope of ^{40}K.

For conducting energy estimates, we will assume per unit values of the energy release by the radioactive isotopes after D. Turcot and J. Schubert [150]: $^{40}K = 0.279$; $^{238}U = 0.937$; $^{235}U = 5.69$; $^{232}Th = 0.269$ erg/g·s. Then the fraction of the radiogenic heat flow associated with the radioactive potassium isotope decay is $0.146 \cdot 10^{20}$ erg/s. We will now assume that in the continental crust, its average ratio is $Th/U \approx 4$. In this case, from total rate of radiogenic energy generation in the crust ($0.91 \cdot 10^{20}$ erg/s) may be determined the uranium content $U = 0.367 \cdot 10^{20}$ g and the thorium content $Th = 1.52 \cdot 10^{20}$ g. In this case, the ratio $K/U \approx 1.2 \cdot 10^4$ and $K/Th \approx 3.0 \cdot 10^3$.

The determination of radioactive element contents in the mantle is much more difficult and may be done only by indirect methods. One such indirect technique of potassium content determinations in the mantle was proposed independently of one another by P. Gast [140, 151] and P. Hurley [152]. In their thinking, the contents in Earth of radioactive potassium isotope ^{40}K (therefore, also of total potassium) may be determined from the concentration in the atmosphere of a radiogenic argon isotope ^{40}Ar getting in this geosphere in transit of potassium from the mantle in Earth crust. At this, Gast believed that the potassium mobility is the same as rubidium mobility which may be determined from the strontium ratios $^{87}Sr/^{86}Sr$ in the crustal and mantle rocks. Using this method, Gast concluded that the potassium concentration in the mantle is exceptionally low, about $6.5 \cdot 10^{-5}$. In our publications [17–19, 153], this method was somewhat upgraded by the use of Earth's evolution model and comparison of the isotope ratios of radiogenic elements in Earth's and lunar basalts. The determination result was that the most likely potassium concentration in the mantle is approximately two times higher than the one determined by Gast and reaches 0.012%. Therefore, the potassium contents in the present-day mantle are $4.81 \cdot 10^{23}$ g and $5.62 \cdot 10^{19}$ g of the radioactive isotope ^{40}K, and the total in Earth is $9.31 \cdot 10^{23}$ g of potassium and $1.086 \cdot 10^{20}$ g of ^{40}K.

For comparison, after A.P. Vinogradov [154], the mantle rocks contain about 0.03% of potassium; after G. Tilton and G. Read [138], 0.01%; after A. Ringwood [50, 92], 0.03%; after S. Taylor [155], 0.015% and after P. Gast [140], fewer than 0.01%. Later data are also within these limits. So, our determination is close to the average of these values.

The estimate of contents in the mantle of uranium and thorium may be performed only by indirect methods, for instance, based on potassium/uranium and potassium/thorium ratios. Usually, relatively refractory elements (uranium and thorium) concentrate in the continental crust to a noticeably greater extent than alkali metals [140]. This is a reason to expect that in the present-day mantle both the potassium/uranium and potassium/thorium ratios will be higher than in the crust. On the other hand, summary contents in Earth of the uranium and thorium must exceed their mass in the continental crust. Herefrom, the limits of these element contents in Earth are

$$\begin{aligned} 3{,}76 \cdot 10^{19} < U_g < 7{,}76 \cdot 10^{19} \text{ g} \\ 1{,}51 \cdot 10^{20} < Th_g < 3{,}10 \cdot 10^{20} \text{ g} \end{aligned} \tag{6.7}$$

The quoted limits of possible changes in total mass of uranium and thorium in Earth in and of itself are not too great but in real conditions they

must be even narrower. Indeed, the lower limits of inequalities (6.7) are simply unrealistic as a conclusion follows from them about total absence of U and Th in the mantle, which is absurd. The upper limits are also quite unlikely as due to higher mobility of Th and U compared with K, the ratios K/Th and K/U in the mantle must be notably higher and the ratio Th/U, lower than in the crust. Even if we disregard this limitation and use for the determination of radiogenic energy released in Earth the right-hand limits of inequalities (6.7), the total heat generation by these elements (combined with ^{40}K) is approximately $1.89 \cdot 10^{20}$ erg/s. That is substantially lower than the total heat loss by Earth of $\dot{Q} \approx 4.3 \cdot 10^{20}$ erg/s. Unavoidably, an important conclusion follows from this: an additional and quite powerful source of endogenous energy must act in the subsurface of our planet: $E_g > 2{,}41 \cdot 10^{20}$ erg/s. Such a source of energy, as we showed above, may be functioning even currently process of gravity (chemical-density) Earth differentiation resulting in the separation in its central areas of a high-density iron-oxide core and exciting in its mantle of intense convective flows.

In our estimates, expounded in more detail in our publications [17, 19] we assumed for the mantle $K/U = 4.5 \cdot 10^4$ and $K/Th = 1.7 \cdot 10^4$. Then the uranium content in the mantle is equal to $U_m = 1.05 \cdot 10^{19}$ g and thorium $Th_m = 2.89 \cdot 10^{19}$ g. Together with potassium, these elements generate in the mantle approximately $0.34 \cdot 10^{20}$ erg/s of heat energy. Altogether, Earth is currently releasing approximately $1.25 \cdot 10^{20}$ erg/s of radiogenic energy.

Therefore, the estimates set forth above, derived by a methodology independent of a hypothesis of exclusively radiogenic Earth heating, show that the contribution from radioactive elements in Earth's energetics turned out much more moderate than believed earlier (and sometimes even now) but still quite noticeable (see Table 6.1).

The estimates above show that currently the major mass of radioactive elements is concentrated in the continental crust. Earlier, this was clearly demonstrated by P. Gast [140]. However, it should be remembered that it is possible to determine more or less accurately the contents of radioactive elements only in Earth crust whereas the estimate of their concentration in the mantle remains quite approximate. Nevertheless, a major conclusion that in the mantle is dispersed much less radiogenic heat than in Earth's crust may still be considered quite reliable.

Radioactive elements carried out from the mantle into Earth crust are concentrated more in its upper granite layer or in the sedimentary shell. For this reason, the heat they generate is rather rapidly lost through Earth's surface and practically does not participate in the heating of Earth's deep subsurface. Therefore, of special interest in the identification of endogenous energy sources feeding Earth's tectonic activity is only a fraction of

Table 6.1 Contents of radioactive elements in Earth.

	Continental crust, mass $2.25 \cdot 10^{25}$ g		**Mantle, mass $4.07 \cdot 10^{27}$ g**		**Earth as a whole, mass $5.98 \cdot 10^{27}$ g**	
	Content of elements	**Release energy erg/s**	**Content of elements**	**Release energy erg/s**	**Content of elements**	**Release energy erg/s**
^{238}U	$3.64 \cdot 10^{19}$ г	$0.341 \cdot 10^{20}$	$1.047 \cdot 10^{19}$ г	$0.098 \cdot 10^{20}$	$4.69 \cdot 10^{19}$ г	$0.439 \cdot 10^{20}$
^{235}U	$0.026 \cdot 10^{19}$г	$0.015 \cdot 10^{20}$	$0.008 \cdot 10^{19}$г	$0.004 \cdot 10^{20}$	$0.034 \cdot 10^{19}$г	$0.02 \cdot 10^{20}$
^{232}Th	$15.18 \cdot 10^{19}$г	$0.408 \cdot 10^{20}$	$2.89 \cdot 10^{19}$ г	$0.078 \cdot 10^{20}$	$18.07 \cdot 10^{19}$ г	$0.486 \cdot 10^{20}$
^{40}K	$5.24 \cdot 10^{19}$ г	$0.146 \cdot 10^{20}$	$5.62 \cdot 10^{19}$ г	$0.157 \cdot 10^{20}$	$10.86 \cdot 10^{19}$ г	$0.303 \cdot 10^{20}$
K/U	$1.23 \cdot 10^{4}$	–	$4.6 \cdot 10^{4}$	–	$1.98 \cdot 10^{4}$	–
K/Th	$3 \cdot 10^{3}$	–	$1.67 \cdot 10^{4}$	–	$5.16 \cdot 10^{3}$	–
Th/U	4	–	2.74	–	3.83	–
E_g	–	$0.91 \cdot 10^{20}$	–	$0.337 \cdot 10^{20}$	–	$1.248 \cdot 10^{20}$

radiogenic energy released in the mantle. As the estimate above shows, currently this fraction of the radiogenic energy ($0.337 \cdot 10^{20}$ erg/s) is only about 8% of total heat loss of Earth ($4.3 \cdot 10^{20}$ erg/s) or approximately 10% of the depth heat generated in the mantle ($3.39 \cdot 10^{20}$ erg/s). However, during past geological epochs radiogenic energy release in the mantle might have been substantially higher.

For the determination of this fraction of the energy it is necessary to take into consideration that the concentration of radioactive elements in the mantle had been decreasing with time not only due to the decay of these elements but also by means of their dominant transit in the continental crust. For this reason, the content in the mantle of i^{th} radioactive element R_i had been declining over time under a somewhat more complex resulting pattern. As a first approximation, it may be assumed that the transit of radioactive elements in the continental crust is proportionate to the rate of the convective mass exchange in the mantle which, in turn, according to (5.48), is characterized by the rate of heat energy release in the mantle.

For a quantitative estimate of the radioactive elements transit processes from the mantle into the continental crust it is convenient to introduce, by analogy with the evolution parameter of Earth x also tectonic parameter of Earth z (see section 5.4) in Eqs. (5.48) and (5.48'). We will repeat these equations:

$$z = (Q_m - Q_{4,0}) / (Q_{m0} - Q_{4,0}), \tag{6.8}$$

where $Q_{4.0} \approx 1.6 \cdot 10^{37}$ erg is heat loss by Earth by the beginning of its tectonic activity about 4 BYa; $Q_{m0} \approx 10.77 \cdot 10^{37}$ erg is total heat loss by Earth mantle by present. In this case, Earth's tectonic activity will be characterized by the time derivative of this parameter which is

$$\dot{z} = \dot{Q}_m / \dot{Q}_{m0} \tag{6.8'}$$

where $\dot{Q}_m$ is the current value of the mantle heat flow; $\dot{Q}_{m0} = 3.39 \cdot 10^{20}$ erg / s is present-day value of the depth heat flow. From where, the present-day value of parameter $z_o = 1$ and the derivative $\dot{z}_0 = 1$ (for comparison, $x_o = 0.864$ and $x_0 = 0.664 \cdot 10^{-10}$ year^{-1}).

In this case, the transit rate of i^{th} element from the mantle into Earth crust (hydrosphere or atmosphere) is

$$\dot{m}_i = -m_{0i} \cdot \chi_i \cdot \dot{z} \tag{6.9}$$

From where

$$m_i = -m_{0i}(1 - e^{-\chi_i z}) \tag{6.9'}$$

where m_i is mass of i^{th} element that transited from the mantle in a different geosphere; m_{0i} is the initial mass of this element in the mantle; c_i is the i^{th} element mobility parameter. As the parameter z is normalized, all mobility parameters c_i, become nondimensional values and the derivative $\dot{z}$ acquires a dimension of 1/time.

In this case, the contents of i^{th} radioactive element R_i in the mantle is

$$R_i = R_{0i} \cdot e^{-(\chi_i z + \lambda_i t)} \tag{6.10}$$

where λ_i is the decay constant of the element R_i; t is the time from, the moment of Earth formation; i is an index of one of four radioactive elements ^{238}U, ^{235}U, ^{232}Th or ^{40}K. In this case, the rate of the radiogenic energy release $\dot{E}(R)$ in Earth and in the mantle is determined from equations

$$\dot{E}(R_i)_g = \sum_{i=1}^{4} R_{0i}\dot{q}_i \cdot e^{-\lambda_i t} \tag{6.11}$$

$$\dot{E}(R_i)_m = \sum_{i=1}^{4} R_{0i}\dot{q}_i \cdot e^{-(\chi_i z + \lambda_i t)} \tag{6.11'}$$

where $\dot{q}_i$ is heat generation by a unit mass of a radioactive element R_i per unit time (^{238}U = 0.937; ^{235}U = 5.69; ^{232}Th = 0.269; ^{40}K = 0.279 erg/g·s). The total radiogenic energy released in Earth and in the mantle over the time t may be found now by integrating equations (6.11) and (6.11') for all radioactive elements

$$E(R_i)_g = \sum_{i=1}^{4} R_{0i} \frac{\dot{q}_i}{\lambda_i}(1 - e^{-\lambda_i t}) \tag{6.12}$$

$$E(R_i)_m = \sum_{i=1}^{4} R_{0i}\dot{q}_i \int_0^t e^{-(\chi_i z + \lambda_i t)} dt \tag{6.12'}$$

At this, initial masses of the radioactive elements are found from a simple correlation

$$R_{0i} = R_i e^{\lambda_i t_g} \tag{6.13}$$

where R_i is total mass of i^{th} element in the present-day Earth; $t_g = 4.6 \cdot 10^9$ years is the age of Earth.

For the estimates from equations (6.10) – (6.12) it is necessary first to determine the values of mobility parameters c_i from equations (6.9'). Using this equation and the contents of radioactive elements in the mantle and continental crust determined above, the searched for mobility parameters of these elements may be estimated: $\chi_K \approx 0.79$; $c_U \approx 1.8$; $c_{Th} \approx 2.2$. The z function values are assigned by Eq. (6.8) and had been determined in the monograph [18].

Judging by the data in the monograph by G. Fore [133]: $^{40}K/(^{39}K+^{41}K) = 1.167 \cdot 10^{-4}$; $^{238}U/^{235}U = 137.88$; $\lambda_{238} = 1.551 \cdot 10^{-10}$ years^{-1}; $\lambda_{235} = 9.849 \cdot 10^{-10}$ years^{-1}; $\lambda_{232} = 4.948 \cdot 10^{-11}$ years^{-1}; $\lambda_{40} = 5.543 \cdot 10^{-10}$ years^{-1}. Then we find $^{238}U_0 = 9.76 \cdot 10^{19}$ g; $^{235}U_0 = 3.22 \cdot 10^{19}$ g.; $^{232}Th_0 = 2.22 \cdot 10^{20}$ g; $^{40}K_0 = 1.39 \cdot 10^{21}$ g.

Using these and quoted above data about concentrations of the radioactive elements in the continental crust, the evolution of the contents of such elements in Earth, mantle and continental crust (see Figs. 6.3, 6.4 and 6.5) may now be determined.

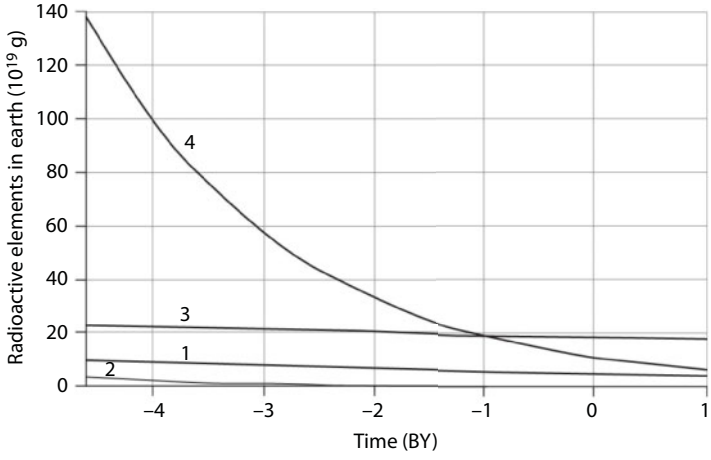

Fig. 6.3 Evolution of radioactive element contents in Earth (element masses are iv 10^{19} g): 1. ^{238}U; 2. ^{235}U; 3. ^{232}Th; 4. ^{40}K.

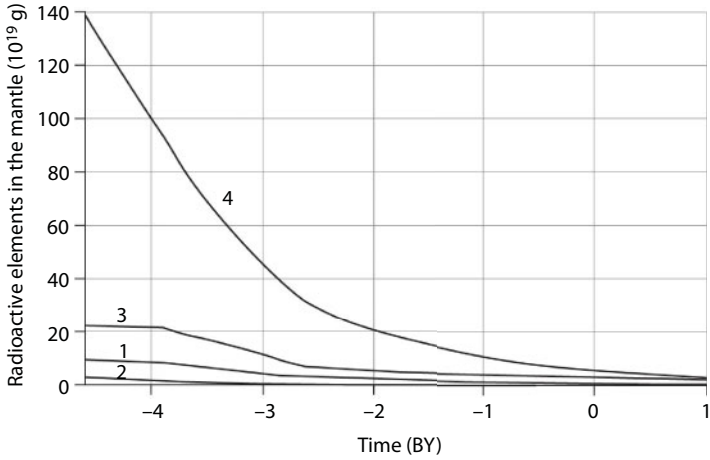

Fig. 6.4 Evolution of radioactive elements content in the mantle (elements' masses in 10^{19} g): 1. ^{238}U; 2. ^{235}U; 3. ^{232}Th; 4. ^{40}K.

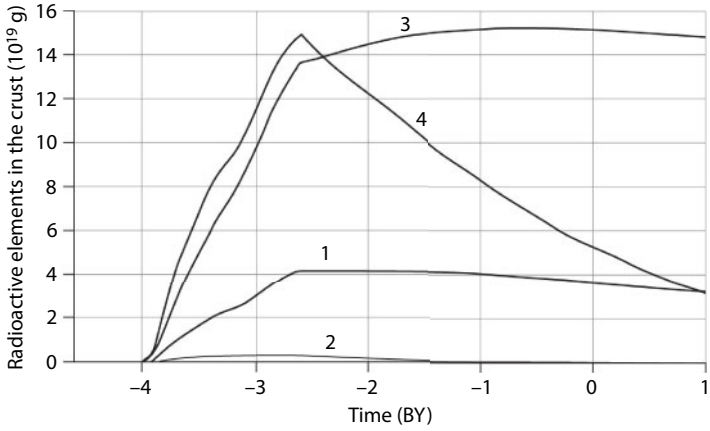

Fig. 6.5 Evolution of radioactive elements' contents in threcontinent crust (element masses in 0^{19} g): 1. ^{238}U; 2. ^{235}U; 3. ^{232}Th; 4. ^{40}K.

The diagrams above show that the contents of radioactive elements in Earth had been gradually declining appropriately to their constant decay values λ_i. The decline rate of these elements in the mantle is somewhat greater as a notable part of them transited in the continental crust. Whereas in the continental crust, when it had been forming in Archaean and in the mantle still had been preserved relatively high concentrations of radioactive elements, their contents in the crust had been growing at the

largest rate and in it intense accumulation of such elements had still been occurring. Due to a sharp decline of Earth's tectonic activity and the rate of continent formation after the formation of Earth core about 2.6 BYa, in Proterozoic and Phanerozoic had been observed some stabilization in ^{238}U and ^{232}Th concentrations, whereas the contents of ^{235}U and ^{40}K, because of the elevated values of their decay constants, after Achaean had been only declining.

Of interest are the diagrams of radioactive elements' relative concentrations in the mantle and Earth shown in Fig. 6.6. As a unit in these diagrams are laid down the concentrations of subject elements in the primordial Earth matter. A sharp distinction between their concentrations in the mantle and Earth is associated with the transit of these elements into the continental crust.

Now substituting parameters of subject radioactive elements and their per unit heat generating capacity in equations (6.11) and (6.11') shown above, we find that in young Earth initially had been being released about $7.18 \cdot 10^{20}$ erg/s of radiogenic energy. By present time its release had declined to $1.25 \cdot 10^{20}$ erg/s. Fig. 6.7 includes evolution diagrams of radiogenic energy release in Earth, mantle and continental crust. These diagrams show that the radiogenic energy release intensity in the mantle notably declined, especially in Archaean, because exactly at this time radioactive elements had been at the greatest rate transited in the continental crust. Currently,

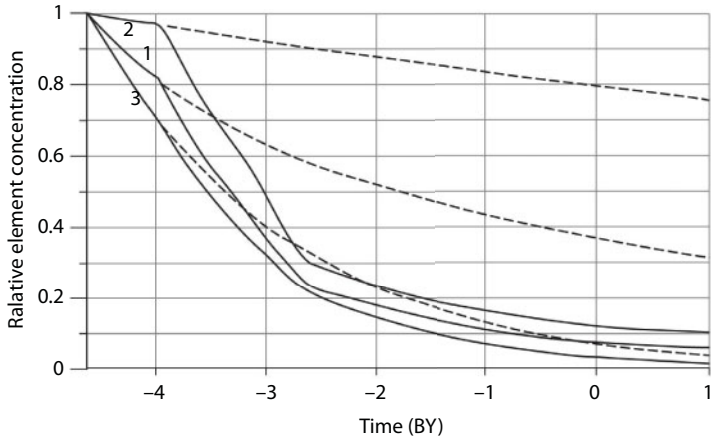

Fig. 6.6 Relative concentrations of radioactive elements in the mantle (solid lines) and in Earth (dashed lines). Concentrations of the subject elements in primordial Earth matter are taken for the unit: 1. Total concentrations of ^{238}U and ^{235}U; 2. Concentration of ^{232}Th; 3. Concentration of ^{40}K.

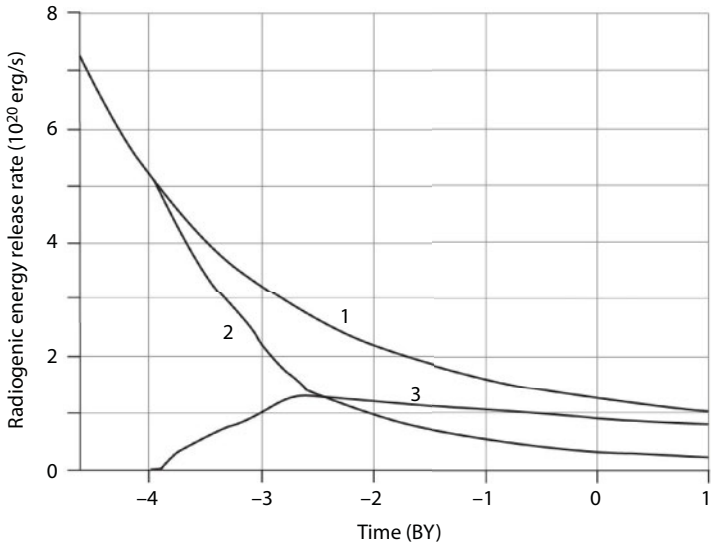

Fig. 6.7 Radiogenic energy release rate (in 10^{20} erg/s units): 1. Earth; 2. Mantle; 3. Continental crust.

the radiogenic energy release in the mantle does not exceed $0.337 \cdot 10^{20}$ erg/s, i.e., just 4.7% of the initial level and 8% of the total heat loss by present-day Earth. Estimated total energy from equations (6.12) and (6.12') testifies to the same. It is estimated that in the entire Earth lifetime in its subsurface had been released about $4.33 \cdot 10^{37}$ erg of radiogenic energy. Out of those in Katarchaean (i.e., in the first 600 MY, before the beginning of Earth's geological evolution) had been released approximately $1.16 \cdot 10^{37}$ erg. During the entire Archaean, 4 to 2.6 BYa, in Earth had been released approximately $1.67 \cdot 10^{37}$ erg of radiogenic energy, of them in the mantle $1.35 \cdot 10^{37}$ erg and in the continental crust $0.32 \cdot 10^{37}$. During the remainder of geological evolution of our planet, i.e., the last 2.6 BY, in Earth mantle had been released only $0.6 \cdot 10^{37}$ erg or approximately 14% of the radiogenic energy (see Fig. 6.8). Overall, in the mantle had been released approximately $3.11 \cdot 10^{37}$ erg and in the continental crust, $1.22 \cdot 10^{37}$ erg of radiogenic energy.

6.3 Earth's Deceleration Tidal Energy

It is known that the total kinetic momentum in a system of a planet with the satellite joined between themselves by gravity-tidal forces remains constant, although at this occur redistributions of the moments between

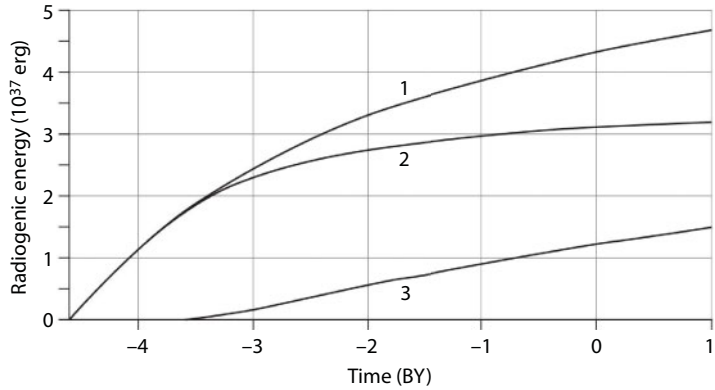

Fig. 6.8 Radiogenic energy release (in 10^{37} erg): 1. Earth; 2. Mantle; 3. Continental crust.

the planet and its satellite. However, such changes emerge only under the influence of a release and dissipation of kinetic energy originally stored in the system [19].

After the Moon formation, Earth's axial revolution angular velocity always exceeded the angular velocity of the Moon axial movement, $\Omega > \omega$. That is why dissipation of the tidal energy in Earth body caused a decline of both Ω and ω. Therefore, under Kepler's third law, the distance L between the Moon and Earth had been continuously increasing [19]. At this, the changes of subject system parameters had substantially depended on rate of tidal energy dissipation $\dot{E}_t$ in Earth's body.

Currently, the major part of the tidal energy is being released in shallow-water seas and much less, in deep oceans and Earth asthenosphere. As determined by G. McDonald [446], the rate of tidal energy release is now equal approximately to $\dot{E}_t \approx 0.25 \cdot 10^{20}$ erg/s, at that about 2/3 of the tidal energy is dissipated in shallow-water seas due to the friction of intense near-bottom tidal currents about the sea floor. According to our estimates, $\dot{E}_t \approx 0.287 \cdot 10^{20}$ erg/s and in the hydrosphere is dissipated about 94% of the tidal energy. As the present-day total heat flow through Earth surface reaches approximately $4.3 \cdot 10^{20}$ erg/s (see section 2.1), it appears that currently the fraction of the tidal energy dissipated in the "solid" Earth does not exceed 0.5 – 1% of total energy generated within its subsurface. This shows that the lunar tides are now playing a very modest role in feeding Earth's tectonic activity, although the tidal deformations themselves of the lithospheric shell (whose amplitude reach a few dozen centimeters) in some cases perhaps can serve as "trigger mechanisms" of earthquakes.

Even less significant for the tectonics of Earth are Solar tides whose effect does not exceed 20% of the lunar tides.

However, whereas the amplitude of the Solar tides had always been insignificant, the action of lunar tides in the past geological epochs had been much greater. The tide theory says that the intensity of such action is inversely proportionate to the sixth power of the distance between the planets [64, 156, 157]. It means that at remote geological times, when the Moon was positioned much closer to Earth, its tidal actions on our planet had been much stronger. Moreover, it may be assumed that at the very early stages of Earth's evolution, when the lunar tide amplitude, according to Eq. (4.3), had reached 1.5 km (almost a mile!), the tidal energy had dominated all other sources of endogenous energy and for this reason had been to a large extent defining the tectonic evolution of Earth.

As is known [64, 157], the heat released by means of tidal deformations is extracted from kinetic energy of Earth's axial revolution. Currently, this energy is relatively low and is equal $(E_\Omega)_{0.0} = 0.214 \cdot 10^{37}$ erg but in the beginning of Earth – Moon system evolution path about $4.6 \cdot 10^9$ years ago it had been much greater and had reached $(E_\Omega)_{4.6} \approx 4.019 \cdot 10^{37}$ erg. Part of this energy released in the process of the deceleration of Earth revolution is expended for increasing the energy of orbital Moon movement and the rest is dissipated in Earth itself. As in the moment of Moon formation its distance from Earth had been $L_{4.6} \approx 1.72 \cdot 10^9$ cm [19], we will find the initial orbital energy of the Moon $(E_\omega)_{4.6} = -8.54 \cdot 10^{36}$ erg (a note: the energy of the Moon orbital movement is a potential energy and for this reason $E_\omega < 0$). Similarly, currently $L_{0.0} = 3.844 \cdot 10^{10}$ cm and $(E_\omega)_{0.0} = -0.38 \cdot 10^{36}$ erg. Therefore, during the lifetime of the system Earth – Moon, i.e., in $4.6 \cdot 10^9$ years, the time kinetic energy of Earth revolution had decreased by $\Delta E_\Omega = 3.81 \cdot 10^{37}$ erg and the kinetic energy of Moon orbital movement, on the contrary, had increased by $\Delta E_\omega \approx 0.81 \cdot 10^{37}$ erg. Therefore, during the same within Earth had dissipated and converted to heat

$$E_t = \Delta E_\Omega - \Delta E_\omega \tag{6.14}$$

Nearly $3 \cdot 10^{37}$ erg of tidal energy.

The rate of the tidal energy release may be determined by differentiating Eq. (6.14). Then:

$$\dot{E}_t = I \cdot \Omega \cdot \dot{\Omega} - \gamma \frac{M \cdot m}{2L^2} \dot{L} \tag{6.15}$$

where I is momentum of Earth inertia; Ω is angular velocity of its own revolution; γ is gravity constant; M and m are respectively masses of Earth and Moon; L is the distance between centers of mass in Earth and Moon.

The evolutionary correlation of products $\dot{\Omega}$ vs. parameters of the system Earth – Moon may be from the equation by N.N. Pariysky [156] by substituting in it tide lag angle with the dissipative function $\sin 2\delta \approx \mathrm{tg}2\delta = Q_{\mu}^{-1}$

$$\dot{\Omega} = -\frac{3}{2} \cdot \frac{k_2 \gamma \cdot m^2 R^5}{I \cdot Q_{\mu} \cdot L^6} \tag{6.16}$$

where k_2 is the second Love number; R is Earth radius; Q_{μ} is mechanical Q-quality factor for Earth.

Now we may determine the sought for correlation of Earth's tidal energy release rate [17]

$$\dot{E}_t = -\frac{3}{2} \cdot \frac{k_2 \cdot \gamma \cdot m^2 R^5}{Q_{\mu} \cdot L^6} (\Omega - \omega) \tag{6.17}$$

In ([19], Chapter 3) is shown that Earth's tidal Q-quality factor Q_{μ} had been substantially changing in time in the entire evolution history of our planet. Based on an analysis of geological material and the condition of age equality of Earth and Moon, in this publication was substantiated an approximal model of Q_{μ} changes with time. Estimated from Eq. (6.17) $Q_{\mu}(t)$, rate of Earth's tidal energy release $\dot{E}_t(t)$ is included in Fig. 6.9 and the value of the tidal energy $E_t(t)$ estimated from Eq. (6.14) is shown in Fig. 6.10.

The tidal energy had been being released in Earth most intensely in the very beginning of its formation, before Moon formation. Those remote times, immediately after having captured the Proto-Moon about 4.65 BYa, the release rate of tidal energy had reached a giant value, approximately $5.2 \cdot 10^{24}$ erg/s, which is almost 13 thousand times greater than the generation rate of endogenous heat energy in present-day Earth. A reminder: the height of the tides in the "solid" Earth then had been close to a mile and the seismic activity might have probably been three orders of the magnitude over its present-day level (see section 4.9).

However, at the moment of the Moon transit on a stationary Roche limit's orbit the tidal energy release, according to Eq. (6.17), had dropped practically to zero because on such Roche limit orbit $\Omega = \omega$. Still, already

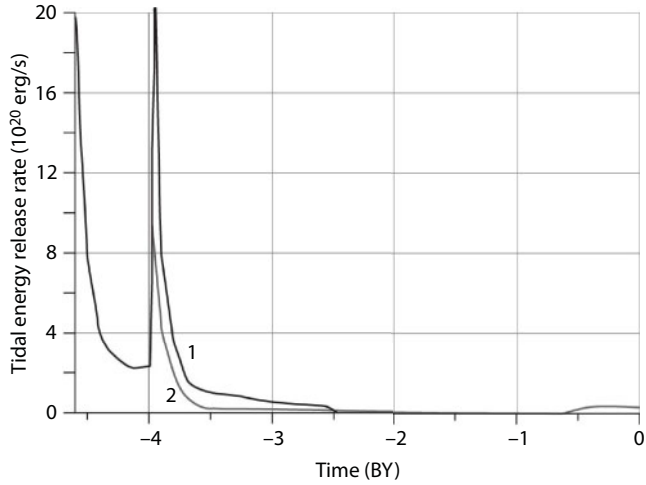

Fig. 6.9 Tidal energy release rate in Earth: 1. Tidal energy release rate in the mantle and hydrosphere; 2 Energy release in the mantle.

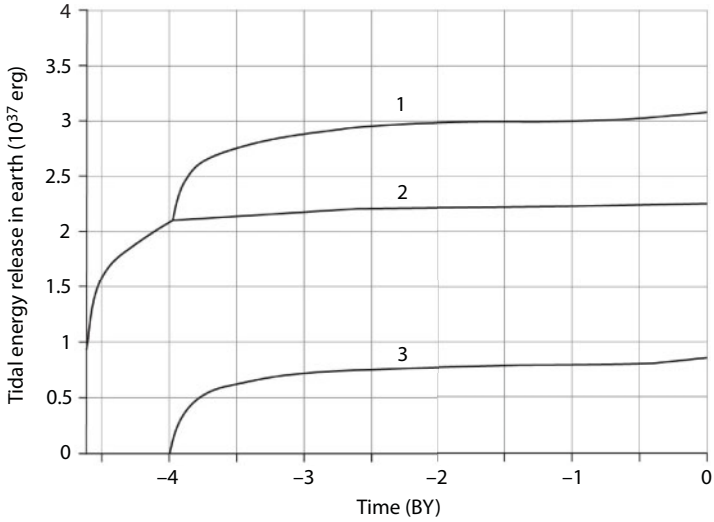

Fig. 6.10 Tidal energy release: 1. In Earth; 2. In the mantle; 3. In hydrosphere.

in 1 MY (million years) the tidal heat generation had again risen approximately to $20 \cdot 10^{20}$ erg/s and after 100 MY more it had again dropped to the level of $7 \cdot 10^{20}$ erg/s only to the double of the present-day total heat generation in Earth. Further on, the tidal energy dissipation had continued to decline smoothly approximately to $2.2 \cdot 10^{20}$ erg/s at the end Katarchaean

about 4 BYa (billion years ago). As already noted in the previous chapter, the young Earth in Katarchaean did not yet have the asthenosphere and hydrosphere. For this reason, the tidal energy then had been distributed in Earth body more uniformly and appropriately to the amplitudes of tidal deformations defined by Eq. (4.3). It follows from this equation that the maximum tidal deformations in Katarchaean had occurred on the equator and in the low latitudes. At latitude of about 55° they had turned to zero and at higher latitudes, the deformations had reversed the sign but had become weaker, and at the poles their variable component had again turned to zero. For this reason, most of the tidal energy in Katarchaean had been released within the equatorial belt and in low latitudes. As a result, within this belt Earth in Katarchaean might have additionally heated by approximately 600°C and on average for its entire mass, by 400°C. However, this additional heating, perhaps, should be relegated to Earth's primordial heating.

The second "heat strike" of the tidal origin had occurred at the boundary Katarchaean/Archaean about 4.0 BYa immediately after the emergence of the asthenosphere on Earth's equator and appearance of first shallow-water sea basins. An explanation of this is in that the tidal deformations of the planet are mostly concentrated in the layers with lowermost values of moduli of rigidity and of viscosity, i.e., in layers most easily subjected to deformation. But after Earth's heating in Katarchaean and beginning of mantle degassing with the formation of the hydrosphere in Early Archean, tidal deformation had begun concentrating mostly in shallow-water seas of the low-altitude equatorial belt ring, partially in asthenosphere of the upper mantle underneath this belt. The tidal energy released at this had resulted in an additional mantle matter overheating and melting and also in an expansion of the asthenospheric layer. This, in turn, had lowered Earth's tidal Q-quality and, therefore, increased even more the rate of tidal energy release. The amplitude of the second tidal energy peak in the very beginning of Archean had been significantly lower than the Early Katarchaean one but still reached $1 \cdot 10^{22}$ erg/s, i.e., had been approximately 20 times greater than the present-day generation rate of endogenous energy in Earth. However, this energy had no longer been being released in the entire Earth's mass but mostly in seas of that time and in the upper mantle asthenospheric layer (see Fig. 5.1). As a result of such avalanche-like release of the tidal energy, the upper mantle matter in the equatorial ring belt had turned out molten, and in it started a new and most powerful energy process with the gravity differentiation of Earth matter.

The tidal energy release in Late Archean and even more so, in Proterozoic had become more quiescent. By that time, real oceans had appeared on Earth and for this reason most tidal energy and had begun dissipating in

Earth's hydrosphere. The rate of the tidal energy release had somewhat increased only in Phanerozoic. However, this time such activation of tidal interaction with Moon had been quite insignificant, associated only with the evolution of Earth hydrosphere, with the first broad oceanic transgressions on the continent and formation of shallow-water epicontinental seas in which most of the tidal energy is expended now.

The change in time of Earth effective Q-quality enables, in principle, an approximate estimate of the energy fraction being currently dissipated in shallow-water seas, oceans and the mantle. The current Earth's tidal Q-quality factor is equal approximately 13. So, it is possible to determine that currently in Earth is dissipated about $0.287 \cdot 10^{20}$ erg/s of the tidal energy. Using now the condition of dissipative function additivity, we find that in the hydrosphere is dissipated about $0.27 \cdot 10^{20}$ erg/s, whereas in the mantle, only $0.018 \cdot 10^{20}$ erg/s. Therefore, currently about 93% of the tidal energy is dispersed in the hydrosphere and only 7% in Earth's mantle. Thus, the tidal energy fraction in Earth endogenous energetics ($3.39 \cdot 10^{20}$ erg/s) is currently approximately 0.5%.

The total tidal origin heat energy released in Katarchaean, in the first 600 MY of Earth existence, had been about $2.1 \cdot 10^{37}$ erg (see Fig. 6.10). In Archean, Proterozoic and Phanerozoic, in Earth had been released approximately $1.2 \cdot 10^{37}$ erg of tidal energy. From this amount, in hydrosphere had been released about $0.96 \cdot 10^{37}$ erg, whereas in Earth mantle, only $0.24 \cdot 10^{37}$ erg. The total tidal energy release in Earth since the moment of Moon formation on the circumterrestrial orbit about 4.6 BYa had been approximately $3.08 \cdot 10^{37}$ erg. Out of this amount, about $2.24 \cdot 10^{37}$ erg belonged with the mantle (see Fig. 6.10).

The quoted estimates show that the tidal energy had been dominant only in Katarchaean and in the very beginning of Archean. The contribution from lunar tides in the total Earth's energetics in Late Archean, Proterozoic and Phanerozoic had remained quite modest and never exceeded 1÷2 %.

6.4 Earth's Heat Losses

As shown in the previous sections, over Earth's lifetime within its subsurface had been released $E_{gT} \approx 16.95 \cdot 10^{37}$ erg energy of Earth matter gravity differentiation, about $3.11 \cdot 10^{37}$ erg of radiogenic energy and approximately $2.24 \cdot 10^{37}$ erg of tidal energy to the total of about $22.3 \cdot 10^{37}$ erg. This amount, $17.94 \cdot 10^{37}$ erg of heat energy and $4.36 \cdot 10^{37}$ erg of additional Earth compression energy released at the formation of Earth's core, would have been quite sufficient for additional heating and overheating of Earth by approximately 4,000 °C.

However, this overheating had not occurred. Which means that most of this heat had been lost by Earth with its heat radiation into the outer space. In the next section this fraction of the radiation heat will be quantitatively determined. Here, we will review only the present-day heat loss by Earth.

At present, over 40 thousand experimental determinations of the heat flow measured in various points of Earth surface have been accumulated. However, to estimate from them average heat loss value and based on that to determine the total heat flow $\dot{Q}$ for the entire Earth would be methodologically wrong.

The present-day heat loss by Earth may be determined only by semi-empirical, semi-theoretical method. The reason for this is in that a significant portion of the depth heat flow from the mantle is carried out by hydrothermal water. Whereas on continents the role of hydrothermal heat release is relatively small, the heat release with ocean water circulating in Earth crust fractures in the oceanic rift zones and on the slopes of mid-oceanic ridges reaches tremendous values. Our estimates are that such heat release may amount to 24% of the total heat loss by Earth [15]; however, so far it was impossible experimentally to measure the total convective heat flow. Exactly for this reason at the determination of the heat loss by Earth, beside empirical data, it is necessary to resort to theoretical estimates of the depth heat flow convective component.

It is known that the oceanic lithospheric plates form by means of cooling and total crystallization of a partially molten upper mantle matter [158, 159]. A continuous movement of the ocean lithospheric plate conveyor from rift zones at the crest of mid-oceanic ridges (where they emerge) to plate subduction zones underneath the island arcs and active continental margins (where they again submerge into the hot mantle) results in that the major heat loss by our planet occurs exactly through oceanic floor [160]. Whereas the role of the continents and continental plates in the process of regulating Earth's heat balance is significantly more modest and mostly passive. The heat flow through the ocean floor exceeds the total heat flow of the continents more than 2.5 times. If, however, to consider that most heat on continents is generated by radioactive elements' decay, the elements concentrated in the upper layers of the continental crust, then it turns out that through the ocean floor is lost more than 90% of endogenous (mantle) heat of Earth [96, 101].

From the crystallization formation model of the oceanic plates it follows that the heat flow through a plate is inversely proportionate to the square root of its age t

$$q = \lambda_l \frac{T_m}{\sqrt{\pi \cdot a \cdot (t_0 + t)}} \tag{6.18}$$

where t_0 is effective formation time of the oceanic crust in a rift zone of a mid-oceanic ridge (usually about 30 – 40 thous. years); λ_l is the lithosphere heat conductivity; a is its heat conductivity; $T_т$ is the upper mantle temperature. Based on the data in the reference book [147], for lithosphere of a lherzolite composition may be assumed: $\lambda_l \approx 6.2 \cdot 10^{-3}$ cal/cm·s·deg and $a \approx 5.7 \cdot 10^{-3}$ cm^2/s. Average temperature next to the focus of molten basalts underneath the rift zones may be assumed equal 1,300–1,400°C [19]. If we now measure the lithospheric plate age in millions of years (1 MY ≈ $3.156 \cdot 10^{13}$ s) and heat flow, in units of 10^{-6} cal/cm^2·s, then

$$q \approx \frac{12}{\sqrt{t_0 + t}} \tag{6.19}$$

A comparison of the theoretical correlation (6.19) with experimental data of the heat flow measurements in the quiescent areas of the ocean floor (outside of transform faults and volcanic areas) included, for instance, in publications [15, 161, 162] shows that the theoretical curve as if averages only maximum value of the measured heat flow (see Fig. 6.11). This is because Earth crust of the mid-oceanic ridges is broken by a dense network of fractures and faults emerging at expansion of lithospheric plates in the process of their moving apart from the rift zones. In these fractures draining the oceanic crust freely circulate the oceanic water carrying from not yet cooled down lithospheric plates a significant part of heat from crust in the oceans. The result is that the total heat flow through the ocean floor is broken into two components: conductive and convective ones. The possibility of convective heat release from mid-oceanic ridges and of existing the hydrothermal sources has been predicted purely theoretically [15, 158, 163], i.e., way before the discovery of the sources themselves on the ocean floor in 1977–78 [164–167]. Also at that time, was for the first time conducted the estimate of the capacity of the process of hydrothermal heat release through the ocean floor which turned out equal approximately to $2.4 \cdot 10^{12}$ cal/s ≈ $1 \cdot 10^{20}$ erg/s. This is about 23% of total Earth heat loss [15].

Similar correlation of heat flow value vs. the oceanic floor age has been done by A.M. Gorodnitsky and O.G. Sorokhtin [161] on significantly broader factual data collected in the Pacific, Atlantic and Indian oceans. Averaging has been conducted based on Eq. 6.19 with somewhat larger values of aproximation coefficients: 13, 14 and 15 (see Fig. 6.12).

The appearance of convective component results in an increase of the oceanic crust heat conductivity λ_{cr}, effective value, therefore in a decrease of temperature gradient in it. Experimental heat flow measurements may be done

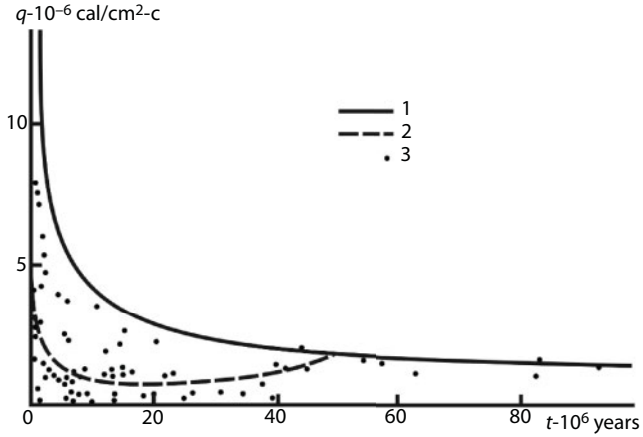

Fig. 6.11 Heat flow through the ocean floor vs. lithospheric plate age [15]: 1. Theoretical curve of total heat flow from Eq. (5.19); 2. Heat flow's conductive component (average value based on experimentyal determinations); 3. Experimental determinations of the heat flow in Southern Atlantic and Pacific.

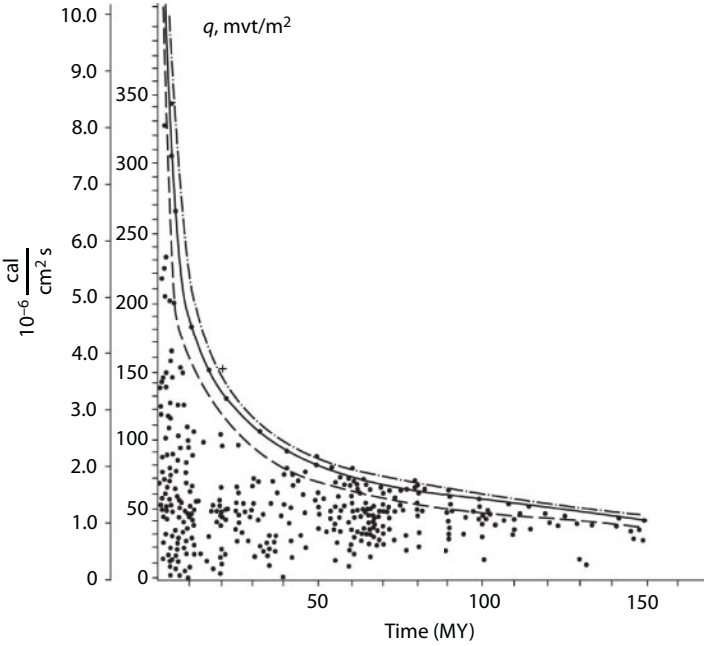

Fig. 6.12 Heat flow through the ocean floor vs. its age. Experimental data on this diagram have been collected in rift zones and quiescent areas of the ocean floor between transform faults and off young intraplate volcanic areas [161].

only in the ocean floor areas sprinkled with deposits. At this, the heat flow value is determined from measured temperature gradient in deposits and heat conductivity coefficient λ_s of the deposits. However, in the presence of convective heat release always $\lambda_{cr} < \lambda_s$, and for this reason heat flows measured by thermal probes under conventional technique in filled with deposits topographic pockets of mid-oceanic ridges are as a rule less than the genuine (total) flows. Only in relatively rare cases (under favorable conditions) in the bottom floor areas with fractures completely filled with deposits measured conductive components correspond with the total heat flow. Exactly for this reason, theoretical curves of the heat flows through the ocean floor are always above "the cloud" of experimental points. In fact, a curve of the total heat flow through mid-oceanic ridges and the ocean floor must average maximum values of experimental flow measurements. Taking into consideration this and the data shown in Fig. 6.12, it is possible to fine-tune Eq. (6.19) defining the correlation of the heat flow through the ocean floor vs. its age:

$$q \approx \frac{13.2}{\sqrt{t_0 + t}}, \tag{6.19'}$$

where q is in 10^{-6} cal·s, t is in MY. In this case, average per unit heat flow through the ocean floor is equal

$$\bar{q} = \frac{26.4}{\sqrt{\tau}}, \tag{6.20}$$

where τ is average lifetime of the oceanic plates.

For the present-day oceanic lithospheric plates, average maximum age apparently is close to $\tau \approx 120$ MY. In this case, average per unit heat flow through the ocean floor is approximately $q_{ок} \approx 2.64 \cdot 10^{-6}$ cal/cm²·s. Assuming total area of the oceanic crust (without the area of shelf and marginal seas with continental or transitional type crust) equal to $3.06 \cdot 10^{18}$ cm², the total heat flow through the oceanic crust is equal $\dot{Q}_{ок} \approx 8.08 \cdot 10^{12}$ cal/s $= 3.09 \cdot 10^{20}$ erg/s.

Judging by the empirical data, average per unit heat flow through continents is approximately equal to $1.42 \cdot 10^{-6}$ cal/cm²·s [148]. Assuming the area of the continental crust equal to $2.04 \cdot 10^{18}$ cm² (this time including the area of shelf and marginal seas with the continental type crust), we find total heat flow through the continental crust $\dot{Q}_{кк} \approx 2.9 \cdot 10^{12}$ cal/s $= 1.21 \cdot 10^{20}$ erg/s. As the radiogenic heat flow of the continents is equal to $0.91 \cdot 10^{20}$ erg/s and

total Earth's heat flow is equal to $4.3 \cdot 10^{20}$, then through the continents is going $1.21 \cdot 10^{20} - 0.91 \cdot 10^{20} = 0.3 \cdot 10^{20}$ erg/s. Coming from the mantle total depth heat flow in this case is equal

$$\dot{Q}_m = 3.09 \cdot 10^{20} + 0.3 \cdot 10^{20} = 3.39 \cdot 10^{20} erg/s \tag{6.21}$$

Therefore, total heat loss by the present-day Earth reaches $\dot{Q}_G \approx 4.3 \cdot 10^{20}$ erg/s. It should be mentioned that similar estimates of total heat loss by Earth have been published earlier: $4.2 \cdot 10^{20}$ erg/s [15, 148] and $4.3 \cdot 10^{20}$ erg/s [161].

6.5 Earth's Energy Balance and Tectonic Activity

Earth's energy balance in an integral form is defined by a simple equation

$$W_T = E_g + E_R + E_t - Q_G \tag{6.22}$$

where W_T is heat store of Earth; E_g is Earth's gravity differentiation energy; E_R is energy of radioactive elements' decay; E_g is tidal energy in "solid" Earth; Q_G is total heat loss through Earth surface. Major components of Eq. (6.22) have been determined above (see Fig. 6.2, 6.8 and 6.10). Original and present-day Earth heat stores may be determined from Eq. (6.2) in which heat capacities for the young and present-day Earth are shown in Fig. 4.2 and density and temperature distributions are borrowed from ([19], sections 2.7 and 2.8). As a result, they turned out equal respectively to $W_{4.6} = 8.38 \cdot 10^{37}$ and $W_{0.0} = 15.915 \cdot 10^{37}$ erg. Analyzing temperature distribution at the end Archean, in consideration of potential energy released at the formation of Earth core $\Delta U_c = -8.08 \cdot 10^{37}$ erg and virial theorem maintaining that half of such energy (with the opposite sign) transits in heat energy, it was possible to determine the value of Earth heat store at the end Archean. It is equal to $W_{2.6} = 14.69 \cdot 10^{37} + 4.04 \cdot 10^{37} = 18.73 \cdot 10^{37}$ erg. It follows from that, that after the Archaean overheating of the mantle and the formation of Earth core, Earth had begun gradually cooling down: its heat store over this time declined by $\Delta W_T = 2.81 \cdot 10^{37}$ erg (see Fig. 6.13, curve 3). Having determined separately and in total the size of major energy sources in Earth ($E_g + E_r + E_t$) and Earth's heat store change character (W_T), we will now determine Earth's heat loss

$$Q_G = E_g + E_R + E_t - W_T \tag{6.22'}$$

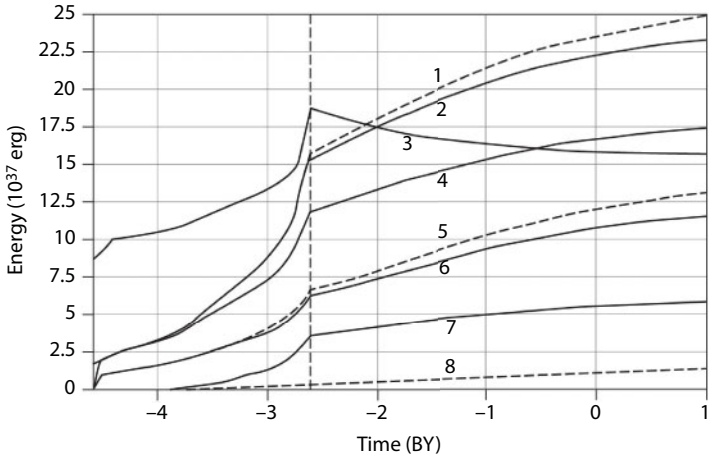

Fig. 6.13 Integral form of Earth's energy balance: 1. Total energy released in Earth after its formation (without the tidal energy dissipated Earth's in seas and oceans) E_G; 2. Energy released in Earth's mantle E_m; 3. Earth's total heat store W; 4. Heat component of energy released in the mantle E_{mI}; 5. Earth's total heat loss Q_G; 6. Heat loss of the mantle caused by depth heat flow, Q_m; 7. Energy of Earth's additional compression associated with the process of Earth's core separation, E_{com}; 8. Radiogenic energy dissipated in Earth's crust, E_{rcr}.

Similarly, may be determined total heat loss by Earth's mantle Q_m, at this, their difference will describe the heat loss by the continental crust Q_{cr} associated with the decay of contained in it radioactive elements $Q_G - Q_m = Q_{cr}$.

Therefore, over Earth's lifetime in its mantle had been released $16.95 \cdot 10^{37}$ erg of Earth's matter gravity differentiation energy (together with energy of Earth's subsurface compression), about $3.11 \cdot 10^{37}$ erg of radiogenic energy and approximately $2.24 \cdot 10^{37}$ erg of tidal energy (not considering its dissipation in Earth's hydrosphere), i.e., in toto about $22.29 \cdot 10^{37}$ erg. This heat would have been sufficient for additional Earth's heating and overheating by almost 4,400 °C. However, this overheating of our planet had not occurred. Therefore, most heat had been lost by Earth with its heat radiation in the outer space. Appropriate estimates including total energy generation in Earth's mantle and also its original and present-day heat stores, allowed to determine that during Earth's lifetime with its heat radiation had been lost about $10.77 \cdot 10^{37}$ erg of depth (mantle) heat. This value represents total energy of tectono-magmatic processes on Earth. For the determination of Earth's total heat loss, to the mantle component is necessary to add radiogenic energy released in continental crust $E_{rcr} \approx 1.22 \cdot 10^{37}$ erg (curve 8 in Fig. 6.13). Including this energy, total heat loss by Earth by present time reaches approximately $10.77 \cdot 10^{37} + 1.22 \cdot 10^{37} = 11.99 \cdot 10^{37}$ erg.

Summing up all data of energy release rates in Earth's subsurface shown in Figs. 6.1, 6.7 and 6.9, we come up with total generation rate of endogenous energy in Earth: curve 4 in Fig. 6.14.

As the diagrams of Fig. 6.14 show, after the formation of the system Earth–Moon, at the highest rate the energy had been generated in Earth subsurface only in Archean, especially in Late Archean when at the peak of endogenous energy release it had approximately 17 times exceeded its present-day level. Starting in Proterozoic, the endogenous energy release rate had been only declining. This decline will continue in the future until in 1.5 – 2 BT Earth again will have turned into a tectonically passive planet. At the earliest stages of Earth's existence (in Katarchaean), its energetics had been clearly dominated by the tidal energy and starting in Archean, only by the gravity energy. The radiogenic energy, especially its part dissipated in the mantle, contrary to a common opinion, practically never had defined the energy regime of Earth evolution. This is a very important conclusion of the theoretical geology which may no longer be disregarded.

Earth's heat balance in the differential form, defining for instance the total rate of heat energy accumulation in the mantle, may now be presented in such format:

$$\dot{E}_{mT} = \dot{E}_{gT} + \dot{E}_R + \dot{E}_t, \tag{6.23}$$

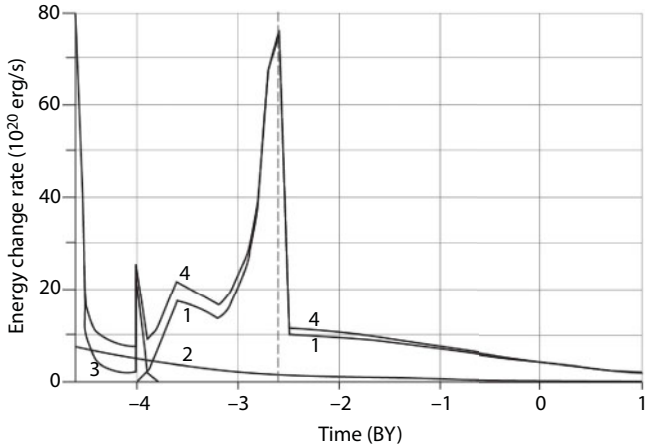

Fig. 6.14 Endogenous energy release rate in Earth's mantle: 1. Energy of Earth's gravity differentiation; 2. Radiogenic energy; 3. Energy of lunar tides; 4. Total energy; the dashed line marks the moment of Earth core formation.

Or coming from Earth's mantle depth heat flow $\dot{Q}_G$

$$\dot{Q}_m = \dot{E}_{mT} - \dot{W}_T = \dot{E}_{mT} - \dot{W}_T \qquad (6.23')$$

where $\dot{E}_{mT}$, $\dot{E}_{gT}$, $\dot{E}_R$ and $\dot{E}_t$ are, respectively: rate of release in the mantle of total heat energy, heat component of the mantle gravity differentiation energy, radiogenic and tidal energy in the mantle; $\dot{Q}_m$ is coming from the mantle depth heat flow (see Fig. 6.15); $\dot{W}_m$ is rate of change in the mantle of heat content (its heat store). The present-day depth heat flow value is easy to determine by subtracting rate of radiogenic energy generation in the continental crust ($0.91 \cdot 10^{20}$ erg/s) from Earth's total heat loss ($4.3 \cdot 10^{20}$ erg/s). Therefore, the present-day depth heat flow is equal to $\dot{Q}_0 = 3.39 \cdot 10^{20}$ erg/s. At this, the change of Earth's heat store $\dot{W}_0$ introduces $\dot{W}_0 = -0.27 \cdot 10^{20}$ erg/s (i.e., $\dot{W}_0 < 0$). This means that after the Archaean overheating of the upper mantle, as already mentioned above, Earth had still been continuing to cool down weakly at a rate about 0.015°C in 1 MY.

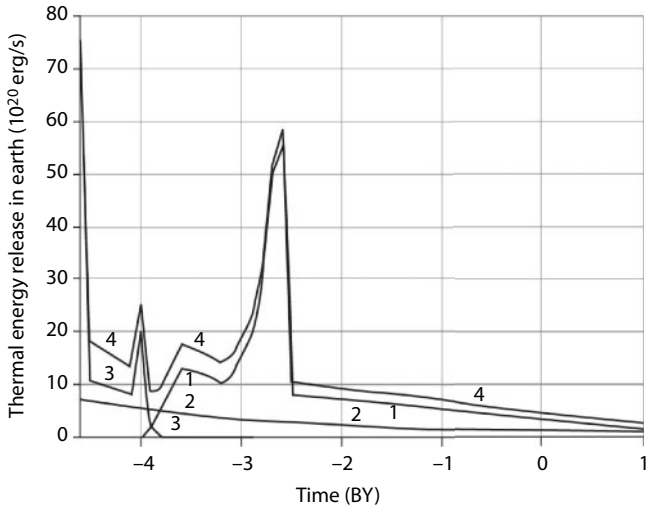

Fig. 6.15 Earth's mantle heat energy release rate: 1. Heat component of Earth gravity differentiation energy and $\dot{E}_{gT}$; 2. Radiogenic energy release $\dot{E}_R$; 3. Tidal energy release $\dot{E}_t$; 4. Total Earth's heat energy generation rate $\dot{Q}_G$.

6.6 Calculation Parameters of Earth's Tectonic Activity

Considering the above estimates, теперь may now determine from Eq. (6.23') Earth's tectonic activity in units of the mantle heat flow $\dot{Q}_m$. At this, it is necessary to remember that the oceanic crust area had been growing first, in connmection with the expansion in Archean of Earth matter differentiation belt from the low altitude to high ones, and at post-Archaean time, on the contrary, had been gradually shrinking by means of growth of the continent areas (see Fig. 8.4). With these patterns in mind, now may be estimated average per unit heat flows penetrating in past geological epochs the oceanic crust, $\overline{q}_{occr}$ and the surface of ancient continents $\overline{q}_{concr}$. In consideration of such corrections was put together a diagram of Earth's relative tectonic activity (see Fig. 6.16).

As this Figure shows, Earth's total tectonic activity (curve 1) is a double-hump curve with a strong domination of the second activity maximum. This maximum in Early Archean describes the process of zonal separation of the metallic iron from the mantle's silicate matrix, whereas a sharp activity increase in Late Archean had been associated with two causes: with the inclusion in the differentiation process (beside the metallic iron) also of its oxides and with the beginning at the end Archean of Earth's core formation process. The manifestation of tectonic activity on Earth surface is described in this Figure also by a double-hump curve 2, but with different parameters. The first maximum of this curve is significantly higher than the

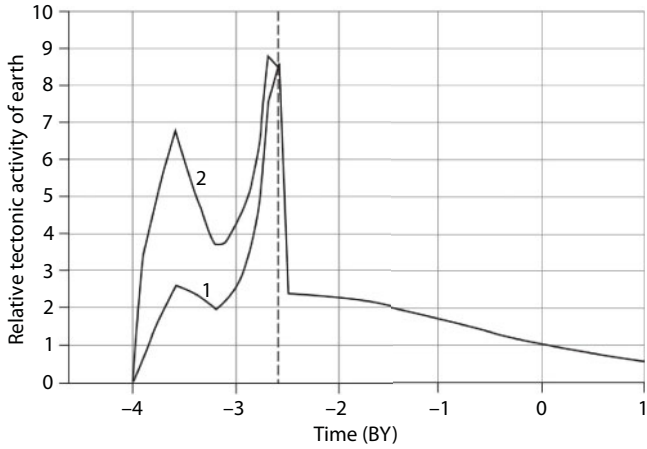

Fig. 6.16 Earth's relative tectonic activity (for unit is taken tectonic activity of present-day Earth): 1. In average for Earth as a whole; 2. Archean tectonic activity in the latitudinal ring belt over Earth's matter differentiation zone.

maximum of curve 1, whereas the second is commensurate with the major maximum of total Earth's tectonic activity. This is not so much because of the intense generation in that time of endogenous energy as because of a relatively small area of its exposures on the surface within a relatively narrow equatorial latitudinal belt of such activity manifestation (see Fig. 5.3). The largest intensity of local tectonic activity in Early Archean, about 3.6 BYa, had exceeded the present-day activity of our planet more than 6.5 times, whereas average Earth's activity at that time had been higher than the present-day one only 2.5 times. The reason for this is that the area of a ring belt of Earth's matter zonal differentiation at that time had been only 0.37% of Earth area at the level of Earth's matter zonal differentiation front. For this reason, local activity on Earth at that time had been approximately 2.5/0.37 = 6.73 times the present-day one. In mid-Archean, average local tectonic activity had turned out to be substantially lower due to a slow-down in the rate of Earth's matter differentiation as described in section 5.3. However, in Late Archean had occurred a new and most intense splash up of tectonic activity exceeding the amplitude of the present-day level almost 8.5 times (see Fig. 6.16). This had been associated with the beginning about 2.8 BYa of Earth's core formation process (see Fig. 5.1). Both splash ups in Earth's tectonic activity in Archean well correlate with the change in the upper mantle surface temperature at the time its overheating episodes in Archean (see Fig. 5.5). In quantitative form, Earth's tectonic activity is convenient to express through total rate of endogenous energy generation in the mantle (see Fig. 6.17).

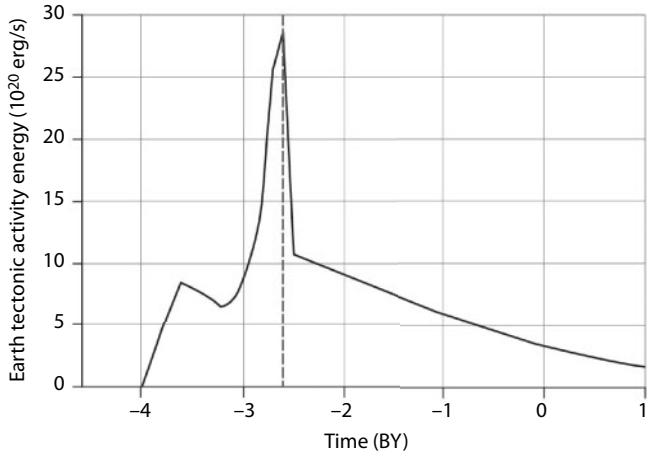

Fig. 6.17 Energy expression of Earth tectonic activity (the dashed line is the moment of Earth's core formation).

The gravity energy generation in Proterozoic and Phanerozoic had been occurring in a significantly more quiescent regime under the mechanism of barodiffusion mantle matter differentiation. For this reason, Earth's tectonic activity had become more quiescent, although it shouldn't be forgotten that the curve shown in Fig. 6.17 reflects its averaged values, with the averaging scale on the order of tectonic cycles' duration (i.e., on the order of hundreds of millions of years). The real correlation of Earth's tectonic activity vs. time is more complex, although the amplitude of tectonic cycles superimposed over averaged fluctuation curve is substantially lower than the major maximum at the time about 2.6 BYa (see Fig. 7.8). In connection with a gradual exhaustion of the "core matter" stores in the mantle, tectonic activity in Proterozoic and Phanerozoic had also gradually faded. This trend will continue in the future.

For the determination of Earth's heat loss in Katarchaean, i.e., before the beginning of its tectonic activity, we assume that in the period of ending the process of Earth's formation and mass torrent on its surface of large planetesimals, any volume of near-surface Earth's layer had been going through a melting stage (by means of planetesimal strikes). In this case

$$\dot{Q} \approx \frac{\lambda \cdot T_m \cdot S_g}{\sqrt{\pi \cdot a(t + t_0)}} \tag{6.24}$$

where $\lambda \approx 5 \cdot 10^{-3}$ cal/cm·s·deg is coefficient of heat conductivity; $T_m \approx$ 1,000°C is Earth's matter melting temperature under pressure $P = 0$; $S_g = 5.1 \cdot 10^{18}$ cm^2 is Earth area; $a \approx 5 \cdot 10^{-3}$ cm^2/s is coefficient of heat conductivity; $t_0 \approx 10^7$ years $\approx 3.16 \cdot 10^{14}$ s is the time of the completing stage of Earth formation, at which time its mass increased from 97 to 100%. Substituting the quoted parameter values in (6.24), remembering that 1 cal $\approx 4.19 \cdot 10^7$ erg, we will find the heat flow in the beginning of Katarchaean $\dot{Q}_{4.6} \approx 4.8 \cdot 10^{20}$ erg/s, whereas by the end of this epoch it declined to $0.6 \cdot 10^{20}$ erg/s. As we see, average heat flow in Katarchaean had been quite modest compared with the value of the present-day flow $\dot{Q}_0 \approx 4.3 \cdot 10^{20}$ erg/s. By integrating Eq. (6.24), we determine that total heat loss by Earth in Katarchaean had been exceptionally low and had not exceeded $0.2 \cdot 10^{37}$ erg. During this very time, Earth's я heat запас store had grown from $8.38 \cdot 10^{37}$ to $9.98 \cdot 10^{37}$ erg, i.e., by $1.6 \cdot 10^{37}$ erg.

Evaluation of energy release rate in Earth (see Fig. 6.14) and of total energy, in consideration of a change in own heat store of Earth (Fig. 6.13), enables estimating heat flows existing in the past $\dot{Q}(t)$. As the first approximation, such flows had been proportionate to the intensity of the

convective mass exchange in the mantle. In a general case, intensity of the convective mass exchange in the mantle or, which is the same, of Earth/s tectonic activity, may be described by Eq. (6.23').

The major part of Earth's total heat loss had always been occurring through the oceanic crust (see section 6.4). Over 4 BY, i.e., in the time of Earth's geologic evolution, through its surface (minus the heat loss in Katarchaean) had been lost approximately $10.77 \cdot 10^{37} - 1.6 \cdot 10^{37}$ erg = $9.17 \cdot 10^{37}$ erg of the heat energy, at this through the oceanic crust, about 90% of this energy.

Under the mechanisms of endogenous energy generation reviewed here and according to major patterns of heat loss by Earth, it was possible to determine the heat flow evolution through the ocean floor. It turned out close to curve 2 in Fig. 6.16. A reminder: an elevated value of heat flows through the ocean floor in Early Archean had been associated with a narrow equatorial belt in which at that time a young oceanic crust had been forming.

6.7 Convecting Mantle Temperature Evolution

As shown above, in Archean a significant overheating of the upper convecting mantle had existed (see Fig. 5.5). The convecting mantle in Early and Middle Archean had covered only a small area of Earth and only in its very end, at the moment of Earth core formation, its mass had grown substantially (see Fig. 5.1). The estimates in section 5.3 enable the determination of the convecting mantle's average temperature evolution in Archean. The result of these estimates is displayed in Fig. 6.18. In Proterozoic and

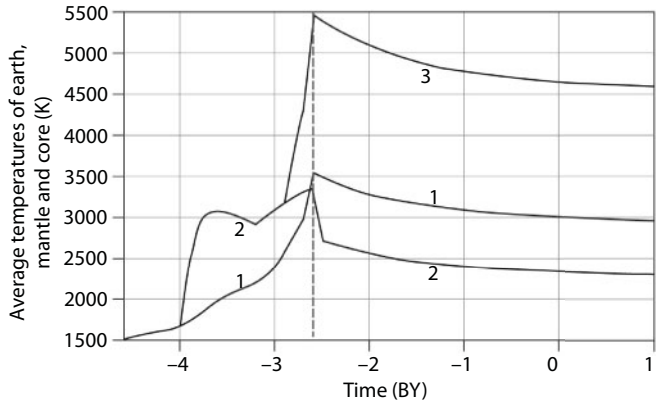

Fig. 6.18 Average temperature of Earth (curve 1), mantle (curve 2) and Earth's core (curve 3).

Phanerozoic, as the energy balance of our planet, included above, shows, Earth had begun gradually cooling down and its heat store W, declining (see Fig. 6.13, curve 3). Knowing the value of Earth's heat store, average temperature of the entire Earth as a whole and of its mantle may be determined. Average Earth's temperature is easy to find from its mass M_G and heat store W_G:

$$T_G = \frac{W_G}{M_G \cdot c_{PG}}, \tag{6.25}$$

Here, the heat store of Earth W_G is set by the curve 3 in Fig. 6.13, the mass of Earth $M_G = 5.9772 \cdot 10^{27}$ g and average heat capacity of Earth is assumed at $0.887 \cdot 10^7$ erg/g.

As a first approximation, heat store of the mantle and Earth core may be determined as follows:

$$W_m = W_G \cdot \frac{M_m}{M_G}, \tag{6.26}$$

$$W_C = W_G \cdot \frac{M_C}{M_G}, \tag{6.26'}$$

where M_m and M_C are, respectively, the mantle and Earth's core masses. Then average temperatures of these geospheres are found through these equations:

$$T_m = \frac{W_G}{M_G \cdot c_{Pm}}, \tag{6.27}$$

$$T_C = \frac{W_G}{M_G \cdot c_{PC}}, \tag{6.27'}$$

where $W_G = 15.915 \cdot 10^{37}$ erg is the present-day Earth's heat store; $C_{PG} \approx 0.89 \cdot 10^7$; $C_{Pm} \approx 1.106 \cdot 10^7$ and $C_{PC} \approx 0.574 \cdot 10^7$ erg/g·deg are assumed values of average heat capacity, respectively, of: Earth as a whole, the mantle and Earth core.

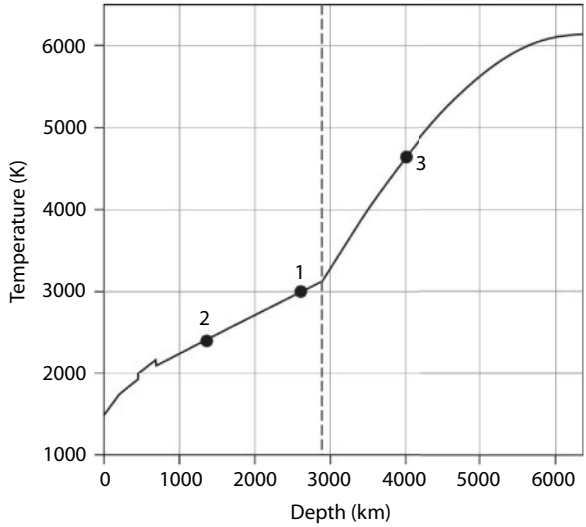

Fig. 6.19 Temperature distribution subsurface of the present-day Earth as compared with average temperature values in Earth geospheres: points 1, 2 and 3 are average temperatures of Earth, mantle and Earth core (the dots are intersections of the determined average temperature levels with the distribution diagram of Earth temperature); the dashed line is the boundary between the mantle and Earth core.

Using equations (6.25), (6.27) and (6.27') and the diagram in Fig. 5.2, may be approximately determined average temperatures of the present-day Earth (≈ 3,000 K), mantle and (≈ 2,400 K) and Earth oro core (≈ 4,600 K). The received estimates, as compared with the temperature distribution in the present-day Earth, are displayed in Fig. 6.19. As may be seen in this Figure, the derived estimates of average temperatures nicely match the temperature distribution in the present-day Earth meaning that the determined above values of Earth's heat content in Fig. 6.13, curve 3 as well as the values of Earth's geospheres heat capacity included in Fig. 5.2 are close to reality.

7

The Nature of Earth's Tectonic Activity

7.1 Possible Causes of Earth's Tectonic Activity

After the collapse of a number of speculative tectonic hypotheses of only historical value now, in the mid-20th century appeared a hypothesis of the continental drift which subsequently transformed the theory of the lithospheric plate tectonics. However, some of the hypotheses preceding the new paradigm, despite clear contradictions with geologic data and the laws of physics, turned out to be extremely resilient with some geologists. This relates in particular to the hypotheses of Earth crust basification, expanding, pulsating and hydride Earth.

Many publications are devoted to criticism of these hypotheses, including some of our publications [17, 168]. For this reason, without breaking stride for their detailed analysis, we will mark only the major drawbacks and often simply the absurdity of such hypotheses. Thus, in any versions of the hypothesis of expanding or "pulsating" Earth are usually not described and even more so not estimated quantitatively physically acceptable mechanisms capable of providing for a change in Earth's volume at a suggested scale. Most of the proposed mechanisms are in a clear contradiction with the laws of modern physics or experimental data about the matter behavior in conditions of high pressure and temperature (for instance, the hypothesis of hydride Earth), and for this reason cannot be perceived today as serious hypotheses. In particular, many options of the hypotheses of expanding Earth using an assumption of changing value of the gravity constant or self-expansion of the mass of celestial bodies (ostensibly by means of "the mass birth from vacuum") do not take into consideration that the same factors must have affected not only Earth but also the Sun. Whereas any noticeable changes in the Sun's definitive parameters unavoidably resulted in catastrophic consequences for it and for Earth, up to the Sun explosion and emergence of a black hole in its place.

Sometimes, for an explanation of Earth's tectonic activity, purely exogenous effects are utilized, for instance, the Solar system revolution around the mass center of the Galaxy or the nonuniformity of Earth's own

N. O. Sorokhtin (ed.) The Origins of Natural Diamonds, (145–174) © 2019 Scrivener Publishing LLC

revolution. If we are speaking about the former mechanism, it is necessary to take into consideration that Earth, the same as other cosmic bodies, is moving in space only on equipotential surface of the gravity field. At this, any deformation actions of such field on Earth may emerge only in a case of existence of noticeable exciting field's gravity gradients generating the tidal forces. The action of the tidal forces on Earth was reviewed in Chapters 4 and 5. It was shown that in the present-day epoch their effect from the Moon (the largest "troublemaker") is negligibly small and does not exceed 1%. Nevertheless, the gradient of the lunar tides' gravity acceleration ($1.7 \cdot 10^{-13} s^{-2}$) is substantially greater than the Solar one ($7.87 \cdot 10^{-14}$) and by many orders of the magnitude exceeds the gradients created by the galactic gravity field ($1.5 \cdot 10^{-30}$ s^{-2}). Therefore, gravity gradient of the lunar tides is approximately 10^{17} times greater than the gradient caused by the galactic gravity field and for this reason any influence of the "galactic year" on Earth's tectonics is out of the question.

The same may be said about the effect of the nonuniformity in Earth's own revolution on its tectonic activity. Total revolution energy of the present-day Earth is known to be approximately $2.1 \cdot 10^{36}$ erg. At Moon formation about 4.6 BYa this energy had reached $3.4 \cdot 10^{37}$ erg. Therefore, during Earth's lifetime, about $3.19 \cdot 10^{37}$ erg of its revolution energy could have been released this way, out of this amount, $2.24 \cdot 10^{37}$ erg in Earth's subsurface, and over the time of Earth's geological evolution (i.e., after 4 BYa), only $0.2 \cdot 10^{37}$ erg. At that, all this energy is accounted for in the shown energy balance in disguise of the tidal interaction energy between Earth and Moon (see Chapter 6). About $0.95 \cdot 10^{37}$ erg more must have been released in the hydrosphere. A reminder: during the same time in Earth had been released about $23.5 \cdot 10^{37}$ erg of the heat energy. As for nonuniformities of its revolution caused both by tectonic movements themselves and by fluctuations of the Solar-Earth ties, the power of such energy actions does not exceed $1.6 \cdot 10^{17}$ erg/s. This is almost by 3.5 orders of the magnitude smaller than the total power of endogenous energy sources feeding Earth's tectonic activity.

A similar critical analysis may be made about some other speculative hypotheses, for instance, a hypothesis of oceanization (basification) of the continental crust which is clearly breaking the Archimedes' law, but perhaps this may be avoided as in recent years such hypotheses on their own had an opportunity to move from the sphere of science to the shelf of history.

Therefore, except for the lunar tides, all other factors of exogenous action on the tectonic activity of Earth may be disregarded. However, lunar tides, as demonstrated in Chapter 4 and sections 6.3 and 6.5, had

made a notable contribution in total heating of Earth only in Katarchaean (i.e., even at a pre-geologic stage of its history) and in Early Archean, and had therewith served as if a trigger mechanism starting the tectonic evolution of Earth. The rest of the time the contribution from lunar tides in the tectonics of our planet had remained quite modest. Therefore, Earth's tectonic activity starting at 3.8 BYa had practically always been fed only by endogenous energy.

Noting a small effect of external factors on the tectonic activity of our planet, at the same time must not be forgotten a great and often definitive effect on the general geological evolution of Earth by the Solar radiation, i.e., an exogenous factor. This is understandable as total flow of the Solar energy on Earth surface (around $1.75 \cdot 10^{24}$ erg/s) is approximately 4,000 times greater than the amount of the depth heat flow of Earth itself ($4.3 \cdot 10^{20}$ erg/s). Whereas the upper Earth's geospheres (its atmosphere, hydrosphere, Earth crust and even the lithosphere) are in a continuous mass exchange with one another. At this, what should be remembered is that these outer geospheres had been formed on Earth only due to the action of endogenous processes of degassing and differentiation of Earth's subsurface. However, the existence on Earth of the liquid water, comfortable climatic conditions, highly organized life forms, evolution of the rock weathering processes, sedimentogenesis, formation of evaporites, combustible and other exogenous commercial minerals, all these are associated exclusively with the Solar radiation.

The evolution of Earth and its tectonic activity must be controlled by the mightiest endogenous processes to the maximum extent lowering its potential (inner) energy. With such processes belong only chemical-density differentiation of Earth matter, decay of radioactive elements and lunar tides. At this, the lunar tides had made their noticeable contribution only at the very beginning stages of Earth's evolution. Whereas at the geological stage, i.e., starting approximately 4.0–3.8 BYa, chemical-density (gravity) differentiation of Earth's matter had become such process. It had resulted in Earth's stratification into a high-density iron-oxide core and a residual silicate mantle.

This process had been accompanied by the emergence in the mantle of large-scale convective movements embracing the entire mantle (upper and lower) with the formation of convection cells whose size is commensurate with the size of the mantle itself. This had been the cause of the very fact of continental drift and the existence of large lithospheric plates whose size often reaches many thousand kilometers. As a result of lithospheric plate motions had emerged a complex of geological processes and phenomena with which we usually associate the concept of Earth tectonic activity

(for instance, earthquakes, volcanic activity, orogeny, etc.). A graphic measure of Earth tectonic activity may serve average rate of relative lithospheric plates displacements (the present-day value of this rate is close to 4.5–5 cm/year). However, as the energy of any dynamic (tectonic) processes in Earth subsurface eventually converts in heat, the most natural measure of Earth tectonic activity remains coming from the mantle depth heat flow whose total value reaches today $3.39 \cdot 10^{20}$ erg/s (see Fig. 6.17).

As discussed in Chapter 6, the most powerful endogenous process controlling Earth's tectonic activity had been the chemical-density differentiation process resulting in the separation in Earth's subsurface depths of the core and generating in the mantle of matter's convective movements. Apparently, for the first time an important role of Earth core formation process in the planet's tectonic activity was emphasized by S. Runcorn [81, 82]. Later, this issue was analyzed in publications by E.V. Artyushkov [169, 170], O.G. Sorokhtin [15, 91, 171], A.S. Monin [172, 173], A.S. Monin and O.G. Sorokhtin [93, 110], O.G. Sorokhtin and S.A. Ushakov [17, 18, 101], [19, 112], etc.

Currently, numerous proofs are available of a direct association between tectonic processes in Earth's lithospheric shell and matter's convective movements in mantle depths. Major of them may be considered: the continental drift, the young age of the ocean floor, the presence of a global rift zone systems in which the mantle matter rises to the surface and forms a young oceanic crust; the existence of global compression belts under which the oceanic crust submerges into the mantle. There are a number of other facts supporting this conclusion; some of them will be reviewed in more detail in subsequent sections of this monograph.

Analyzing the nature of mantle convection, the leading role in the emergence of Earth matter chemical-density differentiation process should be taken into consideration. However, a contribution of convection's heat component in this should not be overlooked. This contribution is defined both by the matter heating due to convective currents' energy dissipation in a viscous mantle matter and by additional heating of the mantle matter due to radioactive elements decay and the action of tidal disturbances. Based on the energy estimates in Chapter 6, the radiogenic heat contribution in energetics of convective mantle matter mass turnover currently does not exceed 10% and the tidal deformations contribution in heating of this matter now is less than 1%. The major portion of endogenous energy feeding Earth's tectonic activity (almost 90%) is drawn from Earth matter differentiation process. Taking into consideration these estimates, the nature of tectonic (or more accurately, tectono-magmatic) activity of Earth has

to be associated not simply with gravity but with gravity-heat convection. Later on, as a synonym of this concept, we will be commonly using the term chemical-density convection, meaning that density nonuniformities in the mantle emerge not only by means of changes in the matter chemical composition but also due to its temperature nonuniformities.

7.2 Possible Mechanisms of Lithospheric Plates Drift

Addressing an issue of lithospheric plate drift, it is necessary to review the motivating forces emerging in the lithospheric shell. Disregarding the side pressure acting from the side of adjacent lithospheric plates, usually two major causes of plate displacing relative one another and the mantle are identified. The first is ocean plate sliding from the slopes of asthenospheric lenses positioned underneath the mid-oceanic ridges (Fig. 7.1). The second cause is associated with the submergence of cold and for this reason heavier oceanic plates in the hot mantle through the subduction zones. At this, the edge of the lithosphere descending into the mantle as if is pulling behind it the major portion which is still "afloat", i.e., on the plate's surface (see Fig. 7.3).

A lithospheric plate sliding off the asthenospheric uplift, if it bumps into another plate, causes compression of its peripheral areas. The compression pressure Δp created by the oceanic plate by means of its sliding from the asthenospheric lens underneath a mid-oceanic ridge in the absence of friction at plate's base may be estimated from the condition of hydrostatic equilibrium. In this case, compression pressure acting on the base of the plate has the age of about 100 MY and reaches approximately 800 kg/cm^2, i.e., it is close to the limit of long-term shear strength of rocks (on the order of 1 t/cm^2). Apparently, exactly this kind of overpressure is

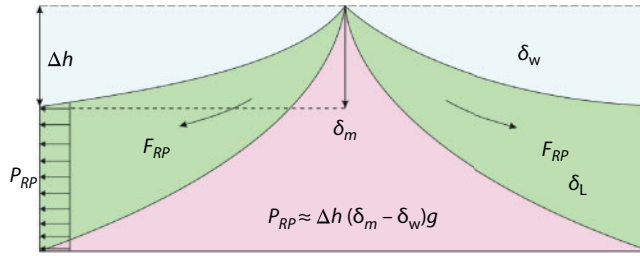

Fig. 7.1 The mechanism of oceanic lithospheric plate sliding from a mantle upheaval area underneath a mid-oceanic ridge.

an explanation of a somewhat elevated seismicity on passive oceanic and continental margins of the Atlantic type. This phenomenon must be especially manifested in the Northern Atlantic as in this region, under pressure of positioned there ascending mantle flow, oceanic lithospheric plates turned out raised relative their average level by 2–2.5 km, and in the area of Iceland, the ocean floor even rises above the ocean level. This creates an additional pressure of approximately 200–400 kg/cm^2, and therefore total pressure on the flanks of the mid-oceanic ridge in the Northern Atlantic may exceed long-term strength of the lithospheric rocks. Perhaps, such was the nature of the renowned Lisbon earthquakes of 1531 and 1755 in Portugal as well as some earthquakes in the USA east coast and the west coast of Northern Europe.

The forces pulling the oceanic lithospheric plates into the mantle may be substantial. However, for their estimation it is necessary to consider the existence in the mantle of phase transitions in mineral associations of its matter (Fig. 7.2). The restructuring itself of such associations in the mantle emerges under the influence of high pressure and temperature. This occurs with pressure increase due to restructuring of minerals' crystalline grids into their ever higher density modifications (phase transits). Such mantle mineral associations crystalline structures' restructuring may occur with the release or absorption of heat. In the former case, transition is exothermal and the position of its boundary on the pressure – temperature plain has a positive gradient (phase transits I, II, IV and V in Fig. 7.2). In the latter case, transition is endothermal and is characterized by a negative pressure gradient (phase transits III and VI in the same Figure).

When the oceanic lithosphere submerges through a subduction zone to some depth h in the mantle (Fig. 7.3), then due to a greater density of its cold rocks, compared with the density of the mantle hot matter, a negative Archimedes force emerges. In the absence of friction, this pulling-in force generates tensile stress in the near-surface cross-section of the lithosphere. For instance, if a submerging plate descended to the depth of 400 km, tensile stress in the oceanic lithosphere in front of a deep-water trough, depending on the submergence angle, may reach 2–3 kbar. At this, it must be remembered that the submergence of a cold oceanic lithosphere to the level of exothermal phase transition in hot mantle results in an increase of its density above this boundary, thereby strengthening the pull-in effect of plate in the mantle. For instance, at reaching the IVth phase boundary at depth 400 km corresponding with transition of olivine affected by high pressure from rhomboid syngony (α-phase) in the spinel modification (β-phase), mineral density increases approximately by 8% [178]. The temperature of the descending plate at the depth of the subject phase transition

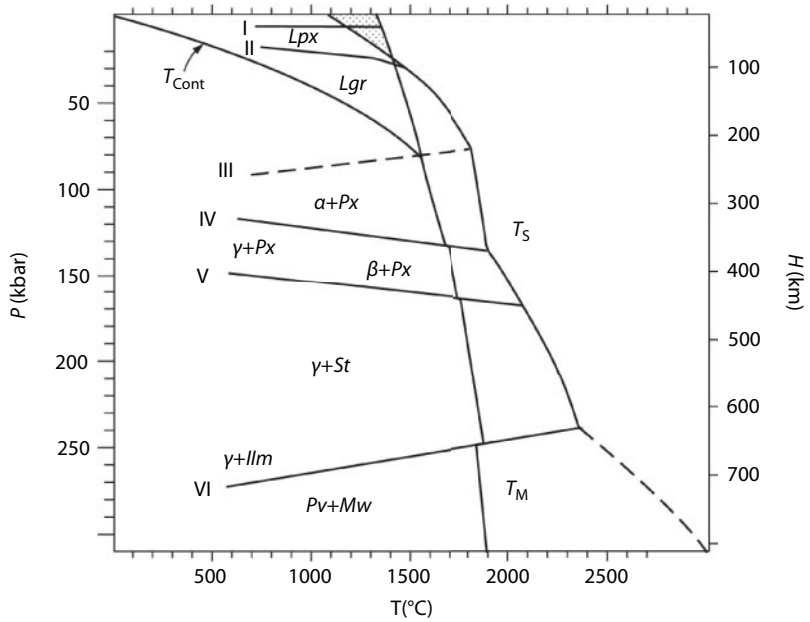

Fig. 7.2 Temperature distribution in the mantle and phase transitions in the mantle matter: T_S is temperature of the mantle matter solidus (using the data by [40] and [174]); T_M is adiabatic temperature in the convecting mantle [175, 176]; T_{Cont} is continental geotherm under Archaean cratons [55]; speckles indicate the existence area of juvenile melts in the mantle. Exothermal phase transits: I. Transition from plagioclase to pyroxene lherzolites (*Lpx*); II. Transition from pyroxene to garnet lherzolites (*Lgr*); IV. Transition of olivines (α) to spinel structures (γ and β); V. Transition of the silica in the stishovite structure (*St*) and of pyroxenes in ilmenite structure (*Ilm*). Endothermal transitions: III. Suggested by us transition of a rigid poly-crystalline matter to its plastic state [112]; VI. Transition of pyroxenes to perovskite (*Pv*) and magnesio-wustite (*Mw*) structure. Phase transits I and II, after the data by Green and Ringwood [174], generalized transits IV, V and VI, after the data by Kuskov and Fabrichnaya [177].

(about 400 km) is still approximately 500°C lower than the temperature of the enclosing hot mantle. For this reason, the subject exothermal polymorph transition of its matter and its appropriate "heaving" of the plate occurs at a somewhat shallower depth, approximately by 380 km (see Fig. 7.2). Therefore, at these depths emerges additional pressure of about 0.2 kbar strengthening even more the pulling of a lithospheric plate into the mantle. A similar picture will emerge also at the intersection by the descending plate to phase boundary V at a depth about 470 km – the pressure will increase by approximately the same amount. Contrary to this, at intersection by the plate of endothermal boundary at the depth of 670 km

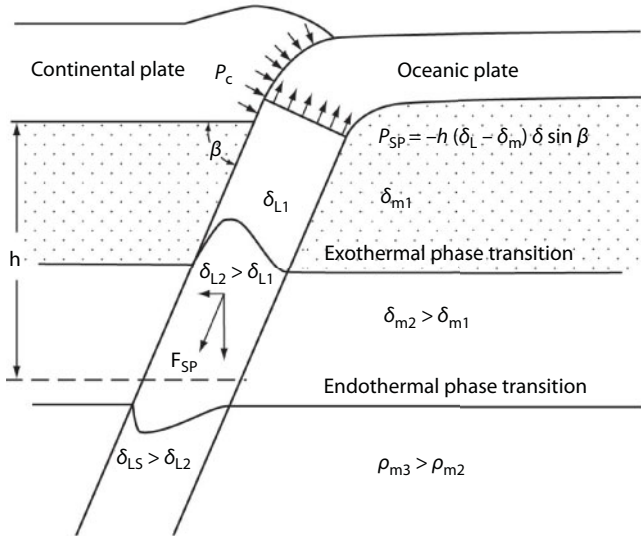

Fig. 7.3 Pulling the ocean lithosphere in the mantle through a subduction zone.

its pressure will decline by about 0.2 kbar. However, at this level the total excess pressure of the submerging plate is equal approximately 5–6 kbar. For this reason, the phase transition endothermal boundary at depth 670 km, although weakening pulling in gravity force of the oceanic lithosphere plate, does not prevent at all its submersion to depths of the lower mantle. Similarly, exothermal phase transitions in the mantle matter will only facilitate the rise of hotter ascending flows in the mantle and endothermal, on the contrary, will somewhat slow down the movement but still not prevent this rise.

For the estimation of existing temperature gradient between the ascending convective flow and its descending branch, we will assume that under equilibrium conditions, excess of the heat energy of the ascending flow is almost totally radiated by oceanic plates over the time of their movement from rift zones to the subduction zone, i.e., during their average lifetime $\tau \approx 120$ MY or $3.8 \cdot 10^{15}$ s. The present-day average depth (mantle) heat flow through the ocean floor, as determined in Chapter 6 (see Eq. 6.20), is equal to $\dot{Q}_m \approx 3.09 \cdot 10^{20}$ erg/s. Then average temperature difference between the ascending convective flow and the enclosing mantle, in first approximation, may be recorded as

$$\Delta T \approx \frac{\dot{Q}_m \cdot \tau_m}{Mm \cdot (c_p)_m}, \tag{7.1}$$

where $M_m \approx 4 \cdot 10^{27}$ g is mass of the present-day mantle and $(c_p)_m \approx 1.11 \cdot 10^7$ erg/g·deg is average value of convecting mantle heat capacity. Then $\Delta T \approx 26$ °C.

In this case, for instance, the transition boundary of olivine from α-phase in β-phase (boundary IV in Fig. 7.2) will drop in the ascending flow approximately by 2.5 km and in it will emerge an additional lifting force with excess pressure of about 0.07 kbar. Whereas the endothermic phase transition boundary at a depth 670 km (boundary VI in Fig. 7.2), on the contrary, will rise approximately by the same amount and will result in the appearance of a locking stress about 0.1 kbar, and it will cause some slowdown of the ascending flow.

The difference in average mantle matter densities on the core surface before and after its differentiation (i.e., in the descending and ascending flows) is equal approximately to 0.01–0.02 g/cm^3. As the ascending flows in the mantle formed on the surface of Earth core at a depth of about 3,000 km, their lifting force is equal approximately to 1.0–1.5 kbar and much exceeds "blocking" action of the endothermal boundary at a depth 670 km. For this reason, the global convection remains the same for the upper and lower mantle although the "blocking" action of such boundary may somewhat complicate the convection and result in a pulsating regime of its functioning.

The quoted estimates of pulling-in forces of the oceanic plates in the mantle enabled D. Forsyth and S. Uyeda [179] to suggest that observed lithospheric plate movement rates depend on the length of their begridding subduction zones. Indeed, the "fast" plates are purely oceanic plates with relatively small thickness of the lithosphere (60 to 80 km) and relatively extensive subduction zones. However, under this very classification in the category of "slow" get almost all continental plates of a large thickness (up to 250 km) and the oceanic plates attached to them. An interesting pattern was discovered. The greater the continental plate area, the smaller the rate of its drift. Perhaps this indicates that thick continental plates, like icebergs stranded in low water are submerged by their roots in the mantle mesosphere, and the horizontal components of the mantle currents in them either too small or their influences over the large area of big continents become mutually balanced.

In essence, this is the same heat convection whose motivating beginning is not heating from the bottom of a colder matter but on the contrary, cooling down from the top of a hotter matter. Therefore, we can see that the gravity instability of oceanic lithospheric plates on its own may engender their movement and create convection in the mantle. In this connection, the observations of movements of cooled lava crusts on the surface

of a molten lave lake in the volcano Kilauea in Hawaii conducted more than 110 years ago by Reverend O. Fisher [180] should be recalled. He observed as these cooled down and heavier crusts, like micro-lithospheric plates were sliding down from the surface of liquid-molten lava forming on the one hand structures reminding mid-oceanic ridges and on the other a semblance of subduction zones in which cooled down crusts again submerge in incandescent magma and totally remelt in it. At that time, based on these observations, O. Fisher made far-reaching conclusions about the nature of tectonic activity on Earth [180]. Approximately 80 years later, at the same volcano, these well-forgotten observations were repeated by V. Duffield [181] who compared the movements of lava crusts with displacements of the lithospheric plates already discovered by that time.

In real conditions, however, both the compression pressure of the oceanic lithosphere on its contact with the passive continental margins and the expansion stresses in the lithosphere in front of plate subduction zones may substantially differ from simple estimates. This is associated with the interaction of moving plates with other plates and with the mantle matter. As in this movement model the plates move relative to the immobile mantle, viscous friction with mantle matter forces must emerge and retroacting their displacements tangential slowing down stresses. The plate friction in subduction zones and active portions of transform faults also make their slowing down contribution. As a result, the plate movement is significantly slowed down and the appropriate forces of pulling plates in the mantle are substantially weakened. As the viscous slowdown forces increase with increasing rate of the plate motion, their movement occurs approximately at a constant rate about a few centimeters a year. In a stationary case, the sum of moving forces is completely balanced with the sum of slowing down forces.

Let us now review a nature of the mantle convection in a broader sense and attempt to answer a question whether the described "self-motion" mechanisms of the oceanic lithospheric plates are sufficient for its agitation. What must be taken into consideration at that is that the reviewed mechanism of lithospheric plate motion might have operated only starting at 2.6 BYa as in Archean, as now on Venus, most likely there had been no subduction zones and their functions had accomplished huddling zones and zones of thrusting basalt slabs over the continental shield edges (see Fig. 8.5).

For a long-term operation of the described convection, as for any heat convection, it is necessary to supply the mantle matter with the energy no smaller than heat loss associated with it. At this, convective mass exchange intensity in the mantle, and in our case also average movement

rates of the oceanic plates (i.e., average intensity of Earth's tectonic activity) would apparently be totally controlled by the rate of the energy generation in the mantle. This is associated with a strong exponential correlation between the mantle matter viscosity and the temperature, and therefore, heat energy supply to it. At declining the heat generation rate in the mantle, its viscosity would increase and would appropriately grow the viscous friction forces hampering the plate movement under mechanisms here considered. And on the contrary, with a supply of additional energy the mantle viscosity and friction forces would decrease and the plate "self-movement" rate would decrease.

For this reason, a tectonic activity of Earth within the framework of the model of plate movement considered here is rigidly defined by heat energy generation in depths of the mantle, i.e., actually defined by the heat flow through the ocean floor. The major contribution to the depth heat flow, as shown above, is from the major energy process on Earth, the process of chemical-density differentiation of Earth matter into high-density oxide-iron core and a residual silicate mantle. Therefore, the heat convection in the mantle must also be mostly defined by the same process, i.e., by Earth core formation.

Currently, through the subduction zones in the mantle submerge approximately $7.6 \cdot 10^{17}$ g/year or about 230 km^3/year of cooled down rocks of the oceanic lithospheric plates. Analysis of Earth heat loss (see section 6.4) indicate that major loss of endogenous energy occurs, and had always been occurring, through the ocean crust in the process of oceanic plate formation. It was mentioned in Chapter 6 that Earth tectonic evolution under the laws of lithospheric plate tectonics had begun only in Early Proterozoic after the separation of Earth core about 2.6 BYa. In Archean, no mechanism of lithospheric plate "self-movement" might have existed. Overall, in recent 2.6 BY this way had been lost about $4.5 \cdot 10^{37}$ erg of heat energy (see section 6.5). Presently, through the ocean floor is lost about $3.09 \cdot 10^{20}$ erg/s (see section 6.4), or approximately $9.7 \cdot 10^{27}$ erg/year of heat energy. However, as the oceanic lithospheric plates form by means of crystallization and cooling down of the mantle matter, and their average temperature at that changes little, then as a first approximation it may be assumed that the heat losses quoted here are proportionate to the masses of the lithospheric plates formed and submerged in the mantle. As average oceanic lithospheric plate density approximately equals to 3.3 g/cm^3, it may be estimated that over the recent 2.6 BY in the mantle had submerged about $1.25 \cdot 10^{12}$ km^3, or $4.13 \cdot 10^{27}$ g of the lithospheric plate mass. The mass of the present-day convecting mantle (without the continental crust) is approximately equal to $4 \cdot 10^{27}$ g. Therefore, over the time of operation of

the lithospheric plate tectonic mechanism, i.e., during the recent 2.6 BY, in Earth mantle had submerged the lithospheric plate mass somewhat greater than the mass of the mantle itself. Which makes it obvious that the entire mantle matter at least once had totally run through in the convective cycle over the time of its existence.

7.3 The Nature of the Mantle Convection

Let us now review physical mechanisms capable of exciting convective movements in the mantle matter. Most geophysicists traditionally prefer to consider only the heat convection in a classical arrangement, believing that it is fed by energy decay of radioactive elements or gradual cooling of Earth. Among the early researches should be mentioned once again the publication by O. Fisher [180] who believed that the subcrustal matter convection was caused by general cooling down of Earth, and the publication by A. Holmes [182] who noted that the heat convection causing continental drift might be begotten by the decay of radioactive elements.

A strict solution of the problem of finding the field of the rates of convective movements in Earth matter mantle may be obtained only through the joint solution of the Navier Stokes equation for a compressible liquid with the continuity equations. The boundary conditions for the problem solution must be structure of the real mantle in consideration of existing in it phase transitions and equation of state for the mantle matter. However, it is very difficult to comply with all these requirements, besides, not all patterns of Earth structure and evolution have been known with sufficient accuracy. For this reason, in earlier attempts undertaken to study the process of heat convection, starting with the fundamental study by S. Chandrasekhar [183] and other scientists, this was not always taken into account, and the solutions found of the problem, might be mathematically correct but for very coarse Earth models. For instance, for models in which the mantle viscosity was either assumed constant or a monotonous function of the radius, or it was believed that the mantle was "heated" from the bottom by Earth core. Results have been cumbersome solutions only schematically reflecting the nature of real phenomena.

In the application to mechanisms of lithospheric plate tectonics, the heat convection in the mantle was studied by F. Richter [184], D. McKenzie, F. Richter [185], D. Turcot, J. Schubert [150], etc. In Russia, Earth mantle heat convection was studied most exhaustively, using more realistic distribution of physical parameters in the mantle, by V.P. Trubitsin and V.V. Rykov [186].

We may remember that for the determination of the heat convection emergence condition in the mantle is usually used Rayleigh criterion (number)

$$R_a = \frac{\rho \cdot H^3 \cdot \Delta T \cdot \alpha \cdot g}{a \cdot \eta} \tag{7.2}$$

where ρ is density in the mantle; H is the mantle layer thickness; ΔT is super-adiabatic temperature difference in the layer; α is coefficient of the mantle matter volume expansion; g is gravity acceleration; a is coefficient of heat conductivity; η is mantle matter dynamic viscosity. For a spherical layer, the critical value of Rayleigh number, after which the heat convection may begin, is equal approximately 2,000 [187]. According to currently accepted views, the value of Earth mantle effective viscosity is between 10^{23} and 10^{24} poise [188]. For this reason, for the emergence in it of a flow-through heat convection is sufficient a temperature super-adiabatic difference of only 1–10 °C. At this, however, only a very flabby convection emerges but real value of super-adiabatic temperature difference quite may reach a few dozen degrees.

This shows that in Earth mantle indeed may be excited the heat convection in its classic understanding, i.e., by means of heating the mantle matter from below or within the volume of mantle itself as long as there are sufficient heat sources in it. Radioactive elements are too little for this. The only adequate energy source is the process of the mantle matter chemical-density differentiation. However, this process, besides simple heat generation in the mantle, results also in the emergence in its body of density variations substantially exceeding the effects of matter expansion at heating. For this reason, for approaching real conditions, it is necessary to contemplate not simply heat or purely chemical-density convection in the mantle but their combination in the form of the chemical-heat-density convection.

The condition of chemical-density convection emergence may be found by analogy with the Rayleigh criterion for heat convection. Indeed, the nondimensional Rayleigh's criterion (7.2) is the ratio of two factors, the lifting force emerging at heat expansion of the matter and the factor hampering the convection and describing the dissipation rate of the medium's heat nonuniformities and its resistance to shear deformations. Taking the said into account, the product $\Delta T \cdot \alpha$ in equation (7.2) may be substituted with its equivalent ratio $\delta\rho/\rho$, where $\delta\rho$ should be understood as average density difference emerging by means of a change in the mantle matter's chemical composition after

its differentiation on the core surface (see Eq. 5.21). Using then the analogy between the diffusion equation defining the dissipation rate of chemical composition variations with the equation of heat conductivity defining the rate of temperature levelling in the medium, the heat conductivity coefficient a in the denominator of Eq. (7.2) may be replaced with the diffusion coefficient D. In this case, the modified Rayleigh number defining the evolution of chemical-density convection in the mantle [15], may be written as

$$R_g = \frac{\delta\rho \cdot H^3 \cdot g}{D \cdot \eta} \tag{7.2'}$$

In (7.2'), most indefinite is the value of the product $D{\cdot}\eta$. For its estimation we will use the theory of diffusion viscosity [109] under which the viscosity of a crystalline matter and the diffusion coefficient are connected between themselves as follows

$$\eta = A \cdot \frac{k \cdot T}{D \cdot d}\left(\frac{l}{d}\right)^2 \tag{7.3}$$

where A is a constant equal approximately to 0.03; $k = 1.38{\cdot}10^{-16}$ erg/deg is Boltzmann constant; $T \approx 2{,}500$ K is average temperature of the mantle; $l \approx 0.1$ cm is the characteristic size of the mantle matter crystals; $d \approx 3{\cdot}10^{-8}$ cm is a characteristic parameter of the crystalline grid cell in the mantle matter. In this case, $\eta{\cdot}D \approx 3.8{\cdot}10^6$ dyne.

Substituting now in (7.2') the determined value of $\eta{\cdot}D$ product and assuming, according to definition (5.21), $\eta\rho \approx 0.02$ g/cm^3; g $\approx 10^3$ cm/s^2; H $\approx 2.9{\cdot}10^8$ cm, we will find that a new modified Rayleigh's number is about $1.3{\cdot}10^{20}$ which is by many orders of the magnitude exceeds its critical value $2{\cdot}10^3$ and may be assumed infinite.

So large value of the modified Rayleigh's number does not mean at all a greater intensity of the convection. It simply shows that the intensity of chemical-density convection is completely defined only by the medium viscosity η and density differences $\eta\rho$ in its chemical variations and absolutely does not depend on the process of these density variations' diffusion. Therefore, with the assigned η and $\eta\rho$, the chemical-density convection in the mantle will always be developing at maximum possible rate. But it may be very flabby if the mantle viscosity η is sufficiently high and density differences $\eta\rho$ generated on the core surface, are insignificant. In real conditions,

however, the rate of chemical-density convection must self-regulate so that the rate of Earth's potential energy decline was maximum and the energy expense for overcoming the viscous friction forces in the medium, minimal. At this, the convection structure is organized so that these two conditions are most satisfied.

If the mantle matter responds to slow deformations similar to viscous liquid, then an important conclusion follows from the above reasoning. Practically any change in the mantle matter chemical composition emerging at its differentiation on the core surface, unavoidably results in the appearance in the mantle of convective movements. Even if caused by such differentiation density fluctuations only slightly disturb the gravity stability of the mantle. At this, the evolution rate of such process will be totally defined by density differences in the mantle matter and its viscosity.

The intensity of the mantle convective stirring was changing with time according to a formula close to the tectono-magmatic activity of Earth (see Fig. 6.17). However, on Earth's surface in Archean are identified two periods of elevated convective and tectono-magmatic activity (see Fig. 6.16, curve 2). The first of them coincides with the beginning of Archean and is associated with the zonal differentiation of metallic iron. Convective mass exchange at that time had mostly the heat nature and embraced only the upper mantle and its transitional layer at the depth of 400 to 800 km in a narrow tropic belt of Earth. At this, the Early Archaean splash up in Earth of the convective (and tectonic) activity turned out relatively high not so much due to a high rate of Earth matter gravity differentiation as due to a fact that this entire energy dissipated at that time in small volumes of convecting mantle under the narrow tropic belt. That is why convective structures existing in Early Archean must have been small, with the size not exceeding a few hundred or a few thousand kilometers. A simple estimate shows that in Early Archean might have existed at least 80 convective strictures on the perimeter of Earth. If, however, we take into consideration that the first embryos of future continental shields formed above the descending flows of such convective structures, a conclusion may be that in Early Archean formed at least 80/2 = 40 such continental nuclei (see Figs. 7.4 and 9.1). Interestingly, approximately the same number of primary, most ancient (composed by gray gneisses, trondhjemites and tonalites) nuclei of the continental crust (37) are identified based on geological data [99, 189].

With the submergence of the differentiation front, the convective cell size must have been increasing, the individual nuclei must have merged with one another and their number must have shrunk. For this reason, by the end of Early Archean the number of such continental embryos should not already have exceeded 20 (Fig. 7.4).

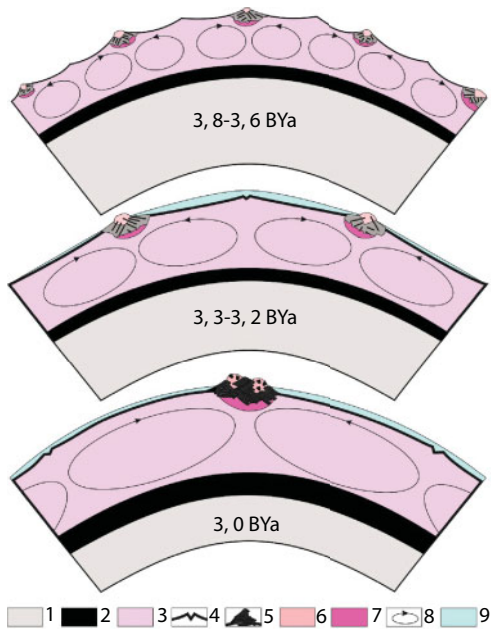

Fig. 7.4 Change in the cell number in the convecting mantle in Archean and the formation of embryos (nuclei) of Archaean continental shields (the cross-dections in the equatorial plain and at arbitrary scale); 1. Primordial Earth's matter; 2. Iron and iron oxides' melts; 3. Archaean depleted mantle impoverished in iron, iron oxides and siderophillic elements; 4. Mid-oceanic ridges; 5. Piling-up areas of the oceanic lithosphere; 6. Continental crust domains; 7. Oceanic crust melting areas; 8. Directions of the mantle convective flows; 9. Earth's hydrosphere.

The second period of a drastic increase in the convective and tectono-magmatic activity in Late Archean, as mentioned above, had been associated with the beginning of Earth core separation and involvement in the process of zonal differentiation, beside the iron oxide, also the formation of eutectic alloys Fe·FeO. A new splash up in Earth's tectono-magmatic activity had been stimulated already by a significant increase in the release rate of the "core" matter and formation of the core itself (see Fig. 5.13). These processes had caused a proportionate increase in the rate of Earth matter gravity differentiation generation energy (see Fig. 6.1). By that time, the differentiation belt had substantially expanded; therefore, the mass of the convecting mantle itself had increased, whereas the number of continental massifs (future Archaean shields), had probably decreased to 12–14. After such transition, the process of Earth matter differentiation had significantly activated. It had especially strengthened after the

beginning of the process of Earth core formation in the second half of Late Archean, starting approximately 2.8 BYa. At this very time, the most significant restructuring of convective flows in the mantle had occurred and a most powerful single-cell convective structure had begun forming that had led at the end Archean to a collision of all earlier emerged continental massifs into a single supercontinent we called Monogea (see Fig. 5.1) [19, 112]. According to the laws of mechanics about a stable revolution of free bodies mentioned in section 5.2, the supercontinent formed above a descending mantle flow center must have been positioned on Earth's equator. This has happened, most likely, 2.6 BYa and is marked in the geological chronicle of Earth by its most grandiose diastrophism of the Kenoran orogeny.

Despite the approximate nature of conducted estimates it is believed that the general pattern identified here of change in the number of convective cells in Archean correctly presents a general evolution picture of convective processes in this most ancient eon. In particular, it follows from these estimates that in Early Archean might have formed only small convective cells with brief lifetimes – tectonic cycles. In connection with a small scale of Early Archaean convection (on the order of a few hundred kilometers), individual cycles had been overlapping in time thereby creating a continuous succession of pulsating but globally not correlating with one another processes (in separate cores of growing continents). Appropriately, numerous tectonic cycles in Early Archean in most ancient cores of various continents had been forming a mosaic manifestation picture of individual not synchronous with one another splash-ups of tectonic activity.

First global-synchronous tectonic cycles might have emerged only in Late Archean when the zonal differentiation front of Earth matter had already submerged in the mantle to significant depths and because of this sizes of convective cells had substantially increased, to a few thousand kilometers. However, most clearly the synchroneity of tectonic processes must have been manifested only at the very end Archean, at the moment of Earth's core separation. As show geological data analyzed by K. Condi (Fig. 7.5), a noticeable global correlation of tectonic events in Archean granite-green stone belts on various shields had appeared only about $2.9 \cdot 10^9$ years ago. However, it had been manifested most clearly in the age interval 2.7–2.6 BYa. At this, the last Archaean convective cycle coinciding in time with the moment of Earth core separation, simultaneously had been the first most grandiose global tectono-magmatic event in Earth history which had left its indelible footprint in the epoch of the Kenoran diastrophism.

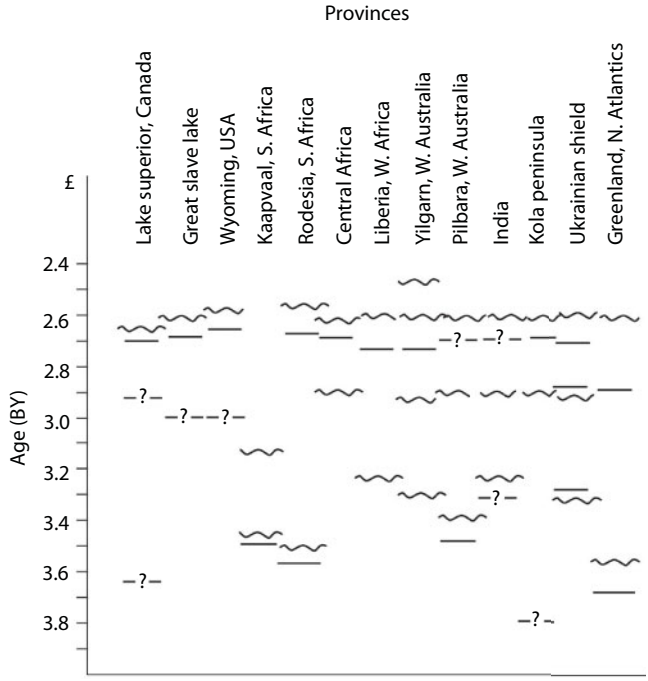

Fig. 7.5 Correlation of tectonic events at formation of granit-greenstone belts of Archean. After K. Condi [190], modified: straight lines are green stone belts' formation times; wavy lines are times of orogenies.

After transition of Earth matter gravity differentiation process from a mechanism of "core" matter zonal separation to a relatively slow-operating barodiffusion differentiation mechanism, the mantle convection, starting in Early Proterozoic, had become substantially more quiescent. For this reason, after tempestuous Archean tectonic events a relatively quiet and more long-drawn Earth evolution stage emerged, which by analogy with the terminology from the stellar evolution may be called the main sequence in the evolution of Earth group planets.

With a gradual fading of the mantle matter barodiffusion differentiation mechanism due to exhaustion of the "core" matter store, in the mantle a gradual decline in the intense of endogenous energy release had begun occurring. Thus, judging by estimates, the release of endogenous energy after transition of gravity differentiation to barodiffusion mechanism about 2.5 BYa had declined approximately by 2.3 times. Currently, compared to Late Archaean peak, it declined by approximately 7–8 times. This decline will continue in the future.

Since the time of Earth core formation about 2.6 BYa, its mass had been regularly increasing (see section 5.5), whereas the mass of Earth mantle had been appropriately declining from $4.76 \cdot 10^{27}$ g at the Archean/Proterozoic boundary to $4.035 \cdot 10^{27}$ g at present. Under chemical-heat-density convective mass exchange, alternation of single-cell and double-cell convective structures apparently had been occurring in the mantle [15, 191, 192]. As at the emergence of single-cell convective structures in the mantle, unified supercontinents must have been formed (judging by geological data, there had been four of them: Monogea, Stille's Megagea, Mesogea (Rodinia) and Wegener's Pangea). Thus, starting at 2.6 BYa, in Proterozoic and Phanerozoic had existed 4 complete single-cell convective structures and between them had been dual-cell convective structures with which had occurred the destruction of supercontinents with centrifugal drift of the released continents from one another (see Fig. 7.7).

The above estimate of the number of convective cycles in the mantle is certainly approximate. It may be fine-tuned, for instance, by using synergetic approach to the issue and coordinating estimate results with geological data. The convecting mantle is an open dissipative system embraced by strong positive and negative feedbacks. This enables a suggestion of existence in the mantle of a trend to self-organization of convective processes with the emergence of intermediate quasi-stable states defined by its most general parameters. Such parameters may be, for instance, mass of the mantle, concentration in it of the "core" matter, energy generated in it and also the balance of operating in the mantle positive and negative feedbacks.

Thus, we will depart from a view that the process of convective mass exchange in the mantle had been controlled by the operation of strong positive and negative feedbacks in the system. An example of positive feedbacks may be the convection rate vs. heat generation. At this, with temperature increase of the mantle, viscosity of its matter had been exponentially declining and appropriately growing had been the rate of chemical-density convection. Simultaneously with this, the diffusion rate of iron oxides from silicate crystals into intergranular spaces had increased, therefore, the "core" matter transit rate into Earth core (see section 5.4). This, in turn, had resulted in the density increase of the mantle variations and in a new activation of the mantle mass exchange.

A strong negative feedback had emerged by means of the heat loss by Earth. For instance, with an increase in the convective mass exchange rate had increased the rate of the oceanic lithospheric plate movement, had increased heat flows through the ocean floor and total loss of heat by

Earth. Due to this, average mantle temperature had declined, viscosity of its matter had grown and this, in turn, had led to a decrease in the rate of convective mass exchange in the mantle. Another negative feedback mechanism had been in the very process of the mantle matter barodiffusion differentiation. The iron oxide diffusion from silicate crystals into intergranular spaces had occurred only in the lower mantle at depths exceeding 2,000 km (see section 5.4). For this reason, the higher the convection rate, the shorter time the mantle matter would have been in the lower mantle active layer, the less "core" matter would have diffused in this time from silicate crystals and overflowed into Earth core.

Therefore, Earth's heat machine is an open nonlinear dissipative system with feedbacks defining the possibility of emergence in it of self-oscillating processes and self-organization of geodynamic processes. Therefore, chemical-density convection in the mantle in its nature had been a non-stationary process with continuously changing distribution of the heavy fraction concentration in the mantle matter and associated with this continuously changing structure of convective cells. For this reason, it should be expected that the self-organization of convective cells in the mantle would be continuously disrupted by non-stationarity of the process. Nevertheless, such self-organizing states, on average corresponding with minimal dissipation rate of the endogenous energy, must have emerged from time to time.

It is shown in the publication by Sorokhtin and Ushakov [101] that at a constant mass of the mantle and the absence of its heating or cooling, average convective mass exchange rate in this geosphere over large time intervals would remain constant, although its fluctuations associated with structure modifications of convective cells might have been quite significant. As the mantle after Archaean overheating still had been cooling down on average, then average convection rate had to be gradually lowered; therefore, the periods of complete mass exchange convective cycles in the mantle had to increase gradually. However, as with time the mass of the mantle had been decreasing (by means of Earth core separation), and this had resulted in an acceleration of the mantle mass exchange, then a stabilization of convective processes in the mantle might have occurred. This conclusion is apparently supported by geological data. If this is so, an important geodynamical law follows: Earth's energy balance had on average stabilized the evolution of convective processes in the mantle.

How it had been actually occurring and which factor (mantle cooling down or the decrease in its mass) had been dominating, may be determined from Earth's geological chronicle. Thus, the formation moments of supercontinents Monogea, Megagea, Mesogea (Rodinia) and Pangea should

be juxtaposed with the completion times of the Kenoran, Svecofennian, Grenvilian and Hercynian tectonic eras (orogenys), respectively 2,600 ± 100; 1,800 ± 100; 1,000 ± 70 and 230 ± 10 MYa. If this is so, the periodicity interval of the supercontinent formation in Precambrian had been slightly fluctuating within 800 to 780 MY. As we may see, the megacycle periodicity in post-Archaean time, accurate within the determination of orogenic ages, in Proterozoic had remained approximately constant. This is an indication that, simultaneously with a decrease of the mantle mass (see Fig. 7.6) resulting in the accelerated convection, had been occurring its weak cooling down (see Fig. 6.13, curve 3) which had been increasing its viscosity, therefore, slowing down convection. As a result, both these factors operating in opposite directions, had been stabilizing the mantle convection and keeping the periods of supercontinent formation megacycles approximately constant.

Thus, the effect of Earth's fading tectonic activity as a result of a declining generation of endogenous energy in the mantle, therefore, the mantle temperature, in real conditions of Proterozoic had been compensated by a decrease of mantle's mass, thereby stabilizing periodicity of tectonic events on Earth. However, in the future, due to exhaustion of Earth's energy reserves and deceleration of the mantle matter differentiation process, the factor of mantle cooling will begin playing a more important role. As a

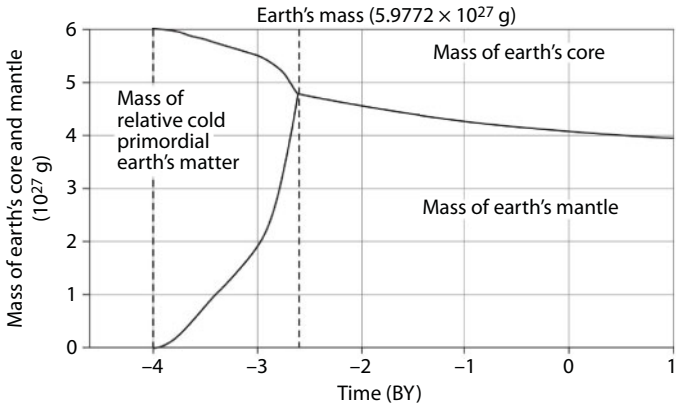

Fig. 7.6 Gradual increase of the mantle mass in Archean as a result of expansion of Earth matter differentiation zone and a decrease of its mass in Proterozoic and Phanerozoic due to the growth of Earth core. Dashed lines mark the moments of "core matter" separation start about 4 BYa and of the formation in Earth's center of a high-density oxide-iron Earth core about 2.6 BYa. After Earth formation about 4.6 BYa and to the very and of Archean, in Earth's composition had been preserved primordial Earth matter saturated with ore elements.

result, the convective mass exchange in the mantle will slow down and the periods of tectonic megacycles will again notably increase.

As noted above, the Archaean history had completed with the formation of a real high-density Earth's core and the emergence in its mantle of the mighty single-cell convective structure. For this reason, it is convenient to assume exactly this natural boundary, the moment of the final formation in subsurface of our planet of a heavy core about 2.6 BYa, as point zero of Post-Archaean geological history corresponding with the main sequence of Earth evolution. This is also supported by the fact that at the end Archean had been formed first in Earth history supercontinent Monogea. This boundary is most clearly recorded in geological chronicle as with it had been associated the change of mechanisms and geochemistry of the continental crust formation. Besides, it had been directly preceded by a mighty tectonic process (Kenoran orogenesis) of the formation of the first in Earth's history supercontinent Monogea.

In this case, taking into consideration alternating single-cell and dual-cell convective structures in the mantle and quoted geological data of the supercontinent formation times, may be fine-tuned the estimate derived above of a number of convective cycles in Proterozoic and Phanerozoic. It turns out that to the present time approximately 6.3 convective cycles had completed, each lasting 380 to 420 MY. If we assume the Kenoran orogeny, completing tectonic events of Archaean epoch, the zero time of all subsequent cycles (both single-cell and dual-cell), it turns out that by present time at $N_0 \approx 6.3$ to whole-number values *No.* = 0; 1; 2; 3; 4; 5; 6 in Post-Archaean time had corresponded ages: 2.6; 2.22; 1.84; 1.45; 1.05; 0.65 and 0.23 BYa. These reference age values closely match ages of the main tectonic events in Proterozoic and Phanerozoic (Figs. 7.7, 7.8). As noted above, in the future, due to exhaustion of Earth energy reserves, the factor of its declining tectonic activity will play a more important role. For this reason, in the future will have to substantially slow down the convective mass exchange in the mantle and, as a consequence, will have to noticeably increase periods of tectonic megacycles.

If we assume that at chemical-density convection in mantle, one convective cycle had corresponded with a total mantle matter turnover then we find that in Proterozoic and Phanerozoic had existed about 6.3 convective cycles.

The formation time of the first supercontinent in Earth's history (see Fig. 9.2) corresponds with the value $N_C = 0$. By analogy with the unified continental massifs Megagea (by Stille) and Pangea (by Wegener) that emerged in subsequent geological epochs, we named this first supercontinent in Earth's history Monogea [19, 112].

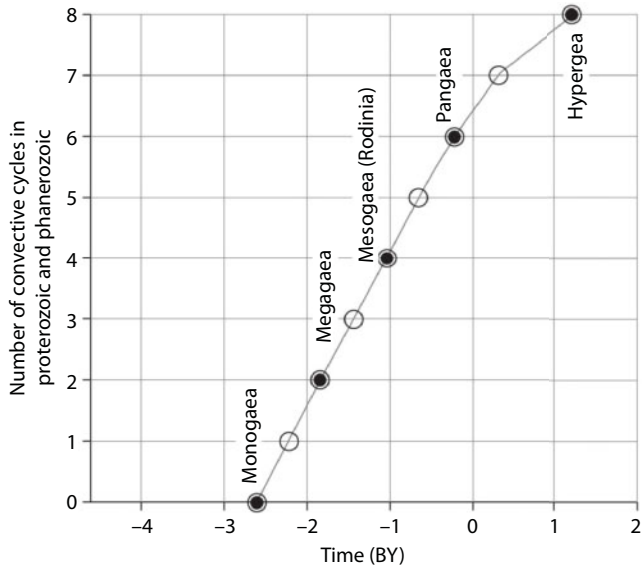

Fig. 7.7 A number of convective (tectonic) megacycles in Proterozoic and Phanerozoic $N_C(t)$ vs. time: solid circles are single-cell structure moments of supercontinent formation; transparent circles are dual-cell convective structures at the time of maximum split supercontinents.

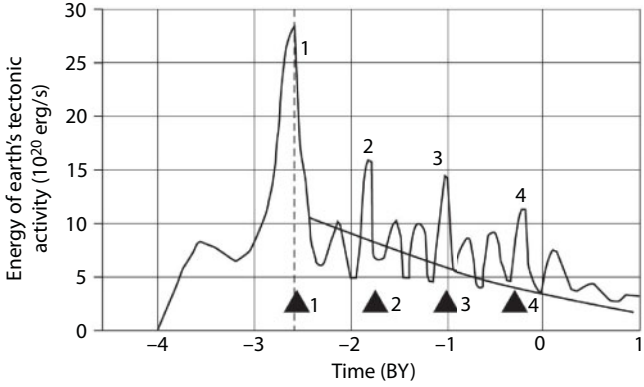

Fig. 7.8 The complete Earth's tectonic activity diagram under the subject model (see Fig. 6.17) with using the estimates by V.P. Keondjan and A.S. Monin [123] considering cyclicity of endogenous energy release. Each significant maximum of this curve at the times 2.6; 1.8; 1.0 and 0.2 BYa corresponds with a single-cell convective structure in the mantle and the formation of supercontinents. The genuine positions of the supercontinents is marked by triangles: 1. Monogea; 2. Megagea; 3. Mesogea (Rodinia); 4. Pangea. The dashed line indicates the moment of Earth's core formation.

However, the supercontinents had been unstable mosaic agglomerations of heterochronous structures. After the formation they had rapidly split of supercontinents and fragmented into separate parts (the appropriate possible reconstructions of supercontinents and continents – fragments of their decomposition are reviewed in Chapter 9).

This had been associated with a change in the structure of convective flows in the mantle and emergence, instead of a descending mantle flow underneath a former supercontinent of a new ascending flow, the direct cause of its decomposition and fragmentation. But each time when a single-cell convective structure had emerged in the mantle, had also emerged a new supercontinent.

Considering a relatively brief life of supercontinents, it may be assumed that at $N_C = 1$ by the moment in time 2.22 BYa a more complex, possibly dual-cell convective structure had set up in the mantle. At this, in compliance with the laws of mechanics requiring for a stable Earth's revolution the coincidence of its main axis of the moment of inertia with own revolution axis, Earth must have turned so that mass centers of most continents of that time, for instance, Monogea fragments had turned out on the equator or in low latitudes.

The next supercontinent, Megagea by Stille (see Fig. 9.3) had begun to form about 2.0–1.9 BYa but had finally formed only 1.84 BYa as a result of a global Svecofennian (Karelian) orogeny. Therefore, at that very time with which might have been associated the value of a parameter $N_C = 2$, in the mantle again must have been functioning a single-cell convective structure. Considering the conclusion included in section 5.2 of the association of Earth's moment of inertia's orientation with the positions of continental masses on Earth's surface [193], it may be concluded that the second supercontinent Megagea had formed in low latitudes with the mass center on the equator. This is also supported by the geological data (see section 9.3).

The Megagea existence had also been short-lived: Already the beginning of Riphaean had been marked by general fragmentation of the continental crust. The value of parameter $N_C = 3$ in time (1.45 BYa) had matched Early Riphaean. Whereas the beginning of the Megagea split had occurred somewhat earlier, at about 1.6 BYa, and had closely coincided with the next outstanding tectonic epoch of a great renewal in Earth's structural plan from which is sometimes counted the beginning of the Neogean epoch.

The value $N_C = 4$ corresponds with the time 1.05 BYa, which closely corresponds with equally radical Grenville epoch of tectono-magmatic activation as a result of which from Megagea fragments had begun forming

a new, third in succession supercontinent, Mesogea, sometimes called Rodinia (see Fig. 9.4). The new supercontinent, same as Megagea, had been positioned near the equator and had existed a relatively short time, about 100–150 MY. Soon thereafter, this single-cell convection in Earth's mantle had been replaced by a dual-cell convective structure with two descending flows near Earth's poles and one ring-like ascending flow underneath its equatorial belt. Such situation at the value of parameter N_C = 5 and time 800 MYa had corresponded to Mesogea split into two large supercontinents, Laurasia and Gondwana (see Fig. 9.5). However, already about 650 MYa, underneath Laurasia (the northern fragment of Mesogea) had emerged a secondary ascending mantle flow which had literally torn apart this supercontinent with the formation of Pra-Atlantic ocean Yapetuis and Paleo-Uralian ocean. The Gondwana at this had experienced only partial destruction but already in Katanga (Pan-African) orogeny it had welded again into a single supercontinent (see section 9.7).

For the fourth time, a single-cell convective structure had occurred in Earth and had again formed a united supercontinent, Wegener's Pangea (see Fig. 9.8) at the boundary of Paleozoic and Mesozoic about 230 MYa. This event corresponded with the parameter value N_C = 6 and estimated time 230 MYa and also maximum tectonic activity of Hercynian orogeny in Phanerozoic. The Pangea, as all other supercontinents, also had not existed long and already early in Mesozoic (about 200 MYa) had experienced first destructive impulses, and approximately 190 MYa had occurred first transcontinental ruptures which had then grown into young oceans: Atlantic, Indian and Arctic.

The quoted estimates of $N_C(t)$ are certainly approximate, especially considering substantial instability of the mantle convection. Still, they apparently correctly reflect the main feature in the evolution of Earth's tectonic activity, its cyclicity. Judging by the above estimates (see Fig. 7.8), in the post-Archaean geological history are identified six alternations of the convective cycle structures from single-cell to double-cell ones, and the other way around: 2.6–2.22–1.84–1.45–1.05–0.65–0.23 BYa, with the duration about 380–420 ± 10 MY.

If we extend this pattern in the future but in consideration of a progressive fading of Earth convective activity, it turns out that the next complete convective cycle will have completed approximately in 300 MY at N_C = 7. At last, the last, fourth megacycle with N_C = 8 may be completed approximately in 1.2 BY in the future. However, due to a gradual fading of the process of Earth matter barodiffusion mechanism of the differentiation and the appropriate decline of the mantle convective activity, it is not clear whether weakening mantle convection

will have enough power for the formation of the last суперсontinent, a hypothetic Hypergea.

The energy approach enables an estimation of the total mantle matter mass that had made it through the differentiation and participated in convection. Thus, it was determined above that the rate of present-day convective mass exchange in the mantle is equal approximately to $6 \cdot 10^{18}$ g/year, or $1.9 \cdot 10^{11}$ g/s.

Over the entire time of Earth tectonic activity (from $4.0 \cdot 10^9$ years ago to the present) its heat loss associated with the convective heat transfer had composed approximately $10.773 \cdot 10^{37}$ erg (see Fig. 6.13) and the present-day depth heat flow, minus the effect of post-Archaean Earth cooling, is equal to $3.39 \cdot 10^{20} - 0.27 \cdot 10^{20} = 3.12 \cdot 10^{20}$ erg/s. This allows us to determine the total mass of the mantle matter that had participated in convective mass exchange. It turns out equal to $5.2 \cdot 10^{28}$ g. Whereas the mass of Earth and of the present-day mantle are respectively $5.977 \cdot 10^{27}$ and $4.035 \cdot 10^{27}$ g. From this, we find that by present time the total mass of mantle matter gone through convective mass exchange is approximately 8.7 times the mass of Earth itself and approximately 13 times the mass of the present-day mantle. The included estimate, despite its approximate nature, is still very graphic and shows that the convective mass exchange in the mantle had indeed been huge and for this reason it must not be neglected.

It was also possible to estimate the matter overheating ΔT in the ascending mantle flows as compared with average mantle temperatures. As the mantle convection is "heating" entire Earth including the surface of Earth's core, it may written:

$$\Delta T = \frac{\Delta Em_{2.6-0}}{M_G \cdot 8.7 \cdot (c_p)_G}, \tag{7.4}$$

where $\Delta Em_{2.6\text{-}0} = 4.576 \cdot 10^{37}$ erg is heat component of energy released in the mantle after Archean; $M_G = 5.977 \cdot 10^{27}$ g is the mass of Earth; $(c_p)_G \approx 1 \cdot 10^7$ erg/g·deg. Herefrom, $\Delta T \approx 88^{\circ}C$, i.e., the temperature of ascending mantle flow exceed average temperature of the mantle less than by 100 °C.

At this, the scale of the mantle matter differentiation may be determined. Indeed, the rate of gravity energy release is associated with the rate of mantle matter differentiation on the surface of Earth core $\dot{M}_m$:

$$\dot{E}_g \approx \dot{M}_m \cdot \left[\Delta \bar{h}_c \cdot \frac{\Delta \rho_{cm}}{\bar{\rho} c} + H_m \cdot \frac{\Delta \rho_m}{\bar{\rho}_m} \right] \cdot g_c \tag{7.5}$$

The present-day rate of the release of heat component of the gravity energy of Earth differentiation is $\dot{E}_g \approx 2.77 \cdot 10^{20}$ erg/s. Average topography contrast at the core surface $\Delta\bar{h}_c$ is approximately 7 km; $\Delta\rho_{\text{cm}}$ is the matter density difference on the mantle – core boundary, ($\Delta\rho_{cm}$ = 9.92 – 5.6 = 4.32 g/cm^3); $\bar{\rho}_c \approx 10.6 g/cm^3$ is average density of Earth core; $H_{\text{m}} \approx$ 2,875 km is average mantle thickness; $\bar{\rho}_m \approx 4.54 g/cm^3$ is average mantle density; g_c = 1,067 cm/s^2 is the gravity acceleration at the core surface. The density difference between the matter in a descending and ascending flow $\Delta\rho_{\text{m}}$ may be determined from condition of their isostatic equilibrium (considering that $\Delta h_{\text{c}} << H_{\text{m}}$)

$$\Delta\rho_m \approx \Delta\bar{h}_c \cdot \frac{\rho_c - \bar{\rho}_m}{H_m} \tag{7.6}$$

Herefrom we find $\Delta\rho_{\text{m}} \approx$ 0.0165 g/cm^3. In the section 5.4 (see Eq. 5.21) a somewhat different although close estimate of the value $\Delta\rho_m \approx$ 0.019 g/cm^3 was derived. Substituting now all determined values in Eq. (7.5), we will find the transition rate of Fe·FeO alloy from the mantle in the core of Earth $\dot{M}_m \approx 2.8 \cdot 10^{11} \div 3.2 \cdot 10^{11}$ g/s or $8.8 \cdot 10^{18} \div 10.1 \cdot 10^{18}$ g/year, which gives, recalculated on the metallic iron, respectively $7.7 \cdot 10^{18} \div 8.8 \cdot 10^{18}$ g/year or $7.7 \cdot 10^{12} \div 8.8 \cdot 10^{12}$ t/year.

7.4 Evolution of Earth's Tectonic Activity Parameters

As mentioned earlier, Earth's tectonic activity is understood as the manifestation intensity within it of the entire multitude of geological processes resulting in deformations of its lithospheric shell (including Earth's crust) and in any forms of magmatism within this shell. After the appearance of the theory of lithospheric plate tectonics it became clear that as a demonstrative estimate of average tectonic activity of Earth may serve some movement measure of the lithosphere plate ensemble, for instance, the rate of their relative displacement. However, most general, convenient and physically substantiated estimate of Earth tectonic activity, apparently, should be considered its energy measure defined in the final analysis by coming from the mantle depth heat flow $\dot{Q}_m$. Indeed, any displacements of Earth masses and magmatic matter transformations resulting in the tectonic activity of our planet eventually convert in heat and are lost by Earth with its heat radiation. Exactly for this reason such depth heat flow $\dot{Q}_m$ may serve as a natural measure of Earth's tectonic activity.

In mid-Archean, about 3.2 BYa, some weakening of Earth tectonic activity had been observed with the formation of more stable oceanic plates. At that time, the rate of lithospheric plate movement had declined approximately to 20–25 cm/year. The decline of tectonic activity in mid-Archean is explained by that at this time the front of Earth matter zonal differentiation had approached the depths (about 800–1,000 km) at which had substantially increased the difference between melting temperature of the metallic iron and Earth geotherm (see Fig. 5.4). As a result, starting at that time (approximately 3.4 BYa) a significant part of gravity energy released at the separation of iron melts from silicates, had begun to be expended not only for excitation of convective movements in the upper mantle (i.e., not only for Earth's tectonic activity) but also for heating of the underlying and still relatively cold primordial heart of young Earth.

In Late Archean, at the time of Earth core formation, had been observed a new and most drastic splash up of Earth tectonic activity. The rate of oceanic plate movement then had exceeded 350 cm/year and at the peak had reached almost 400 cm/year, which is 70 times the present-day plate rate of movement! The drastic splash up of Earth tectonic activity in Late Archean had been associated with two causes. First, with the transition process of Earth matter differentiation from separation of metallic iron (in Early Archean) to differentiation more abundant eutectic melts Fe·FeO. Second, a catastrophic process of Earth core separation about 2.8–2.6 BYa accompanied by release of a large additional energy, about 5·1037 erg (see Chapter 6). A combined action of these processes had caused a colossal splash up of Earth tectonic activity which had left in its geological chronicle an indelible footprint of a radical reworking of almost all continental crust formed by that time.

Starting in Early Proterozoic, the average rate of lithospheric plate movement had been continuously declining from 50 cm/year to its present-day value of about 5 cm/year, although at the moments of Earth tectonic activity splash ups the rate of their movement had been sharply increasing (see Fig. 7.8). The decline of average rate of plate movement will have occurred in the future, up to a moment when, due to a gradual transition of iron oxides in Earth core, their reserves in Earth mantle will have exhausted. This will have occurred, however, most likely only in 1–1.5 BYa.

The first and perhaps major consequence from the theory of Earth global evolution reviewed here is a clear subdivision of Earth tectonic evolution into four large and conceptually different stages: 1) Passive Katarchaean; 2) Exceptionally active Archaean; 3) Moderately active (quiescent) Proterozoic-Phanerozoic and 4) Future stage of Earth tectonic death.

The most ancient of these stages (pregeological or Katarchaean) had lasted about 600 MY, i.e., from the moment of Earth formation 4.6 BYa to the beginning of its tectonic activity in Early Archean approximately 4.0 BYa. At that time, tectono-magmatic manifestations of endogenous origin had been completely absent as Earth still had been a relatively cold cosmic body and all matter within its subsurface had been at the temperatures substantially lower than the temperature of beginning of its melting. Nevertheless, at the Katarchaean epoch Earth had not been a tectonic dead planet. First, its subsurface at that time had been gradually heated by the energy of radioactive element decay and tidal interaction with the Moon, thereby preparing conditions for Earth transition to tectonically active evolution stages. Second, in Katarchaean (especially in Early Katarchaean) a substantial role had played exogenous tectonic of a tidal origin causing swarms of strongest earthquakes. In general, this stage may be called crypto-tectonic.

First clear and intense manifestations of Earth endogenous tectono-magmatic activity had been reliably recognized only in the beginning of Archean about 3.8 BYa [84, 85]. This beginning of Earth tectonic activity had been prepared by radiogenic and tidal Earth matter heating to a level of appearance in the upper mantle of the primary asthenosphere. Following this sharp and even "shock" activation of the tectono-magmatic activity on Earth had occurred first by means of "pumping" in the emerged asthenosphere of the tidal energy of Moon-Earth interactions and then, due to the release of Earth matter gravity differentiation energy (see Chapter 6 and section 5.3).

Describing the specifics of tectonic processes in Archean, it is important to emphasize that "pumping" tidal energy in the asthenosphere had occurred mostly in the equatorial belt of Earth. For this reason, first embryos of continental massifs, on the whole about 40, in the beginning of Early Archean might have emerged only in near-equatorial areas (see section 7.3 and Fig. 7.4). However, after the beginning of operation by a new and very powerful energy source, release of the gravity energy under the mechanism of Earth matter zonal differentiation, the belt of tectonic activity on Earth had begun gradually broadening capturing ever higher latitudes, and the number of continental shields, on the contrary, had begun shrinking and simultaneously increasing in mass.

In Archaean, the entire Earth's primordial matter within the expanding low-altitude hot upper mantle belt must have gradually been assimilated by the mantle and totally remelted. Thereby it must have deleted from Earth's geological chronicle practically all direct footprints of the Katarchaean (Hadean) stage of its evolution (see Figs. 5.1 and 7.9). It is possible that

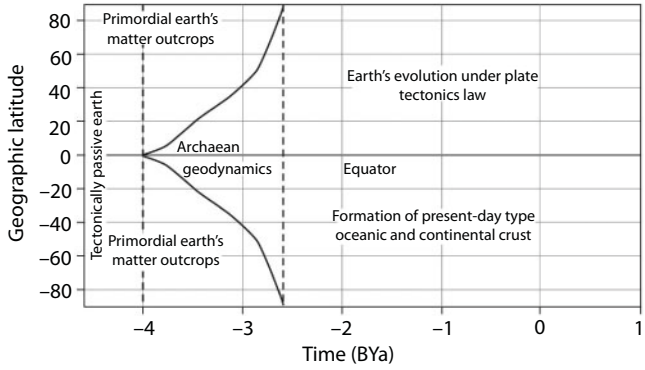

Fig. 7.9 Evolution of tectonic environments on Earth: in Katarchaean (4.6 to 4 BYa), Earth had been a tectonically passive planet. Earth's tectonic activity had begun only in Archean after the process of Earth core separation had begun about 4 BYa in the narrow equatorial belt, by the end Archean, about 2.6 BYa, this belt expanded over the entire Earth. During entire Archean a significant Earth's surface area had been still composed of primordial Earth's matter. For Archean geodynamic are typical granite-green stone belts. After Earth core formation about 2.6 BYa, Earth evolution had begun under the laws of lithospheric plate tectonics with the formation of oceanic and continental crust of present-day type.

some redeposited sediments may be the bearers of a material memory about the initial stage of Earth's evolution. Besides, gray gneisses of most ancient Archean complexes may be remelted and substantially altered residues of the primordial matter.

Earth's core separation in the end Archean had resulted in a significant decline of average tectonic activity (see Fig. 5.16), after which had drastically declined the ocean plate formation rate and equally drastically had increased the duration of their existence and cooling down on Earth's surface (see Fig. 8.11). In a cooled-down state their density had grown compared to the mantle matter. As a result, oceanic plates had been able to submerge in mantle depths; subduction zones had emerged after which Earth's tectonic evolution had been developing under the laws of the lithospheric plate tectonics. However, during approximately 100–200 MY between 2.6 and 2.5–2.4 BYa, Archean tectonics apparently had still been showing. Therefore, this relatively short Earth's evolution period may be described as transitional from Archean geodynamics to the lithospheric plate tectonics of Proterozoic and Phanerozoic. It is important to stress that exactly Earth's core formation about 2.6 BYa had predetermined the transition of Earth's tectonic evolution from Archaean geodynamic to post-Archaean lithospheric plate tectonics.

8

Earth's Crust Evolution

8.1 Patterns in the Formation of Oceanic Lithospheric Plates

The oldest stage of Earth's evolution (pre-geological or Katarchaean) lasted about 600 MY, i.e., from the moment of Earth formation 4.6 BYa and to the beginning of its tectonic activity in Early Archaean, approximately 4.0 BYa. At this time, tectono-magmatic endogenous origin manifestations had been completely absent as Earth was still a relatively cold cosmic body and the entire matter within its subsurface was at a temperature substantially lower than the temperature of the beginning of its melting. Nevertheless, Earth during the Katarchaean epoch had not been a tectonically dead planet. First, its subsurface at that time had been gradually warmed up at the expense of the energy of radioactive element decay and tidal interaction with the Moon, thereby preparing conditions for Earth's passing to tectonically active stages of its evolution. Second, in Katarchaean (especially in Early Katarchaean), a substantial role had been playing exogenic earthquakes of a tidal origin. In general, this stage may be called crypto-tectonic.

The first clear and intense manifestations of Earth endogenous tectono-magmatic activity are reliably recorded only at the beginning of Archaean about 3.8 BYa [84, 85]. At this, the beginning of Earth's tectonic activity had been prepared by the radiogenic and tidal heating of the primordial Earth's matter to the appearance level in its upper mantle of primordial melts. Following this sharp and even "shock" activation of tectono-magmatic activity on Earth had been occurring initially at the expense of "pumping" in the formed asthenosphere of the tidal energy of Moon-Earth interactions and then, due to the release of Earth's matter differentiation gravity energy (see section 5.3 and Chapter 6).

A rapid overheating of the asthenosphere with almost total melting of its matter had resulted at the boundary Katarchaean/Archaean in an equally sharp decline in the thickness of the overlying lithosphere. But the density of the rich in iron and its oxides (Fe ≈ 13% and FeO ≈ 24%) primordial lithosphere ($\rho_o \approx 3.9$ g/cm^3) at that time had substantially exceeded the

N. O. Sorokhtin (ed.) The Origins of Natural Diamonds, (175–247) © 2019 Scrivener Publishing LLC

density of a matter that had already passed by that time the differentiation of a young asthenosphere ($\rho_a \approx 3.3–3.4$ g/cm^3). For this reason, the primordial lithosphere above Earth matter differentiation zone must have immersed in the molten upper mantle and there to have been completely remolten. However, the differentiation zone only had gradually expanded and covered the entire Earth only by the end of Archaean (see Fig. 7.9 and 8.4). Thus, during the entire Archaean, on Earth surface still had been preserved the primordial Earth matter overlain by a Moon-like porous ground, regolith. but this entire primordial Earth matter, in the process of expansion of a zone of tectono-magmatic activity, turned out in Archaean to have been completely destroyed and, therefore, had not gotten in Earth's geological chronicle. The only exceptions are this matter erosion products which in form of deposits had been getting in younger sedimentary-volcanogenic Archaean complexes and had been preserving their relic memory of pre-geological Earth history.

Describing the specifics of tectonic processes in Archaean, it is important to emphasize that the "pumping" tidal energy in the asthenosphere had been occurring mostly in Earth equatorial belt. For this reason, first marine basins as well as embryos of continental massifs, to the total of about 40 in the beginning of Early Archaean, might have emerged only in near-equatorial areas (see Fig. 5.3 and 7.4). However, after the beginning of operation of a new and very powerful energy source, release of the gravity energy under the mechanism of Earth matter zonal differentiation, the belt of tectonic activity on Earth had begun gradually to expand encroaching in higher latitudes, and the number of emerging at that continental shields, on the contrary, had begun shrinking and simultaneously increasing in mass. By the end of Archaean, about 2.6 BYa, tectonic movements had already involved the entire Earth, and all continents that had emerged in Archaean joined in a united supercontinent Monogea. Exactly for this reason, during almost the entire Archaean on Earth surface, beside the emergence of the oceanic crust areas and embryos of the future continents, had been preserved areas of its primordial surface covered with a thick layer of regolith with the original composition of Earth matter. Taking this into consideration as well as a fact that in Archaean had been formed about 70% of the continental crust and in subsequent epochs only 30% [85], it was possible to estimate approximately the growth of the oceanic crust area in Archaean and the subsequent evolution in Proterozoic and Phanerozoic (see Fig. 8.4).

At a first approximation, average volume of basalt eruption on the ocean floor is proportionate to penetrating it heat flow. It follows from here that in Archaean as well the thickness of the oceanic crust basalt eruptions $H_b \sim \dot{Q}_m$ (see Fig. 6.17) might have reached a quite substantial size. If we

accept that the basalt layer thickness in the present-day oceanic crust is approximately 2 km, we find that in Early Archaean the thickness of the basalt layers might have reached 9 km and in Late Archaean, exceeded 32 km. However, in those faraway times, the mass of erupting basalts had been limited by the depth of the beginning of the mantle matter melting and thicknesses of the consolidated layers (analogs) of the oceanic crust, by the surface cooling and the penetration depth in basalts of the oceanic water. In Archaean, according to our estimates, their thickness had been approximately 4 km. In Middle Archaean, about 3.2 BYa, the thickness of consolidated slabs had exceeded the basalt layer thickness and reached 11 km, and in Late Archaean, had declined to 8 km. In Proterozoic, the thickness of the basalt layer (including the gabbro layer) of the oceanic crust had been gradually declining from 6 to 4 km (Fig. 8.1).

The quoted interrelations enable important geological conclusions. First, subduction zones could not have existed in Archaean; the oceanic plate compression had been compensated by their piling-up and obduction over the margins of continental plates (see Fig. 8.5). Second, plate subduction zones might have emerged only in Proterozoic, about 2.5 BYa. Therefore, Earth's tectonic evolution in Archaean had been proceeding under deformation mechanisms of thin lithospheric slabs whereas the present-day type lithospheric plate tectonics on Earth had begun operating only in Early Proterozoic (starting approximately 2.5 BYa).

In Fig. 8.1, a model of the oceanic crust structure evolution is displayed. The Figure shows that in Archaean the oceanic crust had been substantially basalt, with only a thin layer of overlying deposits. At the moments of maximum overheating of the upper mantle (see Fig. 5.5), the composition of crust's base rocks had been becoming basalt-komatite. As opposed to this, in Proterozoic and Phanerozoic, consolidated oceanic crust had

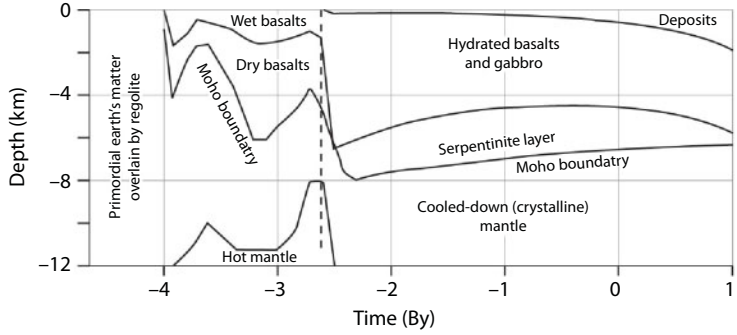

Fig. 8.1 Generalized model of the oceanic crust structure evolution.

acquired present-day features of a triple-layer structure: the upper sedimentary layer, then basalt (together with gabbro) layer and in the lower parts of the oceanic crust, the serpentinite layer.

We showed above (section 6.4) that the major part of the depth heat coming from the mantle (Fig. 6.15) is lost through the oceanic plates. At present, this fraction is 92%; in the past geological epochs it had been even higher. Therefore, it may be assumed that after the emergence of Earth's endogenous tectonic activity, parameter $\dot{Q}_{\mathrm{m}}$ first of all and always was describing the oceanic lithospheric plate formation and destruction regimes. Average heat flow through the ocean floor approximately is equal to a ratio $\overline{q} = \dot{Q}_m / S_{oc}$ and is inversely proportionate to a square root of average life span of the oceanic plates $\overline{q} \propto 1/\sqrt{\tau} = \sqrt{u/S_{oc}}$, where u is average formation rate of oceanic plate area (km²/year) and S_{oc} is total area of the oceanic plates (km²). Thus, average rate of oceanic plate formation is proportionate to a ratio $u_l \sim \dot{Q}_m^2 / S_{oc}$ [101]. The heat flow through the oceanic crust was estimated in section 6.5 by Eq. (6.23`) and imaged in Fig. 6.15 by curve 1 in Archaean and curve 4 after Archaean.

Considering that the present-day average formation rate of oceanic plates is equal approximately to 3 km²/year (or about 5 cm/year at the length of all oceanic rift zones of 60 thous. km) and remembering that the area of oceanic plates in Archaean had been gradually increasing together with expansion of Earth's low-latitude tectonically active belt, it is possible to estimate average formation rate of these plates in the past geological epochs (see Fig. 8.2).

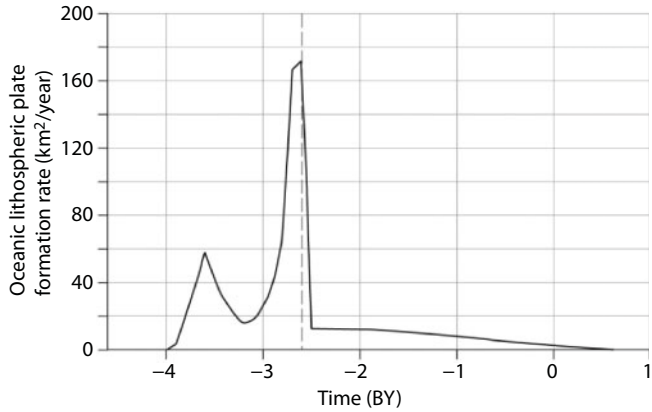

Fig. 8.2 Evolution of average oceanic lithosphere plate formation rate (the present-day value is approximately 2.6 km²/year).

As the included diagram shows, the first substantial splash up of Earth's tectonic activity had occurred in Early Archaean, when the mechanism of iron zonal differentiation had begun operating. Average formation rate of oceanic plates at that time had reached 40–50 km^2/year, i.e., 16–20 times the present-day rate of their formation. So high rate of the plate formation had been defined to a large extent by that in Early Archaean their area was still insignificant and for this reason, the heat flow density through them had been, on the contrary, quite large.

In mid-Archaean, about 3.2 BYa, a substantial weakening of Earth tectonic activity with the formation of more stable oceanic plates had been observed. At that time, the rate of lithospheric plate movement had declined approximate to 20–15 am/year. The decline of tectonic activity in mid-Archaean had been due to the fact that at this time the front of Earth matter zonal differentiation had approached those depths (about 800–1,000 km) at which the difference between the metallic iron melting temperature and Earth geotherm had substantially grown (see Fig. 5.4). As a result, beginning at this time (approximately 3.2 BYa), a significant part of gravity energy released at iron melt separation from silicates had begun to be expended not only on excitation of convective movement in the upper mantle (i.e., not only on Earth tectonic activity) but also on heating the underlying and still relatively cold primordial heart of young Earth.

In Late Archaean, at a time of Earth's core formation, had substantially grown a new and sharpest splash up of Earth tectonic activity had substantially grown. The movement rate of oceanic plates had reached at that time 170 km^2/year, i.e., more than 50 times the rate of present-day plate movement! A splash up so sharp of Earth tectonic activity in Late Archaean had been associated with two causes. First, with the transition of Earth matter differentiation from the metallic iron separation process (in Early Archaean) to the differentiation of more abundant eutectic melts Fe·FeO. Second, with a catastrophic Earth core release process approximately 2.7–2.6 BYa. This process had been accompanied with a release of a huge additional energy, about $5 \cdot 10^{37}$ erg (see Chapter 6). Combined action of these two processes had caused a colossal splash up of Earth's tectonic activity which had left in its geological chronicle an indelible footprint of a radical reworking of almost the entire continental crust formed by that time.

Beginning in Early Proterozoic, the rate of lithospheric plate movement had been continuously approximately from 13 km^2/year to its current value of about 3 km^2/year (around 5 cm/year). The decline in plate movement average rate will be continuing in the future up to a moment when, due to the oceanic plate thickness increase and their friction about each other, it will have completely stopped. But it will have happened apparently only in 1–1.5 BY.

Fig. 8.3 is the diagram of lifetime τ evolution of average oceanic plate and of the appropriate average thickness of these plates.

At the determination of the oceanic crust (oceans) area, should be kept in mind its substantial growth in Archaean due to the expansion of tectonic activity belt from the equatorial zone in the very beginning of Early Archaean practically to the area of the entire Earth (together with continental crust blocks) and the appropriate growth of continent's area (see Fig. 8.4).

The first and perhaps the main consequence of the review of Earth's global evolution theory is a clear subdivision of Earth tectonic evolution into four large and conceptually different stages: 1) Passive Katarchaean;

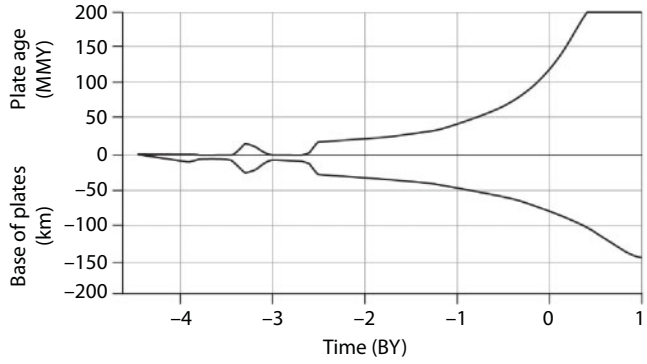

Fig. 8.3 The evolution of lifetime and average thickness of the oceanic lithospheric plates.

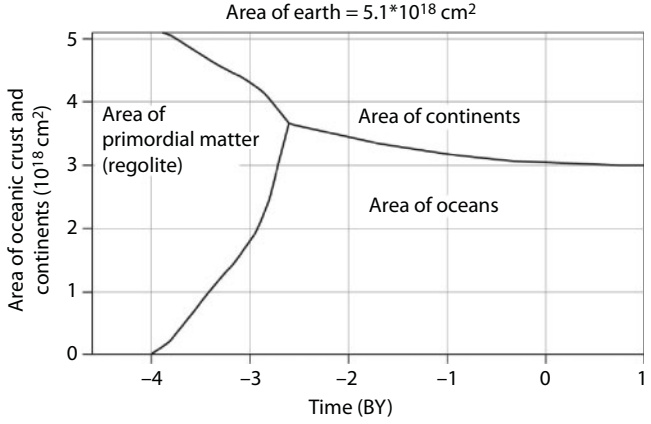

Fig. 8.4 Evolution areas of oceanic and continental crust.

2) Exceptionally active Archaean; 3) Moderately active (quiescent) Proterozoic-Phanerozoic and 4) Future stage of Earth's tectonic death.

8.2 Formation of the Continental Crust in Archaean

It follows from the lithospheric plate theory that the continental crust is forming currently only above the lithospheric plate subduction zones at the expense of dehydration and partial remelting in these zones of the oceanic crust overlying deposits. However, only those plates may intrude the mantle through subduction zones, whose average density, in consideration of a lower crust density (2.9 g/cm^3) compared with the lithospheric one (3.3 g/cm^3), is greater than the hot mantle density (3.2 g/cm^3). Presently, this condition satisfy the plates whose thickness (together with the oceanic crust $H_{oc} \approx 6.5$ km) exceeds approximately 26 km. In the past geological epochs, values of such critical oceanic plate thickness might have been different (see Fig. 8.22, curve 3). A reminder: the continental plates, despite their great thickness (about 200–250 km), had never invaded the mantle as they, due to low rock density of the continental crust, always maintained positive buoyance reaching 0.02–0.03 g/cm^3.

Using a known correlation of oceanic plate thickness vs. their age $H_l \approx k \cdot \sqrt{t}$ (where H_l is in km, t is in MY, and $k \approx 6.5–7.5$) described in section 8.2, it may be determined that the plate thickness greater than 26–30 km corresponds with ages older than 16–21 MY. Average lifetime of the present-day oceanic plates, judging by the data of paleomagnetic geochronology, is approximately equal to 120 MY. For this reason, under conditions existing at present, such plates, older than 16–20 MY, not only may but really are intruding the mantle through subduction zones. As the estimates of oceanic plate thickness evolution show (see Fig. 8.22), their invasion of the mantle had become possible only in Proterozoic and Phanerozoic. This is associated with the fact that the thickness of the lithosphere (curve 4) in Proterozoic had exceeded the thickness' critical value (curve 3) after which the cooled down oceanic plate had become heavier than the hot mantle and begun descending in it through subduction zones. This enables us to suggest with certainty that, starting in Early Proterozoic (around 2.5 BYa) all oceanic lithospheric plates, after their formation in rift zones of mid-oceanic ridges, after some time mandatorily invaded the mantle through the existing at that time plate subduction zones. Thus, it is possible to conclude that Earth's tectonic evolution at the boundary of Archaean and Proterozoic had entered the epoch of the laws of lithospheric plate tectonics. Naturally, the process of transition from Archaean geodynamic to the lithospheric plate tectonics of Proterozoic and Phanerozoic had not

been instantaneous. The entire Early Proterozoic (approximately 2.5 to 1.7 BYa) is marked by typical features of withering away of the old geodynamic style and the emerging of the new one [194].

For most of Archaean, the average lifetime of lithospheric plates had been substantially less than 16 MY and their thickness had been 20-40 km. This is much smaller than critical parameters after which the subduction process had been possible [112]. For this reason, thin Archaean plates, which it is better to call basalt composition lithospheric slabs, in Early and Late Archaean had lower density than the mantle. Therefore, such slabs at that time might not have invaded the mantle. Thus, a major tectonic conclusion: during most Archaean customary for us subduction zones had not existed. Instead of them, in compression areas of the lithospheric shell (i.e., above the descending convection flows of the mantle matter) zones of pileup and clustering of thin oceanic lithospheric slabs had been emerging.

Affected by compression forces caused by convective flows in the mantle matter, total thickness of piled up lithospheric slabs, naturally, had been increasing. For this reason, the roots of such "pileup" structures had still invaded the hot mantle to a depth of 50–80 km under the mass of piled up slabs. In Archaean, the upper mantle had been substantially overheated, its temperature at that time had by 400–500°C exceeded the present-day one (see Fig. 5.5). As a result, invading the overheated mantle roots of piled up thin oceanic slabs must have been molten again. The melting of containing water basalts of the former oceanic crust and subsequent differentiation of melts had resulted in the formation of lighter tonalite, trondhjemite and plagio-granite melts. These relatively light melts, naturally, had to float and rise up in form of diapirs and domes breaking through the entire structural-material complex of piled up oceanic slabs and formed sedimentary-volcanogenic sequences forming thereby renowned granite-greenstone Archaean belts, the most ancient components of the continental crust (Fig. 8.5). A theoretical substantiation of the formation of Archaean continents through piling up and partial melting of a relatively thin (no thicker than a few kilometers) oceanic lithosphere had been provided already in 1991-1994 [17, 195]. In 1992-1998, this Archaean continental shield formation model was confirmed at a study of Caapvaal Archaean craton by Wit and Roering *et al.* [196] and Wit [197] who also believed that the Archaean oceanic crust could not have subducted due to its elevated buoyancy.

In this connection, one more feature of Archaean continental massifs' formation is remarkable. Because of high heat flows in Archaean, a thick and high density mafic composition lithosphere might not have formed under continental crust of these massifs. A relatively light continental crust as if had been "floating" directly in the hot mantle. For this reason,

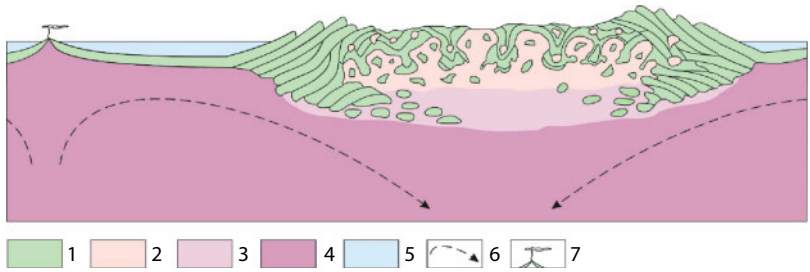

Fig. 8.5 The mechanism of continental crust formation in Archaean. 1. Oceanic type crust; 2. Forming domain of the tonalite-trondhjemite composition continental crust; 3. Oceanic type crust's melting and differentiation zone; 4. Convecting mantle; 5. Earth's hydrosphere; 6. Convecting flow directions; 7. Fracture volcanism in mid-oceanic ridges.

the continent standing level during the entire Archaean and beginning of Early Proterozoic had been exceptionally high. The surface of the continents at that time had towered over the ocean level by 6–4 km [198] and even higher in the pileup zone of basalt slabs, by about 8–10 km. This is part of explanation to a high erosion level on practically all without exception Archaean shields.

Thus, the Archaean continental crust had been forming due to the action of two major tectonic processes, the formation at the first stage of thin basalt slabs of oceanic crust and their piling up with secondary remelting at the second stage. These two tectonic stages in the continental crust formation correspond with two different petrogenesis processes identified by V.M. Moralev and M.Z. Glukhovsky [199] from empirical data at a study of the Aldan shield rocks' structure and composition. The first is the formation of primordial basite crust at the expense of partial melting and differentiation of the mantle matter. The second is a partial (15–20%) material melting in the lower portion of the basite crust at 7–8 kbar, i.e., at a depth of about 25–30 km, with the release of silica and alkalis in amounts sufficient for the formation of the first in Earth history high-temperature low-potassium enderbites and tonalites, i.e., rocks of tonalite-trondhjemite series. Similar paragenesis is perhaps appropriate for some types of ancient anorthosites formed already at the third stage at the expense of secondary melt differentiation.

With the above considerations, the Archaean tectonic may be defined as the **tectonics of thin basalt slabs,** thereby underscoring its conceptual difference from customary present-day tectonic regimes of Earth evolution. Only in mid-Archaean, at the time of a sharp decline in Earth's tectonic activity about 3.2 BYa, had possibly begun forming conditions for emergence of structures like plate subduction zones. It is so far unclear, however, whether these structures had been materialized.

Thus, contrary to the process of the lithospheric plate tectonics unchallenged on Earth starting with Early Proterozoic, tectono-magmatic processes in Archaean had been evolving under different mechanisms, perhaps, close to those currently operating on Venus. Judging by radiolocation images of its surface, there are clearly identified rift zones there and semblances of mid-oceanic ridges but no structures similar to Earth's plate subduction zones. What is observed instead are zones of compression and pileup of crustal material with characteristic structures of small scales (tesseras) or extended ridges as if wrapping over large and hilly plateaus, analogs of Archaean continental massifs and shields. A characteristic formation on Venus' surface is, for instance, the merging area of Lakshmi Plateau with Maxwell Mountains (see Fig. 8.6). The boundary between these different structures is a sharp transition from the plateau plain elevated by 4–5 km above the average level of the planet to a steep slope of Maxwell Mountains reaching the elevation of 10–11 km and encircling the plateau from east and northeast. At this, within Maxwell Mountains in the ridge topography the slopes facing massif Lakshmi are often steeper than the opposite slopes, i.e., similar to what is shown in Fig. 8.5.

The described formation mechanism of Archaean crust is nothing new. Similar models at first approximation were mentioned in many publications [85, 190, 200]. What is important here is that the model of Earth tectonic evolution in Archaean reviewed here fairly describes many known patterns of Earth crust formation in that distant epoch. In particular, the

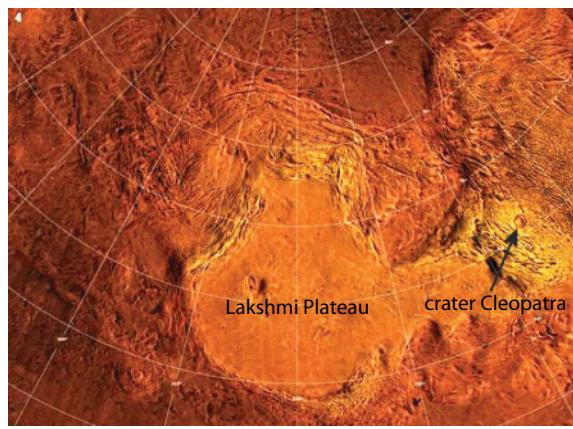

Fig. 8.6 Radiolocation image of Venus surface areas, at the merger of the Maxwell Mountains (an analog of thin basalt slabs pileup zones), with the Lakshmi Plateau (an analog of the continental massif). In the central right-hand part of the image is seen a large meteorite crater Cleopatra).

model perhaps correctly explains bimodality of magmatic rocks in the Archaean crust dominated by base (tholeiite basalts and komatites) and acidic rocks (granitoids of tonalite composition) with very much subordinated amount of medium volcanites (andesites). The model also explains the origin of the oldest Archaean migmatites – gray gneisses; mechanisms of the continental crust build up from the bottom by a granitoid material; a notable age difference between basaltoids and relatively younger granitoids in Archaean granite-greenstone belts. This model also explains the origin of granulite massifs formed at a depth of about 30 km but then floating to the surface as giant domes or overthrusting of lower stages of the crust on faults on Earth surface as well as broad occurrence in Archaean of migmatites and many other patterns in the evolution of Archaean crust.

8.3 The Continental Crust Growth

After the completion at the end Archaean of a tempestuous process of the release in Earth subsurface of oxide-iron core in which at that time had been concentrated up to 63% of the present-day core mass, the further tectonic regime of the planet evolution had become much more quiescent. A sharp decline in Earth tectonic activity in Proterozoic had resulted in an equally sharp increase in the lifetime and thickness of oceanic lithospheric plates (see Fig. 8.3). As a result, plate density had become higher than the mantle density and, as a consequence, pileup zones of thin basalt slabs, so typical for Archaean, had been replaced by normal plate subduction zones of a present-day type. Besides, about 2.5 BYa had substantially changed the composition and structure of oceanic crust and instead of purely basalt and komatiite Archaean oceanic crust had already formed in the beginning of Proterozoic its third, serpentinite layer, the major reservoir of bonded water in the oceanic crust. All these changes had resulted in firm establishment on Earth, starting in Proterozoic, of the evolution tectonic regime described by the theory of lithospheric plate tectonics.

Developed by the author theory of Earth global evolution enables the identification of major patterns in the continental crust growth. Let us assume that growth of the continental crust mass starting $4 \cdot 10^9$ years ago had been proportionate to generated in the mantle heat component of the total energy E_{mT} minus heat energy $\Delta E_{mT} \approx 3.2 \cdot 10^{37}$ erg accumulated in the mantle in Katarchaean as shown in Fig. 6.13

$$m_{\text{Ccr}} \sim E_{mT} - \Delta E_{mT}. \tag{8.1}$$

In our estimates we assume mass of the present-day continental crust after A.B. Ronov and A.A. Yaroshevsky [73]: $m_0 \approx 2.25 \cdot 10^{25}$ g.

The theoretical curve of continental crust growth based on this value is displayed in Fig. 8.7 in comparison with most popular model of its accumulation proposed by S. Taylor and S. McLennan [85] in consideration of geochemical data, estimates of deposit accumulation rate in the oceans and rate of absorption of these very deposits in plate subduction zones. As Fig. 8.7 shows, the theoretical curve of continental crust growth based on our geodynamic model (curve 1) very well matches the empirical model by S. Taylor and S. McLennan (curve *2*). As these models, although equal in the values of present-day continental crust mass, have been built based on different approaches using independent prerequisites and data but nevertheless resulted in similar outcomes, their fit with each other may be considered a testimony in favor of verity of both models. This is important as our theory of Earth tectonic activity certainly requires checks and proofs and included in Fig. 8.7 curve comparison is an example of such checking.

The continental crust formation rate is now easy to determine by differentiating Eq. (8.1) (i.e., curve 4 in Fig. 6.13). The result is presented in Fig. 8.8. As this diagram shows, in Early Archaean the crust growth rate had been relatively high, reaching almost $8 \cdot 10^{15}$ g/year or about 3 km^3/year. With time, it had been gradually declining due to descending Earth's matter zonal differentiation front in depth of the mantle. In mid-Archaean, about 3.3–3.2 BYa, during the period of a general decline in Earth tectonic activity (see Fig. 6.17) the rate of Earth crust formation had been also declining.

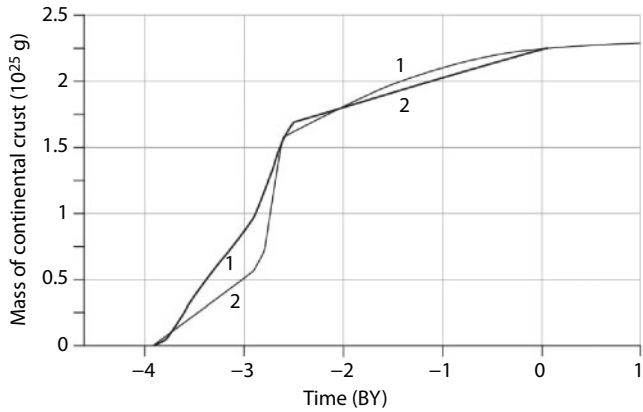

Fig. 8.7 Continent crust mass growth: 1. Our opinon; 2. Curve by Taylor and McLennan [85].

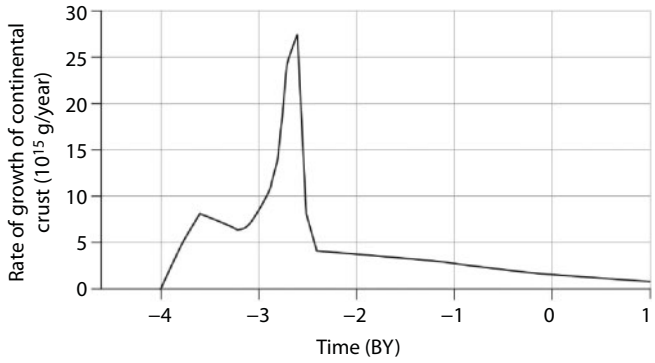

Fig. 8.8 Continental crust growth rate evolution.

It cannot be excluded that in this brief time interval which may be called the litho-plate period in Archaean crust evolution, in some places might have emerged typical for lithospheric plate tectonics geodynamic environments with normal plate subduction zones and island-arc calcareous-alkaline magmatism close to the present-day analogs. Along with this, at this very litho-plate period the formation of Archaean greenstone belts must have shrunk and instead might have emerged even some ophiolite nappes usual for Phanerozoic.

In Late Archaean, the continental crust formation rate had sharply increased at the expense of the transition from the metallic iron differentiation process to the separation of a eutectic alloy Fe·FeO and, the main thing, due to Earth core formation process begun at the end of Late Archaean (see Fig. 5.1). Based on the estimates, at the peak of Late Archaean splash up in Earth tectonic activity, the continental crust formation rate had risen to $27 \cdot 10^{15}$ g/year or 10 km^3/year.

The greenstone belts and associated with them granitoid diapirs' (intrusions') formation rate must have substantially increased in Late Archaean. These intrusions have often been enriched in potassium. At the same time must have significantly grown heat flows piercing the oceanic slabs and, as a consequence of this, increased the melt-out volume of komatiite lavas with simultaneous growth basicity of their composition. At that very time had sharply increased intensity of tectonic deformations clearly identified in the structure of numerous Late Archaean greenstone belts on ancient shields of practically all continents. At this, apparently for the first time in Earth history had been observed approximately synchronous, 3.0–2.9·BYa correlation of tectonic deformations and magmatic manifestations on most of the ancient shields (see Fig. 7.5).

However, tectonic regime of the continental crust formation must have reached the maximum stress only at the end Archaean, at the moment of Earth core separation catastrophic process evolution. Judging by geological data, this event had occurred between 2.7 and 2.6 BYa. It had been accompanied on all continents by practically simultaneous and very intense activation of all tectono-magmatic processes on Earth: the formation of huge area greenstone belts, the melt-out of giant volumes of granitoids among which a notable role had already played potassium granites (charnokites), the formation of strained fold deformations, etc. [85, 190, 195]. A major tectonic subsequence of Earth core separation process must have been the formation about 2.6 BYa of the first united supercontinent in Earth history, Monogea. In combination, tectono-magmatic formations of this age are manifestations of most ancient and most intense on Earth Kenoran or White Sea global diastrophism epoch. Exactly this process had resulted in the formation of a mosaic ensemble of Archaean age continental crust.

With the end of the young Earth core formation process about 2.5 BYa, Earth tectonic activity had declined in Early Proterozoic. Along with it, the formation rate of continental crust had also dropped to $6 \cdot 10^{15}$ g/year, or approximately 2 km^3/year. In Proterozoic and Phanerozoic, the rate of continental crust mass buildup had been continuing to decline – to $4.2 \cdot 10^{15}$ g/year 2.4 BYa. At present, based on estimates, it does not exceed $0.8 \cdot 10^{15}$ g/year (0.28 km^3/year). On average, in Phanerozoic it had been $1.4 \cdot 10^{15}$ g/year (0.5 km^3/year).

Having estimated Earth tectonic activity defined by the mantle heat flow, we may now estimate the average thickness of lithospheric plates underneath the ancient continents. It follows from solution of heat conductivity equation that the cooled down part of a hot semi-space pierced with heat flow q (in our case, the thickness of a lithospheric plate underneath the continents) is inversely proportionate to the value of coming from the mantle depth heat flow, penetrating such continents. We will assume that average thickness of the continental crust in Archaean had been no less than average crust thickness of the present-day Archaean shields, i.e., at least 40 km. On the other hand, theoretical estimates considering overheating of the upper mantle in Archaean and possible heat flows through the continental crust, show that the thickness of subcrustal lithosphere in Early Archaean had been varying between 15 and 23 km. In mid-Archaean, at the time of decreased Earth tectonic activity, it had increased to 40 km but in Late Archaean it had again dropped to 5–8 km (Fig. 8.9). Exactly for this reason, the staying height of continental shields above the ocean level during almost entire Archaean had been exceptionally high,

on average close to 6.5 km. This defines a high base level of erosion of practically all Archaean shields.

In Proterozoic, the continental lithospheric plate thickness had reached the depth of endothermal boundary of subcrustal lithosphere solid matter transition in the plastic state (see boundary III in Fig. 7.2). After this moment (about 2 BYa), the Precambrian continental lithospheric plate thickness, in consideration of average continental crust thickness of about 40 km, had practically stopped changing and remained at depth of about 240–250 km (see Fig. 8.9).

Due to a change in the continental crust melt out regimes in Proterozoic and cool down of the upper mantle after its overheating in Archaean, the continent stand level had substantially changed. A reminder: in Archaean, due to high heat flows under the continental crust, might not have formed thick and high-density lithospheric plates of mafic composition. As a result, Archaean continental massifs, as lighter formations, had towered high over average stand level of mid-oceanic ridges and the ocean surface. As opposed to Archaean, in Proterozoic and Phanerozoic, the upper mantle had substantially cooled down, and under the continental crust formed welded to it thick and high-density lithospheric plates (see Fig. 8.9) notably "inundating" the continental blocks. Simultaneously with this, due to a rise of the ocean surface level (see Fig. 10.6), under the Archimedes law had increased acting on continents' buoyancy in water. As a consequence of a balance of oppositely directed forces, average stand level of the continents above the ocean surface had been changing with time as shown in Fig. 8.10.

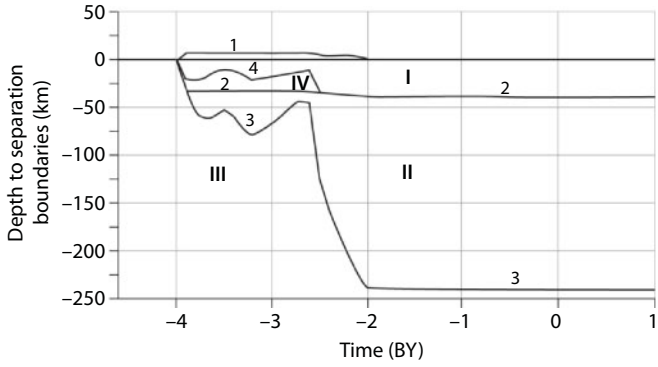

Fig. 8.9 Evolution of continental plate structure: I. Continental crust; II. Continental lithosphere; III. Sublithospheric (hot) mantle; IV. Lower, partially molten layer of continental crust; *1.* Surface of continents; *2.* Continental crust base (Moho boundary); *3.* Base of continental lithosphere.

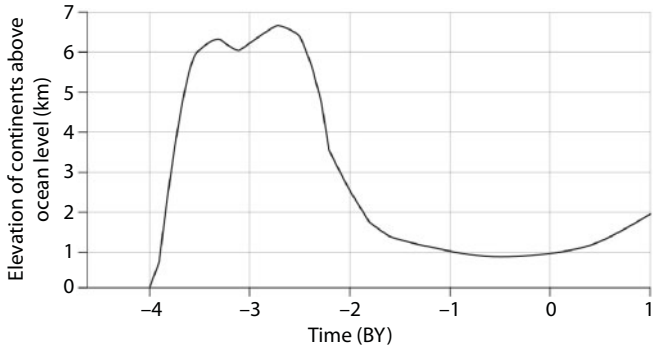

Fig. 8.10 Average continental massifs' stand level above rift zones in Archaean and above the ocean surface in Proterozoic and Phanerozoic.

By the present time, a significant part of the Archaean crust had already been denuded, and on the cratons' surface are exposed its most ancient and depth areas, often metamorphosed to amphibolite and granulite facies.

8.4 Major Features in the Composition of the Continental Crust in Archaean

A young and primitive continental crust might have existed only at the expense of remelting of the water-saturated basalts, i.e., might have had a tonalite and trondhjemite composition. Other crustal components simply might not have formed as young Earth still had not made it through the differentiation and had been composed of ultramafic primordial planet matter out of which, without a radical differentiation, might have melted out only basalts. For the emergence of more differentiated rocks, a deeper differentiation of Earth rocks had been needed or an addition to them of a new material with different geochemical properties. For instance, for the melt-out of granitoids very common in Archaean, had been absolutely necessary the addition of a sedimentary material that had made it through the stage of a preliminary weathering under diverse geodynamic conditions.

An important geological consequence follows from the estimates above. Due to a high continent stand and elevated erosion of their crust, large depositional masses should have accumulated in Archaean. However, very few Archaean deposits had been preserved. To where to had they vanished? Obviously, the major mass of deposits must have been accumulated on the oceanic plates (slabs) at the foot of continental massifs (see Fig. 8.5). However, the movement rate of oceanic slabs in Archaean had been

exceptionally high, reaching even a few meters per year; their "life time", on the contrary, had dropped to a few million and even few hundred thousand years (see Fig. 8.2). Exactly for this reason, clastic deposits had not had time to accumulate in large amounts at the foot of continental massifs and together with the oceanic slabs had been rapidly getting in overthrusting and piling up zones shown in Fig. 8.5. Subsequently, under the burden of the oceanic crust fragments newly thrust over, the entire packet of earlier piled up slabs with overlying deposits had again been immersing in a hot mantle. At this, sedimentary rocks had also been remolten, creating a tonalite-trondhjemite melts which in form of diapirs and huge granitoid crustal intrusions had invaded the continental massifs (see Fig. 8.5). Thus, a large part of Archaean deposits, due to the recycling processes, had converted in Archaean granitoids of the granite-greenstone belts, and their mass had been huge indeed.

A special attention should be paid to the origin of Late Archaean potassium granitoids which had somewhat pushed aside sodium granodiorites and granitoids of a tonalite-trondhjemite composition typical for the entire Archaean. An issue of the origin of this type granitoids from a geochemical position was minutely reviewed in the publication by S. Taylor and S. McLennan [85]. Accepting many of their conclusions, we will review this issue in terms of an Early Precambrian geodynamics model proposed here.

The mantle origin of major mass of these granitoids is supported by a low primordial ratio $^{87}Sr/^{86}Sr \approx 0.702$ to 0.703, only slightly exceeding the mantle level of that time (0.701 to 0.7015). The very fact of this excess might probably have been a result of a partial involvement in the processes of their melt-out of older crustal rocks (including Early Archaean Na-granitoids) with some addition of a sedimentary material [85]. The mantle origin of Canadian Late Archaean granites is also supported by the analysis results of their intrinsic Sm/Nd ratios. In such situation, a substantial enrichment of the Late Archaean granitoids with potassium, beside contamination with a crustal material, may be explained only by the melt-out of the corresponding sialic magmas from water-saturated basalts at great depths, possibly exceeding the transition level of basalt in eclogite or in the area of granulite facies' high pressure. For the development of such magmatic processes, naturally, specific tectonic conditions had been required.

Exactly in Late Archaean, in connection with the change in Earth matter differentiation regimes, had been observed a strong splash up of Earth's convective, therefore, tectonic activity (see Fig. 6.16). Simultaneously with this, about 2.7–2.8 BYa had been also occurring maximum overheating of the upper mantle with the temperature rise up to 1,800–1,850°C (see Fig. 5.5). Besides, due to a gradual water accumulation in the hydrosphere,

the oceanic surface in the course of almost entire Late Archaean had completely overlain the crests of mid-oceanic ridges and rift zones located in them, This, naturally, had resulted in a substantial water-saturation increase of basalts in Late Archaean oceanic crust. In fact, the hydration of oceanic basalts at that time had reached its maximum.

All that undoubtedly had to influence both the composition and the growth tempo of the continental crust being formed in Late Archaean. In particular, at that time, the lithospheric slabs' pile-up and clustering processes had to increase sharply. For this reason, the roots of pile-up structures at that time might have deeply immersed in a hot mantle and remolten there. Presently, the maximum existence depth in juvenile mantle melts does not exceed 80–100 km. However, in Late Archaean the mantle overheating had reached 400–500°C and a partial melting of the mantle matter had spread up to a depth of about 350–400 km. For this reason, if at that active time the roots of the oceanic slabs being piled-up, together with water-saturated basalts of the oceanic crust, had immersed to depths exceeding 80–100 km**,** the sialic magma melt-out might have been occurring at pressures allowing conversion of the basalts into garnet amphibolites, pyroxenites and eclogites. At this, the eclogites, as a heavy fraction, must have been descending in depths of the mantle carrying with them most of MgO, FeO, CaO, TiO_2 as well as any excess of Al_2O_3, thereby enriching the residual melts with silica and alkali [174]. It had also been a possibility that the silicate magmas engendering potassium granitoids had been subjected to an additional fraction differentiation with the separation at intermediate lower crust depths of Na-containing pyroxenes and amphiboles of the omphacite, jadeite and aegirine type. As a result, a light residual melt would have been mandatorily enriched in K_2O. Besides, the maximum hydration of the oceanic crust basalts had also caused sialic magmas' melt-out in that time lithospheric slabs pile-up zones in the presence of water. Water is the strongest mineralizer actively transferring into the melts all lithophilic (hydrophilic) elements, first of all, potassium, rubidium, uranium and thorium. In conditions of sharply increased heat flows and most stressed tectonic deformations in already formed continental crust, part of the crustal matter including deposits could have been getting again in the lithospheric slab pile-up zones and being again remolten there, going therewith through additional differentiation and enrichment with lithophilic elements. All this combined had obviously resulted in the formation in Late Archaean of the first continuous series of potassium granodiorites from granodiorites, monzonites to adamellites and genuine potassium granites.

The rare earth elements' distribution spectra observed in the major mass of Late Archaean potassium granitoids may serve as a confirmation of a great melt-out depth (Fig. 8.11). Thus, if granitoids had indeed been molten out at the existence levels of garnet lherzolites (garnets are known for being major concentrators of heavy elements in this group), then after the melts separation, the spectrum of rare earth elements in granitoids themselves must have been substantially impoverished in heavy rare earth elements. This is exactly what is observed in actuality: all Late Archaean granites have relatively high values of ratios La/Yb ≈ 20–30 whereas shallower depth Early Archaean and Proterozoic granitoids have lower ratios of La/Yb ≈ 5–10.

Here, however, attention should be paid to a fact that, despite Earth's tectonic evolution passing after Archaean under the laws of lithospheric plate tectonics, in Early Proterozoic had been occurring a sharp suppression or even almost total disappearance of calcareous-alkali (andesite) magmatism [201, 202]. Most likely, this had been associated with the specifics of Early Proterozoic oceanic deposits' composition as at that time a massive deposition of iron ore formations had been going on. Having gotten in plate subduction zones, heavy ferruginous deposits couldn't already be able to be squeezed out of the gaping between the plates and had played

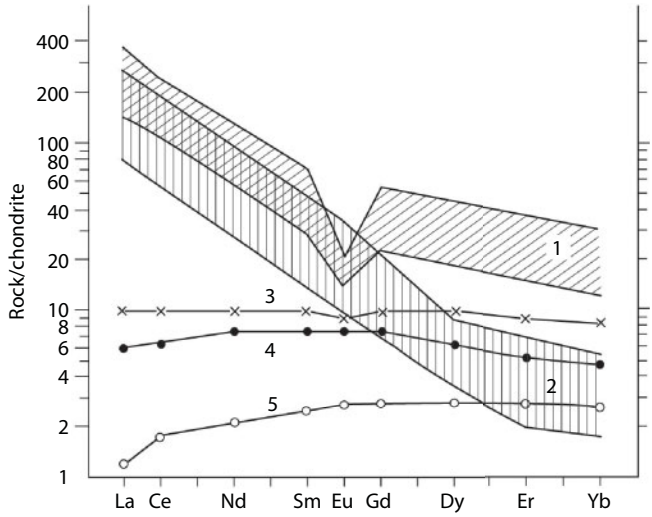

Fig. 8.11 Rare earth elements' distribution in Archaean rocks: *1.* Field of Early Archaean Na-granitoids; *2.* Field pf Late Archaean K– granitoids; *3.* Minesotta tholeite basaltsx *4.* Komatiites Onverwacht; *5.* Peridotite komatiites (after [85]).

there a role of a "lubricant" preventing thereby the heating and remelting base rocks of the subducted oceanic crust at the expense of its dry friction with the obducted plate. Exactly for this reason, the calcareous-alkali magmatism in the plate subduction zones in its present-day form had appeared only in Middle Proterozoic after weakening of the iron ore formations deposition processes.

Another distinctive feature in forming the continental crust composition in post-Archaean time had become melting-out of crustal magmas and running processes of regional metamorphism in conditions of excess of water coming from the plate subduction zones at dehydration there of the oceanic crust serpentinites. It was estimated that over the entire Proterozoic and Phanerozoic, through plate subduction zones had filtered about $2.3 \cdot 10^{25}$ g of water, which is approximately 16 times its mass in the present-day World ocean! This is a very important factor as water is a strong chemical reagent and mineralizer actively carrying in the continental crust all lithophilic and hydrophilic elements.

Altered conditions of the continental crust formation in post-Archaean time are clearly manifested in geochemical interrelations identikit rocks of different ages. Ya. Weizer data (1980) of changes in K_2O/Na_2O ratio in various ages crustal igneous rocks are demonstrative (Fig. 8.12) [453]. All Early Archaean igneous rocks indeed have typically basalt ratios $K_2O/Na_2O \approx 0.5$. In Late Archaean, these ratios had been gradually growing (in connection with the started melt-out of potassium granitoids). Especially rapid potassium accumulation in crustal rocks had been occurring in Early Proterozoic. At that time, a newly formed oceanic crust serpentinite layer had begun to be saturated with water. Already by the end of Early

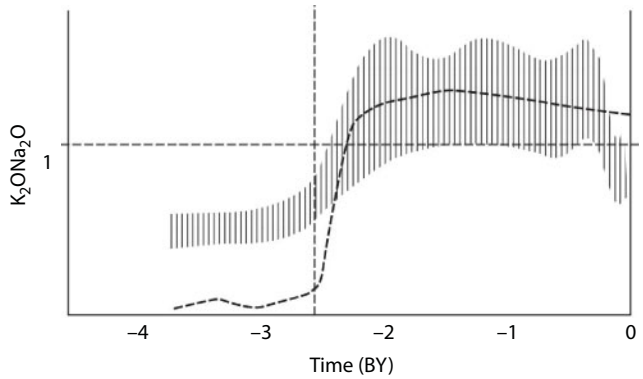

Fig. 8.12 Evolution of K_2O/Na_2O ratios in continental crust rocks (after [203]) compared with bonded water concentration curve in oceanic crust (dashed line).

Proterozoic, in connection with maximum saturation by that time with oceanic crust water, the ratios K_2O/Na_2O had reached the equilibrium value of 1.2–1.5. A local minimum of the subject ratios in Mesozoic, most likely, had been associated with a global marine transgression on the continents and, as a consequence, with the decline in crustal material supply in ocean and further on, together with the deposits, in plate subduction zones.

No less demonstrative are ratios of strontium isotopes $^{87}Sr/^{86}Sr$ in oceanic origin limestones (Fig. 8.13). This is associated with that in oceanic water occurs efficient averaging of continental rock isotopic marks, the rocks currently subjected to weathering and runoff with river water in the ocean. For this reason, the isotope composition of the deposits formed in equilibrium with water must reflect the isotope composition of the matter supply sources. In this case it is average isotopic composition of continental crust and oceanic basalts erupted in rift zones of mid-oceanic ridges.

As in the previous case, $^{87}Sr/^{86}Sr$ correlation in Fig. 8.13 demonstrably shows that in Early Archaean, primordial $^{87}Sr/^{86}Sr$ ratios in crustal rocks had been completely coincident with the mantle source. In Late Archaean, due to the melt-out of potassium granitoids and started recycling of crustal material (that had resulted in predominant accumulation in the crust of potassium and rubidium crust), the value of $^{87}Sr/^{86}Sr$ ratio in crustal rocks had increased somewhat. However, the contribution of this process in general composition of the Late Archaean crust had still remained insignificant and overall it, as previously, had had approximately mantle level of primordial $^{87}Sr/^{86}Sr$ ratio. Only beginning in Early Proterozoic, i.e., after the restructuring of Earth evolution tectonic regime, the $^{87}Sr/^{86}Sr$ ratios had risen sharply, marking thereby the accelerated accumulation in the crust of that time of rubidium, and therefore potassium. This had been

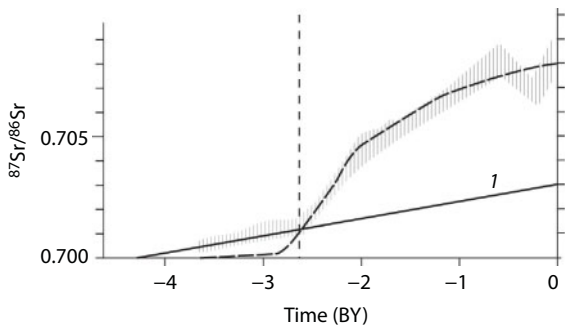

Fig. 8.13 Evolution $^{87}Sr/^{86}Sr$ ratios in oceanic deposits (after [203]) vs. age trend of these ratios in mantle rocks (*1*) and with bonded water concentration in continental crust (dashed line).

associated with the emergence of the oceanic crust serpentinite layer and, mainly, with the appearance of subduction zones in which had started to be pulled deposits washed off from continents.

The Archaean/Proterozoic boundary is the line of a sharp change in the trace element concentrations [85]. For instance, the ratio of summed up concentrations of the rare earth group elements' light portion and their heavy portion in fine-grained deposits had sharply increased approximately from 6 to 11. The ratio Th/Sc had grown from 0.4 to 1.1; La/Sc, from 1 to almost 3 and thorium concentration had risen from $1.5 \cdot 10^{-6}$ to $3.5 \cdot 10^{-6}$.

As the quoted examples show, geochemical indicators clearly mark the transition from Archaean to Proterozoic. Considering in addition to it tectonic factors as well as theoretical constructions quoted here, it may be stated today with great certainty that the nature of the most profound geological boundary between Archaean and Proterozoic had been associated with the completion of the dense core formation process in Earth's center. By that time, in Earth's core had been concentrated about 63% of Earth's present-day mass. At this, after the young core separation has happened, also a transition had happened from the endogenous Earth matter differentiation regime mechanism of iron and its oxides zonal separation to a more quiescent mechanism of their barodiffusion differentiation. The direct cause of drastic changes in geochemical and tectonic condition of Earth crust formation between Archaean and Proterozoic had been the passage from the thin basalt slab tectonics in Archaean to the lithospheric plate tectonics with subduction zones in Proterozoic and Phanerozoic. Due to the formation in Early Proterozoic of the oceanic crust serpentinite layer, water regime of the continental crust melt-out also had substantially changed. After Archaean it had begun forming in conditions of excessive overheated water fluids coming from plate subduction zones. A large role in the melt-out of crustal magmas, especially of granitoid and alkali composition, had begun playing at that time deposits pulled in the subduction zones.

8.5 Tectonic Regimes of the Continental Lithosphere Formation in Early Precambrian

We will now review tectonic regime specifics of the continental crust formation in Archaean. As the tectonic activity of Earth first had to manifest only in its equatorial zone, the first continental crust volumes, the oldest embryos of future continents, might have formed only in low latitudes. In Early periods of Archaean, when the front of Earth matter zonal differentiation had still been positioned at relatively shallow depths, 400 to

1,000 km, in the mantle overlying this front must have emerged only small convective structures. The horizontal size of these convective cells had not exceeded a few hundred, maximum 1,000 km. Therefore, several most ancient embryos of the continental crust (similar to Isua formation in West Greenland) might have simultaneously existed and evolved. Every one of them had been mandatorily positioned above the center of one of descending convective flows in the mantle (see Fig. 7.4 and 9.1).

With the deepening of Earth matter zonal differentiation front, the size of mantle convective cells must have increased and Earth tectonic activation belt must have expanded in the areas of higher latitude. As a result, already emerged by that time cores of future continental shields had increased in mass and had moved away from one another. The proposed model (Fig. 6.16) suggests that in mid-Archaean, about 3.2 BYa, must have been observed some quieting down of Earth tectonic activity. It is even possible that for a short time then, instead of pile-up and clustering zones of thin basalt slabs had emerged lithospheric plate subduction zones, as already mentioned above. If so, then in mid-Archaean the continental crust might for some time have been built up at the expense of island arc (andesite) magmatism. However, already in the beginning of Late Archaean, about 3.0 BYa had occurred a new and this time exceptionally strong activation of all tectonic processes.

Starting at this moment, all processes of the continental crust formation had sharply activated. Especially significant changes in the tectonic regimes of Archaean crust formation had occurred at the end of Late Archaean, 2.8–2.6 BYa, when in Earth subsurface had begun evolving a catastrophic process of Earth core formation (see section 5.1). This had resulted in the establishment in the mantle of a single-cell convective structure with exceptionally intense mantle matter flow directed from the equatorial zone of one planet's hemisphere to another one, antipodal hemisphere. As a result, at the end of Late Archaean all individual until this time continental massifs had begun tempestuously moving to the center of the descending flow at Earth equator, colliding with one another, substantially deforming and merging in a unified continental massif. Perhaps, that had been exactly the way Monogea, the first supercontinent in the history of our planet, had emerged (see Fig. 5.1-*e*).

If this had been so indeed, then at the end of Late Archaean, about 2.6 BYa, must have happened practically simultaneous deformation of almost all basalt slab pile-up zones (future greenstone belts) of end Archaean surrounding the continental massifs. Approximately at that very time, only with a small delay, must have occurred also most powerful granitization impulse accompanied by "squeezing out" (due to intense compression of

continental margins) of huge granitoid melt masses from under the pile-up zones of basalt slabs into the upper structural floors of a newly forming continental crust. According to K. Condie [190], that was how it had been in actuality. Fig. 7.5 clearly shows that the first certain correlation of the subject tectonic events had occurred practically on all Archaean continental shields only at the and Archaean, about 2.7–2.6 BYa.

The correlation of tectono-magmatic events in Middle Archaean is much weaker. Tectonic events of this period had been far from always synchronous on different continents. In Early Archaean, it is difficult to identify synchronous tectonic events on all continents as the Early Archaean continent embryos had been evolving to a large extent independently from one another, each of them had been positioned in a separate area of descending upper mantle flows' multi-cell convective structure. Considering latitude dependence of convective processes intensity in the Archaean mantle, the observed time difference in the manifestation of one or another tectonic event on different continents in Early Archaean and the first half of Late Archaean may be explained by different latitudinal positions of continental massifs already existing at that time.

A.S. Monin [172, 173] showed that under the laws of mechanics, the planet revolution becomes stable only at the time when the "center of gravity" of the supercontinent is positioned on its equator. If initially such a supercontinent formed in a different place, for instance, in high latitudes, then, affected by the inertia forces, the entire body of the planet would turn with respect to its revolution axis so that the "center of gravity" of such supercontinent would get on the equator. This means that the Monogea also had to be positioned on Earth's equator. Nevertheless, in Early Proterozoic, about 2.4–2.5 BYa, in all its expanses had occurred the first in Earth's history Huronian glaciation that had shown up simultaneously on several shields, in Canada, South Africa, India, West Australia and Baltic shield [204]. An explanation is that in Early Proterozoic, after the beginning of ultramafic rocks' hydration and formation of the serpentinite layer of the oceanic crust, bonding had happened in carbonates of a high-density carbon dioxide Archaean atmosphere and disappearance of the greenhouse effect. A consequence of this had been sharp climate cooling, with establishing of average for entire Earth temperature about +30°C (instead of +60 to +70°C in Archaean). The continent elevation stand above the sea level after Archaean, in the first half of Early Proterozoic still had remained relatively high, about 5–2.5 km (see Fig. 8.10 and 10.6). For this reason, the Huronian equatorial glaciation had been in substance a moderate climate Alpine glaciation [198], although costal glaciers might have perhaps crept to the ocean level.

Simultaneously with the crustal rocks' melt-out process in plate subduction zones and buildup of the continental crust, had always operated the opposite process of the continental crust denudation resulting in its erosion and the runoff of clastic sedimentary material in the oceans. After the completion of a full Wilson cycle in some specific ocean (from its opening to the total closing), the entire sedimentary material that had gotten in an oceanic basin would have eventually unavoidably been reworked again in plate subduction zones or crushed into folds, overthrust on the continental margins, consolidated and again welded with the continental crust. However, this process had been quite nonuniform. During the larger part of the cycle, the continents' denudation rate had substantially exceeded the buildup rate of the continental crust in plate subduction zones. Thus, based on the data about the present-day clastic material runoff [439], the total amount of a matter brought currently in the oceans, is approximately $25 \cdot 10^{15}$ g/year (about 10 km^3/year). At the same time, the present-day crust buildup rate in plate subduction zones is only 0.5–1.1 km^3/year [85]. A material brought from continents is mostly deposited in the continental slope zones and on shelfs [205], i.e., it continues to preserve connection with the continental crust and formally may be considered as its part. Whereas the fraction of pelagic deposits completely torn off the continental crust is just about $3 \cdot 10^{15}$ g/year, or equivalent of 1.1 km^3/year of crustal rocks. For this reason, present-day mass of the continental crust is currently rather decreasing than growing. In the end of tectonic cycles, at closing of the Atlantic type oceans, all previously accumulated on the bottom oceanic deposits turn out involved in the process of crust formation, crushing, granitization, metamorphism and consolidation. In such orogenic phases, the rate of crust formation sharply increases and its buildup becomes dominating. In Phanerozoic, this had been happening, for instance, at closing of the Paleo-Atlantic Ocean (Iapetus) in Caledonian time, Paleo-Uralian ocean in Hercynian epoch or Tethys ocean in Mesozoic and Cenozoic at the formation of the Alpine-Himalayan fold belt. According to our theoretical estimate, the continental crust's mass buildup, averaged in timescale on the order of 1 BY, at present is still positive, approximately $0.65 \cdot 10^{15}$ g/year (0.26 km^3/year).

As a result of averaging the continental crust formation effects over various phases of this process and assuming the total return (recycling) of the sedimentary material in the crust in about 800 MY, it is possible to suggest that until now the continental crust growth balance remained positive. Moreover, until the middle of Phanerozoic this condition apparently had been practically completely realized. In the future, due to a decline in Earth's tectonic activity, the balance between deposit accumulation in the

oceans and their recycling in the crust formation processes will have to be ever more broken. This will facilitate also an increase of the dry land basis of erosion as average ocean stand level in the future will be progressively becoming lower (see Fig. 10.6). For this reason, in the future, especially after almost total fading of Earth's tectonic activity, the consolidated continental crust mass will only have to decrease.

Thus, as Fig. 8.8 shows, under our Earth's tectonic activity model, the continental crust formation had been occurring at the highest rate in Late Archaean. Thus, most of the present-day crust mass (around 70%) had been formed by the end Archaean, i.e., already 2.6 BYa. At this, in Early Archaean, within 800–600 MY (4.0–3.8 to 3.2 BYa) only 20% of the crust had emerged and in Late Archaean, approximately during an equal time duration (3.2 to 2.6 BYa) had been formed approximately 50% of the crust. In the entire remaining longest Earth history (in 2.6 BY) had been formed about 30% of the crust and during the recent part of Phanerozoic (about 600 MY), only slightly over 3% (considering the deposits recycling). In the future, the continental crust growth will have stopped and a phase of irreversible destruction will have onset, although it will have occurred in a very distant future.

In connection with a change in the continental crust melt-out regime in Proterozoic and the upper mantle cooling after its overheating in Archaean, the continent stand level had substantially changed. A reminder: in Archaean, due to high heat flows under the continental crust might not have formed thick and high-density lithospheric plates of ultramafic composition. As a result, Archaean continental massifs, as lighter formations, had towered high over average stand level of mid-oceanic ridges and ocean surface. Contrary to Archaean, in Proterozoic and Phanerozoic the upper mantle had notably cooled down, and underneath the continental crust had formed welded to it thick and high-density lithospheric plates that had substantially sunk the continental blocks. Simultaneously with this, due to a rise of the ocean level surface (see Fig. 10.6), under the Archimedes law had grown acting on continents water buoyant lift. As a result of the balance in oppositely directed forces, average continent stand level over the ocean surface had been changing it time as this shown in Fig. 8.10.

In connection with the tectonic regime change of the oceanic crust conversion in the continental, in post-Archaean time the very process of the continental crust formation had cardinally altered. The area-wide crustal magmatism of mostly tonalite-trondhjemite composition had been replaced by emerged in the oceanic crust pile up zones calcareous-alkali magmatism of linear plate subduction zones. The granitoid formation processes had also changed. In the post-Archaean time they, as a rule, had been formed from crustal matter sources and mostly, perhaps, either at the expense of a repeated

remelting of clastic sandy-clayey deposits pulled into plate subduction zones or due to metamorphic reworking of sedimentary sequences in the rear of the plate subduction zones by overheated fluids as this is shown in Fig. 8.29.

8.6 Early Pre-Cambrian Continental Lithosphere Formation Mechanisms

As shown earlier, high heat flow in Archaean had resulted in existence in the mantle of mostly heat convection which, in view of small thickness of mantle lenses at that time, had had finely meshed structure organized under the principle of Benard cells (see Figs. 7.4 and 8.14). At this, above the descending convective flows in the mantle had occurred piling-up of such thin basite plates and their sinking in the hot mantle where they had partially melted again thereby engendering granitoids of future continent embryos (see Fig. 8.5). Most favorable for this apparently had been the joining areas of the Archaean mantle convective cells which in turn had defined their isometric, sometimes even close to polygonal shape (Figs. 8.15 and 8.16).

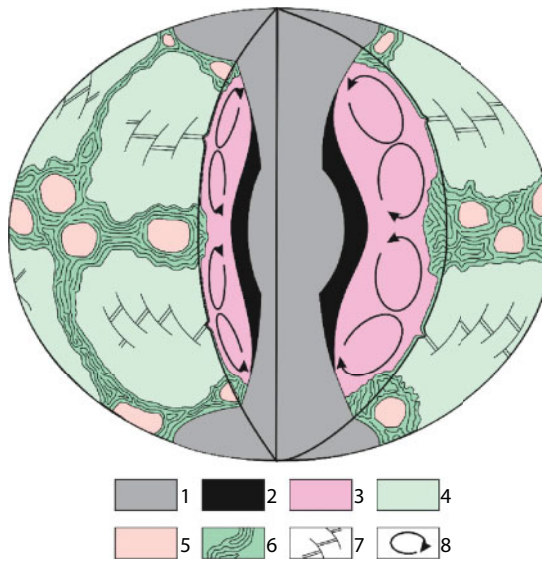

Fig. 8.14 Volume model of Earth's structure in Middle Archaean. 1. Primordial Earth matter; 2. iron and iron oxide (core matter) melts; 3. Depleted mantle impoverished in iron, ero oxides and siderophile elements; 4. Crust of proto-oceanic type; 5. Continental crust; 6. Pile-up areas of proto-oceanic crust; 7. Mid-oceanic ridges; 8. Direction of convective flows in the mantle. (The Figure scale substantially distorted for illustrative purposes.)

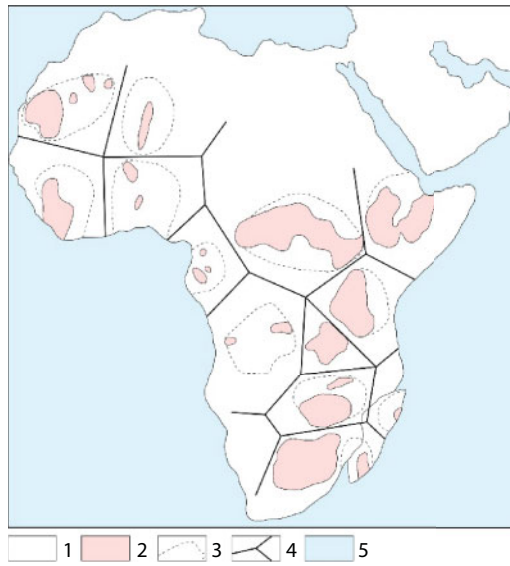

Fig. 8.15 Spatial placement of Archaean age continental micro-plates in Africa [454]. 1. Continental lithosphere; 2. Surface exposures of Archaean rocks; 3. Outlines of Archaean massifs; 4. Generalized strike of Late Archaean and Lower Proterozoic age mobile belts; 5. World ocean.

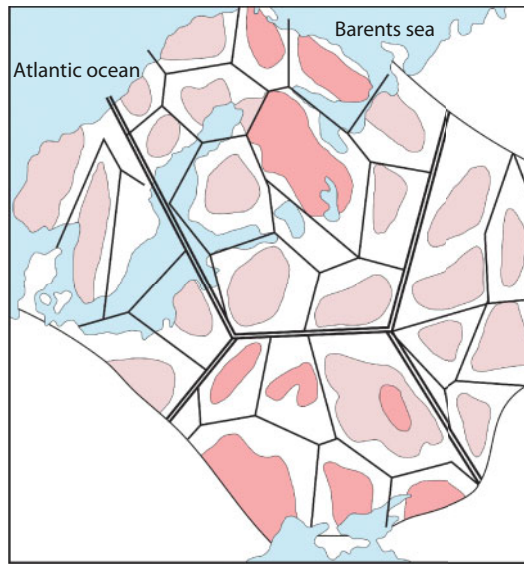

Fig. 8.16 Location scheme of Archaean age continental plates of the Russian plate [454]. Solid, single and double lines are generalized strikes of Archaean and Lower Proterozoic age mobile belts.

So obvious apparent similarity in the configuration of individual crust domains with Benard cells may be a result of a rather simple pattern: these domains had indeed emerged above the descending flows of Benard type convective cells (Fig. 7.4 and 8.14). It should be noted that the described similarity is typical of both large crustal segments as a whole and of their component domains. This, for instance, may be observed within the Russian plate (Fig. 8.16) and in Baltic shield's Karelian granite-greenstone area (Fig. 8.17), which is its composite part. Within the latter, axes of greenstone structures form two polygonal segments clearly separated in space and different from one another in age.

Continental crust formation above the descending convective flows in the mantle had resulted in the emergence of small continental plates whose

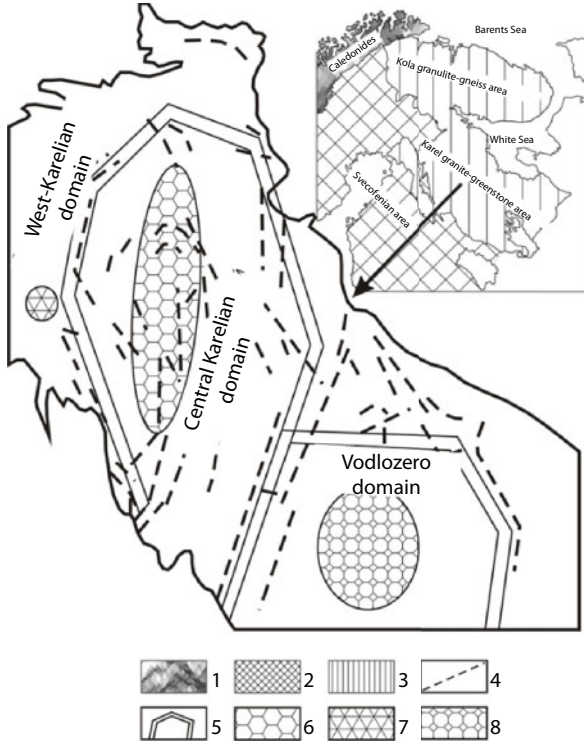

Fig. 8.17 Schematic map of Archaean greenstone structures in Karelian granite-greenstone area and Vodlozero domain. Insert is a position scheme of heterochronic continental crust areas in the central and eastern Baltic shield: 1. Paleozoic, 2. Early Proterozoic, 3. Archaean, 4. Greenstone belts axes, 5. Boundaries of identified polygonal structures; 6–8. Heterochronic cores of the continental crust (Early Precambrian..., 2005); 6. Continental crust area with age 3.0–2.9 BY; 7. Continental crust older 3.1 BY; 8. Continental crust ≈ 3.1 – 3.5 BY old.

evolution had been occurring in relatively detached from one another places up until Late Archaean [17, 50, 85]. Remarkable is a fact that continental formations 3.8–3.2 BY-old do not carry any noticeable traces of a collision interaction with one another. Only in rare cases intense collision processes with the age of about 3.5 BYa are noted [190]. This phenomenon is easily explainable considering that intense heat convection had been materialized in form of Benard cells which are quite stable in space and time. Embryos of the continental crust being formed at that time had to be disconnected and their lateral drift on Earth surface had been out of the question. The available facts of lateral motions at about 3.5 BYa, as well as in the other epochs, as was discussed earlier, may indicate spasmodic enlargement of the Archaean mantle cellular structure and the result of its spatial expansion (see Fig. 7.4).

Modeling processes of the continental crust-formation in Early Precambrian enabled the identification and substantiation of structural nonuniformity of the Archaean continental lithosphere [175, 195]. As will be shown later, a powerful heat flow through the continental crust must have resulted in the emergence and long-time existence in the lower crust of expansive zones of a partial substrate melting. The thickness of these zones might have reached 20–30 km at a total thickness of the crust close to the present-day one (about 40–45 km). Thus, the continental lithosphere in Archaean had been a macro-laminated system of different in physicochemical parameters media regularly positioned in space.

The upper position had belonged with a rigid crystalline crust layer; below it had been a highly plastic lower crust layer. Lower yet there had been a layer of a relatively rigid and completely crystallized subcrustal lithosphere sitting on a partially molten substrate of the mantle asthenosphere [206]. This structure of continental lithospheric plates had been appropriate only for Archaean and is completely different from its present-day status.

Based on all the aforementioned, it is reasonable to attempt considering the effect of Earth tectonic activity and of depth heat flows on the evolution in the structure of continental lithospheric plates and on particulars of their formation in Early Precambrian.

To simplify the model, it is possible to disregard the duration of the formation process of any continental crust areas and to consider its thermal history only since the moment t_0 marking the end of the crustal matter release process. We will also assume that after its formation, the continental crust thickness had changed little and on average remained close to $H_{cc} \approx 40$ km [85]. Besides, we will assume that starting with the moment $t > t_0$, underneath a newly emerged continental crust embryo was beginning to form a rigid subcrustal lithosphere separating the crust from the

direct contact with the hot mantle. The lithosphere formation had been occurring due to cooling and complete crystallization of a partially molten mantle matter. In this case, the lithosphere thickness H_l and the position of its base had been defined by crystallization (solidus) geotherm T_s of the mantle matter.

For the determination of heat regimes of Earth crust existence and lithospheric plate formation it is necessary to solve the heat conductivity equation substituting in the general solution the boundary condition corresponding with geodynamic environments that had existed in the past geological epochs. At this, in the simplified plate model assumed by us may be used a single-dimensional approximation for a horizontally laminated medium. In this case, the heat conductivity equation has its simplest form

$$\rho \cdot c_p \frac{\partial T}{\partial t} = \frac{\partial}{\partial Z}[\lambda \frac{\partial T}{\partial Z}] + \Theta \tag{8.2}$$

where $T(z,t)$ is medium temperature; ρ is medium density; c_p is the matter heat capacity at permanent pressure; λ is heat conductivity; Θ is volume density of radiogenic heat sources in the medium; t is time; Z is the vertical coordinate directed down from Earth's surface.

As we assumed a horizontally laminated representation of the medium, we will be searching a solution for Eq. (8.2) individually for each identified layer. At this, it is possible to consider within such layers the values of definitive parameters ρ, c_p, λ, Θ to be constant. If we also disregard temperature jumps at phase transition boundaries in the convecting medium (at low rates) then it is possible to perform sewing together separate particular solutions in the general one. We will also assume that within the layer containing radioactive elements:

$$\Theta = q_R / h_R \tag{8.3}$$

where q_R is the heat flow created by the decay of radioactive elements at the top of the layer; h_R is the thickness of this layer.

The correlation temperature $T(z)$ vs. depth in Eq. (8.2) may be determined from its stationary solution $\partial T/\partial t = 0$ considering also that the laminated medium, beside radiogenic heat flow, is also penetrated by a depth (subcrustal) heat flow q_m. At that time, the total heat flow on the crust surface at $Z = 0$ is equal to

$$q_0 = q_m + q_R \tag{8.4}$$

In this case it is easy to determine that the temperature at depth Z at $Z \leq h_R$ is equal to:

$$T = T_0 + \frac{q_m}{\lambda} \cdot Z + \frac{q_R}{\lambda}[Z - \frac{Z^2}{2h_R}] \tag{8.5}$$

where T_0 is Earth's surface temperature. At $Z \geq h_R$, the stationary crust temperature is determined from equation

$$T = T_0 + \frac{q_R}{\lambda} \cdot \frac{h_R}{2} + \frac{q_m}{\lambda} \cdot Z \tag{8.5'}$$

Whereas the temperature at the crust base (or at the top of the lithosphere) is equal to:

$$T_0^{cc} = T_0^l = T_0 + \frac{q_R h_R}{2\lambda} + \frac{q_m}{\lambda} H_{cc} \tag{8.5"}$$

where H_{cc} is the crust thickness.

Radioactive element distribution in Earth is quite nonuniform (see Chapter 6). Thus, radioactive element contents in the present-day mantle is so small that their energy contribution in the mantle depth heat flow does not exceed 10% [17]. For this reason, at solving Eq. (8.2) for the medium subcrustal layers, subcrustal lithosphere and convecting mantle may be assumed $q_R \approx 0$ (at this, the radiogenic heat contribution in the mantle will be indirectly included in the flow $\tilde{q}_m$). The distribution of radioactive elements in the continental crust is also very nonuniform, most of them, most likely, are concentrated only in the upper crust layer [85, 139]. Indeed, should the concentration of radioactive elements in the continental crust have been uniform and equal to near-surface levels, the surface heat flow on the ancient continents would be at least double the observed one.

Considering this, we will assume that the entire significative radioactivity of the continental crust is concentrated only in its upper layer, h_R thick. For the remaining layers in the section we will assume $q_R \approx 0$ at $q_m \neq 0$. In this case, the general solution of Eq. (8.2) for the subcrustal lithosphere may be expressed in the classical form like, for instance, in [207]. Then, for the depth interval $H_{cc} \leq Z \leq H_{cc} + H_l$, where H_l, is the subcrustal lithosphere thickness, we find

$$\left[T - T_0^l - \frac{\tilde{q}_m}{\lambda} \cdot \left[Z - H_{cc}\right]\right] = \left[T_m - T_0^l - \frac{\tilde{q}_m}{\lambda} \cdot \left[Z - H_{cc}\right]\right] \cdot erf \frac{\left[Z - H_{ccf}\right]}{2\sqrt{at}} \tag{8.6}$$

where $erfx = \frac{2}{\sqrt{\pi}} \cdot \int_0^x e^{-\xi^2} \cdot d\xi$ is the error range; $\tilde{q}_m$ is heat flow coming from the depth convective mantle; a is heat conductivity factor; T_m is the mantle temperature at depth Z. Then the stationary solution of the heat conductivity equation (8.2) may be written in the following form

$$T - T_0^l = \frac{\widetilde{q_m}}{\lambda} \cdot \left[Z - Hcc\right] \tag{8.7}$$

The temperature distribution in sub-lithospheric mantle will not be possible to determine by a simple solution of Eq. (8.2) as it depends on the structure of convective flows in the mantle and especially on parameters of the boundary layers emerging underneath the lithosphere. That is where is generated most of heat flows $\tilde{q}_m$ (at the expense of viscous friction energy dissipation in the deformed mantle matter).

If temperature in the lower crust nowhere exceeds the melting temperatures of it rock solidus, i.e., $T_0^l < T_s^{cc}$ and the matter of this layer preserves its effectively rigid state, then temperature at the crust base (i.e., top of the subcrustal lithosphere) is determined from Eq. (8.5"). However, if $T_0^l \geq T_s^{cc}$, then in partially molten (migmatized) lower crust rocks with the thickness H_2^{cc} unavoidably should emerge heat convective movements with establishing of temperature distribution close to adiabatic

$$\frac{dT}{dZ} = \frac{\alpha \cdot g}{C_p} \cdot T \tag{8.8}$$

where g is gravity acceleration; α is volume expansion factor; C_p is heat capacity of the crustal rocks. Then:

$$ln \frac{T_0^l}{T_s^{cc}} = \frac{ag}{C_p} H_2^{cc} \tag{8.8'}$$

where T_s^{cc} is temperature of the crustal rocks' solidus at the boundary of the upper and lower crust (at depth e H_1^{cc}).

With real parameter values in Eq. (8.8') $g = 981$ cm/s^2; $\alpha \approx 3 \cdot 10^{-5}$ deg^{-1}; $c_p \approx 1.2 \cdot 10^7$ erg/g·deg and $H_2^{cc} \approx 25$ km, the adiabatic distribution temperature changes little in the depth interval of the lower crust, i.e., $T_0^{cc} \approx T_s^{cc}$. However, the temperature T deflection from its adiabatic distribution (8.8) in the lower crust convecting layer may be estimated based on Rayleigh criterion

$$R_a = \frac{\alpha \rho g \Delta T (H_2^{cc})^3}{a} \tag{8.9}$$

where η is crustal rocks viscosity after beginning of their melting. For the emergence of a noticeable convection is necessary for the Rayleigh number $R_a \geq 1{,}500 \div 2{,}000$. Therefore, for the existing of a stable heat convection in the lower part of Archaean crust must be fulfilled conditions

$$\Delta T \geq 2 \cdot 10^3 \cdot \frac{a \cdot \eta}{\rho \cdot g \cdot \alpha \cdot (H_2^{cc})^3} \tag{8.9'}$$

Assuming ideal viscosity of partially molten (migmatized) rocks in the lower crust equal $\eta \approx 10^{18}$ poise (П), we find that for the emergence of heat convection in this layer is necessary for the super-adiabatic temperature difference at its surface to exceed just 9°C. At a lower viscosity, such difference becomes even smaller, and temperature distribution in the layer approaches the rule (8.7), i.e., becomes practically isometric at the level $T \approx T_s^{cc}$.

However, the reasoning above envisions the instantaneous temperature levelling in the crust at its increasing or decreasing in the area of heat generation, i.e., in the mantle. If temperature of the medium sharply increased for some reason, the establishing of a stationary temperature distribution in the crustal astheno-lens might have turned impossible. The heat removal through the external crust shell is proportionate to some average value of temperature difference T-T_0 in the crustal astheno-lens and the external medium regardless of the heat release nature within it. For this reason, if temperature of the medium had been increasing sufficiently rapidly in Archaean crust, then operating at this this moment certain type of heat removal (for instance, convection) may have been insufficient for achieving the system equilibrium. At such time in an individual crustal block might have occurred a heat "explosion" expressed as breaking the rigid crystalline layer of the crust and instantaneous heat release from the area of heat generation (upper mantle) in the atmosphere. Naturally, temperature

rise in the mantle in Late Archaean might not have resulted in an instantaneous heat regime reaction in the entire lower crust layer and must have been occurring with some delay. A qualitative estimate of a time interval needed for levelling may be found with the help of a dimensional relationship proposed by V.N. Zharkov [109] $\Delta t \sim \frac{(\Delta L)^2}{a}$ where ΔL is the distance between the heat source and the observation point, a is heat conductivity factor ($5 \cdot 10^{-3} cm^2/s$). Assuming the thickness of the crustal asthenosphere convecting layer at 20–30 km, it is easy to find that $\Delta T \sim 25 \cdot 10^6 - 50 \cdot 10^6$ years.

However, such kind of a process might have occurred only near the ascending convection flow within the crust and resulted in overheating of its lower layer matter. Overall, due to the process of convective stirring, average temperature at the base of the continental crust might have been close to 600°C. This conclusion does not rule out at all that in the crust's lower portion might have existed broad areas of more heated matter.

The granitoid series' aluminosilicates with low contents in them of bonded water in conditions of elevated pressures $p > 2–3$ kbar begin melting already at temperature about 600–650°C [208]. At this, the matter viscosity under the Arrhenius law sharply declines. If we assume that at temperature about 400°C continental crust rocks practically maintain their rigidity with effective viscosity on the order of $10^{23} - 10^{24}$Π, their viscosity at T ≈ 600°C would have sharply declined to the values $10^{16} - 10^{17}$Π. In this environment, in the lower crust unavoidably had to emerge convective flows removing heat excess from the lower crust base to the base of the upper crust layer. Indeed, according to Rayleigh criterion (Eq. 8.9), the convection emerges even at relatively small superadiabatic temperature differences $\Delta T \approx 10$°C and in relatively thin layers ~10 km, saying nothing about the entire lower crust with thickness of up to $H_2^{cc} \approx 25-30$ km.

The thickness of underlying Archaean subcrustal lithospheric layer may be determined using the condition $Z–H_{cc} = H_l$ at $T = T_s^l$, where H_l is thickness of the lithosphere; T_s^l is temperature of the mantle lithospheric matter solidus. At that time

$$[T_s^l - T_0^l - \frac{\tilde{q}_m}{\lambda} \cdot H_l] = [T_m - T_0^l - \frac{\tilde{q}_m}{\lambda} \cdot H_l] \cdot erf \frac{H_l}{2\sqrt{at}} \qquad (8.10)$$

where $\tilde{q}_m$ is the depth heat flow coming to the base of the lithosphere from the sub-lithospheric convecting mantle. At this, the stationary solution of Eq. (8.10) defining maximum thickness of the subcrustal lithosphere is

$$T_s^l - T_0^l - \frac{\tilde{q}_m}{\lambda} \cdot H_l = 0 \qquad (8.10')$$

A heat flow generated by the cooling lithosphere is defined by a derivative with respect to Z of the function $T(z,t)$ defined by Eq. (8.2) at $Z - H_{\kappa\kappa} = 0$

$$q_m = q_l + \tilde{q}_m = \lambda \cdot \frac{[T_m - T_0^l]}{\sqrt{\pi \cdot a \cdot t}} + \tilde{q}_m \qquad (8.11)$$

The (8.10) solution is derived on an assumption of a constant depth heat flow $\tilde{q}_m$. Nevertheless, under real conditions this heat flow had substantially changed. However, considering that such changes had been occurring quite slowly (compared with the changes in vertical temperature gradient), this solution may be used but only as an approximate one. Due to slow changes of $\tilde{q}_m$, stationary regime of the lithosphere (8.10') may have been established over a finite time. If at this $T_s^l - T_0^l - \frac{\tilde{q}_m}{\lambda} \cdot H_l < 0$, then the subcrustal lithosphere would have begun gradually melting from the bottom and getting thinner until a new equilibrium had occurred at a greater value of the heat flow $\tilde{q}_m$ and smaller thickness of the lithosphere H_l. The approximate heat flow value at this maintains the format of Eq. (8.11).

Beside the heat flow associated with cooling of the lithosphere, its formation had been accompanied also by a release of the latent heat of melting (crystallization) of the lithospheric matter

$$q_s = \mu \cdot \vartheta \cdot \rho_l \cdot \frac{dH_l}{dt} \qquad (8.12)$$

where μ is partial melting of the sub-lithospheric hot mantle; ϑ is the latent heat of melting lithospheric (mantle) matter; ρ_l is density of the lithosphere; dH_l/dt is rate of the crystallization front movement at the base of the lithosphere. The amount of a heat flow associated with the release of the mantle matter crystallization latent heat is relatively small and the patterns of this flow change in time are completely coincident with changes of the flow q_l determined from Eq. (8.11). Taking this into consideration as well as an approximate nature of major heat physical process parameters (λ, a, μ, and ρ) determinations, at the first approximation, the effect of composite q may be disregarded (indirectly, its effect is taken into consideration in the flow associated with the lithosphere cooling q_l).

The solutions (8.6) and (8.10) remain valid also at the time when $T_m(z)$ and $T_s^l(z)$ are linear functions of depth. This allows as the first approximation to consider real correlations of the boundary temperature vs. depth. At present, the total thickness of lithospheric plates (crust + subcrustal lithosphere) on ancient continental platforms apparently is equal approximately to 220–250 km and is possibly marked by the Lehmann seismic boundary [17]. If we disregard heat effects associated with polymorphic phase transitions in the mantle matter, then temperature distribution in convecting mantle must obey the adiabatic Eq. (8.8). In this case:

$$T_m = T_m^0 \exp\left[gaZ / C_p \right] \tag{8.13}$$

where T_m^0 is mantle temperature normalized for the surface. $T_m^0 \approx 1{,}300°C$; g is 981 cm/s^2 and the ratio $\alpha/c_p \approx (5.16–4.77)\cdot 10^{-12}$ g/erg [187]. Then we find that at depth 200 km ($2\cdot 10^7$ cm) the mantle temperature must have reached T_m = 1,461°C and at depth of 220 km T_m = 1,477°C.

However, starting at surface and to the depth of 220 km, the mantle matter experiences at least two polymorphic transitions: from plagioclase to pyroxene and garnet lherzolites. At every transition, in the convecting mantle should occur a positive temperature leap

$$\Delta T = W / c_p \tag{8.14}$$

where W is exothermal phase transition per unit heat. After A. Ringwood [50], densities of the plagioclase, pyroxene and garnet pyrolith (close in composition to lherzolite) at normal pressure and temperature are respectively $\rho_1 = 3.26$; $\rho_2 = 3.33$; and $\rho_3 = 3.38$ g/cm^3, whereas at sub-solidus temperature, the phase transitions occur at pressure P about 7.5 and 25 kbar. Considering that $W = \Delta V \cdot P$, where ΔV is volume effect of the phase transitions, it may be determined that temperature leaps at these levels are respectively 4 and 9°C.

Thus, in consideration of phase transitions heat effects, the mantle temperature at depth of 220 km may reach 1,500°C, and that was accepted for the estimates. At that time, the correlation of $T_m(z)$ sought for may be written in the following format

$$T_m = T_m^0 [1 + 7 \cdot 10^{-9} Z] \tag{8.15}$$

Unfortunately, as of today there are no reliable direct determinations of thickness for present-day lithospheric plates under ancient continents.

Perhaps, this is due to transparence for seismic waves and other geophysical fields of the transition boundary from the rigid lithosphere underneath the continents to its underlying viscous convecting mantle. As opposed to a simple physical model of the oceanic lithosphere as rigid holocrystalline plate sitting on a plastic layer of partially molten mantle matter, the transition nature of the continental lithosphere in its underlying plastic mantle is more difficult to define unambiguously. A possible nature of such transition was reviewed in section 7.2 and a position of the continental lithosphere's lower boundary in the section is shown in Fig. 7.2 (boundary III).

In connection with this, it is possible to assume that at a given temperature, polycrystalline silicates acquire properties of effectively viscous liquids only in a case when the external pressure exceeds the long-term strength of intercrystaline bonds in the matter. Usually, the long-term strength of polycrystalline materials is approximately by one order of the magnitude lower than their instantaneous modulus of rigidity [109]. At that time, by the rate of shear wave advance in the upper mantle at depths about 220 km ($U_s = \sqrt{\mu / \rho} \approx 4.6$ km/s) it may be determined that such critical pressures of ~70 kbar are currently reached at depths about 220–250 km (see Fig. 7.2). The maximum thickness of continental lithospheric plates of 220-250 km is supported also by petrological determinations of maximum depth of formation of the mineral associations in depth xenoliths of diamond-bearing kimberlites.

Thus, the entire multitude of the quoted considerations and data enables us to maintain with sufficient certainty that the lithospheric plate thickness underneath ancient continental massifs is within the range of 200 to 250 km and on average may be assumed at 220 km. It follows from this that in the existence area of mantle melts at depths to 100 km it is possible to use the classical definition of the lithosphere and to consider that its base's position is defined by the temperature of mantle matter solidus T_s^l. At greater depth it is allowable to use only the concept of its effective thickness keeping in mind that the depth to its base is defined by the temperature of mantle matter transition from the solid to viscous-plastic state. For a depth of 220 km the effective value of this temperature may be assumed at $\tilde{T}_s^l \approx 1{,}450 - 1{,}460$°C, at $T_m \approx 1{,}500$°C. In this case, averaged correlation of $\tilde{T}_s^l$ (z) at first approximation of the linear function may have the following format:

$$\widetilde{T_s^l} = T_s^0 \left[1 + 17 \cdot 10^{-8} \cdot Z \right] \tag{8.16}$$

where $T_s^0 \approx 1{,}060$°C is temperature of the mantle matter solidus on Earth's surface.

We will now review the evolution of depth heat flow $\tilde{q}_m$ and radiogenic heat flow $\bar{q}_R$ coming through continental lithospheric plates. The depth flow $\tilde{q}_m$ is proportionate to the mantle heating, i.e., the temperature difference $T_m^0 - T_s^0$. It may be assumed that the solidus temperature T_s^0 had been little changing with time and on average had been 1,060°C. Whereas the normalized to the surface mantle temperature T_m^0 in the course of Earth's geological history had been changing quite substantially (see Fig. 5.5). These changes, most likely, had been caused by the process of metallic iron zonal differentiation that had been going on in Early and Middle Archaean (see section 5.3). As Fig. 5.5 indicates, the upper mantle surface temperature in Early Archaean had exceeded 1,500°C, by mid-Late Archaean it had risen to 1,700°C, then, at the boundary of Archaean and Proterozoic had rapidly declined to 1,400°C and presently is 1,300 – 1,320°C. The Archaean mantle overheating, in particular, is an explanation of abundant komatiite lavas in greenstone belts of Late Archaean.

It is possible to determine the proportionality coefficient in $\tilde{q}_m \sim [T_m^0 - T_s^0]$ by inputing the present-day value of the depth heat flow $\tilde{q}_m$. For that, however, it is necessary to know initially the temperature at the top of the subcrustal lithosphere T_0^l (or, which is the same, at the base of Earth crust T_0^{cc}). According to Ya.B. Smirnov [209], the temperature at the Moho boundary underneath the Archaean platforms and shields ($H_{cc} \approx$ 40 km) is close to $T_0^l \approx 400$°C. Considering now approximate stationarity of heat flows underneath the ancient shields, it may be determined from Eq. (8.16) that at depth $(H_{cc}+H_l) \approx 220$ km $\tilde{T}_s^l \approx 1{,}456$ °C. And from Eq. (8.10'), at $\lambda \approx 5 \cdot 10^{-3}$ cal/cm·s·deg and $H_l \approx 180$ km we find $\tilde{q}_m = 0.29 \cdot 10^{-6} \approx 0.3 \cdot 10^{-6}$ cal/cm^2·s.

Another independent estimate gives the total released in the continental crust about $0.91 \cdot 10^{20}$ erg/s of radiogenic energy (see Table 6.1). The total area of the present-day continental crust is approximately equal to $2.04 \cdot 10^{18}$ cm^2, from where average radiogenic origin heat flow is $\bar{q}_R \approx 1.06 \cdot 10^{-6}$ cal.cm^2·s. At average heat flow through continents of $\bar{q}_{KK} \approx 1.4 \cdot 10^{-6}$ cal/cm^2·s [16], average depth flow turns out equal to $q_m \approx 0.34 \cdot 10^{-6}$ cal/cm^2·S.

For ancient shields the present-day heat flow q_m must be somewhat lower than the average value for the entire continental crust. For this reason we assumed for further estimates the average value of the present-day depth heat flow equal to $\tilde{q}_m \approx 0.3 \cdot 10^{-6}$ cal/cm^2·s. Then the sought for correlation may be

$$\widetilde{q_m} \approx 1.25 \cdot 10^{-9} \left[T_m^0 - T_s^0 \right] \qquad (8.17)$$

As this equation shows, in Archaean, during the epoch of upper mantle overheating to $T_m^0 \approx 1{,}600-1.700$°C, stationary depth heat flows had approximately 2–2.5 times exceeded the present-day value.

Having determined the present-day parameters of the depth heat flow through the continental crust, we may from (8.4) estimate also average values of radiogenic component on the ancient shields and platforms. For most Archaean shields $q_0 \approx (0.8–0.9)\cdot 10^{-6}$ cal/cm^2·s, thus $q_R \approx (0.5–0.6) \cdot 10^{-6}$ cal/cm$^2 \cdot$ s.

For estimating heat flows of the radiogenic origin, it is necessary to know the accumulation rate of radioactive elements in the continental crust. We assume that the accumulation rate of radioactive elements in the crust had been proportionate to the mass of these elements in convecting mantle and the formation rate of the continental crust itself. In Archaean, the mantle mass M_m had been continuously increasing at the expense of a gradual heating and involvement in convective mass exchange of Earth primordial matter still preserved at that time in depth of the subsurface in the central areas of our planet, and the formation rate of the continental crust M^{cc} had been completely defined by Earth tectonic activity $\dot{Q}$. Taking this into consideration, it may be written

$$\sum \dot{m}_R^i = -\sum (m_R^i)_0 \cdot e^{\lambda i t} \cdot \frac{M_m}{M_g} \chi_i \cdot M_N^{cc} \tag{8.18}$$

where m_R^i is mass of ith radioactive element (^{238}U; ^{235}U; ^{232}Th; and ^{40}K); $(m_R^i)_0$ are beginning contents of these elements in Earth; λ and χ_i are respectively half-life periods and mobility parameters of radioactive elements; M_m is the mass of convecting mantle; Mg is Earth mass; $M_N^{cc} \doteq \dot{M}^{cc}/M_0^{cc}$ is relative formation rate of continental crust normalized by the present-day mass of this crust M_0^{cc}; a dot over the parameter, as usually, means time derivative of this parameter.

Remembering now that the generation rate of radiogenic energy is always proportionate to the mass of radioactive elements $\dot{\xi}_R \sim m_R^i$, the solution of Eq. (8.18) for Archaean is

$$\dot{E}_R^{cc} = \sum (\dot{E}_R^i)_0 \cdot e^{-_i t} \cdot \left[1 - e^{-_i \mu}\right] \tag{8.19}$$

Where $\mu = \int_0^{M^{cc}} \frac{M_m \cdot dM^{cc}}{M_g \cdot M_0^{cc}}$, $\dot{E}_R^{cc}$ is radiogenic energy dispersed in Earth crust; $(\dot{E}_R^i)_0$ is the starting generation level of radiogenic energy by i^{th} radioactive element at the moment of Earth formation.

After Archaean al radioactive elements had already concentrated in the mantle or crust, and for this reason, the solution of Eq. (8.18) should be written in a somewhat different format

$$\dot{E}_R^{cc} = \sum (\dot{E}_R^i)_{AR} \cdot e^{-\lambda_i \Delta t} + \sum (\dot{E}_R^i)_0 \cdot e^{-\lambda_i t} \left[1 - e^{-\chi_i \Delta M_N^{cc}} \right] \quad (8.19')$$

where $(\dot{E}_R^i)_{AR}$ is radiogenic energy generation at the end Archaean; Δt is time counted from the end Archaean; $\Delta M_N^{cc} = M_N^{cc} - (M_N^{cc})_{AR}$ is relative change of dimensionless (normalized) mass of the continental crust after Archaean.

In the section 6.2 were included beginning masses of radioactive elements in Earth $(m_R^i)_0$: $^{238}U_0 = 9.76 \cdot 10^{19}$ g; $^{235}U_0 = 3.22 \cdot 10^{19}$ g; $^{232}Th = 2.22 \cdot 10^{20}$ g; $^{40}K_0 = 1.39 \cdot 10^{21}$ g, as well as their contents in the present-day continental crust: $^{238}U = 3.64 \cdot 10^{19}$ g; $^{235}\mathrm{U} = 0.026 \cdot 10^{19}$ g; $^{232}Th = 15.18 \cdot 10^{19}$ g; and $^{40}K = 5.24 \cdot 10^{19}$ g. These data enabled an estimation of radiogenic energy generation in the continental crust during the entire history of its existence (see Fig. 6.7 and 6.8).

Now we will review the continental crust heat regimes evolution in some more detail. The thickness of the upper rigid crust H_1^{cc} is defined by a position of melting start geotherm in the continental crust water containing rocks we tentatively assumed equal to $T_s^{cc} \approx 600°\mathrm{C}$. The depth to this geotherm is determined from Eq. (8.5') by substituting in it $T = T_s^{cc} \approx 600°\mathrm{C}$ and $Z = H_1^{cc}$ on condition that the temperature at the crust's base $T_0^{cc} = T_0^l > T_s^{cc} \approx 600°\mathrm{C}$. In this case the lower crust matter is in a partially molten (migmatized) state and is intensely stirred by heat convection. And the greater the depth to heat flow q_m, the more intense its convection and mass exchange in the lower crust layer $H_2^{cc} = H_{cc} - H_1^{cc}$.

The determination results of phase transition boundary positions from a rigid upper crust to partially molten lower crust are shown in Fig. 8.9. It shows that in Archaean, the continental lithosphere everywhere had been very thin (its subcrustal part had not exceeded 40 km) and at the time of the mantle maximum overheating about $2.8 \cdot 10^9$ years ago it had declined to 20–25 km.

The convection in lower crust had been transferring the already differentiated light sialic material in the upper crust. However, a high efficiency of convective heat release, as already noted above, had been supporting in the lower crust a sub-solidus temperature at which might have melted out only eutectic melts. This Archaean plates certainly might not have been as strong as the present-day ones whose thickness reaches 180–200 km in its subcrustal portion. For this reason, it must be expected that in Archaean,

the continental plates had been plastic enough and might have been subjected to quite substantial deformations both in oceanic basalt slabs pile-up zones and at collision of neighboring continental massifs. This had been manifested with a particular strength in the epoch of the mantle maximum heating and formation of the first supercontinent, Monogea, in Earth's history, about 2.7–2.6 BYa [17].

In a wide range of aluminum silicate components of crustal rocks, only granitoids have eutectic properties. This is perhaps an explanation of exceptionally broad development of granitoids and real granites invading in Archaean the upper crust from the lower one. Together with granitoids, into it had been passing many lithophilic components including alkali, rare earths and radioactive elements. At this, the lower crust matter had been gradually losing all these elements, silica and, appropriately, had been enriching in magnesium and calcium oxides. As a result, after the formation of primordial and primitive tonalite-trondhjemite continental crust, this process still in Archaean had been leading to its gradual stratification in two layers: the upper, enriched in lithophilic elements, mostly of the granitoid composition, and impoverished in lithophilic elements lower layer of enderbite-charnokite-diorite composition (the Archaean granulite layer). The estimates showed that the lower crust anatectic layer (continental-crustal asthenosphere) had existed underneath all without exception ancient shields during the entire Archaean as this is shown in Figs. 8.5 and 8.9.

In Proterozoic and Phanerozoic, the continental crust formation had been occurring under the mechanism of lithospheric plate tectonics. The crust had been forming above the plate subduction zones on the earlier emerged lithosphere. Depth heat flows on such plates are usually small, $q_m < (0.5–1)\cdot10^{-6}$ cal/cm^2·s, whereas radiogenic components of heat flows, although reaching $q_R \approx (1–2)\cdot10^{-6}$ cal/cm^2·s, still had been generated only in the uppermost and thin layers of the continental crust. For this reason, they might not have introduced a substantial contribution in the heat regime of the crust as a whole. That is exactly why underneath the Proterozoic and Phanerozoic age crust, as opposed to the Archaean crust, usually had not been emerging continuous and stable layers of the crustal asthenosphere (see Figs. 8.5, 8.9). A ubiquitous evolution and long existence of such partially molten layers in the crust is a typical feature only of Archaean. This is one of the major and conceptual distinctions of the Archaean crust areas from the continental crust of a younger age.

Specific conditions of Archaean had been no less radically affecting also the lithospheric plate structure of those faraway epochs. As follows from the solution (8.10), formation of the subcrustal lithosphere had been to

a certain extent affected by temperature conditions in the mantle T_m, at the base T_s^l and at the top T_0^l of the lithosphere as well as by the depth heat flow $\tilde{q}_m$. T_m and $\tilde{T}_s^l$ parameters, temperature-dependent at depth, are estimated from Eqs. (8.15) and (8.16). The temperature on the lithosphere surface T_0^l is found from (8.4") and (8.7') at $T_s^{cc} \approx 600$°C, the depth heat flow $\tilde{q}_m$ – from (8.17), and the radioactive component q_R, from Eqs. (8.19) and (8.19').

At the end Archaean and in Proterozoic, the continental lithosphere thickness had begun rapidly increasing. Its strength had been increasing appropriately and the tectonic evolution of continents had changed from geodynamics of thin and mobile basalt slabs to the lithospheric plate tectonics. At this very time had emerged also present-day type plate subduction zones. With a decline in the depth heat flow, the rate of young lithospheric plates thickness increase had been notably growing. By the end of Early Proterozoic (about $1.8 \cdot 10^9$ years ago) the continental lithospheric plate thickness underneath Archaean crustal blocks had already grown to 180–200 km. (Due to an approximate nature of the performed estimates, it is possible that their total thickness might have reached even 220 km.) Further on, the thickness of ancient plates had been remaining approximately constant. At present, only relatively young Phanerozoic continental plates remain relatively thin. Exactly for this reason, young areas of Earth's crust similar for instance to the West Siberian Epi-Paleozoic or the Sea of Okhotsk Epi-Mesozoic platforms experience at present a stable submerging trend.

The strength of a holocrystalline matter is defined by its elastic rigidity modulus μ. The same modulus defines the rate elastic shear wave spread in such matter

$$\vartheta_s = \sqrt{\mu / \rho} \tag{8.20}$$

If external pressure exceeds the elastic modulus value of a crystalline matter, such matter should pass in the amorphous state of overcooled liquid although the viscosity of such liquid may be very high. For the crystalline silicates, such transition in the amorphous state may occur only at pressure exceeding 2–3 Mbar, i.e., way out of the mantle pressure range.

However, as was shown in Chapter 7, the effectively amorphous state for a polycrystalline matter may have emerged already at the time when the external pressure exceeded the strength of intergranular bonds defined by the value of the long-term strength $\tilde{\mu}$ of such matter. In this case, at $P > \tilde{\mu}$ the matter remains polycrystalline but its component individual crystals

get an opportunity of mutual displacements under the influence of even small excess shear stress

$$\tau \approx \eta \cdot \dot{E} \tag{8.21}$$

where η is matter viscosity; $\dot{E}$ is rate of emerging plastic deformations. For this reason, such plastic state of the stressed polycrystalline matter may be considered as effectively liquid, although its temperature remains substantially lower than the melting temperature. At this, under Arrhenius law the temperature still remains the definitive factor of matter viscosity.

Usually, the long-term strength $\tilde{\mu}$ of polycrystalline matter is by one order of the magnitude lower than the "instantaneous" (elastic) strength μ [109]. Judging by the spreading rate of shear waves in the upper mantle underneath the continents $\vartheta_s \approx 4.6$ km/s, the "instantaneous" value of the elastic rigidity modulus is equal to $\mu \approx 7 \cdot 10^{11}$ dyne/cm^2. From this, it may be approximately assumed $\tilde{\mu} \approx 7 \cdot 10^{10}$ dyne/cm^2. Considering this, it is now easy to determine that the critical pressure $\tilde{P} = \tilde{\mu} \approx 7 \cdot 10^{10}$ dyne/cm^2 is reached at depths about $\tilde{H} \approx 216$ km. In view of the approximate nature of estimates, it is possible to assume that the critical pressure in the mantle is reached at the level of the Lehmann boundary [210], i.e., at the depth of about 220–250 km (see Fig. 7.2, boundary VI).

It needs to be mentioned here that the continental lithosphere in its structure and composition is sharply heterogenous. The reason is that the lithosphere underneath continents in post-Archaean time had been numerously fragmented, merged again, reworked and newly formed together with the continental crust near the plate subduction zone, into which had been pulled oceanic plates together with oceanic crust and overlying deposits. In these zones had been occurring dehydration and remelting of the oceanic crust rocks as well as had been developing complex metamorphic and metasomatic processes transforming the lithospheric matter in former plate subduction zones and forming the composition of the continental crust above them. As a result of multiple superposition of such processes one over another, in the continental crust must have emerged a complex mosaic of blocks welded with one another in the depth suture zones most of which are former plate subduction zones.

All these suture zones are naturally the zones of weakness. For this reason, at any changes of the lithospheric state of stress (caused, for instance, by a restructuring of the system of convective flows in the mantle), the very first intra-plate motions must have occurred along such zones of weakness or already existing faults. This, in particular, is the reason for the pattern well-known by geologists of tectonic motions inheritance from ancient faults and suture structures.

8.7 Formation Mechanism of Lithospheric Plates and the Origin of Mid-Oceanic Ridges

Earth's lithospheric shell is a cooled and completely crystallized part of the upper mantle underlain by a hot, and underneath the oceans although partially molten asthenospheric matter. In this case it is natural to assume that the oceanic lithospheric plates had formed at the expense of cooling and total crystallization of a partially molten asthenospheric matter, similar to the way this happens, for instance, on a river at water freezing and ice formation. The crystalline lithospheric rocks are in effect the same "silicate ice" for the partially molten silicate matter of the asthenosphere. The only difference is that the usual ice is always lighter than water, whereas the crystalline silicates are always heavier than their melt. If this is indeed so, the further solving of a problem of oceanic lithospheric plate formation would not already present a great difficulty as the process of water crystallization is well studied.

It is more difficult to suggest such analogy for the continental lithosphere as it is underlain albeit by a "hot" mantle but with the temperature below the melting temperature of the mantle matter (see Fig. 7.2). In particular, this explains the fact of the continental lithospheric plates solid state to a depth of about 250 km (deeper is already a plastic mantle). The physical nature of a rigid to a plastic state transition from the upper mantle underneath continents may be associated with the mantle matter disintegration under high pressure. Indeed, it may be expected that with the pressure increase to a level at which the energy of additional mantle matter activation $\Delta W = p \cdot \Delta V$ will exceed the energy of bonds between crystals in a polycrystalline matter, must occur the disruption of inter-crystalline bonds with the preservation unchanged of the crystalline structure of mineral grains themselves. As a result of such disintegration occurring with the absorption of energy ΔW, a rigid and strong polycrystalline mantle matter as if "crumbles" into individual small grains and turns into a "loose granular" body behaving similarly to a high viscosity plastic matter. In this case, a phase transition at the continental plate base must have properties of an endothermal boundary (see Fig. 7.2).

The oceanic lithospheric plate formation process under the model of a crystallization mechanism may be imagined as follows. Through the gap between the divergent plates rise hot basalt melts released from partially molten asthenospheric matter. Getting on the ocean floor surface, the basalts cool down, solidify and crystallize turning in lithospheric rocks. As the plates diverge further, earlier formed areas of the lithosphere "freeze out"

ever deeper, and underneath the basalt composition rocks already crystallize a mantle matter of the asthenosphere. To replace it, new basalt and asthenosphere matter portions enter new rift gaps, and the process is repeated. Begun in rift zones, the process of lithospheric plate formation continues under the slopes of mid-oceanic ridges and abyssal bowls at the expense of a gradual cooling and complete crystallization of the source hot mantle matter sequentially "frozen" form the bottom to the base of lithosphere. The longer the mantle matter risen on Earth surface cooled down, the greater is depth of its "freezing" and crystallization. Therefore, under the older areas of the ocean floor located farther from rift zones, the lithosphere thickness (i.e., the layer of cooled and crystallized mantle) will be greater.

Apparently, the first to voice the suggestion of a variable thickness of the oceanic lithosphere were Dewey and Bird [145] who tied increasing depth of the ocean with the distance from rift zones with increasing thickness of the lithosphere. However, these authors did not study physical causes of such descendance of the ocean floor quantitatively. Such studies were conducted somewhat later. It turned out that "freezing" depth of a melt (be it water, basalt magma or partially molten asthenospheric matter) was determined by the solution of the heat conductivity equation [159].

The formation and geodynamics of oceanic lithospheric plates to a large extent depend on thermodynamic parameters of the upper mantle matter and on the regime of its cooling. For this reason, it is necessary to pay special attention to temperature distribution in the upper mantle and lithospheric plates. It is known that Earth mantle is involved in an intense convection mass exchange which is supported for instance by the facts of lithospheric plate movement in the oceans and the continental drift. For this reason, temperature T_m in the convecting hot mantle must be close to the adiabatic distribution defined by the following equation:

$$\frac{dT}{dr} = -\frac{g \cdot \alpha \cdot T}{c_p} \tag{8.22}$$

where g is gravity acceleration; α is volume expansion factor; c_p is heat capacity at constant pressure; r is current value of Earth radius. The lithospheric thickness may be determined from the Kelvin solution of the heat conductivity equation

$$T_s = T_l erf \frac{H_L}{2 \cdot \sqrt{a \cdot t}} \tag{8.23}$$

where T_s = 1,060° is temperature of the basalt solidus; T_l = 1,320°C is temperature of asthenosphere (basalt liquidus); H_L is thickness of the lithosphere; a is heat conductivity factor; t is time since the moment of asthenosphere matter rise on Earth surface. We find from (8.23)

$$erf\frac{H_L}{2\cdot\sqrt{a\cdot t}}=\frac{T_s}{T_l}=0.803 \tag{8.24}$$

From the reference book of special functions [455]

$$\frac{H_L}{2\cdot\sqrt{a\cdot t}}=0.915 \text{ or } H_L=1.83\cdot\sqrt{a\cdot t} \tag{8.24'}$$

Equation (8.24') enables to derive a simple correlation of the thickness of oceanic lithosphere H_1 vs. its age t [159, 211]

$$H_1=k\cdot\sqrt{t}. \tag{8.25}$$

From here, it is easy to find a generalized model of the oceanic lithospheric plate structure (Fig. 8.18).

The heat conductivity factor (coefficient) is found as $a=\lambda/(c_p\rho_L)$, where λ is heat conductivity factor; c_p is per unit heat capacity, ρ_L is density of the lithosphere. The per unit heat capacity of the lithosphere for the assumed lherzolite composition at average lithospheric temperature T_L = 730° C is found using formulae in the reference book [212] to be equal to $\bar{c}_p=0.28$cal/g·deg.

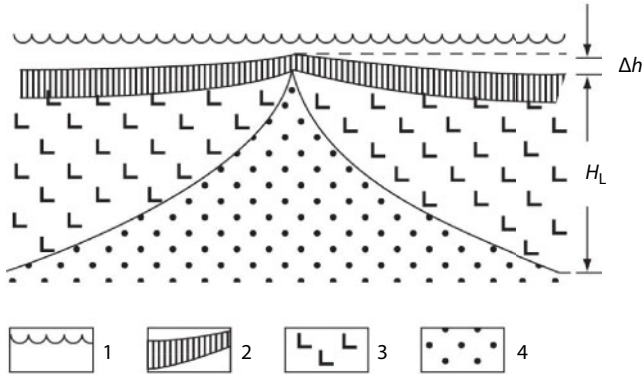

Fig. 8.18 Generalized model of the oceanic lithosphere structure: 1. Ocean surface; 2. Oceanic crust; 3. Oceanic lithosphere; 4. Mantle asthenosphere.

By the extrapolation of heat conductivity factor values for gabbro and dunnite to average temperature of the lithosphere it was found $\overline{\lambda}_L = 5.0 \cdot 10^{-3}$ cal/cm·s·deg. The density of the lithosphere may be assumed ρ_L = 3.3 g/cm^3, therefore, average heat conductivity factor for the lithosphere is equal to $a_L = 5.41 \times 10^{-3}$ cm^2/s. The a_L factor is determined in the CGS system although it is much more convenient to express the time t in millions of years and the lithosphere thickness H_L in kilometers. Then we are getting a simple expression

$$H_L = 7.56 \cdot \sqrt{t}, \tag{8.26}$$

where H_L is already in kilometers and t in MY.

At basalt (diabase) crystallization, its density increases by about 8.6% [212]. Taking this value, average temperature of the lithosphere and assuming the volume expansion factor for lithospheric rocks equal to $a = 3.0 \cdot 10^{-5}$ deg^{-1}, we find ρ_L = 3.3 g/cm^3, r_a = 3.21 g/cm^3 and $\Delta\rho$ = 0.09 g/cm^3.

Some other authors got different although close estimate results shown in Fig. 8.19.

Using most likely values of these parameters, it was possible to conclude that the real correlation of lithospheric plate thickness vs. their age is within the following range (see Fig. 8.9)

$$6{,}5\sqrt{t} \le H_l \ge 8{,}6\sqrt{t}. \tag{8.27}$$

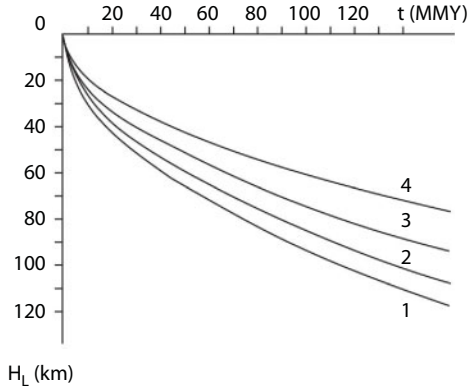

Fig. 8.19 The oceanic lithosphere thickness vs. its age: *1.* Parker-Oldenburg [211] model, $k \approx 9.4$; *2.* Sorokhtin [158] model, $k \approx 8.6$; *3.* Yoshii [213] model, $k \approx 7.5$ and current Sorokhtin's model, $k \approx 7.56$; *4.* The curve based on seismic data of lithospheric thickness underneath Hawaii Isl. (60 km): $k \approx 6.3$.

For the determination of factor k in Eq. (8.25) may also be used empirical data. Thus, based on seismologic data, thickness of the lithosphere underneath the Isl. of Hawaii is approximately $h \approx 60$ km (from the ocean floor surface) and the crust age is 85 – 90 MY. Solving the inverse problem, the result is $h \approx 6.3 \cdot \sqrt{t}$ (see Fig. 8.19). Fig. 8.20 is a typical section of the oceanic lithospheric plate in consideration of their composition and the penetrating heat flows. The heat flow value (in 10^{-6} cal/cm^2·s) was determined from the equation in [161]

$$q = \frac{13,2}{\sqrt{t + t_0}}, \tag{8.28}$$

where $t_0 \approx 100$ thous. years is the consolidation time of the rift zone.

Thus, the crystallization model nicely corresponds with the real mechanism of oceanic lithospheric plate formation. In this model, the lithospheric thickness is defined by the cooling and crystallization depth of the mantle matter; therefore, it depends on the time of the mantle matter exposure on Earth surface. For this reason, the lithosphere thickness underneath mid-oceanic ridges is not constant but regularly increases with the distance from rift zones. In the center of rift valleys, the thickness of the lithosphere is minimal and the asthenosphere is almost exposed on

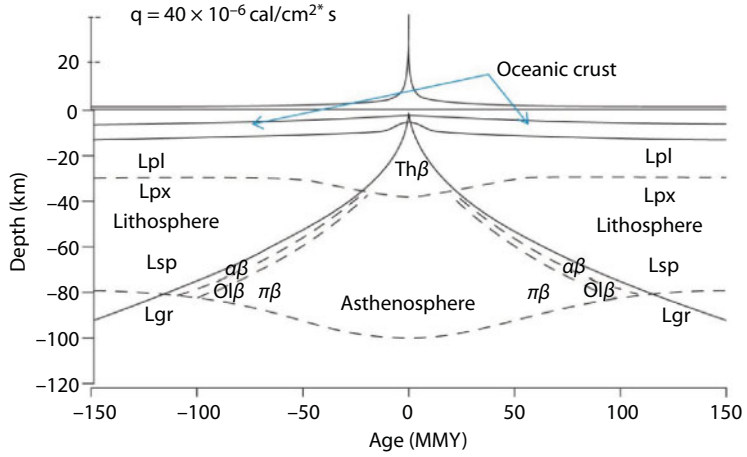

Fig. 8.20 Cross-section of oceanic lithospheric plates, at the top are heat flows q penetrating these plates. Areas of existence: Lpl – plagioclase lherzolites; Lpx – pyroxene lherzolites; Lsp – spinel lherzolites; Lgr – garnet lherzolites. Areas of melt-out: Thβ – tholeiite basalts; aβ – alkali basalts; Olβ – olivine basalts; πβ – picrite basalts.

Earth surface. As opposed to the oceanic plates, ancient continental lithospheric plates at the time of their existence (t >$1 \cdot 10^9$ years) had already cooled down to the level of establishing in them stationary heat flows. For this reason, their thickness practically had not been changing with time remaining approximately equal to 200 – 250 km.

Lithospheric rocks are heavier of their underlying hot asthenospheric matter (by about 0.1 g/cm^3). Therefore, the thicker the oceanic lithosphere, the greater the depth of its immersion in the mantle and the lower its surface goes down. For this reason, the descending rule of the ocean floor is defined by the same root correlation vs. the age of the lithosphere, i.e., vs. the age of the ocean floor itself. Under this correlation, the highest ocean floor stand level must be where the lithosphere is youngest and thinnest, i.e., in the oceanic rift zones positioned on the crests of mid-oceanic ridges. With the increasing distance from crests of these ridges, the ocean depth must increase proportionate to the lithospheric thickness increase, i.e., according to the rule

$$\Delta h = \frac{\rho_L - \rho_a}{\rho_a - \rho_w} H_l \tag{8.29}$$

where Δh is the difference in average topographic levels of a mid-oceanic ridge between its crest and any given point on the slope; ρ_L; ρ_a and ρ_w are densities of, respectively, lithosphere, asthenosphere and oceanic water. In consideration of heat flow values (8.28), we assume, according to Eq. (8.26), $H_L = 7.56\sqrt{t}$, and set most likely average lithosphere and asthenosphere densities equal to ρ_L = 3.3; ρ_a = 3.2 g/cm^3. Average oceanic water density is possible to determine from the ratio of the ocean mass M_{oc} to its total volume V_{oc}. According to the geochemical reference book [72], M_{oc} = 1,420·10^{15} t and V_{oc} = 1,370·10^6 km^3, then ρ_w = 1,036 g/cm^3, from where

$$\Delta h \approx 0.35 \cdot \sqrt{t} \tag{8.30}$$

If the described formation model of the oceanic lithospheric plates is true, then the quoted theoretical rule derived based on it must correctly average a real topography of the ocean floor. It is easy to verify this. The results of such verification are included in Fig. 8.21-*a* and 8.21-*b*. As these Figures and numerous other examples show, averaged profiles of all mid-oceanic ridges are indeed very nicely approximated by a single

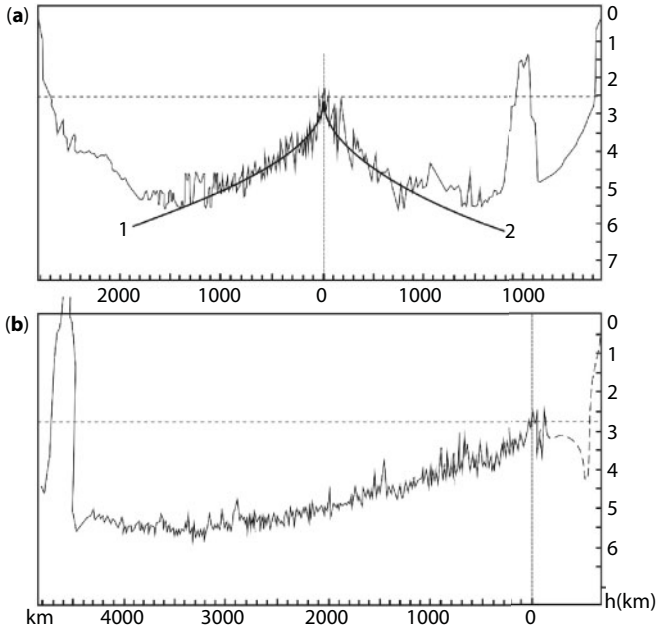

Fig. 8.21 Approximation of the ocean depths on the slopes of mid-oceanic ridges from equation $\Delta h \approx 0.35 \cdot \sqrt{t}$ [158]: *a* is the Mid-Atlantic Ridge in the southern Atlantic (plate spreading rate 2×1.8 cm/year); *b* is the East Pacific High, a latitudinal cross-section through Hawaiian Islands (rate of plate spreading about 2.5 cm/year).

equality $\Delta h \approx 0.35 \cdot \sqrt{t}$. As we see, the theoretical value of the proportionality factor in the found rule is pretty close to its averaged empirical values. The ocean depth is estimated from an equally simple equation

$$h_{oc} \approx h_0 + 0.35\sqrt{t} \qquad (8.30')$$

where h_0 is the depth of an oceanic rift zone. Usually, on average $2.5 > h_0 > 2$ km but in some cases $h_0 \approx 0$ or even somewhat above the ocean level as this, for instance, is observed in Iceland or in the Afir province in Northern Ethiopia.

As the ocean floor volcanoes are fed by the basalt magmas of directly underlying oceanic lithospheric plates, naturally, the height of underwater volcanoes and oceanic islands must be defined by the thickness of these plates. Among the first who paid attention to this phenomenon was P.R. Vogt [214] and independently from him A.M. Gorodnitsky [215].

In particular, A.M. Gorodnitsky derived a simple equation defining both the height of underwater volcanoes and Hawaiian-type oceanic islands H_m

$$H_m = H_L \cdot \frac{\rho_a - \rho_b}{\rho_b - \rho_w}, \tag{8.31}$$

where $H_L = 7.56 \cdot \sqrt{t}$ is the lithospheric plate thickness (see Eq. 8.5); ρ_a = 3.21; ρ_b = 2.9; and ρ_w = 1.03 g/cm^3 are respectively densities of the lithosphere, basalt and sea water.

The estimate results of the underwater volcanoes' and oceanic islands' maximum height estimated from (8.31) very well agree with the observed data. Indeed, substituting in (8.31) the data for the Island Hawaii: $t \approx$ 85 MY, $h_w \approx$ 5 km and ρ_w =1.03 g/cm^3, we find the island's elevation above the ocean floor equal 10 km; it is actually H_m = 9.7 km. A known pattern follows from the same equality (8.31): the closer a volcano is to a rift zone, the lower it is [215].

Using Eqs. (8.22)–(8.26) in combination with the equation for Earth tectonic activity (6.23'), it is possible to find major evolution patterns of the oceanic lithospheric plates for the entire Earth history (Fig. 8.3). In the very beginning of Earth tectonic evolution, about 3.8 BYa, maximum thickness of the lithospheric plates above Earth matter differentiation zone had exceeded 12 km. By 3.6 BYa, the plate thickness declined to 10 km, and the time of their existence (i.e., their "lifetime") had not exceeded a million years (as the ocean width at that time had been very small, as this is shown in Fig. 5.3). In mid-Archaean, about 3.2 BYa, the maximum oceanic plate thickness had increased again to 27 km, and their "lifetime", approximately to 10 MY. In Late Archaean, about 2.9 BYa, the plate thickness had dropped again approximately to 8 km and their "lifetime", due to a great rate of displacement, had again decreased to a few million years. At this, the ocean width had notably increased.

In Fig. 8.22 together with the oceanic plate thickness evolution, is also shown the critical thickness estimated based on their density. With its greater thickness, it had become heavier than its underlying hot mantle and for this reason may immerse in it, i.e., subduct. At the oceanic lithospheric plate thickness less than its critical value, it might not have subducted in the mantle but in a compression environment such plate might have obducted over another plate or a continental margin.

The determination of a depth heat flow $\dot{Q}_m$ (see Fig. 6.17) enables the estimation of other important parameters of Earth tectonic activity. Ne such parameter is average lifetime of the oceanic plates τ_l. It is proportionate

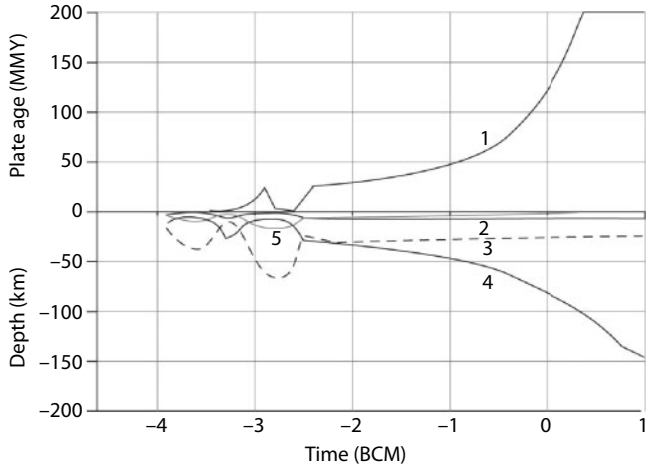

Fig. 8.22 Evolution of the oceanic lithospheric plate structure and average time of their being on Earth surface: *1.* Average plate's lifetime; *2.* Oceanic crust thickness; *3.* Critical thickness of lithospheric plates defining the likelihood of immersion in the mantle of thicker plates; *4.* oceanic plate thickness by the end of their average lifetime; *5.* The basalt layer thickness.

to squared ratio of the oceanic plate area and the penetrating heat flow $\tau_l \sim S_{oc}^2 / \dot{Q}_m^2$ (see Fig. 8.3 and Fig. 8.22). Another parameter is average thickness H_l of the oceanic plate at reaching by it maximum age τ_l. It is proportionate to the ratio of the total oceanic plate area and the same heat flow $H_l \sim S_{oc} / \dot{Q}_m$ (curve *4* in Fig. 8.22). If we assume that the present-day average lifetime of an oceanic plate is approximately $\tau_l \approx 120$ MY and $H_{oc} \approx 7.56 \cdot \sqrt{\tau_l} \approx 80\ km$ then in Early Archaean the thickness of such plate at the peak activity about 3.6 BYa had declined to 6.2 km and its lifetime, to 700 thous. years! In mid-Archaean, about 3.2 BYa, maximum oceanic plate thickness had risen to 27 km and their lifetime almost to 14 MY. In Late Archaean, about 2.8 BYa, the area H_l area had again declined approximate to 8 km and the oceanic plate lifetime, to 1.2 MY.

At first approximation, average volume of basalt eruptions on the oceanic floor is proportionate to its penetrating heat flow. For this reason, similarly may be determined the thickness of the oceanic crust basalt layer $H_b \sim \dot{Q}_m$ (see Fig. 8.1). However, in Archaean, the basalt layer thickness had been restricted not by basalt eruption volumes but by the depth to the beginning of the mantle matter melting, i.e., by the lithospheric plate thicknesses which in Early and Late Archaean respectively had been 6.2 and 8 km. Therefore, at that time thin basalt slabs, with average density about 2.8–2.9 g/cm^3, had been sitting directly on the molten mantle with

the density of at least 3.3–3.2 g/cm^3. In the beginning of Archaean and in its middle about 3.2 BYa the lithospheric plate thickness had exceeded the thickness of the basalt layer. In Proterozoic, the oceanic crust's basalt layer thickness (not including the gabbro layer) had been gradually declining from 6.5 to 2 km (Fig. 8.22, curve *5*).

If oceanic lithospheric plates had indeed been heavier than the asthenospheric matter, then a question emerges why at that time they had not sunk in the hot mantle on their own. In regard of the oceanic plates this question is not totally correct as they all sooner or later had immersed in the mantle and sunk in it underneath of plate subduction zones. It is a well-known fact that the present-day oceanic lithosphere is younger than 150 MY as its older fragments had already been pulled in subduction zones and had sunk in the hot mantle. However, within 150 MY the oceanic lithosphere had been preserved afloat similarly to metal vessels floating on the surface of water. Indeed, stable (not sinking in the mantle) oceanic plates remind by their structure giant dishes bounded from all sides by raised boards (crests of the mid-oceanic ridges and by continental margins, for instance, the lithosphere underneath the Atlantic Ocean). Due to this, such plates acquire a neutral buoyancy as under the Archimedes law the density of the asthenosphere displaced from under them turns up equal of the combined density of plates themselves and water filling up the lithospheric "dishes" (abyssal kettle depressions). The faults emerging in such plates usually rapidly self-heal by the crystallization of basalt magmas penetrating them.

In the oceanic lithospheric plate bodies, at their immersion in the asthenosphere emerge excessive stresses. The value of these stresses is the greater, the deeper such plates sink in the mantle, i.e., the older the plates are. From the correlation of the oceanic depth vs. the age of its floor, as quoted above, it is easy to estimate that in the lithospheric plates older than 150 MY must have emerged the stresses exceeding 1 t/cm^2, i.e., the strength of the lithosphere itself. Maybe this is exactly the reason why the maximum age of oceanic plates is approximately 150 MY.

As for the continental plates, they do not sink as their heavy mantle portion is "welded" on the top a light continental crust with a reserved "positive buoyance". As a result, average density of the continental plates is always smaller than average density of the hot mantle and in which such plates are immersed.

Detailed studies of mid-oceanic ridges established that their crests and rift valleys extend along the ridges not continuously but as if torn into separate segments by transform faults on which usually occurs only strike-slip plate displacements. These are third type plate boundaries or transform

faults. As a rule, they are always perpendicular to the strike of rift fractures. At this, active areas of the faults are only their segments joining two neighboring rift zones (transforming one of them into another one). Outside the limits of these active segments, no plate motions occur on the transform faults. The offset amplitude on most of such faults does not exceed ten of few dozen kilometers although sometimes it may reach hundreds of kilometers.

Transform faults sometimes cross plate subduction zones or extend from them to rift zones. But most of them cross only mid-oceanic ridges. The largest of them are the faults Gibbs, Atlantis, Vima and Romanche in the Atlantic Ocean; the faults Owen and Amsterdam in the Indian ocean; the faults Eltanin, Challenger and Udintsev in the Pacific. Besides, in the northern half of the Pacific remain the traces of now extinct but giant in the past faults, offsets on which had reached many hundreds and even 1,200 km. These are the so-called great fault of the Pacific floor: Mendocino, Pioneer, Murrey, Molokai, Clarion and Clipperton. An example of the third type boundary on continents is the San-Andreas fault in California.

Topographically, oceanic transform faults clearly display conjugated parallel structures of narrow ridges and valleys with a steep common wall (Fig. 8.23). At this, due to "welding" of the lithospheric plates with one another on the passive flanks of transform faults and more rapid immersion of the young plates, the transform faults are always framed by narrow ridges only on the side of younger plates, and on the contrary, the

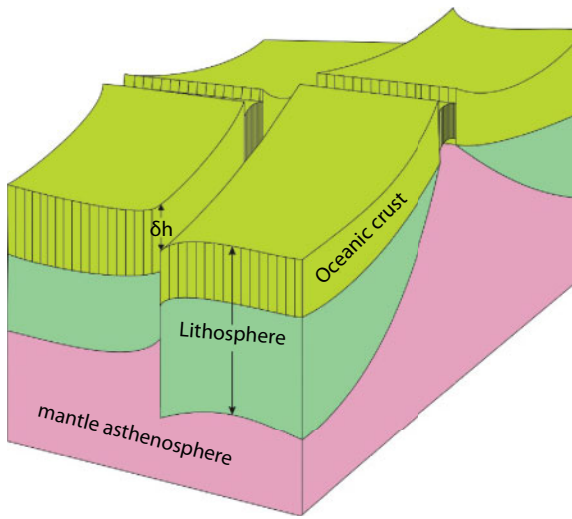

Fig. 8.23 Block diagram of a trasansform fault in the oceanic lithosphere.

valleys emerge only on the side of older plates. As a rule, transform faults are amagmatic although in some cases (with the presence of an expansion component in the plate movement) on their flanks may emerge basalt volcanoes of alkali orientation.

Lithospheric plate displacements are accompanied by their friction about one another and by earthquakes on plate boundaries. For this reason, lithospheric plate boundaries may be identified not only by geomorphological indicators but also by the zones of elevated seismicity. At this, different earthquakes correspond with different plate boundaries. Thus, in oceanic rift zones all earthquakes occurring under the crests of mid-oceanic ridges are shallow-focus, with the focus depth of up to 5–10 km and have the extension mechanism. The earthquake depth in transform faults reach 30–40 km and their mechanism is purely strike-slip. Most seismically active are plate subduction zones. In these zones are recorded the shallow-focus earthquakes with depth to the focus up to 30 km, intermediate earthquakes at depths of 30 to 150–200 km and deep-focus earthquakes with depth to the focus of up to 600–700 km. The main seismic focal surface of plate subduction zone is usually dipping at an angle about 30–50° to the axis of the deep-water trough underneath the island arc or the continental margin thus fringing the body of the immersing in the mantle subducting oceanic plate. Various types of earthquakes occur in the subduction zones. The shallow-focal earthquakes are dominated by strike-slip and reverse fault-overthrust mechanisms and average and deep-focal ones, by the strike-slip and compression mechanisms.

As a rule, maximum depth of the deep-focus earthquakes corresponds with the position of endothermal phase boundary at depth about 670 km (see Fig. 7.2). Deeper this boundary occurs the disruption of crystalline ties in the mantle matter and it apparently acquires the properties of amorphous matter. Nevertheless, the data of seismic tomography reveal the traces of subsiding oceanic plates even deeper, in the lower mantle, up to Earth's core. This is reflected in the topography of its surface: everywhere under the plate subduction zones, the plate depression zones fringing, for instance, the Pacific and Indian oceans are observed depressions in the core surface with the amplitude of up to 4 km. Under the ascending flows in the centers of the same oceans, as well as under the Northern Atlantic, on the contrary, are observed the lows of topography with the amplitude up to 6 km.

Solving the heat conductivity equation also allows us to determine the heat flow penetrating the ocean floor. It also depends on the lithospheric plate age although in this case it is inversely proportionate to its square root. By comparing theoretical estimates with the observed heat flows in the ocean floor areas with their undistorted values at t >50 MY

(see Fig. 6.12), it was possible to determine empiric correlation of the per-unit area heat flows q in heat flow units 10^{-6} cal/cm^2·s vs. the ocean floor age t in million years $q \approx 13.2/\sqrt{t}$ [161]. Using this correlation, it is easy to find average value of the heat flow through the ocean floor with the age from 0 to τ: $\bar{q} \approx 26.4/\sqrt{\tau}$. According to our estimates, average lifetime of oceanic plates is equal approximately to 120 MY. In this case, average heat flow through the ocean floor is equal to $\bar{q} \approx 2.41 \cdot 10^{-6}$ cal/cm^2·s. The area of all oceans and marginal seas with the oceanic crust is equal approximately to $3.06 \cdot 10^{18}$ cm^2, thus through the ocean floor at present is lost about $7.375 \cdot 10^{12}$ cal/s or $3.09 \cdot 10^{20}$ erg/s of heat.

8.8 Structure of Lithospheric Plate Subduction Zones

Proposed by O. Fisher, the idea of possible ocean floor subduction underneath island arcs was supported about 50 years after the conducting in the mid-1930s by F. Vening Meinesz [216, 217] of measurements of gravity field above these structures and their adjacent deep-water troughs. It was determined that near-island slopes of the deep-water troughs and the troughs themselves correspond with negative gravity anomalies reaching 200 mGal whereas above the island arcs themselves in most cases are observed positive anomalies with the amplitude of up to 100–150 mGal. F. Vening Meinesz tied the origin of these conjugated gravity anomalies with the dynamic effect of compression and subduction of the ocean floor under the island arcs.

The next step in the study of active transition zones from the oceans to the continents was made by a Japanese seismologist K. Wadati [218]. He established a depth seismofocal surface dipping from the ocean under the island arcs. The second great scientist was an American seismologist, H. Benioff [219, 220], who studied these zones in more detail and showed that on them occurs thrusting of continental crust and upper mantle blocks over the oceanic crust. At about the same time academician A.N. Zavaritsky [221] noted a genetic connection of the andesite volcanism with the inclined depth seismofocal zones identified by K. Wadati, tying thereby the continental crust formation process with tectonic movements. Considering this interconnection and the contribution by scientists to the studies of depth seismoactive zones usually called Benioff zones, it would be fair to call them Wadati–Zavaritsky–Benioff (WZB) zones.

The current model of the structure and evolution of the Kuril type plate subduction zone based on the consideration of the lithosphere elastoplastic

properties was developed in the USSR Academy of Sciences Oceanology Institute [15, 222] and modeled in Moscow State University (MGU) [223]. According to this model, the lithospheric plate subduction process reminds piling up, hummocking of river ice under compression. As with ice, the subducted plate experiences a strong pressure from the plate obducted over it. Affected by the excess pressure created by a horizontal compression stress and the weight of upper plate's obducted part, in the lower (subducted) plate are developing plastic deformations. It changes the direction of its movement and begins to descend steeply into the mantle. At this, the major distinction between the compared processes is that the ice is lighter than water whereas the oceanic lithospheric plates are always somewhat heavier than the asthenospheric matter.

The slippage of lithospheric plates on the inclined surface of the subduction zones causes a breakdown of the isostatic equilibrium and the appearance above the island arcs of conjugated positive and negative gravity anomalies (see Fig. 8.24). Using the condition of force equilibrium in the plate subduction zone, it is possible to find a correlation between the amplitude of the emerging gravity anomalies and lithosphere strength. Estimates performed

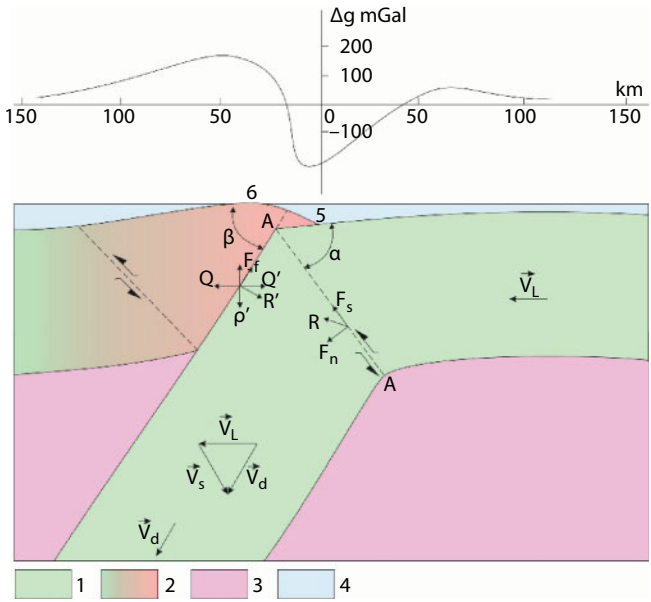

Fig. 8.24 Mechanical model of a plate subduction zone [222]: 1. Subducted lithospheric plate; 2. Obducted plate; 3. Asthenosphere; 4. Water of the ocean and marginal basin; 5. Deep-water trough; 6. Island arc; β is Wadati-Benipff zone dip angle; α is dip angle of the plastic deformation zone; Δg is "free air" gravity anomaly.

using such correlation showed that this strength is close to the value 1 t/cm^2 matching empirical data of the shear strength for ultramafic rocks.

In the cross-section of Fig. 8.24, the plastic deformation zone is marked by line AA although it may be quite wide; the angle β is the inclination of the plate subduction zone; α is the inclination angle of the shear deformation surface; V_L is the rate of the oceanic plate onward movement; V_d is the rate of the descending plate branch onward movement; V_s is shear rate of layers' displacement in the plastic deformation zone. Thus, it may be recorded in a vector format

$$V_d = V_l + V_s \tag{8.32}$$

The moving lithospheric plate deformation in the subject model is developing according to a scheme resembling metal cutting process where the function of a cutting bit is performed by the frontal part of the obducted plate and the role of shaving is played by the descending branch of the subducted plate. We denote H_L the thickness of the oceanic plate before the subduction zone under the island arc, and H_d, the thickness of the same plate after the subduction zone. Then

$$H_d = H_L \frac{\sin(\alpha+\beta)}{\sin\alpha}, \tag{8.33}$$

which shows that generally $H_d \neq H_L$.

From (8.32) may be determined correlations of absolute values of shear rate V_s and immersion V_d of the lithospheric plate vs. its subduction V_L

$$\begin{aligned} V_d &= V_L \frac{\sin\alpha}{\sin\left(\alpha+\beta\right)} \\ V_s &= V_L \frac{\sin\beta}{\sin\left(\alpha+\beta\right)} \end{aligned} \tag{8.34}$$

A model of plate subduction by L.I. Lobkovsky and O.G. Sorokhtin [224] described here enables determination of the gravity anomalies above the plate subduction zones. Indeed, a tangential stress τ_s may be expressed through the shear angle α and internal friction angle ϕ as well as through a vertical force P of excess pressure from the uplifted edge of the obducted plate:

$$\tau_s = \frac{P}{H_l} \cdot \frac{\sin\alpha \cdot \sin(\alpha+\phi)}{\left|\cos(2\alpha+\phi)\right|} \tag{8.35}$$

At this, the excess pressure is

$$p = \frac{P}{H_L \cdot ctg\beta} \tag{8.36}$$

And from this

$$p = \tau_s \frac{\left|\cos(2\alpha + \phi)\right| \cdot tg\beta}{\sin\alpha \cdot \sin(\alpha + \phi)} \tag{8.37}$$

However, excess pressure p value is tied with the gravity anomaly amplitude above the island arc, as gravity anomaly Δg in free air reduction above a layer of density ρ and of thickness h is found like this:

$$\Delta\rho = 2 \cdot \pi \cdot \gamma \cdot \rho \cdot h \tag{8.38}$$

where $\gamma = 6.67 \cdot 10^{-8}$ cm^3/g·s^2 is gravity constant. The excess pressure created by this layer is $p = \rho \cdot g \cdot h$, where g is gravity acceleration. Then

$$p = g \cdot \Delta g / 2 \cdot \pi \cdot \gamma \tag{8.39}$$

It follows from (8.16) – (8.18) that the gravity anomaly in free air reduction above the island arc is

$$\Delta g = \frac{2 \cdot \pi \cdot \gamma \cdot \tau_s}{g} \cdot \frac{\left|\cos(2\alpha + \phi)\right| \cdot tg\beta}{\sin\alpha \cdot \sin(\alpha + \phi)} \tag{8.40}$$

For the quantitative estimate of Δg we assume that average value of the maximum shear stress τ_s of the lithospheric material in a plate subduction zone is approximately equal to $\tau_s \approx 10^9$ dyne/cm^2 (1 t/cm^2). Substituting now in (8.40) the values of angles, for instance $\alpha = \beta = 40^o$ $\phi = 30^o$, we find $\Delta g \approx 200$ mGal. This matches quite well the average values of Δg anomalies in free air reduction above the island arcs. The found Δg anomaly value $\Delta g \approx 200$ mGal corresponds with a vertical displacement of the obducted plate frontal block of approximately $h \approx 2.8$ km (with the lithospheric ledge density of about $\rho_s \approx 2.7$ g/cm^3).

Upon getting in the plate subduction zone, the oceanic crust is dehydrated, heated and partially melted. This results in lowering of the crustal

matter effective viscosity and allows the consideration of the crustal layer in plate subduction zones as a lubricant between rubbing rigid surfaces (this process will be reviewed in more detail, on an example of pulling deposits in the plate subduction zones, in the next section, 8.9). In this case, the crustal matter will be experiencing shear deformations of the Couette flow type [225], therefore:

$$\eta_{cr} \approx \frac{\tau_c \cdot h_{cr}}{u_d} \tag{8.41}$$

where h_{cr} is the oceanic crust thickness in the plate subduction zone (~ $6.5 \cdot 10^5$ cm); τ_c is tangential stress in Couette flow; u_d is the lithospheric plate immersion rate in the mantle (on the order of 5 cm/year ≈ $1.58 \cdot 10^{-7}$ cm/s).

Tangential stresses at the oceanic crust deformation when it is composed of basalt pillow lavas and serpentinite, must be much lower than in a massive material of the lithospheric plates (which we assumed equal to 10^9 dyne/cm^2). Judging by the crustal earthquakes, causing them tangential stresses reach 10^8 dyne/cm^2. Then the oceanic crust viscosity is equal approximately to $4 \cdot 10^{20}$ poise.

The plate friction in a subduction zone releases a large amount of heat expended for heating and remelting rocks near this zone. The heat release increases with depth and for this reason, the lower and middle parts of the obducted plate are subjected to a much stronger magmatic reworking and destruction than the upper part. Due to this, in front of the obducted plate is gradually forming a relatively thin wedge-like lithospheric (crust) ledge overlying like a giant overhang above the subducted plate over the areas between the deep-water trough and the plate subduction zone (see Fig. 8.25). Besides, at the expense of a continuous erosion of the obducted plate frontal parts, this process under the Kuril type island arcs results in their displacement toward positioned behind them continents and in gradual closing (at a rate of about 0.3 cm/year) of the back-arc basins if such exist. Examples of such currently closing back-arc basins are South Okhotsk deep-water kettle basin and the Sea of Japan.

Beside the Kuril and Andean type plate subduction zones which are dominated by horizontal compression stress "breaking" the subducted plate, there are also plate subduction zones where the descent of a heavy oceanic lithosphere in the mantle occurs simply under the effect of the force of gravity and the pressure from the island arc. A typical example of such plate subduction zone structure is the Mariana island arc in the Pacific (subducted under it is a plate whose age is very close to a maximum

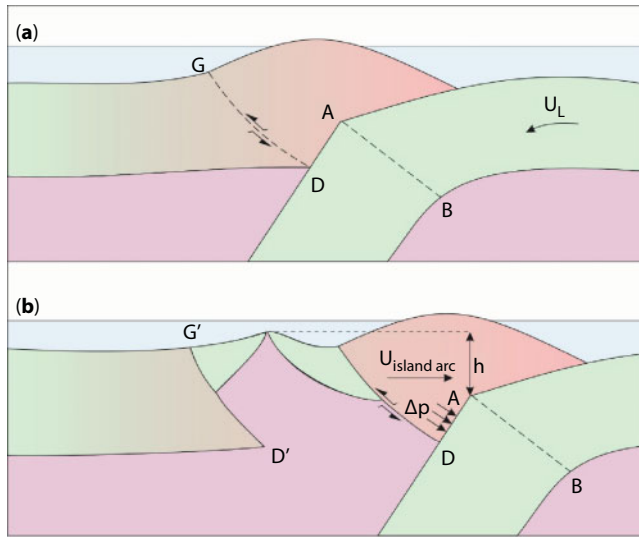

Fig. 8.25 Formation mechanism of a secondary rift zone in the island arc rear (a) and the spreading of the back-arc basin bottom (b).

stability age of the oceanic plates, 150 MY, as quoted above). These arcs are different from the previous type in that positive gravity anomalies above them are either completely absent or low in amplitude whereas negative anomalies above deep-water troughs are equally clearly expressed. Besides, as opposed to the Kuril type zones, back-arc basins in the rear of the Mariana type islands do not close but on the contrary actively expand with emerging in them secondary rift zones.

At a descent of the lithospheric plates in the mantle under their own weight, tensile stresses emerge in the island arcs' rear. Due to these stresses, along the faults feathering the plate subduction zone (*DG* in Fig. 8.25-*a*) may occur moving away of the island arc body from the rear parts of the island-arc plate. As a result, in the rear of such arc emerges a secondary rift zone, moving away of a newly born plate and the compensating move away by the island arc body towards the subducted oceanic plate and buildup of young plates (Fig. 8.25-*b*). At this, the excess pressure by the island arc on the subducted plate (at $h \geq 20$ km) exceeds the subducted plate's rock shear strength, deforms it and gradually pushes the plate subduction zone toward the ocean.

The distinction in evolution dynamics between Mariana and Kuril type island arcs is defined mostly by the plate subduction rate. At a great plate conversion rate emerge island arcs of the Kuril type, at a small rate

emerge the Mariana type arcs. The critical plate subduction rate appears to be close to 5 cm/year. The only exception is the Тонга-Kermadec island arc with a spreading back-arc basin Law where the subduction rate of the Pacific plate under this arc exceeds 5 cm/year. Perhaps, this is associated with a dynamic effect of the upper mantle matter "squeezing" in the asthenosphere at the northeastward movement of the Australian continental plate or with the existence under the Fiji kettle basin of a local ascending mantle flow. In any case, this exception from the rule does not break the general pattern but simply requires an individual consideration.

8.9 Geodynamics of the Plate Subduction Zones

Friction of a subducted plate about the base of the lithospheric ledge of the obducted plate in the frontal zone of island arc or active continental margin is naturally accompanied by earthquakes. A solution of the problem of earthquake repetition frequency Δt in the model of elastoplastic medium was published by Magnitsky [105]

$$\Delta t \approx \frac{\sigma_s}{\mu \cdot \dot{\varepsilon}} \tag{8.42}$$

where σ_s is material tensile strength; μ is material's modulus of elasticity (shear); $\dot{\varepsilon}$ is rate of material deformation. Using the publication [15], we will determine the deformation rate by the ratio u_L/L, in which u_L is the plate displacement rate and L is the width of a crustal ledge (frontal overhang) of an island arc or active continental margin. For a wide range of materials and rocks, the σ_s/μ ratio is approximately equal to 10^{-4}. The average plate subduction rate may be assumed equal to 7 cm/year $\approx 2.22 \cdot 10^{-7}$ cm/s and the width of a crustal ledge, equal to 100 km. Then time intervals between earthquakes are equal approximately to $\Delta t \approx 140$ years.

In 1988, L.I. Lobkovsky proposed a new and more sophisticated model of the structure of plate subduction zone frontal parts [226]. He noticed that the overhang of a lithospheric ledge from the side of island arcs and active continental margins was broken not only by lengthwise but also by crosswise fractures removed from one another by 100 – 200 km. As a result, the lithospheric ledge of island arcs and active continental margins turns out to be broken into separate pressed to one another blocks – keys capable of independent motions (see Fig. 8.26).

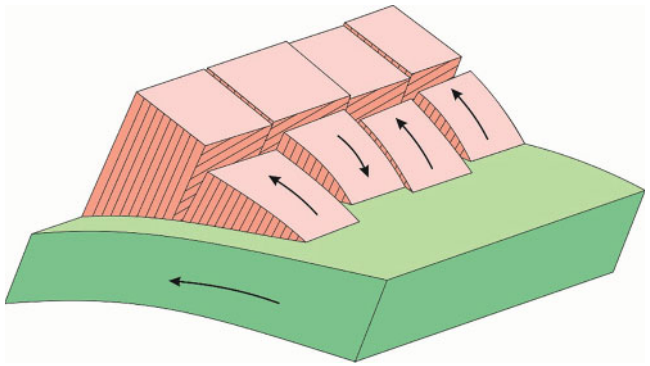

Fig. 8.26 A key-like model of a crustal ledge block structure above a plate subduction zone in the frontal part of an island arc [226].

It follows from the key-like model proposed by L.I. Lobkovsky that crosswise faults are purely crustal and extend in depth only to the top of a subducted plate. An interaction of the neighboring blocks with one another and with the subducted plate causes various manifestations of seismic motions and their corresponding sources of tsunami. Besides, what is also important is that the model allows to understand observed spatial and temporal distribution patterns of the strongest earthquake foci, including those causing tsunami. It follows from this model, in particular, that if in some part of an island arc or active continental margin for a long time have not been an earthquake whereas in the neighboring areas of the active zone the earthquakes were frequent, then in such zone called a seismic breach very strong earthquakes should be expected. This pattern has earlier been summarized in an empirical concept of "seismic breaches" serving at present the basis of a long-term forecast of catastrophic earthquakes and strongest tsunamis in island arcs and active continental margins. However, only now, after the development of the physical basis of this concept, the pattern became understandable.

Displacements of crustal overhangs of the key-like blocks in frontal zones of island arcs, as already mentioned, occurred due to their friction about the subducted lithospheric plate. At this, deformations of the key-like blocks results in the accumulation in them of elastic compression energy and emergence of shear stresses. As soon as these stresses exceed the rocks' shear strength, a discharge happens of the block's state of stress, it "straightens up" and assumes its original (unstressed) state under which the frontal part of a block sharply protrudes forward displacing its adjoining oceanic water toward the ocean.

That is exactly the way the strongest tsunamigenic earthquakes emerge [227]. Examples are the Chilean earthquake of 1960 and Indonesian

earthquake of 2004. The tsunami of the latter caused catastrophic consequences not only on Sumatra Island and nearby islands but also over almost the entire Indian ocean shore. A distinctive feature of such tsunami waves is a strongest withdrawal of oceanic water above the epicenter of earthquakes that engendered them replaced in a short time by the collapse on the coast of a giant wave sometimes exceeding 30–40 m in amplitude.

There is also another mechanism of tsunami emergence, although somewhat smaller in amplitude. Such earthquakes emerge when, under pressure by the subducted lithospheric plate, overthrusting occurs of the island arc frontal part on the edge of the arc itself. Under such mechanism of wave stimulation, as opposed to the preceding case, initially happens an uprush of the tsunamigenic wave on the island arc shore and after that, its withdrawal.

According to the Lobkovsky model, most dangerous are the so-called "seismic breaches", i.e., areas of island arcs and active continental margins above lithospheric plate subduction zones where earthquakes did not happen for a long time. At this, zones of the oblique plate subduction have great danger, as this was observed in the northern part of Sunda island arc. Indeed, in the catastrophic earthquake of December 26, 2004, the starting jolt occurred near the northern end of Sumatra Island and further on, the domino effect took place, which brought into action the adjacent key-like blocks lengthening thereby the focus of a tsunamigenic earthquake by almost 1,300 km [228]. There is such a danger zone in Russia, a seismic breach approximately in the center of the Kuril-Kamchatka island arc. Although only a direct (orthogonal) plate subduction has occurred there but large earthquakes were absent there at least for about 150 years. This zone was a dangerous area, and a very strong tsunamigenic earthquake was predicted there in a short time [228], and it happened indeed on November 25, 2006. Thus, the emergence of this earthquake was forecast.

The tsunami waves' movement rate in the open ocean is huge and is determined from the following equation

$$V_{ts} = \sqrt{g \cdot H_{oc}} \tag{8.43}$$

where V_{ts} is rate of tsunami wave advancing in the ocean; g is gravity acceleration; H_{oc} is the open ocean depth. If $H_{oc} \approx 5{,}000$ m then $V_{ts} \approx 211$ m/s $\approx$ 760 km/hr. The tsunami wave height in the open ocean is usually not great, just about one meter, but their length reaches 500 and even 1,000 m. In shallow water, the wave rate sharply decreases and their height is equally sharply gows.

8.10 The Mechanism of Pulling Oceanic Deposits in Subduction Zones

Together with the oceanic lithosphere, pelagic deposits also move toward plate subduction zones. At this, in most cases deposits stripping and crushing does not occur. As a rule, also not observed is excessive deposit accumulation in deep-water troughs, although the sedimentation rate there reaches a few centimeters per thousand years. At such deposition rate, most troughs would be completely filled already in a few dozen million years whereas in actuality they remain unfilled despite some of them existing and continuing to evolve for hundreds of millions of years in a row. Examples are the Japanese or Peruvian-Chilean troughs. This is an indication of operating in deep-water troughs of an efficient deposits removal mechanism from the surface of the ocean floor. This natural mechanism, as it became clear now, is their pulling in plate subduction zones. This is similar to lubricating of the moving mechanisms with liquid lubricants when they get in gaps between the rubbing rigid parts.

A possibility of pulling unconsolidated pelagic deposits into gaps between the moving rigid plates in subduction zones was in the past causing numerous doubts in geologists. Initially, this problem was solved theoretically [222], then the fact of pulling deposits in the plate subduction zones was supported by seismic studies [229] and eventually proven by drilling data on the island arc slopes of the Lesser Antilles [230]. Somewhat later, a problem of pulling in pelagic deposits to great depths under the continents was theoretically solved [56].

The deposits getting in the gap between lithospheric plates are under the influence of oppositely directed actions one of which is the subducted plate movement and another is process of pushing deposits back from the zone at the expense of excessive weight of the obducted continental lithospheric block (Fig. 8.27). The interaction results of these oppositely directed forces defined the evolution process. If the force dominates pulling deposits in the gap, they will be absorbed in a plate subduction zone without "stripping", "scraping" effect. In the opposite case, excessive volume of deposits will be pushed back out of it, crushed in front of the obducted plate edge and will form a folded structure of the accretion prism.

For determination of the nature of viscoplastic flows in a deposit layer between the moving plates, it is necessary to solve the Navier-Stokes equation for a given structure of the plate subduction zone. It is appropriate to search the solution for a case of a steady (stationary) viscous liquid flow in a flat gap between two rigid plains moving relative one another

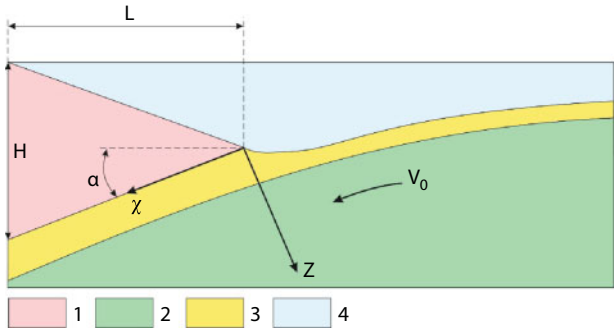

Fig. 8.27 A model of pulling deposits in a plate subduction zone: 1. Frontal ledge of the obducted plate, H and L are thickness and length of this ledge; 2. Subducted plate; 3. Deposits; 4. Oceanic water; α is the plate subduction zone dip.

(in hydrodynamics, such flows are called Couette flows [225]. We will take an option of structure of a plate subduction zone imaged in Fig. 8.27. The x axis is directed along the plate subduction zone from its frontal edge in the zone depth and the z axis is perpendicular to the plate subduction zone top and down. The origin may be selected at the frontal edge of the obducted plate. It may be assumed that the subducted plate is displacing at a constant rate u_0. Then the Navier-Stokes equation may be recorded as follows

$$\eta \cdot \frac{d^2u}{dz^2} = \frac{\partial P}{\partial x} - \rho_s \cdot g \cdot \sin\alpha \tag{8.44}$$

where u is rate of deposits flow in the gap between plates; η is deposits viscosity; P is pressure; ρ_s is deposits density; g is gravity acceleration; α is plate subduction zone dip angle.

The boundary conditions in the problem are

$$\begin{aligned} u &= 0 \text{ at } x = 0 \\ u &= u_0 \text{ at } z = h \end{aligned} \tag{8.45}$$

where h is gap thickness between the plates. In this case, the solution of Eq. (8.44) is:

$$u = \frac{z}{h} \cdot u_0 - \frac{z}{h} \cdot \left(1 - \frac{z}{h}\right) \cdot \frac{h^2 \cdot \Delta\rho \cdot g}{2 \cdot \eta} \cdot \sin\alpha \tag{8.46}$$

where $\Delta\rho = \rho_l - \rho_s$; ρ_l is density of the obducted lithospheric plate; ρ_s is density of deposits. Then average flow rate of the sedimentary matter in the gape between plates is:

$$\overline{u} = \frac{u_0}{2} - \frac{h^2 \cdot \Delta\rho \cdot g}{12 \cdot \eta} \cdot \sin\alpha \tag{8.47}$$

Obviously, pulling deposits in plate subduction zones may occur only in a case when $\overline{u} > 0$. For usual pelagic deposits whose density is much lower than average density of the lithospheric plates $\rho_s < \rho_l$, this condition is fulfilled only when

$$\frac{h^2 \cdot \Delta\rho \cdot g}{6 \cdot \eta} \cdot \sin\alpha < u_0 \tag{8.48}$$

In the absence of scraping deposits from the ocean floor and their crushing in front of the plate subduction zone, a flow of sedimentary matter on the ocean floor in the beginning of the plate subduction zone must be equal, i.e., $h_0 \vartheta_0 = h\overline{u}$ where h_0 is deposit thickness on the ocean floor. In this case,

$$h_0 \cdot u_0 = \frac{u_0}{2} \cdot h - \frac{h^2 \cdot \Delta\rho \cdot g}{12 \cdot \eta} \cdot \sin\alpha \tag{8.49}$$

On the other hand, it follows from the solution (8.46) that in a gap between the plates may emerge reflected flows of the sedimentary material pushed out under the weight of the obducted plate. For such flows emerging at low and average z values may be $u < 0$. The condition of absence of such flows, therefore of pushing the deposits out of the plate subduction zone, is an inequality $u \geq 0$ observed in the gap at all levels of Z. From this condition at $\rho_l > \rho_s$ and from Eq. (8.48):

$$0 < \frac{h^2 \cdot \Delta\rho \cdot g}{2 \cdot \eta \cdot u_0} \cdot \sin\alpha \leq 1 \tag{8.50}$$

Eq. (8.50) may be recorded in a different format

$$3 \cdot \left(1 - \frac{2 \cdot h_0}{h}\right) = \frac{h^2 \cdot \Delta\rho \cdot g}{2 \cdot \eta \cdot u_0} \cdot \sin\alpha \tag{8.51}$$

Comparing now expressions (8.51) and (8.50), we find that at a positive pressure gradient ($\rho_l > \rho_s$) and unchanged deposits viscosity η, their thickness in the gap h is always

$$2h_0 < h \leq 3h_0 \tag{8.52}$$

In practice, the condition (8.52), especially at shallow depths, usually is always observed (see Fig. 8.28). However, this inequality belongs only to the width of the frontal part of the plate subduction zone. In deeper portions of this zone the gap width between the plates h may substantially change depending on alterations experienced by the deposits and the appropriate changes of their viscosity, as well as at melting of the deposits; on permeability for the melts of overlying the plate subduction zone areas of the obducted plate.

Indeed, in the process of pulling in the deposits between the moving plates deformation of the sedimentary material occurs, accompanied by viscous friction energy dissipation. As a result, the deposits viscosity in depth of the plate subduction zone rapidly decreases under the Arrhenius law

$$\eta = \eta_0 \cdot e^{\frac{W}{R \cdot T}} \tag{8.53}$$

where $\eta_0 \approx 10^{-5}$ Π is viscosity of a strongly overheated silicate matter; W is per unit volume activation energy of viscous deformations; R is the gas constant; T is absolute temperature, K. At this, the inequality (8.52) is broken and, together with the decline in viscosity of the sedimentary material pulled in the plate subduction zone, must substantially decrease the equilibrium width of the gap h between the plates. Practically, this means that the light sedimentary material ρ_s, in the course of its heating and decline of viscosity must be pushed out of

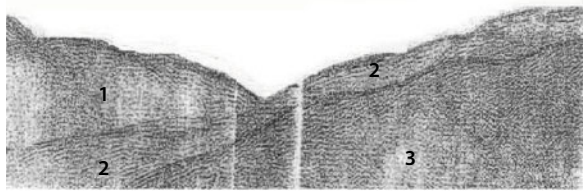

Fig. 8.28 Seismic cross-section displaying pulling of the oceanic deposits (2) together with the oceanic plate (3) under the body of the Kuril island arc (1) [231].

the plate subduction zone through a system of faults conjugated with it which are usually abundantly cutting the body of island arcs or active continental margins. An estimate of heat generation in the deposits may be performed using the dissipative function q defining the viscous friction energy release per unit volume of the matter per unit of time according to Eq. (8.54) [56]

$$q \approx \frac{2 \cdot \eta}{h} \int_0^h \left(\frac{du}{dz} \right)^2 dz = 2 \cdot \eta \cdot \frac{u_0^2}{h^2} + \frac{(h \cdot \Delta\rho g \cdot \sin\beta)^2}{6 \cdot \eta} \qquad (8.54)$$

It is also obvious that in the time of deposits immersion to a depth H, per each gram, of their matter will be released heat

$$Q = q \frac{H}{\rho_s \cdot u_0 \cdot \sin\beta} \qquad (8.55)$$

The estimates using Eqs. (8.53–8.55) show that within a wide range of initial viscosity values of the deposits pulled in plate subduction zones, these deposits heat up to the melting temperature of water-containing silicates already at depths of 20 to 30 km. Thus, regular light deposits with density of about $\rho_s \approx 2 \div 2.5$ g/cm^3 do not get deeper than this limit but are pushed out from the plate subduction zone and as magmatic intrusions invade rear zones of island arcs or active continental margin (see Fig. 8.29).

As in a case of lubrication, the amount of deposits getting in a gap between the rubbing plates must depend on the rate of the plate movement and viscosity of the deposits pulled into the gap. The appropriate estimates based on the mechanisms' lubrication theory showed that the deposits may be pulled in under the island arcs without scraping and crushing only if their thickness does not exceed some critical value dependent on the rate of the plate subduction and deposits viscosity [232]. At this, the thickness of the deposits pulled in a gap between the plates increases two to three times. The very critical thickness value of the deposits h_0, depending on their viscosity η_s and the rate of the plate subduction u_o, is determined as follows

$$h_0 \leq 5{,}5 \cdot 10^{-8} \cdot \sqrt{\eta_s \cdot u_0} \qquad (8.56)$$

where h_o is in meters; u_o is in cm/year; η_s is in poise

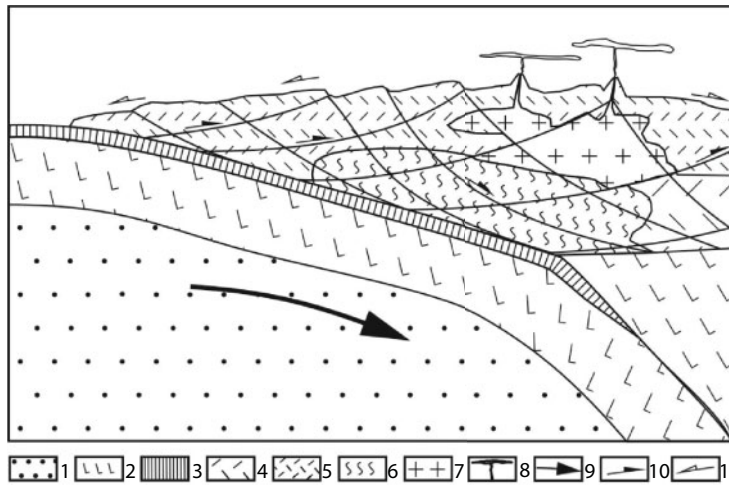

Fig. 8.29 Formation of the continental crust in Proterozoic and Phanerozoic at the expense of partial remelting and dehydration of the oceanic crust and overlying pelagic deposits in the zones of the oceanic plates subduction under the island arcs. 1. Mantle's asthenosphere, 2. Oceanic and subcrustal continental lithosphere, 3. Sedimentary-volcanogenic layer of the oceanic crust, 4, 5. Continental crust of island arc or continental-marginal type, 6. Area of remobilizing and melting of the crustal matter, 7. Granite intrusions, 8. Volcanic buildups, 9. Movement directions of the oceanic lithosphere, 10. Shear (strike-slip) deformations in the continental crust, 11. Direction of sedimentary matter runoff.

Under such arcs as Kuril, Japanese and Tonga, may be pulled in without scraping and crushing up to 500–520 m of pelagic deposits and under Peruvian-Chilean, Aleutian and Java troughs may be pulled in without scraping only up to 400–430 m of the deposits. Near the Kuril, Japanese and the central part of the Java deep-water troughs, the thickness of sedimentary layers does not exceed 300–500 m, near the Tonga trough the deposit thickness declines to 100–300 m, and in front of the major part of the Peruvian-Chilean trough the sedimentary layer thickness drops to 100 m and thinner. For this reason, the plate subduction under these structures occurs without scraping and crushing of the deposits before the frontal portion of the obducted plate. If we assume that 500 m of deposits may be pulled in the listed plate subduction zones without scraping, it means that viscosity of the Pacific pelagic deposits is equal approximately to 10^{19} Poise.

A totally different situation is observed in the Alaska Bay in the east of the Aleutian arc and in the north of the Java trough. In these areas both the rate of plate subduction is not very high, about 2–3 cm/year, and the deposit thickness exceeds 500–700 m, sometimes even reaches 1,000 m,

i.e., everywhere exceeds estimated for these structures critical values of subducted deposit thickness. A similar picture is observed also near the subduction zone of the Atlantic plate under the Lesser Antilles islands. For this zone a critical thickness of deposits which still may be pulled in the plate subduction zone without scraping is equal to about 250 m. However, the real thickness of sedimentary sequences there reaches 500–1,000 m. Therefore, in all these areas the lithospheric plate subduction must be accompanied by scraping the deposits from the ocean floor and crushing them in front of the lithospheric ledge of island arcs, i.e., formation of accretional sedimentary prisms. Exactly this process must be the explanation of the emergence of outer nonvolcanic ridges near these plate subduction zones formed by Kodiak islands in the Aleutian arc, lesser Antilles Island in the Atlantic and Andaman Islands in the Indian Ocean.

Through the dissipation of the viscous friction energy, the deposits that got in a gap between the rubbing plates, gradually heat up and even begin slightly to melt. Thus, their viscosity in the plate subduction zones sharply (by many orders of the magnitude) decreases and the maximum thickness substantially declines. That is exactly why most deposits, with density lower than the lithospheric density, may not be pulled in plate subduction zones at depths deeper than 20–30 km**.** Such deposits are usually pushed up through their feathering faults and invade as migmatite granite-gneiss domes or granitoid batholiths the body of island arc structures or active continental margins above such subduction zones (see Fig. 8.29).

The deposits may be pulled in at great depths and under the continental lithospheric plates only if their density is close or exceeds the lithosphere density. In such a case, average rate of deposits pull in the subduction zones is always higher than the subduction rate of the plates themselves. Therefore, heavy deposits must "collapse" in the plate subduction zones on their own [56]. The density of any present-day deposits is always smaller than the density of the lithosphere ($\rho_1 \approx 3.3$ g/cm^3). For this reason, they may not be pulled in at great amounts to a substantial depth under the island arcs or active continental margins. As will be shown later, some amount of the sedimentary matter and fluids still may immerse in the mantle together with the oceanic lithosphere and further be dispersed by its convective flows forming the geochemical train of carbon's characteristic isotope marks.

Contrary to this, in Earth's Pre-Cambrian history had existed epochs when on the ocean floor and on the continental shelfs had been abundantly deposited iron ore formations (jaspilites) with density reaching 4–4.5 g/cm^3 that had substantially exceeded the density of the lithosphere. Such deposits might have been unhindered pulled in ("collapsed") at great

depths underneath the continents. After melting of these deposits, their differentiation with the formation of silicate-carbonate melts, and after the separation from them of iron compounds (going in the mantle), at the lower levels of the continental lithosphere at depths of 100 to 220–250 km, might have formed the foci of kimberlite, lamproite, carbonatite or alkali-ultramafic magmas. Further on, at a change of compression tectonic regimes by the extension ones, these magmas (now lighter after liquation of the melts and separation of iron from them) might have again risen on the surface and invaded the continental crust.

9

Continental Drift in Earth's Geological History

It was shown in previous chapters that the continental crust formation had begun around 4.0–3.8 BYa, i.e., with the delay of approximately 600–800 MY in regard to the moment of the formation of Earth itself. After the beginning of continental crust formation, a continuous and quite nonuniform buildup of its mass up to the present-day size had occurred. The crust formation occurred most intensively in Late Archaean. However, during almost the entire Archaean eon, no large continents had existed and their embryos (nuclears and ancient shields), most likely, had been evolving isolated from one another (see Figs. 7.4 and 9.1). The first large supercontinent, Monogea, apparently had been formed only on the boundary of Archaean and Proterozoic, about 2.6 BYa, at the moment of formation in Earth of a high-density oxide-iron core. In subsequent epochs, numerous other supercontinents had been emerging (see Fig. 7.7), which then split into individual continents drifting apart from one another. Studies conducted showed that supercontinents had formed with periodicity about 800 MY and only after Archaean. At that, in the entire post-Archaean time they had emerged only four times (see section 7.3). In this section we will undertake an attempt to reconstruct the spatial positions of these supercontinents and continental (and oceanic) drift in the Pre-Cambrian Earth's history. At that, we will be conducting a review of such reconstructions in a historical sequence, from ancient situations to the present-day ones, although in actuality the reconstructions were conducted the other way around: from the present-day positions of the continents to the ancient.

9.1 Continental Shields' Evolution in Archaean

As we have already noted (see section 8.2, Fig. 8.5), in Archaean, the continental crust had formed by means of the secondary remelting of partially hydrated basalt and komatiite slabs (proto-oceanic crust) in places of their

N. O. Sorokhtin (ed.) The Origins of Natural Diamonds, (249–270) © 2019 Scrivener Publishing LLC

pileup and clustering above descending convective flows in the mantle. The mantle convection in Early and Middle Archaean had mostly a thermal nature with heating from below at the front of the Earth matter zonal differentiation and for this reason must have organized itself in a system of stationary Benard cells (see section 7.3, Fig. 7.4). That is why the number of ancient continental crust embryos in Early Archaean, most likely, had corresponded with the number of then existing convective cells and might have reached 40 "nuclears" (in the terminology of M.Z. Glukhovsky and V.M. Moralev, [99]). At that time, the shields themselves had been forming isolated from one another and as if staying in place, without any noticeable continental drift, and gradually acquired the outline of roundish polygonal structures. At that, however, with the immersion of Earth's matter zonal differentiation front and the expansion of the differentiation zone, the size of stable Benard cells had also grown, which must have resulted in the restructuring of convection and in corresponding merging of the nuclears in larger shields. Nevertheless, by mid-Late Archaean, at least 10–12 not connected with one another centers of the future continents (Archaean shields) formation still had to be preserved.

It does not appear possible now to reconstruct precisely mutual positions of ancient shields on Earth surface in Archaean. However, general patterns in the distribution of continental massifs at that distant epoch are possible to trace. Most likely, first most ancient embryos of the future continental shields had appeared about 3.8 BYa in the equatorial belt of Earth's lithospheric shell above most ancient Earth matter differentiation zone (see Fig. 5.1). Many such embryos of the future continents, most likely, had not been preserved until our time but some of them, as for instance gray-gneiss complexes in West Greenland or the rocks of Engr series of the Aldan shield not only have been preserved but also are stratotypical examples of the most ancient Earth crust formations. Further on, during almost entire Archaean the zonal differentiation of Earth matter had already been fed mostly by only gravity energy and continued to evolve within the same expanding latitudinal Earth belt (see Chapter 8). About 3.6 BYa the widths of tectono-magmatic activity belt had already reached 4,000 km (see Fig. 9.1). A mutual drift of the Archaean shields relative to one another still had been remaining insignificant as all they had formed then more or less independently in the environment of stationary Benard type thermal convection (see Fig. 7.4 and 8.14).

A catastrophic event of Earth's core separation at the end Archaean, as already noted, must have been accompanied by stimulation in the mantle belt above Earth matter differentiation zone of exceptionally strong

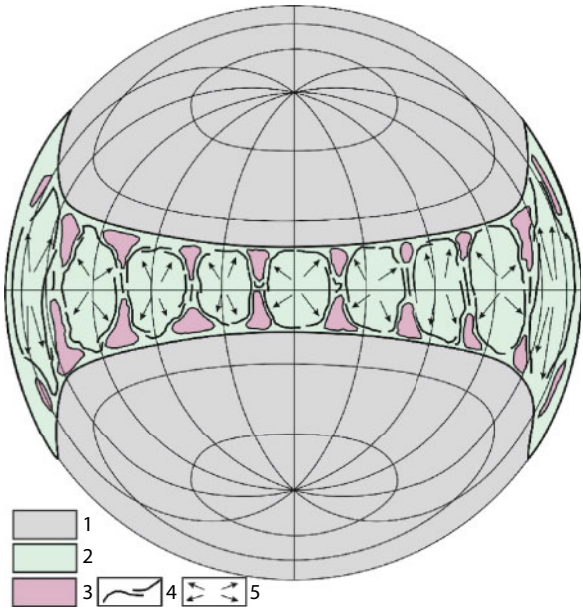

Fig. 9.1 Schematics of possible positions of most ancient (embryonal) continental crust blocks in Earth's equatorial belt about 3.6 BYa (Lambert projection): 1. Primordial Earth's matter of ultramafic composition (overlain from above by a finely-porous regolith of the same composition); 2. Basalt and komatiite surface of convective cells in the latitudinal zone of Earth's tectono-magmatic activity; 3. Embryos of the continental crust composed of greenstone rocks and sodium composition granitoids; 4. Folding at the edges of convective cells; 5. Basalt slabs' movement directions.

convective flows that had completely restructured the entire previously existing tectonic plan. It is clear from geometry of the described motions that at that time must have emerged a single-cell convective structure with a single ascending flow above the emersion (surfacing) place of the former Earth's heart and a single descending flow above the "core" matter runoff area to the planet center (see Fig. 5.1-*d* and *e*). That is why there is every reason to believe that exactly above this descending mantle flow on the boundary between Archaean and Proterozoic about 2.6 BYa from previously separated continental shields had formed the first supercontinent in Earth's history. We called it Monogea [96, 100]. Exactly due to this process on all Archaean continental shields of the planet had been formed a characteristic mosaic structure of heterochronal, variously denudated crust blocks. A possibility of existence on the boundary between Archaean and Proterozoic of a single supercontinent based on geological data was also proposed by V.E. Khain and N.A. Bozhko [102] who called this hypothetic continent Pangea 0.

Considering all the aforementioned, it appears enticing to tie the described geodynamic catastrophe with the most outstanding Kenoran epoch of the planetary tectono-magmatic diastrophism that had completed the Archaean stage of Earth geological evolution. The prime cause of such radical geological events had been a catastrophic process of Earth core formation.

The density of iron and its oxides, i.e., "core matter" at normal pressure (7.8–8 g/cm^2) is approximately twice the density of primordial Earth heart matter also at normal pressure (about 3.9–4.0 g/cm^3) and the density of gone through the differentiation mantle matter (about 3.2–3.3 g/cm^3). That is why the core formation about 2.7–2.6 BYa might have occurred only under the influence of excess pressure acting from the side of the forming core on the former Earth heart which must have not only surfaced but also risen high (by a few kilometers) above its equilibrium surface (see Fig. 5.1-*d*). At that, surfacing of Earth's heart in conditions of revolving Earth must have been occurring in its equatorial plain. Therefore, there is every reason to believe that the then emerging supercontinent Monogea had also been positioned on the equator and at low latitudes on the opposite side of our planet.

9.2 Formation of Monogea Supercontinent at the End Archaean

Beside the specifics of Monogea formation, as already mentioned, the very position of continents on the surface of revolving Earth substantially distorted the symmetry of its momentum of inertia, thereby forcing Earth body to turn so that the center of gravity of the continents had been on the equator [173, 193]. Exactly for this reason all subsequent supercontinents must have been positioned only at low latitudes with the geometrical center on the equator of revolution. Apparently, for all supercontinents that had been exactly so. At least, no traces of glacier cover deposits were discovered, until now, in the territories of subsequent supercontinents Megagea, Mesogea or Pangea [204]. However, in Archaean and Early Proterozoic, the average stand level of continents above rift zones and oceans had been still very high (see Fig. 8.10): in Archaean, up to 6 km and in Early Proterozoic, up to 5 –3 km. That is why, despite even a hot climate in Archaean and substantially cooler but still warm climate of Early Proterozoic, on continents of that time might have evolved high-mountain type glacier covers [198]. An indirect support of this is a broad development in Early Proterozoic of conglomerates (of Witwatersrand formation

type in South Africa) deposited then in abundance on the margins of many other ancient cratons.

The fact that the first in Earth history almost global Early Proterozoic (2.5–2.2 BYa) Huron glaciation had covered most shields of ancient continental platforms may be explained only by that after Archaean a high-density carbon dioxide atmosphere with the pressure about 6 atm. turned out almost completely bonded in carbonates (see Chapter 10), and the total pressure of already almost purely nitrogen atmosphere declined to 1.5 atm. (see Fig. 10.24). A reminder: this drastic decline in the atmospheric pressure had occurred at high average level of the continent stand, about 5 – 3 km. That is why a decline of the atmospheric pressure at still high stand of the continents had been the main cause of the emergence of the expansive high-mountainous glaciation of Early Proterozoic [198]. In Early Proterozoic, the emergence of expansive glaciations might have occurred also on continents positioned at low latitudes.

Unfortunately, all paleomagnetic data related to Pre-Cambrian and in particular to Early Proterozoic are so far not very reliable and their ties with age horizons leaves plenty to be desired. That is why for the reconstruction of Pre-Cambrian supercontinent positions, and within them, of individual continental massifs and continents, we in principle did not use paleomagnetic data as that might distort such reconstructions beyond recognition. We built all reconstructions based only on geological and paleoclimate data by aligning with each other homochronous and identikit geological structures, formations and climatic provinces. For that, we used geological data quoted in special literature on geology of Early Pre-Cambrian [102, 190, 201, 233, 234].

In particular, for the Monogea reconstruction we utilized the data of tillite and tilloid development on Early Proterozoic continents [204]. At that, we used a criterion of compact positioning of known exposures of the Early Proterozoic tillites in consideration of possible inheritance of the continents' positions on Earth surface during subsequent geological epochs. At such reconstruction, the "center of gravity" in geographic locations of the identified tillites and tilloids approximately defines the mass center of a supercontinent itself. Besides, we took into consideration the development and strike of the belts of Kenoran and its homochromous orogeneses (~2.6 BYa) and also the fact that in Early Proterozoic, the eastern part of the South America (Brazilian craton) had been still an organic whole with the Central and possibly South Africa but had been separated from the western part of the South American (Amazon) platform. Besides, the West Africa at that time, most likely, had been still attached to the Guyanese shield of South America. Apparently, at the boundary of Archaean and Proterozoic, the other ancient platforms had been broken into parts, and their fragments

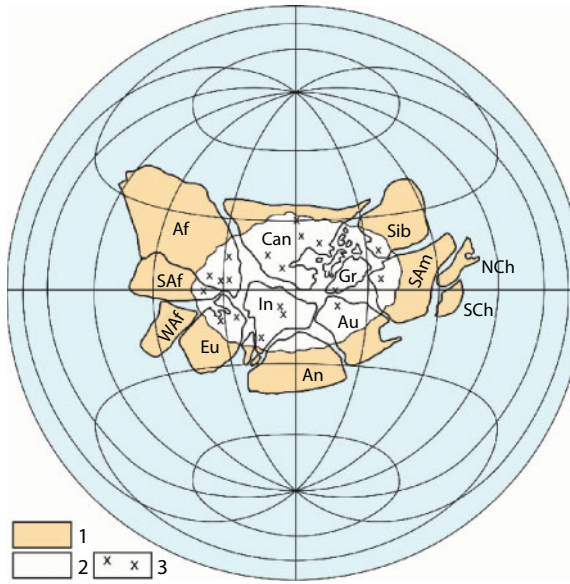

Fig. 9.2 Reconstruction of the Monogea supercontinent (2.5–2.4 BYa) in Lambert projection: 1. Consolidated continental crust free of tillites and tilloids; 2. Areas of glacial covers although they might have been more expansive; 3. Tillites, tilloids and glacial striation. Au - is Australia; NAm and SAm - are North and South America; An- is Antarctic; WAf, CAf and SAf - are West, Central and South Africa; Eu - is Europe; In is Indostan; Kz - is Kazakhstan; NCh and SCh are North and South China; Sb - is Siberia; Gr – is Greenland.

(Archaean shields) might have held then different positions from current ones. However, now there is no reliable geological data about possible displacements of other shields at the end Archaean. That is why on the Monogea reconstruction we made (Fig. 9.2), other platforms are tentatively shown with their present-day configuration and with the same as at present time mutual positions of their component Archaean shields.

9.3 Monogea Disintegration and the Formation of Megagea Supercontinent in Early Proterozoic

An asymmetrical distribution of high-density matter in the mantle that had emerged after Earth core formation at the boundary of Archaean and Proterozoic (see Fig. 5.1-d) must have resulted in an equally strong action asymmetry of the mantle matter barodiffusion differentiation process on the surface of the newly formed core. Due to the fact that the primordial matter had been rich in iron (about 13%) and its oxides (about 24%), most

intense differentiation then must have been occurring under the "dense" hemisphere with the formation there of powerful descending convective flow. Contrary to that, in the "light" hemisphere under Monogea must have emerged equally powerful ascending convective flow leading eventually to the split of a new supercontinent in Earth history.

First extension impulses had been likely to have appeared already about 2.4 BYa, which is indicated by the age of the Great Dyke in Zimbabwe. However, the main phase of supercontinent fragmentation had occurred somewhat later, about 2.3 BYa. After the epoch of Archaean mantle overheating, continental lithospheric plates had still remained relatively thin (no thicker than 100–150 km) and not as strong as the plates of present-day continents whose thickness together with Earth crust reaches underneath Archaean shields 250 km. That is why there are reasons to believe that, against the background of still relatively strong tectonic activity in Early Proterozoic, Monogea split had occurred for small blocks – cratons mostly on the old sutures that had welded in Kenoran diastrophism epoch Archaean shields into a single supercontinent. As a result, in mid-Early Proterozoic many shields had separated again and begun drifting in centrifugal directions off the center of the former Monogea.

The consideration of Karelian (Svecofennian) and its homochronous orogenies' development belts also helps restoring the formation process of a new supercontinent in Early Proterozoic from fragments of continental cratons of former Monogea. The Svecofennian phase of folding had welded individual Archaean cratons about 1.9–1.8 BYa into a new supercontinent Megagea. For taking this pattern into consideration, a sufficiently complete synthesis by V.E. Khain and N.A. Bozhko [102] and Khain [127, 235] was used for Pre-Cambrian continental tectonics as well as additional criteria for the determination of Archaean shields and proto-platforms in Early Proterozoic edge zones. For instance, it was considered that the largest iron ore deposits of that age had formed, most likely, on the passive margins of continental blocks in upwelling zones of that time.

Thus, based on geological data [102], within the North-American platform, Archaean cratons Wyoming, Churchill, Kaminak and Slave on the one side and cratons Superior and North-Atlantic (South Greenland) on the second and third sides had been cut by Trans-Hudson and Labrador orogens with the folding age of 1.9–1.8 BY. With this in mind, the North-American platform turns out to be broken into three parts: eastern, western and Greenland with Baffin Land and Newfoundland provinces.

Similarly, the European platform is also broken into three cratons: Kola-Karelian, Central Russian (including the Southwestern Fennoscandian,

Voronezh massif, Dnieper and Azov blocks of the Ukrainian shield) and the third craton, Kirovograd and Belozersk blocks of the Ukrainian shield as well as the basements of Belorussia and Baltics.

The Siberian platform is tentatively sectioned into four parts: the Anabar and Aldan shields with the attached territories although there might have been more of such Siberian platform fragments.

Australia is broken into three cratons: blocks Yilgarn and Pilbara with adjacent territories and a group of blocks in the north of the continent (Pine-Creek, Kimberly, etc.).

Africa is sectioned into four cratons: Southern shield Kalahari, proto-platform Congo in the equatorial Africa, Central-African proto-platform possibly joining several independent shields and proto-platform of West Africa.

Within the South America are identified two proto-platforms: Guiana shield with the Amazon craton and East Brazilian craton including a number of smaller blocks with Archaean crust at the foundation. At that, the East Brazilian craton is joined with the Congolese craton of South Africa as a clear separation of these blocks had occurred relatively recently, only in Mesozoic.

Thus, in the middle of Early Proterozoic, at the time of Monogea disintegration the Archaean continental crust had turned out broken into numerous individual small plates. In our estimate, there had been 28 of them; V.E. Khain [127] believed that there had been more than 30 such individual plates then. (That is why he proposed to call Early Proterozoic the era of small plates.)

In connection with the aforementioned sharp nonuniformity in the composition of Early Proterozoic mantle, the descending flow of the next single-cell convective structure formed about 1.9 BYa must have been located antipodally to the former supercontinent Monogea. With this in mind, the reconstruction of the second supercontinent was built by way of moving the continental blocks of Monogea onto the opposite side of Earth with their subsequent centripetal drift to "gumming" into a single continental massif. At that, turned out merged into one also all ancient blocks of the continental crust surrounded by the Karelian and its homochronous folding and by activation and reworking areas of the Archaean crust which had occurred about 1.9– 1.8 BYa (Fig. 9.3).

Concerning the formation at the end Early Proterozoic of a single supercontinent, V.E. Khain and N.A. Bozhko [102] wrote: "By 1.7 BYa practically all proto-geosynclinal basins had vanished, all eocratons merged and had to have emerged a single massif of continental crust – a supercontinent which is logically to call Pangea I as opposed to a younger, Wegenerian Pangea II".

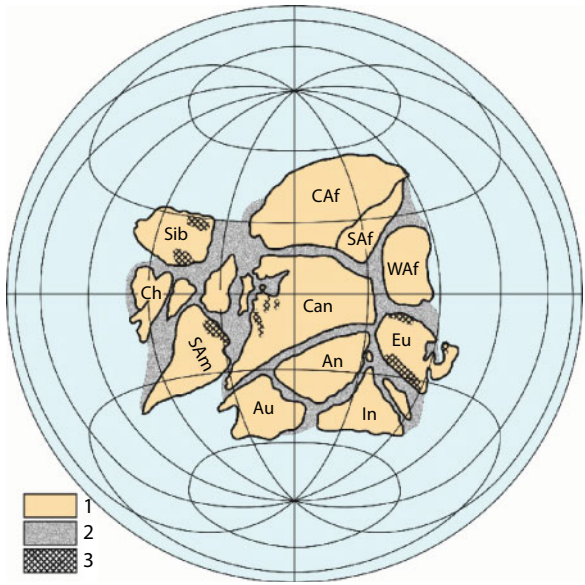

Fig. 9.3 Reconstruction of a supercontinent Megagea (Stille) 1.8 BYa: *1.* Archaean continental shields; *2.* Fold belts; *3.* Redbeds; Ch is China; CAf is Central Africa; (for other symbols see Fig. 9.2).

Simultaneously with the continental drift a reorientation had occurred of Earth's momentum of revolution axes as already mentioned above. As a result, a newly formed supercontinent had to move into low latitudes again. Judging by abundant development at that time of red-bed weathering crusts [236], that is exactly what had happened in actuality (see Fig. 9.3).

Reviewing the reconstruction of a supercontinent Megagea, it should be remembered that first to suggest the existence of this hypothetic ancient supercontinent was H. Stille in 1944. He also proposed to call it Megagea. His proposal was based on the observations of a great similarity in the geological structure of various ancient blocks often united by homochronous folding at the time of "Algonkian revolution" of late Early Proterozoic. As a result, H. Stille came to a correct conclusion "about unusually thick post-Algonkian continental massif 'Megagea'. It had included not only most ancient continents of the subsequent Earth evolution but also later ortho-geosynclinal regions that had emerged as most ancient geosynclines within this continent. This had occurred as a result of a global scale regeneration, and most ancient continents may be considered residual blocks of Megagea" [237, p. 383].

H. Stille was no mobilist. That is why he considered the origin of Megagea from purely fixist position, believing this supercontinent to have been an ancient formation of Earth crust and the disconnection of many

present-day continents a result of a subsequent destruction of the continental crust and not of a continental drift.

A more modern geological substantiation of Megagea existence based on more accurate and mass absolute age determinations of geological event ages through the mobilist approach to the issue is provided in a publication by V.E. Khain and N.A. Bozhko [102] in which, though, this supercontinent is called not Megagea but Pangea I.

In our work essentially the same mobilist approach and the same geological data taken mostly from the monograph by V.E. Khain and N.A. Bozhko were used. Nevertheless, the Megagea reconstruction quoted here (see Fig. 9.3) is substantially distinct from Pangea I reconstruction in the publication by V.E. Khain and N.A. Bozhko. The latter circumstance probably says that currently proposed continent reconstructions for geological epochs so remote from us in time are still far from perfect. Unfortunately, due to a low reliability of paleomagnetic determinations for Proterozoic rocks it did not appear possible so far to use this method for the reconstruction of the Pre-Cambrian history of the continental drift.

9.4 Disintegration of Megagea and Formation of Mesogea (Rodinia) Supercontinent in Middle Riphaean

Similarly to Monogea, Megagea had existed for a short time, no longer than 100–150 MY as already about 1.7 BYa, the first indication of a split of the Early Proterozoic supercontinent had appeared. For instance, in place of folded structures, in the North American cordillera at that time had been laid down first riftogenic formations and aulacogens. However, the fault tectonic and split of continents had showed up most explicitly about 1.5–1.4 BYa. At that time, almost on all platforms had emerged riftogenic troughs and numerous aulacogens. Over some marginal riftogenic structures about 1.5–1.4 BYa had been forming huge anorogenic volcano-plutonic belts, often unprecedented in scale as it is observed along the eastern framework of the North-American platform or Western margin of the Russian platform. These broad belts extending for up to a few thousand kilometers, in Early Riphaean had been invaded by hundreds of large (up to a 100 km across) plutons of anorthosites, sienites, gabbro, granite-porphyry, rapakivi granites and normal potassium granites.

This Early Riphaean phenomenon, so unique and never repeated thereafter, apparently is still waiting its detailed explanation. However, already now a suggestion may be voiced that all these plutons had emerged at the

expense of secondary remelting of sedimentary rocks accumulated over 200–300 MYa on passive continental margins, fragments of split about 1.7–1.6 BYa supercontinent Megagea. As likely as not, involvement in the remelting of shelf sediment masses so giant (thickness up to 12–15 km) had been facilitated by high initial contents in them of iron oxides. After all, the end of Early Proterozoic and beginning of Early Riphaean had been epochs of massive iron ore formations' deposition on the continental shelves and slopes. If, however, density of such sediments exceeded density of the mantle matter (about 3.3 g/cm^3), which is possible as density of jaspilites is greater than 4 g/cm^3, then at the moment of riftogenesis such sediments could have easily "collapsed" into a hot mantle through subduction zones.

This is even more likely as the thickness of Middle-Proterozoic oceanic plates had not then exceeded 40 km, i.e., had been about two times thinner than the present-day ones (see Fig. 8.3). After remelting of sediments and melt liquation, iron had immersed in the mantle and light silicate magmas had emerged on the surface and crystallized there at shallow depths as granitoid or alkaline plutons [18]. Primary sedimentary origin of the anorthosite-rapakivi-granite magmas is also indicated by strontium ratios in the subject rocks. Thus, primary ratios $^{87}Sr/^{86}Sr$ in fifteen anorthosite bodies of North America and Norway are within the range of 0.703–0.706, for the Vyborg rapakivi massif this ratio is 0.704. That is strontium isotope ratios typical of the sediments in the very end of Early and Middle Proterozoic whereas the mantle ratios of same age these isotopes are within a narrow range of 0.7015–0.702 (see Fig. 8.13).

For this reason, at reconstructions we considered anorogenic volcano-plutonic belts as indicator complexes of passive continental margins. Besides, at the reconstruction of Megagea disintegration, its partition into individual continents was conducted by Grenville orogeny collision sutures. It had emerged at the next consolidation stage of the third in succession supercontinent, Mesogea or Rodinia, as it is called in many publications. It was also assumed that fallen apart fragments of Megagea had been centrifugally drifting in various directions from the former supercontinent's center of gravity.

At reconstructing of the next supercontinent, Mesogea (Rodinia) we worked based on an assumption that the newly emerged descending flow of a single-cell convective structure, as in the case of Megagea formation, had emerged in the opposite Earth hemisphere in the equatorial plain. This theoretical assumption was considered when combining the continents into a single structure of a new supercontinent. Besides, the inherited nature of continent motions and paleo-climatic data of red-bed weathering crust distribution in Middle Riphaean was also considered [236]. What was

also considered was that subsequently, about 800 MYa, had been observed simultaneous glaciations in the South and Central Africa, on the Brazilian craton of South America and in the Eastern Australia. For this reason, Australia in Mesogea reconstruction is shown in a position of approach with South Africa (Fig. 9.4).

Paleomagnetic latitude determinations for Middle Riphaean still remain very unreliable. That is why it does not make sense to use them for Mesogea (Rodinia) reconstruction. However, the paleomagnetic declinations apparently may be used as auxiliary information. For this purpose, it is expedient to take directions for the poles for each subcontinent at the time 1 BYa from the reconstructions built based only on paleomagnetic data by L.P. Sonenshein *et al.* [238] and by J. Piper [239]. These directions are shown as arrows on our reconstruction.

A distinctive feature of Middle Riphaean had been a drastic weakening of typical of the previous epoch riftogenic processes and on the contrary, equally drastic increase of orogenic ones. The Grenville epoch diastrophism in Middle Riphaean, about 1 BYa, had showed up on the periphery of

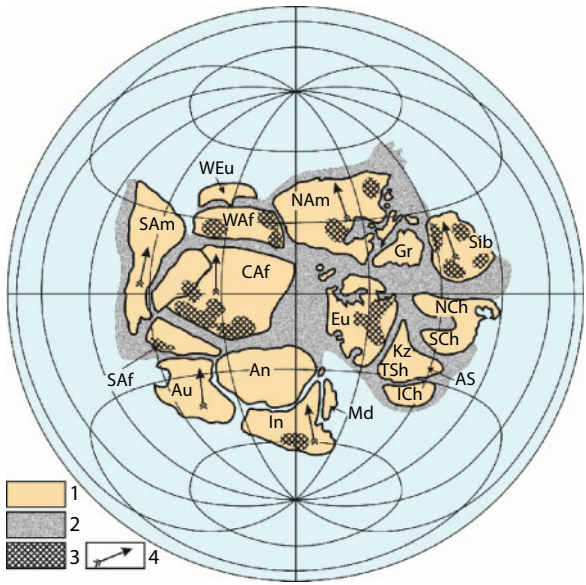

Fig. 9.4 Reconstruction of Mesogea (Rodinia) supercontinent for the epoch about 1 BYa: *1.* Archaean continental shields; *2.* Fold belts; *3.* Red-bed weathering crusts; *4.* Vectors of paleomagnetic inclinations borrowed from the publication by Zonenshain *et al.* [238]; NAm is North America; TSh is the Tien Shan block; AS is the Altay-Sayan domain; ICh is Indochina; WEu is Western Europe; Md is Madagascar; see Figs. 9.2, 9.3 for the rest of the symbols.

practically all Early Proterozoic platforms. Among the main criteria for building the Mesogea (Rodinia) reconstruction, were used fold belts of the Grenville orogeny. At that, same type mobile Grenville age belts manifested on the margins of adjacent continents were merged with one another. For instance, in the eastern North America at that time had emerged the Grenville mobile belt which is, most likely, the zone of collision with North Europe. On this subject, V.E. Khain [127] noted that about 1 BYa Grenville mobile belt had merged into a single continental plate North America, Greenland, Ireland, North Great Britain, Scandinavia and Northwestern France. We may add that attached to North America through these areas had been the Baltic shield and the Russian platform. However, the West Europe with the Armorican massif still had been separated from the rest of Europe and most likely adjoined the West Africa.

With Middle Riphaean also belongs setting up of the Timan structure and in the South Urals, a subduction origin Maksyutov metamorphic complex. The Grenville tectogenesis that had manifested itself in Kazakhstan and in the basement of West Siberian platform, through a fold system of the Yenisei Range had actually joined the Russian and Siberian platforms. Grenville age orogenesis had involved territories of Kazakhstan-Tien-Shan, Altay-Sayan and Baikal-Vitim fold areas as well as North Mongolia. At the end of Middle Riphaean, sedimentary sequences in riftogenic troughs and framework of the Chinese platform had experienced an intense folding and besides, in place of the South Chinese craton had existed island arc and marginal sea basins' environments.

As is obvious from the quoted brief geographic distribution list of collision fold belts welding together adjacent platforms, in Middle Riphaean (about 1 BYa) all north continents had been merged in a single supercontinent Laurasia, although even its configuration had been still different from a classical Wegenerian_Laurasia that later had entered the composition of Pangea. Such distinction had been associated with probable position at that time of the Chinese platform between the Siberian and Kazakhstan plates which, in particular, is supported by homochronous cover glaciations in Europe, Kazakhstan and on the Chinese platform about 650 MYa [204, 240].

The southern continents had turned out about 1 BYa merged in the second supercontinent Gondwana. Thus, at that time the Amazon plate had joined through a sub-longitudinal fold system Arasha–Estrondy the Brazilian platform and through it, the Central Africa. Simultaneously, South Africa through the Kibaride buildup had been welded with the Central African platform. It had also been joined with the West Africa through a folded zone of the Central Hoggart. Whereas the Eastern

Gondwana including Australia, Antarctic and India had been attached to the eastern margin of the African mega-shield by Kibara folding of a set up by that time Mozambique mobile belt and fold system of the Somalia Horn and Arabian Peninsula. In Antarctic, a zone of tectono-thermal basement reworking in the area of the Tran-Antarctic mountains (Eastern Antarctic) corresponds with this belt.

Both Middle Riphaean supercontinents most likely had been merged into a single larger supercontinent Mesogea. This is supported by intense folding and magmatic activity in the Arabian-Nubian Gondwana area and in a fold belt of the Dalsland orogeny of Laurasia's South-European framework. From the European side to the relics of this branch of the Grenville belt belong the basement of the Pannonian depression, the central part of Rhodopes and possibly Serbian-Macedonian massifs. Extension of this belt is probably observed up to the Crimea. The result of the performed reconstruction based on the consideration of all mentioned building criteria is imaged in Fig. 9.5.

As seen from the conducted constructions, the supercontinent Mesogea turned out a rather compact formation little resembling in its configuration the Paleozoic Pangea imaged in Fig. 9.8. The exceptions are only the

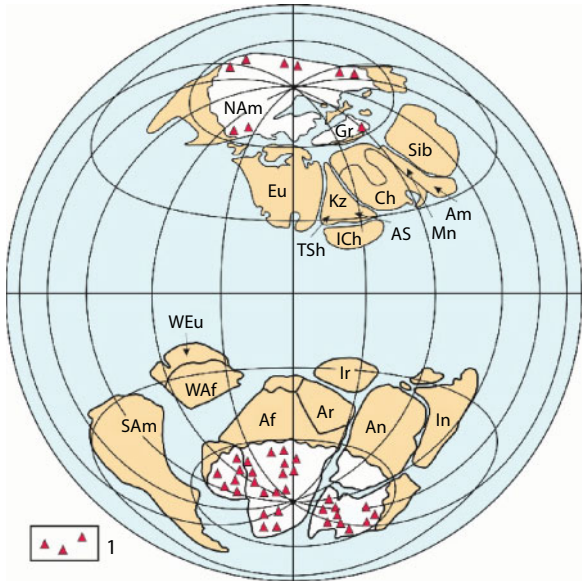

Fig. 9.5 Mesogea disintegration into Laurasia and Gondwana about 800–750 MYa: *1.* Riphaean tillites and tilloids position after N.M. Chumakov [204]; Mn is the Mongol Plate; Am is the Amur Plate; Ir is the Iranian Plate; Ar is the Arabian Plate; for the other symbols see Figs. 9.2-9.4.

orientation of Eastern Gondwana turned 90° compared with its position on the Wegenerian Pangea reconstruction and position of the Chinese platform positioned on our reconstruction between the Siberian and Kazakhstan plates.

9.5 Mesogea Disintegration in Late Riphaean and Formation of Pangea Supercontinent at the End Paleozoic – Early Mesozoic

As all previous supercontinents, Mesogea (Rodinia) had existed for a short time (no longer than 100–150 MY), and already sometime about 900 MYa had begun its disintegration into two parts, the northern, Laurasia and the southern, Gondwana. Approximately 850 MYa, a wide oceanic basin, Proto-Tethys had emerged between them. About 800–750 MYa, Laurasia had moved in the northern circum-polar area and Gondwana, to the South pole, a testimony to which are numerous Late Riphaean tillite and tilloid finds of these two supercontinents [204] (Fig. 9.5).

A substantial climate cooling had onset at the end Proterozoic. The snow-line had significantly dropped and in high latitudes had even reached below the continent stand level. A new era of glaciation epochs had onset on Earth [19]. Besides, through the convection, the mantle composition had become rather uniform. As a consequence, the orientation of Earth main inertia momentum axes and its body position in regard to the revolution axis had already been defined only by the position of continents and oceans on Earth's surface.

The establishment at the end Riphaean and in Vendean of a cold climate in Laurasia and Gondwana had been clearly facilitated not only by the position of continental massifs in the circumpolar Earth's areas but also by emerging at that time a broad ring-like oceanic basin in low latitudes. That had been favorable for establishing in it of a single and powerful equatorial trade wind current with weak branches of anti-trade wind currents in temperate latitudes. A result had been that the "water-heating" system of Earth's continental sectors at the end Riphaean had sharply weakened. That had facilitated the emergence in the second half of Late Riphaean of the African-Australian glaciation in Gondwana and the Canadian glaciation in Laurasia and also of expansive Lapland glaciation in Europe, Kazakhstan and China in Late Riphaean or Vendean (Figs. 9.5 and 9.6).

In Late Riphaean and Vendean, as in Early Riphaean, most former orogenic mobile belts in Middle Riphaean age Mesogea had extinguished. In their place had often been emerging riftogenic structures. On continental

platforms at that time had emerged a network of aulacogens. They had usually been inheriting ancient suture zones of Svecofennian (Karelian) age. Along younger suture zones of Grenville age fold belts had begotten new oceanic basins. Thus, in place of a Grenville mobile belt which had welded in Middle Riphaean the east coast of North America and Greenland with the European platform, had emerged about 800 MYa a new Paleo-Atlantic ocean called Iapetus ocean.

At the same time, the West Gondwana had been crossed by narrow oceanic troughs of West African and Brazilian sub-oceans (Red Sea type) with Katanga Bay. Between the West and East Gondwana had emerged a rapidly expanding African-Australian oceanic basin. Due to its evolution apparently had occurred restructuring of Gondwana general structure plan (see Fig. 9.6). Geology of the present-day eastern margins of Africa and Australia and also Trans-Antarctic mountains does not contradict a hypothesis of existing in Late Riphaean of oceanic basin between these continents. Indeed, the Mozambique belt in Africa, the Adelaide geosyncline in Australia and the Trans-Antarctic mountains at that time had been passive continental margins.

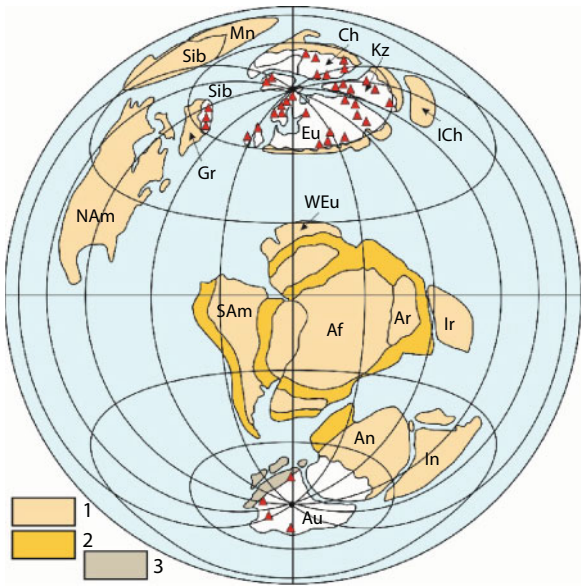

Fig. 9.6 Disintegration of Laurasia and Gondwana about 650 MYa: *1.* Continental shields and platforms; *2.* Fold belts; *3.* Fold belts covered at that time by glaciation; for other symbols see Figs. 9.2-9.5.

A very severe precondition for making Gondwana reconstructions in Late Riphaean, and therefore for earlier geological epochs is actual data on the distribution of cover glaciation traces (tillites and tilloids) on the southern continents in Late Pre-Cambrian. According to the data systematized by N.M. Chumakov [204], about 750 MYa had practically simultaneously existed glaciation covers in South and Central Africa, in Australia and in the eastern South America. That is why at making reconstructions of the southern continents' positions in Late Riphaean we are forced always to place all glaciated continents closely near the south geographic pole. At that, it must be remembered that geological formations – indicators of glaciation periods – are much more reliable than paleomagnetic data for Pre-Cambrian. That is why on our reconstructions of a Middle- and Late Riphaean Gondwana the juncture of the eastern and western fragment of the supercontinent is shown not the conventional way but along the contact line with Africa of Australian and Antarctic continents (see Figs. 9.4 and 9.5). The same goes with the positions of the northern continents on Laurasia Riphaean reconstructions. On our reconstructions of Late Pre-Cambrian, the Chinese platform is placed not in the southern Laurasia but in the territory adjacent to Northern Europe (see Fig. 9.6).

In some cases, paleoclimatic data are helpful at estimation of the intercontinental oceanic basin width. Thus, it may be estimated that in Late Riphaean the width of circum-equatorial Proto-Tethys had reached approximately 6–10 thous. km (see Fig. 9.5). Similarly, it may be estimated that in Vendean the width of Iapetus paleo-ocean had been at least 2,000 km whereas the width of the Paleo-Urals ocean had been still insignificant (see Fig. 9.6).

Folding deformations in the second half of Late Riphaean had occurred in limited regions of both supercontinents. Thus, orogenic movements in Laurasia had occurred only in the parts of Indochina adjacent to the Chinese platform and in the Yenisei range massif. In Gondwana, mobile fold belts had continued to form only in the eastern Arabian craton and adjacent to it portions of the Antarctic platform on the side of the present-day Weddell Sea.

In Vendean, practically all Laurasia continents and cratons had continued to remain in an environment of evolving riftogenic structures. Passive continental marginal regimes had established on their periphery. Only in Timan-Pechora, mobile belt at the end Vendean had been evolving folding dislocations and overthrust structures. But in general, continental massifs of Laurasia in Vendean, as in Late Riphaean, had continued their centrifugal drift.

Contrary to this, in Late Riphaean (Vendean), Gondwana had already moved in the existence area of a descending convective flow in the mantle.

That had predetermined a complete change of the tectonic development regime of this supercontinent. As a result, South America and Africa had been embraced in the process of intense compression with the closing of all earlier existing narrow oceanic troughs in whose place had now emerged inter-cratonic folded structures of Pan-African orogeny. At the same time Eastern Gondwana had again merged with the Western along the Mozambique belt on the eastern margin of Africa. This, in particular, explains the origin of intense orogenic movements that had embraced at the end of Vendean (approximately 630–600 MYa) the entire Mozambique belt. However, the final Gondwana consolidation, apparently, had occurred somewhat later, only in Cambrian and Ordovician, after completion of the last activation phase of this belt about 550–450 MYa. This time outlines of the Southern supercontinent become the same as in customary to us reconstructions of the Wegenerian Pangea (see Figs. 9.7 and 9.8).

A position of a single supercontinent in the near-polar zone, as we saw above, causes strong instability of revolving Earth. As a result, its body tends to turn so that the center of gravity of such continental massif would eventually turn out on the equator. Only in this case the momentum of inertia maximum value's main axis for the planet will coincide with its revolution axis. However, at non-symmetric position of the two approximately equi-sized supercontinents near the poles but in the same hemisphere, a quasi-stable

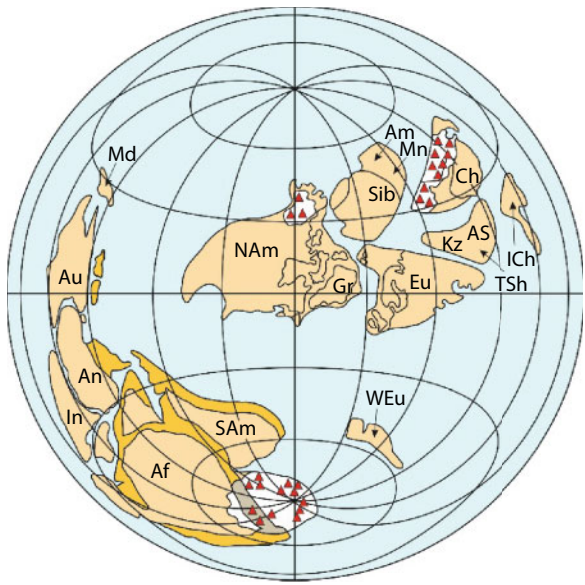

Fig. 9.7 Gondwana and Laurasia evolution about 550 MYa. See Figs. 9.2-9.6 for the symbols.

Fig. 9.8 Reconstruction of A. Wegener's supercontinent Pangea about 200 MYa based on the data by [242]. See Fig. 9.6 for symbols.

situation may emerge when the common center of mass of these continental massifs lies in the equatorial plain of revolving Earth. Besides, Earth revolution also may be stable in case of the coincidence of its revolution axis with the third axis of the momentum of inertia that has the minimum value. In this case, under the laws of mechanics, Earth's revolution remains stable. That is exactly the situation observed for the present-day Earth: the major axis of its main momentum of inertia is positioned somewhere in the central Pacific south of the equator and the minor axis, in the North Arctic basin near the geographic pole. Considering this, in Figs. 9.6 and 9.7 are imaged the reconstruction options satisfying exactly this condition.

The emergence in Late Riphaean and Vendean of this quasi-stable situation, apparently, may be an explanation of a relatively long (about 200 MY) stay of substantial continental masses in Earth's circumpolar areas without a notable turn of its body into a position where both supercontinents, Laurasia and Gondwana, would have been on the equator. Should these supercontinents have been positioned in the near-polar areas more symmetrically with regard to the geographic poles, such turn of Earth and a displacement of the supercontinents on the equator, at average mantle viscosity about 10^{23} Π, would have happened in less than 150 MY.

Nevertheless, existed in Late Riphaean and Vendean drift continents had been gradually changing the orientation of Earth's momentum of

inertia axes. In connection with this had to occur the adequate with this turns of its body relative to geographic poles. It is possible that such "drift-caused" Earth turns relative its revolution axis, in combination with the continental drift, might be used for the explanation of frequent alternation of the glacial and warm climates in Late Riphaean and Vendean on one and the same continents [240]. In particular, at the Vendean/Cambrian boundary in the process of the final formation of the Paleozoic Gondwana about 550 MYa, due to general turn of Earth approximately by 90°, West Africa had turned out on the South pole and North America, Europe and Australia had moved on the equator (Fig. 9.7).

By that time part of West Europe had possibly separated from West Africa and had been drifting toward the European platform with which it had merged in Paleozoic on an Early Hercynian suture zone. As a result, most continents in Cambrian had been positioned at low latitudes, and that had predetermined the emergence of Earth's warm climate so typical of that period (inland glaciations had been evolving then only in a limited territory of West Africa). This phenomenon perhaps may be an explanation of a rapid (at a rate of about 5 cm/year) apparent pole movement in the Gondwana continents from West Africa in Late Ordovician to Antarctic in Early Permian.

Paleomagnetic data of Phanerozoic, especially its second half, become much more reliable. That is why the configuration of the last supercontinent Pangea, whose existence was predicted by A. Wegener [241] already in 1912, is usually determined from geomorphological structural features of coastal zones of adjacent continents and from paleomagnetic data. One of the most perfect reconstructions made by A. Smith and J. Brieden [242] is displayed in Fig. 9.8.

As with the previous supercontinents, Pangea's center of gravity had been positioned in low latitudes, although the continents were really expanding by that time, and had sprawled in a wide band almost from one pole to the next. If we believe this reconstruction, it turns out that Pangea emerged at the end Paleozoic had also been in a quasi-stable state in regard to Earth's revolution axis at which the third, minor axis of the planet's momentum of inertia had coincided with the revolution axis. With such configuration, Pangea might have preserved its orientation in regard to Earth's revolution axis indefinitely but about 150 MYa had begun its disintegration and a new period of centrifugal continental drift.

In more detail and quantitatively, the continental drift influence on Earth's position in Phanerozoic was reviewed by A.S. Monin and V.P. Keondzhyan in a monograph Geodynamics (oceanology, geophysics of the ocean) [243]. A reminder: the minor axis of major momentum of inertia

coincides with the revolution of the present-day Earth. Nevertheless, our planet is continuing the stable revolution without any trend to a significant apparent pole drift.

Summarizing the formation and destruction of supercontinents, they may be lined up by the time of their formation:

1. Monogea (2.5 –2.4 BYa);
2. Megagea by Stille (1.8 – 1.7 BYa);
3. Mesogea – Rodinia (1.0 – 0.9 BYa);
4. Pangea by Wegener (230 – 150 MYa).

As already mentioned above, the formation and disintegration of supercontinents in Earth's history had been caused by a restructuring of mantle convective flows. At the emergence of a single-cell convective structure, all continental massifs had been drifting towards the single descending flow forming above it a single supercontinent of Monogea, Megagea, Mesogea (Rodinia) or Pangea type. At that, a splash up had always occurred of Earth's tectonic activity (see Fig. 7.8). After the formation of such supercontinent, it had been naturally as if surrounded from all sides by subduction zones by which the oceanic plates of flowing around joint ocean Panthalassa had been immersing in the mantle. At a usual plate subduction rate of about 5–10 cm/year, already in a few dozen million years these plates had subsided to the core level, where they had been subjected to a total destruction (disintegration) due to the operation of barodiffusion differentiation mechanism of iron oxides (see section 5.4).

The effect of the mantle matter barodiffusion differentiation had depended on the length of its stay in the environment of high pressure (greater than 0.9 Mbar). The matter itself of the immersing plates had always remained somewhat colder and therefore always had a greater density compared with the surrounding mantle. That is why it is natural to expect that under subduction zones, the mantle matter would be sinking in the core, forming there a semblance of descending flow roots (Fig. 9.9). It follows from this that after the differentiation, the disintegrated mantle matter of these roots as a liquid "magmatic gruel" would have to be "flowing" off these roots (i.e., rising) in all directions from the immersion areas of former oceanic lithospheric plates in the core. For this reason, under the center of a supercontinent emerged shortly before that had gradually begun accumulating large masses of the mantle matter that had experienced differentiation and because of this of lower density. As a result, after some time (on the order of a few dozen million years) under the supercontinent, in the location of former descending flow, had emerged a powerful ascending convective

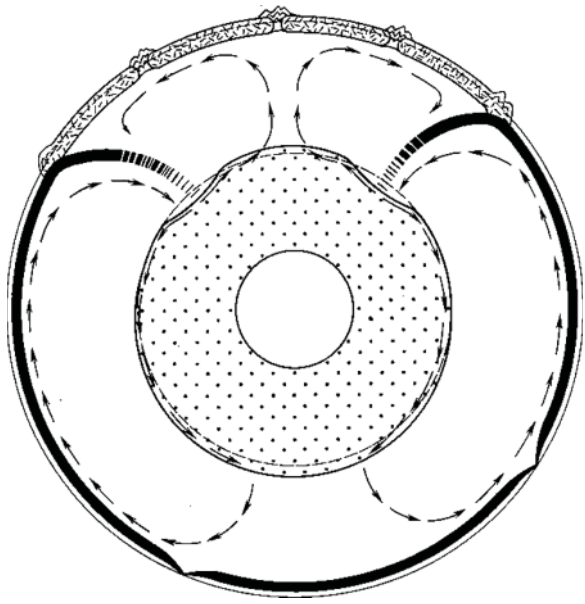

Fig. 9.9 Supercontinent destruction mechanism at the expense of emergence under of a new ascending mantle flow instead of earlier existed descending flow.

flow. It had lifted and broken positioned above it lithospheric shell. This, in turn, had caused a supercontinent split and centrifugal drift of its continental fragments in all directions from its former center. This phenomenon is apparently the explanation of the instability of all supercontinents that emerged in the past geological epochs and a very short time (no greater than 100 MY) of their existence as single continents. Actually, this correlation, and in fact the rule may be explained only in the context of the global chemical-density convection mechanism.

10

Mantle Degassing and the Formation of Earth's Hydrosphere and Atmosphere

The hydrosphere and atmosphere evolution regimes on Earth are of first-rate significance in determining Earth's climate evolution, origins and evolution of life on Earth and also as the solution of an issue of mineral resources' origin, in particular, combustible mineral resources. This is a reason to review the formation of these external geospheres in somewhat more detail.

10.1 The Primary Mantle Degassing

As mentioned earlier, a young Earth in Katarchaean had been devoid of the hydrosphere and atmosphere. For this reason, it is natural to assume that these external and quite volatile geospheres had emerged on Earth only due to its degassing. However, this process might have started only after heating up of the upper parts of Earth's section and emergence in it of molten matter foci. Heating up of Earth's subsurface in those distant epochs had been occurring only at the expense of a release of the tidal energy of interaction with the Moon and radioactive elements' decay in its subsurface. At that, the tidal energy had been released mostly in the upper parts of Earth's section. Exactly for this reason the first melts of Earth matter had appeared at relatively shallow depths, 200 to 400 km, approximately 600 MY after the formation of Earth itself. Soon after the first melt appearance Earth matter differentiation had immediately begun and the first indications of endogenous tectono-magmatic activity had appeared. This had occurred around 4 BYa. Subsequently, Earth matter differentiation had begun feeding on most powerful process, gravity energy separation of high-density molten iron masses from Earth matter silicates (see section 5.3). It is also anticipated that Earth, or rather its mantle degassing had substantially depended not only on temperature defining the intensity of convective movements in

N. O. Sorokhtin (ed.) The Origins of Natural Diamonds, (271–323) © 2019 Scrivener Publishing LLC

it but also on its chemical composition. Major features of the convecting mantle chemical composition's evolution are shown in Figs. 5.15 and 5.16.

After developing the fundamentals of Earth's global evolution concept described above, a real opportunity emerged for a quantitative description of the ocean formation processes on Earth. First quantitative models of Earth's World oceanic water and gas shell mass growth based on most general concepts of Earth's global evolution have been proposed as early as the mid-1970s [15]. These models assumed that Earth's degassing rate had been directly proportionate to the rate of convective mass exchange in the mantle and that a major contribution to the mantle convection had come from a most powerful energy process, gravity chemical-density differentiation of Earth's matter onto the high-density oxide-iron core and residual silicate mantle. However, in these early publications the beginning of Earth degassing was traditionally placed at the moment of ending the process of our planet formation around 4.6 BYa.

Somewhat later (Monin, Sorokhtin, 1984); [17, 18] more sophisticated models of the hydrosphere formation have been developed based on zonal and barodiffusion differentiation mechanisms of Earth's matter reviewed above (see sections 5.3 and 5.4). In these models, the primordial Earth after its formation was assumed to have been a relatively cold planet. Within this context, Earth's degassing might have started approximately 600 MY after its formation time. This process had started up after a preliminary heating of the initially cold Earth subsurface to melting temperature of the upper mantle silicates and the emerging in young Earth of the first asthenosphere.

The initial mantle degassing had been likely associated with the decline of volatile component solubility in silicate melts at lowering their temperature and relatively low pressure. As a result, erupted on Earth surface mantle melts, mostly basalts and in Archaean also komatiite magmas, had boiled releasing excessive volatile elements and compounds in the atmosphere. Besides, part of the volatiles might have been released at weathering of igneous rocks after their destruction under surface conditions. However, the main mechanism of water degassing had been a decline of its solubility at cooling and crystallization of water-containing basalt melts at low pressure (Fig. 10.1).

It follows from this that Earth's degassing rate is proportionate to the mass of the mantle rocks erupted on Earth surface within unit time, to their content of volatile components and their mobility. As a first approximation, the rate of mantle rocks eruption is proportionate to Earth's tectonic activity defined by the rate of its total heat loss $\dot{Q}_{m}$ (see Fig. 6.17) or time derivative from Earth's tectonic parameter $\dot{z} = \dot{Q}_{\mathrm{m}} / Q_{\mathrm{m0}}$; where

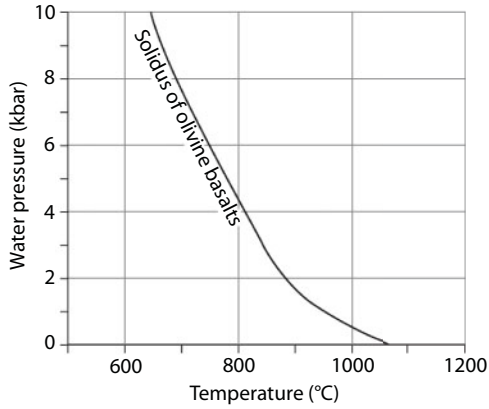

Fig. 10.1 Solidus of olivine basalts vs. pressure of water dissolved in basalt melt, after H. Yoder [244]. At basalt crystallization occurs a release of water dissolved in basalt melts.

$z = Q_m/Q_{m0}$ is Earth's tectonic parameter and Q_m and Q_{m0} are the depth heat flow (Fig. 6.13) and the present-day values of the mantle summary heat loss. The rate of Earth tectonic parameter change vs. time is shown in Fig. 10.2 and the tectonic parameter value is shown in Fig. 10.3.

Therefore, rate the mantle degassing is proportionate to its content of a given component $(m_i)_m$, its mobility exponent c_i and the rate of convective mass exchange in the mantle $\dot{z}$

$$\dot{m}_i = -(m_i)_m \cdot \chi_i \cdot \dot{z}. \tag{10.1}$$

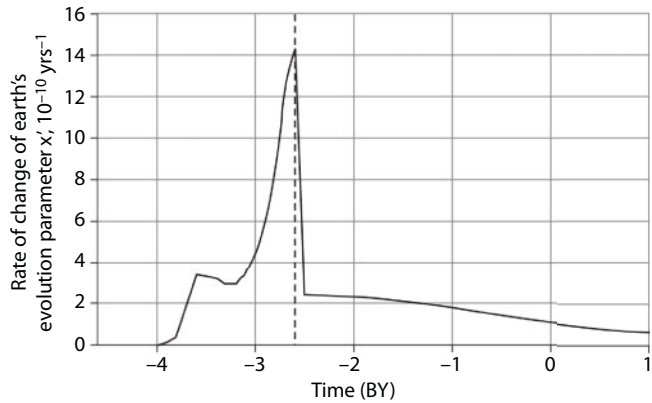

Fig. 10.2 Rate of change of Earth tectonic parameter $\dot{z}$ defining the rate of eruption on Earth surface of basalt melts and rate of the mantle degassing (the dashed line is the separation moment of Earth's core).

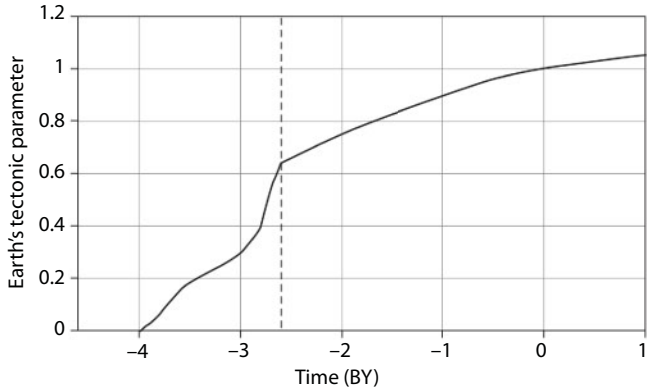

Fig. 10.3 Earth tectonic parameter z defining the accumulation of Earth's magmatic activity products and mass of volatile matter degassed from the mantle. Dashed line marks the moment of the end of Earth core separation process.

Then the mass of a degassed i^{th} volatile component and its accumulation in Earth's external geospheres is determined from the following equation:

$$m_i = (m_i)_0 \cdot \left(1 - e^{-\chi_i \cdot z}\right), \tag{10.2}$$

where $(m_i)_0$ is total mass of the i^{th} volatile component in Earth (in the mantle and external geospheres). In Archaean, when the mass of the degassing mantle had been gradually increasing, it is necessary to consider its growth from $M_m = 0$ to its total amount at the end Archaean $M_{m\Sigma}$. The mass of the mantle was estimated earlier (see Fig. 7.6), then for degassing water and any other volatile elements and compounds (for instance, N_2 and CO_2) in Archaean should be used another equation

$$m_i = (m_i)_0 \cdot (1 - e^{-\chi_i \cdot z}) \cdot \frac{M_m(t)}{M_{m\Sigma}}, \tag{10.2'}$$

where $M_m(t)$ is mass of the mantle at the time $4 < t < 2.6$ BYa. At that, for Proterozoic and Phanerozoic, the equation (10.2) remains valid.

To determine the mass of a volatile component m_i, degassed from the mantle, for instance water, in Eqs. (10.2) and (10.2') it is necessary to substitute the initial and boundary conditions for the contents of this component (water, nitrogen or carbon dioxide) in Earth's external geospheres.

10.2 Seas and Oceans Formation on Earth Surface

Taking into account that Earth matter differentiation mechanism in Archaean and after Archaean had been conceptually different, it should be expected that volatile components' mobility parameters χ_i, at least for some of them, may also have been substantially different from one another. In Archaean, all silicate matter in the convecting mantle, together with volatile components contained in it, had unavoidably passed through a layer of molten iron (see Fig. 5.1). At that, oxides with smaller formation heat than bivalent iron oxide (63.64 cal/mole), must have dissociated releasing their oxygen for oxidizing of iron to the bivalent state. Formation heat of water molecules (water vapor or fluid) is equal to 57.8 kcal/mole, therefore, water must not have been dissociated on the metallic iron melts in Earth matter differentiation zones.

$$Fe + H_2O \rightarrow FeO + H_2 + 5.84\,\text{kcal/mole} \tag{10.3}$$

As opposed to water, carbon dioxide formation heat is equal to 94.05 kcal/mole, for this reason carbon dioxide might have crossed this layer of zonal differentiation unhindered. It thereby follows that in Archaean, the water mobility parameter in the degassing equations (10.1) and (10.2) had been substantially smaller than in post-Archaean time, whereas the mobility parameter for carbon dioxide might have remained constant for the entire time of its degassing from the mantle. Please note in passing that together with water, on iron melts in Archaean had dissociated also many other oxides and sulfides with low formation heat value, reducing at that to native elements.

As water mobility parameters in Archaean and post-Archaean might have been drastically different from one another, it is necessary for the estimation of the mantle degassing to compose two degassing equations (10.2) and (10.2') with different mobility parameters. For this, it is necessary to join them by the continuity condition of the degassing process at the boundary between Archaean and Proterozoic. In this case, two equations include three variable parameters: two water mobility parameters and initial mass of water in Earth's matter $(m_{H_2O})_0$. Therefore, for a quantitative solution of the problem, it is necessary to determine and insert in the equations three independent boundary conditions.

The first boundary condition may be the total mass of water in the present-day ocean, continental and oceanic crust combined. Our estimates, based on the works by A.B. Ronov and A.A. Yaroshevsky [73], amended with

our own observations and computations, showed that for the present time the following values of water mass in hydrosphere may be assumed. The ocean currently contains $1.42 \cdot 10^{24}$ g of water, the continental crust together with continental water and glaciers, $0.446 \cdot 10^{24}$ g, and the oceanic crust, approximately $0.358 \cdot 10^{24}$ g of bonded water. The total in external Earth geospheres (in its hydrosphere) is currently $2.23 \cdot 10^{24}$ g of water. This quantity of water had been degassed from Earth subsurface over the entire time of its geological life, i.e., over the recent 4 BY in the history of the planet. Strictly speaking, this assertion is not totally right because in Proterozoic and Phanerozoic most of the water that had reached Earth surface, had again been constantly returning in the mantle through the plate subduction zones. Some part of it had been dissociating at the oceanic crust rock hydration in the upper layers of the atmosphere (as affected by the solar radiation). However, if we consider not the absolute mass but only its effective value (equal to the difference between the masses of degassed and subducted water), then all estimates are valid. Only the effective value of the mobility parameter χ turns out somewhat smaller than their real values.

For the determination of the second boundary condition of the problem, which is the total mass of water on Earth $(m_{H_2O})_0$, is necessary preliminarily to determine its mass in the present-day mantle. The problem of determining water concentration in the mantle matter in and of itself is fundamental for global petrology and, unfortunately, is not solved conclusively. The absence of the solution is due to the fact that practically all mantle rocks, upon getting on Earth's surface, right away (while in the process of rising and reaching the surface) are intensively contaminated by the surface water. Even the deepest xenoliths, for instance, garnet peridotites or eclogites of kimberlite diatremes, virtually turn out to be only fragments of the ancient oceanic crust pulled to great depths underneath the continents through the former subduction zones [11, 55, 58]. Nevertheless, fresh basalts of the oceanic islands, despite a possible capture by them of sea water filtering through stratovolcano bodies, usually contain very little water, no greater than 0.3% hydroxide (OH) [442]. These and other considerations of a theoretical nature make most of the present-day petrologists studying rocks of the mantle origin believe that there is very little water in the mantle. Thus, A. Ringwood [50] assumes that the mantle contains around 0.1% water. V.A. Pugin and N.I. Khitarov [245] believe that it is smaller, 0.025–0.1%. According to our estimates treated in more detail in monographs [17–19, 112], water concentration in the mantle matter does not exceed the same 0.05–0.06%, i.e., Earth mantle is indeed maximum dry. Then the total water content in the present-day

mantle reaches $2.007 \cdot 10^{24}$ g, and the total mass of water on Earth is approximately $(m_{H_2O})_0 \approx 4.23\,10^{24}$ g.

As the third reference point of the estimate might have served the water mass determination in the hydrosphere at an intermediate moment in time. With the use of complementary geological data, this is a quite solvable problem. As the ocean had been gradually increasing in volume, in its evolution history unavoidably must have occurred a moment when the ocean water eventually had reached the crests of mid-oceanic ridges with their Earth's rift zones. After that, the extent of oceanic crust rocks' hydration and release of ore elements in the ocean from rift zones must have been rapidly increasing. Therefore, after the described event the geochemistry of oceanic deposits must have sharply changed. In their composition must have appeared in abundance ore elements carried away from the mantle. The most typical such elements and clear indicators of the sought for boundary (a moment of oceanic crust saturation with water) is undoubtedly iron. After all, in the Precambrian mantle, there had still been notable quantities of the free (metallic) iron (see Fig. 5.16). Rising together with a hot mantle matter in the rift zones, it had been reacting there with sea water forming in a non-oxygen medium but in the presence of carbon dioxide gas well-soluble in water iron bicarbonate:

$$Fe + H_2O + 2CO_2 \rightarrow Fe(HCO_3)_2, \qquad (10.4)$$

After the crests of mid-oceanic ridges had been under the oceanic surface, the soluble iron hydroxide had begun spreading in the entire ocean. Having gotten in the shallow water, the bivalent iron, with the participation of bacteria, especially cyanobacteria, oxidized to the trivalent state, settled forming thereby thick sequences of iron ore deposits

$$2Fe(HCO_3)_2 + O \rightarrow Fe_2O_3 + 2H_2O + 4CO_2. \qquad (10.4')$$

Due to this process of the iron release from oceanic rift zones into the World ocean, it is possible to identify at least two unique epochs of mass accumulation of the iron ore formations. The first one had been manifested at the end Archaean when Kivatin type iron ore deposits had been forming (around 3.0 – 2.8 BYa). The second one had been formed at the end of Early Proterozoic around 2.2 BYa (Krivoy Rog type ores). The second stage of iron accumulation in Earth's geological chronicle is most clearly identified.

The ocean area in Proterozoic obviously had been equal to Earth area minus the area of the continents. If it is assumed that the thickness of the continental crust had changed little with time then it may be expected that the area of continents is proportionate to their mass, and the evolution of continents' mass is shown in Fig. 8.7. The area of oceans 2.2 BYa had reached $3.48 \cdot 10^{18}$ cm^2. It will be shown below (see Fig. 10.6) that average depth of the oceans then had been reaching 930 m, from which follows that the mass of water in the World ocean 2.2 BYa had been approximately $0.325 \cdot 10^{24}$ cm^2.

The mass of water bonded in Earth's crust 2.2 BYa was possible to determine from made in [18] reconstruction of the oceanic crust structure imaged in Fig. 8.1 and from the continental crust mass at that time (see Fig. 8.7). By the end Archaean, by our estimates, average concentration of bonded water in the continental crust had risen to 0.6% and by the present-day, to 2%. In this case, we find that 2.2 BYa in the continental crust had been contained around $0.109 \cdot 10^{24}$ g of bonded water. We will now assume that average density of pelagic deposits is approximately 2.2 g/cm^3 and that they contain up to 20% water. In hydrated basalts and gabbro, density around 2.9 g/cm^3, is contained around 2.5% and in serpentinites, density 3 g/cm^3, the bonded water concentration reaches 11%. This enables us to determine that in the oceanic crust 2.2 BYa had been contained around $0.385 \cdot 10^{24}$ g water. In this case, 2.2 BYa the total mass of water in the hydrosphere had been $0.325 \cdot 10^{24} + 0.385 \cdot 10^{24} + 0.109 \cdot 10^{24} = 0.819 \cdot 10^{24}$ g.

Making now a system of two equations like (10.2) and (10.2') separately for Archaean and post-Archaean time, it is possible to substitute in them the values found above of the water mass in hydrosphere of present-day Earth and in Early Proterozoic (around 2.2 BYa). As these equations include different values of water mobility parameter, it is necessary to join them into the common system by the continuity condition of the degassing process at the boundary of Archaean and Proterozoic. Only after that is it possible to find the correlation of the mass of water degassed from mantle vs. time. At that, water mobility parameter in Archaean had been equal to $c_1 = 0.245$ and in Proterozoic and Phanerozoic, as suggested, almost 5.2 times greater: $c_2 = 1.27$.

The results of water accumulation estimate in Earth hydrosphere are shown in Fig. 10.4. As we see from the Figure, water accumulation regime in Earth external geospheres had substantially changed at the boundary of Archaean and Proterozoic. This change had been especially drastic in water accumulation in the oceanic crust. This had been caused by the formation early in Proterozoic of the oceanic crust serpentinite layer which is the main and most capacious reservoir of the bonded water on Earth.

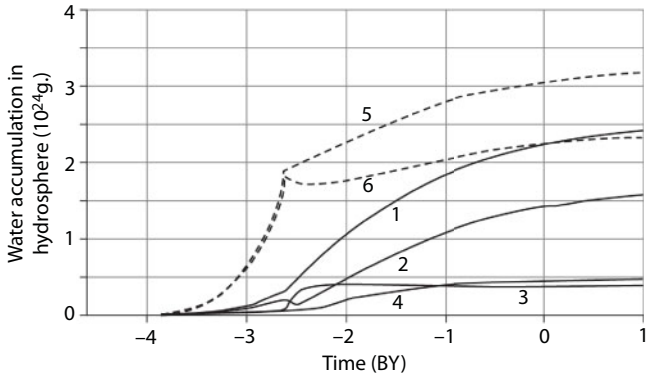

Fig. 10.4 Water accumulation in Earth hydrosphere: 1. Total mass of water degassed from mantle; 2. Water mass in the ocean; 3–4. Water mass bonded in oceanic and continental crust; 5 - 6. Mass of water degassed from mantle and ocean in a hypothetic case of the absence of its dissociation in differentiation zones of Earth matter in Archaean under reaction (10.3).

After we managed to determine the total mass of water in Earth and the value of water mobility parameters in Archaean and post-Archaean time, from Eq. (10.1) we will determine the rate of water accumulation in Earth hydrosphere. The diagram (constructed this way) of rate of water degassing from mantle is shown in Fig. 10.5. It is clear from the diagram that maximum rate of water degassing had occurred 2.5 BYa, i.e., in the

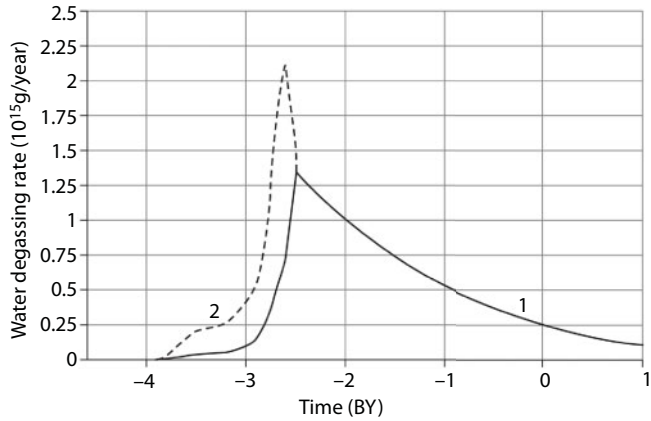

Fig. 10.5 Water degassing rate from Earth mantle into the hydrosphere: 1. In consideration of water dissociation in Archaean Earth matter differentiation zone; 2. Without the consideration of such dissociation.

beginning of Proterozoic, whereas the maximum of Earth's tectonic activity is observed in Archaean. This apparent disagreement is a result of that in Archaean, as was already mentioned, most of the degassed water still in the mantle had dissociated on iron melts in Earth matter differentiation zones under reaction $H_2O + Fe \rightarrow FeO + H_2$. At that, the heavy oxygen isotope had been bonded mostly with iron and the light one had been preserved in degassed water. In Proterozoic and more so in Phanerozoic, there had been no longer water dissociation in the mantle and in total compliance with Eq. (10.1) it had been coming without losses into Earth hydrosphere. Currently, from the mantle is degassed around $2.6 \cdot 10^{14}$ g/year or 0.26 km^3/year of water.

Average depth of the oceanic depression may be determined from Earth tectonic activity (see Fig. 6.17), Eqs. (8.30), (8.30') and average oceanic plates' life duration (see Fig. 8.3). After having determined this way average depth of oceanic depressions and their areal extent (in consideration of the fact that in Early Archaean the oceans had been placed only in low latitudes), from the determined mass of water in the ocean it is now possible to find the position of the oceanic surface relative to average stand level of mid-oceanic ridge crests. The results of appropriate estimates compared with the continents' stand levels are shown in Fig. 10.6.

As the Figure shows, depths of oceanic depressions in Early Archaean compared with the mid-oceanic ridge crests stand level had been shallow, 80 to 200 m. But there had been very little water in the oceans. In Early and Middle Archaean there had been no real oceans but only numerous isolated shallow-water basins. Above levels of these seas had towered the crests of mid-ocean ridges and areas of Earth primordial matter. Especially outstanding had been pile-up zones of lithospheric slabs in whose centers at that time had been only emerging cores of the future continental massifs (see Fig. 8.5). The elevation of these microcontinents had reached 6 km and they, like giant table mountains, had dominated the landscape of that time (see Figs. 8.10 and 10.6).

It will be recalled that so high continent stand in Archaean had been caused by high heat flows coming from the mantle. As a result, under Archaean continental shields might not have formed thick (and heavy) lithospheric plates and the crust itself, as a "light cork" had towered high above average surface of the mantle. As opposed to this, the present-day continental crust is underlain by welded to it thick (up to 200 km) and high-density (around 3.3 g/cm^3) ultramafic composition lithosphere which substantially sinks them in the upper mantle (see Fig. 8.9).

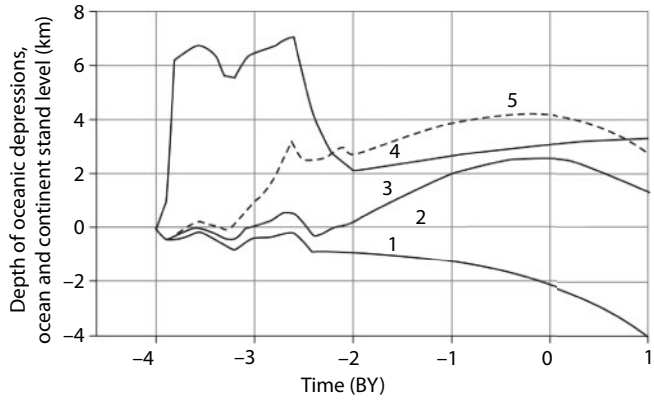

Fig. 10.6 Evolution of oceans and continents' surface position compared with average stand level of mid-oceanic ridge crests: 1. Average depth of oceanic depressions; 2. Stand level of mid-oceanic ridge crests; 3. Elevation of the World ocean surface; 4. Average continent stand levels (compared with the elevation of mid-oceanic ridge crests); 5. Position of the ocean level in case if in Archaean would not have occurred water dissociation on iron melts under reaction 10.3.

As mentioned in Chapter 8, high stand of the continental shields in Archaean had resulted in an intense physical erosion of its surface. This is obvious even in the present-day structure of many Archaean shields on whose surface are now exposed amphibolite and granulite depth metamorphism facies formed in the past at depths 5–10 km. There are also examples of deep metamorphism of the epidote-amphibolite facies in Late Archaean sedimentary rocks, for instance, in Keyv block of the Kola Peninsula. It was shown in section 8.2 that huge sedimentary rock masses which mandatorily had to have been deposited at high stand of Archaean continental blocks on the ocean floor, after their remelting in pile-up zones of oceanic slabs, had turned into tremendous granitoid intrusions of granite-greenstone Archaean belts (see Fig. 8.5).

At the end Proterozoic, the surface of growing ocean had risen to an average level of continental plain after which (already in Phanerozoic) the first global marine transgression on continents had occurred. They had significantly shrunk river runoff areas and delivery of continental rocks in the oceans.

Interestingly, should water dissociation in Archaean Earth matter differentiation zones not have occurred, its mass in the oceans would have exceeded the present-day amount almost by the factor of 1.5 ($3 \cdot 10^{24}$ g rather than $2.2 \cdot 10^{24}$ g) (see Fig. 10.4). At that, the ocean level after Archaean would have been above the present-day level approximately by 2 km. This would

have resulted in flooding in Proterozoic and Phanerozoic of a larger part of continents (see Fig. 10.6). Only summits of highest mountains would have appeared above the ocean surface.

10.3 Hydrothermal Processes on the Ocean Floor

Estimating the intensity of Earth primary degassing process, we noted that it had occurred only together with eruptions on Earth surface of juvenile basalt magmas mostly coming through the rift zones of mid-oceanic ridges. At the very beginning of Archaean, at boiling of basalts erupted from the mantle, vapor sources and hot fluids indeed had been juvenile. Subsequently, however, numerous hydrothermal springs within rift zones pouring from the so-called "black smokers" had not been juvenile at all as the entire water passing through them had exclusively oceanic origin. Such mineralized springs may create an illusion of primary which is totally wrong. For this reason, we will review the issue of a secondary Earth degassing in more detail.

The discovery at the end of the 1970s on the ocean floor of an intense hydrothermal activity associated with functioning of the most active belt of underwater volcanism in the World ocean rift zones resulted in a reconsideration of many views on the problem of the origin of a number of economic minerals. This concerns, for instance, hydrothermal deposits of sulfides and other mineral formations in the ophiolite zones of Earth's fold belts. These very discoveries enabled the identification of a large role of exogenous matter in the processes of hydrothermal ore formation. For instance, hydroxyl groups in hydrosilicates or sulfate sulfur in sulfides. This also enabled the determination of a formation mechanisms of abiogenous methane in hydrothermal springs.

By now, large amounts of fundamental studies of hydrothermal activity on the ocean floor have already been done. Since 1978, after the discovery of hydrothermal springs in the Galapagos rift [165], the number of works devoted to ocean floor hydrotherms, massive sulfide ores and other hydrothermal mineral formations drastically increased. We will mention here only three synoptical studies published in Russia. They include studies by A.P. Lisitsin, Yu.A. Bogdanov and E.G. Gurvich "Hydrothermal formations of rift zones" [246], P. Rona "Hydrothermal mineralization in the ocean spreading areas" [247] and a fundamental work by Yu.A. Bogdanov *et al.*, "Hydrothermal ore-genesis of the ocean floor" [248]. These large monographs include exhaustive present-day bibliographies devoted to the study of these objects.

However, the first assumption of the existence of powerful hydrotherms in Earth ocean rift zones and the conclusion about exogenous nature of water circulating in them was proposed theoretically already in the early 1970s by K. Lister [163] and independently by O.G Sorokhtin [15]. This was well before the actual discovery of hot springs on the ocean floor in 1977–1978. In the latter work, by the way, the total power of hydrothermal processes in Earth mid-oceanic ridges was evaluated. This theoretical forecast of the existence in rift zones and on the slopes of mid-oceanic ridges of a powerful hydrothermal springs' system was made by way of comparing the estimated correlation of per-unit heat losses through the oceanic lithospheric plates vs. their age with empirically measured heat flows piercing those mid-oceanic ridge slopes (Fig. 6.12). At that, it was taken into consideration that empirical data enabled measuring only of the heat flow conductive component whereas theoretical estimates accounted for the entire heat flow. Thus, their difference defined the convective heat removal by the oceanic water circulating in Earth crust fractured medium in rift zones and on the slopes of mid-oceanic ridges. The grandiose nature of the convective component of the oceanic crust "flushing" phenomenon by the sea water may be judged based on the estimates of appropriate heat loss. It was found that through the activity of hydrothermal springs a total of around 30% of the entire endogenous energy radiated by Earth was lost, which is estimated at about $\dot{Q} = (4.2 \div 4.3) 10^{20}$ erg/s [15]. Therefore, thermal waters are currently removing at least $\dot{\theta} = 1.29\, 10^{20}$ erg/s or around $3.07 \cdot 10^{9}$ kw of Earth heat energy (30% of $4.3 \cdot 10^{20}$ erg/s).

In hot springs of a "black smoker" type encountered in the rift valleys of mid-oceanic ridges the maximum water heating is always limited by its critical temperature T_{cr} = 374°C. This is associated with that at a temperature exceeding the critical value water turns into a gas fluid whose volume V is inversely proportionate to the pressure p. As for such fluid pV = const, this leads to a rapid and very efficient removal of overheated water fluids from the system of open fractures at the expense of the fluid density decline at its rise proportionate to the pressure decrease. Besides, at $T > T_{cr}$ water completely loses its capillary properties playing the definitive role in its soaking the crustal rocks. As a result, in a system of fractures communicating with surface of the bottom, water physically cannot get on the levels with the temperature exceeding 374 °C. This defines maximum temperatures of the greenstone metamorphism of the oceanic crust rocks emerging due to the functioning of "black smokers" type hot springs.

Geological data completely confirm this conclusion. For instance, study of the ophiolite complexes' composition (they are fragments of oceanic crust thrust over the continents – [141]) indicates that the rocks

composing these complexes (basalts, dolerites, gabbro and serpentinites) alter only to the facies of greenstone metamorphism with maximum temperature not exceeding 400°C (in round numbers). This indicates that oceanic crust rock metamorphism indeed occurs under the existence conditions of open (communicating with the surface) paths of water penetration into the crust. It follows from this that all higher extents of temperature metamorphism, for instance, amphibolite and granulite facies, may emerge only under closed conditions obstructing water removal from the system of rock reacting with it. Such conditions usually emerge in subduction zones saturated with water due to dehydration of pulled in them oceanic crust rocks. Sometimes, very rarely, in rift zones also may arise conditions for the emergence of metamorphism's amphibolite facies. For instance, at the formation of faults bounding rift valleys of slowly spreading ridges. Within them, dyke complex rocks altered by greenstone metamorphism may again immerse in a magmatic complex under the rift zone. As in the rocks of greenstone metamorphism the entire water is only in bonded state, then at that will happen progressive metamorphism with the formation of amphibolite facies. But in any case, the rocks of amphibolite metamorphism facies play an insignificant role in the oceanic crust structure.

Due to gradual covering of oceanic crust fractured rock surface with pelagic deposits and their diagenesis, and also at the expense of plugging existing fractures and other water migration paths in the crust with chemical deposits of hydrotherms themselves, the crust permeability for oceanic water gradually declines. A comparison of the observed (conductive) heat flows with theoretical estimates (see Fig. 6.12) shows that almost complete discontinuation of oceanic water circulation in crust rocks occurs approximately in $\tau = 50$ MY after the formation moment of crust in the rift zone of a mid-oceanic ridge. Therefore, hydrothermal springs, including warm and "cool" seepages (springs seeping through the deposits), mostly exist only in the ocean floor areas with the age $\tau < 50$ MY. Within this age range of the oceanic floor, average temperature of hydrothermal springs is equal approximately to $\overline{T}_{ht} \approx 42°C$ whereas maximum temperature of the "black smokers" in rift zones reaches 370 – 400°C.

An estimate of the total water mass washing in unit time through the ocean crust may be performed based on the balance of heat flows. It was found that totally through mid-oceanic ridges and their slopes is filtering around $2.3 \cdot 10^{18}$ g/year (2,300 km^3/year). At such rate of a hydrothermal water-exchange, the entire mass of water in the ocean ($1.42 \cdot 10^{24}$ g) passes through hydrotherms and seepages of mid-oceanic ridges with their expansive and low-angle slopes approximately in 600 thous. years. At the same time, the

rate of rift zone "wash-through" by hot hydrotherms is equal approximately to $2.2 \cdot 10^{16}$ g/year (22 km^3/year). Therefore, through hot springs of the "black smokers" the entire oceanic water is filtered in approximately 60–70 MY. At a rate of oceanic crust in rift zones forming around $1.46 \cdot 10^{16}$ g/year, the water/rock ratio in "hot zones" is equal to 1.5 (not including water bonded with rocks in the process of reactions). However, the formation continues as well outside the rift zones. For this reason, total rate of its formation is somewhat greater and reaches $4.7 \cdot 10^{16}$ g/year. Then the water/rock ratio in the subject total system of hydrotherms (including seepages) reaches almost 50. This is an indication of quite complete hydration of the oceanic crust rocks.

Therefore, estimates included here of the exogenous water exchange mass in the oceanic crust of mid-oceanic ridges, is 8,500 times the present-day level of juvenile water degassing from the mantle, which is approximately equal to $0.26 \cdot 10^{15}$ g/year (0.26 km^3/year). Even if we determine average rate of the juvenile water degassing in the entire evolution time of this process (4 BY) based on total mass of the hydrosphere of $2.18 \cdot 10^{24}$ g (including water bonded in rocks of Earth's crust), even in this case average rate of juvenile water coming from mantle at 0.54 km^3/year is approximately 4,000 times lower than the total rate of hydrothermal springs on the ocean floor.

All these certainly testify in favor of the exogenous nature of oceanic hydrotherms water. Similarly, in the subduction zones at oceanic crust heating at the expense of lithospheric plate heating, its dehydration is accompanied by the release of water and carbon dioxide gas getting there before that from the ocean.

$$\underset{\text{serpentine}}{2Mg_6(Si_4O_{10})(OH)_8} + \underset{\text{calcite}}{CaCO_3} + 164\text{cal/mole} \rightarrow$$
$$\rightarrow \underset{\text{olivine}}{5Mg_2SiO_4} + \underset{\text{enstatite}}{MgSiO_3} + \underset{\text{diopside}}{MgCASi_2O_6} + 8H_2O + CO_2. \quad (10.5)$$

Total flow of the secondary water degassing in island arcs and on Andean type active continental margins reaches 2.5–3 km^3/year which is also approximately 10 times the present-day level of juvenile water degassing. Summing up water mass released this way through Earth's subduction zones during its lifetime reaches $1.4 \cdot 10^{25}$ g (14 billion km^3) of water or approximately 10 times its amount in the present-day ocean. Therefore, all without exception currently observed on Earth surface hot mineralized water springs are not juvenile, their water, ultimately, always comes from Earth hydrosphere.

Based on reasonably well-preserved ultramafic rock samples from East Pacific high, quantitative interrelations between the primary minerals in the mantle rocks there are: 70–75% olivine, 15–20% enstatite, 5–7% diopside and 1–2% chromspinelide (Savelyeva, 1987). The serpentinization may develop only over olivines and enstatite, i.e., over 85–90% of the source matter. The hydration of major silicates in conditions of greenstone metamorphism usually develops in reactions like

$$\underset{\text{forsterite}}{4Mg_2SiO_4} + 6H_2O \rightarrow \underset{\text{serpentine}}{Mg_6(Si_4O_{10})(OH)_8} + \underset{\text{brucite}}{2Mg(OH)_2} + 33\,\text{kcal/mole}, \tag{10.6}$$

and in the presence of carbon dioxide gas

$$\underset{\text{forsterite}}{4Mg_2SiO_4} + 4H_2O + 2CO_2 \rightarrow \underset{\text{serpentine}}{Mg_6(Si_4O_{10})(OH)_8} + 2\underset{\text{magnesite}}{MgCO_3} + 65.05\,\text{kcal/mole}. \tag{10.7}$$

$$\underset{\text{anorthite}}{2CaAl_2Si_2O_8} + 4H_2O + 2CO_2 \rightarrow \underset{\text{kaolin}}{Al_4(Si_4O_{10})(OH)_8} + 2\underset{\text{calcite}}{CaCO_3} + 110.54\,\text{kcal/mole}, \tag{10.7'}$$

Hydration of ferruginous silicates goes on with the release of hydrogen and in the presence of carbon dioxide gas, even with the formation of abiogenous methane

$$\underset{\text{fayalite}}{Fe_2SiO_4} + 3\underset{\text{forsterite}}{Mg_2SiO_4} + 5H_2O \rightarrow \underset{\text{serpentine}}{Mg_6(Si_4O_{10})(OH)_8} + \underset{\text{hematite}}{Fe_2O_3} + H_2 + 21.1\,\text{kcal/mole}, \tag{10.8}$$

$$\underset{\text{fayalite}}{4Fe_2SiO_4} + \underset{\text{forsterite}}{12Mg_2SiO_4} + 18H_2O + CO_2 \rightarrow 4\underset{\text{serpentine}}{Mg_6(Si_4O_{10})(OH)_8} + \underset{\text{hematite}}{4Fe_2O_3} + CH_4 + 183.4\,\text{kcal/mole}. \tag{10.9}$$

The oceanic water contains in notable quantities (up to 2.7‰) the sulfate ion SO_4^{2}. For this reason, a reaction of such water with hot rocks may be accompanied by the formation of hydrogen sulfide, for instance, under reaction:

$$\underset{\text{fayalite}}{4Fe_2SiO_4} + \underset{\text{forsterite}}{3Mg_2SiO_4} + CaSO_4 + H_2O \rightarrow$$

$$\rightarrow \underset{\text{enstatite}}{5MgSiO_3} + \underset{\text{hematite}}{4Fe_2O_3} + \underset{\text{diopside}}{CaMgSi_2O_6} + H_2S + 33.0\,\text{kcal/mole}. \quad (10.10)$$

Due to a high reduction potential of hydrogen sulfide, sulfur is again rapidly bonded with transitional metals forming their sulfides, for instance, pyrrhotine

$$\underset{\text{Fayalite}}{Fe_2SiO_4} + \underset{\text{forsterite}}{Mg_2SiO_4} + 2H_2S \rightarrow \underset{\text{entstatite}}{2MgSiO_3} + \underset{\text{pyrrhotine}}{2FeS} + 2H_2O$$

$$+26.6\,\text{kcal/mole}. \quad (10.11)$$

A confirmation of abiogenous origin of methane and the formation of sulfides at the expense of sulfate sulfur are their isotopic offsets (shifts). Usually, the isotopic offsets (shifts) of sulfur $\delta^{34}S$ in sulfides of the "black smokers" are within the range of +3 to +5‰. It is different in hot springs emerging on serpentinites. In this case, the range of offsets (shifts) is much broader, +4 to +16‰. Perhaps, this distinctions in isotope composition of sulfides might be explained by the sources of the sulfate sulfur and sulfur isotope fractionation conditions in hydrotherms. It is known that due to a strong temperature effect of isotope fractionation, their separation occurs by mineral phases:

$$^{32}SO_4^{2-} + H_2^{34}S \leftrightarrow {}^{34}SO_4^{2-} + H_2^{32}S. \quad (10.12)$$

This is exactly the reason why under usual conditions of chemical equilibrium must occur impoverishment of the sulfide phase with an isotope ^{34}S and enrichment with it of the sulfate phase. However, if sulfides form at the expense sulfate reduction, they inherit the sulfate values of $\delta^{34}S$. In "black smokers" emerging over hot basalt crust, the sulfate reduction occurs on the iron from basalts. It is possible that the juvenile sulfur may also appear there. In hot springs above the serpentinites, whose ferruginosity is

significantly higher than that of basalts, the major mass of sulfur is coming from the oceanic water and is reduced under reactions (10.10 and 10.11). As a result, apparently the isotopic density of sulfur in the oceanic water ($\delta^{34}S$ around +18.86‰) is splitting so that the H_2S isotopic offset (shift) in a hot fluid declines to +2.4…+3.2‰ and in metal sulfides to +4…+14‰.

We will now review major patterns of carbon isotope offsets (shifts) in the system of "black smokers" emerging on serpentinites. Negative offsets (shifts) of $\delta^{13}C \approx -13\ldots -14$‰ in methane of such springs compared with average value of the isotopic composition of HCO_3^- and CO_2 in the oceanic water of $\delta^{13}C = -5.5$‰, as with hydrogen sulfide, apparently might be explained by fractionation of carbon isotopes at methane formation from carbon dioxide gas.

It follows from a fundamental Le Chatelier principle that an exothermal chemical reaction occurring with heat release always tends to develop along the way of maximum internal energy (enthalpy ΔH_T^0) decline. It follows from this that from carbon dioxide gas with a mix of light and heavy carbon isotopes in CH_4 formation reaction must participate mostly the atoms of a light isotope ^{12}C. Indeed, a heat effect of carbon fractionation reaction at "assimilation" of ^{12}C by methane, compared with ^{13}C isotope, reaches 0.412 kcal/g (CH_4). This is a notable effect certainly working towards carbon "lightening" in formed methane. Thus, the exchange isotope reaction

$$^{12}CO_2 + {}^{13}CH_4 \rightarrow {}^{13}CH_4 + {}^{12}CH_4 + 0.412 \text{ kcal/g} \qquad (10.13)$$

mostly goes left to right.

Now we will review to what extent carbon isotopic ratios in methane and carbonates of "black smokers" emerging at serpentinization of oceanic crust rocks are complementary with the same ratio in the oceanic water. As the ratio $^{12}C/^{13}C = 88.99$ in the belemnite shells B. Americana are taken as standard carbon isotope ratio, it is possible to determine that carbon isotope composition in the sea water $\delta^{13}C = -5.5$‰ corresponds with the ratio $^{12}C/^{13}C = 89.48$ and the isotope composition of the dissolved methane formed above the "serpentinite springs" ($\delta^{13}C = -13.4$‰) corresponds with the ratio $^{12}C/^{13}C = 90.2$. In the process of carbon bonding in methane occurs the change of the isotope ratio for $\Delta^{12}C_{mt}$. Then, converted per unit of mass, $\Delta^{12}C_{mt}/^{13}C = 90.2 - 89.48 = 0.72$. But CH_4 concentration in fluids of such springs is approximately equal to 0.14 mmole/l. In this case, after the methane formation, the ratio of isotopes in a fluid, from which formation of carbonates under reactions (10.9) will be $89.48 - 0.143 \cdot 0.72 = 89.38$. This corresponds with the isotopic

offset (shift) $\delta^{13}C = -4.35‰$. Usually, the offsets (shifts) like this are observed in carbonates of this type "black smokers". At that, in the remaining fluid at the outset of the hydrothermal system must practically totally be missing free carbon dioxide which is often observed in real conditions.

But in any case, the entire methane formed in hydrotherms is only exogenous. Whereas at great depths in the mantle methane is simply unstable, it must have been oxidized there by oxygen released in the formation process of the "core matter" under reaction:

$$8FeO + CH_4 \rightarrow 4Fe_2O + CO_2 + 2H_2O. \quad (10.14)$$

To conclude, we will recall about the existence of mantle cycle of volatile element and compound turnover. This is due to the fact that in the subduction zones incomplete dehydration and decarbonizing of the oceanic crust rocks may have occurred. For this reason, part of remaining water, carbon dioxide gas and other volatile and mobile elements together with oceanic plates had been immersed in the depths of the mantle and again included in the general convective mass exchange of the mantle matter. That is why the Earth's own mantle degassing upon closer analysis turns out not purely juvenile and includes some elements and compounds repeatedly getting on Earth's surface.

Unfortunately, at this time it is still difficult reliably to estimate what part of the degassed volatile and mobile elements is genuinely juvenile and what part had been repeatedly captured in the mantle mass exchange and only after that had gotten again in the external geospheres. For this reason, subsequently, speaking about juvenile degassing of Earth, we will always keep in mind its effective value, remembering that the scale of genuinely primary mantle degassing had been somewhat lower than the effective one as part of the released at that volatiles had been again immersed in the mantle through the plate subduction zones. However, differences in mass between the juvenile mantle degassing and its effective value, possibly, is not too great and for water, according to our estimates, does not exceed 20% and for other compounds and elements, even smaller.

10.4 The Nature of Global Marine Transgressions on Continents

In the aforementioned reconstructions of Earth tectonic activity, only averaged parameters of this process have been used, and its periodic

fluctuations have not been taken into consideration. Such intensity fluctuations of the convective mass exchange in the mantle and of the movement rate of lithospheric plates in real-life conditions certainly must have occurred. For instance, due to instability of chemical-density convection and changing its structure or at the expense of the effect of the continent collision and lithospheric plate destruction processes on the rate of their mutual displacement. For instance, based on age identification of banded magnetic anomalies on the ocean floor, average movement rate of the Pacific plate in Late Cretaceous had been almost 50% above the present-day one, whereas in Late Jurassic and Early Cretaceous it had been close to the current one.

Traces of marine transgressions on and regressions off the continents help restore fluctuations of tectonic activity on Earth. It was shown in publications by G. Menard [249], W. Pitman, J. Heys [250], O.G. Sorokhtin [120] and D. Turcotte and K. Burke [251] that global marine transgressions on continents and their back regressions might have been caused by pulsations of Earth's tectonic activity. At that, beside relatively slow changes in the World ocean level with periods on the order of dozens of millions of years have been identified shorter eustatic oscillations of its level that had lasted dozens of millennia. Apparently, they have been associated with the accumulation or melting of significant water volumes of cover glaciers formed at the time of glacial periods on Earth.

Until the mid-20th century, it was customary to explain the nature of global marine transgressions and regressions on continents by vertical fluctuation movements of continental platforms which ostensibly had experienced periodical uplifting and subsidence. The tradition of such an approach traces its origin to the times of ancient philosophers Strabo and Aristotle. Due to its apparent obviousness, this idea has been accepted as an axiom and often was not even discussed, entering in almost pure and simple form in many textbooks on geology and tectonics. The possibility of the existence of large vertical fluctuation movements of platforms resulting in global marine transgressions and regressions was as a rule tied with periodic heating and cooling of the upper mantle matter underneath the continents [252, 253]. At that, the very nature and especially mechanism of cyclic mantle overheating remained unclear and eluded quantitative estimates.

The theory of lithospheric plate tectonics offers a totally different approach to the explanation of global marine transgressions' origin. This approach was first outlined in publications by marine geologists. For instance, G. Menard in 1964 proposed an idea of significant fluctuations of the World ocean level at the expense of changes in the volume of mid-oceanic ridges. In particular,

he showed that the formation of present-day ridges might have resulted in the ocean level rise by more than 300 m.

It follows from the lithospheric plate tectonics theory that the thickness of oceanic lithosphere is controlled by the depth of the mantle matter cooling and crystallization. Therefore, it depends on the time exposure of hot mantle matter on Earth surface (see Eq. 8.26). In rift zones is occurring gradual spreading of the oceanic lithospheric plates and continuous buildup of their edges at the expense of cooling and crystallization of the rising asthenospheric matter because the lithosphere thickness under mid-oceanic ridges regularly increases with distance from their crests. The silicate crystallization is known to be accompanied by the increase in density. For this reason, with an increase of the oceanic lithosphere thickness, the level of its surface decreases as a function of square root from the age of the lithosphere (see Eqs. 8.25 and 8.26). Therefore, the faster the spreading of the ocean floor in rift zones occurs, i.e., the higher Earth's tectonic activity, the flatter mid-oceanic ridges become (see Fig. 8.21). The volume of oceanic depressions appropriately decreases and the larger volume of water is displaced from the oceanic areas on the continents. It shows that the amplitude of eustatic fluctuations of the ocean level associated with tectonic causes is completely defined by average movement rate of the oceanic lithospheric plates, i.e., by Earth's tectonic activity.

10.5 Earth's Tectonic Activity vs. Fluctuations of the World Ocean Level

This problem may be resolved if eustatic fluctuations of the World ocean surface known are based on independent geological data. Therefore, they may be used for the determination of fluctuations in Earth's tectonic activity. At the same time, the amplitude of eustatic ocean level fluctuations practically for entire Phanerozoic may be established based on the coverage areas of marine deposits on continents and on analysis of seismostratigraphic cross-sections of sedimentary sequences on continental margins of the ocean. So constructed curve of the ocean level eustatic fluctuations [254] is included in Fig. 10.7.

When interpreting the curve of the ocean level eustatic fluctuations, it is necessary to keep in mind that they had occurred for four major reasons. First, due to a gradual increase in degassing of the mantle, the mass of water in the oceans had increased. Over the time of Earth geological history (around 4 BY) the ocean level had risen for this reason on average by 4.5 km. Second, due to evolution changes in Earth's tectonic activity.

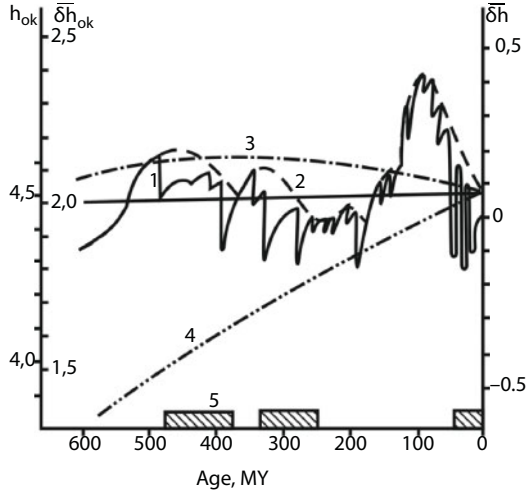

Fig. 10.7 Eustatic fluctuations of the World ocean level in Phanerozoic: 1. After [254]; 2. Averaged (enveloping) curve; 3. Curve of the ocean level evolutionary change $\delta\bar{h}$ (see Fig. 10.6); 4. Curve of the evolutionary increase of ocean depth counted from average stand level of mid-ocean ridge crests $\bar{h}_{OC}$; 5. Glaciation periods.

These changes also had been very slow, with typical periods of the ocean level fluctuations on the order of a billion years (except Archaean when the fluctuation period had declined to 100 MY). Their amplitude had been also significant, up to ±1–2 km. Third, these fluctuations of Earth's tectonic activity had been associated with periodical restructuring of chemical-density convection in the mantle resulting in the formation and destruction of supercontinents. The appropriate fluctuations of the ocean level had occurred with typical periods of 100 to 800 MY and amplitude dh ≈ ±200–400 m. Lastly, the fastest changes in the ocean level, just in a few millennia, had occurred for a fourth reason, the emergence and melting of cover glaciers on the continents positioned in circum-polar areas of Earth. Periods of glacio-eustatic fluctuations of the ocean surface had been usually on the order of 100 thous. years, their amplitude had reached ±100–150 m.

We averaged curve 1 of eustatic ocean level changes presented in Fig. 10.7 keeping in mind that sharp regressive hops of the ocean level shown by it had been associated either with rapid glacio-eustatic changes or are simply apparent (quasi) due to missing and erosion of regressive sedimentary series. Recalculation results of the averaged World ocean level eustatic fluctuation curve (curve 2) for average movement rate of the oceanic lithospheric plates are included in Fig. 10.8. The heat flow through the ocean

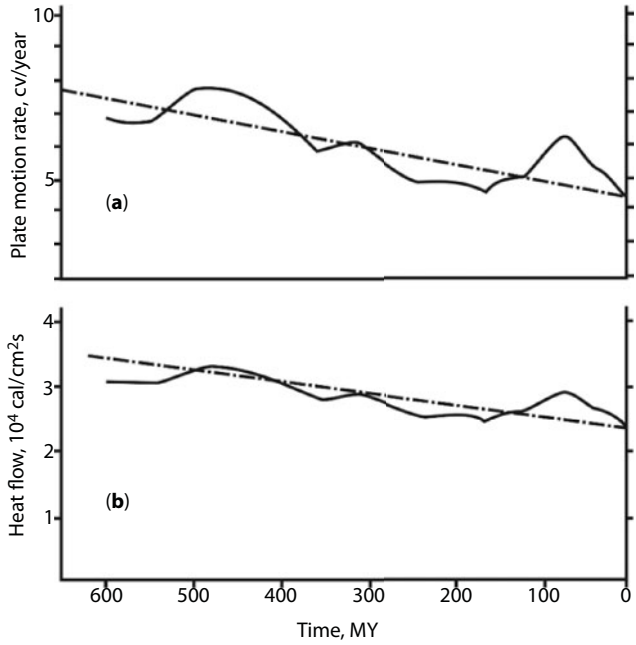

Fig. 10.8 Phanerozoic tectonic activity [17]: a. Recalculated for average movement rate of lithospheric plates; b. Recalculated for average heat flows through the ocean floor; dash-dotted lines are evolution changes, respectively, of oceanic plate movement rate and heat flows through the ocean floor.

floor is proportionate to square root of average rate of oceanic plate spreading. Therefore, it is possible to determine at the same time the average heat flows piercing oceanic plates in Phanerozoic (Fig. 10.8).

The diagrams show that some pulsations in Earth tectonic activity may have reached 15–20%. Three maxima of such pulsations had occurred in Phanerozoic. The main of them had manifested in Ordovician and Silurian in the epoch of the Caledonian orogeny around 500–400 MYa, when the Wegenerian Pangea had begun forming. The second, less significant maximum had occurred during Carboniferous, at the time of Hercynian orogeny continued forming of Pangea. These active orogenic epochs had been replaced in Triassic-Jurassic by a relatively quiescent and short period of a stable existence of supercontinent Pangea. The last, Late Cretaceous splash-up of Earth's tectonic activity had been associated with Pangea disintegration and closing of Tethys paleo-ocean in whose place had emerged a grandiose Alpine mountain belt.

Global transgressions and regressions of marine basins on continents may have resulted and may result in substantial restructurings of biotic

communities. For instance, well known is a mass and rapid extinction of many coral species on oceanic islands early in Late Cretaceous. And exactly at this time had occurred the last global transgression caused by an increase in average rate of oceanic lithosphere buildup. This buildup had led to "repumping" of carbonates and phosphorus compounds from the ocean in shallow-water unprecedently expansive epicontinental seas and to depositing on their bottom Cretaceous sediments and phosphorites. That is why corals and many mollusk species (for instance, rudists) had extinguished on oceanic islands in the middle of Cretaceous period due to impoverishment of the open ocean water in calcium carbonate and phosphorus compounds.

10.6 Earth's Primordial Atmosphere

Reviewing the origin and evolution of Earth's atmosphere, it is necessary to remember that Earth matter (compared with the Sun matter) had been strongly impoverished in volatile and mobile elements and compounds. Otherwise, the present-day atmosphere and hydrosphere would be much thicker. According to estimates by B. Mason [77], the relative hydrogen content on Earth (in relation to silicon) is smaller than in the outer space by the factor of $10^{6.6}$, nitrogen, $10^{5.9}$, carbon 10^{4}, noble gases 10^{6}–10^{14}. For this reason, despite commonality in the outer space of such volatile compounds as H_2, He, N_2, H_2O, CO_2, CH_4, NH_3, etc., in Earth matter there was exceptionally little of them. Perhaps, so significant primordial differentiation of Earth matter had occurred already at the preplanetary stage of the Solar system evolution (while passing by the Sun the evolution stage of τ-Taurus type stars) at the expense of intense wiping out of volatile and highly mobile components from internal parts of the protoplanetary gas-dust cloud to its periphery, in the formation area of giant planets.

Those volatile compounds and elements (H_2O, CO_2, N_2, HCl, HF, HI, etc.) found in Earth might have gotten in it only in bonded state (water with hydrosilicates, nitrogen with nitrides and nitrates, carbon dioxide gas with carbonates, halogens with haloids, etc.). For this reason, in the process of Earth growth such components had been buried in its subsurface and those remains of reaction-active volatile compounds released in impact explosions of planetesimals falling on Earth must have been intensely sorbed by ultramafic regolith on the surface of growing planet and also being buried under new layers of meteorite matter falling on Earth.

With this consideration in mind, we may assume that primordial Earth's atmosphere had included only inert and noble gases. Thus, due to a short time of helium release from Earth atmosphere (around 10^6 years), its partial pressure in the primordial Earth atmosphere during the time of its formation, around 10^8 years, had time to come to equilibrium. In this regard, it should have been no higher than the present-day one. Also, should not have been present in the atmosphere at that time significant quantities of ^{40}Ar, a decay product of radioactive potassium ^{40}K. Thus, it may be expected that partial pressure of noble gases in primordial Earth atmosphere had not exceeded $2 \cdot 10^{-5}$ atm [255].

It is much more difficult to determine partial pressures of other active components in primordial atmosphere (H_2O, N_2 CO_2 and CO) because for that it would be necessary to know sorption and reaction capability of gas by the regolith of ultramafic composition which had included native metals (Fe, Ni, Pt, Co, Cr, etc.). However, our estimates suggest that their pressure might be expected not to have exceeded 10^{-4} atm.

10.7 Evolution of the Degassing Process of Carbon Dioxide Gas

At the geological stage of Earth evolution, carbon suppliers for the rocks might have been only carbon dioxide gas, products of its transformation (carbonates), hydrocarbons and organic matter. However, the primordial carbon might have come in Earth's crust, hydrosphere and atmosphere only due to degassing of the mantle. Dealing with degassing of carbon dioxide gas from the mantle, it is necessary to remember that, as opposed to water, the formation heat of carbon dioxide gas is equal to 94.05 kcal/mole which is much higher than for iron oxide 63.05 kcal/mole. For this reason, the mobility parameter of carbon dioxide gas $\chi(CO_2)$, as for nitrogen, did not have to depend on Earth matter differentiation mechanism (zonal separation of iron or barodiffusion mechanism of Earth core matter release). This makes the task of the determination CO_2 degassing pattern from mantle substantially easier as it preordains in advance constant nature of carbon dioxide mobility parameter and the proportionality of its degassing rate and Earth tectonic activity as displayed in Fig. 6.17.

As one of boundary conditions, it may be assumed after A.B. Ronov and A.A. Yaroshevsky [73] that in Earth's crust carbonates is bonded around $3.91 \cdot 10^{23}$ g CO_2. Besides, the crust contains around $1.95 \cdot 10^{22}$ g more of organic carbon (C_{org}). With this amount of C_{org}, prior to its reduction

by biologic processes, was bonded $5.2 \cdot 10^{22}$ g of oxygen. Therefore, the total mass of buried if Earth crust CO_2 is $m(CO_2) \approx (3.91 + 0.72) \cdot 10^{23} = 4.63 \cdot 10^{23}$ g.

A much more difficult task is to determine carbon content (or CO_2) in Earth's mantle. According to experimental data, high-temperature distillation in oxygen atmosphere fractions of volatile components from tempering glass of tholeiite basalts in oceanic rift zones usually produces 20 to 170 g/t of mantle origin carbon with isotopic offsets (shifts) around –5 ‰ [256–258]. E.M. Galimov [52] indicates that encountered in all igneous rocks trace carbon has minuscule concentration (10 to 100 g/t) and significant shortage of the heavy isotope ($\delta^{13}C \approx -22$ - –27‰). As opposed to this, carbon concentrated in Earth crust is isotopically heavier, with $\delta^{13}C \approx$ –3 - –8 ‰, on averaghe, –5 ‰. What should also be remembered is that part of the mantle carbon is in atomic state dispersed in silicate crystalline grids [256]. For this reason it is not a volatile component of basalt melts. Therefore, carbon content in CO_2 gas phase of basalt melt-outs may be significantly smaller than values of summary carbon concentrations quoted here. To be specific, we will assume the mobile carbon content in the mantle around 30 g/t or, converted to carbon dioxide gas, 110 g/t ($1.1 \cdot 10^{-4}$). In this case, the mantle contains around $m(CO_2) \approx 4.48 \cdot 10^{23}$ g CO_2.

Now we will estimate the total mass of CO_2 in Earth (converting C_{org} in CO_2), which is $m(CO_2) \approx 9.11 \cdot 10^{23}$ g. In this case, from equation (10.2) we find $\chi(CO_2) \approx 0.71$. From equations (10.1) and (10.2) it is easy to build curves of carbon dioxide gas degassing rate from the mantle (Fig. 10.9) and of CO_2 accumulation in Earth's external geospheres (atmosphere, hydrosphere and Earth's crust - Fig. 10.10).

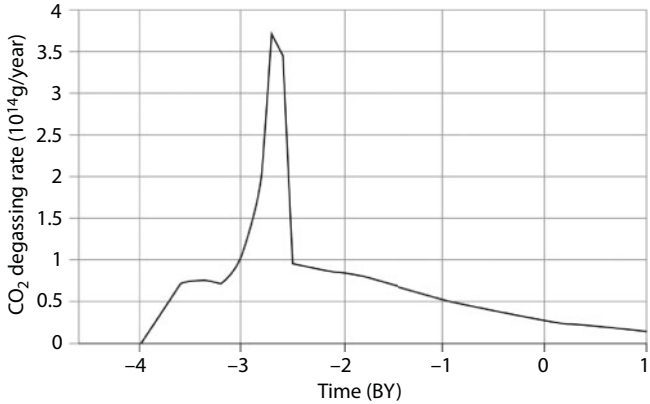

Fig. 10.9 Carbon dioxide gas degassing rate from the mantle.

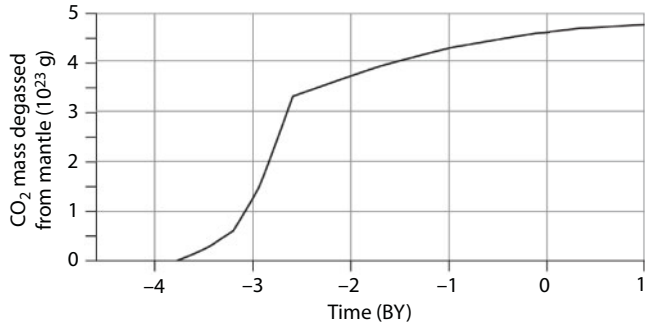

Fig. 10.10 Mass of carbon dioxide gas degassed from Earth's mantle.

Conspicuous is the fact of a sharp difference between the carbon dioxide gas degassing curve and water degassing (see Figs. 10.9 and 10.5). As mentioned earlier, this is due to smaller water formation heat (for molecular water $\Delta H^0_f = 57.8$, for CO_2 $\Delta H^0_f = 94.05$, for FeO $\Delta H^0_f = 63.6$ kcal/mole) and its dissociation on metallic iron in the process of zonal differentiation of Earth matter in Archaean. The peak of CO_2 degassing rate had fallen on the time of Earth maximum tectonic activity, around 2.6 BYa, whereas maximum water degassing rate had occurred around 2.5 BYa.

Should have the entire degassed carbon dioxide gas been preserved in the atmosphere, its partial pressure would have now reached approximately 91–100 atm., i.e., would have been the same as on Venus. Luckily for the life on Earth, simultaneously with the entry of CO_2 in the atmosphere had been occurring its bonding in carbonates. But for passing of this reaction, water in the liquid phase is necessary, as only in this case is the hydration of silicates accompanied by the absorption of CO_2 with the formation of carbonate according to a reactions of 10.7 and 10.7' type. For this reason, history of the ocean evolution on Earth had rendered substantial influence on the evolution of carbon dioxide gas partial pressure in the atmosphere (see Figs. 10.4 and 10.6). Beside carbonates, hydration of ferruginous mafic rocks in the oceanic crust is usually accompanied by the release of a free hydrogen and generation of abiogenous methane (see Eqs. 10.8 and 10.9).

One can see from type reactions (10.7) and (10.7') that for each two molecules of CO_2 bonded in carbonates are expended four water molecules for hydration of rock-forming minerals in the oceanic or continental crust. It follows herefrom that with the excess of carbon dioxide gas in the atmosphere and hydrosphere, practically all reactions of rock hydration will be accompanied by bonding of CO_2 in carbonates. At that, per unit mass of water bonded in rocks, approximately 1.22 of carbon dioxide gas mass will accrue. Under the shortage of CO_2, hydration of some silicates

will be occurring without bonding the carbon dioxide gas, for instance, according to the reaction of brucite formation (10.6).

In Late Archaean (around 2.8 BYa) the World ocean had already emerged covering the mid-oceanic ridge crests (see Fig. 10.6). As a result of this, hydration of a substantially basaltic oceanic crust had significantly increased and the rate of CO_2 partial pressure growth in the Late Archaean had somewhat declined. However, most radical drop of carbon dioxide gas pressure had occurred only at the Archaean/Proterozoic boundary after the separation of Earth core and associated with this sharp decline in Earth tectonic activity (see Fig. 6.17). Due to this, in Early Proterozoic the melt-out of oceanic basalts had shrunk equally sharply. The basalt layer of the oceanic crust had become significantly thinner than in Archaean, and underneath it for the first time had been formed the serpentinite layer, the main and constantly renewed reservoir of bonded water on Earth (see Fig. 8.1). It will be recalled that the serpentinites may contain up to 12% of constitutional (bound) water.

Exactly for this reason, by the time around 2.4 BYa, i.e., by the beginning of the Huron glaciation, the carbon dioxide gas partial pressure in the Early Proterozoic atmosphere had sharply dropped (approximately by the factor 10,000) to equilibrium level of about 1.0 – 1.5 mbar. Total atmospheric pressure at that had declined from 5 – 6 bar at the very end of Archaean to 1.4 bar in Early Proterozoic (see Fig. 10.23). At that, the process of CO_2 removal from the atmosphere at the boundary Archaean/Proterozoic had taken perhaps no longer than 100 – 150 MY. As a result, the composition of the Early Proterozoic atmosphere had become substantially nitrogen (with a small addition of argon around 9 mbar). A natural reaction to these events had become a significant climate cooling, although average stand level of continents at that had still remained sufficiently high, 4 to 2–3 km. Exactly this had been the main cause of the emergence of Huron glaciation: onset of cooling at high continental stand level [198, 259]. As a result of this practically all continents merged then in a single supercontinent Monogea (Fig. 9.2), despite even its equatorial position, had turned out above the snow line and for this reason had been covered by giant inland glaciers.

Subsequently, carbon dioxide gas partial pressure in the atmosphere had been controlled by the oceanic water average temperature and Henry's law. Thus, in glaciation epochs it had been dropping to 0.3 mbar (its current value is approximately 0.46 mbar) and in warm Mesozoic, on the contrary, had been rising to 0.7 – 1 mbar.

We earlier estimated total mass of water bonded in Earth crust rocks (this is the sum of curves 3 and 4 in Fig. 10.4). One can see from this Figure that maximum rate of Earth crust rock hydration had apparently

occurred in Early Proterozoic. During the same period must have occurred also mass bonding of the atmospheric carbon dioxide gas in carbonates, especially dolomites. Based on this it is possible to estimate also the mass of carbon dioxide gas that might have been bonded in carbonates. As the life in the ocean is limited by the phosphorus content in the oceanic water, and phosphorus solubility is relatively low [260], it may be assumed that absolute mass of organic matter in the ocean is proportionate with the oceanic water mass. That is why the mass of organic carbon (converted to CO_2) in Archaean and Proterozoic may be evaluated with an assumption that as a first approximation it had been proportionate to the mass of water in the World ocean shown in Fig. 10.4, curve 2.

Fig. 10.11 is a comparison of the mass of carbon dioxide gas degassed from the mantle (curve 1) with the mass of CO_2 bonded in carbonates (curve 2) and the mass of organic carbon (converted into the mass of CO_2) in biosphere (curve 3). Separately shown is also the evolution of CO_2 mass in the atmosphere (curve 4). One can see from this Figure that in Proterozoic and Phanerozoic almost the entire carbon dioxide gas degassed from the mantle had turned out bonded in a carbonate (as C_{carb}) or biogenic (C_{org}) reservoirs.

A different situation had existed in Archaean. Due to a small amount of water in Archaean oceans, the mass of bonded CO_2 at that time had been substantially smaller than the mass of carbon dioxide gas degassed from the mantle. It follows herefrom that in Archaean a noticeable part of carbon dioxide gas must have been concentrated in the atmosphere (see curve 4 in Figs. 10.11 and Fig. 10.12) and dissolved in the oceanic water.

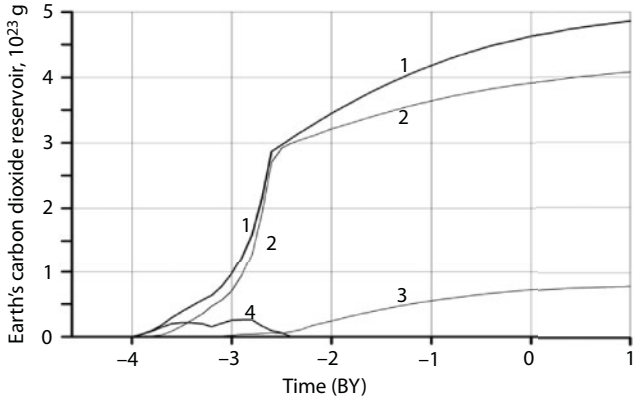

Fig. 10.11 Mass of carbon dioxide gas bonded in Earth crust and in Archaean atmosphere: 1. Mass of CO_2 degassed from the mantle; 2. Mass of the carbon dioxide gas in the carbonate reservoir of Earth crust; 3. Mass of organic carbon converted to CO_2; 4. Mass of CO_2 in Archaean atmosphere.

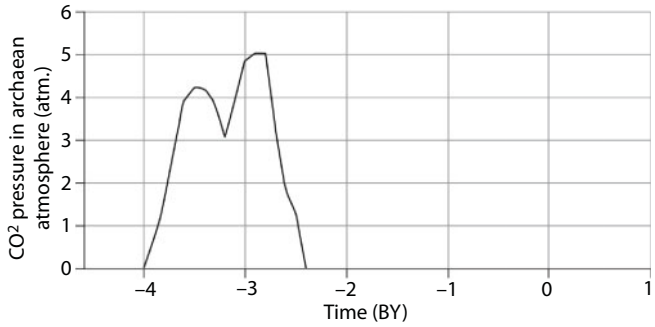

Fig. 10.12 Carbon dioxide gas partial pressure evolution in Earth atmosphere in Archaean.

The emergence at the Archaean/Proterozoic boundary of the oceanic crust's serpentinite layer (see Fig. 8.1) had resulted in a sharp increase of carbon dioxide gas bonding rate in carbonates according to reactions (10.7) and (10.7') and their accumulation in the oceanic deposits. As a result, in Late Archaean a significant increase in the amount of carbonate sediments had already occurred, for instance, marble and calciphyre at Slyuydanka ["Mica"] series in the Trans-Baikalian. In Early Proterozoic, from carbon dioxide gas of the former Archaean atmosphere and from carbon dioxide dissolved in oceanic water had been deposited huge mass of carbonate sediments. At that, because of a low resistance of carbonate rocks to weathering [439], most of them subsequently had turned out redeposited in younger sedimentary formations (Fig. 10.13).

Simultaneously with these events the partial pressure of carbon dioxide gas had sharply declined and, as a consequence, total atmospheric pressure of Early Proterozoic. As a result, a hot Archaean climate had given way to the moderately warm Proterozoic epoch. As mentioned earlier, the emergence of Early Proterozoic Huron glaciation had been a result of high positions of the continents in Early Proterozoic [198].

Beside CO_2 bonded in rocks, part of carbon dioxide gas (in the form of HCO_3^- anions) had always been dissolved in the oceanic water. For this we have to keep in mind that carbon dioxide gas solubility in water, under Henry's law, is directly proportionate to its partial pressure in the atmosphere:

$$C(CO_2)_{OC} = H(CO_2) \cdot p(CO_2), \tag{10.15}$$

where $C(CO_2)_{oc}$ is the carbon dioxide gas concentration in oceanic water; $H(CO_2)$ is Henry's constant; $p(CO_2)$ is carbon dioxide gas partial pressure

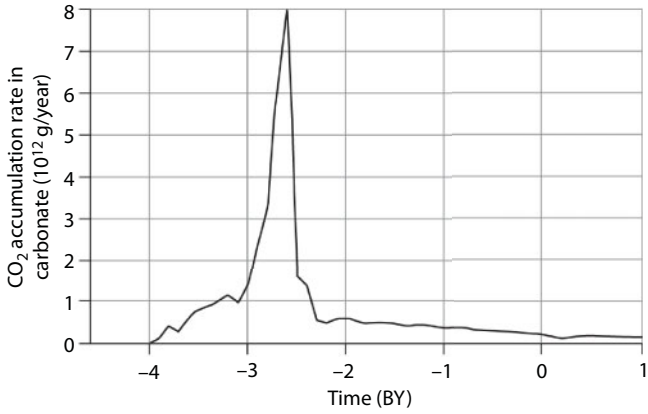

Fig. 10.13 Rate of carbon dioxide gas bonding (accumulation) in carbonates. In Early Precambrian, predominantly dolomites.

in the atmosphere. There is an exponential correlation of gas solubility in water vs. water temperature T:

$$H(CO_2) = H_0 \cdot e^{\frac{-V(CO_2)\cdot p(CO_2)}{R\cdot T}}, \qquad (10.16)$$

where $V(CO_2)$ is partial molar volume of water-dissolved CO_2 (in infinitely diluted solution); R = 1.987 cal/mole·deg is the gas constant; H_0 is the normalization factor.

Taking into account that in the present-day ocean is dissolved approximately $1.4\cdot10^{20}$ g CO_2 and partial pressure of this gas in the atmosphere is 0.46 mbar, from Eq. (10.15) we will estimate the effective value of Henry's coefficient for the present-day ocean: $H_{oc} \approx 0.213$. Average surface temperature of the present-day Earth is equal to 288 K (≈ 15 °C). Thus, we'll find the value of normalizing coefficient in (10.16) H_0 = 0.803. Now it is the time to find mass of carbon dioxide gas dissolved in ocean water:

$$\delta m(CO_2) = m(H_2O)_{OC} \cdot H(CO_2) \cdot p(CO_2). \qquad (10.17)$$

In Late Archaean, around 2.7 BYa the mass of carbon dioxide gas dissolved in the ocean, according to estimates, had reached 10^{23} g. What this means is that at average temperature of the Archaean oceans around 55°C (see below), the oceanic water in Late Archaean had been hot and

acidic, therefore, quite aggressive solvents of many compounds (including ore elements).

Be it noted that conditions for the emergence of a high-density carbon dioxide atmosphere had existed in the past only in Archaean. In Proterozoic, after Earth core separation and sharp decline in Earth tectonic activity, a serpentinite layer had emerged in the oceanic crust (see Fig. 8.1) and processes of bonding carbon dioxide gas in carbonates according to reactions of (10.7) and (10.7') type had sharply activated. As a result, in Early Proterozoic quite rapidly (within approximately 100–150 MY) practically the entire carbon dioxide gas had been removed from the atmosphere, and it had become nitrogen with total pressure of around 1.4 atm. Whereas carbon dioxide gas from Archaean atmosphere and hydrosphere had almost completely passed in carbonates and some of it, in organic matter.

As one may see from Fig. 10.12, partial pressure of carbon dioxide gas had reached in Archaean 4–5 atm. An explanation is that there had been little water in Archaean oceans and for this reason at that time the mass of bonded CO_2 had been substantially smaller than the mass of carbon dioxide gas degassed from the mantle (see Fig. 10.11). It follows from this that major mass of carbon dioxide gas degassed from the mantle in Archaean must have been in the atmosphere and dissolved in the ocean water.

Due to the pressure of carbon dioxide gas in the Archaean atmosphere, redox potential pH in the Archaean oceanic waters had declined at that time to 6–5.5. After Archaean and after the decline of CO_2 partial pressure in the atmosphere, the redox potential had increased practically to a present-day level around 8 (see Fig. 10.14).

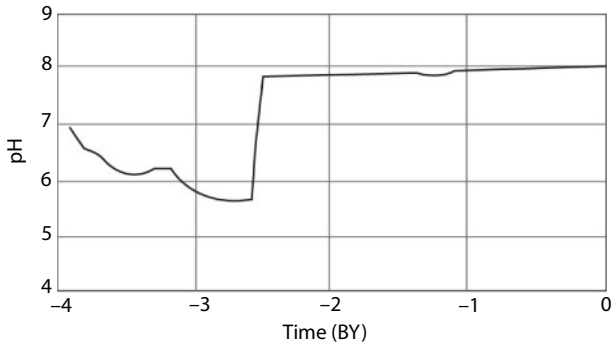

Fig. 10.14 The evolution of redox potential pH in waters of the World ocean defined by the partial pressure of carbon dioxide gas in the atmosphere [261].

10.8 Evolution of Nitrogen Partial Pressure

Nitrogen is a moderately active element weakly reacting with natural inorganic compounds. However, there are nitrogen-fixing bacteria capable of assimilating and bonding this gas in organic matter. The first and most primitive bacteria (Archaean prokaryotes) had possibly appeared soon after life nascency on Earth. As likely as not, nitrogen-fixing bacteria might have already existed among them. In connection with this, already in Archaean, bonding of this gas in organic matter and its burial in oceanic deposits might have begun, and after the life exit on the dry land, also in continental deposits. Besides, nitrogen also might have been fixed in nitrates and nitrites and due a thunderstorm activity. For this reason, life activity of organisms and thunderstorm activity over a long time of Earth's geological evolution might have substantially lowered nitrogen partial pressure in Earth's atmosphere thereby changing the climate. The available estimates indicate that nitrogen bonding by the thunderstorm activity had substantially conceded to the biogenic effect. So bonded in nitrites and nitrates, nitrogen, upon their decomposition, may have again entered the atmosphere. Nevertheless, we will consider that nitrogen removal from the atmosphere has been occurring both at the expense of bacteria and due to the thunderstorm activity. When estimating the effect of nitrogen absorption, what must be taken into account is that the organic nitrogen (Norg) of oceanic deposits together with the deposits had been continuously withdrawn from the oceanic aquatoria through the oceanic crust pile-up zones in Archaean or through plate subduction zones in Proterozoic and Phanerozoic. After this it had been partially included in metamorphic rocks of the continental crust or vanishing into the mantle and partially had been degassed again and entered the atmosphere.

It is perhaps possible to evaluate the quantities of nitrogen buried in oceanic deposits based on the data about the mass of organic carbon Corg buried in them. What is necessary for this is only to determine the proportionality coefficient between Norg and Corg. A.P. Lisitsin and M.E. Vinogradov [262] found that the ratio Corg/Norg in the open ocean bottom deposits is equal approximately to 1:0.04. E.A. Romankevich [263, 264] estimated this ratio at 1:0.1. G. Fore data [133] give Corg/Norg ratio close to 1:0.05. The estimate we use in this our publication is an intermediate value of Corg/Norg ≈ 1:0.09.

The data by A.B. Ronov and A.A. Yaroshevsky [73, 265] is that in the ocean deposits (pelagic zone plus shelves) is currently preserved around $(2.7 \div 2.86) \cdot 10^{21}$ g of Corg and in continental deposits, around

$(9.2 \div 8.09)\cdot 10^{21}$ g of Copr. Taking into consideration studied by A.P. Lisitsin [205] avalanche deposition effect of a solid clastic runoff in near-shore oceanic regions and an elevated concentration in them of the organic carbon, we assumed for our estimate a somewhat greater value of the present-day mass of the oceanic deposits and, appropriately, the mass of organic carbon Corg $\approx 3.36\cdot 10^{21}$ g.

Then the present-day content of Norg in the ocean floor deposits and on shelves is equal approximately to $2.35\cdot 10^{20}$ g and in the continental deposits around $5.0\cdot 10^{20}$ g.

The quoted quantities of the organic nitrogen had been deposited over the average existence time of the present-day oceanic crust, i.e., over the recent 120 MY and on the continents, approximate over 400 MY. To determine nitrogen Norg accumulation rate in the past geological epochs we will take into account that the element limiting life evolution in the ocean is phosphorus and its solubility in oceanic water is limited [260]. Despite the oceanic life evolution mostly occurs in the photic layer of the ocean, due to the existence of upwelling zones, saturated by phosphorus depth water is still reaching this habituated by life oceanic layer. It follows herefrom that the oceanic biomass always remained approximately proportionate to the mass of the ocean itself as shown in Fig. 10.4, curve 2. Considering this, it was possible to evaluate the oceanic biomass itself (Fig. 10.15).

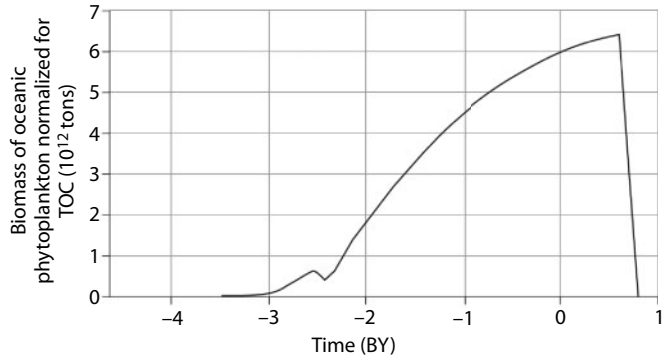

Fig. 10.15 Biomass evolution in the World ocean (decline to 0 biomass after 600 MY in the future is due to degassing from the mantle in large amounts of ruinous for all living abiogenous oxygen according to reaction (5.45) and substantial greenhouse effect associated with this [15, 112].

Considering this assumption about proportionality of the biomass in the ocean and the mass of oceanic water, it is possible to account aspproximately also for the mass of organic nitrogen N_{org} bonded in deposits

$$\left(N_{org}\right)_{OC}^{\Sigma} \approx \frac{\left(\dot{N}_{org_2}\right)_{OK}}{(m_{OC}^{w})_0} \cdot \int_{t=-4\cdot10^9}^{t} m_{OC}^{w} \cdot dt, \qquad (10.18)$$

where $\left(N_{org}\right)_{OC}^{\Sigma}$ is total mass of organic nitrogen withdrawn from the oceanic reservoir over the time of t = –4 BY to the present-day time t = 0; $\left(\dot{N}_{org}\right)_{OC} = \left(N_{org}\right)_{OC} / \tau$ is present-day rate of N_{org} burial in the oceanic deposits; $\tau \approx 120$ MY is average age of the present-day ocean floor; m_{OC}^{w} is current value of water mass in the World ocean (see Fig. 10.4).

Numerically integrating Eq. (10.18) over the assumed parameters, it is possible to determine that over the time of Earth's geological evolution (i.e., over the recent 4 BY) due to life activity of the marine biota from Earth's atmosphere had been withdrawn around $4.3\cdot10^{21}$ g of nitrogen. To this quantity should be added the mass of $N_{org} \approx 5.0\cdot10^{20}$ g, preserved in continental deposits accumulated there over the time of about 400 MY. Therefore, total amount of nitrogen withdrawn over the time of Earth's life from its atmosphere is approximately $4.82\cdot10^{21}$ g, which is equivalent to a decline in the atmospheric pressure by 945 mbar, i.e., somewhat more than the pressure of nitrogen preserved in the atmosphere by the present time (765 mbar).

When estimating, it is necessary to remember that in the Middle Proterozoic, 2 to 0.8 BYa, when Earth's atmosphere had also been almost purely nitrogen with only a small admixture of a radiogenic argon, it had been much warmer than now, and nowhere on continents had glacier covers emerged [266]. Therefore, at that time, at medium elevations of continents annual average temperature had nowhere, even on Earth's poles, dropped below 0° C. Based on the adiabatic theory of the greenhouse effect, in order for positive temperatures to have reigned on the surface of continents with the average elevation of 1 to 1.7 km that had gotten in Middle Proterozoic on Earth's poles, it is necessary for the atmospheric pressure to have exceeded 1.2 atm.

How then is it possible to explain a change in the nitrogen partial pressure of approximately 0 atm. in Katarchaean to 1.4 atm. in Proterozoic and its further decline to 0.755 atm. at present time? This is possible only one way, by assuming that beside nitrogen degassed from the mantle had existed an efficient mechanism of this gas removal from the atmosphere [19, 255, 267].

These conditions are best satisfied if we assume that in the present-day atmosphere is contained approximately 40% of nitrogen degassed from the mantle. In this case, the evolution of nitrogen partial pressure in Earth's atmosphere is illustrated by curve 2 in Fig. 10.16.

In and of itself, the rate of nitrogen removal from the atmosphere is exceptionally low. At present time it is only around $7 \cdot 10^{-7}$ mbar/year, which is certainly below the accuracy of our observations. This estimate results in the total for the entire Earth of about $3.6 \cdot 10^{6}$ t/year, which is not a negligibly small value. If we take into account that nitrogen fixing bacteria and thunderstorms have been "operating" for almost the entire time of Earth's geological evolution, i.e., on the order of a few billion years, the effect becomes quite noticeable. By present time it so happened that from the atmosphere had been withdrawn nitrogen amount necessary for creating the pressure of 945 mbar. In our estimate, the withdrawal from Earth's atmosphere such amount of nitrogen and, the main thing, conversion of it in organic compounds of Earth's sedimentary shell without the participation of nitrogen-fixing bacteria and thunderstorm activity would have been purely and simply impossible. There are no natural chemical reactions for this, bonding an inert nitrogen with non-dissociating organic compounds. Although the thunderstorm activity introduces its contribution in bonding nitrogen, so-produced compounds (nitrates and nitrites) are less stable and at weathering again partially convert in gaseous state.

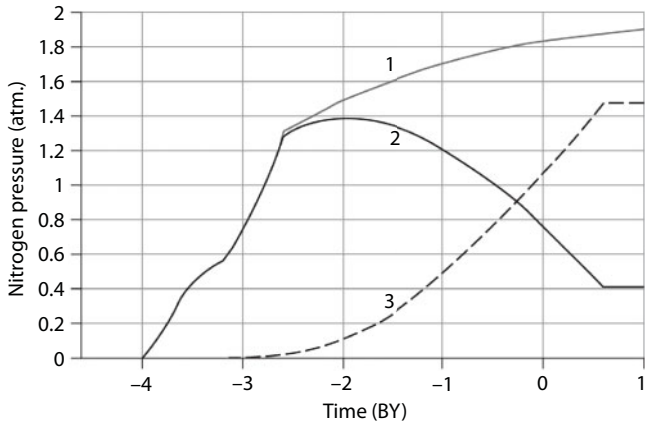

Fig. 10.16 Nitrogen origin in Earth's atmosphere and the evolution of its pressure: 1. Nitrogen degassed from the mantle; 2. Pressure of atmospheric nitrogen's summary composition; 3. The mass of nitrogen withdrawn from the atmospher (converted to the pressure).

10.9 Evolution of Oxygen's Partial Pressure

At estimating oxygen partial pressure, we will assume that in Precambrian it had been generated due to life activity of micro-algae and some species of bacteria (for instance, cyanobacteria) that had inhabited then the ancient oceans and in Phanerozoic also at the expense of macroalgae and dry land plants.

In the process of photosynthesis, oxygen is released in the chlorophyll at the expense of carbon dioxide gas dissociation according to the reaction

$$CO_2 + H_2O \rightarrow CH_2O + O_2, \tag{10.19}$$

where CH_2O is a generalized representation of organic matter [260].

Beside a biogenic origin of the major oxygen mass, it may be released also abiogenously at the expense of dissociation by water vapor affected penetrating radiation of the Sun:

$$H_2O + (h\nu)_1 \rightarrow OH + H \text{ and } OH + (h\nu)_2 \rightarrow O + H, \tag{10.20}$$

where the energy of the Sun UV-radiation $(h\nu)_1 = 5.11$ ev and $(h\nu)_2 = 4.4$ ev [268]. However, this source of oxygen appears to be low-efficiency [269]. Thus, this way is presently generated only one millionth part of the atmospheric oxygen [270], although in Early Precambrian, at a low oxygen partial pressure, the fraction of its abiogenous photodissociation might have been somewhat greater.

After the extinction of oxygen-generating organisms had occurred, a reverse reaction had occurred of oxidizing the organic remains and oxygen absorption with a new formation of carbon dioxide gas (this time, of biogenic origin)

$$CH_2O + O_2 \rightarrow CO_2 + H_2O. \tag{10.21}$$

However, if organic remains had gotten in a nonoxygen medium and subsequently had been buried in sediment sequences, the organic matter decomposition had occurred without absorption of oxygen but with the release of organic carbon C_{org}:

$$CH_2O \rightarrow C_{org} + H_2O, \tag{10.22}$$

or hydrocarbons:

$$2CH_2O \rightarrow C_{opr}H_4 + CO_2 \qquad (10.22')$$

Comparing now (10.19) with the reaction (10.21), we see that per every buried carbon atom come two atoms of a released biogenic origin oxygen. For this reason, burial of the organic carbon also leads to the accumulation in the atmosphere of biogenic oxygen [269].

The atmospheric oxygen is also participating in rock at their weathering or at oxidizing of mineralized water solutions. That is why biogenic oxygen is also accumulating in the deposits. At that, accessible for the observation are only oxidized deposits and organic carbon buried on the continents and on the bottom of the present-day oceans. Whereas it is impossible to directly account for carbon and some oxides immersed in the mantle through ancient subduction zones. Nevertheless, indirect estimates of the amounts of these elements immersed then in the mantle are still possible using, for instance, theoretical models of accumulation of iron ore formations. This is possible because iron is most active and major absorbent of the atmospheric oxygen.

In Precambrian, oxygen had been generated by marine microorganisms only in the ocean. The mass of oxygen released this way must have been proportionate to the oceanic biomass (see Fig. 10.15) or the mass of water in the ocean (see Fig. 10.4, curve 2). In Phanerozoic, after the vegetation coming on dry land around 400 MYa, this source had been supplemented also by oxygen generation by land plants. For this reason, in general terms mass of oxygen coming in the atmosphere from the ocean must have been proportionate to the mass of water in the ocean and inversely proportionate to the mass of the iron ore formations on Earth. In Phanerozoic, a contribution from the land plants has also to be accounted for:

$$p(O_2) = \frac{a \cdot M_{wo}}{b \cdot \dot{Fe} + c} + p(O_2)_{cont}, \qquad (10.23)$$

where M_{wo} is the mass water in the ocean (see Fig. 10.4); $\dot{Fe}$ is the iron ore formation ccumulation rate which was determined above (see Fig. 10.5); $p(O_2)_{cont}$. is the contribution from the dry land vegetation after 400 MYa ito oxygen total partial pressure (in our estimates we assumed $p(O_2)_{cont} \approx 0.1$ atm.); factors a, *b* and c are so selected that oxygen partial pressure in the present-day atmosphere would be equal to 0.231 atm.

and in the atmosphere 600 MYa would be lower by one order of the magnitude ≈ 0.0231 atm. The estimate results according to equation (10.23) at logarithmic scale are included in Fig. 10.17.

Comparing results of theoretical oxygen partial pressure estimate with geological data, we are forced to recognize that O_2 partial pressure in Archaean and Early Proterozoic atmosphere indeed had been very low. Although in Archaean, due to a lower content of free iron in the convecting mantle above the areas of Earth matter zonal differentiation (see Figs. 5.1 b–c and 5.16), oxygen partial pressure could have been somewhat higher than in Early Proterozoic at the times of mass deposition of iron ore formations. Besides, in Early Precambrian, processes of abiogenous oxygen generation as affected by the penetrating Sun radiation according to reaction (10.20) also might have contributed. However, according to our estimates, the partial pressure of photodissociation oxygen at that time had not exceeded 0.1 mbar.

Usually, as arguments in favor of a low oxygen partial pressure are used geochemical parameters of ancient sedimentary formations which may be interpreted as parameters of the existence of a reducing environment and practically total absence of free oxygen in the atmosphere up to 2.0 BYa. For instance, in Late Archaean and Early Proterozoic conglomerates, Witwatersrand type in South Africa or Elliot Lake in Canada,

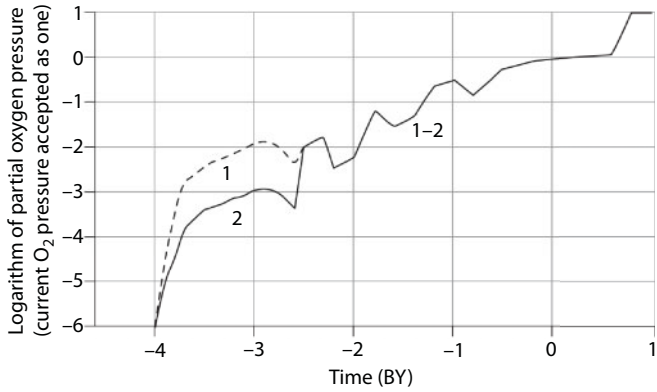

Fig. 10.17 Evolution of oxygen partial pressure in Earth atmosphere. At logarithmic scale. In Precambrian, oxygen had been generated only by the oceanic biota. In Phanerozoic, oxygen from the land plants had been added. 1. Biogenic oxygen pressure (assuming the intensity of its generation by the Archaean prokaryotes had been the same as by eukaryote micro-algae; 2. The same, assuming the intensity of its generation by the Archaean prokaryotes had been one order of the magnitude lower than those by eukaryote micro-algae after Archaean.

commonly developed on many ancient shields and formed in the time interval of 3 to 2.1 BYa, are contained large quantities of clastic uraninite UO_2 and pyrite FeS_2. The formation of these minerals cannot be explained by stagnation phenomena in deep oceanic water. Besides, in the emergence period of the expansive Huron glaciation (around 2.4–2.2 BYa) stagnant water must not have existed at all. Therefore, at the moment of their formation, uraninite and pyrite of the Early Proterozoic conglomerates had been in geochemical equilibrium with aerated oceanic water, i.e., with the atmosphere. High values of ratios bivalent/trivalent iron in Early Precambrian sediments and weathering crusts as well as chemogenous siderite massive deposits indicate reducing environments of the ancient atmosphere.

It must be specially emphasized that the fact of a simultaneous deposition at that time of oxide iron ore formations does not contradict with the above-stated conclusions about exceptionally low oxygen partial pressure in the atmosphere of those remote geological epochs. Moreover, the very existence of sedimentary iron ore formations in Precambrian supports these conclusions. Indeed, under oxidizing environment in the atmosphere and ocean, the solubility of iron oxides sharply declines, therefore, equally sharply must have declined iron's migratory capability. In such a case the entire iron would have been oxidized to trivalent insoluble state directly in the rift zones of Earth and would have been deposited there forming metal-bearing sediments of ophiolite complexes. Thus, on contact of iron with water in the presence of carbon dioxide gas, according to reaction (10.4) would have emerged iron bicarbonate well soluble in water. This iron bicarbonate had been spread all over the ocean, and in a shallow water, with the participation of microorganisms, according to reaction (10.4') had been occurring iron oxidizing to the insoluble trivalent oxide, and exactly this oxide had formed main masses of iron ore deposits. From such iron oxidizing mechanism follows, in particular, that at the moment of iron ore accumulation splash-up oxygen partial pressure in Earth atmosphere must have declined lower yet as exactly in those periods almost the entire oxygen had been absorbed by the oxidizing iron. As opposed to this, in the periods of fading processes of iron ore accumulation the oxygen content in the Precambrian atmosphere might have been slightly increased. It is difficult to determine the scale of these oxygen partial pressure fluctuations in the atmosphere, but it is not impossible that they might have exceeded one order of the magnitude.

Oxygen partial pressure in Middle and Late Precambrian had continued to grow slowly. As a result, after 2 BYa on the surface of continents and continental margins had appeared red-bed weathering crusts and clastic

origin red-bed deposits [236, 271]. Exactly red-beds are indisputable evidences of free oxygen appearance in the atmosphere (and hydrosphere), as at that iron migratory capability sharply declines. After its oxidizing to the trivalent state in the process of silicate or carbonate weathering or had been preserved *in situ* in products of rock destruction giving them characteristic brownish red hues. The parameter characteristic of redox conditions change in the ancient atmosphere is passing of Europium oxides in sediments from Eu^{2+} to Eu^{3+} which had also occurred in the time interval 1.9 to 0.8 BYa [272].

An increase in oxygen partial pressure after 2 BYa had occurred also in Earth biota. Exactly at this time had been tempestually evolving numerous species of single-cell bacteria and algae. After a total disappearance of metallic iron from the mantle at the boundary Proterozoic/Phanerozoic, a new and most significant raise had begun of oxygen partial pressure which had resulted in most significant restructuring of the entire Earth biota.

The third sharp geological-biological boundary at the transition from Proterozoic to Phanerozoic had been clearly expressed not only in Earth biologic history but also had radically changed the entire ecological environment on its surface. From then on, Earth atmosphere had converted from neutral to oxidizing. In this new environment already most efficient had turned out those life forms whose metabolism was built on oxidizing reactions of organic matter synthesized by the plant kingdom. Appropriately to this, oxygen generation for Vendean in Phanerozoic may be accepted as shown in Fig. 10.18.

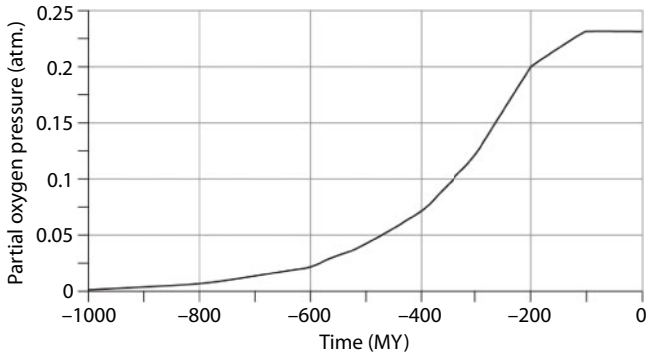

Fig. 10.18 Assumed oxygen partial pressure evolution in the recent billion years (present-day oxygen pressure is 0.2315 atm).

10.10 Abiogenous Methane Generation Patterns

Among minute additions to the major composition of the atmosphere attention should be paid to methane, even more so that at early stages of Earth evolution it had substantially affected the conditions of life emergence on Earth. Besides, the abiogenous methane might have served a nutritive base for the bacterial biota and perhaps had played a noticeable role in the formation of gas hydrate accumulations in the oceanic deposits.

In the foundation of iron ore formations emergence in Precambrian had laid processes of iron oxidizing at the expense of thermal dissociation of CO_2-saturated oceanic water and hydration by this very water of iron-containing oceanic crust rocks. In the process, methane had been generated according to the following reaction

$$4Fe + 2H_2O + CO_2 \rightarrow 4FeO + CH_4 + 41,8\,\text{kcal/mole} \quad (10.24)$$

Currently, the mantle does not contain the free iron, and for this reason, methane generation in the oceanic rift zones occurs only at hydration of containing bivalent iron rocks of the oceanic crust, mostly according to reactions like

$$\underset{\text{fayalite}}{(4Fe_2SiO_4} + \underset{\text{forsterite}}{12Mg_2SiO_4} + 18H_2O + CO_2 \rightarrow \underset{\text{serpentine}}{4Mg_6(Si_4O_{10})}\ \underset{\text{hematite}}{(OH)_8} + 4Fe_2O_3 + \underset{\text{methane}}{CH_4} + 183,4\,\text{kcal/mole}) \quad (10.24')$$

Due to fractionation reactions of isotopes between carbon dioxide gas and methane, the latter must have been enriching in a light carbon isotope ^{12}C; the heavy isotope ^{13}C must have mostly changed to carbon dioxide gas. Such carbon isotopic shifts are observed, for instance, in hydrothermal springs of the "black smokers" emerging on serpentinites. For methane this is usually $\delta^{13}C \approx -13\ -14‰$ whereas the composition of dissolved in oceanic water HCO_3^- and CO_2 is characterized by shifts (offsets (shifts)) close to $\delta^{13}C = -5.5‰$ [19, 273]. This shows that the isotope exchange reaction between carbon dioxide gas and methane, as this follows from reaction (10.13), occurs in the direction of declining $\delta^{13}C$ in methane.

Obviously, epochs of maximum rate of iron withdrawal into the ocean must have had to come together with maximum methane generation rate which, in turn, had resulted in a mass increase of methane-absorbing

bacteria. Carbon isotope fractionation had always been leading to a lightening of methane isotope composition, therefore, to lightening composition of carbon in the organic matter (C_{org}) of the bacteria that had grown on this methane. This phenomenon is probably an explanation of the fact that the organic matter of methane absorbing bacteria usually has extremely low values of $\delta^{13}C_{org}$ offsets (shifts) to –50‰ and even to $\delta^{13}C_{org} \approx -80‰$. This phenomenon is probably applicable to the emergence of local minima in $\delta^{13}C_{org}$ distribution exactly at the deposition moment of the largest iron ore formation masses at the end Archaean and in Early Proterozoic.

In Chapter 11 we will determine the accumulation rate of iron ore deposits in Precambrian. Here we will reproduce the diagram of Fig. 11.9 in comparison with the isotopic offsets' (shifts') distribution curve of the organic carbon borrowed from the publication by M. Schidlowski [274] (see Fig. 10.19). As anyone can see from this comparison, each epoch of a

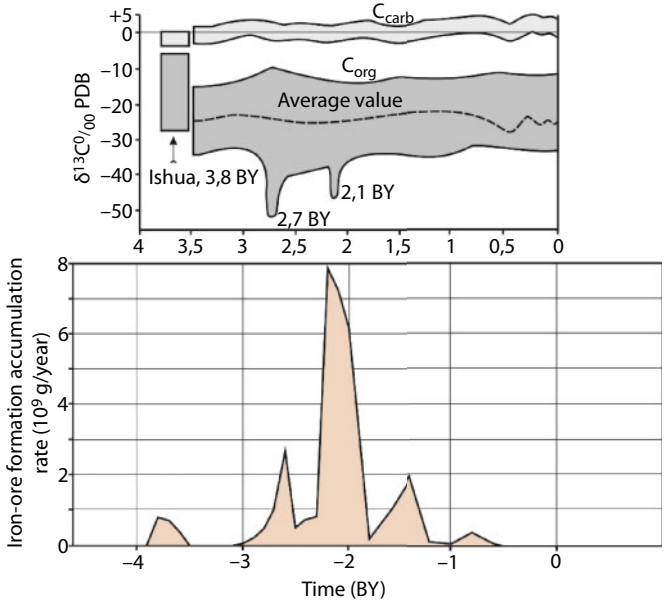

Fig. 10.19 Correlation of carbon isotopic ratio shifts in organic matter vs. the accumulation epochs of iron ore formations in Precambrian. The upper diagram is distributions of $\delta^{13}C_{org}$ and $\delta^{13}C_{caeb}$ in Earth's history [274]. The lower diagram is the rate of iron ore formations' emergence in Precambrian imaged in Fig. 11.9. Two most outstanding iron ore formations' accumulation epochs in Precambrian clearly correspond with two local minima on the enveloping curve of minimum $\delta^{13}C_{org}$ values. Unfortunately, the upper diagram does not include their complementary $\delta^{13}C_{carb}$ positive anomalies that had reached in Early Proterozoic +8…+11 ‰ PDB [275].

mass iron ore deposition on the ocean floor had corresponded with a minimum of the organic carbon $\delta^{13}C_{org}$ isotopic shift. Interestingly, despite a smaller intensity of the jaspilite formation process in Late Archaean, amplitude of the isotopic minimum of $\delta^{13}C_{org}$ at that time turned out maximum. Probably, this had been associated with the fact that in Archaean, a dense carbon dioxide atmosphere had still existed, whereas in Early Proterozoic CO_2 partial pressure had already declined and as a result, the rate of methane generation had declined as well.

It is also interesting that accumulation moments of iron ore deposits in Late Archaean and Early Proterozoic had corresponded with two periods of a broad stromatolite evolution (Fig. 10.20). The nutrition base for such stromatolites, most likely, had served the same abiogenous methane generated by metallic iron oxidizing processes according to reaction (10.24) and by hydration of iron-containing silicates.

At an estimation of abiogenous methane generation it is reasonable to presume that its rate $\dot{m}_i(CH)_4$ had been usually controlled by the formation rate of the oceanic crust [273, 276]. It is equal to $U\cdot(H_b + H_{sp})\cdot\rho$, where

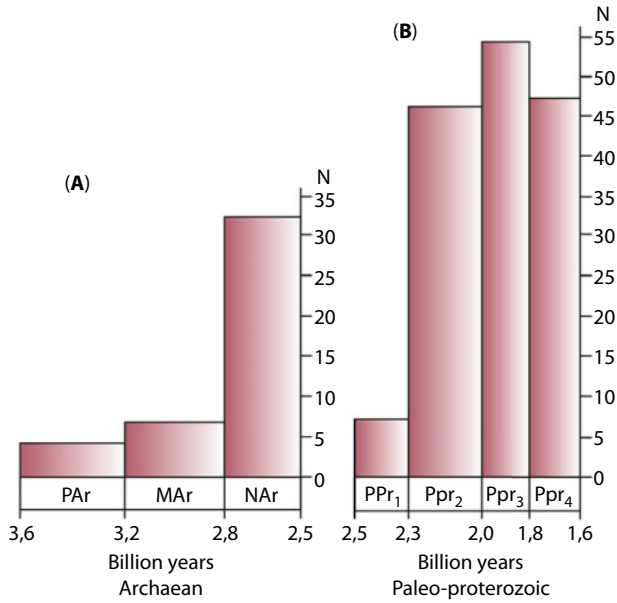

Fig. 10.20 Histograms of stromatolite formations' amount change in Archaean (A) and Proterozoic (B), after M.A. Semikhatov *et al.* [275]: *N* is the number of formations with stromatolites. When comparing these histograms, it is necessary to remember that the mass of Archaean stromatolites is substantially smaller than that of Early Proterozoic ones (Paleo-Proterozoic in M.A. Semikhatov's terminology).

U is the rate the oceanic crust build-up area in Earth's rift zones (see Fig. 8.2); H_b and H_{sp} are respectively thicknesses of basalt–gabbroid and serpentinite layers of the oceanic crust (see Fig. 8.1); $\rho \approx 2.9$ g/cm^3 is average density of oceanic crust. Besides, in epochs of a mass deposition of iron ore formations had occurred additional methane release at a rate proportionate to iron accumulation $\dot{F}e$ in such formations.

In the Precambrian rift zones, methane generation had been occurring as well due to hydration of iron-containing silicates according to reactions like (10.9), as with the participation of free (metallic) iron according to reaction (10.24). Both reactions had been taking place in the thickness of oceanic crust at hydration of its rocks by the oceanic water. It is also likely that these reactions had been occurring in Archaean due to soaking of Earth's primordial regolith with the rain water saturated by carbon dioxide gas (see Fig. 5.1 b–c and 8.4).

For adjusting the estimate results to a single scale, it was necessary to reduce all methane formation reactions to its unit of mass. Thus, under the reaction of iron oxidizing (10.24) in rift zones and primordial regolith, one mole of methane (16 g) had formed at the expense of a recombination of 304 g of source reagents. Therefore, the scale factor of this reaction is $k = 16/304 = 0.0526$. Similarly, to a hydration reaction of the oceanic crust iron-containing rocks and regolith as described by Eq. (10.9), corresponds fudge factor $n = 16/2{,}876 = 0.00556$. With these notes in view, the rate of abiogenous methane generation reaction (at surplus of CO_2) is as follows

$$\frac{d(CH_4)}{dt} = U \cdot \rho \cdot n \cdot C_{FeO} \cdot 0{,}8 \cdot (H_{sp} + 0.12H_b) \cdot \frac{S_O}{S_G} \cdot 10^{15} + k\frac{D(Fe)}{dt} \cdot 0{,}1 \tag{10.25}$$

where S_O is the oceanic crust area (see Fig. 8.4); $S_G = 5.1 \cdot 10^{18}$ cm^2 is the area of Earth; C_{FeO} is iron oxides' concentration in the mantle matter and in the oceanic crust (see Fig. 5.16); factors 0.1 and 0.8 describe the extraction extent of a given component (Fe or FeO from the oceanic crust layers). The methane generation in the present-day oceanic crust, judging by Eq. (10.9), is equal to $1.86 \cdot 10^{12}$ g/year. This is close to the determinations by Dmitriyev and his colleagues [276]: approximately $2 \cdot 10^6$ t/year (or $2 \cdot 10^{12}$ g/year). The results of methane generation rate estimate according to (10.25), in comparison with the organic carbon isotopic shifts, are included in Fig. 10.21.

One can see from the Figure that the generation of abiogenous methane in the oceanic crust had begun around 4 BYa and had reached

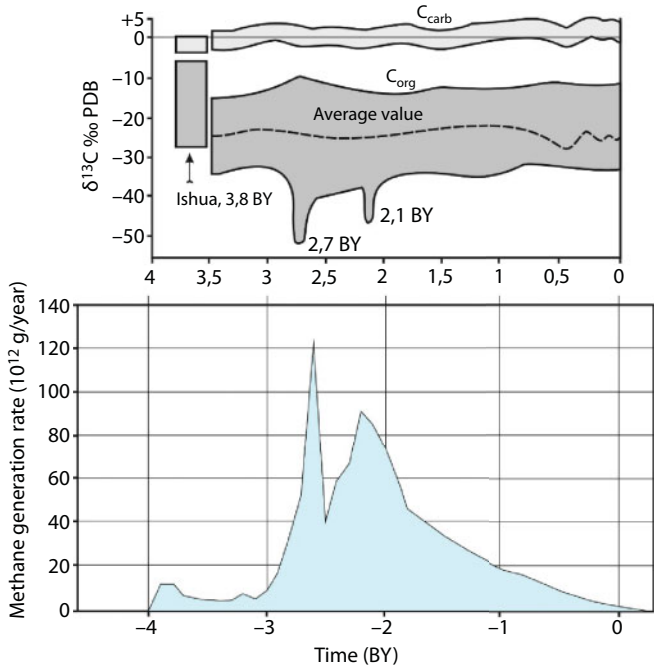

Fig. 10.21 Abiogenous methane generation rate evolution in the oceanic crust rocks based on theoretical correlation (10.25), as compared with carbon in organic matter isotopic ratios' shifts. The upper diagram is $\delta^{13}C_{org}$ and $\delta^{13}C_{carb}$ distributions in Earth's history [274]. The lower diagram is abiogenous methane generation rate. Two most outstanding epochs of Precambrian iron ore formation and methane accumulation clearly correspond with local minima on the enveloping curve of minimum $\delta^{13}C_{org}$ values.

approximately 10 million t/year but quite rapidly dropped again to a few million t/year in mid-Archaean. Then, in connection with the started process of Earth's core separation (see Fig. 5.1 d–e) and a significant increase in Earth's tectonic activity (see Fig. 6.17), methane generation had sharply grown again and by the end Archaean had reached its absolute maximum of around 120 million t/year. At the Archaean/Proterozoic boundary, due to a new sharp decline in Earth's tectonic activity, the rate of methane generation had dropped again to 40 million t/year. However, mass deposition of iron ore formations begun in Early Proterozoic (see Fig. 10.19) around 2.2 BYa had resulted again in a new rise of methane generation intensity approximately to 90 million t/year. Subsequently abiogenous methane formation had only been shrinking and by the present-day had declined to 1.8 million t/year. In approximately 500 MY, when in connection with the regime of Earth's core formation, bivalent iron had totally vanished from

the mantle (see Fig. 5.16), the very process of abiogenous methane generation had stopped.

Conspicuous is the fact of a strong correlation between organic carbon isotopic shifts and the methane generation rate, therefore, the mass of iron ore formations deposited in Early Precambrian. This is understandable as iron oxidizing under reaction (10.24) and its subsequent accumulation in iron ore formations had been accompanied with the generation of abiogenous methane. Methane had served a nutrition base for cyanobacteria and methane consuming bacteria. So, such correlation must have left a noticeable footprint in Earth's geological scripture. At that, due to carbon isotopic fractionation in exchange reactions of carbon dioxide gas with methane according to reaction (10.13), methane had always been enriched in the light carbon isotope, and the remaining carbon dioxide gas which then had passed in carbonates, on the contrary, had grown isotopically heavier. For this reason, the organic matter formed from methane-absorbing bacteria, must always have had a relatively lighter carbon isotopic composition dropping sometimes to $\delta^{13}C_{org} \approx -50‰$ and lower. Perhaps, this phenomenon is exactly the explanation for the emergence of local $\delta^{13}C_{org}$ distribution minima squarely at the moments of maximum rates of iron ore formations deposition at the end Archaean and in Early Proterozoic.

An intensified methane generation during epochs of iron ore formations mass deposition must have reflected also in the evolution intensity of stromatolite buildups, which are remains of bacterial mate (film) accretion. If so, and a noticeable part of such films had indeed been formed by methane-consuming archaebacteria, then in the periods of mass iron ore formations' accumulation and abundant methane generation, a bloom of these lifeforms must have occurred. Exactly at these moments in time, according to A.M. Semikhatov with colleagues [275], sharp flash-ups in the growth mass of stromatolite buildups had occurred (see Fig. 10.21).

Perhaps, some part of the abiogenous methane might have concentrated in form of gas hydrate accumulations in the oceanic deposits. Exactly in Late Yatulian time (i.e., in the second half of Early Proterozoic) in Karelia had occurred a mass deposition of shungites (a coaly matter, most likely, graphitized remains of hydrocarbon accumulations).

Beside methane generation in the oceanic rift zones, in the very beginning of Archaean had occurred a single spew of abiogenous methane in the atmosphere due to hydration of the ultramafic regolith still covering most of Earth's surface at that remote time (see Fig. 5.1 *b-c* and 8.4). The intensity of this spew is possible to evaluate, for instance, by assuming that in the first 100 million years (4.0 to 3.9 BYa) the entire layer of primordial regolith with beginning

iron concentration in it around 13% and its oxides around 23% (see Fig. 5.16), had been saturated with carbon dioxide rainwater. In this case, under CO_2 surplus, the original methane pressure is determined as follows:

$$p(CH_4) = \rho_r \cdot H_r \cdot (0.13 \cdot k + 0.23 \cdot n) \cdot \frac{S_r}{Sg \cdot 10^3} \text{ bar}, \qquad (10.26)$$

where $\rho_r \approx 2$ g/cm^3 is regolith's density (by analogy with the lunar regolith); H_r is an unknown thickness of the regolith layer soaked with rainwater; S_r is the regolith-covered area (see Fig. 8.4); $S_G = 5.1 \cdot 10^{18}$ cm^2 is Earth's area. However, a limiting factor in reactions (10.9) and (10.24) of methane formation is mass of degassed carbon dioxide gas. Our estimate is that by the moment 3.9 BYa around $m(CO_2) = 6.4 \cdot 10^{20}$ g of the carbon dioxide gas had been degassed from the mantle. Assuming that all this this gas had been spent on the methane generation, its mass would have been $m(CH_4) = m(CO_2) \cdot 16/44 \approx 2.33 \cdot 10^{20}$ g, the partial pressure of methane would not have exceeded $p(CH_4) \approx 46$ mbar. This methane pressure in Eq. (10.26) corresponds with carbon dioxide water-soaked regolith layer around 38 m thick. This $p(CH_4)$ estimate is perhaps maximum whereas the real methane partial pressure at the very beginning of Archaean had been somewhat lower but still no less than 20 mbar.

However, in places of its generation (in primordial regolith and outside of depositional sequences) methane might not have been accumulated in water of that time marine basins and had entered the atmosphere directly, giving it sharply reducing nature. Thus, the atmosphere at the beginning of Early Archaean had been substantially reducing and carbon dioxide-nitrogen-methane in its composition. Subsequently, in approximately 100 million years, after total hydration of primordial regolith, the reducing potential of Archaean atmosphere must have declined due to methane photodissociation under the Sun radiation and the formation of formaldehyde.

$$CH_4 + CO_2 + h\nu \rightarrow 2HCOH. \qquad (10.27)$$

Besides, in a humid and warm atmosphere of Early Archaean, affected by the Sun UV radiation, methane had also oxidized ($CH_4 + H_2O + h\nu \rightarrow CO + 3H_2$), and hydrogen had volatilized. As a result, the Archaean atmosphere had become a carbon dioxide-nitrogen one with only a small admixture of methane at equilibrium moisture content.

As E.M. Galimov [277] showed, for the emergence of life abiogenically, some precursors, simple organic compounds must have initially

accumulated. One such compound might have been formaldehyde emerging, same as methane, at iron oxidizing

$$2Fe + H_2O + CO_2 \rightarrow 2FeO + HCOH + 3.05\,\text{kcal/mole}. \quad (10.28)$$

Beside formaldehyde, in a humid nitrogen and methane-containing reducing atmosphere of Early Archaean, due to lightning discharges, also the formation of another "building brick" of the primordial life, hydrogen cyanide must have occurred:

$$N_2 + 2CH_4 + Q \rightarrow 2HCN + 3H_2, \quad (10.29)$$

where Q = 26.6 kcal/mole is absorbed by the reaction (10.29) part of lightning discharge energy.

At the very beginning of Archaean around 3.9 BYa, bacteria possibly had not had time to emerge. In this case, the isotopic shifts of that time organic matter had been defined only by properties of the reactions like (10.9) and (10.24) without adding the isotopic shifts at the expense of bacterial metabolism. This, in particular, may be an explanation why carbon isotopic ratios around 3.9–3.8 BYa in Shidlowski diagram are somewhat higher compared to $\delta^{13}C$ values of subsequent epochs (see Fig. 10.19 and 10.21).

Using the estimates obtained from Eqs. (10.25) and (10.26), it was possible to derive the partial pressure evolution of abiogenous methane in Earth's atmosphere shown in Fig. 10.22. However, for a complete description of methane generation rate on Earth, the correlation (10.26) had to be amended with the generation of this gas in the swamps of Eurasia northern areas, of Canada and in Earth's soils and also methane seeping from hydrocarbon accumulations on continents. Assuming the beginning of this process approximately 1.8 BY and methane partial pressure in the present-day atmosphere approximately $p_0 = 1.216 \cdot 10^{-6}$ bar ($\log(p_0) = -5.92$), it is possible to determine total methane pressure in Earth's atmosphere. Our estimates are that the current methane generation on continents is approximately 3.3 times of that in the oceanic crust rocks. As methane partial pressure in the entire Earth history had varied by more than 4 orders of the magnitude, estimate results in Fig. 10.22 are to the logarithmic scale:

Methane is a quite unstable gas and usually rapidly decomposes in a free environment. For instance, degassing from the oceanic water and getting in the stratosphere, it is affected by high energy Sun radiation and

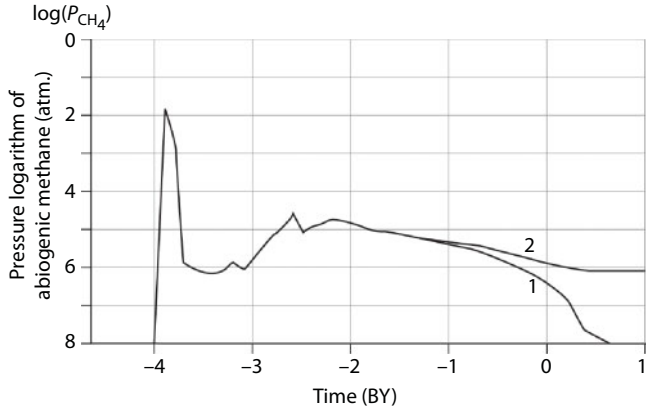

Fig. 10.22 Methane partial pressure evolution in Earth's atmosphere: 1. Methane generation in the oceanic crust; 2 Summary methane generation in the oceanic crust and on continents.

rapidly decomposes, and carbon returns in the atmosphere carbon dioxide reservoir.

$$CH_4 + 2H_2O + h\nu \rightarrow CO_2 + 4H_2, \tag{10.30}$$

$$CH_4 + 2OH + h\nu \rightarrow CO_2 + 3H_2. \tag{10.31}$$

And at last, in Late Precambrian and especially in Phanerozoic direct methane oxidizing reaction had begun developing:

$$CH_4 + 4O_2 \rightarrow 2H_2O + CO_2 + 131.2\,\text{kcal/mole} \tag{10.32}$$

In the oceanic water, methane is consumed by bacteria with the release of the same carbon dioxide gas (especially after the extinction of microorganisms)

$$CH_4 + \text{bacteria} \rightarrow CO_2 + (\text{OM}). \tag{10.33}$$

In active metamorphism zones of Early Precambrian, perhaps, might have occurred also direct reactions of carbon reduction from methane with the formation of coaly matter (oil shales, shungites and even graphite).

Despite all these losses, methane remaining in sedimentary sequences, especially without an access of oxygen, might have formed individual hydrocarbon accumulations, for instance, gas hydrates [278]. Synthesis of more complex hydrocarbons from methane is also a possibility. For instance, A.Yu. Lein and her colleagues [279, 280] believe that sulfide ores of "black smokers" are a unique target for studying organic matter genesis. The chemical peculiarity of hydrothermal systems with H_2, H_2S, CH_4, NH_4, Fe^{2+}, Mn^{2+}, CO, CO_2 and NaCl (electrolyte) in the composition of their solutions and sulfide minerals (electrode) in the solid phase allow to suggest the process of organic compounds' bacterial synthesis on the sulfide mineral matrix in this giant electrochemical cell. In particular, the study by A.Yu. Lein with her colleagues [279] of lipid fractions in hydrothermal springs by the methods of single-dimensional and bidimensional chromatography showed that all samples had a wide range of neutral lipids and phospholipids; protein and nucleic acids (DNA) were discovered in the water-methanol phase.

Mass-spectrometry of organic matter's lipid fraction composition from sulfide ores confirmed present in them components of biogenic structures including cellular material of microorganisms. Fatty acids extracted from the present-day sulfide ores are close in composition to lipids from the biomass of chemoautotrophic bacteria of the hydrothermal community in the active fields of mid-oceanic ridges [279–281].

10.11 The Evolution of Earth Atmosphere Composition and Pressure

Summing up partial pressures of all major components of Earth's atmosphere (carbon dioxide gas, nitrogen, argon, oxygen and atmospheric moisture), it was possible to build a summary picture of chemical composition and atmospheric pressure change for the entire Earth's history and even with a forecast for the future (Fig. 10.23).

At the beginning stage of Earth formation its atmosphere had been composed by insignificant quantities of the inert nitrogen with noble gas traces. The atmospheric pressure had not exceeded 1 millibar. No additions of chemically active gases (for instance, CO_2, CO, O_2, H_2O or OH) had existed in Katarchaean primordial atmosphere as all such active components had been rapidly absorbed then by regolith of still growing Earth.

After Earth's degassing had begun in Early Archaean, partial pressure of carbon dioxide gas, nitrogen and methane had begun rapidly growing

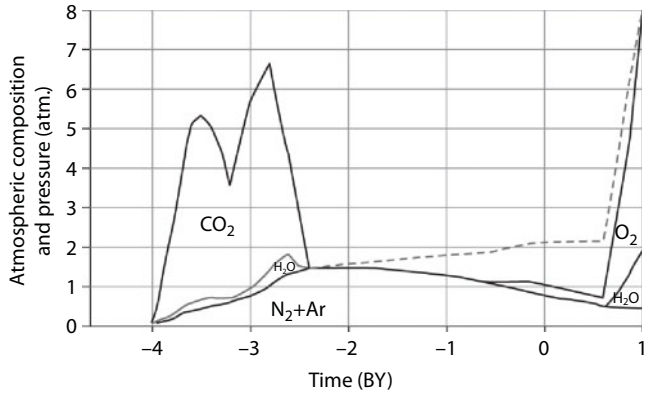

Fig. 10.23 Evolution of Earth's atmosphere composition and pressure. The dashed line shows the atmospheric pressure in an assumption of nonexistence of nitrogen bacterial absorption.

(methane had been associated with reducing CO_2 on iron). The atmosphere first had turned carbon dioxide-nitrogen-methane and substantially reducing. Starting approximately at 3.5 BYa, after a significant rise of the atmospheric average temperature, a significant partial pressure of water vapor had added to its carbon dioxide-nitrogen composition. After methane dissociation approximately 3.8 BYa, the atmosphere had become neutral carbon dioxide-nitrogen gas shell of Earth.

Due to the degassing of nitrogen from the mantle, nitrogen partial pressure in Late Archaean had significantly grown. At the same time, carbon dioxide gas pressure at the end Archaean had begun declining as the atmospheric carbon dioxide gas after this time had been intensely bonding in carbonate deposits. At last, after Earth core separation and formation of the oceanic crust serpentinite layer (see Fig. 8.1), almost the entire atmospheric carbon dioxide gas had been bonded with carbonate rocks, and the composition of the Proterozoic atmosphere had become almost purely nitrogen with only small admixture of argon and methane (see Fig. 10.23).

In Early Proterozoic, nitrogen partial pressure might have reached 1.4–1.5 atm. Starting in Middle Proterozoic, nitrogen partial pressure had begun significantly declining in connection with the life activity of nitrogen-fixing bacteria. Simultaneously with this, in Late Riphaean, especially after the total disappearance of metallic iron from the Precambrian mantle, oxygen had begun accumulating in the atmosphere.

In Phanerozoic, nitrogen partial pressure had continued to decline, although in Paleozoic and Mesozoic it had been much compensated by the accelerated generation of the biogenic oxygen. And after broad evolution

of flowering plants (main "producers" of oxygen) at the end Mesozoic, its partial pressure had reached its stationary value of around 230 mbar, and together with nitrogen, around 1 atm = 1,013 mbar. After this, already in Cenozoic, the atmospheric pressure had begun declining again. At that, it should not be overlooked that an atmospheric pressure decline results in the climate cooling. This factor may significantly suppress life activity of nitrogen-fixing bacteria. This, in turn, should have led to a decrease in nitrogen partial pressure rate decline in the future.

A drastic increase in oxygen partial pressure in a distant future will have been associated with degassing of abiogenous oxygen due to the process of Earth core separation after a complete mantle iron oxidizing to stoichiometry of magnetite under reaction (5.45). As a result, 600 MY in the future the pressure of Earth's atmosphere will have rapidly risen much over 10 atm. causing therewith the strongest greenhouse effect on Earth.

11

Some Patterns of Economic Minerals' Formation in Earth's History

Major patterns of ore matter concentration in Earth's crust and the origin of commercial minerals are closely tied with the processes of Earth's global evolution and its climate. At that, the identified patterns in distribution of the commercial minerals in space and time are often reliable indicators of the very process of Earth's evolution. That is why many metallogenic concepts were based in toto on reigning in olden times theoretical perceptions about the evolution of geotectonic and petrological-geochemical processes.

An analysis was conducted of the accumulated factual material on formation environments and spatial-temporal interrelations between geologo-petrological features and tectonic environments of commercial mineral deposit formation. It indicated that metallogenic epochs are inimitable moments in the evolution history of our planet. Overall, this is understandable as from thermodynamic position Earth is an open dissipative system irretrievably losing its endogenous energy to the outer space. It follows herefrom that its evolution must be conceptually irreversible. Using this approach and based on presented in the monograph most general physical theory of Earth's global evolution, the problem of the commercial minerals' origin and major patterns in their distribution in space and time are considered from a unique theoretical position.

The problem of ore genesis in Earth's crust was numerously considered in publications. Serious contribution in the solution of this problem have been introduced by the studies of N.L. Dobretsov, Kirdyashkin [282], V.A. Zharikov [283], A.E. Kontorovich [284], D.S. Korzhinsky [285], A.A. Marakushev [286, 287], D.V. Rundquist [288, 289], V.I. Smirnov [290], V.I. Starostin [291, 292], O.G. Sorokhtin [112, 293], G.A. Tvarchelidze [294], A.I. Khanchuk [295, 296], A.D. Shcheglov [297] and many others. These fundamental studies dealt in detail with various aspects of ore formation, however, as a rule, did not touch upon the issues of transformation and redistribution of ore components in different time periods and in different geodynamic environments.

N. O. Sorokhtin (ed.) The Origins of Natural Diamonds, (325–368) © 2019 Scrivener Publishing LLC

11.1 Mechanisms of Riftogenic Earth's Crust Benefication with Ore and Lithophilic Elements

A major difficulty in explanation of formation causes of large local accumulation in Earth's crust of ore and some other trace elements is in that their concentration in the mantle is negligibly small, whereas in deposits it grows sometimes hundred- and thousand-fold. For instance, uranium and gold concentration in the present-day mantle does not exceed $2 \cdot 10^{-9}$, mercury and thorium, $8 \cdot 10^{-9}$, lead, $9 \cdot 10^{-8}$, silver, tungsten and platinum, on the order of 10^{-7}, lithium, niobium, molybdenum and tin, 10^{-6}, etc. Besides, as it follows from the present-day concepts of the origin of Earth and its evolution, the matter of the entire mantle (both upper and lower) over 4 BY of Earth's tectonic activity had been well stirred by convective flows and on average is uniform in its composition at different levels. That is why one should not expect the existence in the mantle of any local nonuniformities with an elevated content of ore elements. Only most common among the mantle ore elements (for instance, chromium) may create their purely endogenous deposits by way of a direct differentiation of mantle melts. An example may be chromite deposits in Earth's ophiolite belts.

Besides, it is significant that, judging by the melt-out environments of oceanic basalts and juvenile water content in them, Earth's mantle is practically dry, its water content does not exceed 0.05 %. Therefore, any fluid flows in the mantle capable of bringing ore elements in Earth's crust are out of the question. The major mass of endogenous commercial minerals in the continental crust might have formed only through the operation of a multistep process of beneficiating the crust with ore elements. At that, the first step of Earth's beneficiating occurs in rift zones on the ocean floor.

Thus, it so happened that in the ocean rift zones and on the slopes of mid-oceanic ridges (Fig. 11.1) are operating most powerful hydrothermal processes through which Earth is losing more than 30% of endogenous heat [15]. We estimated that average total water exchange rate of all oceanic hydrothermal springs in mid-oceanic ridges is approximately 2,300 km^3/year. At such rate of hydrothermal water exchange, the entire mass of water in the ocean ($1.42 \cdot 10^{24}$ g) passes through the active hydrotherms and seepages of mid-oceanic ridgesов with their wide and flat slopes in approximately 0.6–1.0 MY.

Hydrothermal systems of rift zones carry out giant masses of endogenous matter in the oceanic crust and hydrosphere, including chalcophile ore elements and silica, there are formed sulfide shows of zinc, copper, lead

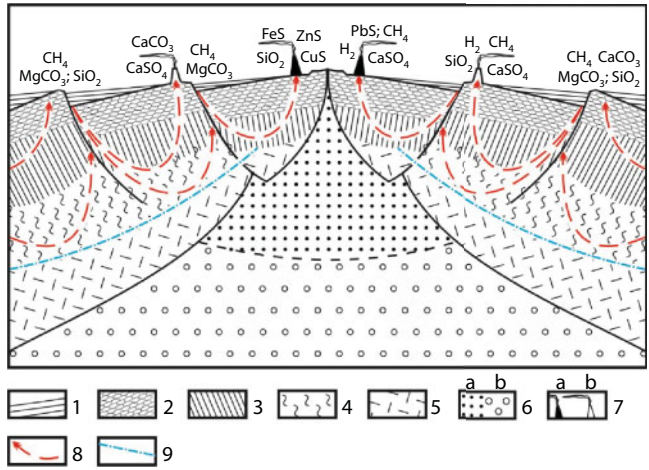

Fig. 11.1 Formation environments of the oceanic crust and geochemistry of hydrothermal processes in rift zones of mid-oceanic ridges: *1.* Sediment cover; *2.* Basalts (pillow lavas); *3.* Dolerite dykes; *4.* Serpentinite layer; *5.* Subcrustal lithosphere layer; *6.* The mantle: a. A magmatic focus underneath the crest of a mid-ocean ridge, *b.* Convecting mantle; *7.* Hydrothermal buildups: a. "black smokers", *b*- "white smokers"; *8.* The direction of ocean water movement within the body of the oceanic crust; *9.* Critical level of water temperature stability.

and other metals [246]. Thus, over the recent 150 MY only into the Pacific Ocean this way had been brought through hydrothermal springs around (10–15) 10^{12} t of polymetallic ore matter [298].

In rift zones, hydration of the near-surface mantle layers occurs and goes a number of chemical reactions important for the support on Earth of stable ecological environments as well as for the formation of carbonate and siliceous facies. All these reactions are irreversible as they are unfolding with energy release. The main of them are the reactions of oceanic crust rock hydration bonding the carbon dioxide gas in carbonates which are then consumed by living organisms and buried in oceanic deposits:

$$\underset{\text{olivine}}{4Mg_2SiO_4} + 4H_2O + 2CO_2 \rightarrow \underset{\text{serpentine}}{Mg_6(Si_4O_{10})(OH)_8} + \underset{\text{magnesite}}{2MgCO_3} + 721.34\,\text{kcal/mole}, \quad (11.1)$$

$$2CaAl_2Si_2O_8 + 4H_2O + 2CO_2 \rightarrow Al_4(Si_4O_{10})(OH)_8 + 2CaCO_3 +$$
$$\text{anorthite} \qquad\qquad \text{kaolin}$$
$$+ 110.54\,\text{kcal/mole}. \qquad\qquad (11.2)$$
$$\text{calcite}$$

Due to these reactions, in Earth atmosphere, on the one hand, is supported equilibrium and relatively low partial pressure of carbon dioxide gas and on the other, into the ocean is continuously delivered the source material for the normal life activity of skeletal organisms (among them corals, mollusks, foraminifers and coccolithophores) leading to the formation of carbonate rocks.

At hydration of pyroxenes, from rift zones silica is abundantly withdrawn

$$6MgSiO_3 + 4H_2O \rightarrow Mg_6(Si_4O_{10})(OH)_8 + 2SiO_2 + 27.38\,\text{kcal/mole},$$
$$\text{enstatite} \qquad\qquad \text{serpentine} \qquad\qquad \text{silica}$$
$$(11.3)$$

This silica serves a source of material for organisms with silica skeleton and for deposition of siliceous sediments, formation of flints and jaspers. At oxidizing bivalent silicate iron to trivalent state in the presence of carbon dioxide gas forms abiogenous methane (see reaction 10.24'), and at oxidizing iron without CO_2, hydrogen emerges

$$Fe_2SiO_4 + 3Mg_2SiO_4 + 5H_2O \rightarrow Mg_6(Si_4O_{10})(OH)_8 + Fe_2O_3 +$$
$$\text{fayalite} \quad \text{forsterite} \qquad\qquad \text{serpentine} \qquad\qquad \text{hematite}$$
$$+ H_2 + 30.72\,\text{kcal/mole}. \qquad\qquad (11.4)$$

Appropriate estimates indicate that at rock hydration in the present-day oceanic crust is generated 2 to 9 million tons a year of CH_4 and approximately the same amount of H_2. At such rate of methane generation, every million years would have emerged more hydrocarbons than there are today on Earth. It follows herefrom that most of this gas is oxidized by the methane-consuming bacteria or together with hydrogen is removed

in the atmosphere. However, a substantial part of these volatiles may be preserved in the oceanic deposits forming in them hydrocarbon accumulations, for instance in the form of gas-hydrates [299].

Together with the oceanic water, gases dissolved in water including helium are getting in rift zones. In particular, G.N. Savelyeva and her colleagues [300] showed that the variations in helium isotopic composition in rocks are caused by a different extent of mixing juvenile and atmospheric He. At that, an increase in the atmospheric He fraction in rocks of the oceanic crust reflects the involvement of the sea water in magmatic and post-magmatic processes. For instance, the high-temperature hydration of ultramafic rocks (their amphibolization) is accompanied by an increase of the mantle helium fraction, whereas the low-temperature one (serpentinization), by its sharp decline. Serpentinization is also accompanied by an increase in $^{87}Sr/^{86}Sr$ ratio. However, for most gabbroids are observed stable ratios $^{143}Nd/^{144}Nd \approx 0.5130$ and $^{87}Sr/^{86}Sr \approx 0.7035$. This, in the view of the authors of the quoted publication is a testimony of a single source of melts which may be the depleted mantle.

In the oceanic rift zones occurs release from the mantle into the ocean of numerous ore elements including iron, zinc, lead, copper, manganese and other trace elements. Sulfur is although released from the mantle, it forms sulfides of these ore element, it must be borne in mind that notable part of sulfur enters the rift zone sulfides through the reduction of the sulfate sulfur of the oceanic water on methane and hydrogen from the same zones under the reaction

$$\underset{\text{magnesium}}{MgSO_4} + \underset{\text{methane}}{CH_4} \rightarrow \underset{\text{magnesite}}{MgCO_3} + H_2S + H_2S + H_2O + 11.35\,\text{kcal/mole}. \quad (11.5)$$

The released hydrogen sulfide is exceptionally "aggressive" mineralizer (releasing large amount of energy in reaction). That is why it is immediately reducing iron and other ore metals (copper, zinc, lead) to sulfides literally "pulling them out" of basalts and ultramafic rocks of the oceanic crust, for instance, under the following reaction

$$\underset{\text{fayalite}}{Fe_2SiO_4} + 2H_2S \rightarrow 2\underset{\text{pyrrotine}}{FeS} + SiO_2 + 2H_2O + 56.68\,\text{kcal/mole}. \quad (11.6)$$

All compounds getting in water eventually turn in a deposit forming around rift zones' hot springs ("black smokers") sulfide deposits of ore elements and on the oceanic crust, a layer of metal-bearing deposits [248, 299]. Sulfide accumulations are oxidized in the course of time and their ore matters pass into metal-bearing deposits.

Beside hydrothermal benefication of the oceanic crust by ore elements, in its lower section, on contact of gabbroids with dunnites and peridotites, usually emerge deposits of banded magmatogene and chromite ores. Their origin is associated with the direct differentiation of the mantle matter immediately in the magmatic focus under rift zones. Sometimes these ores are "residues" of high-density phase chromite accumulations of basalt melts descended on the bottom of a magmatic focus underlain by restite mantle rocks. This process is observed, for instance, in Early Precambrian laminated massifs of Bushveld, Still Water and Pechenga (Baltic shield). In younger deposits the chromite ore position is usually fixed in the bodies of ophiolite complexes. Good examples of such deposits are the Kempirsay Paleozoic chromite deposit in the Southern Urals and Mesozoic chromite deposits on the Balkan Peninsula. Another example is the Voykaro-Synyin massif in the Polar Urals. According to the publications by G.N. Savelyeva and her colleagues [300–302] who studied the structure of this massif and flow structures in its rocks, its chromite formation had taken place at the final stage of deformations and plastic flow in a high-temperature mantle mass. At that, chromite ores of the massif had turned out composed of chromospinelides and olivine with accessory diopside, amphibole, Fe-Ni sulfides and platinum group minerals. The formation of this association had been caused by basite melt migration through restite peridotites in the lithospheric mantle and active interaction of the enclosing peridotites with the melt which caused the formation of dunnite and chromites in place of harzburgites or lherzolites.

11.2 The Subduction Zone Metallogeny

The second stage of continental Earth's crust benefication with lithophilic as well as with ore elements occurs in plate subduction zones under the island arcs and active continental margins at the expense of their removal from the oceanic crust. Mobilization of ore elements and their transfer into the continental crust occurs due to dehydration and remelting processes in plate subduction zones. At that, plenty of water bonded in hydrosilicates is released and emerge very powerful hot and mineralized fluid flows transferring large amount of previously dispersed elements in the continental crust.

An important role in Earth's geological history play intercontinental mountain belts joining with one another the adjacent heterochronic lithospheric plates. Most of them had for a long time already been denuded, however, a mosaic structure of the Post-Archaean continental crust is marked exactly by them. The main among Phanerozoic mobile belts of this type are Early Paleozoic North Atlantic Caledonides of the Appalachians in Scotland and Norway as well as Ural-Kazakhstan Hercynian folded buildups that had welded nearly 230 MYa the continents into a single supercontinent Pangea. With younger structures of the similar type should be attributed the Mesozoic Verkhoyansk-Kolyma fold belt emerging in the place of East Siberian paleo-ocean and merging Kolyma accretion massif and Chukotka with the ancient Siberian platform. At last, the youngest Alpine-Himalayan Cenozoic mountain system had formed at closing Tethys paleo-ocean and joined the Eurasian continent with Africa, Arabia and India.

All known folded mountain belts and tied with them ore areas had been formed as a result of closing oceanic basins and collision of continental lithospheric plates or island arcs (Fig. 8.29). In the process of their collision young continental-crust formations had always obducted the margin of an older continent with the sedimentary sequences accumulated over the entire time of ocean's existence partially absorbed in the subduction zone. Besides, often in the process of island arc obduction over the passive continental margin, ophiolite covers had formed.

At the orogenic stage of a fold system evolution in a relatively short time (on the order of a few million years), the sediment cover in the miogeosynclinal zone of a former continental margin had been crushed into folds. At the same time, under the influence of ever-growing pressure by the plate, emerging folded buildups had begun intensively rising and in the eugeosynclinal zone, i.e., in the body of the former island arc had formed numerous overthrust and fold-fault deformations. Remelting of sedimentary sequences of the former continental margin caught in the plate subduction zone had led to changing of calcareous-alkali (typical island arc) magmatism for acidic one with abundant invasions of granite intrusions and broad evolution of regional metamorphism.

Subsequently had occurred consolidation of a mountain system, its extinction, denudation and levelling-off which might have lasted hundreds of millions of years. Eventually the junction zone of lithospheric plates had ended standing out in topography, had been overlain by sediment cover and had converted in an internal platform structure. Formed clastic sedimentary sequences containing ore matter had been partially washed off by rivers and temporary streams on the continental margins where they had

been deposited on continental slopes due to a phenomenon of the avalanche sedimentation [205]. At the base of so formed sections are often positioned evaporite sequences emerged on passive continental margins. They are known, for instance, on both coasts of the Atlantic Ocean, in the Red Sea, in the Gulf of Mexico and in other regions. At getting such deposits in a plate subduction zone or zone of collision between two continents, from them might have melted out a broad spectrum of crustal igneous rocks, granites to sienites and alkali-ultramafic rocks with their appropriate mineralization.

Due to the destruction of a folded system and sedimentogenesis, redeposition had occurred of ore matter accumulations of magmatic, hydrothermal and sedimentary genesis and benefication by them of newly emerged sedimentary sequences. Redeposited on the margin and at the foot of a continent, placers in the termination phase of a new geodynamic cycle (decomposition of the previous supercontinent and the formation of a new one) might have gotten again in a subduction or collision zone where they had transformed again and involved in the benefication process of the continental crust. If a similar mechanism had been working more than once, the later ore deposits of the same type, as a rule, had turned out richer because their ore matter during the time of Earth's geological evolution had managed to have gone through a greater number of transformation and benefication cycles. An example may be the tin whose concentrations in younger deposits are usually higher than in older ones. For instance, the total content of the tin in the Mesozoic deposits more than by two orders of the magnitude exceeds its content in Archaean ore manifestations [303]. A similar situation is observed with molybdenum and tungsten. As a result of magmatic processing of the sedimentary sequences, the concentration of these metals in deposits had been continuously growing from ancient to younger ones [304]. It follows herefrom that, it would appear, "endogenous" economic minerals in point of fact had made it through the stage of a natural separation by way of the crustal rocks destruction and their sedimentogenesis in clearly exogenous environments. This conveyor type mechanism had been operating in mother nature already for a few billion years and is an example of functioning of Earth's global "concentrating plant".

In the subduction process of the oceanic lithospheric plate, in the body of allochthone had formed two dipping one toward the other systems of strike-slip faults, along which had been occurring main deformations and transport of remobilized matter (Fig. 11.2). Along these faults had also been going circulation of the mineralized hydrothermal solutions emerged due to thermal-metamorphic processes in the area of friction and tectonic erosion of the base of the lithospheric ledge overlying the subducted oceanic plate.

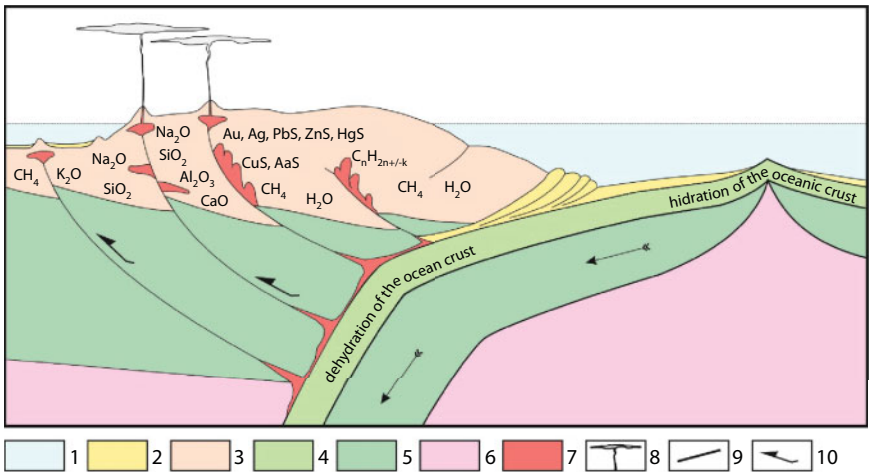

Fig. 11.2 A conceptual scheme of continental crust formation in Phanerozoic at the expense of a partial remelting and dehydration of the oceanic crust and its overlying pelagic deposits in the oceanic plate subduction zones underneath the island arcs [15, 112]. 1. Ocean level; 2. Sedimentary sequences; 3. Sedimentary-volcanogenic complexes of island arc type; 4. Oceanic crust; 5. Subcrustal lithosphere; 6. Mantle; 7. Melting area of crustal matter and intrusive bodies; 8. Volcanic buildups; 9. Movement direction of lithospheric plates; 10. Vector of strike-slip deformations.

At the expense of viscous friction energy dissipation, the deposits gotten in a gap between the rubbing plates had been gradually heating up and unavoidably beginning to melt. This process had been accompanied by the release of a large amount of heat energy, nearly 500–700 cal. per 1 g of the oceanic crust rock [112]. Should have a given system been closed (without heat dumping), the oceanic crust structure-material complexes might have heated to 1,500–2,400°C. At this, melting of water-saturated silicates occurs at much lower temperature, nearly 700–800°C, and of the deposits, at 450-500°C. Therefore, in such environments, the oceanic crust matter would be experiencing partial (nearly 10%) melting whereas the deposits would be practically completely remolten. Any further removal to the surface of the emerged magma and gas-liquid fluids had played the role of a system's thermal control and must have resulted in the medium temperature decline to a level of 1,100–1,200°C. It is necessary to mark here that the deposit density is substantially lower than the lithosphere density and their viscosity in plate subduction zones and maximum thickness drastically decrease. Due to this, they mostly vanish at depths up to 30 - 40 km being remolten and squeezed away up through their feathering faults invading as migmatite granite-gneiss domes or granitoid batholiths in a body of the island arcs or active continental margins (Fig. 11.2).

Magmatism of the subduction zones is mostly represented by medium and acid rock associations. Main of them are andesites and andesite-basalts and their intrusive analogs (quartz diorites and diorites). At obduction of island arcs over the continents' passive margins, various granitoids had formed. For these environments is also typical a contrasting in alkalinity magmatism of the base series, although its amount is not comparable with the acidic and medium varieties. The andesites and even more so granitoids are characterized by the elevated content of silica, alkalis, especially potassium, and of the other lithophilic elements and also by lowered contents of magnesium, calcium, iron and other metals. In this connection it is necessary to mention that in most cases alkali andesites and granodiorites had emerged due to a complex reworking and assimilation of the crustal, mantle and sedimentary rocks at deep lithospheric horizons.

The processes of oceanic crust dehydration and anatexis occurring in plate subduction zones had been developing according to a rather complex and multistep scheme. All stages of its transformation are not yet totally clear however, a general direction of the processes may be already perceived. Spatial-temporal variability of metamorphic transformations is in that the rock associations of a subducting oceanic lithospheric plate had experienced a progressive metamorphism in the contact zone with an obducting continent. At that, they had sequentially passed transformation stages from the lower steps to the higher. Forming in these environments mineralized and gas-saturated fluid had been moving up through the faults and, cooling down, had been causing retrograde contact-metasomatic alterations in the enclosing rocks. Numerous protrusions of ultra-mafic composition and ophiolites, having gone through the peak of alterations, had also experienced retrograde processes. Along with this, sedimentary sequences of the passive continental margin over which the island arc had obducted, had experienced a progressive metamorphism and been washed with saturated hydrothermal solutions. In the process of metamorphic transformations of the oceanic crust rocks, olivine, enstatite, magnetite and its other refractory minerals as well as the garnets emerged at depths of the eclogite transition had been removed from the system together with the lithospheric plate immersing in the mantle. At this, water fluids, silica and lithophilic compounds had been assimilated by the silicate melts forming in plate subduction zones and squeezed up.

All chemical reactions in plate subduction zones are irreversible, proceeding with heat absorption or release and in certain redox environments. An important role in the implementation of all listed processes had played geologic time which had eventually led fold system evolution physicochemical parameters to the equilibrium state.

Loose depositional sequences on the seafloor contain to 20-40% water whereas in its diagenetic varieties water content had declined to 10-15%. At this, in clayey rocks had formed hydromicas (illite, smectite, montmorillonite, kaolin and diaspore).

The deposits pulled in subduction zones, at early stage of metamorphic transformations had experienced processes of intensive dehydration. The first lost had been pore water, then crystallization water after which in them had developed a complex series of endothermal (associated with heat absorption) metamorphic transformations accompanied with the release of water, CO_2, silica, alkali (especially potassium) and lithophilic elements. The rocks in maximum compression zones had been compacted and had partially sealed the formed solutions thereby having created high fluid pressure and expanded the water-containing minerals stability field [305].

A large part of so formed fluid streams had been moving from the bottom up and to the side, perpendicularly to the long axis of the folding from the area of high pressure to the zones of tectonic shadow. At the existence of tangential pressure gradient in a permeable medium is always observed its movement and transition from one metamorphic facies to another one (Fig. 11.3). The suggested scheme favorably expresses the interrelation specifics between the fields of metamorphic facies where separating them (these fields) zones are transition areas from one facies to the next one. Exactly in these zones had begun and intensively unfolded the mineral

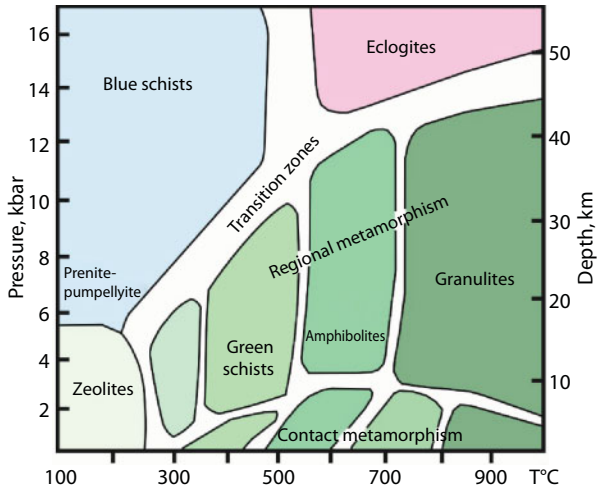

Fig. 11.3 Distribution scheme of metamorphic facies in PT coordinates after Yardley [306].

phase recrystallization processes. An analysis of this scheme enables to make one more very important geodynamic conclusion. At great depths, in subduction zones the contact line between the lithospheric plates had been fading and mineral associations had been dwelling in the environment of physicochemical equilibrium. This may have led to encapsulation of some crustal melt volumes, metamorphosed crustal rocks and fluid solutions and to transfer them deep into the mantle and over great distances together with the immersing lithospheric plate. This aspect is extremely important for understanding the nature of diamond formation and of crust-mantle carbon transfer.

Substantial influence on the formation of commercial mineral deposits render hydrothermal processes. As water content in the mantle is minuscule, all without exception hydrothermal deposits (regardless of their type) had been formed either at the expense of mobilizing meteoric water and (or) hydrosphere bathing hot intrusive bodies or at the expense of releasing by the cooling magma dissolved in this magma water in the form of a fluid solution.

The formation of hydrothermal solutions is closely tied with processes of progressive stress-metamorphism and the overheating of water-saturated system in the rocks. For instance, sodium chloride abundantly contained in sea water, interacting with sulfuric acid solutions at temperatures nearly 250°C, decomposes onto water solution of the hydrochloric acid and the sodium sulfate (mirabilite) according to the following reaction:

$$NaC1 + H_2SO_4 + H_2O \rightarrow Na_2SO_4 + HCl + H_2O. \qquad (11.7)$$

An example of deriving hydrogen sulfide is a number of sequential reactions running at temperature nearly 100°C, first by way of decomposing sodium chloride, then antimonite and at the end, tioantimonite:

$$NaC1 + 2H_2O \rightarrow 2NaOH + Cl_2 \uparrow + H_2 \uparrow; \qquad (11.8)$$

$$Sb_2S_3 + 4NaOH \rightarrow Na_3SbS_3 + NaSb(OH)_4, \qquad (11.9)$$

$$2Na_3SbS_3 + 3C0_2 + 3H_20 = Sb_2S_3 + 3Na_2CO_3 + 3H_2S \uparrow. \qquad (11.11)$$

The oceanic water contains notable amounts (up to 2.7‰) of the sulfate ion SO_4^{2-} so the reaction of such water with base composition rocks at their heating may also be accompanied by the formation of hydrogen sulfide, for instance, according to a reaction:

$$4Fe_2SiO_4 + 3Mg_2SiO_4 + CaSO_4 + H_2O \rightarrow 5MgSiO_3 + 4Fe_2O_3 +$$
fayalite forsterite enstatite hematite
$$+ CaMgSi_2O_6 + H_2S\uparrow$$
diopside (11.12)

Due to a high reducing potential of hydrogen sulfide, sulfur again is rapidly bonding with transitional metals, forming sulfides, for instance pyrrhotine:

$$Fe_2SiO_4 + MgSiO_4 + 2H_2S \rightarrow 2MgSiO_3 + 2FeS + 2H_2O.$$
fayalite forsterite enstatite pyrrhotine

(11.13)

In the process of deserpentinization of heated ultra-mafic composition rocks are released carbon dioxide gas and water:

$$2Mg_6(Si_4O_{10})(OH)_8 + CaCO_3 \rightarrow 5Mg_2SiO_4 + MgSiO_3 + MgCaSi_2O_6 +$$
serpentine calcite olivine enstatite diopside
$$+ 8H_2O + CO_2\uparrow.$$ (11.14)

Sulfuric hydrothermal solutions in epithermal environments form according to the reaction:

$$4H_2S + 8O_2 = 4H_2SO_4 \quad (11.15)$$

or:

$$4SO_2 + 4H_2O = 3H_2SO_4 + H_2S\uparrow. \quad (11.16)$$

At the interaction with hot water solutions of other oxidizers some sulfides pass into sulfates:

$$PbS + 4H_2O_2 = PbSO_4 + 4H_2O. \quad (11.17)$$

Manganese settled in great amounts on the seafloor in the form of crusts and concretions, when getting in a subduction zone, under certain conditions easily dissolves in a water sulfuric acid solution with the formation of manganese sulfate

$$Mn^{2+} + H_2SO_4(\text{diluted}) = MnSO_4 + H_2\uparrow. \quad (11.18)$$

At temperature over 450°C and high sulfuric acid concentration of fluid solution, manganese dioxide (pyrolusite) also forms sulfates with the release of oxygen and water:

$$2MnO_2 + 2H_2SO_4(\text{разб}) = 2MnSO_4 + O_2\uparrow + 2H_2O, \quad (11.19)$$

And at temperature 850-1,150°C manganese sulfate passes into hausmannite:

$$MnSO_4 = Mn_3O_4 + 2SO_3\uparrow + SO_2\uparrow, \quad (11.20)$$

Which is very common in scarn and high-temperature hydrothermal manganese manifestations in association with tephroite (Mn_2SiO_4) and braunite ($Mn_2O_3 \cdot MnSiO_3$).

Under the influence of overheated carbon dioxide solutions in the base and ultra-mafic rocks occurs the decomposition of olivine, pyroxenes and amphiboles with the formation of talc, quartz and magnesia-ferruginous carbonates (dolomite, braunnerite, ankerite, etc.) Field spars are replaced by muscovite mica or sericite. At high CO_2 partial pressure, pyrophyllite ($Al_2Si_4O_{10}(OH)_2$) is crystallized.

With temperature and pressure increase in a subduction zone the concentration of metals dissolved in hydrotherms also grows. In supercritical environments, at the peak of metamorphic processes manifestation, a fluid solution pass in gas-saturated pneumatolytic solution. Within it may be concentrated the smallest solid particles of various silicates, oxides and some other compounds. Subsequently, at the removal and cooling down of

hydrothermal solutions in a discharge area, these particles become concentrators of emerging ore deposits.

Most processes in the subduction zones run in an environments of allochemical metamorphism and are characterized by redistribution of matter and change in rock chemical composition. Thus, water-carbon dioxide fluids are a medium which transfers components participating in dehydration and decarbonizing reactions. On the progressive branch of the metamorphism occur recrystallization and replacement of low-temperature minerals by higher-temperature ones. After reaching the peak, its parameters begin going down and the inverse process of mineral associations change is realized.

Thus, for instance, in shaly rocks are sequentially replaced sericite, pyrophyllite, muscovite, andalusite, garnet, potassium feldspar and in base schists, chlorite is replaced by actinolite, hornblende and pyroxene.

The minerals so typical of the rocks of metamorphism's green schist facies as pyrophyllite, chlorite and chloritoid ($(Fe_2+,Mg,Mn)_2Al_4(SiO_4(OH)_2O)_2$), getting in the environment of the amphibolite facies, transform with the loss of water and silica:

$$\text{pyrophyllite} + Q \rightarrow \text{andalusite} + \text{silica} + \text{water};$$

$$\text{chlorite} + \text{muscovite} + Q \rightarrow \text{staurolite} + \text{biotite} + \text{silica} + \text{water};$$

$$\text{chloritoid} + \text{andalusite} + Q \rightarrow \text{staurolite} + \text{silica} + \text{water};$$

where Q is heat absorbed by the reaction.

Calcite in the presence of chlorite and quartz pass in the actinolite ($Ca_2(Mg,Fe)_5Si_8O_{22}(OH)_2$) and epidote ($Ca_2(A1, Fe)_3(Si_2O_7)(SiO_4)O(OH)$) with the release of H_2O and $CO_2\uparrow$.

According to V.S. Antipin and V.A. Makrygina [305], in pelites and dark-colored schists, the following endothermal reactions may occur:

$$\underset{\text{chlorite}}{(mg,Fe)_6(AlSi_3O_{10})(OH)_8} + \underset{\text{sericite}}{KAl_2(AlSi_3O_{10})(OH)_2} + \underset{\text{rutile}}{TiO_2} \rightarrow$$

$$\rightarrow \underset{\text{biotite}}{K(Mg,Fe)_2(Fe,Al,Ti)(AlSi_3O_{10})(OH)_2} + \underset{\text{Ilmenite}}{FeTiO_3} + H_2O, \qquad (11.21)$$

$$\underset{\text{pyrophyllite}}{Al_4(Si_4O_{10})(OH)_8} \rightarrow \underset{\text{andalusite}}{2Al_2SiO_5} + 2SiO_2 + 4H_2O, \tag{11.22}$$

$$\underset{\text{chlorite}}{(Mg,Fe)_6(AlSi_3O_{10})(OH)_8} + SiO_2 \rightarrow \underset{\text{garnet}}{(Mg,Fe)_3\,Al_2Si_3O_{12}} + H_2O, \tag{11.23}$$

$$\underset{\text{muscovite}}{KAl_2(AlSi_3O_{10})(OH)_2} + SiO_2 \rightarrow \underset{\text{orthoclase}}{(K,Na)(AlSi_3O_8} + \underset{\text{sillimanite}}{Al_2SiO_5} + H_2O. \tag{11.24}$$

In dark-colored schists (metavolcanics, tuffites and sandstones with a carbonate cement) the reactions are somewhat different:

$$\underset{\text{calcite}}{CaCO_3} + \underset{\text{albite}}{NaAlSi_3O_8} \rightarrow \underset{\text{plagioclase}}{(Na,Ca)\,Al\,2\,Si_2O_8} + CO_2 \tag{11.25}$$

$$\underset{\text{chlorite}}{(Mg,Fe)_6(AlSi_3O_{10})(OH)_8} + \underset{\text{calcite}}{CaCO_3} + SiO_2 \rightarrow \underset{\text{actinolite}}{Ca_2(Mg,Fe)_5(Si_8O_{22})} \cdot$$
$$\cdot(OH,F)_2 + H_2O + CO_2 \tag{11.26}$$

$$\underset{\text{actinolite}}{Ca_2(Mg,Fe)_5(Si_8O_{22})(OH,F)_2} + \underset{\text{biolite}}{K(Mg,Fe)_2(Fe,Al,Ti)(AlSi_3O_{10})}$$
$$(OH)_2 \rightarrow$$

$$\rightarrow \underset{\text{hornblende}}{(Ca,Na,K)_2\ (Mg,Fe)_5\ (Al_2Si_6O_{22})(OH,F)_2} + \underset{\text{diopside}}{Ca\,(Mg,Fe)(Si_2O_6)}$$
$$+ H_2O. \tag{11.27}$$

In epidote-amphibolite metamorphism facies, rocks of a base composition oceanic crust, under the action of hot gas-saturated water solution recrystallize according to a reaction:

$$4(NaAlSi_3O_8 \times CaAl_2SiO_8) + 5(Mg,Fe)SiO_3 + 5H_2O \rightarrow$$
$$\text{labrador} \qquad\qquad \text{pyroxene}$$

$$\rightarrow 2Ca_2Al_3Si_3O_{12}(OH) + (Mg,Fe)_5\,Al_2Si_3O_{10}(OH)_8 + 4NaAlSi_3O_8 + 4SiO_2. \quad (11.28)$$
$$\text{epitode} \qquad\qquad \text{chlorite} \qquad\qquad \text{albite}$$

At increasing temperature, ever denser and more waterless parageneses develop and a rock on the whole is losing 10-15% of water and 5-10% of the volume. Water released in the reaction pass in the fluid and most of the fluid is squeezed in the area of lower pressure.

At temperature nearly 500°C and high pressure (the amphibolite facies of metamorphism, see Fig. 11.3) the deformations become plastic, a solid-phase separation of the minerals into leucosome and melanosome occurs in rock associations. This process is running with mineral recrystallization "in situ". The leucosome is most often presented by quartz and plagioclase and the melanosome is composed of dark-colored minerals, mainly amphibole and biotite. As a result, the rock acquires metamorphic striation and gneissose structure.

In supercritical environments (temperature 400—500°C and higher) pneumatolith-hydrothermal processes are realized, which act upon structure-material complexes surrounding them through high-temperature gas-liquid solutions (super-critical fluids) and have mostly metasomatic nature, i.e., are expressed in the replacement of primary minerals with newly-formed associations.

Thus, from shaly deposits form alkali aluminosilicates which are subsequently removed into the continental crust enriching it with alkali and other lithophilic elements, for instance, in the reaction of albitization:

$$Al_4(Si_4O_{10})(OH)_8 + NaCl + \rightarrow Na(AlSi_3O_8) + HCl + 2H_2O + 3A1O(OH).$$
$$\text{kaolin} \qquad\qquad \text{albite} \qquad\qquad \text{diaspore}$$

(11.29)

At high depths and temperature of the medium, aluminosilicates are enriched in potassium:

$$\underset{\text{kaolin}}{Al_4(Si_4O_{10})(OH)_8} + KCl \rightarrow \underset{\text{orthoclase}}{K(AlSi_3O_8)} + HCl + 2H_2O + SiO_2 + \underset{\text{diaspore}}{3AlO(OH)}. \quad (11.30)$$

At this, a significant role of chlorine in hypogenous processes is proved not only by the formation of hydrochloric hydrothermal solutions or some chlorine-containing silicates (scapolites, sodalites) but also by the release in huge amounts of gaseous HCl in the areas of active volcanism.

In the plate subduction zones, occurs the dissociation of carbonates with alkali earth elements entering the silicate composition and with the release of free carbon dioxide, for instance, as follows:

$$\underset{\text{serpentine}}{Mg_6(Si_4O_{10})(OH)_8} + 4SiO_2 + 2CaCO_3 \rightarrow \underset{\text{diopside}}{2CaMg(Si_2O_6)} + \underset{\text{enstatite}}{4MgSiO_3} + \underset{\text{calcite}}{} + 4H_2O + 2CO_2 \uparrow. \quad (11.31)$$

Under this reaction, enstatite and diopside, as refraction minerals, together with immersing lithospheric plate are removed into the mantle as restite and water and carbon dioxide passing in the fluid (pneumatolith) solution.

At high temperature, copper oxide in a sulfuric solution forms copper sulfate:

$$Cu_2O + H_2SO_4 \rightarrow Cu_2SO_4 + H_2O \quad (11.32)$$

$$2Cu_2SO_4 + O_2 + 2H_2SO_4 = 4CuSO_4, \quad (11.33)$$

And at temperature 600-650°C, muscovite is decomposed into orthoclase, sillimanite and water:

$$\underset{\text{muscovite}}{KAl_2(AlSi_4O_{10})(OH)_2} + SiO_2 \rightarrow \underset{\text{orthoclase}}{KAlSi_2O_8} + \underset{\text{sillimanite}}{Al_2SiO_5} + H_2O. \quad (11.34)$$

At even higher temperature typical of the metamorphism's granulite facies, biotite turns high in titanium (up to 5-6% TiO_2). Subsequently, in the presence of silica, it decomposes into feldspar, hypersthene and water:

$$\underset{\text{biotite}}{2K(Fe,Mg)_3(AlSi_3O_{10})(OH)_2} + 6SiO_2 = \underset{\text{orthoclase}}{2K(AlSi_3O_8)} + \underset{\text{hypersthene}}{3(Fe,Mg)_2(Si_2O_6)} + 2H_2O \quad (11.35)$$

According to S.Z. Smirnov with coauthors [307], in the environment of metamorphism's eclogite facies (Fig. 11.3), which corresponds with depths nearly 40 km, the deposits and water solutions vanish practically completely and rock complexes become "tentatively dry". Fluids are replaced with pneumatolith gas-saturated solutions, mineral recrystallization and phase changes occur. For instance, plagioclase in the presence of pyroxenes becomes unstable and is transformed into a specific garnet with the elevated Ca content and a solid solution of diopside, jadeite and aegirine, which is called omphacite. Silica released as a result of the reaction has overpressured quartz modification and is represented by coesite:

$$\underset{\text{base plagioclase}}{(Ca(Al_2Si_2O_8) + Na(AlSi_3O_8))} + \underset{\text{clinopyroxene}}{CaMg(Si_2O_6)} + \underset{\text{orthopyroxene}}{Mg_2(Si_2O_6)} \rightarrow$$

$$\rightarrow \underset{\text{pyrope grossular}}{(Mg,Ca)_3Al_2(SiO_4)_3} + \underset{\text{omphacite}}{(Na,Ca)(Al,Mg)(Si_2O_6)} + \underset{\text{coesite}}{SiO_2} \quad (11.36)$$

Hydrothermal solutions are a powerful factor in the formation of commercial mineral deposits. Deposits of this type contain such metals as Fe, Mn, Cu, Pb, Ag, Au, Hg, Sn, Ge, Ti, Mo, W, Zn, Cd, Co, etc. Water feeding the hydrothermal systems is abundantly enters them at dehydration of the crustal matter. Mineralized solutions closely associate with magmatic activity of orogenic systems bathing hot intrusive bodies and saturating with ore components.

Genetically, it is possible to identify two major types of hydrothermal ore deposits. The first one may include ore buildups of most fumaroles and hot springs in volcanic areas. It also includes sulfide deposits by "black smokers" in the rift zones of mid-oceanic ridges. The second type of hydrothermal processes is often accompanied by a pegmatite mineralization emerging, for instance, above granitoid massifs or due to the rise of hot mineralized water from the plate subduction zones. In Phanerozoic, granite magmas had mostly formed due to remelting of sandy-clayey water-saturated deposits in continental collision zones and water, as earlier shown, had gotten in the plate subduction zones together with the oceanic crust rocks and pelagic deposits. Therefore, the hydrothermal system water participating in the formation of various commercial mineral deposit comes from the hydrosphere, i.e., is an exogenous reagent.

Hydrothermal systems are highly aggressive media and powerful mineralizers. The movement of a hot, mostly water fluid from the depth of a subduction zone results in a repeat hydration of the near-surface crust layers and the occurrence of a number of chemical reactions in the retrograde metamorphism environments. Among the leading are hydration reactions of base and ultra-mafic protrusive complexes and ophiolites which are often encountered in fold systems and producing a whole number of common ore minerals. All reactions are irreversible and occur with energy release:

$$\underset{\text{olivine}}{3Mg_2(SiO_4)} + \underset{\text{orthopyroxene}}{Mg_2(Si_2O_6)} + 3H_2O + 2CO_2 + O_2 \rightarrow$$

$$\rightarrow \underset{\text{serpentine}}{Mg_3(Si_2O_5)(OH)_4} + \underset{\text{brucite}}{3Mg(OH)_2} + \underset{\text{magnesite}}{2MgCO_3} + 3SiO_2, \quad (11.37)$$

$$4Mg_2SiO_4 + 4H_2O + 2CO_2 \rightarrow Mg_6(Si_4O_{10})(OH)_8 + 2MgCO_3,$$
olivine serpentine magnesite

(11.38)

$$(Mg,Fe)2(SiO4) + 3H2O \rightarrow Mg3(Si2O5)(OH)4 + SiO2 +$$
olivine serpentine
$$+FeFe2O4 + H2\uparrow,$$
magnesite (11.39)

$$2CaAl_2Si_2O_8 + 4H_2O + 2CO_2 \rightarrow Al_4(Si_4O_{10})(OH)_8 + 2CaCO_3$$
anorthite kaolin (11.40)

The formation of quartz-feldspar vein complexes occurs due to the saturation of solutions with the silicon oxide which is released at hydration of pyroxenes:

$$6MgSiO_3 + 4H_2O \rightarrow Mg_6(Si_4O_{10})(OH)_8 + 2SiO_2.$$
enstatite serpentine (11.41)

At oxidizing the bivalent silicate iron to trivalent state, in the presence of carbon dioxide gas forms abiogenous methane (reaction 10.24') and at oxidizing iron without CO_2, hydrogen is released (see reaction 11.4).

According to A.A. Marakushev [287], at interaction between fayalite and CO_2, water and hydrogen sulfide also form methane and iron sulfides:

$$2Fe_2SiO_4 + 8H_2S + CO_2 = 4FeS_2 + 2SiO_2 + 6H_2O + CH_4\uparrow;$$

(11.42)

$$4Fe_2SiO_4 + 4H_2S + CO_2 = 2FeS_2 + 2Fe_3O_4 + 4SiO_2 + 2H_2O + CH_4\uparrow; \quad (11.43)$$

$$6Fe_2SiO_4 + 2H_2O + CO_2 = 4Fe_3O_4 + 6SiO_2 + CH_4\uparrow. \quad (11.44)$$

The formed methane and hydrogen have abiogenic nature and may mix with hydrocarbons of biogenic origin migrating from subduction or collision zones into the sediment cover of peripheral areas. A strong fractionation of isotope composition of these light, chemically-active elements in a broad spectrum of geological processes results in shifting of their marks both in the direction of "heavying" and "lightening" [308]. This effect may create an illusion of their genetic bimodality.

Formation processes of commercial mineral deposits in fold areas are closely tied with ore components which get in a plate subduction zone and then in a collision zone of mid-oceanic ridges and abyssal plains. Emerged on the ocean floor sulfide ores at high temperature and with availability of sulfuric water fluid are transformed. The copper sulfide (chalcosite) transformation reaction is running with the release of chalcanthite, sulfur dioxide and water:

$$Cu_2S + 6H_2SO_4 \rightarrow 2CuSO_4 + 5SO_2 \uparrow 6H_2O. \quad (11.45)$$

At 650°C dehydration of chalcanthite and its turning into bonattite occurs, the bonattite then decomposes with the formation of the bivalent copper oxide (tenorite) and sulfur bioxide:

$$2CuSO_4 \rightarrow 2CuO+2SO_2\uparrow +O_2\uparrow. \quad (11.46)$$

Lead, copper and zinc sulfides (galena, chalcopyrite and sphalerite) at high temperature of the acidic fluid solution decompose as follows:

$$PbS + 2HCl \rightarrow PbCl_2 + H_2S\uparrow. \quad (11.47)$$

At that, limestone dololmitization occurs under the action of hot solutions containing magnesium sulfate:

$$2CaCO_3 + Mg(SO_4) \rightarrow CaMg(CO_3)_2 + CaSO_4. \quad (11.48)$$

The resulting hydrous magnesium sulfate (kieserite) may then interact with methane forming magnetite, hydrogen sulfide and water

$$MgSO_4 + CH_4 \rightarrow MgCO_3 + H_2S\uparrow + H_2O. \quad (11.49)$$

At a temperature drop, hydrogen sulfide contained in the solution is a very strong and "aggressive" mineralizer (releasing in a reaction plenty of energy). That is why in such cases it again reduces various ore metals (copper, zinc, lead, iron) to sulfides taking them from the solution and also from base and ultra-mafic rock under reaction (11.6).

The lead chloride and chlorides of some other metals in these environments again pass back in sulfides, for instance, $PbCl_2 + H_2S \rightarrow PbS + 2HCl$, thereby forming deposits of polymetallic ores of hydrothermal origin.

Hydrothermal processes in mid-oceanic ridges lead to a removal of large amounts of the alkali earth metals which deposit on the sea-floor as sulfates and carbonates. Getting then in subduction zones, they easily dissolve passing from one state to another and eventually again form sulfates and carbonates which deposit in hydrothermal discharge zones.

For instance, barium carbonate (witherite) may emerge at high temperature by acting on it with a mineralized by a hydrochloric solution:

$$BaCO_3 + 2HCl \rightarrow BaCl_2 + H_2O + CO_2\uparrow. \quad (11.50)$$

Subsequently, at interaction of the dissolved salts, barium sulfate (barite) and sodium chloride (halite) form which then are removed up by hydrothermal solutions and deposited in Earth's crust near-surface zones:

$$BaCl_2 + Na_2SO_4 \rightarrow BaSO_4 + NaCl. \quad (11.51)$$

Calcium sulfate behaves similarly and passes in hydrothermal systems from the no-water form (anhydrite) to dihydrate $CaSO_4(2H_2O)$ (gypsum, selenite).

As a result of a fold system evolution, along with intensive geodynamic processes in its body occur powerful in scale and complex multistep in nature spatial-temporal manifestations of metallogenic events leading to the formation of a unique in its specialization ore area.

Spatial-temporal localization patterns of a whole number of endogenous and exogenous deposits in fold belts are closely tied with geodynamic processes proceeding on the boundaries of lithospheric plates.

Thus, at closing of the Paleo-Urals ocean and obduction of the Uralian island arc over the passive margin of the East-European ancient (Archaean) platform in Late Paleozoic, in the body of the latter had been formed a structure-material ensemble of specific magmatic, metamorphic and sedimentary complexes. Besides, the island arc system overlie multi-kilometer Riphaean-Paleozoic sedimentary sequences which had experienced powerful processes of hydrothermal change. Part of these deposits had been remolten in the subduction zone and invaded upper structural stages as granite intrusions. All these processes had led again and again to a benefication of the Urals belts with ore elements and to the formation of a whole number of rich commercial mineral deposits (Fig. 11.4).

Evolution of the Urals fold system in the Caledonian tectogenesis phase had been accompanied by a multistage and nonuniform convergence and subduction of the ancient East-European platform (EEP) under the active margin of the West Siberian plate (WSP). This resulted in the formation of a complex configuration collision structure during the period of Late Devonian - Early Carboniferous (nearly 360 MYa) in the south through Late Permian – Early Triassic (nearly 265-245 MYa) in the north. The northern edge of the forming fold system had been thrown over the Siberian craton making the Taymyr fold system and Yenisei-Khatanga (Taymyr) foredeep.

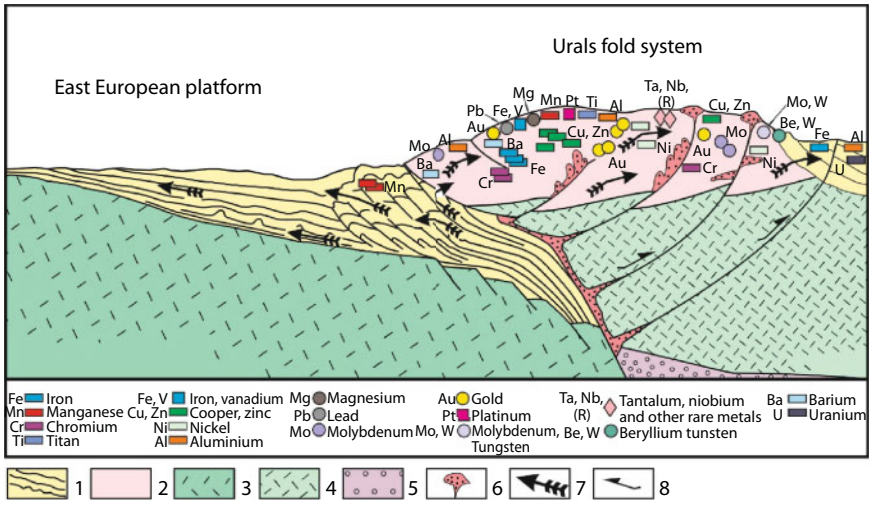

Fig. 11.4 Metallogeny of the Urals fold system. 1. Heterochronic sedimentary cover; 2. Sedimentary-volcanogenic complexes of island arc type; 3. Crystalline basement of the East-European platform; 4. Subcrustal lithosphere of the Urals island arc; 5. Mantle's asthenosphere; 6. Areas of melting deposits, crustal-lithospheric matter and granitoid intrusions; 7. Direction of fluid migration; 8. Vectors of major strike-slips.

Complete closing of the Paleo-Urals ocean had been marked by the evolution of post-collision granites with the age 264 MY (Explanatory…, 1996). As a result, the Urals orogen structure had been formed between the EEP and WSP. It has vari-directional, sometimes arcuate, up to oxygonally oriented fold zones, sometimes cut with transform type faults.

The Urals minerals-raw material potential is characterized by various deposit types regularly positioned in spatial and temporal interval of their formation (Fig. 11.4). The distribution of ore elements in the junction zone of lithospheric plates may be demonstrated by an example of sulfide type deposits' evolution. These deposits are broadly developed in the region.

Thus, the pre-collision evolution stage of the Urals belt had been distinct in the manifestation of intensive hydrothermal, sometimes even skarn processes forming in the sediment cover of the East-European platform (EEP) accumulations of sulfide, copper-skarn, vanadium-iron-copper, skarn-magnesite, copper-porphyry and iron-manganese-lead-zinc ores. At the same time, on the passive EEP margin had been occurring the accumulation of platform clastic-carbonate sequences with stratiform lead-zinc and iron-manganese mineralization [309]. At that stage, the Paleo-Urals ocean closing processes had had the character of reflected tectono-thermal events which, however, had resulted in activization of the region. In Devonian, at the stage of orogenesis, Uralian fold system obducting the passive EEP margin had been characterized by a dominant sulfide metallogenic specialization leading to the formation of copper- and iron-skarn deposits. In Late Devonian – Early Carboniferous, a collision joining of the plate in the Middle and Southern Urals had been generally completed and the process had begun of the entire continental-crustal system cratonzation. This had resulted in the destruction of island arc type sedimentary-volcanogenic structures and in broad occurrence of graywackes and in manifestations of a tonalite-granodiorite magmatism with which are closely tied gold deposits. Early and Middle Carboniferous had been marked by the accumulation of platform type coaliferous and carbonate sequences. With carbonates are closely tied stratiform lead-zinc manifestations and sedimentary-hydrothermal type manganese deposits. Simultaneously with this had been forming iron deposits connected with volcano-plutonic associations of post-orogen stage and sulfide-polymetallic and copper-porphyry ores spatially coinciding with granitoid intrusions [309]. On average, in Late Carboniferous and Permian a relaxation had been observed of the fold system, its isostatic levelling and, as a consequence, invasion of large masses of palingenic-anatectic granites. At the same time, the accumulation had been occurring in sedimentary sequences on the East-European and West-Siberian

platforms of variegated clastic-carbonate deposits with manganese ores, copper sandstones, salts, coaliferous sequences, often uranium containing, fluorite, etc. (Fig. 11.4).

Clear examples of the influence by exogenous factors on the origin of, it would appear, endogenous commercial minerals may be tin-bearing, rare-metal and gold ore deposits in the Verkhoyan-Kolyma fold zone if East Siberia. Indeed, in Early Paleozoic the Kolyma massif had split off the East Siberian platform and the East Siberian paleo-ocean had emerged between them (Fig. 11.5). At that, thick sequences of clastic deposits brought off the Anabar shield's Early Paleozoic sediment cover in the north and off the Aldan shield and Vitim-Patoma highland in the south by paleo rivers Paleo-Vitim, Paleo-Lena, Paleo-Vilyuy and Paleo-Olenek. They had been carried eastward and deposited on the eastern passive margin of the Siberian platform. In these deposits, as near-shore placers, had been gradually accumulated carried off the ancient shields heavy fraction including cassiterite, gold, niobium, tantalum and other rare metal minerals. Over 250–300 MY existence of the East Siberian ocean, on its western margin

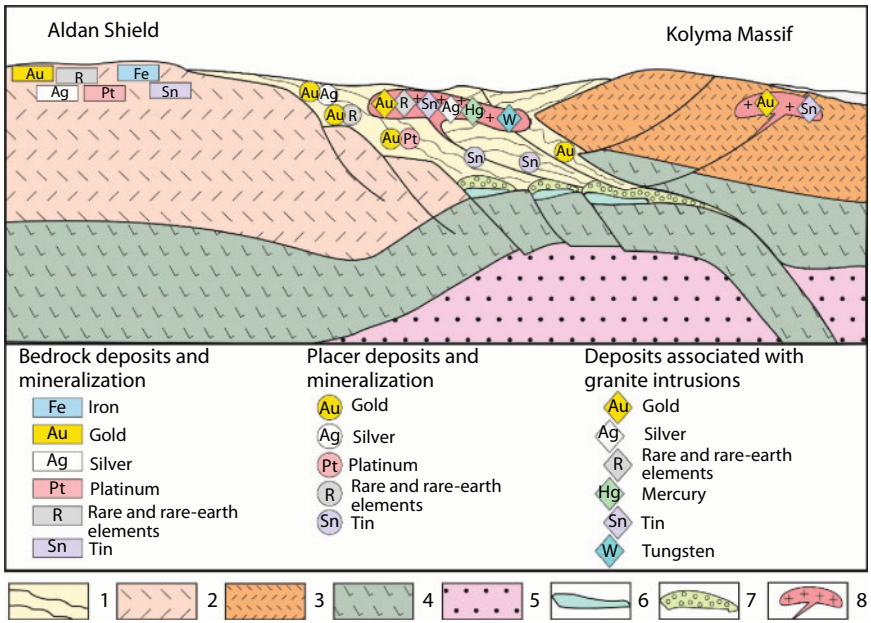

Fig. 11.5 Schematic metallogenic zoning of the east part of the Siberian craton and Verkhoyan-Kolyma fold zone. 1. Sediment cover sequences; 2. Continental crust of the Siberian craton; 3. Volcanogenic-sedimentary complexes of island arc type in the Kolyma accretion massif; 4. Subcrustal lithosphere; 5. Mantle; 6. Base composition magmatism; 7. Deposits' melting and remobilization area; 8. Intrusive complexes of granitoid composition.

(i.e., in the east of the Siberian platform) had accumulated this way at least 12 to 15 km of clastic (including deltaic and channel) deposits beginning from Devonian (although mostly from Carboniferous) through Jurassic.

In mid-Mesozoic, the convergence of Kolyma massif with the Siberian platform had been continuing, the East-Siberian ocean had begun narrowing down. Its closing in the middle of Mesozoic had been accompanied by crushing of the entire accumulated by that time thick continental marginal sedimentary sequences and by their obduction over the Siberian platform. As a result, small accretion terranes of island arc type had been welded by belts of granitoid batholiths and overlain by volcano-plutonic belts.

Under the pressure from the Kolyma massif steamrolling over the lithospheric relic of the East-Siberian paleo-ocean and the margin of the Siberian craton, in the oceanic lithosphere must have emerged crosswise tension fractures. Through them, from the mantle into the lower part of the sedimentary sequences had invaded basalt melts (Fig. 11.5) with density of approximately 2.8 g/cm^3, which is substantially higher than average density of deposits, 2.45–2.7 g/cm^3. For this reason, basalts might have invaded only the lower part of the sedimentary section. Basalt magma temperature at depths about 12–15 km reaches 1,350–1,400°C whereas the melting temperature of water-saturated deposits at these depths does not exceed 700–750°C. It follows herefrom that the deposits of the subject sequences on contact with hot basalt magmas must have melted. As a result of thermal transformations, their density and viscosity had been substantially lowering, and further on they had been invading the upper structural stages as granitoid intrusions and diapirs. Average composition of these granitoids varies from granite-porphyry to liparite and corresponds with average composition of the Verkhoyan-Kolyma fold zone's sedimentary rocks. Hydrothermal processes accompanying magmatism had converted some ore elements in pneumatolith-hydrothermal solutions which had been rising together with granite intrusions. As a result, a characteristic ore specialization had emerged of granitoids and their corresponding hydrothermal manifestations. In the north of the Verkhoyan-Kolyma fold zone (where to deposits from the Anabar shield mostly had been carried) is common the tin and tantalum-niobium mineralization. In the southeast, in the area where deposits from the Aldan shield and Vitim-Patoma highlands had been brought in, predominantly gold manifestations are observed.

The gold ore mineralization within the Aldan-Stanovoy shield of Archaean and Early Proterozoic growth is represented by numerous bedrock and placer gold deposits, some of them with platinum.

Mesozoic gold mineralization is associated mostly with quartz vein hydrothermalites, a notable role among them belongs to carbonates

and feldspars. The gold-rare-metal-quartz, gold-silver and gold-copper-molybdenum type mineralization is sometimes encountered [295]. In the southeastern margin of the Siberian craton platform cover is observed a spatial-temporal conjugation of gold mineralization with volcano-plutonic activity polycyclically manifested in Jurassic-Cretaceous time. In Yana-Kolyma fold area, i.e., in the rear zone of the Verkhoyan-Kolyma fold system (Fig. 11.5), is developed gold- (sulfide-, carbonate-)-quartz, more rarely gold-rare metal-quartz mineralization with bismuth and some other mineralization [295].

Metallogenic evolution of the Verkhoyan-Kolyma fold system enables us to identify and describe another very powerful natural process of Earth's crust conveyor benefication with ore elements. Within the framework of this process, magmatic and metamorphic deposits of commercial minerals formed at the first stage are destroyed and pass in the sedimentary deposits where they form placers. Then, after the emergence of specific geodynamic prerequisites, they enter the composition of volcano-plutonic associations and form at first sight typical magmatogene ores. A cyclical benefication of Earth's crust by a similar way might have shown up numerously in Earth's history and might have resulted in the benefication of ore deposits from ancient complexes to young ones.

With the deposit which had experienced similar cyclical transformations may be attributed magmatic and metasomatic Urals type iron ore complexes of Kochkanar titan-magnesite deposits, mounts Magnitnaya and Blagodat. The emergence of these iron ore deposits had been associated with closing of the Paleo-Urals ocean, obduction of the Uralian island arc over the east margin of the Russian platform and pulling Riphaean and older thick sedimentary sequences of Taratash type iron ore complexes in the subduction zone.

Something similar had been going on also with the formation process of gas-condensate accumulations' on the Barents Sea shelf in the Russian Arctic. The Barents Sea lithospheric plate's basement had been formed nearly 1.55 – 1.3 BYa [127, 310]. It is composed of polyfold and metamorphosed gneisses and crystalline schists, marbles, dolomites and conglomerates in the environments of epidote-amphibolite metamorphism facies. Later, continental crust in the region had experienced the process of denudation and peneplanation, and beginning in Cambrian and Silurian, the platform cover had begun accumulating on its surface. Currently, the Barents Sea shelf is a large petroleum basin where, according to a whole number of scientists [311, 312], most likely oil source rock complexes of the primary migration hydrocarbons are Late Devonian – Early Permian sediments. The manifestation of Late Permian -Early Triassic (257-228 MYa)

and Late Jurassic - Early Cretaceous (159-131 MYa) syn- and post-collision magmatism in the region had resulted in invasion of oil source rock sequences by huge masses of basaltoids forming layered bodies (sills) in the lower part of the sediment cover [313]. E.V. Shipilov [314] notes that the formation of the Shtokman and some other gas-condensate fields had been going practically simultaneously with intrusive magmatic activity of a certain age. At this, gas-condensate accumulations belong with high-temperature secondary- migratory formations which migrate up the section as a result of superposed tectono-thermal processes. It so happens that in the nature, under certain conditions, may function a huge in scale and manifestation capacity process of oil thermal separation and its partition into gas-condensates and bitumens.

Similar but slightly different processes must have been occurring in the sediment cover of an ancient Siberian platform when water-saturated oil source rocks of the Riphaean sedimentary sequences had been overlaid with trap magmatism's hot melts in Triassic which also had to result in the formation and conservation of gas-condensate accumulations.

All aforementioned processes had been occurring along with those processes that had accompanied diamond formation. That is exactly why a study of formation and transformation processes of structural-material complexes in compression geodynamic environments (subduction and collision) is highly important for understanding Earth's crust ore genesis processes in general and diamond formation in particular. Most endogenous deposits are closely tied with the magmatism and hydrothermal activity processes and as a rule had been formed on lithospheric plate margins. At that, different types of plate boundaries correspond with a different composition of magmatites and different ore complexes, which are regularly positioned in space relative to them. Geodynamic evolution of all Earth's shells had been doing so that the spatial-temporal parameters of their interaction in matter are a complex and multistep functioning mechanism of a number of global natural "benefication factories".

The described ore genesis mechanisms in plate subduction zones touch upon only a part of natural benefication processes of Earth's crust commercial mineral deposits. Along with ore genesis issues in plate subduction zones we were able to approach a solution of the problem of hydrocarbons' abiogenic genesis and consider at the heels of [273, 315] that their overwhelming majority have nothing to do with the mantle sources. According to our concept, the entire abiogenic methane and hydrogen form at hydration of base and ultra-mafic composition rocks of the oceanic lithosphere in crustal environments of riftogenesis and subduction zones.

As we have already shown, the reprocessing mechanism of the oceanic crust in the continental one has a clearly expressed conveyor nature, i.e., it is accumulative and very powerful. For instance, only in the time interval of active lithospheric plate tectonics (about 2.6 BY), the total mass of water-fluid flows in subduction zones had exceeded the mass of the entire Earth's hydrosphere 8–10-fold and the mass of oceans and seas together, 13–16-fold! This theoretical estimate is especially important as it shows that the real fluid-water flows in plate subduction zones are million-fold more powerful than juvenile ones.

Nevertheless, benefication of the continental crust with ore elements occurring in subduction zones results in more or less uniform increase of their content along the lithospheric plate subduction zones. Of course, in this case as well commercial accumulations of some commercial mineral types, for instance, sulfide ores might have formed. This is especially strongly manifested in long-functioning plate subduction zones as therein occurs a tectonic erosion of the obducted plate frontal areas and a repeat processing (recycling) of the crustal rocks and deposits overlying the subducted plate. That had likely been the formation way of unique copper-molybdenum-porphyry ores in the South American Andes. Based on paleo-geodynamic reconstructions, the Pacific and Pre-Pacific oceanic crust under them had been subducting almost without interruptions for at least 1.5 BY.

Beside described above two mechanisms, there is also a third mechanism of benefication the deposits of endogenous commercial minerals with ore elements. It is a fact that weathering and deposit accumulation exogenous processes, often passing with active participation of live organisms and plants extremely strongly affect redistribution of elements within Earth's crust. Sedimentogenesis is usually accompanied by intensive differentiation of the matter. Clear examples are sedimentary sequences of phosphorites, carbonates, sandy-clayey and other differentiated deposits possessing a specific, intrinsic only to them peculiar mineralization. For instance, the Russian platform clayey deposits, compared with the mantle composition, contain on average 11-fold tin, 20-fold lead, 200–250-fold potassium, a few hundred-fold rare earth elements, 500–700-fold rubidium, up to 1,500-fold barium, 3,000–3,500-fold uranium. Wherever sandy-clayey sediments had been deposited in stagnant basins infected with hydrogen sulfide (such environments had been especially common in Precambrian), in sedimentary sequences might have accumulated iron, copper, zinc, lead and molybdenum sulfides and in some cases, uranium oxides, tungsten hydroxides and gold. The same goes for the other deposits. Carbonates, for instance, contain a few hundred-fold strontium compared to the mantle, sodium, potassium, calcium, sulfur, chlorine and

fluorine concentrate in evaporites. It is a fact that living organisms accumulate in themselves many trace elements including uranium and rare earth elements (lanthanum, cerium, neodymium, etc.). That is why their elevated content in the phosphorites is always observed much exceeding their concentrations in the mantle (for uranium, 20–25 thousand-fold, for rare earth element, 500–1,000-fold).

As noted above, the mountain systems destruction had led to runoff by rivers and ephemeral streams of clastic deposits on the continental margins and their deposition on the continental slopes. At their entering plate subduction or collision zones, the entire spectrum of crustal igneous rocks (granites to sienites and alkali-ultra-mafic rocks) with their peculiar mineralization might have been melted out from them. That makes understandable often observed motley character in the territorial positions of commercial mineral deposits.

Due to a renewed crustal rock destruction and the repetition of sedimentogenesis process, the fourth stage of the continental crust benefication with ore elements sometimes occurs. For this reason, younger ore deposits of such type may at the same time turn out richer as their ore matter for the time of Earth's geological evolution might have gone through a greater number of recycling cycles. An example is tin whose concentration in younger deposits is usually higher than in ancient ones. For instance, total tin content in the Mesozoic deposits more than by two orders of the magnitude is exceeding its content in Archaean ore manifestations [303]. A similar situation is observed with molybdenum: as a result of magmatic processing of sedimentary sequences, with time the concentration in young deposits of molybdenum and tungsten had been continuously growing [304]. It follows herefrom that, it would appear, clearly "endogenous" economic minerals in actuality had made it through the stage of the recycling, i.e., benefication due to the destruction of crustal rocks and subsequent sedimentogenesis under clearly exogenous environment.

Another no less demonstrative example of a substantial influence by exogenous factors on the formation of commercial mineral deposits is hydrothermal commercial mineral deposits. As water content in the mantle is negligibly low, all without exception hydrothermal deposits (regardless of their type) had been formed either at the expense of mobilizing surface and ground water bathing hot intrusive bodies or at the expense of releasing by a cooling magma of water dissolved in it. However, even in the latter case the water-saturated magma in the process of its formation had been capturing water only from water-saturated deposits or from the hydrosphere.

11.3 Metallogeny of Early Stage in Earth Evolution and the Nature of a Unique Early Proterozoic Ore Formation Epoch

Along with Earth's geological evolution, naturally, had been changing formation environments and regimes of Earth's crust and commercial minerals concentrated in it. As already mentioned, the evolution processes on Earth are irreversible. That is why, when exploring major evolution patterns in the formation of commercial minerals in distant past, it is necessary to use very cautiously the concept of uniformitarianism (the present is the key to the past) continuously introducing evolution corrections in it. For instance, it is now becoming clear that in Archaean, plate subduction zones had not existed yet (see. Fig. 8.5). That is why the continental crust formation regimes, and together with them of most types of endogenous commercial minerals, had been then totally different and absolutely unlike the present-day environments of their formation. With this in mind, it is possible to review an issue of commercial mineral evolution in time. In its foundation is a concept of the main energy process controlling Earth evolution as a whole is the process of formation and growth of Earth's core.

As already mentioned in Chapter 4, according to the present-day concept based on the ideas of O.Yu. Schmidt [68, 71] further developed by V.S. Safronov [61], Earth, same as other Solar system's planets, had formed due to accretion of a "cold" gas-dust protoplanetary cloud. That is why the young Earth right after its emergence had been a "cold", tectonically passive planet uniform in composition and structure. As a consequence, all ore and other elements had been more or less uniformly distributed in the volume of just emerged Earth, with their own "Clarke" contents and had not formed accumulations which might have been attributed with the commercial mineral deposits. It follows herefrom that commercial mineral deposits in young Earth might not have existed at all.

It had been totally different with the benefication processes of Earth's crust with ore elements in Archaean. At the boundary 4 BYa, an intensive magmatic activity had begun which had started up the commercial mineral accumulation formation mechanism on Earth's surface.

You will recall that in Early and Middle Archaean, at the separation of the core matter, together with iron and its oxides most siderophile and chalcophile elements had been passing in the ring-like layer of melts from Earth's primordial matter. For this reason, the convecting mantle

above the immersing ring-like layer of Earth's matter zonal differentiation in Early and partially in Middle Archaean had been impoverished in iron and other siderophile elements (see Figs. 5.15 and 5.16). That is exactly why the Early Archaean continental shields and greenstone belts in them have relatively low metallogenic potential [235, 316] and relatively modest metallogeny, with not too large iron and other commercial mineral reserves.

The process of moving high-density oxide-iron melts toward Earth's center and displacement the primordial heart (Fig. 5.1-*d* and -*e*) must have been accompanied by squeezing out ore element rich primordial Earth's matter from its central areas (from the "heart" of young Earth) into the upper mantle. As a result, the Late Archaean oceanic plates had started forming at the expense of the mantle matter substantially enriched in ore elements. That is why greenstone belts in Late Archaean had turned ore-bearing, saturated by many siderophile and chalcophile elements including gold, copper, nickel, platinum, platinoids and polymetals. At remelting of greenstone rocks in the lower parts of Archaean crust (see Fig. 8.5) even the Late Archaean granitoids had been becoming ore-bearing.

The processes of a final Earth's heart destruction (it had been composed of primordial matter of planetesimals) had increased at the very end of Archaean and in Early Proterozoic (see Figs. 5.1-*d*,-*e*). A result had been a very substantial benefication of the upper mantle with ore elements. At that, the upper mantle composition had radically changed. As we already mentioned earlier, this had been connected with the addition then in the convecting mantle of the former Earth's heart matter with primordial concentrations in it of iron (nearly 13–14%), its oxides (nearly 23–24%) as well as siderophile elements, sulfides of chalcophile metals and other ore elements including platinoids. As a result, at the end Archaean and especially in Early Proterozoic most favorable environments had emerged for the formation of unique deposits of endogenous ore commercial minerals, and the very epoch of Early Proterozoic had become most outstanding period of endogenous ore formation.

A direct evidence of these events is differentiated base and ultra-mafic rock intrusions that had invaded in the middle of Early Proterozoic (nearly 2.4–2.3 BYa) many ancient shields at the very first impulses of the split of Archaean supercontinent Monogea. Most typical and classical formation of this type is the Great Dyke intrusion in Zimbabwe which is a stratified complex of the Early Proterozoic mantle matter. Chromite deposits in the Great Dyke are common in its lower levels and are associated with dunites and harzburgites whereas platinum in the

form of sperrylite ($PtAs_2$) and platinoids are encountered in sulfide layers between ultra-mafic rocks and gabbro-norites.

High concentrations in Early Proterozoic ultra-mafic and gabbro-norite intrusions of Bushveld stratified magmatic massif (RSA) reach iron, titanium, chromium and vanadium whereas in sheet-like deposits of copper-nickel sulfides, platinoids reach commercial concentrations. The Bushveld pluton had invaded a thick sedimentary-volcanogenic sequence of the Early Proterozoic Transvaal system. As a result, the upper (gabbro-norite) portion of the mantle intrusion is contacting the crustal granites formed at the expense of remelting the pluton enclosing sedimentary-volcanogenic rocks. That is why with Bushveld granites is also associated tin and fluorite lithophile (hydrothermal) mineralization.

The other examples of this type mantle intrusions may be Sudbury norite invasions of Early Proterozoic Huron sedimentary-volcanogenic sequences in Canada (sulfides of copper, cobalt, nickel, platinum), Stillwater deposit in Canada (chromium, titaniferous magnesite, platinoids) and Kambalda deposit in Australia (nickel, copper, platinoids). In Russia, this is the Burakov intrusion in southeastern Baltic shield with the chromite, nickel, vanadium, platinum and possibly gold metallogeny. Similar type formations are apparently gabbro-norite intrusive complexes of Pechenga and Monchegorsk (Baltic shield) with their sulfide copper-nickel and cobalt mineralization and also the Pan intrusion on the Kola peninsula and magmatic formations of the Olonga group in Karelia with platinum mineralization.

Be it noted that intrusive formations of such type with high concentrations of ore elements had never again emerged either before Early Proterozoic or after. This is an indication in favor of the subject convecting mantle benefication model at the boundary Archaean/Proterozoic with the primordial Earth's matter by risen from Earth central areas in the core formation process at the end Archaean as shown in Fig. 5.1-*e*.

Beside intrusive ore-bearing rocks, quite typical of Early Proterozoic are sedimentary ore deposits. A classic example are sedimentary iron ores of well-known jaspilite formation and ore-bearing of the sedimentary sequences in Witwatersrand, RSA (see below). Thus, in Fig. 11.6 is shown the distribution in time of gold reserves in the entire Earth's geological history [293]. As this Figure shows, in Early Proterozoic had been indeed observed a drastic splash up of the amount of deposited gold, at that, its significant part is found exactly in deposits of a Witwatersrand type.

Conspicuous is the fact of a drastic activation in Phanerozoic of chalcophile elements (including gold) recycling processes. This had been

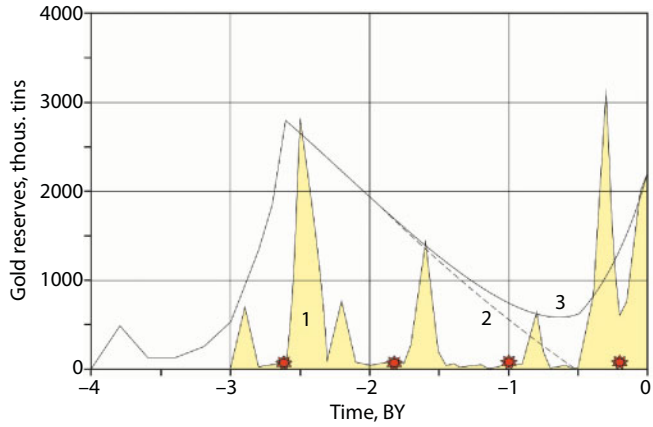

Fig. 11.6 Gold reserves distribution in Earth's geological history, after [293]. 1. Gold reserves; 2. Relative concentration of metallic iron in the mantle imaged in Fig. 5.16; 3. The curve accounting for gold recycling in young formations; the stars indicate supercontinent formation moments.

associated with large mobility of chalcophile elements and their lower resilience to weathering processes. That is why chalcophile elements had been gradually removed from ancient rocks and redeposited in younger sediments. Should have such deposits gotten in a plate subduction zone or contacted hot mantle melts, their remelting would have occurred and the formation on new (young) magmatic deposits. At that, the ore matter in them had remained ancient. Clear examples of such deposits are tin, rare metal and gold ore deposits in Verkhoyan-Kolyma fold zone found in Mesozoic age rocks but ajoint with Precambrian formations described in detail above. However, the ore matter in them is ancient and derived from the matter of Archaean and Early Proterozoic age redeposited in Paleozoic and Mesozoic in near-shore deposits of the East Siberian paleo-ocean.

After the formation in Earth of a high-density oxide-iron core, its subsequent growth had been going already under a more quiescent barodiffusion mechanism. In this connection, in Proterozoic Earth's tectonic activity had notably declined, the chemical-density convection had emerged, the spreading rate of the ocean floor had decreased, thicker and "heavy" lithospheric plates had emerged, oceanic plate subduction zones had appeared and the mechanism of lithospheric plate tectonics had begun operating.

The chemical-density convection had been quite unstable and changing its structure. This had resulted in periodical (over time intervals on

the order of 800 MY) emergence in Earth's mantle of single-cell convective structures with one powerful ascending and one descending flows (see Chapter 7). At that, all existing continents had been drifting to the center of such descending mantle flows forming above them giant supercontinents similar to Wegenerian Pangea. Overall, four such supercontinents had existed in Earth's geological history (see Figs. 9.2, 9.3, 9.4 and 9.8): Monogea (2.6 BYa), Stille's Megagea (1.8), Mesogea or Rodinia (1.0) that had later disintegrated (in 120–200 MY) into two large continents, Laurasia and Gondwana, and Wegenerian Pangea (nearly 220 MYa).

Sequential stages of supercontinent formation and destruction had predetermined manifestations of various metallogenic environments on Earth. Thus, at the moments of supercontinent formation, ophiolite covers had usually emerged with typical chromite type deposits of the Kempirsay massif in South Urals and continental collision environments with the melt-out of huge granite masses. At that, huge numbers of hydrothermal and pegmatite deposits and polymetallic and sulfide ore deposits had also been formed (Fig. 11.4).

The lifetime of supercontinents as single continents usually had not exceeded 100–120 MY which is explained by specifics of the chemical-density convection in the mantle. That is why the supercontinent compression had been rapidly replaced by the environments of their expansion with manifestations of younger alkali-ultra-mafic, sienite, carbonatite and diamond-bearing kimberlite magmatism. Most kimberlite diatremes in the world are found exactly in association with periods of such initial supercontinent expansion. Their further expansion and split had resulted in vast invasions in the continental crust of trap basalts and as a consequence, in the formation of continental rifts with their bimodal volcanism. Usually this process had been ending in the split of supercontinents into a number of smaller and centrifugally drifting continents with the formation between them of the Atlantic type young oceans.

In this connection, it is necessary to take into consideration that the open faults – depth magma release channels might have sometimes appeared even at the supercontinent formation stage in generally compression regime of the continental lithosphere, especially if one of the colliding lithospheric plates had wedge-like outlines as, for instance, at the consolidation of Laurasia and closing of the North Paleo-Atlantic (Iapetus ocean) in Devonian (see Fig. 16.7 and 16.8). Perhaps, exactly through such faults in Devonian and Carboniferous Earth's crust had been invaded with alkali-ultra-mafic intrusions of the Kola Peninsula and diamond-bearing kimberlites in Archangelsk Province.

11.4 The Influence of the Ocean and of Earth Climates on the Formation of Sedimentary Commercial Minerals in Early Proterozoic, the Major Iron Ore Accumulation Epoch

A large influence of the atmosphere and hydrosphere on the evolution of metallogenic environments on Earth's surface, including in Early Precambrian, was known for a long time ([317, 318]; Strakhov, 1963, 1973; [319], etc.). However, only in recent years it was possible to evaluate a grand scale of these processes and to uncover the nature of their influence on endogenous and exogenous Earth's metallogeny.

As was shown in Chapter 10, carbon dioxide gas partial pressure had reached in Archaean 4–5 atm. (see Fig. 10.12). It had been caused by a small water amount in Archaean oceans, and that is why at that time the mass of bonded CO_2 had been substantially smaller than the mass of carbon dioxide gas degassed from the mantle (see Fig. 10.11). It follows herefrom that in Archaean the major mass of carbon dioxide gas degassed from the mantle must have been in the atmosphere and dissolved in the ocean water. That is why it is important to keep in mind that the Archaean ocean had been quite heated ([112], Chapter 14). Due to a high partial pressure of carbon dioxide gas in the Archaean atmosphere reaching 5 atm. (see Fig. 10.12), its water had been saturated with carbonic acid H_2CO_3 had had the acid reaction (pH ≈ 5–6) [261]. Hot acidic water is quite an aggressive reagent capable of dissolving many ore elements and compounds. Therefore, it may be expected that the Archaean ocean water had been saturated with many ore components including gold, uranium, sulfides of iron, copper, lead, zinc, manganese oxides, bivalent iron oxides, etc. It is possible that all these compounds had been coming in the hydrosphere at hydration of the oceanic crust basalts and at interaction of hot and acidic rainwater with rocks of the greenstone belts and continental granitoids.

After a substantial climate cooling and pressure decline of the Archaean carbon dioxide atmosphere in Early Proterozoic (se Fig. 10.23), the oceanic water had become neutral (pH ≈ 7–8) and ore elements dissolved in them had precipitated out. Exactly this is way, in our view, at the very end of Archaean (nearly 2.7–2.6 BYa) and in Early Proterozoic (nearly 2.5–2.3 BYa) largest stratiform accumulations of gold, uranium, copper, polymetals, cobalt, iron sulfides and carbonates, manganese oxides and other commercial minerals had formed (see Fig. 11.7). An example of such deposits are deposits in Witwatersrand whose mineralization in greenstone rocks had manifested itself already nearly 3 BYa and ore-bearing

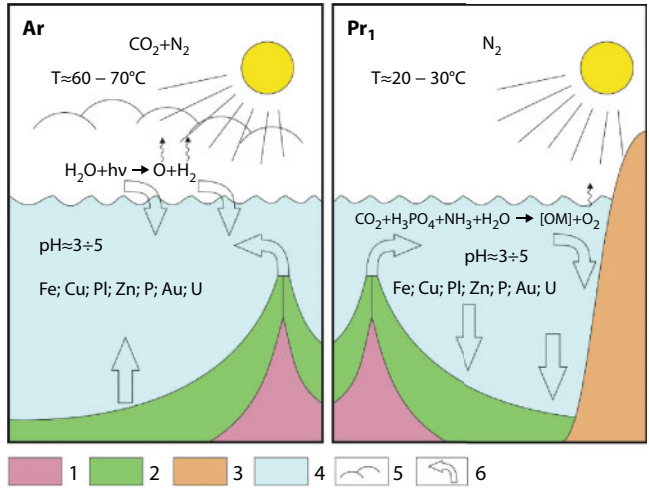

Fig. 11.7 Formation of unique Early Proterozoic ore-bearing stratiform deposits.
1. Mantle astenosphere; 2. Unsubdivided oceanic lithosphere; 3. Continental lithosphere; 4. World ocean water layer; 5. Intense cloud cover caused by the greenhouse effect; 6. Direction of ore element supply in the oceans and their deposition in Early Proterozoic; [OM] is organic matter.

sedimentary conglomerates containing gold and uranium had appeared beginning only 2.5 BYa. At the same time had been deposited Early Proterozoic gold bearing conglomerates on other ancient platforms, copper sandstones of the Katanga-Rodesian copper-bearing belts in Africa, Udokan copper sandstones in Siberia, etc.

In the context of the subject concept, the origin of unique iron ore formations of end Archaean and Early Proterozoic are easily explainable. Iron concentration in the convecting mantle during most of Archaean had been relatively low (see Fig. 5.16) as at that time it almost in toto had been passing in Earth's matter differentiation zone underlying the convecting mantle (see Fig. 5.1). However, already by the end Archean the primordial matter with high concentrations of iron and its oxides squeezed out of Earth's central areas had started arriving in the convecting mantle (see Fig. 5.1-*d* and -*e*). Our estimates are that at the end Archaean and in the beginning of Early Proterozoic, average concentration of metallic iron in the mantle might have reached 5.5% and of the bivalent iron, 15%. In oceanic rift zones, the metallic iron had been rising to Earth's surface and making contact with ocean water. There, the hot iron had been oxidized in an anoxic medium at the expense of water dissociation and further on had aggregated with carbon dioxide gas forming iron bicarbonate well soluble in water:

$$4Fe + 2H_2O + CO_2 \rightarrow 4FeO + CH_4 + 41.8\,\text{kcal/mole}, \quad (11.52)$$

$$FeO + 2CO_2 + 2H_2O \rightarrow Fe(HCO_3)_2. \quad (11.52')$$

In this form iron apparently had been spread all over the ocean, whereas in near-surface environments, due to cyanobacteria and microalgae life activity the bivalent iron had been oxidized to trivalent state and precipitated:

$$2Fe(HCO_3)_2 + O \rightarrow Fe_2O_3 + 2H_2O + 4CO_2. \quad (11.53)$$

At that, as a result of iron-reducing bacteria metabolism a new restoration of trivalent iron might have occurred but now only to stoichiometry of magnesite [320]. Simultaneously with iron, silica had also been withdrawn from rift zones. It had been released, for instance, at pyroxene hydration according to a reaction (11.3). This makes understandable the paragenesis of iron oxides with silica in jaspilites from Precambrian iron ore formations (see Fig. 11.8).

Obviously, mass removal of iron and other metals from the mantle in the hydrosphere might have occurred only when in the mantle matter had been contained a noticeable amount of these metals and when the oceanic surface had overlain average level of rift zones in the crests of mid-oceanic ridges. It is important that only the combination of these two factors might have assured iron removal from the mantle into the hydrosphere and further on in Earth's sediment cover. Besides, the oceanic crust composition had been of great significance. Thus, the iron content in the Precambrian basalt crust had been substantially lower (approximately 10 times lower) than in serpentinites emerged at the hydration of the mantle matter restite areas. In consideration of all these factors it was possible to estimate relative rate of ore formations accumulation in Precambrian on condition that these formations had contained on average about 50% iron and from the oceanic crust rocks had also been extracted only 50% of iron.

Beside the described mechanism of iron ore formations emerging in Early Precambrian at the expense of iron removal from rift zones, early in Archaean might have functioned a different mechanism. Indeed, as already mentioned, Earth's crust formation in Early Archaean had been occurring only within a relatively narrow ring equatorial belt, whereas the rest of its surface still had been composed of primordial Earth's matter (see Fig. 8.4) containing about 13% metallic iron and nearly 23% of

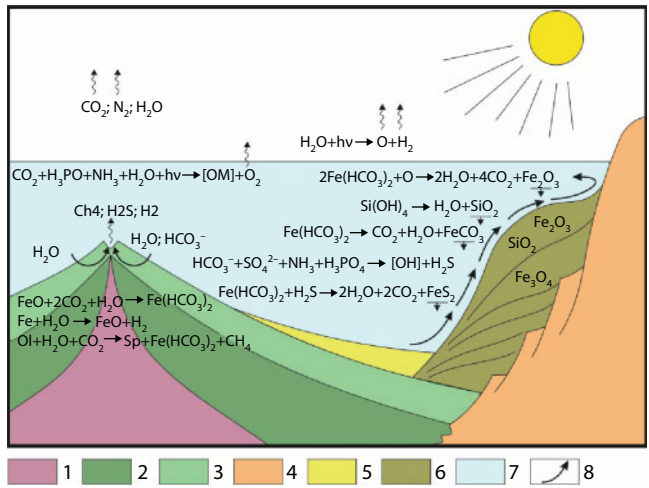

Fig. 11.8 Geochemistry of iron transfer processes from the mantle into rift zones and oceans. Iron ore deposit formation environment on the oceanic continental margins in Early Proterozoic. 1. Mantle astenosphere; 2. Oceanic lithosphere; 3. Basalt layer of the oceanic crust; 4. Continental lithosphere; 5. Pelagic deposits of oceanic abyssal plains; 6. Sedimentary accretion prism of the continental slope and foot; 7. World ocean water layer; 8. Cold water movement direction in upwelling zones and water circulation direction in the mid-oceanic ridge rift zone; [OM] is organic matter, Ol is olivine, Sp is serpentine.

its bivalent oxide (silicate iron). After Earth degassing start and emerging of a carbon dioxide atmosphere, iron from the surface layers of these primordial areas had begun being removed by acid rain water into young marine basins and deposited there forming Early Archaean iron ore formations.

A tie between the iron ore formations accumulation, the biosphere evolution and generation of abiogenous naftides, in particular, methane was described by E.M. Galimov [52]. Besides, it is noted in the same publication that the oceanic water in Archaean, compared with the present-day ocean, had been substantially impoverished in ^{18}O isotope. In our concept, isotope ^{18}O had been mostly bonded with iron already in the mantle environment at passing of water molecules through the molten iron zone (see Fig. 5.1-*b* and -*c*) under the following reaction:

$$Fe + H_2O \rightarrow FeO + H_2. \qquad (11.54)$$

In the estimates described here it was also assumed that iron removal from the oceanic crust into oceanic water had been proportionate both

with the water content in serpentinites m_{sp}^{w} (nearly 11%) and basalts m_{bs}^{w} (nearly 2.5%), and with average buildup rate of the oceanic lithospheric plates area $u_{oc} = k \cdot \dot{Q}_{\mathrm{m}}^{2} / S_{okk}$, where the heat flow $\dot{Q}_{m}$ defines the characteristic of Earth's tectonic activity imaged in Fig. 6.17, and S_{occ} is the oceanic crust area (Fig. 8.4)

Taking this into account, relative iron ore accumulation rate in Precambrian may be described by the following equation:

$$\dot{m}\left(Fe\right)_{s} \approx C\left(Fe\right)_{m} \cdot \left|\delta h\right| \cdot \left[m_{sp}^{w} + m_{bs}^{w}\right] \cdot u_{oc} \qquad (11.55)$$

where the delta-function $|\delta h| = 1$ at $\delta h_{\text{ок}} > 0$, i.e., when the ocean surface overlies the crests of mid-oceanic ridges and $|\delta h| = 0$ при $\delta h_{\text{ок}} \leq 0$, i.e., when the ocean surface is below average crest levels of these ridges or exactly coincides with it. The estimate results of the iron removal rate from the mantle into the sediment cover according to Eq. (11.55) in units of 10^9 t/year are displayed in Fig. 11.9:

As the diagrams indicate, in Precambrian, four or five periods of mass iron ore deposits accumulation might have occurred. The deposition of the earliest iron ores had been going nearly 3.8 BYa (the Isua formation in West Greenland). The second epoch of iron accumulation had been Late Archaean. At that time had been deposited sedimentary-volcanogenic iron ore sequences of the Keewatin type (Canada) and in Russia, Kostamukshi ores and of other areas in Karelia and Kola Peninsula, iron ore complexes

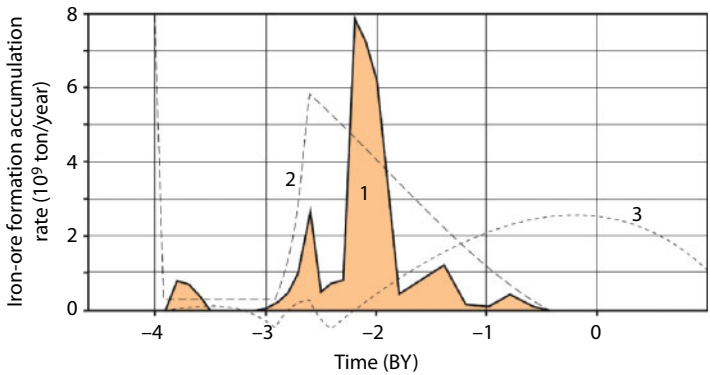

Fig. 11.9 Theoretical estimate of Precambrian iron ore formation accumulation rate: *1.* Total iron ore deposition rate, 10^9 t/year: *2.* Metallic iron concentration in the convecting mantle, % (see Fig. 5.16); *3.* Ocean surface position relative average stand level of mid-oceanic ridge crests, km (see Fig. 10.6).

Taratash in the Urals and Staro-Oskol series in the Voronezh crystalline massif.

However, most outstanding period of the iron ore accumulation had been undoubtedly the epoch at the end Early Proterozoic, 2.2 to 2.0–1.8 BYa. The iron ore deposits of this age are known practically on all continents and many of them had been almost homochronous. With them belong unique jaspilite deposits of Krivoy Rog in the Ukraine, Kursk Magnetic Anomaly in Russia, Karsakpay in Kazakhstan, Hamersley in West Australia, deposits in the area of Lake Superior in the USA and Canada, in Guyana (South America) and in other regions. Conspicuous is the fact that the silica saturated ferruginous deposits from which the jaspilites had later formed might have been deposited only in Earth's high latitude boreal and polar zones. Perhaps it had happened because in Early Proterozoic, same as in the present time, in Earth's tropical belt mostly would have to be deposited carbonate rich deposits then having served the basis for the formation of siderite iron ore. However, the siderites, same as other carbonates, are less resistant to weathering and redeposition processes. That is perhaps a reason why there are much less ancient siderite iron ores than jaspilite ones.

In the second half of Early Proterozoic taking just 5–7% of the total time of Earth's geological evolution had formed at least 70–75% of world iron ore reserves. Our estimates are that at the emergence time of Early Proterozoic iron ore formations, the iron deposition rate had reached 3.3 billion tons a year which is close to earlier estimates of $(1–3)\cdot10^9$ y/year [321]. The total of the ferruginous formations so deposited in Precambrian must have been nearly $3.3\cdot10^{18}$ t which exceeds by many orders of the magnitude the identified iron ore resources (nearly $3\cdot10^{12}$ t after N.A. Bykhover [322]) and more than 30 times of the amount of iron oxides in sedimentary rocks on the continents (nearly $0.1\cdot10^{18}$ t after A.B. Ronov and A.A. Yaroshevsky [73]). Possibly, somewhat more iron is in metasedimentary rocks and "granite" layer of the continental crust. This indicates that most of the sedimentary iron already in Precambrian had immersed again in the mantle through ancient subduction zones.

A characteristic feature of this unique iron accumulation epoch is that its beginning had been practically homochronous on all continents (about 2.2 BYa). This is understandable under our model (the common cause) as exactly at that time the oceanic crust had been completely "sated" with water after which the ocean surface had risen over the crests of mid-oceanic ridges (curve *3* in Fig. 10.6). At that, soluble iron hydroxides from the rift zones had begun coming into the ocean as shown in Fig. 11.9.

By the end Early Proterozoic (about 1.8 BYa) the mass accumulation of sedimentary iron ores had stopped almost as sharply as it had begun.

Most likely that had been associated with the fact that by the time 1.8 BYa the ocean level had already risen over the crests of mid- oceanic ridges by approximately 400 m, i.e., by the height exceeding thickness of the ocean's active layer. The ocean in Middle Proterozoic and Riphaean, most likely, had been displaying a stable stratification with the deep-water stagnation which is supported, in particular, by a broad development at that time of black shales. As a result, coming from the rift zones hydroxides of bivalent iron had been getting only in stagnant deep water and might not have oxidized there to the insoluble state whereas iron ore formations of that age might have been deposited only in zones of oceanic upwelling.

As already mentioned in Chapter 9, in Early Riphaean nearly 1.6–1.4 BYa, a split of Stille's supercontinent Megagea had been going on. At that time might have been observed one smaller splash up of the iron ore accumulation. The cause had been the emergence on the territory of the former supercontinent of a large number of riftogenic structures overgrowing then in relatively shallow-water intercontinental oceans. Shallow-water nature of young oceans had been due to the split of Megagea developing above the emerging under this supercontinent powerful ascending convection flow (see Fig. 9.9). A similar geodynamic environment is presently observed in the North Atlantic where the ocean floor is even rising on the surface (Iceland).

Due to the shallow-water nature of Early Riphaean intercontinental oceans, the metallic iron brought in the oceanic rift zones after hydration had been getting in the ocean's active layer and then spread over its entire aquatorium. By that time about 2–2.5% of it had remained in the mantle (see Fig. 5.16), After oxidizing in well aerated water of continental margins it had been precipitating, gradually forming iron ore deposits there. However, such situation might have been preserved for a relatively short time (1.6 through 1.4 BYa), i.e., only until such time when in the place of a split Megagea continents had emerged a descending mantle flow that had subsequently formed (nearly 1.0 BYa) a new supercontinent, Mesogea.

A stagnant water stratification of the World Ocean had perhaps continued until a new glaciation impulse had covered in Late Riphaean a number of Laurasia and Gondwana continents (see Figs. 9.5, 9.6). As is well-known, oceanic water stirring occurs in glaciation periods, therefore, at the end Riphaean, iron oxides from rift zones might have again gotten in the oceanic active layer. However, by that time in the mantle had remained much less than 1% of the free iron (as most of it had already passed in the growing Earth's core). As a result, the last of the Precambrian iron ore accumulation impulses had been the weakest.

At the foundation of Precambrian iron ore formation emergence had been processes of iron oxidizing at the expense of thermal dissociation of

the CO_2-saturated oceanic water and hydration by this water of the oceanic crust's iron-containing rocks. At that, abiogenic methane generation had been occurring according to reaction (11.52). Obviously, the epochs of maximum rate of iron removal in the ocean must have been accompanied by maximum methane generation rate, which in turn had led to increasing the mass of methane-absorbing bacteria. As follows from reaction (10.13), a fractionation of carbon isotopes always causes lightening of methane isotopic composition, therefore, also lightening of carbon composition in organic matter C_{org} in bacteria grown on this methane. This perhaps explains why the organic matter in the methane-absorbing bacteria usually has extremely low content of the heavy carbon isotope $\delta^{13}C_{org}$ of up to –50‰. May be this is the explanation of emerging local minima in $\delta^{13}C_{org}$ distribution exactly at the moments of deposits with maximum iron ore formation reserves at the end Archaean and in Early Proterozoic (see Fig. 10.19). At this, despite a lower intensity of the jaspilite formation process in Late Archaean, the amplitude of $\delta^{13}C_{org}$ isotope minimum at that time had been at its maximum. Probably it had been associated with the existence in Archaean of a high-density carbon dioxide atmosphere, whereas in Early Proterozoic, CO_2 partial pressure had already declined and as a result, methane generation rate had also declined (Fig. 10.21).

As for the formation of iron ore deposits in Early Archaean, it had to have been accompanied by the formation of methane. However, methane might not have accumulated in its generation places (outside of the sediment sequences) and had been released directly in the atmosphere. In a humid and hot Early Archaean atmosphere under the influence of the solar UV radiation methane had been oxidized in a reaction $CH_4 + H_2O + UV \rightarrow CO + 3H_2$, and hydrogen had volatilized. In Early Archaean, most likely, bacteria had not yet existed capable of consuming methane, therefore, isotope shifts of the organic matter at that time had been caused only by chemical reactions (possibly abiogenic), without addition of methane isotope shifts (see Fig. 10.19).

12

Diamond Origin and the Formation of Kimberlite and their Affine Rocks

In the context of lithospheric plate tectonics, diamond-bearing rocks might have formed only at the immersion of the oceanic crust and its overlying heavy (ferruginous) pelagic deposits underneath the continental plates at depths of 150 to 200-220 km. In Archaean, as we have seen above, continental plates had still been too thin for it. That is why such conditions on Earth had first emerged only about 2.2–1.8 BYa, at the time of Early Proterozoic massive accumulation epoch of heavy ferruginous deposits (see Fig. 11.9) when the continental lithospheric plate thickness increased to 200–250 km (see Fig. 8.9). At that time, Earth's atmosphere had been still almost oxygen-free because the entire oxygen produced by then existing phytoplankton had been actually spent for oxidizing bivalent iron dissolved in water to the trivalent state. Beside a mass accumulation of ferruginous deposits, this circumstance must have resulted in hydrogen sulfide stagnation of the Early Proterozoic oceans; therefore, on their floor, beside usual deposits and iron hydroxides then in abundance had been deposited sulfides of iron and of other metals, siderite and organic matter. Besides, the Early Proterozoic oceans had not been deep. According to estimates, their average depth at that time had not exceeded 1.5 km (see Fig. 10.6) and only in narrow deep-water troughs had reached 4-5 km, i.e., almost everywhere had been less than the depth of sedimentation carbonate compensation. Therefore, at that remote epoch simultaneously with iron compounds on the ocean floor, at least in the tropical zone might have been deposited carbonate oozes saturated with organic and abiogenous methane emerged under reactions similar to 10.9 or 11.52.

The density of most ferruginous minerals in the composition of Early Proterozoic deposits had been very high. For instance, goethite density is 4.0-4.4, hematite 5.0-5.2, magnetite 4.9-5.2, pyrrhotine 4.6-4.7, pyrite 4.9-5.2 and siderite 3.9-4.0 g/cm^3. That is why, after the diagenesis of such deposits and pulling them in plate subduction zones (where pore and crystallization water had been squeezed out of them), deposit density had risen substantially. Estimates showed that whereas the ferruginous compound content in pelagic

N. O. Sorokhtin (ed.) The Origins of Natural Diamonds, (369–396) © 2019 Scrivener Publishing LLC

deposits of Early Proterozoic had reached 40% which is typical of lean (about 28-30% iron) jaspilite ores, then their density had become higher than average density of the continental lithospheric plates ($\rho_l \approx 3.2$ g/cm^3). Therefore, such deposits, as was shown above, had been easily pulled in subduction zones to great depths regardless of their viscosity, and at low viscosity might have even "collapsed" in the gap between plates and immersed down to the base of the continental lithospheric plates at depths of about 250 km (Fig. 12.1).

Melting of deposits within the subduction zones had occurred mostly at the expense of viscous friction energy dissipation of deposits themselves and friction between the lithospheric plates. However, at pulling heavy deposits in Early Proterozoic plate subduction zones such heating had been quite insignificant. The deposits had been heated more by the depth heat flow permeating the continental plates. It follows thence that the deposit stream temperature in the gap between plates then had corresponded with geotherm of the continental plate. That is why heavy deposits gotten in the subduction zone had begun melting only at depths where the continental lithosphere geotherm had intersected the deposit melting temperature (see Fig. 12.2). It is known that the melting temperature of most silicates in the presence of water, with pressure increase to 5-10 kbar sharply declines to 600-700°C [208]. Water-saturated carbonates behave similarly, the same as many other compounds. In a case of a system saturation by a complex

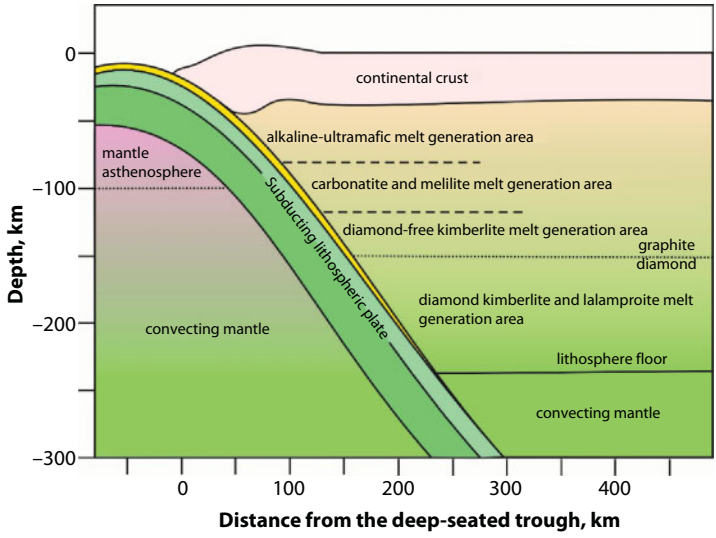

Fig. 12.1 Pulling oceanic crust sedimentary complexes in the plate subduction zone at great depth (up to 250 km) and the position of depth rock melts formation areas.

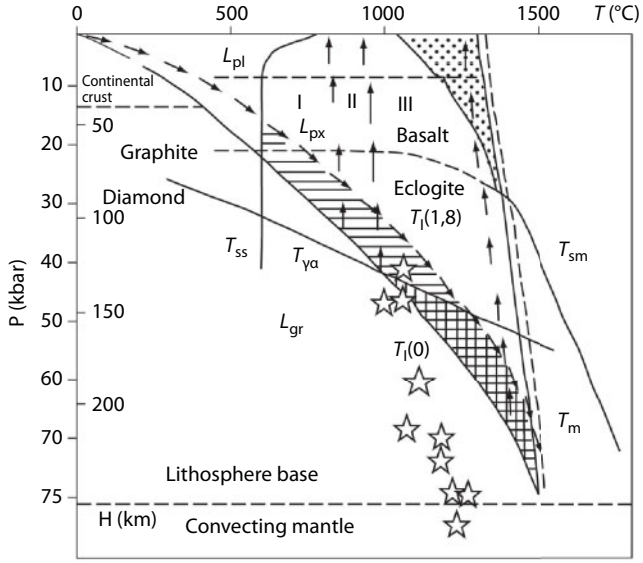

Fig. 12.2 Depth-temperature conditions of melting out alkali-ultramafic and kimberlite magmas [55]: T_m is mantle temperature; T_{sm} is mantle matter solidus temperature; $T_{g\alpha}$ is transition temperature graphite/diamond; T_{lk} is present-day continental geotherm (the ancient geotherm is marked by descending arrows); L_{pl}, L_{px} and L_{gr} re areas of stable existence of plagioclase, pyroxene and garnet lherzolites; T_{ss} is melting temperature of water-saturated deposits; horizontal hatch work is existence area of alkali-ultramafic, alkali-carbonatite and calcium-carbonatite melts; cross hatch work is existence area of diamond-bearing kimberlite and lamproite depth melts under the proposed mechanism; stars are positions of natural diamond P-T conditions after F.V. Kaminsky [37]; arrows are P-T conditions of heavy ferruginous deposits movement about 2–1.8 BYa and of magma rise in Phanerozoic; *I.* Area of formation and rise to the surface of alkali-ultramafic intrusions; *II.* Carbonates, melilites and no-diamond kimberlites; *III.* Diamond-bearing kimberlites and lamproites.

water-carbon dioxide fluid, rock melting temperature with the pressure increase also declines first but then smoothly grows. At that, the position of the temperature minimum depends on the ratio of fluid H_2O and CO_2 and usually is close to 5÷10 kbar.

Considering the noted patterns and the above-defined temperature distributions underneath the Archaean plates during the process period of pulling heavy Early Proterozoic deposits in subduction zones, it is reasonable to expect that silicate water-saturated deposits must have been melted already at a depth of about 50–70 km and the carbonate ones, about 80 km. With time, temperature gradients underneath the Archaean continents had been gradually declining (see Fig. 12.2). That is why by now,

molten silicates in ancient subduction zones might have been preserved only at depths exceeding 70–80 km and the carbonatite magmas, deeper than 100 km.

Deeper than the critical level of the continental geotherm intersection with the sedimentary matter melting start curve, the deposit melting extent had drastically increased. That is why at great depths must have been occurring liquation of the emerged melts and their differentiation by density. Heavy ferruginous and sulfide fractions had been descending and eventually had immersed in depths of the convecting mantle being gradually assimilated by its matter. Whereas the light fractions composed of separated fluids, carbonatite and silicate melts, in a general compression environment typical of the plate subduction process, had not had an opportunity to rise and must have accumulated (and conserved) at lower stages of the ancient continental plates (see Fig. 3.1 and 8.1). Gradually, they had been forming there the foci of alkali-ultramafic, carbonatite and lamproite-kimberlite magmas.

The subduction process often had been ending in continent collision. This situation had been especially typical of the Karelian diastrophism epoch about 1.9–1.8 BYa when from numerous fragments of the most ancient supercontinent Monogea (formed at the Archaean/Proterozoic boundary) had emerged a new supercontinent Megagea (see Fig. 9.3). Due to this, in numerous then acting plate subduction zones had been "sealed" the melts formed there. By force of coming from the mantle depth heat flows supporting stationary levels of ancient continental plates heat regimes, such melts might have been preserved in lithospheric "traps" for hundreds of millions of years practically without cooling.

During a long conservation of silicate-carbonatite magmas, especially in conditions of their overheating typical of lower stages of Archaean continental plates, magma differentiation by density had been unavoidably occurring. That is why emerged in plate subduction zones depth melt foci mandatorily had to be substantially differentiated. In the upper parts of such magmatic foci had been concentrated water-gas fluids, underneath had been positioned the lightest alkali (sienite) melts, somewhat lower, potassium-alkali aluminosilicate magmas and lower yet, carbonatite melts. Underneath carbonatites had usually been positioned highest density magnesia-silicate and potassium-magnesia-silicate melts of kimberlite and lamproite composition.

Therefore, in the proposed mechanism of depth rock melts formation the specifics of their composition and geochemistry substantially depend on the nature and type of Early Proterozoic ferruginous deposits pulled in plate subduction zones. However, no smaller role in this regard had played

also mentioned above depth melt differentiation and liquation processes and hydrodynamic regimes of rise by silicate-carbonatite magmas from great depth to Earth's surface.

Thus, at slow opening of extension fractures and, as a consequence, slow rise of depth melts with laminar flow establishing in them, the order of coming fluids and magmas on the surface had completely corresponded with the succession of their density differentiation in the source depth foci.

In these situations, first to rise had been pneumatolytic and strongly mineralized hydrothermal fluids causing intense fenitization of the encircling rocks and abundant formation of alkali (sienite) pegmatites. On the heels of overheated hydrothermal solutions had been rising sienites saturated with volatile elements' lightest alkali melts of agpaite and sienites enriched in sodalite and apatite. Then enriched in albite, the nepheline and leucite monzonites had invaded. After the silicate melts had often invaded carbonatite magmas, usually in order of increasing density. The alkali (sodium) carbonatites had been replaced by much more abundant volumes of calcite carbonatites (soevites). After them had been rising magnesial (dolomitic) carbonatites. The process had completed with the invasion of highest density ankerite carbonatites. Naturally, such slow laminar flows could not have brought and had never brought on the surface xenoliths of the dense rocks – fragments of ancient oceanic crust and subcrustal lithosphere as well as of depth rocks torn from the walls of a fracture channel in which magmas had been rising.

Usually, the described succession of invasion by differentiated magmatic series is characteristic only for the melts rising from intermediate levels of the continental lithospheric plates, 80 to 120-150 km. The cause of this phenomenon will be considered below. Here, we will only note that a quiescent at depth, rising regime of such magmas might have been followed by explosive spew of the melts in near-surface conditions. This had occurred at lowering lithostatic pressure acting upon the rising melts below 1–2 kbar. After that, it will be recalled, had occurred the "ebullition" of water-saturated magmas with the release of volatile elements and fluids whose overpressure had been exactly what had caused the destruction and explosive spew of surface rocks with the emergence of the eruptive channel – diatreme, in which rising melts had rushed.

If viscosity of the melts emerged near the base of lithosphere at high pressure had remained very low and their saturation with fluids, high, such melts had turned out capable rapidly to fill the emerged fractures. It may be expected that kimberlite magmas had such properties. In this case, after the emergence of tensile stresses in a continental plate, fracture opening in the body of the lithosphere had been especially blistering, at a filling-up rate of the expanding

fracture with low viscosity fluids and liquid (overheated) melts. At that, the lower had been magma viscosity, the faster the fracture had been opening. In a situation like this, in a few meter-wide magmatic channel had unavoidably emerged turbulent flows efficiently stirring all earlier differentiated melts. As a result, instead of differentiated silicate and, separately, carbonatite melts had been coming on the surface mixed silicate-carbonatite magmas similar in their summary composition with silicate-carbonatite fractions emerged at melting of the source Early Proterozoic ferruginous pelagic deposits. A blistering (at the speed of an express train) rise of depth magmas and a turbulent vorticity of magma flows had unavoidably led to abrasion of the magmatic channel walls and to tearing off of them bedrock pieces. These rocks had been carried on the surface as "rounded" (boulder-like) xenoliths of depth rocks.

That had been, most likely, the origin of enigmatic pseudo-mantle kimberlites with their specific composition and exotic inclusions of xenoliths some of which may have a mantle origin.

A study of diatremes on the Kola Peninsula (the Baltic shield, Russia) showed that an invasion of melilitite and kimberlite magmas in a crystalline basement lacking the sediment cover had resulted in the formation of specific magmatic bodies. Archaean age crystalline formations had been ruptured by the dykes of alkali-ultramafic composition and characteristic arachnoid shape. These dyke bodies fanning out in different directions form isometric, close to roundish, body in the place of their convergence. The central body diameter may reach 5-10 meters and the length, 50-100 m with the thickness of 1-3 (5) m. Petrographic analysis of samples from these bodies indicates that they all are finely crystalline unvitrified mass with the chemical composition of kimberlite and melilitite melt-outs. Naturally, they cannot include any diamond grains although their chemical composition in some cases corresponds with diamond-bearing kimberlites. Based on this, an important conclusion may be made that diatremes had emerged only when depth magmas of such composition had invaded a thick sedimentary sequence. Otherwise, dyke bodies of the described shape had formed. The author studied these specific magmatic formations on the coast of the White Sea Throat on the Baltic Shield's Kola Peninsula.

Reviewing the lamproite origins' issues, similar features of these rocks with kimberlites should be marked, which was noted by N.V. Sobolev in the foreword to the monograph by A. Jakes, J. Louis and C. Smith [2]. This is a similarity of magma formation fluid regime, closeness of early crystallization stage parageneses of inclusions and a similarity of geochemical features in high-potassium phlogopite kimberlites with olivine lamproites, etc. Despite a low CO_2 content in lamproites, it was reliably established that at early stages of lamproite magma formation, same as in the kimberlites, the main fluid

component had been carbon dioxide. Based on inclusions' parageneses, temperature in both types of depth melts had not exceeded 1,200°C. Practically in all lamproite diatremes and bodies are established chromium-containing pyropes with the composition completely analogous to pyropes from the inclusions in kimberlite diamonds. The lamproite diamonds themselves are also similar to the kimberlite types. Most of them had crystallized in eclogite, some of them in ultramafic paragenesis minerals, i.e., in the mineral associations totally different in their chemical composition to the lamproites themselves. Besides, both in lamproites and kimberlites are observed close and practically overlapping distributions of rare earth elements (Fig. 12.3).

We may add to it that the composition of kimberlites recalculated for no-carbonate residue often corresponds very closely with the composition of lamproites, except maybe somewhat lower content of potassium in kimberlites (see Table 12.1). Besides, there are also transitional forms

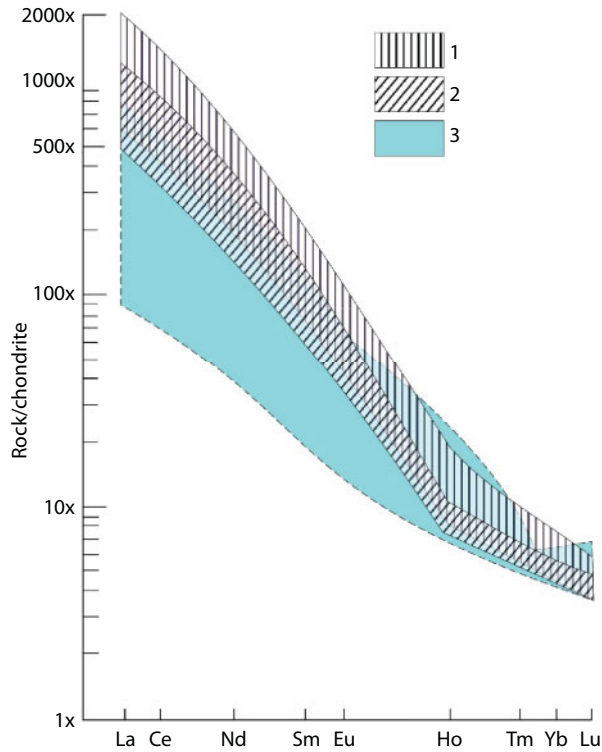

Fig. 12.3 Chondrite-normalized rare-earth element distribution in West Kimberly lamproites (Australia) in comparison with rare earth element distribution in South African kimberlites (after [2]): 1. Field 21 of lamproites; 2. Field 7 of olivine lamproites; 3. The kimberlite field of South Africa.

Table 12.1 Kimberlite and lamproite composition and comparison with the composition of their silicate fraction.

Oxides	**1**	**2**	**3**	**4**	**5**	**6**	**7**	**8**
SiO_2	35.20	31.10	33.55	41.50	41.36	40.28	46.10	44.80
TiO_2	2.32	2.03	1.29	3.62	2.73	2.63	1.77	3.91
Al_2O_3	4.40	4.90	2.94	3.64	5.17	6.35	4.03	3.93
Fe_2O_3	–	–	4.69	–	–	–	6.44	–
FeO	9.80*	10.50*	2.97	8.10*	11.52*	13.60*	4.08	8.75*
MnO	0.11	0.10	0.10	0.13	0.13	0.13	0.14	0.14
MgO	27.90	23.90	25.40	25.00	32.38	30.96	31.31	26.99
CaO	7.60	10.60	9.18	4.99	4.00	2.02	4.92	4.77
Na_2O	0.32	0.31	0.13	0.46	0.38	0.40	0.18	0.50
K_2O	0.98	2.10	0.47	4.12	1.15	2.72	0.65	4.47
P_2O_5	0.70	0.70	0.29	1.68	0.82	0.91	0.39	1.81
CO_2	3.30	7.10	8.50	0.45	–	–	–	–
H_2O	7.40	5.90	9.68	6.36	–	–	–	–
other	–	–	0.45	–	–	–	–	–
Total	100.03	99.24	99.64	100.05	100.04	100.00	100.01	100.05

*- the entire iron is converted to FeO

1. Average kimberlite [48], 2. Average mica kimberlite [48], 3. Average kimberlite from "Mir" diatreme [3], 4. Olivine lamproite from Allendale diatreme West Australia [2]; 5–8. Recalculated analyses 1–4. Per no-carbonate and no-water residue: 5. Recalculated analysis 1, 6. Analysis 2, 7. Analysis 3, 8. Analysis 4.

with the composition equally reflecting the specifics of both kimberlites and lamproites. For instance, the high-potassium phlogopite kimberlites and olivine lamproites [323].

The main difference of the lamproites from kimberlites is small amounts (or complete absence) in them of carbonate phase and high potassium concentrations. Besides, in lamproites large xenoliths of depth eclogites or garnet peridotites are almost never encountered.

Nevertheless, the material composition of lamproites and kimberlites was apparently substantially affected by the original composition of their begetting deposits. Indeed, as the triple phase diagrams of kimberlites and lamproites from various parts of the world demonstrate, beside the common superposing areas of their existing fields, also totally incompatible areas are identified (Fig. 12.4). We believe that these differences on the $CaO–Al_2O_3–(FeO'+MgO)$ diagram are much associated with a different composition of pelagic deposits immersed in depth. Thus, the deposits that served the basis for emerging lamproites and kimberlites in fields 2, 4 and 5 had been strongly enriched in iron and magnesium but impoverished in silica. At that, lamproites in West Australia and kimberlites in South Africa (fields 2 and 4) are impoverished in calcium. On the other hand, beside a ferruginous quartzite, the deposits forming lamproite fields 1 and 3 also included a notable amount of silica (i.e., pelite deposits), whereas deposits begetting the kimberlite had in their composition notable amounts of dolomite or siderite.

Taking into account the data on the diamond formation depths (see Fig. 12.2) and kimberlite mineral associations, it is reasonable to believe that kimberlite magmas had been begotten in the lower parts of the continental lithosphere. Most likely, substantially enriched in water-carbon

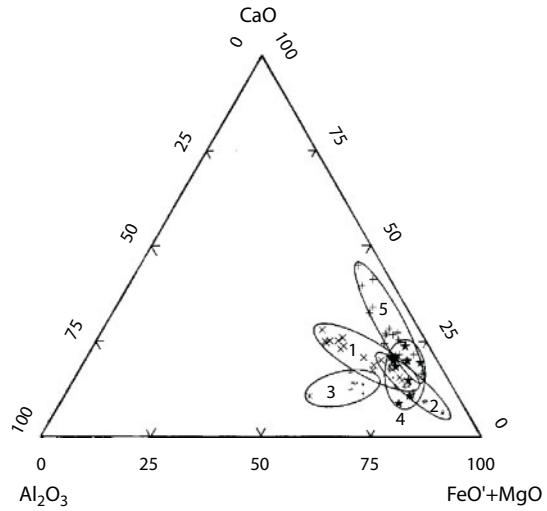

Fig. 12.4 Existence fields of lamproites and kimberlites in the $CaO–Al_2O_3–(FeO_{total}+MgO)$ diagram for various world regions: 1. The lamproite field of the Aldan shield based on data from [4]; 2 and 3. Lamproite fields after [2]; 4. Existence field of the South African kimberlites after [1]; 5. The kimberlite field of the Siberian province after [3].

dioxide fluids and incoherent elements ultramafic kimberlite melts had been emerging due to melting of ferruginous and iron-carbonate deposits. Because of the saturation of these melts with water and especially carbon dioxide gas, the viscosity of kimberlite magmas must have been very low. That is why at the emergence of lithosphere extension conditions and fracture formation, the rise of kimberlite magmas had been occurring exceptionally rapidly and had been accompanied by intense turbulence facilitating carrying to the surface of large and heavy xenoliths.

The lamproites, similarly to the kimberlites, had also been formed at the lower stages of the continental lithosphere in the form of magnesial-potassium, saturated with silica and water alkali silicate melts. However, as opposed to the kimberlites, without a noticeable mixing of these melts with carbonate fractions. That is why it is reasonable to assume that the lamproite magma foci formation had been occurring at the expense of melting non-carbonate deposits, for instance iron siliceous and shaly ones, similar to those from which further on jaspilites had formed. In this connection it is interesting to note that in a classic region of the diamond-bearing lamproites (West Australia) are very common jaspilites as well, for instance in the Hamersly Fm. Due to a silicate composition of the lamproite magmas, their viscosity must have been much higher than the kimberlite silicate-carbonate melt viscosity. In particular, that had been a reason for a more quiescent rise regime of the lamproite melts accompanied by only a weak turbulence incapable of bringing on the surface large depth xenoliths.

The described mechanism of kimberlite and lamproite formation also enables the explanation of the entire gamut of transitional forms between these rocks from the classic kimberlites through micaceous kimberlites to the olivine and leucite lamproites. At the same time, the affinity of carbonatites with kimberlites must be once again emphasized. Thus, according to [1], strontium isotope composition in calcites from kimberlites and carbonatites is very much alike.

We will now review in some more detail what had been going on with the oceanic deposits and oceanic crust rocks gotten at great depths underneath the continents. As already noted, the temperature of heavy ferruginous deposits pulled in subduction zones must have been only slightly exceeding the geotherm of the obducted continental plate (see Fig. 12.2). The oceanic crust rocks would have acquired approximately the same temperature at the appropriate depths. That is why already at the intersection of about 70–80 km level corresponding to the basalt-eclogite transition, the subducted basalts, gabbro and ultramafic rocks of the oceanic crust tripartite section had experienced polymorphic transitions turning appropriately in eclogites and garnet peridotites.

For a reason of the present lubricating effect of adjacent plates by heavy deposits "collapsing" into the depths, in Early Proterozoic plate subduction zones had been absent island arc or Andean type calcareous-alkali magmatism. That is, most island arcs and collision systems of that time had been amagmatic which is supported by numerous geological data (for instance, [127]). At that, the temperature of the oceanic crust rocks had been as if "following" the obducted continental lithosphere geotherm. That is why in such zones neither basalts nor even more so ultramafic rocks and their polymorph analogs had melted and all their metamorphic transformations had been mostly isochemical. This, in particular, is convincingly supported by the coinciding compositions of eclogites from the kimberlite diatremes, dykes and sills with basalts of the ocean floor and islands (see Figs. 12.5 and 12.6). Exceptions are only some high-silica eclogites and relatively rare grospidites that had apparently experienced substantial metasomatic alterations. It is not clear, however, whether this had been occurring at their melting or only at the expense of hydrothermal and diffusion replacement. Be it noted here as well that the sometimes encountered coesite inclusions in diamonds, in the view of N.V. Sobolev [39], are a proof of a relatively low-temperature nature of those rocks in equilibrium with which diamonds and eclogites had formed.

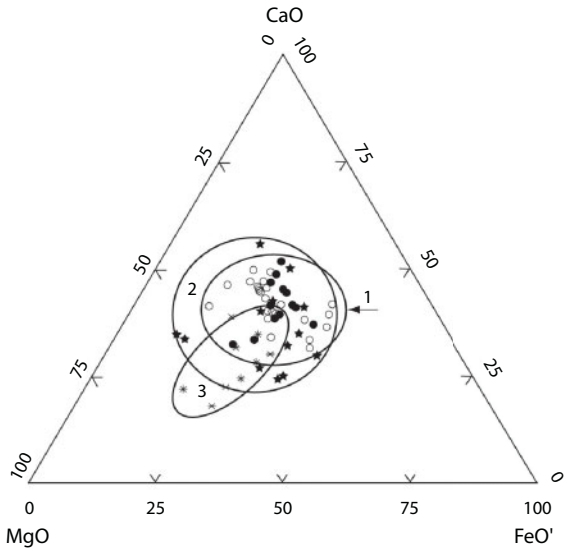

Fig. 12.5 A diagram CaO–MgO–FeO_{total}. 1. Basalt field of mid-oceanic ridges based on the data by [324] and oceanic crust gabbro [325]; 2. South African eclogite field based on the data by [1]; 3. Yakutia eclogite field based on the data [3].

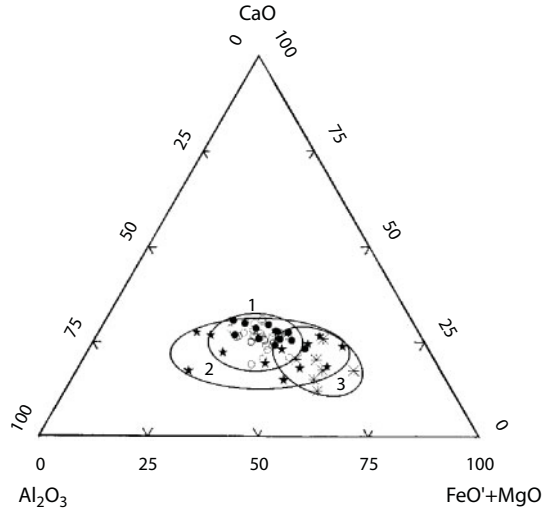

Fig. 12.6 A diagram CaO–Al_2O_3–(FeO_{total}+MgO) of oceanic basalts, gabbro and kimberlites (see Fig. 12.5 for symbols).

Interestingly that Yakutia eclogite field (Russia), compared with the composition of major present-day oceanic crust rocks is noticeably enriched in magnesium. Perhaps this is due to remaining after Archaean mantle overheating.

Our estimates (see Fig. 5.5) show that in the second half of Early Proterozoic the upper mantle temperature had been close to 1,500°C (the present-day temperature is about 1,320°C). Exactly this circumstance might have caused some enrichment of Early Proterozoic oceanic crust basalts with magnesium, therefore, also eclogites emerged from them.

The carbonates in the plate subduction zone had also experienced a number of transformations resulting in the release of CO_2 and bonding some bases in silicate phases and some others in carbonate ones. Thus, siderite formation heat from its component oxides is equal 22.3 kcal/mole, magnesite, 23 kcal/mole, calcite 42.6 kcal/mole. It follows thence that a direct carbonate dissociation might have occurred only in hot areas of a plate subduction zone: siderite and magnesite at depths about 80–100 km, calcite, at depths exceeding 150 km, i.e., only in melting areas of getting in the subduction zones water-saturated deposits (see Fig. 12.2). Whereas, if at carbonate dissociation had formed new mineral formations, then although the reaction would still have remained endothermal, the depth of the process in plate subduction zones might have been much lower:

$$\underset{\text{calcite}}{CaCO_3} + SiO_2 + 21.3\ \text{kcal/mole} \rightarrow \underset{\text{wollastonite}}{CaSiO_3} + CO_2, \quad (12.1)$$

$$\underset{\text{magnesite}}{MgCO_3} + SiO_2 + 15.3\ \text{kcal/mole} \rightarrow \underset{\text{enstatite}}{MgSiO_3} + CO_2, \quad (12.2)$$

$$2\underset{\text{magnesite}}{MgCO_3} + SiO_2 + 34.2\ \text{kcal/mole} \rightarrow \underset{\text{forsterite}}{Mg_2SiO_4} + 2CO_2, \quad (12.3)$$

$$2\underset{\text{siderite}}{FeCO_3} + SiO_2 + 35.8\ \text{kcal/mole} \rightarrow \underset{\text{fayalite}}{Fe_2SiO_4} + 2CO_2, \quad (12.4)$$

$$\underset{\text{calcite}}{CaCO_3} + \underset{\text{magnesite}}{MgCO_3} + 2SiO_2 + 31.4\ \text{kcal/mole} \rightarrow \underset{\text{diopside}}{CaMg(Si_2O_6)} + 2CO_2. \quad (12.5)$$

Carbon dioxide released in reactions (12.1)–(12.5) had dissolved in the formed melts and entered the water-carbon dioxide fluid. The minerals formed in the same reactions had transferred to melts and then (already from the melts) had crystallized, sometimes as a monomineral phase reaching at that the size of mega-crystals (up to 15 cm and greater).

Deposit dehydration in the plate subduction zones might have occurred under the reactions:

$$\text{Sodium montmorillonite} \rightarrow \text{paragonite} + \text{albite} + \text{chlorite} + H_2O \rightarrow \text{sillimanite} + \text{albite} + \text{cordierite} + SiO_2 + H_2O. \quad (12.6)$$

These reaction had been accompanied by the release of silica and water, the silica had bonded with oxide of alkali-earth metals in reactions (12.1)–(12.5), and water, same as carbon dioxide gas, had passed into the fluid. Besides, through the exchange reactions between the sedimentary origin silicates and carbonates, magnesia had mostly concentrated in the silicate phase (mostly in olivine) and calcium, in carbonates.

At reaching by the deposits of the subsolidus temperature two reactions important for the understanding of kimberlite genesis had possibly become possible: crystallization of apatite and formation of phlogopite. It should be expected that in hydrogen sulfide infected oceanic basins of

Early Proterozoic, phosphorites might have made a notable part of the pelagic sapropel oozes deposited on their bottom. After having gotten in a "hot" portion of the plate subduction zone, the phosphorite dispersed in the deposits had been mobilized by circulating there thermal water and crystallized as apatite. A genetic tie between the apatites from kimberlites and sedimentary phosphorites in the oceans is seen in the similarity of their composition. Thus, according to [326, 327], both belong with the fluorine-hydroxyl apatite group, contain elevated concentrations of rare-earth elements (about 0.5% and more) among which light lanthanoids dominate.

At determining phlogopite genesis in kimberlites and lherzolite xenolith is very important to find out the source and arrival paths in these rocks of such dispersed in the mantle elements and compounds as fluorine, potassium and water. The contents of these components in the phlogopite exceed their concentrations in the mantle matter respectively 300–400, 600–1,000 and 50–100 times. The same goes with trace elements, especially rubidium, barium, lithium, strontium and other rare elements. On the other hand, contents of these very elements in pelagic deposits pulled in plate subduction zones usually by dozens and hundreds of times exceed their mantle concentrations (for potassium, for instance, 200 times). Therefore, a conclusion may be made that the phlogopite and apatite had formed in kimberlites metasomatically, affected by the hydrothermal solutions enriched in potassium, fluorine and other trace elements. This conclusion complies with the conclusion by J. Dawson [1] that the phlogopite mega-crystals indeed had formed within the kimberlite melt.

The phlogopite origins in lherzolite xenoliths may apparently be explained by seritization type reactions which had been running already in conditions of oceanic crust hydration. This process had been accompanied by recrystallization of the plagioclase at the expense of the operating hydrothermal solutions bringing magnesium (released at serpentinization of ultramafic rocks), potassium, fluorine and other trace elements.

Hydration (serpentinization) of peridotites and lherzolites near oceanic rift zones had been running only at the expense of the oceanic water penetrating them. Usually, peridotite serpentinization had been accompanied by the release of magnesite, and at shortage of carbon dioxide, of brucite, and by increase in the rocks of the content of alkali metals and some other lithophile elements getting there directly from the oceanic water. This, for instance, is indicated by the fact that alkali, rare earth and other lithophilic elements in the peridotites and eclogite xenoliths are

concentrated mostly in the intergranular spaces (for instance, 54 to 99% of uranium ultramafic rocks). Based on the data by H. Allsopp [328], the potassium and rubidium concentrations in intergranular material of the eclogites from the Roberts-Victor diatreme in South Africa reach respectively 1.6% and 48 g/t, i.e., exceed many times the contents of these very elements in the eclogite minerals.

Beside a primary "contamination" of the basalt and serpentinite layer rocks in the former oceanic crust, in a plate subduction zone, especially at the kimberlite melts formation depth, must have occurred a substantial secondary contamination of these very rocks by the elements dispersed in kimberlites. For instance, Manton and Tatsumoto [329] showed that eclogites from the Roberts-Victor diatreme are strongly "contaminated" by uranium, thorium, lead, rubidium and strontium that had entered them from kimberlites. They estimate that 38 to 96% of lead had been delivered in eclogites from the enclosing rocks.

There are reasons to suggest that phlogopite in peridotite xenoliths had formed at the expense of metasomatic alterations in the oceanic crust hydrated rocks at the time of their descent and gradual heating in the subduction zones. The same process, due to plate friction in the subduction zones, had resulted in intense deformations of the subducted crust, therefore, had formed those fluidal and gneiss-like flow textures in the rocks which are usually very characteristic for xenoliths of garnet peridotites.

At deeper levels, where deposit melting and liquation of the melts begin (i.e., in the formation area of the kimberlite magma silicate-carbonate facies), perhaps, the reaction of forming phlogopite mega-crystals over potassium feldspar had already been possible:

$$\underset{\text{orthoclase}}{K(AlSi_3O_8)} + \underset{\text{magnesite}}{3MgCO_3} + H_2O \rightarrow \underset{\text{phlogopite}}{KMg_3(AlSi_3O_{10})(OH)_2} + 3CO_2, \quad (12.7)$$

and olivines and pyropes, over clay minerals and pyrophyllite

$$\underset{\text{magnesite}}{5MgCO_3} + \underset{\text{kaolin}}{Al_2(Si_4O_{10})(OH)_2} \rightarrow \underset{\text{forsterite}}{Mg_2SiO_4} + \underset{\text{pyrope}}{Mg_3Al_2(SiO_4)_3} + 5CO_2 + H_2O. \quad (12.8)$$

A possibility of running such reactions in the hot portion of the plate subduction zones is supported by the size of olivine and garnet megacrystals exceeding sometimes 3–7 cm and, mainly, by finds of kimberlite inclusions in them [1].

In conditions of high pressure (40–50 kbar) typical of the continental plate lower portions, carbonate decomposition apparently must have been accompanied by oxidizing of bivalent iron with the formation of dense magnetite crystalline structures and by CO_2 reduction to carbon monoxide as this seen in reaction (12.1). However, most magnetite still had to be formed at the expense of iron oxides contained in deposits. The summary saturation of kimberlites by iron oxides reaches on average 10-12%, whereas the magnetite content in the accumulative rocks reaches 30-32% [330]. This indicates that most of magnetite together with other iron oxides had been immersing in the mantle.

The monticellite is often abundantly encountered in the kimberlites. Sometimes its concentration even reaches 80% as, for instance, in the Monticellite diatreme (Yakutia, Russia) but more often this mineral forms fringes around olivine crystals. These very fringes as a rule include magnetite and periclase. The magnetite forms around ilmenite and perovskite grains and perovskite is sometimes in the composition of common kimberlite minerals.

A fact is conspicuous in the kimberlite composition of a sharply increased ration MgO/CaO≥2. In lamproites it is even higher and reaches sometimes 3–4, whereas in their affine rocks of the alkali-ultramafic series this ratio is less than 0.3–0.1 and in carbonates it fluctuates between 0.3 and 0.6. In the present-day oceanic deposits, it is only 0.05–0.12 [331]. Partially, this incoherence may be explained by that in the Early Proterozoic oceans, most likely, not limestones had been deposited but dolomites [260, 265, 439] for which MgO/CaO ≈ 0.7, and also magnetite (containing 46.7% of MgO?) released according to the reaction (11.38).

Nevertheless, $CaCO_3$ is usually dominant in carbonatites and kimberlite carbonates. An explanation of this fact is that in the kimberlite and carbonate melt foci, had been occurring exchange reactions when magnesium had been passing in silicates and calcium, in carbonates, for instance:

$$\underset{\text{diopside}}{CaMg(Si_2O_6)} + \underset{\text{magnesite}}{MgCO_3} \rightarrow \underset{\text{enstatite}}{Mg_2(Si_2O_6)} + \underset{\text{calcite}}{CaCO_3}, \qquad (12.9)$$

At even greater depths had been occurring garnets and corund formation with the release of calcite:

$$\underset{\text{anorthite}}{3Ca(Al_2Si_2O_8)} + \underset{\text{magnetite}}{6MgCO_3} \rightarrow \underset{\text{pyrope}}{2Mg_3Al_2(SiO_4)} + \underset{\text{calcite}}{3CaCO_3} + \underset{\text{corund}}{3CO_2 + Al_2O_3}, \quad (12.10)$$

$$\underset{\text{anorthite}}{3Ca(Al_2Si_2O_8)} + 6FeCO_3 \rightarrow \underset{\text{almandine}}{2Fe_3Al_2(SiO_4)} + \underset{\text{calcite}}{3CaCO_3} + 3\,CO_2 + \underset{\text{corund}}{Al_2O_3}. \quad (12.11)$$

In exchange reactions (12.9)–(12.11), at even higher temperature and pressure, had possibly occurred also the carbonate decomposition with the release of free carbon dioxide, formation of monticellite, perovskite, periclase and magnetite with carbon monoxide

$$\underset{\text{calcite}}{CaCO_3} + \underset{\text{forsterite}}{Mg_2SiO_4} + 29\ \text{kcal/mole} \rightarrow \underset{\text{monticellite}}{CaMgSiO_4} + \underset{\text{periclase}}{MgO} + CO_2, \quad (12.12)$$

$$\underset{\text{calcite}}{CaCO_3} + \underset{\text{enstatite}}{MgSiO_3} + 23.8\ \text{kcal/mole} \rightarrow \underset{\text{monticellite}}{CaMgSiO_4} + CO_2, \quad (12.13)$$

$$\underset{\text{calcite}}{3CaCO_3} + \underset{\text{ilmenite}}{3FeTiO_3} + 78.1\ \text{kcal/mole} \rightarrow \underset{\text{perovskite}}{3CaTiO_3} + \underset{\text{magnetite}}{Fe_3O_4} + 2CO_2 + CO. \quad (12.14)$$

In the framework of our model it was possible to describe from a unified position most of the specific features and sometimes even subtle details in the composition of the diamond-bearing and their affine rocks including the diamonds themselves and mineral inclusions therein. Thus, kimberlites and lamproites under this model are indeed depth rocks although emerged

from pelagic deposits. It follows thence a conclusion that carbon, phosphorus, nitrogen, most of lithophilic elements (Li, B, F, Cl, K, Ti, Rb, Sr, Y, Zr, Nb, Cs, Ba, Ta, Pb, Th, U), water and other fluids in the diamond-bearing rocks are not of mantle but primary-depositional, i.e., purely exogenous origin. This is also indicated by high concentrations and spectra of rare-earth elements, potassium/sodium, thorium/uranium ratios, hydrogen, oxygen, sulfur and strontium isotopes in kimberlites as well as gas-liquid inclusions in the diamonds of H_2O, H_2, CH_4, CO_2, CO, N_2, Ar, C_2H_4 and even ethyl alcohol C_2H_5OH [20, 21]. The same is testified by isotope shifts of carbon in diamond crystals with clear biogenic marks. The existing convention is that kimberlites and their affine rocks are purely mantle formations. It follows from everything stated that kimberlites are not at all mantle but only pseudo-mantle rocks in whose formation a substantial role had been played by exogenous factors.

The same is supported by the xenolith petrology and geochemistry of their component minerals. Thus, conducted by J. Dawson [1] analysis of zoning in garnets and clinopyroxenes from the kyanite eclogites and grospidites in the Roberts-Victor diatreme in South Africa shows that by the composition of outer zones in these minerals, the source eclogite, earlier in a state of equilibrium at moderate pressure, later descended in the high-pressure area. After that, it had gotten in the kimberlite and only then had been brought on the surface again. There are also data supporting the formation of garnet harzburgites from originally spinel peridotites [1] which also supports a preliminary descent of the ultramafic rocks to great depth occurred, as this follows from theory, long before the rise of the rocks to the surface.

Beside kimberlites, similar geochemical features belong also with many less deep but still clearly magmatic alkali-ultramafic rocks. Examples are carbonatite intrusions of Kovdora and Africanda as well as Khibin deposits of apatite-nepheline ores on Kola peninsula (Baltic shield, Russia). For instance, among the minerals of Khibin sienites and apatites (in nepheline, eudialyte and feldspars), hydrocarbon gases are discovered. Some of them are even high-molecular hydrocarbons (up to C_{20}): paraffin series bitumoids, naphthene and aromatic hydrocarbons, derivatives of esters, saturated steroids and carbonic acids. Actually, in the bitumoid composition of these alkali rocks are established compounds of all classes typical of sedimentary rock bitumoids: lubricants, benzene and alcohol-benzene resins, asphaltenes, etc.

The kimberlite formation age, based on strontium and lead isotopic ratios in omphacites and inclusions in diamonds, had also been Early Precambrian and close to 2–2.5 BY [1], which is exactly what follows from the formation model reviewed here of these exotic rocks. Although

recently the information appeared that by samarium-neodymium and rhenium-osmium ratios in diamond inclusions have been determined even more ancient ages of the diamonds, up to 3–3.4 BY. However, at close look into the methodic of these age determinations it became clear that only uniform chondrite reservoir CHUR model parameters have been used in them. This method apparently is quite appropriate for the mantle rocks. According to the conventional interpretation, diamonds are also believed to be mantle formations but, as shown above, the diamonds had formed out of Early Proterozoic oceanic pelagic deposits matter. Therefore, in geochronal equations should be used not the $(^{143}Nd/^{144}Nd)_{CHUR}$ ratio values from the CHUR model but the values of these isotopes in crustal rocks $(^{143}Nd/^{144}Nd)_{crust}$ or better in the oceanic deposits:

$$\left(\frac{143_{Nd}}{144_{Nd}}\right)_{diam} = \left(\frac{143_{Nd}}{144_{Nd}}\right)^{0}_{crust} - \left(\frac{147_{Sm}}{144_{Nd}}\right)^{0}_{crust} \cdot \left(e^{\lambda \cdot t} - 1\right), \quad (12.15)$$

where $\lambda = 6.54 \cdot 10^{-12}$ years^{-1} is samarium ^{147}Sm decay constant; the upper superscript "0" means that the present-day values of isotope ratios are used. If we now substitute in Eq. (12.15), for instance, average crustal values of $(^{143}Nd/^{144}Nd)^{0}_{crust} = 0.5115$ (instead of 0.512638 in the CHUR model) and $(^{147}Sm/^{144}Nd)^{0}_{crust} = 0.2 - 0.22$ (instead of 0.1967 in the CHUR model), then the Early Proterozoic age of the diamonds will be about 2 BY. This result perfectly matches our theoretical constructions. The same goes with all other diamond age determination methods: at age determination should be used parameters of the ancient deposits and not at all of the mantle rocks.

Oxygen isotope shifts and hydrogen/deuterium ratios in hydrosilicates of these rocks well match the reviewed kimberlite formation model. Moreover, according to the data in the publication by J. Dawson [1], lower values of the initial isotope ratios $^{87}Sr/^{86}Sr$ in minerals of kimberlites and their affine rocks, 0.703 to 0.705 (for none-phlogopite samples) are completely within the range of similar ratios for Early Proterozoic deposits (see Fig. 8.13). Maximum values are usually observed in phlogopite-containing, i.e., alkali kimberlites with the elevated rubidium content in them. At that, for the eclogites these ratios are within the range of 0.701–0.703 which for the mantle rocks also corresponds with Early Proterozoic age. That said, the elevated $^{87}Sr/^{86}Sr$ values in some eclogite samples may be due to the alkali contamination of basalts which had happened perhaps as early as at the hydration stage of the source oceanic crust by the chloride water of Early Proterozoic ocean.

As already mentioned, eclogite xenoliths encountered in kimberlites come laden with evidences of the primary-near-surface origin: despite clearly depth mineral associations, their bulk composition nicely matches the oceanic tholeiite basalts and gabbro of the oceanic crust (see Fig. 12.5 and 12.6) molten out only at shallow depths (to 35 km) underneath the oceanic rift zones. All these, in our view, convincingly testify in favor of relatively near-surface formation level of the entire complex of the subject rocks in Early Proterozoic, their subsequent descent at great depths and new blistering rise to the surface (at a rate of about 30–50 m/s) in subsequent geological epochs.

The issues of the diamond origin have been under discussion for more than a century now. Major concepts of this discussion are included, for instance, in the monograph by J. Dawson [1]. According to these publications we will note that most of modern diamond formation hypotheses are based on the assumption that the diamonds are an upper mantle mineral and had been formed at high pressure and temperature. Most popular among these approaches at the end of the 1970s was a hypothesis based on a position that the diamonds are mantle rock disintegration products [23, 332]. This hypothesis survived until the end of the 1980s [2, 333, 334]. For the support of this hypothesis, the attention was drawn to the fact that the composition of inclusions in the diamonds usually was similar to homonymous minerals from depth xenoliths of eclogites and peridotites. According to this view, diamonds are mantle origin xenocrysts and the kimberlite magma is just a transport delivering diamonds and xenoliths from the depth of the upper mantle on the surface.

In the view of A.A. Marakushev [335], Marakushev *et al.* [336], the diamonds had also been crystalized in the upper mantle from ultramafic and base magmas saturated with hydrocarbon fluids whereas the kimberlite magmas then had replaced the depth rocks and inherited diamonds that existed in them. According to S.K. Simakov [337], the source diamond-bearing melt had emerged about 3.5 BYa in liquid iron melts at depths of over 200 km. The appearance of liquid iron was associated with Earth's heating by the radioactive element decay. Without breaking stride for a critical analysis of these and numerous other hypotheses of this kind (their critical review is included in a publication by Garanin *et al.*, [338]), we will come straight to the description of the proposed model.

Under our model, the diamonds had been formed by way of reducing the carbon in the interaction reactions of carbon monoxide and carbon dioxide with methane or other organic and abiogenous origin hydrocarbons, pulled through subduction zones, together with deposits, to great depths. In deep and near-bottom water of the Early Proterozoic oceans,

most likely, had dominated substantially reducing conditions. Therefore, the oceanic deposits of those times must have contained elevated concentrations of the organic matter. Having gotten in a plate subduction zone, the organic matter had been subjected there to thermolysis, hydrolysis and had been passing in an accelerated way all stages of transformation into hydrocarbons, nitrates and ammonia compounds. Some of these mobile compounds together with pore water had been certainly squeezed out of the plate subduction zones already in their most upper horizons. But some part of them, together with deposits, had continued the way in the depth of the mantle.

In the present-day subduction zones, where the water-saturated silicate melts are easily brought out of the plate friction zone, the magma formation temperature in them is rapidly rising to melting level of "almost dry" and even dry basalts. That is why hydrocarbons through such zones cannot penetrate deep in the mantle as long before that they have to practically completely dissociate with the formation of dispersed graphite. That is exactly the way for part of carbon to get in the mantle.

A totally different picture, as we saw, must have been formed in Early Proterozoic plate subduction zones filled up with heavy deposits. The temperature in their upper parts had never exceeded the temperature of partial melting of water-saturated deposits. Only in the lower portion of the continental lithosphere it might have risen to 1,000–1,200°C and higher (see Fig. 12.2). Neither in Late Proterozoic nor in Phanerozoic had ever again emerged the conditions of "cold" subduction zones. All subduction zones of those epochs had been "hot".

It is known [339] that the stability of all without exception hydrocarbons substantially declines with the increase of temperature and pressure. This occurs at the expense of tearing carbon bonds in long chains of complex hydrocarbon molecules. As a result of such cracking-process, in the system gradually decreases the content of complex hydrocarbons and increases the concentration of simple hydrocarbons. Most stable is methane surviving the heating (at usual pressure) of up to 1,200°C. That is why in the process of sufficiently long-time reaction under high temperature and pressure conditions the entire organic matter eventually converted into methane, hydrogen and free carbon. However, the temperature destruction of hydrocarbons is an endothermal process and might not have resulted in the formation of large-crystalline carbon phases. The released carbon had remained finely dispersed and pulverized.

Whereas for the formation of crystalline forms of carbon had been needed its release through an exothermal reaction resulting in the decline of the system's internal energy. These conditions had been satisfied in a

reaction of merging hydrocarbons with carbon monoxide and carbon dioxide running with energy release, for instance (Simakov, 1985); [11]:

$$CH_4 + CO_2 \rightarrow 2C + 2H_2O + 24.6 \text{ kcal/mole}, \quad (12.16)$$

$$CH_4 + 2CO \rightarrow 3C + 2H_2O + 65.9 \text{ kcal/mole}. \quad (12.17)$$

In a general case, the diamond formation may be explained through reactions of interaction between broad range hydrocarbons with carbon oxides [11, 57, 112, 340]

$$4C_nH_{2n\pm k} + (2n \pm k)CO_2 \rightarrow (6n \pm k)C + 2(2n \pm k)H_2O, \quad (12.18)$$

$$2C_nH_{2n\pm k} + (2n \pm k)CO \rightarrow (4n \pm k)C + (2n \pm k)H_2O. \quad (12.19)$$

Carbon dioxide gas must be released at the expense of thermal dissociation of carbonates in hot parts of the plate subduction zone under endothermal reactions of a (12.1)–(12.5) type. Carbon monoxide, possibly, might have generated also under an exothermal reaction at oxidizing, for instance, wustite to stoichiometry of magnetite

$$3FeO + CO_2 \rightarrow Fe_3O_4 + CO + 8.8 \text{ kcal/mole}. \quad (12.20)$$

Beside hydrocarbons of purely organic origin, in diamond formation might have participated also abiogenous methane generated, for instance, in reactions (12.1) and (11.52) as well as hydrogen released according to reaction (11.4). In the later case the reaction of diamond emergence may be written as

$$2H_2 + CO_2 \rightarrow C + 2H_2O + 42.6 \text{ kcal/mole}. \quad (12.21)$$

Reactions like (12.16)–(12.19) and (12.21) run with energy release, that is why they may cause carbon crystallization (at moderate pressure graphite, at high pressure, diamond).

As an illustration, it is easy to calculate from the formation enthalpy of chemical compounds [341] that under normal PT conditions according to the first reaction (12.16) at combining methane with carbon dioxide gas is released 24.6 kcal/mole of energy and according to

the second reaction (12.17) of combining CH_4 with CO, much more, 65.9 kcal/mole. Under greater pressure and temperature this relationship may be somewhat different but always the enthalpy ΔH_t^0 of reaction products under the first scheme will be lower than under the second (a reminder: $\Delta H_t^0 < 0$). It follows thence that out of the gas mix of CO + CO_2 in the carbon crystallization reaction will be coming CO first and only then, CO_2.

Keeping in mind frequent sulfide, especially pyrrhotine, inclusions in diamonds, sometimes as the cause of diamond formation are proposed the following reactions of carbon release:

$$2FeS + CO_2 \rightarrow 2FeO + S_2 + C, \tag{12.22}$$

and, after S. Haggerty *et al.* [342]

$$2FeS + CH_4 \rightarrow 2H_2S + 2Fe + C. \tag{12.23}$$

Besides, emphasizing an important role of nitrogen in the diamond formation process, S.K. Simakov [337] suggests also this reaction

$$3CH_4 + 2N_2 \rightarrow 3C + 4NH_3. \tag{12.24}$$

All these three reactions (12.22)–(12.24) are endothermal, therefore, might not have led to diamond crystallization (at best they might have resulted only in carbon molecular scattering). Besides, at high temperature a product of reaction 12.24, ammonia is unstable and falls into nitrogen and hydrogen.

Beside hydrocarbons of purely organic origin, in kimberlites, eclogites and garnet peridotites formed from the oceanic crust rocks may be present primitive hydrocarbons, especially methane formed at the expense of thermal dissociation of water over iron and reduction CO and CO_2 in the system to methane.

The dissociation of water over iron is an endothermal reaction and in plate subduction zones of Early Proterozoic might have run according to the following scheme:

$$4H_2O + 3Fe + 5{,}9 \text{ kcal/mole} \rightarrow Fe_3O_4 + 4H_2, \tag{12.25}$$

whereas water dissociation through oxidizing of bivalent (silicate) iron to stoichiometry of magnetite, on the contrary, is an exothermal reaction

$$H_2O + 3FeO \rightarrow Fe_3O_4 + H_2 + 8{,}16 \text{ kcal/mole}. \qquad (12.26)$$

It follows thence that free hydrogen in the foci of diamond-bearing kimberlite melt, most likely, had been formed exactly under reactions of (12.26) type and also at oxidizing of the silicate iron to magnetite. You will recall that the magnetite is a spinel phase of iron oxides, therefore, is most stable in conditions of elevated pressure. As likely as not then, that part of magnetite reaction fringes around crystals of olivine and other ferruginous silicates had formed exactly this way.

Methane synthesis is occurring under exothermal reactions through a simple joining of CO and CO_2 with hydrogen or water [343]. In the presence of catalysts, for instance, nickel, nickel carbonate or native iron, these reactions significantly accelerate and start running already beginning with 250-400°C (although at normal pressure). All these reactions run with heat release, so there are reasons to expect that under higher PT conditions typical of plate subduction zones they might have been running without a catalyst:

$$\begin{aligned} CO + 3H_2 &\rightarrow CH_4 + H_2O + 59.8 \text{ kcal/mole} \\ CO_2 + 4H_2 &\rightarrow CH_4 + 2H_2O + 60.5 \text{ kcal/mole}. \end{aligned} \qquad (12.27)$$

At relatively low temperature of the greenstone metamorphism facies (up to 400-500°C), abiogenous methane synthesis might have run under serpentinization reaction of iron-containing olivines in the presence of carbon dioxide gas (see reaction 12.1). At high temperature (over 660-700°C) this reaction, perhaps, had been running as a side reaction at the formation of pyroxene metasomatic mega-crystals:

$$4Fe_2SiO_4 + 4Mg_2SiO_4 + 2H_2O + CO_2 \rightarrow 8MgSiO_3 + 4Fe_2O_3 + CH_4 + \\ + 43.3 \text{ kcal/mole}. \qquad (12.28)$$

Besides, abiogenous methane had been generated also at direct oxidizing of native iron in the presence of carbon dioxide gas (see reaction 11.52).

It is important to note that due to fractionation of carbon isotopes between CH_4 and CO_2 under reaction

$$^{12}CO_2 + {}^{13}CH_4 \rightarrow {}^{13}CO_2 + {}^{12}CH_4 + 1.02 \text{ kcal/mole}, \quad (12.29)$$

in abiogenous methane, same as in methane of organic origin, had always concentrated mostly light carbon isotope ^{12}C. An illustration of the said may be the fact that the epochs of maximum iron formations accumulation in Precambrian had corresponded with minimum $\delta^{13}C_{org}$ values inherited by the organic matter from the source abiogenous methane [19].

Under reducing conditions of deposit accumulation in Early Proterozoic oceans, the decomposition of nitrogen compounds must have been accompanied by the formation of ammonia and its compounds. For instance, in the present-day Black Sea oozes (its stagnant water is known to experience currently a hydrogen sulfide infection) contain elevated nitrogen concentrations in the form of NH_3. As noted above, ammonia is not a very stable compound ($\Delta H_t^0 = -11$ kcal/mole). That is why, having gotten together with pelagic deposits in hot conditions of plate subduction zone, it had decomposed already at moderate temperature into nitrogen and hydrogen. After that, nitrogen and hydrogen had entered the fluid. Further on, some nitrogen had been sorbed by growing diamond crystals and entered its crystalline grid, and most of it had been probably preserved in the fluid.

Marked here some exchange reactions between carbon and hydrogen-containing compounds must have resulted in the formation of a complex composition in kimberlite fluid phase. Of a special interest in this respect are gas-liquid inclusions in diamonds preserving in a sealed state the composition of those fluids from which they had been crystalized in due season. Conducted by K. Melton and R. Giardini [20, 21] studies of the composition of these inclusions showed that they contained 10 to 60% H_2O; 2 to 50% H_2; 1 to 12% CH_4; 2 to 20% CO_2; 0 to 45% CO; 2 to 38% N_2 and about 0.5-1.2% Ar. Besides, it was found that these inclusions sometimes contained ethylene C_2H_4 (about 0.5%) and ethyl alcohol C_2H_5OH (0.05 to 3%). No free oxygen was ever discovered in such inclusions which is another confirmation of sharply reducing conditions of diamond formation. It is our opinion that this entire specific set of gases is a unique testimony of exogenous (not juvenile) origin of the fluid phase from which diamonds in kimberlites had been crystallized.

Therefore, hydrocarbons needed for diamond formation might have been coming in kimberlites both at the expense of thermolysis of organic matter pulled together with carbonate deposits in plate subduction

zones and due to the reduction of carbon dioxide gas at oxidizing iron and iron-containing silicates. However, in all cases, and this is especially important, carbon in diamonds is only of exogenous origin [11, 57].

For many diamonds are typical notable (up to 0.25%) admixtures of nitrogen entering directly the crystalline grid of this mineral [1, 49]. The proposed theory makes its source understandable. Same as carbon, this element had gotten in the diamonds from the fluid phase of kimberlite and lamproite magmas that had formed in due time at the expense of melting the pelagic deposits pulled at great depths underneath the ancient continents.

Beside gas-liquid inclusions, in diamond crystals are often encountered solid inclusions of depth mineral associations dominated by sulfides. Also found are olivine, serpentine, phlogopite, omphacite, pyrope, almandine, magnetite, wustite, native iron, chromite and some other minerals. Practically all solid inclusions in diamonds are high pressure mineral phases of eclogite or peridotite paragenesis.

Of a certain interest, in our view, is the origin of inclusions in diamonds of the native iron and wustite. As shown above, the native iron concentration in the Early Proterozoic mantle had reached 5–4% (see Fig. 8.2). That is why base and ultramafic rocks of the Early Proterozoic oceanic crust must have contained a notable amount of it. At present time, the telluric iron is rarely found in Precambrian rocks due to its instability against the oxidizing processes that had been evolving in conditions of Earth's crust. Nevertheless, in some cases its remains had managed to be preserved as impregnations and even individual lumps in Early Proterozoic base and ultramafic rocks. For instance, in basalts of Disco Island (Greenland west coast) and also in some areas of Karelia [344, 345]. This allows us to suggest that in the oceanic crust rocks pulled in Early Proterozoic underneath the Archaean continents the native iron had also been present. That had been this iron that could have gotten later in diamond inclusions. As for the wustite, it, most likely, had emerged in the hot portions of the plate subduction zones at the expense of oxidizing the metallic iron due to water dissociation over it.

Based on experimental data of artificial diamond synthesis, the main factors controlling shape and quality of crystals are temperature and pressure of the medium wherein the growth of these crystals is occurring [24]. Thus, based on Giardini and Tydings data [346], at minimum temperature and pressure usually form opaque cubic crystals with a large amount of admixtures and accidental inclusions. At high pressure and temperature, i.e., close to the base of the continental lithosphere under the proposed model had formed transparent, without inclusions octahedral crystals.

Considering the diamond formation under the described scheme, it is surprising not so much the possibility of its formation at the expense of exogenous carbon as the fact of this exceptionally rare accessory mineral not having become a rock-forming mineral in conditions of excess of the source carbon-containing compounds (CO_2 and CH_4). There may be two explanations. First, in the overheated and apparently exceptionally liquid kimberlite melt, the diamonds as a heavier fraction (density of about 4 g/cm^3) must have sunk in the focus of kimberlite magma, must have gotten at the sub-lithospheric levels and carried from there by the convective flows all over the mantle. Second, it is as likely as not that the diamonds had crystallized mostly under reaction (12.17) but the amount of carbon monoxide in the system had been limited. This perhaps is also an explanation of exceptional tardiness of the diamond forming process: they had managed over the lifetime of the kimberlite magma foci (i.e., in 1-2 BY) to form only small and even miniscule crystals of this still quite mysterious mineral.

Thus, the suggested theory of kimberlite- and diamond-formation answered all the questions asked in Chapter 2 by J. Dawson. His first question may now be answered with sufficient certainty. Carbon, phosphorus, nitrogen and most other lithophilic elements in the kimberlites as well as the kimberlites themselves, are of exogenous origin. The second paradox mentioned by J. Dawson (calcite domination in kimberlite carbonate phase) also finds confirmation in the suggested theory. The point being that calcite contents in the source deposits had been higher, whereas the magnesite component in the presence of silica and alumina had been spent for the formation of metasomatic olivines, pyroxenes and garnets (pyrope and almandine), for instance, under reactions (12.9)–(12.11). As for the question of why some kimberlites include diamonds and some others do not, one may assume that the depth of kimberlite melt formation foci and processes of isolating diamond crystals in the primary magmatic foci had played certain role. Besides, not a small role had been played by the rate of kimberlite magma rise. At a slow rate diamonds had had time to dissolve in the H_2O+CO_2 fluid or to convert into graphite. There is a quite definite answer to the fourth question: the diamonds are not xenocrysts but typical phenocrysts. An answer to the next question may be as follows. The kimberlites and their affine rocks are found only in mostly Archaean age continental crust because the formation of their begetting melts had occurred in Early Proterozoic when the Archaean continental plate thickness had grown to 200–250 km. A response to the sixth question is as simple as to the first one: water had been pulled to the formation depth of kimberlite melts together with pelagic deposits of Early Proterozoic oceans. Further on, carbon isotope shifts in the diamonds are defined by mixing proportions of

organic and carbonate carbon at crystallization of the diamonds in the kimberlite or lamproite melt foci. A response to the question of the mechanism of tectonic movements deforming the rocks of depth inclusions in the kimberlites is also simple: this is the process of lithospheric plate subduction and friction of rigid plates about one another. And at last, the answer to the last, the ninth of the questions set by J. Dawson about the nature of the energy leading to melting the kimberlite magma is also simple. This is the geothermal heat of coming from the mantle depth in the magma foci easily fusible kimberlite compounds. The cause and effect connections acting in the process of kimberlite formation, have been reviewed in detail above.

13

Carbon's Depth Cycle

The evolution of oceans is closely tied with the processes of Earth's crust conveyor benefication by numerous chemical elements and compounds which are being accumulated on its surface in convergent and divergent Earth areas. Studies of carbon geochemical cycle between different reservoirs traditionally describe the phenomena of its transformation in the crust, hydrosphere and atmosphere where an important role is played by living organisms [347–350]. The issues of this element isotopes' behavior in the geochemical cycle have also been reviewed in detail [53, 351]. A number of scientists [352–354] proposed an interesting and ambiguous option of the nature of carbon depth geochemical cycle with involvement of experimental data. These studies discuss possible mantle flows and carbon reservoirs brought in from contact zones of Earth's core and lower mantle at the expense of its withdrawal by ascending plumes in the presence of water and oxygen.

The author conducted studies of patterns in crust-mantle interaction of the material-structural complexes composing these geospheres. These studies enabled the substantiation of availability of carbon geochemical cycle's depth branch without involving mechanisms of its generation in the external core and lower mantle and also without any substantial amount of water and oxygen in the latter [12]. The major supplier of carbon forming its crust-mantle branch in the global cycle is sedimentary complexes deposited on the sea floor. They contain a great number of this element compounds and are represented by carbonate deposits of biogenic and chemical origin as well as by organic matter from pelagic and clastic sediments and carbonic shales carried away from continental margins. As shown above, sedimentary complexes pulled in plate subduction zones undergo a number of alterations and immerse in the sublithospheric mantle. There, they are almost completely destroyed, remelted and mostly carried up as magmas and fluid solutions. A part of carbon compounds and its monomineral fraction are capsulated, reach the sublithospheric levels of the mantle and are transferred by upper mantle convective flows in the

N. O. Sorokhtin (ed.) The Origins of Natural Diamonds, (397–410) © 2019 Scrivener Publishing LLC

discharge areas under the lithospheric plate rift zones. There, as new compounds they again get in Earth's hydrosphere (Fig. 13.1).

Dehydration and anatexis processes of the oceanic crust occurring in plate subduction zones develop according to a rather complex multistep scheme. Spatial-temporal variability of metamorphic transformation is in that the rock associations of the subducted oceanic lithospheric plate experience progressive metamorphism in the contact zone with the obducted continent. At that they sequentially run through transformation stages from the lower to the upper. A mineralized and gas-saturated fluid formed in this environment is moving up through faults and, cooling down, causes retrograde contact-metasomatic alterations in the enclosing rocks. Numerous ultramafic protrusions and ophiolites, having run through the peak of alterations, are also experiencing retrograde processes. Along with this, sedimentary sequences of the continental margins are running-off into the ocean, mixing with pelagic deposits and together with them are pulled in the plate subduction zone. Clastic deposits substantially increase carbon influx into the general balance and experience progressive metamorphism, being bathed with saturated hydrothermal solutions. In the process of metamorphic transformations of the oceanic crust rocks olivine, enstatite, magnetite and other refractory minerals, and also garnets emerging at depths of the eclogite transition are mostly removed from the system together with the lithospheric plate immersing in the mantle. At this, water fluids, silica and lithophilic

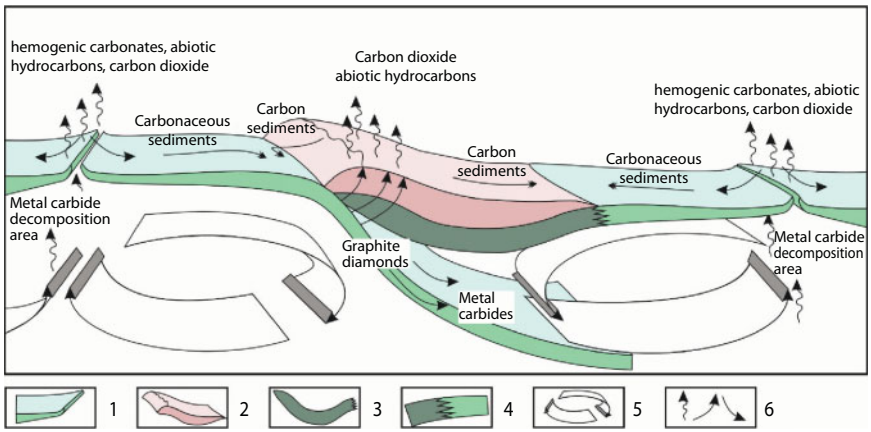

Fig. 13.1 Crust-mantle cycle of carbon in the ocean. 1. Oceanic lithosphere, 2. Continental crust, 3. Continental subcrustal lithosphere, 4. Transition zone of subcrustal lithosphere transition to oceanic type lithosphere, 5. Direction of convective flows in the upper mantle, 6. Direction of carbon compounds migration.

compounds are assimilated by the silicate melts forming in plate subduction zones and mostly are squeezed up.

The deposit and sedimentary rock melting in subduction zones is mostly occurring at the expense of dissipating viscous friction energy within sequences and friction on contact of the lithospheric plates. Added to this is the value of the depth heat flow permeating continental lithospheric plates and the water-saturation of sequences lowering melting temperature. Therefore, temperature in the gap between the plates approximately corresponds with the geotherm of a continental plate or a bit higher. Then the formations having gotten in the subduction zone begin to melt only at those depths where the continental plate geotherm intersects with the deposit melting temperature (see Fig. 2.1). At this, melting temperature of most silicates in the presence of water, with pressure increase to 5-10 kbar sharply declines to 600-700°C [208]. Water-saturated carbonates [355] and many other compounds behave similiarly. The marked patterns enable us to conclude that the aluminosilicate water-saturated deposits begin melting already at depths around 50–70 km and the carbonate ones, around 80 km.

Deeper than the critical level of intersecting the continental geotherm with the melting start curve of a sedimentary matter, the degree of sedimentary rock melting sharply increases. That is why at great depths must occur differentiation of the formed melts and their separation by density. The heavy ferruginous and sulfide fractions go down and eventually, having submerged in depths of the convecting mantle, are gradually assimilated by its matter. Whereas the light fractions composed of the separated fluids, carbonate and silicate melts have no possibility to rise up and are accumulated (conserved) in the bottom horizons of the continental plates (Figs. 12.1, 13.2) gradually forming there the foci of alkali-ultramafic, carbonatite and lamproite-kimberlite magmas.

Within the transition zone from the base of the continental lithosphere to the convecting mantle, at similar chemical parameters of the medium, no significant temperature and density hops are observed. This boundary is rather marking a phase transition of the mantle matter from the rigid state to the plastic one. It is expected that in this zone degassing processes of the oceanic crust and fragments of sedimentary sequences are not running to the full extent so the remaining part of water, carbon, carbon dioxide gas and some other volatile components may immerse in the convecting mantle.

Pulling carbon containing compounds in a subduction zone results in a process of their multistep decomposition and transformation as well as in the release of the monomineral carbon. At depths of about 120-150 km is observed phase transition from graphite to diamond, below which the

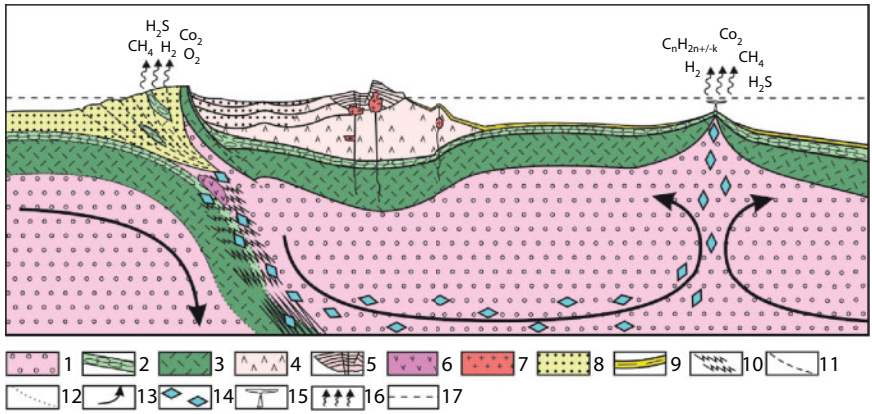

Fig. 13.2 Abiogenic hydrocarbon generating mechanisms in convergent and divergent environments. 1. Mantle asthenosphere; 2. Oceanic type crust; 3. Oceanic lithosphere; 4. Island arc type structure-matter complexes; 5. Caldera type sedimentary-volcanogenic complexes; 6. Depth foci of carbonatite and kimberlite magma melting; 7. Granitoid intrusions; 8, 9. Sedimentary complexes: 8. Undifferentiated complexes of oceanic and island arc type deposits, 9. Oceanic deposits; 10. Zone of maximum stress-metamorphism manifestation; 11. Generalized faults; 12. Zone of partial disintegration of a subducting lithospheric plate; 13. Convective flow direction in the mantle; 14. Capsulated solid and gas-liquid inclusions of the crust composition disintegrated rocks; 15. Hydrothermal buildups on seafloor; 16. Degassing direction of chemical compounds; 17. Ocean level.

stability area of the latter is positioned. Exactly at such depth's diamonds are crystalized and emerge characteristic mineral associations in eclogites and garnet peridotites of diamond-pyrope depth facies [23]. On the other hand, it is known [34] that at depths about 350 km the rhomboid olivine must transition in a denser cubic modification (spinel phase), ringwoodite. However, this mineral has not been encountered anywhere in kimberlite or diamond inclusions which, apparently, is limiting the maximum formation depth of diamond-bearing rocks by 300 km [1] (Fig. 2.1). By synthesizing these data, it was possible more or less certainly to outline the area of equilibrium existence in the mantle of diamond-bearing eclogites and garnet lherzolites [1, 23, 38]. It was found to be quite wide. At pressure (P) about 50 kbar, the temperature range is 1,120-1,380°C, and at 70 kbar, 1,300-1,500°C. For garnet lherzolites this area is no narrower and is limited by temperatures 900-1,400°C (Fig. 2.1).

The quoted data enable a suggestion that at depths exceeding 250-300 km carbon again transits in the graphite phase and, getting in the metal carbide stability area, forms various compounds with them. A small number of minerals - carbides are known in nature which are found in meteorites, kimberlites, metamorphosed ultramafic rocks and in shungites.

Best known are cohenite $(Fe,Ni,Co)_3C$, moissonite (SiC), tantalum carbide (Ta,Nb)C, niobium carbide (Nb,Ta)C, khamrabaevite (Ti,V,Fe)C as well as compounds of vanadium (V_8C_7 and V_2C) and chromium (Cr_2C_3). So limited number of minerals - metal carbides is due to their depth origin and the penchant to decompose in low thermobaric conditions in the presence of water. Most likely, in the upper mantle minerals - metal carbides are more common, therefore, may exist carbides of calcium, aluminum, manganese, iron and a number of other metals.

All chemical reactions in plate subduction zones are irreversible, run with heat absorption or release and under various redox conditions. An important role in the implementation of all listed processes belongs to geological time eventually bringing physicochemical parameters of a fold system evolution in the state of equilibrium.

The present-day sedimentary sequences at the seafloor contain up to 20-40% water and in diagenetized varieties the content drops to 10-15%. At this, in shaly rocks form hydromicas (illite, smectite, montmorillonite, kaolin and diaspore). They also include a large amount of organic matter (0.5 – 1.0%).

At early stages of metamorphic transformations, deposits and sedimentary rocks pulled in a subduction zone undergo processes of intense dehydration. First, pore (free) water is lost, then crystallization water after which in them is evolving a complex series of endothermic (associated with heat absorption) metamorphic transformations accompanied by the release of water, CO_2, silica, alkali (especially potassium) and lithophilic elements. In the maximum compression zones, the rocks compact and partially seal the formed solutions creating high-pressure fluids and expanding the stability field of water-containing minerals.

Most of the so formed fluid flows is moving up and in the direction, perpendicular to the long axis of the folding from an area of high pressure into zones of tectonic shadow. At the existence of tangential pressure gradient, in a permeable medium will be always observed their movement and transition from one metamorphic facies to the other one (Fig. 11.3). Such process unavoidably results in the disconnection and isolation of large and small volumes of the matter, capsulation of crustal melts, metamorphosed crustal rocks, dispersed matter, fluid solutions and gas-liquid inclusions. At this, in the sublithospheric mantle, gas-liquid inclusions become a supercritical fluid and are characterized by the disappearance of differences between these two phases. In conditions of the medium viscous flow, the "capsules" are transferred in the convecting mantle and are spread over great distances, being torn from the lithospheric plate immersing to the core or jointly displacing into the area of an ascending convective flow in case of its flattening (Fig. 13.2).

The formation of hydrothermal solutions is closely tied with the processes of progressive stress-metamorphism and of overheating of a water-saturated rock system. Carbonates that get in a plate subduction zone are transformed and destroyed with the release of CO_2. This causes bonding of some alkali in silicate fazes and some others, in carbonates. Thus, as siderite formation heat out of its composing oxides is equal to 22.3 kcal/mole, magnetite 23 kcal/mole and calcite 42.6 kcal/mole, the carbonate dissociation might have run only in hot areas of a plate subduction zone at 800-100 to 150 km [55] (see reactions 12.1-12.5). Carbon dioxide released at this dissolved in the formed melts and entered water-carbon dioxide fluid.

In condition of high pressure (40–50 kbar) typical of lower parts of the continental plates, garnets, corund and calcite form with the release of carbon dioxide gas (see reactions 12.10 and 12.11). Deeper yet, carbonate disintegration occurs accompanied by oxidizing of bivalent iron with the formation of high-density crystalline magnetite structure and CO_2 reduction to carbon monoxide as in reaction 12.14.

At depths corresponding with continental lithosphere base boundary, at even greater temperature and pressure the carbonate disintegration possibly runs in the presence of olivine or pyroxene with the release of free carbon dioxide, formation of monticellite, perovskite, periclase, magnetite and carbon monoxide (reactions 12.12-12.14).

According to [356], in the presence of carbon dioxide (CO_2) and hydrogen sulfide (H_2S), olivine (fayalite) forms marcasite (FeS_2), magnetite (Fe_3O_4), quartz, water and abiogenic methane:

$$4Fe_2SiO_4 + 4H_2S + CO_2 = 2FeS_2 + 2Fe_3O_4 + 4SiO_2 + 2H_2O + CH_4 \uparrow \quad (13.1)$$

and even heavier hydrocarbons (ethane):

$$3.5Fe_2SiO_4 + 14H_2S + 2CO_2 = 7FeS_2 + 3,5SiO_2 + 11H_2O + C_2H_6 \uparrow . \quad (13.2)$$

At depths greater than 120-150 km, diamonds form by way of carbon reduction according to the interaction reactions of carbon monoxide and carbon dioxide gas with methane or other hydrocarbons of organic and abiogenic origin pulled to great depths through the subduction zones together with the deposits. Their formation mechanism

was reviewed in detail in Chapter 12, so we will not be dealing with this issue here.

It is a known fact that the oceanic deposits and sedimentary rocks brought in from the continental margins often include elevated concentrations of organic matter. Having got in plate subduction zones, the organic matter is subjected to thermolysis and hydrolysis and rapidly runs through all stages of transformation into hydrocarbons, nitrates and ammoniac compounds. Part of these mobile compounds together with pore water is squeezed from the plate subduction zone in its top horizons. But some part thereof, together with the terrigenous rocks, continue their way in depth of the mantle.

In the present-day subduction zones where water-saturated silicate melts are easily withdrawn from plate friction zones, the temperature of magma formation in them rapidly rises to the level of basalt melting. That is why hydrocarbons are unable to penetrate through such zones deep in the mantle and are decomposed with the formation of scattered graphite.

It is a known fact [357] that stability of all hydrocarbons without exception substantially declines with growing temperature and pressure. A result of this process is a gradual decline in the system of the concentration of complex hydrocarbons and an increase in the concentration of simple hydrocarbons. Methane is most stable; it sustains heating (at a usual pressure) up to 1,200°C. That is why at long enough reaction in conditions of high temperature and pressure the entire organic matter eventually may turn into methane, hydrogen and a free carbon.

For the formation of crystalline form of carbon are necessary exothermic chemical reactions resulting in lowering the internal energy of the system (12.16-12.21).

In publications [358, 359] the possibility was experimentally proven of forming complex hydrocarbons up to $C_{10}H_{22}$, using the solid iron oxide, marble and water. This reaction becomes possible at temperature 1,500°C and pressure over 30 kbar, which corresponds with the depths of over 100 km.

As was shown in the previous chapter, descending in the convecting mantle below diamond stability level, carbon and some capsulated solid mineral compounds and gas-liquid inclusions of degraded sediment complexes may not form large accumulations. Most likely these are numerous but small (mm, fractions of mm and molecular compounds) scattered matter particles forming a stable geochemical train of crustal trend in the mantle expanding in the convective flow displacement plain [12].

At depths about 200-300 km carbon may interact with hydrogen under the reaction:

$$2nC + mH_2 \rightarrow 2CnHm, \tag{13.3}$$

where metrices n and m are coefficients.

It is possible that exactly due to this reaction in diamonds are encountered liquid inclusions of complex hydrocarbons, up to alcohol. Further on, the derived compounds enter reaction with oxides of various metals resulting in carbides:

$$(Me)O + CnHm \rightarrow (Me)C + H_2 + H_2O, \tag{13.4}$$

where (Me) is a metal.

Reduction of metal oxides by carbon with the formation of carbides in the oxygen deficiency conditions may run so:

$$(Me)O + C \rightarrow (Me)C + CO. \tag{13.5}$$

For instance, at temperature 700-800°C, the formation of molybdenum carbide in the presence of methane and hydrogen is running according to reaction:

$$Mo + H_2 + CH_4 \rightarrow MoC + H + CH. \tag{13.6}$$

In a similar temperature range may form lithium carbide at the expense of its clinkering with calcite which is present in abundance in plate subduction zones (reactions 7 and 8) [360].

$$Li_2CO_3 + 4C \rightarrow Li_2C_2 + 3C. \tag{13.7}$$

At temperature above 900°C, carbon forms a solid solution with iron with formation of iron carbides (Fe_3C and Fe_2C).

$$3Fe + C = Fe_3C. \tag{13.8}$$

In mantle composition rocks, in the presence of carbon occurs iron reduction and the formation of its telluric phase. Under similar conditions forms also mineral cohenite $(FeNiCo)_3C$.

Immersing in the mantle, metal carbides had been captured by convective flows and eventually brought in the area of ascending flows. There, they had been getting in sub-rift zones and decomposing with the formation of a new generation hydrocarbons [12].

In the process of lithospheric plate spreading in the oceanic rift systems open fractures had been emerging through which basalt melts had risen from the mantle on the surface. The water-covered oceanic lithosphere had been hydrated and in its lower horizons had formed the serpentine layer at the expense of recrystallization of olivine containing ultramafic rocks. The penetration depth of the oceanic water had been limited by lithostatic pressure of about 2.3 kbar. Deeper than this mark the serpentine had become very plastic, healing all fractures emerging in the thickness of the lithosphere and preventing water from penetrating deeper [112]. Higher than that all structure-material complexes of the oceanic lithosphere had been substantially hydrated and containing in hydrosilicates at least 5% of bonded water of the total mass. At this, serpentinites had contained at least 10-11% of bonded water.

Rift zone hydrothermal systems, very common at seafloor, had brought in the hydrosphere huge amount of endogenous matter [361, 362] which had been generated in the oceanic lithosphere and upper mantle. A result of it had been brought out silica, calcium, magnesium, manganese, metal sulfides, methane, carbonates, sulfates and numerous other compounds. In the depression structures in the north of Juan de Fuca ridge in the Pacific Ocean are described manifestations of methane (CH_4), ethane (C_2H_6), propane (C_3H_8), butane (C_4H_{10}), benzene (C_6H_6) and toluene (C_7H_8) in association with H_2O and CO_2 [356]. In hydrothermal fields of Mid-Atlantic Ridge are discovered hydrocarbon shows of methane (CH_4), ethane (C_2H_6), ethylene (C_2H_4), propane (C_3H_8) and butane (C_4H_{10}) [363]. It is only natural to expect that such variety of hydrocarbons could not have been generated in the mantle and all they are products of the crustal (exogenous) matter decomposition or had been formed in processes of near-surface alteration of the mantle composition rocks.

The generation of carbonic compounds in rift zones might have been occurring in two major ways. The first one had been the transport by the mantle convective flows of capsulated and scattered fragments of crust matter compounds and monomineral phases from a subduction zone. The second one had realized due to hydration of the oceanic lithosphere mantle rocks and their serpentinization (Fig. 13.2).

Having moved in sub-rift zones above the ascending convective mantle flows, metal carbides, capsulated solid particles of the crustal matter and gas-liquid inclusions had reached the oceanic lithosphere hydration

levels (Fig. 13.3). Having gotten in the stability area of mineralized water fluids, carbides had easily decomposed with the release of various hydrocarbons and metal hydroxides. At this, it should be noted that the melting temperature of many carbon with metals compounds much exceeds the upper mantle temperature (≈1,300 – 1,600°C) and is in the range of 1,000 – 4,000°C. We believe this fact is of extreme importance and indicating that in a practically "dry" mantle, metal carbide compounds might have been in the state of a stable equilibrium and preserved geochemical markers of their exogenous origin indefinitely. For instance, having gotten in near-surface rift zones and subjected to hydrolysis, calcium and sodium carbides decompose with the release of acetylene [360]:

$$CaC_2 + 2H_2O \rightarrow Ca(OH)_2 + C_2H_2 \uparrow, \tag{13.9}$$

$$Na_2C_2 + 2H_2O \rightarrow 2NaOH + C_2H_2 \uparrow. \tag{13.10}$$

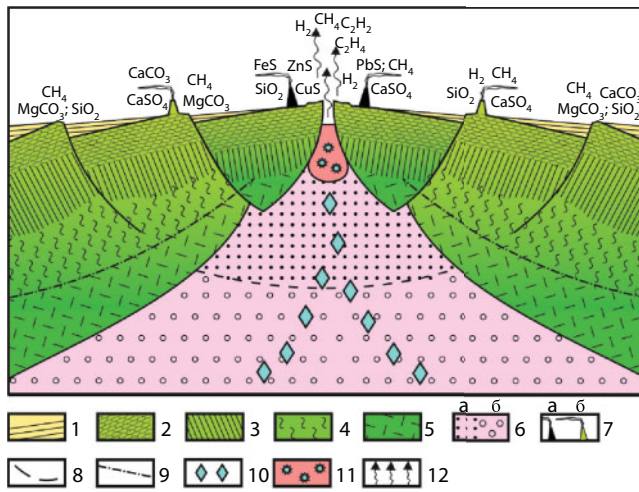

Fig. 13.3 Geochemistry of hydrothermal processes and generation mechanisms of carbon compounds in the rift zones of mid-oceanic ridges. 1. Deposits; 2. Basalts (pillow lavas); 3. Dolerite dykes (dyke in dyke complex); 4. Serpentinite layer; 5. Subcrustal lithospheric layer; 6. The mantle: a. A magmatic focus under the crest of mid-oceanic ridge, b. Asthenosphere; 7. Black (a) and white (b) «smoker» buildups; 8. Oceanic water movement direction in the oceanic crust; 9. Critical level of water stability; 10. Metal carbides and capsulated solid mineral compounds and gas-liquid inclusions of dehydrated sedimentary complexes brought in from a subduction zone; 11. Decomposition area of metal carbides; 12. Degassing of metal carbide decomposition products.

Similar reactions had been running at decomposition of carbides of sodium, potassium (K_2C_2) and a number of other metals. In the presence of metals, the acetylene had been hydrated and might have passed in ethane in two stages:

$$C_2H_2 + H_2 \rightarrow C_2H_4 + H_2 \rightarrow C_2H_6 \uparrow . \qquad (13.11)$$

It is important to note that under usual conditions hydrolysis processes of alkali metal carbides are running highly violently and result in an explosion at their rapid hitting a large volume of water. However, in geological systems these processes had been running exceptionally slowly (hundreds of thousands and millions of years), in a sub-solidus medium, at relatively high pressure (a few kbar) and in the presence of insignificant amount of a free water. This assures certainty of a possible normal running of these chemical reactions.

Thus, the aluminum and manganese carbide hydration is running with the release of methane:

$$Al_4C_3 + 12H_2O \rightarrow 4Al(OH)_3 + 3CH_4 \uparrow, \qquad (13.12)$$

$$Mn_3C + 3H_2O \rightarrow 3Mn(OH)_2 + CH_4 + H_2 \uparrow . \qquad (13.13)$$

Similarly are running reactions of beryllium and lithium (BeC_2) and (Li_2C_2) carbide decomposition. Emerged after the reaction (13.13) manganese hydroxide is easily oxidized in the presence of oxygen which is available in water in sufficient amounts. The reaction is running on a two-step scheme with resulting pyrolusite:

$$2Mn(OH)_2 + O_2 + H_2O \rightarrow MnO(OH)_2 \rightarrow MnO_2 . \qquad (13.14)$$

The decomposition of iron carbide occurs with the ethylene release, however, this reaction most likely had not taken place in nature commonly as the major mass of iron had tended to immerse in lower parts of the mantle and had not formed any perceptible amount of carbides which then would have gotten in the oceanic rift zones. Nevertheless, such reaction is possible:

$$2FeC + 3H_2O \rightarrow Fe_2O_3 + C_2H_4 . \qquad (13.15)$$

The hydration processes of the mantle's near-surface levels in the rift systems had resulted in chemical reactions of rock recrystallization and formation of carbonate and siliceous compounds which had been carried from the depths of the oceanic crust and deposited on the seafloor. All reactions had been irreversible and running with energy release. The majority of them had been reactions of hydrating olivine-containing oceanic crust rocks bonding carbon dioxide gas (CO_2) and forming chemogenous carbonates (see reactions 10.7 and 10.7').

Due to processes described by these reactions in the ocean is continuously brought the source material of normal life activity of skeletal organisms (corals, mollusks, foraminifers and coccolithophorids); the source material having been the dissolved chemical carbonates of biogenic origin rocks.

At hydration of olivines in rift zones, in the process of oxidizing bivalent silicate iron to trivalent state, in the presence of carbon dioxide gas had formed abiogenic methane (reaction 10.9).

Most of formed methane had been oxidized (had served a food base) by methane-consuming bacteria which had participated in the formation of the organic matter (see reaction 10.33).

Part of methane had been brought in the atmosphere, some amount of these volatile compounds might have been preserved in the oceanic deposits and might have formed hydrocarbon gas hydrate accumulations [299].

The mantle matter rising to the surface had contained insignificant amounts of metallic iron (Fe). It had been oxidized by water and generated abiogenic methane and further on had bonded with carbon dioxide gas (CO_2) and formed iron bicarbonate well soluble in water (see reaction 10.4):

$$4Fe + 2H_2O + CO_2 \rightarrow 4FeO + CH_4 + T^{\circ}C, \qquad (13.16)$$

Studying processes of crust-mantle carbon cycle, the issue of its content in Earth's mantle must not be missed. This issue cannot have a unique answer, its solution centers around finding indirect indications that enable finding it with various levels of reliability. Thus, in igneous rocks of base composition the dispersed carbon had very low concentration of 10 to 100 g/t and the deficit of heavy isotope $\delta^{13}C = -22$ to $-27‰$. At this, carbon contained in Earth's crust is heavier, $\delta^{13}C = -3$ to $-8‰$ [52], and included values are typical of isotope shift parameters of diamonds. Tholeiite basalts of the oceanic rift zones contain 20 to 170 g/t of carbon with the isotope shift about –5‰ [258]. At this, two factors must be taken into account which substantially decrease the quoted parameters of the free carbon in Earth's mantle. On the one hand, it had been there in atomic state and had entered

the silicate crystal grid [256]. On the other hand, some part of it had been a product of transfer by mantle convective flows from the plate subduction zone in the rift systems and had participated in the crust-mantle cycle of the exogenous carbon.

The quoted data indicate that in Earth's mantle might have been contained disappearingly minuscule amount of carbon and its total concentrations might have been substantially lower than the accepted ones. After [73], Earth's crust carbonates include about $3.91 \cdot 10^{23}$ g of bonded CO_2 and about $1.95 \cdot 10^{22}$ g of the organic carbon (C_{org}). A substantial part of this matter had been deposited on the seafloor and continental slopes and had participated in the conveyor process of the carbon crust-mantle cycle together with lithospheric plate drift and with the formation of convergent and divergent structures on their boundaries.

Conspicuous is the fact that in rift zones is observed a wide range of hydrocarbon gas manifestations between methane (CH_4), ethane (C_2H_6) and to propane (C_3H_8) and butane (C_4H_{10}). In and of themselves, complex hydrocarbons in the free state at high PT conditions are unstable and tend to disintegrate into simpler ones, up to methane (CH_4). This indicates that the generation of mentioned compounds had happened in the near-surface and low-temperature conditions of the medium, not due to their release from the deep mantle. Apparently, this diversity of hydrocarbon compound composition may be explained by the fact that in conditions of high temperature and pressure in dry mantle metal carbides remained stable, their decomposition had begun only at reaching by them the hydration level, i.e., lower than 400°C.

Jumping ahead, it must be noted that in the rift zone, along with a wide range of forming hydrocarbon gases, is also observed the effect of intensive fractionation of carbon isotopes whose value range may widely vary. The reason for that was that along with *in situ* processes, carbon from subduction zones had been brought in here by the convective flows. This carbon had its own isotope parameters and belonged to a different genetic type. For instance, it may not only distort the radio-carbon data analysis but also lead to obtaining inexplicable age values.

The processes we have studied enable a conclusion that carbon crust-mantle cycle is associated with the formation of this element under some geodynamic conditions and its transfer by the mantle convection under different conditions. As a result of this, it is subjected to a multistage transformation from the chemical state to biogenic one and back, and to immersion in the mantle on levels of its convective stirring and a release on the surface through the rift zones (Fig. 13.1). Practically the entire carbon at this has exogenous origin. This process is closely tied with

the crust-atmospheric carbon cycle as its primary supplier are carbon dioxide gas and transformation products (carbides, carbonates, hydrocarbons, organic matter). Together, they form the global cycle of carbon in the nature.

The amount of thus generated abiogenous origin hydrocarbon gases cannot provide for the formation of large gas and oil fields as a substantial part thereof is released in the atmosphere. Only a small amount of hydrocarbon compounds might have been deposited with the oceanic sediments and formed in them gas hydrate accumulations. It is suggested that the proposed mechanism of carbon depth transformation, including the formation of CH_4, may be used for the explanation of CH_4 origin with radiocarbon age much younger than the present-day one [364]. This is important for a broader understanding also of the nature of a bubble gas massive surges discovered on the shelf of East Arctic seas [365] which is controlled by the state of the underwater permafrost [366].

Among major conclusions of the conducted studies is that there is no need to involve massive water amounts for the implementation of the crust matter physicochemical transformations in the mantle asthenosphere. The data in the article enable a conclusion that the concept of global carbon cycle first proposed in the 1920s by the Academician A.E. Fersman should be expanded with inclusion in it the processes of the mantle carbon transfer from subduction zones in rift systems. Therefore, the crust-mantle component should be added to a conventional branch of carbon crust-atmospheric cycle. The manifestation scale of the crust-mantle brunch of carbon cycle is most likely not very large although numerous small and thinly scattered, up to the atomic dimension, exogenous matter and dispersed carbon particles may form a stable geochemical train of a crustal type in the mantle spreading on the movement plain of convective flows. An indirect judgment about the manifestation scale of this process may be made based on degassing volumes of hydrocarbon and carbon dioxide gases and also hydrogen and its compounds in Earth's crust rift systems.

14

Isotopic Geochemistry of Diamonds and Kimberlites

It follows from the reviewed diamond formation model that the entire carbon had been coming in the kimberlites only from the oceanic crust and deposits. In eclogites, most of the carbon also may have been getting with deposits that have been filling in due time the inter-pillow gaps in ancient lava flows of underwater basalt eruptions. However, some part of carbon in eclogites had been inherited from the carbonates that had emerged at hydration of the source basalts, for instance, under (11.1) type reactions. As opposed to this, the entire carbon might have gotten in garnet peridotites, remnants of the third oceanic crust layer (see Fig. 8.1), only in the process of mantle rock hydration by the oceanic water saturated by carbon dioxide gas. At this, the carbonate formation had been purely chemogenous under the serpentinization reaction (10.7). In the presence of plagioclases and pyroxenes this reaction must have been accompanied by the emergence of pyrophyllite and calcite

$$\underset{\text{anorthite}}{CaAl_2Si_2O_8} + 6\underset{\text{enstatite}}{MgSiO_3} + 5H_2O + CO_2 \rightarrow \underset{\text{pyrophyllite}}{Al_2[Si_4O_{10}](OH)_2} +$$
$$+\underset{\text{serpentine}}{Mg_6[Si_4O_{10}](OH)_8} + \underset{\text{calcite}}{CaCO_3} \qquad (14.1)$$

At elevated temperature in plate subduction zones, hydrosilicates had again dehydrated and part of carbonates had dissociated under reactions (12.1–12.5).

Various carbon sources in diamonds must have certainly resulted in the emergence in them broad variations of carbon isotope composition. According to E.M. Galimov [367], $\delta^{13}C$ variation in diamonds change over a wide range between +2.7 and –34‰; however, the absolute majority of diamonds in kimberlite diatremes in terms of $\delta^{13}C$ variations are in the

N. O. Sorokhtin (ed.) The Origins of Natural Diamonds, (411–432) © 2019 Scrivener Publishing LLC

range between –8 and –3‰ and as a rule had not ventured outside of –10 and –2‰ [368]. It is noted in a publication [369] that in most cases such variations are between –5 and –9‰ with the maximum and minimum value –0.5 and –31.9‰. O.D. Zakharchenko and E.M. Galimov emphasize that in some kimberlite diatremes are encountered diamonds with abnormally high fraction of light carbon isotopes, and such diamonds with $-10‰ > \delta^{13}C > -22‰$ compose 37%. It is noted in a publication [370] that sometimes two maximums are identified on the curve of isotope distribution: one of them appropriate to normal diamonds with $\delta^{13}C \approx -6.8‰$, and another one, to light diamonds with $\delta^{13}C \approx -20.9‰$ (Figs. 14.1 and 14.2).

The experiments of carbon dioxide reacting with alkali silicate melts at 1,200–1,400°C and pressure 5 to 30 kbar indicated that under pressure of about 20 kbar emerge two immiscible melts, the silicate and carbonate ones. At this, fractionation of carbon isotopes does not exceed 2.4‰ [371], whereas in diamonds, observed carbon isotope shifts are greater approximately by one order of the magnitude. This indicates the operation of a different and more efficient carbon fractionation mechanism in the process of their crystallization. From the position of our model, the quoted carbon isotope variations are relatively easy to explain. The entire carbon in the natural diamonds is of exogenous origin. At this, its noticeable enrichment

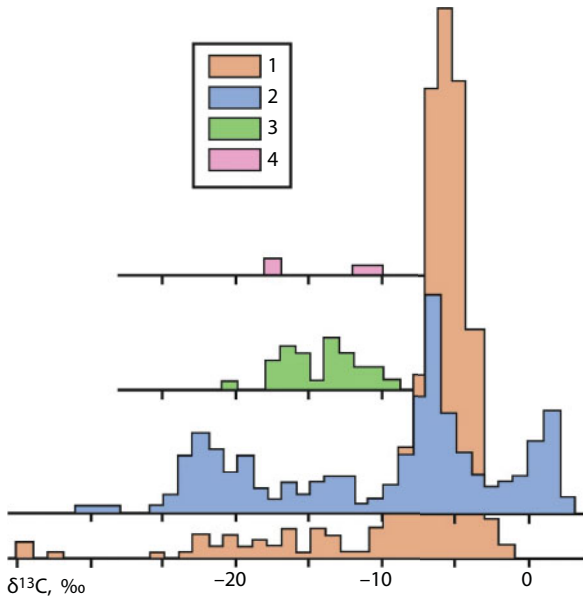

Fig. 14.1 Distribution of carbon isotope composition for various types of their sources [367]: 1. Kimberlite diatremes; 2. Placers; 3. Impact craters; 4. Metamorphic rocks.

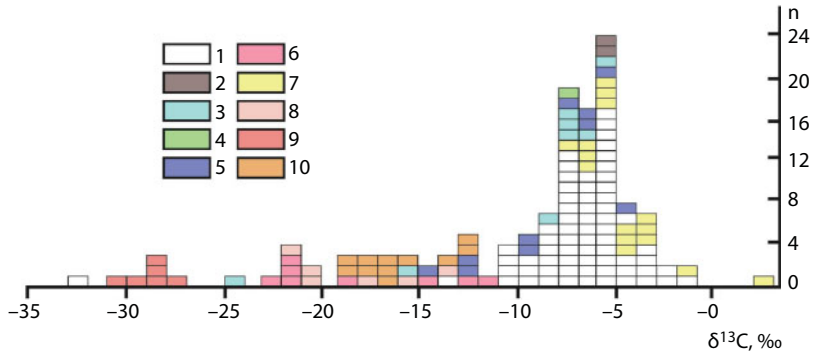

Fig. 14.2 Carbon d^{13}C isotope composition distribution histogram in diamonds and carbonado [3]. Diamonds: 1. From kimberlites of Siberia, Africa, North America; 2. From meteorites; 3–8. Placers (3. Urals, 4. Timan, 5. Sayan, 6. Ebelyakha, 7. Africa, America, Australia, 8. Ukraine); 9. Brazilian carbonado; 10. Cosmogenic diamonds; n is the number of measurements.

in the light isotope C^{12} occurs at the expense of involvement in the diamond formation reaction of the organic carbon C_{org} and carbon of the abiogenous methane which had undergone fractionation under reaction (10.13).

The very idea of C_{org} participation in diamond formation is not new. At various times it has been brought out by V.V. Kovalsky *et al.* [372], E.V. Frantsesson, F.V. Kaminsky [373], V.S. and N.B. Sobolevs [51], F.V. Kaminsky [37] and other authors, and for the graphite, Sv.A. Sidorenko and A.B. Sidorenko [374] and many others. However, it was possible to quantitatively substantiate this suggestion only after a consistent application of the lithospheric plate tectonics theory to the issue of diamond origins [11, 54, 55, 57, 375].

It follows from reactions (12.16)–(12.19) of the diamond (and graphite) formation that their isotope composition must substantially depend on the composition of carbon compounds participating in the reactions. Thus, at diamond formation under reactions (12.16) and (12.17) from abiogenous methane C_{met} and carbonate carbon C_{carb} (as CO_2 or CO), isotope shifts in diamonds are found as follows:

$$\delta^{13}C_{diam} = \frac{\delta^{13}C_{met} + \delta^{13}C_{6carb}}{2}. \qquad (14.2)$$

$$\delta^{13}C_{diam} = \frac{\delta^{13}C_{met} + 2 \cdot \delta^{13}C_{carb}}{3}. \qquad (14.3)$$

If, however, in the diamond crystallization under equations (12.18) and (12.19) participateed organic origin carbon C_{org} from wide range hydrocarbons $C_nH_{2n\pm k}$, the carbon isotope shift in diamonds is determined as follows:

$$\delta^{13}C_{diam} = \frac{4n \cdot \delta^{13}Corg + (2n \pm \kappa) \cdot \delta^{13}C_{carb}}{6n \pm \kappa}, \tag{14.4}$$

$$\delta^{13}C_{diam} = \frac{2n \cdot \delta^{13}C_{org} + (2n \pm \kappa) \cdot \delta^{13}C_{carb}}{4n \pm \kappa}. \tag{14.5}$$

It is usually believed that in the recent 3 BY the isotope variations in carbonate carbon had been quite insignificant $\delta^{13}C_{carb} \approx \pm 2‰$ according to PDB standard [260, 274]. Nevertheless, data were published recently that in the second half of Early Proterozoic (exactly at the time of forming the iron ore deposits) in the carbonate carbon had been observed the so-called Yatulian positive anomaly $\delta^{13}C_{carb}$ of +12 to +15‰ [275]. This anomaly may be explained, for instance, by metabolic activity of methanogenic bacteria producing CO_2 with sharply elevated contents of heavy isotope, to $\delta^{13}C \approx +13‰$. Such a phenomenon was discovered, in particular, in the pore water analyses from fresh-water lakes with abundant methane generation. However, a similar process might have been running in ancient oceans, especially in the epochs of iron ore formations' mass deposition and associated with this phenomenon intense methane generation. That is why for the Early Proterozoic carbonates should be accepted $\delta^{13}C_{carb} \approx (+12\ldots+15)‰$, whereas at the same time isotope shifts in the organic carbon, according to Shidlovsky [274] publication, had been reaching –40…–45‰. Assuming that methane had played the major role in diamond formation, let us substitute these values in Eqs. (14.2) and (14.3). In this case we will find that for the diamonds formed due to CO_2 reduction $\delta^{13}C_{diam}$ is on average minus 12.5 to minus 15‰. However, at the diamond formation through reducing carbon monoxide (CO), isotope shifts in diamonds are noticeably smaller: $\delta^{13}C_{diam}$ minus 5 to minus 5.3‰.

As we see, the derived theoretical estimates of average shifts $\delta^{13}C_{diam}$ in diamonds, despite the use of extreme values $\delta^{13}C_{org}$ and $\delta^{13}C_{carb}$ for their estimation, quite nicely match quoted above empirical values. If we now use for our estimates average values of the experimental distributions $\delta^{13}C_{org}$ and $\delta^{13}C_{carb}$, the match with average $\delta^{13}C_{diam}$ values in diamonds is even better. At this, $\delta^{13}C$ deflections toward increased deficit of ^{13}C

isotope are explained by participation in the reaction of more complex (n > 1) and unsaturated (κ = –2) hydrocarbons and also by isotope fractionation, for instance, under exchange reactions between the gas phase and the solution [376]

$$^{13}CO_{2(gas)} + H^{12}CO_2^-{}_{(solut)} \leftrightarrow {}^{12}CO_{2(gas)} + H^{13}CO_2^-{}_{(solut)} \quad (14.6)$$

E.M. Galimov with coauthors [377] showed that diamond growth from gas methane phase (although at low temperature) also may be accompanied by significant isotope fractionation.

Our model also explains a subtle feature in the isotope distribution in the diamonds of various parageneses. It was identified by N.V. Sobolev, E.M. Galimov and their colleagues [368] at the analysis of the diamonds from eclogite and peridotite xenoliths. It turned out that the described above $\delta^{13}C_{diam}$ distributions in the diamond belong only with crystals formed in kimberlite matrix of eclogites. Whereas the diamonds of peridotite paragenesis display a relatively narrow $\delta^{13}C_{diam}$ distribution (minus 2 to minus 8‰) with average value of minus 6‰. This feature is connected with the fact that in eclogites (same as in kimberlites), the diamonds might have formed from carbon deposits containing both the carbonate phase and organic origin hydrocarbons. Herefrom, a large scatter of $\delta^{13}C_{diam}$ variations in eclogites. As opposed to this, in the peridotite paragenesis diamonds, carbon might have been coming only from chemical carbonates formed at hydration stage of the former oceanic crust rocks under reactions similar to (10.7), and chemical methane generated under reactions of (12.1) type. As carbon had been coming in such carbonates from a single source (from CO_2 dissolved in near-bottom water of the ancient ocean), their isotope composition must have been more uniform.

For the near-bottom water of the present-day oceans, $\delta^{13}C_{oc} \approx +1‰$ [378]. Similar isotope shift value should have belonged with the carbonate carbon in the serpentine layer of the oceanic crust $\delta^{13}C_{carb} \approx +1‰$. The carbon isotope shift in methane emerging at serpentinization of the present-day oceanic crust reaches $\delta^{13}C_{met} \approx -13‰$ [273]. Should isotope shifts in chemical carbonates and methane in Early Proterozoic at descending of oceanic crust to the diamond formation depth have been close, such carbonate and methane (as opposed to the depositional) must have resulted in a narrow spectrum of isotope shifts $\delta^{13}C_{diam} \approx -6‰$ in diamonds. A reminder: according to empirical data [368], maximum distribution of $\delta^{13}C_{diam}$ in diamonds of such paragenesis had been exactly minus 6‰.

If the suggested diamond formation scheme is correct then one more remarkable detail in their subtle structure must have showed up. As mentioned above, complex hydrocarbons under high PT conditions are unstable and decompose into simpler ones [357]. As the per-unit absolute values of the formation internal energy in complex hydrocarbons is lower than in methane, such hydrocarbons must have been the first to enter the diamond formation reaction. So, in the time of diamond crystallization, the fluid phase must have been gradually impoverishing in complex hydrocarbons with high n values (see reactions 14.4 and 14.5) and enriching in the lighter hydrocarbons. However, from the quoted interrelations defining the correlation $\delta^{13}C_{diam}$ vs. composition of hydrocarbons participating in the reaction it is clear that diamonds crystallized from fluids and containing complex hydrocarbons (n>1) should have been characterized by even greater isotope shift values $\delta^{13}C$ than the light and even more so "methanogenic" diamonds.

If during the time of diamond crystallization, the hydrocarbon composition in the fluid phase had substantially changed (i.e., n decreased), the isotope ratios in some layers of such crystal would have changed as well. For this reason, in diamonds crystallized in the kimberlites and eclogites, the least "heavy", i.e., with the lowermost $\delta^{13}C$ values, should have been crystal cores whereas toward their periphery the isotope shift would have declined. For instance, if at an early stage of the diamond crystallization in the fluid had been present organic decane $C_{10}H_{22}$ (with $\delta^{13}C_{org} \approx -40‰$) and carbon monoxide CO of a carbonate origin (with $\delta^{13}C_{carb} \approx +15$), then the isotope composition in the core of such crystal would have value $\delta^{13}C_{diam} = -11.2‰$. If by the end of crystallization of the same diamond, in the fluid phase had still been preserved ethane C_2H_6 and carbon monoxide, carbon isotope composition in its outer layers would have risen to a value $\delta^{13}C_{diam} = -7‰$. If by this time only methane had been preserved, then in the presence of CO would have emerged the shift $\delta^{13}C_{diam} \approx -3.3‰$, and if the diamond growth had been occurring at the expense of CO_2, then its isotope composition would have had the value $\delta^{13}C_{diam} \approx -12.5‰$.

Theoretical estimates of the isotope ratios in diamonds in general match the available experimental data. For instance, in a publication [43] are included the results of a layer-by-layer analysis of variations in carbon isotope ratios in individual diamond crystals. As it happens, in the overwhelming majority of cases (although not in all) is observed a regular trend of carbon isotope ratios from the crystal center to their periphery. Crystal cores are always enriched in light isotope ^{12}C, and toward their outer shells carbon composition is becoming progressively "heavier" due to the isotope ^{13}C. At this, the total shift of isotope composition reaches 4‰

and on average varies between minus 11.01‰ in the diamond centers to minus 7.32‰ on their surface.

In a publication by F.V. Kaminsky and N.V. Sobolev [379] is also mentioned the existence of noticeable variations in carbon isotope composition within individual diamond crystals (up to 5–10‰ in the eclogite paragenesis diamonds). It is noted, however, that such fluctuations may be both toward heavying of the isotopes in the crystal shells and the other way around, toward their lightening. The publication's authors believe that the variations in isotope composition of diamond carbon they identified testified to the formation of some diamonds from exogenous carbon as a result of lithospheric plates immersing in the subduction zones. Further on, diamond growth had been occurring through the mobilization of the endogenous mantle carbon forming relatively heavier (or lightened for heavy seeding cores) shell. In our view, the entire carbon participating in the formation of diamonds is only exogenous and any variations of the diamond isotope composition had been caused by the changes in chemical regime of crystal growth.

No less indicative is the analysis of isotope ratios for other elements. The maximum variations in the kimberlite belong with the hydrogen δD isotopes that vary in a wide range of minus 4 to minus 100‰ under SMOW standard [1]. A sharp change in deuterium for hydrogen containing minerals in the kimberlites (and in other earthly rocks) is easily explained by fractionation of hydrogen isotopes at hydration by outside water of the oceanic crust magmatic and sedimentary rocks which then served the source material for the kimberlite formation. Simultaneously with this, isotope variations of oxygen $\delta^{18}O$ in hydroxyl groups of the serpentine and phlogopite containing most of kimberlite bonded water are within 6 to +12‰ under SMOW standard. Whereas $\delta^{18}O$ variations in the kimberlite matrix (including the carbonate matter) are even wider and reach +24‰ [1]. This pattern is so clear that S. Sheppard and J. Dawson, being proponents of kimberlite mantle origin, came to a conclusion that most of "hydrothermal" water in these minerals is nonetheless of a surficial, not of juvenile origin [380].

As opposed to the kimberlites, values of hydrogen isotope shifts in diamonds are directly opposite and reach $\delta D \approx +180‰$ [381]. It indicates an anomalous enrichment of the diamond hydrogen compared with the sea water ($\delta D = 0$) and deposits (δD minus 30 to minus 100‰). In the author's view, diamond enrichment in deuterium indicates a tie of the diamond formation with a hydrocarbon matter containing fluid (for instance, methane) and had been caused by the process of hydrogen diffusion from the forming diamond crystals.

As opposed to hydrogen (and carbon), for oxygen it is possible to determine quite clearly the mantle ratios of its isotopes based on analyses of fresh basalts from mid-oceanic ridges. Other rocks, including continental and island basalts, are not so well suited for these purposes because of their contamination with ground and crust water. The $\delta^{18}O$ value in such basalts is approximately +5.5 under the SMOW scale [376].

Therefore, all kimberlites, the same as any other metamorphic and sedimentary rocks, are significantly enriched in oxygen heavy isotope. It is very difficult to assume so substantial matter's isotope fractionation in the mantle (speaking truly, just impossible). This is supported also by a very narrow spectrum of $\delta^{18}O$ variations (+5 to +7‰) in the uncontaminated mantle (and lunar) rocks and the absence in kimberlites of complementary minerals equally impoverished in ^{18}O isotope. Besides, should kimberlites indeed have been released from a magma uniform in the isotope composition, then occurring at this exchange reactions, theoretically, would not have substantially changed the composition of the differentiation products. As opposed to this, the reactions' kinetic effects and diffusion of oxygen isotopes in melts would have produced the opposite results, that is, kimberlite enrichment in light oxygen ^{16}O isotope.

Indeed, at degassing water from the hot mantle its isotope composition must have remained in equilibrium with the mantle rocks for which $\delta^{18}O \approx +6\ldots+8$‰. However, in Early Precambrian especially, the isotope composition of the oceanic water, based on isotope composition of the marine flints, had been dropping to $\delta^{18}O \approx -10\ldots-15$ ‰ [367]. At this, with the passing of time had been observed a trend of isotope ratios of the oceanic water from shortage of heavy oxygen isotopes in Early Precambrian to their current normal ratios. However, against the background of a general increase with time of ^{18}O concentration in the oceanic water, some epochs of elevated sedimentation have been identified for which had been observed inverse $\delta^{18}O$ correlation. With this fact in mind, E.M. Galimov [367] came to a conclusion that oxygen isotope composition in the oceanic water is formed as a result of a competition between two processes: isotope fractionation at sedimentation and isotope exchange in the process of lithospheric water circulation, for instance, in oceanic rift zones.

Obviously, hydration of deposits and rocks of the oceanic crust must have resulted in an impoverishment of oceanic water in ^{18}O isotope. In Archaean, had additionally operated developing in the mantle powerful thermal dissociation process of juvenile water on hot metallic iron in layers of zonal melting of the mantle matter (see Fig. 5.1). Mostly "heavy" water $H_2{}^{18}O$ had reacted iron whereas the "light" water had been mostly

degassed from the mantle thereby enriching the water of Archaean ocean in light oxygen O^{16} isotope. Besides, oxygen isotope fractionation between water and carbon dioxide gas which had been saturating Archaean oceanic water, had resulted in "lightening" of water and "heavying" of the carbon dioxide gas:

$$C^{16}O_2 + 2H_2^{18}O \rightarrow C^{18}O_2 + 2H_2^{16}O + 5.82\ \text{kcal/mole}. \qquad (14.7)$$

On the other hand, variations of $\delta^{18}O$ in hydrated basalt material may reach +20‰ and in basalt glass (palagonites) weathering products, even greater (up to +25‰). The main factors affecting the changes in isotope composition of water in the Early Precambrian oceans, apparently, had been isotope fractionation of juvenile and oceanic water with iron, its oxides and carbon dioxide gas and also with hydrated rocks of the oceanic crust and deposits. However, as already mentioned, iron and its compounds concentration in the mantle matter in Archaean and Proterozoic had been significantly higher than now. For this reason, a shift in oxygen isotope ratios then had to have been much more pronounced. If so, the change in $^{18}O/^{16}O$ ratio due to the removal of ^{18}O isotope from the composition of the degassed water had been occurring in proportion with the total iron and its oxide concentration in the mantle. Besides, this change had resulted in a proportionate change of CO_2 partial pressure in the atmosphere and in hydrated rocks and deposits in the oceanic crust.

As the hydration of deposits and bed-rocks in the oceanic water reservoir had resulted in the accumulation of oxygen heavy isotope, then as a compensation, the oceanic water must have become lighter

$$4Mg_2SiO_4 + 4H_2^{18}O + 2C^{18}O_2 \rightarrow Mg_6(Si_4O_{10})(^{18}OH)_8 + \\ +2MgCO_3 + 85.1\ \text{kcal/mole}. \qquad (14.8)$$

The $\delta^{18}O$ variations in marine origin sedimentary rocks cover an even greater range: +10‰ in sandstones to +14‰ and +19‰ in shales (Hoefs, 1997). In the present-day marine carbonates $\delta^{18}O \approx +26‰$ (SMOW standard). However, in the past geological epochs the enrichment of carbonates in heavy oxygen isotope had been less notable and for Early Proterozoic had been approximately +16 …+20‰ [382]. The reason is that in Early Precambrian at iron oxidizing must have been occurring a sufficiently energetic fractionation of oxygen isotopes between bivalent iron

oxide, water and carbon dioxide gas under a reaction of "heavying" the water and CO_2 isotope composition

$$H_2^{16}O + Fe^{18}O \rightarrow H_2^{18}O + Fe^{16}O + 5.83\ \text{kcal/mole}. \qquad (14.9)$$

This reaction, perhaps, might have occurred in rift zone magmatic foci and might have resulted in "heavying" the isotope composition of water and carbon dioxide gas degassed from the mantle.

Therefore, the main factor affecting changes in water and carbon dioxide gas isotope composition in the oceans of Early Proterozoic had apparently been the isotope fractionation of juvenile water and CO_2 with iron oxidizing under reactions (14.7) – (14.9). This approach enables a suggestion of the existence of certain geochemical equilibrium between water degassed from the mantle and the mantle rocks. In this case, the isotope composition of water degassed from the mantle, after its fractionation, had been equal [175] to

$$\frac{^{18}O}{^{16}O} = \left(\frac{^{18}O}{^{16}O}\right)_m \cdot \left[1 - \frac{C(FeO) + \cdot C(Fe)}{So + Sr + k \cdot Mcc} \cdot q\right] \cdot \alpha, \qquad (14.10)$$

where $(^{18}O/^{16}O)_m = 2.0034$ is oxygen isotope ratio in the mantle; C(FeO), C(Fe) are iron oxide and iron concentrations in the convecting mantle; So and Sr are the areas of the oceanic crust and regolith surface in Archaean; Mcc is the continental crust mass; k = 0.5 and q = 0.319 are factors accounting for chemical activity of rock hydration reactions (selected based on experimental data); α = 0.9978 is the isotope separation factor between the mantle and oceanic water reservoirs (selected based on condition $(\delta^{18}O)_0 = 0$, where $(\delta^{18}O)_0$ is the present-day value of oxygen isotope shift in the oceanic water). The oxygen isotope shift estimation results in the oceanic water by Eq. (14.10), compared with evolutionary change curves of isotope composition in flints and carbonates are shown in Fig. 14.3.

Therefore, it follows from the included analyses of oxygen isotope ratios in the oceanic water that in the ancient oceans the $^{18}O/^{16}O$ ratio indeed had been lower. As a consequence, lower values of these ratios in hydroxyl groups of serpentinites and phlogopites in kimberlites (Fig. 14.4).

Kimberlites and their eclogite xenoliths for the rock as a whole have relatively low strontium isotope ratios $^{87}Sr/^{86}Sr \approx 0.703–0.710$, although for individual mineral fractions these ratios may substantially deviate from

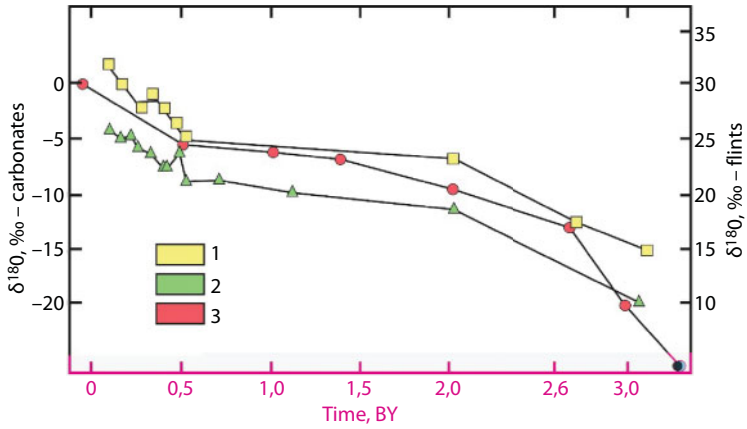

Fig. 14.3 Limestone isotope-oxygen composition ($\delta^{18}O$ relative PDB) after [382] and flints ($\delta^{18}O$ relative SMOW) after [383–385] as a function of the geological age (analysis by T. Schopf [260]); a thin line and dark dots show theoretical $d^{18}O$ estimates for the oceanic water determined from Eq. (14.10) [175].

average values. In eclogites, strontium ratios also vary in a broad range: from 0.701–0.703 in omphacites, 0.708–0.712 in garnets and up to 0.732 in the phlogopite [1, 386]. Low $^{87}Sr/^{86}Sr$ values are usually treated as a proof of the kimberlite mantle origin. It is after all true for the eclogites as they indeed had been formed from the oceanic crust mantle basalts. But it is not

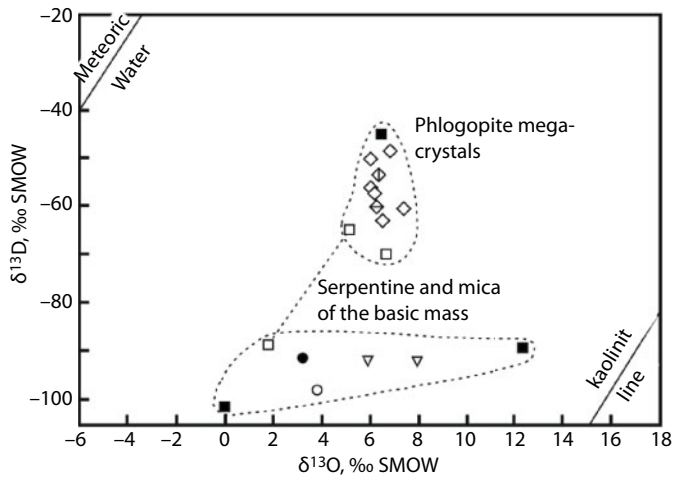

Fig. 14.4 The δD–$\delta^{18}O$ diagram for serpentinites and phlogopites of kimberlite basic mass and phlogopite mega-crystals after J. Dawson [1].

so for the carbonate-silicate matrix of kimberlites. Low strontium ratios in kimberlites are because in ancient oceanic deposits and carbonates these ratios had also been low and only relatively recently they had risen to the values around 0.708–0.709 (see Fig. 8.13). For instance, the Bulavey complex limestones, age 2.95 BY, in South Africa have these ratios at 0.703 and younger Early Proterozoic Transvaal limestones (2 BY) in the same region have these ratios at 0.7044 [387].

Higher $^{87}Sr/^{86}Sr$ ratios are usually fairly tied with elevated contents of radiogenic strontium in phlogopite impregnations often enriched in rubidium. Thus, in phlogopite crystals, strontium ratios sometimes reach the values of 0.715, 0.778 and even 0.959 [386].

In the phlogopite content, South African kimberlites may be subdivided in two groups. In no-phlogopite kimberlites, $^{87}Sr/^{86}Sr \approx 0.7033–0.7049$ whereas in phlogopite-containing kimberlites the strontium ratios rise to 0.7074 - 0.7109 [388]. Even greater values of average isotope ratios are found in West Australian phlogopite kimberlites and diamond-bearing lamproites substantially enriched in Rb. In these rocks, average $^{87}Sr/^{86}Sr$ ratios vary between 0.71037 and 0.71865 [389].

The existence duration of overheated kimberlite melts had been exceptionally long and may have reached 2 BY. That is why over this time exchange reactions between minerals containing Sr and Rb had been continuously running in them. In the process the separation of $SrCO_3$ as a heavier compound had apparently been occurring. As a result, a kimberlite focus had often turned out an incompletely closed system for strontium. This, in turn, may have led to substantially distorted primary $^{87}Sr/^{86}Sr$ ratios under determination (they would be undervalued). Apparently, for this reason the rubidium-strontium method of determining the formation time of kimberlite melts should be used very cautiously. However, it may be used with more certainty for finding the age of the kimberlite breakthrough to the surface. Whereas the timing of the kimberlite melt emergence by the strontium method may be estimated only based on a correlation of primary $^{87}Sr/^{86}Sr$ ratios for basalts and carbonates vs. their age. At this, it should be considered that the minimum values of these ratios in the eclogites and kimberlites had been only slightly distorted with time. Judging by the data on strontium isotopy in basalts and deposits published in the monograph by G. Faure [387], all minimum values of the strontium ratios in the eclogites and kimberlites indeed indicate their Precambrian and even Early Precambrian age. At this, the kimberlite volcanism proper had often manifested itself only in Late Mesozoic.

According to the data summary included in J. Dawson's monograph [1], lead isotope ratios in the South African kimberlites are within the

following ranges: $^{206}Pb/^{204}Pb \approx 17–20$; $^{207}Pb/^{204}Pb \approx 15.7$; $^{208}Pb/^{204}Pb \approx 37.7–39.5$. However, their interpretation is difficult for the same reason as for the strontium ratios as in the foci of long-living kimberlite melts is absolutely impossible to assume the existence of a system closed for U, Th, and Pb. Besides, we do not know in what proportions and primary ratios isotope of Pb, U and Th mixing had been occurring in those deposits from which later the kimberlites themselves had emerged.

The eclogites and peridotites, after their formation (as basalts and restites of the oceanic crust in mid-oceanic ridges) had never melted again. Thus, lead mobility in them must have been substantially lower. This gives a reason to hope in the possibility of using the lead-isochronous techniques for estimating kimberlite ages from analyses of eclogite xenoliths contained in them. For the eclogites from the Roberts-Victor diatreme in South Africa such analysis gave the age in the beginning of Early Proterozoic, 2,465±200 MY. However, it is still not possible to trust these estimates, despite all their attractiveness, for our kimberlite formation model as it was shown that the eclogites exactly in this diatreme are contaminated with U, Th, Pb and Rb from the enclosing kimberlites [329]. The data by these authors show that 38 to 96% Pb had come in the eclogites from their enclosing kimberlites.

Conspicuous is a very close match of the included lead isotope ratios in the kimberlites to the isotope composition of the present-day oceanic deposits: $^{206}Pb/^{204}Pb=18.9$; $^{207}Pb/^{204}Pb=15.86$ and $^{208}Pb/^{204}Pb=38.82$ [390]. Lead isotope composition of the bottom oozes is in equilibrium with the matter of Earth's external geospheres and apparently is the closest to average isotope composition of Earth's crust [390]. Thence, a conclusion that the kimberlites as well had been formed in the past from the crustal matter or the matter equilibrial with it with the same uranium-thorium-lead ratios (for instance, from ancient oceanic deposits). However, some distinctions are observed in the kimberlites. Thus, in Earth's crust, average ratio $Th/U \approx 3.6–3.9$ [390]. According to the data accepted by the author, this ratio in the mantle is also > 1 and is approximately 2.7 [18]. Whereas in the kimberlite, same as in the carbonatites, $Th/U < 1$ [330]. An explanation of this phenomenon may be that the deposits that had been the material for the kimberlite formation, had been substantially enriched in organic matter. And uranium is usually intensely accumulating together with it. For instance, in organic and phosphorus-rich diatomic oozes in upwelling zones, $Th/U \approx 1/7–1/21$ and in the present-day oceanic phosphorites it is even lower, up to 1/11–1/11.7 [326]. In a sharply reducing environment of deep and near-bottom water of the Early Proterozoic oceans, a similar picture must have been appropriate also for the deposition on their bottom

sapropel-rich pelagic deposits from which the kimberlites might have inherited noted for them distribution specifics.

As opposed to the kimberlites, mineral inclusions in the diamonds are closed systems and because of this, the isotope ratios determined from them are of a special interest. In a publication [54], the data are listed of sulfur and lead isotope ratios from sulfide inclusions in diamonds of various African kimberlite diatremes. Analyzing sulfur isotope shift values in diamond inclusions, the authors came to a conclusion of a definite addition in the deep lithospheric levels of the crustal and sedimentary material which had occurred in the past geological epochs through ancient plate subduction zones. Judging by lead isotope ratios, the process of pulling in deposits under the continents had been running up to 1 BYa. Most reliable isotope ratio determinations in peridotite sulfides give the ages of 2 BY.

Very typical for the kimberlites are sharply elevated contents of rare-earth elements reaching 500-800 g/t [1, 391]. Similar rare-earth element concentrations may be encountered only in carbonatites and sienites which have the origin similar to kimberlites, and also in phosphorites and iron-manganese ore-bearing oozes in which their concentration reaches 880-970 g/t [391]. Whereas in the mantle ultramafic rocks, their content is within the range of 2–3 to 20–30 g/t. However, exactly enriched in organics iron ore deposits abundantly accumulating in a reducing environment on the floor of the Early Proterozoic oceans, as we saw, most likely had served a source of the matter for the formation of kimberlites. At this, the rare-earth element distribution in kimberlites and in the present-day oceanic deposits nicely match each other except maybe only heavy rare-earth elements (see Fig. 14.5). However, at such comparison it is necessary to keep in mind that the kimberlite melts in magmatic foci at the existence depths of the garnet metamorphism facies had run through a lengthy differentiation. It is known (see Fig. 14.6) that under high pressure garnets, formed in the kimberlites under reactions (12.8), (12.10) and (12.11), are mostly enriched in heavy rare-earth elements [392]. Garnet density is usually greater than 3.5–4 g/cm^3. That is the reason why they already in magmatic foci had been deposited and removed from the major mass of the kimberlite melt, and together with them had been partially removed heavy rare-earth elements that had gotten in the focus from deposits. As the included comparison shows, after introducing corrections in the rare-earth element spectrum from oceanic deposits for the absorption of heavy rare-earth elements by the garnets from the Premier diatreme, the coincidence with rare-earth elements distribution in kimberlites from the same diatreme substantially improved. A similar picture is observed in carbonates and lherzolites.

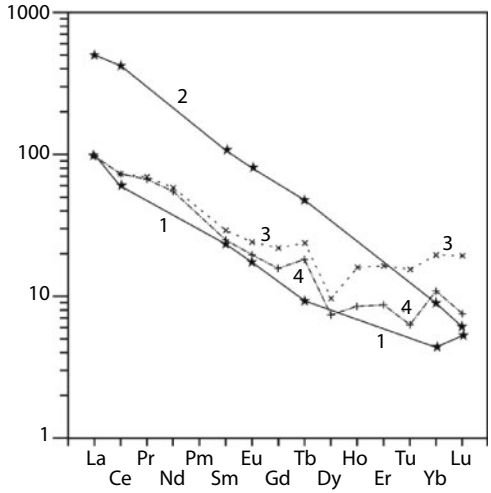

Fig. 14.5 Average rare-earth element distributions in kimberlites and deposits. The data are normalized over the average chondrite distribution (Kheskin *et al*., 1968): 1. and 2. are rare earths elements distributions in kimberlites from the Premier and Wesselton diatremes, South Africa (Dawson, 1983); 3. Rare-earth element distribution in the oceanic deposits estimated based on the data by [392]; 4. Difference between rare-earth element spectrums in the deposits and garnets from the Premier diatreme (see Fig. 14.6).

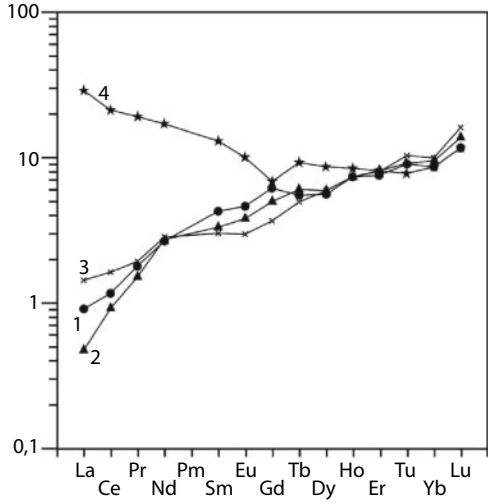

Fig. 14.6 Rare-earth element distributions normalized over the chondrite standard in garnets and pyroxenes from xenoliths of the kimberlite diatremes. The diagrams are based on the data by [393]. Garnets: 1. Premier diatreme, RSA; 2. Udachnaya diatreme, Yakutia; 3. Obnazhennaya [Exposed] diatreme, Yakutia; 4. Pyroxenes, Obnazhennaya diatreme, Yakutia.

It is known that the kimberlites had been formed at depths of garnet lherzolite's stable existence. As opposed to kimberlites, sienites of alkali-ultramafic formations had formed at shallower depths of the pyroxene lherzolite stable existence. However, rare-earth element distributions in pyroxenes are opposite to the garnets as they to the largest extent absorb light rare-earth elements (see Fig. 14.6). Therefore, at comparing the rare-earth element distribution spectrums in the sienites and deposits, it is already necessary to introduce in distributions of the latter, the corrections for absorption of rare-earth elements by pyroxenes. Fig. 14.7 is an example of such comparison taking into consideration that in Early Proterozoic the rare-earth elements concentration in the oceanic deposits might have been approximately 30% higher than their concentration in the present-day deposits.

This Figure shows that average rare-earth element spectrums in the Khibin alkali massif's sienites almost ideally match the distribution of the same elements in the oceanic deposits. Therefore, the rare-earth elements' distribution spectrums in depth rocks once again testify that the sienites of alkali-ultramafic intrusions, same as the kimberlites, carbonatites and lamproites, had formed due to pulling-in oceanic deposits to great depths through ancient plate subduction zones.

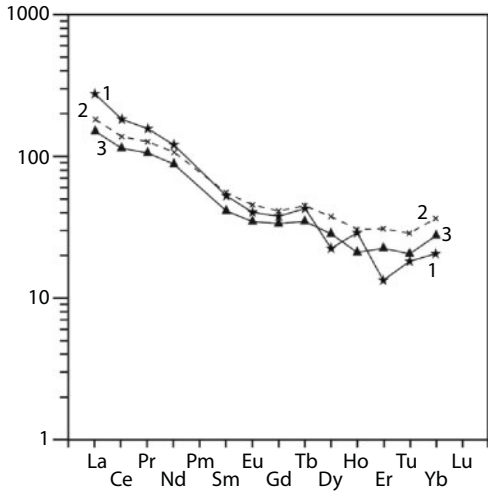

Fig. 14.7 Rare-earth element distributions normalized over chondrites [392]: 1. In the sienites of the Khibin alkali-ultramafic massif; 2. In the oceanic deposits under the assumption that in Early Proterozoic, the rare-earth element concentration in them had been approximately 30% greater than the present-day one; 3. Rare-earth element concentration difference in deposits and in pyroxenes of the Obnazhennaya diatreme [393].

As opposed to kimberlites and their affine rocks, the eclogite matter after its formation had not melted, therefore had not been subjected to so strong differentiation. So, all polymorphic mineral transformations and eclogite metamorphism had mostly to have been occurring isochemically. That is exactly why eclogites had even better preserved major rare-earth element distribution features of their source rocks, the oceanic tholeiite basalts melted out in near-surface environments of the oceanic rift zones (see Fig. 14.8). This is also testified by substantial differences in rare-earth element distribution spectrums between the eclogites and alkali basalts melted out at much greater depths than tholeiite basalts.

Besides the lanthanoids, the kimberlites are significantly enriched also in the other lithophilic elements: Li, B, F, P, Cl, K, Ti, Pb, Sr, Y, Zr, Nb, Cs, Ba, Ta, Pb, Th and U ([1, 14, 389, 330] and other publications). This lithophilic mineralization of kimberlites totally extrinsic to the mantle differentiates is another convincing evidence of a sedimentary-anatectic origin of these unique and highly interesting rocks.

The same is supported by enrichment of the kimberlites in alkalis. At the mantle matter differentiation and basaltoids separation from it, they are as a rule always dominated by sodium ($Na_2O > K_2O$). In the kimberlites, on the contrary, usually $K_2O > Na_2O$ [1]. The potassium enrichment

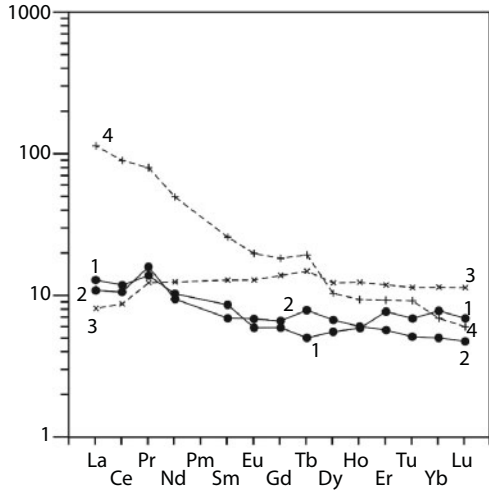

Fig. 14.8 Rare-earth element distributions in the eclogites and basalts normalized over the chondrite standard: 1. Eclogite diatreme Roberts-Victor [1]; 2. Average eclogite; 3. Average tholeiite basalt in the mid-oceanic ridges; 4. Alkali basalt (distributions 2 – 4 are after [391]).

in kimberlites is sometimes so intense that a number of transitions is observed from phlogopite kimberlites through olivine lamproites to leucite lamproites. Exactly such transitions are typical of the rocks on the Plateau Kimberly in the Northwestern Australia [389]. No differences have been discovered in the isotope composition between the diamond-bearing lamproites and kimberlites. This, from the perspective of the study author, is a proof of affinity between these rocks. Whereas the lamproite saturation with potassium under our model had most likely occurred at pulling-in of ferruginous pelagic deposits substantially enriched in illite and other potassium-containing hydromicas in the ancient plate subduction zones. Simultaneously with this had been occurring the metamorphic spinel (or garnets) and talcum formation over dolomites. This process might have been running as follows:

$$4KAl_2(AlSi_3O_{10})(OH)_2 + 7MgCO_3 \rightarrow 4K(AlSi_2O_6) + 4MgAl_2O_4 + \\ \text{illite} \qquad \text{magnesite} \qquad \text{leucite} \qquad \text{spinel}$$

$$+Mg_3(Si_4O_{10})(OH)_2 + 7CO_2 \\ \text{talcum} \qquad (14.11)$$

The spinel and garnets, being higher density minerals ($\rho \approx 3.5–3.7$ g/cm^3), had been subsequently depositing together with iron compounds on the bottom of a magmatic focus and had been gradually withdrawn from the system thus impoverishing the remaining melt in the alumina.

Our kimberlite and carbonatite formation model completely match observed in these rocks' neodymium and samarium isotope distributions. Indeed, as G. Faure [394] noted, partial melting of the mantle in the past had begotten magmas with lower Sm/Nd ratios compared to the mantle matter. So, the rocks formed from such magma, for instance basalts and their transformation products (crustal rocks: granitoids and deposits), currently have lower $^{143}Nd/^{144}Nd$ ratios than in the mantle, they have negative eNd values. On the contrary, these solid phases of the mantle matter, remaining after the removal from it of the formed melts, have higher Sm/Nd ratios than in the primordial mantle reservoir (Fig. 14.9). G. Fore especially emphasized that the rocks formed in the past geological epochs from such residual (restite) solid phases, would also have elevated $^{143}Nd/^{144}Nd$ ratio values. Therefore, carbonates emerged in Early Proterozoic from such ultramafic restites by way of their serpentinization under reactions (10.7) and (10.7'), must also have

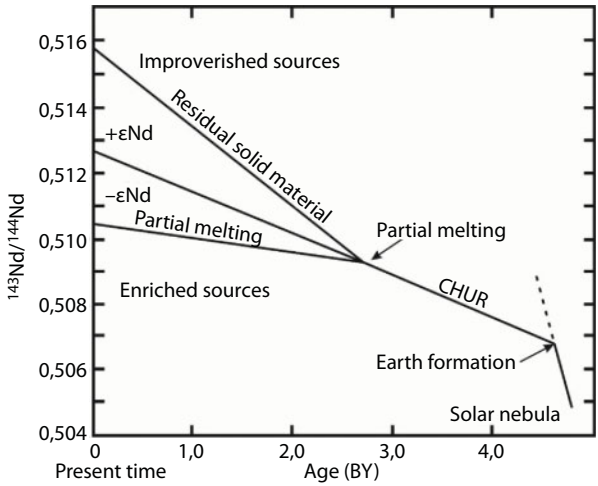

Fig. 14.9 The Nd isotopic evolution in the mantle (in CHUR chondrite reservoir) after G. Faure [394]. The magma formed as a result of partial mantle melting has lower Sm/Nd ratios compared to the mantle reservoir, whereas the residual (restite) solid phase had higher Sm/Nd ratios. As a result, the present-day $^{143}Nd/^{144}Nd$ ratios in the rocks formed from the silicate melt are always lower than in the mantle and in the rocks formed from restites, on the contrary, always higher.

higher $^{143}Nd/^{144}Nd$ ratios compared to the present-day mantle rocks and positive eNd values:

$$\varepsilon Nd = \left[\frac{\left(\frac{^{143}Nd}{^{144}Nd} \right)_{rock} - \left(\frac{^{143}Nd}{^{144}Nd} \right)_{m}}{\left(\frac{^{143}Nd}{^{144}Nd} \right)_{m}} \right] \cdot 10^4, \qquad (14.12)$$

where the subscripts "*rock*" and "*m*" mark the present-day values of $^{143}Nd/^{144}Nd$ ratios in the rock and in the mantle reservoir $(^{143}Nd/^{144}Nd)_m = 0.512638$.

It follows from Eq. (14.12) that negative εNd values correspond with rocks formed from the mantle melt-outs or their reprocessing products, for instance, through the assimilation of ancient crustal rocks. Positive εNd values indicate that in depth rock formation had participated the restite phases of the mantle reservoir [394] remaining after the removal from it of the melt-outs formed at some earlier moment in time (Fig. 14.10).

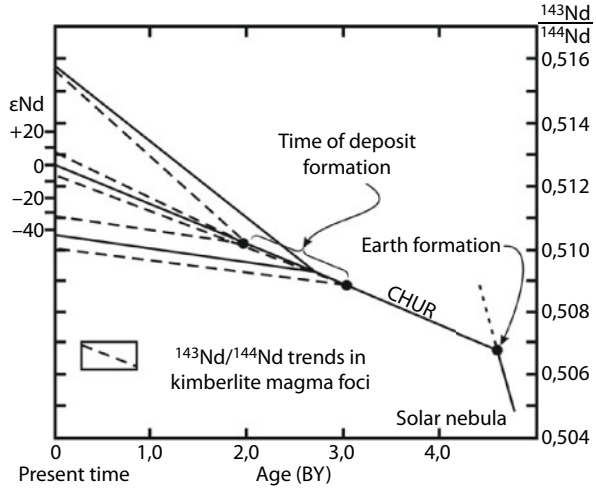

Fig. 14.10 Possible variability limits of $^{143}Nd/^{144}Nd$ ratios and εNd parameter in kimberlites, carbonatites and their affine alkali-ultramafic rocks.

For instance, such "extracts" from the mantle restites may be carbonates formed at hydration (serpentinization) of the oceanic crust ultramafic rocks under reactions of (10.7) type. Whereas real εNd values in the kimberlites, lamproites and carbonatites depend on the extent of mixing these two source matters in depth rocks.

Thus, for Archaean and Early Proterozoic sedimentary rocks formed from mantle differentiates or their derivatives (basalts, tonalites, diorites or granitoids) εNd parameters may be only negative. As opposed to this, carbonate deposits formed from Early Proterozoic ultramafic rocks after their serpentinization under reactions (10.7) and (10.7') must have positive eNd values. As a result of mixing deposits of various genesis in the real kimberlites and carbonatites is observed the entire spectrum of such values between approximately minus 40 to +10…+20 (Fig. 14.10). Including εNd = 0 as it is observed, for instance, in eruption products of some present-day carbonatite volcanoes in South Africa.

In subsequent geological epochs, in the extension environment of ancient shields, the depth magmas so formed, together with diamond crystals had been blisteringly erupted on Earth's surface. At this, the depth rocks had been completely inheriting the elements' isotopic ratio specifics of rare-earth element distribution and typical features of lithophilic geochemistry appropriate for Early Proterozoic pelagic deposits.

The opposite situation must have occurred for strontium distribution as a radioactive rubidium at the mantle melting had mostly concentrated

in basalt melts. It follows thence that in the basalts proper and in their destruction products, i.e., in the deposits, the $^{87}Sr/^{86}Sr$ ratios must have been substantially higher than in the mantle reservoir (see Fig. 8.13). As opposed to this, in samples of rocks and deposits emerged due to weathering of the restite rocks remaining after basalt melt-out, for instance serpentinites and harzburgites of the oceanic crust third layer, the $^{87}Sr/^{86}Sr$ ratios must be lower than in the mantle reservoir. A consideration of these factors enables us to estimate by neodymium and strontium the source of the matter coming in the depth kimberlite melt focus. Thus, if $\varepsilon Nd < 0$ and $\varepsilon Sr > 0$, the kimberlite and lamproite melts had originated from mantle derivatives, i.e., from basalts and their reprocessing products and also from deposits. However, if $\varepsilon Nd > 0$ and $\varepsilon Sr < 0$, then in the formation of depth melts had taken a notable part also the mantle restite matter, for instance, ophiolite complexes' serpentinites and their destruction products. That is the way, for instance, for carbonates formed in the lower parts of the oceanic crust at the hydration of harzburgites under reactions of (10.7) type, to have gotten in the pelagic deposits. Together with carbonates, from the mantle rocks had been carried out their characteristic isotope mark of $\varepsilon Nd > 0$ and $\varepsilon Sr < 0$. If, however, carbonates had formed due to basalt or crustal rocks hydration and weathering, then together with them in the deposits had been coming appropriate isotope marks $\varepsilon Nd < 0$ and $\varepsilon Sr > 0$. In the real environments, because of mixing the destruction products of these two rock types, in the deposits and then in formed from them depth melts, might have emerged intermediate εNd and εSr interrelations as illustrated in Fig. 14.11.

Thus, based on the data in Fig. 14.11, all lamproites of Australia and Aldan, and also some South African kimberlites (group II) had formed only from pelagic deposits emerged through weathering of the crustal rocks. This is also supported, in particular, by an elevated concentration of potassium in lamproites (about 6–10% K_2O). This potassium had been clearly brought into the deposits due to weathering of the continental crust alkali granites.

As opposed to this, most kimberlites in South Africa (group I), Sierra Leone and northern margin of the Russian Platform had perhaps formed with a notable participation of oceanic crust ultramafic rocks and their associated carbonates in the formation of pelagic deposits. Indeed, most carbonates in Early Proterozoic had formed at the hydration of the oceanic crust ultramafic rocks under reaction 10.7 [19]. Thence, elevated magnesium concentrations in the kimberlites, up to 25–29% MgO. Part of magnesium and iron later had bonded with silicates, for instance, under reactions of (12.9), (2.10) and (12.11) types. Calcium released at that had

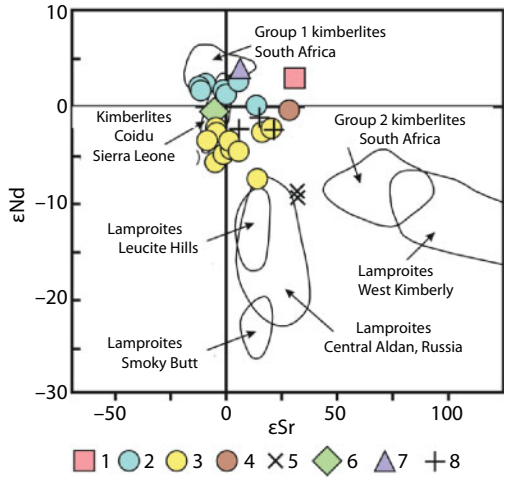

Fig. 14.11 Isotope composition of kimberlites and their affine rocks of the East European Platform and some other regions on the εNd – εSr diagram [395]: 1. Middle Timan; 2–5. Archangel fields: 2. Kepin Field; 3. Zolotitskoye Field; 4. Verkhotinskoye Field, V.Grib diatreme; 5. Pikrites, olivine melilitites; 6. Tersk coast [396]; 7. Kandalaksha [396]; 8. East Finland kimberlites [397].

been passing in the kimberlite carbonate matrix. But simultaneously with these reactions had been passing in a deposit the isotopes of neodymian and strontium at the ratios typical of the ultramafic rocks. This is probably an explanation of grouping kimberlite fields in the εNd–εSr diagram of Fig. 14.11 near the values of εNd ≈ ±10 and εSr ≈ (–20 +40) whereas all lamproites are within the area of εNd ≈ from minus 5 to minus 25 and εSr ≈ from +5 to +120.

15

Kimberlite Magma Rise Mechanism to Earth's Surface

It was mentioned in Chapters 3 (Fig. 3.1) and 12 that at continent collision, the former plate subduction zone between them had turned out squeezed by two thick continental plates. Should heavy (iron-rich) oceanic deposits gotten in the lower portion of such welded plate in Early Proterozoic and should a silicate-carbonate magma focus have emerged there, it might have existed further on without a notable cooling down for hundreds of millions of years as the temperature at those depths had been substantially higher than the melting temperature of water-saturated deposits (see Fig. 12.2).

The plate subduction due to which the oceanic crust and heavy deposits had been pulled under the continents, had been occurring about 1.9–1.8 BYa at the formation time of a supercontinent Megagea (see Fig. 9.3), i.e., in the environment of lithosphere compression above the descending convective flows in Earth's mantle. However, a chemical-density convection in the mantle had been nonstationary and once in a while had been changing its configuration. That is why in the place of former descending convection flows after some time (on the order of a few hundred million years), as a rule, had been emerging their inverse ascending flows. The compression regime had been replaced at that by the extension regime due to "slipping" the continental lithosphere off a mantle uplift (swelling) that had usually emerged above the center of the mantle ascending flow.

Obviously, a specific location of a fault in space had been defined by the configuration of the mantle flows and availability in the lithosphere of weakness zones. The areas adjacent with the former plate subduction zones in particular may have been such zones of weakness. In these zones, two adjacent monolith lithospheric blocks had been separated by a layer of metamorphosed and stratified sedimentary-volcanogenic rocks of the former oceanic crust. So that, all other conditions being equal, the lithosphere would have been faulted exactly along such suture surface.

N. O. Sorokhtin (ed.) The Origins of Natural Diamonds, (433–441) © 2019 Scrivener Publishing LLC

Open fractures might not have emerged at great depth in the lithosphere as under the weight of overlying rocks their walls had experienced plastic deformations. Most publications on the subject of kimberlite volcanism's mechanism [1, 55, 58, 398–400] emphasize that a rapid rise of kimberlite magma on the surface had been facilitated by its low viscosity. Indeed, the lithosphere had been in a state of an intense lithospheric compression, and a liquid melt that had gotten in the fracture had taken this pressure completely on itself thus compensating and unloading the "point" of a fracture off its compressing stress. At that, extension stress exerted to the lithosphere (the stress value had usually significantly exceeded the rock rupture strength) had concentrated on the fracture point. That had caused new fissures in the lithosphere, and liquid melts had instantaneously rushed in and filled in newly emerged fracture systems. The fracture point might not have advanced faster than the fluid in a channel feeding this fracture. Thus, the rate of the split evolution had always been limited by the kimberlite melt viscosity. However, CO_2 release from the magma while it had been rising up the fracture must have lowered the melt viscosity, therewith sharply accelerating its opening and the rate of advance [399]. The real rate of kimberlite magma rise had been so high that it had easily carried with it even heavy xenoliths of eclogites and garnet peridotites.

In our model of kimberlite magma formation, the foci of overheated and for this reason exceptionally liquid melts might have been for a long time (around 1 or 2 BY) preserved without a substantial cooling in lower portions of the continental lithosphere, "expecting" favorable conditions for a breakthrough on the surface. However, in this case, a cross-cutting fracture in the lithosphere had been emerging not immediately after the establishment of its extension regime. Under a relatively small excessive (super-hydrostatic) stress, the lithosphere had behaved as an elastic body. But as soon as the extension stress σ applied to it had exceeded rock's shear strength stress τ_s, the lithospheric matter had converted to a plastic state. Had liquid melts capable of absorbing a confining lithostatic pressure happened to have been within a zone of the lithosphere plastic deformations, further lithospheric deformation would have been developing under the laws of elastic bodies brittle failure.

After a fracture had formed, its maximum opening, i.e., the width of a lithospheric split with all excess tension stresses removed from its walls, had been defined by the value of the continent plate absolute deformation that had caused such a split. Should the magma focus volume have been unlimited, the melt viscosity low and its density equal to enclosing rock density, the maximum opening of a magma-supplying

channel ΔL might have been determined from a simple equation resulting from Hooke's law:

$$\Delta L = \frac{\sigma_0}{E} \cdot L, \tag{15.1}$$

where σ_0 is the lithospheric rocks' tension strength, E is Young's modulus of elasticity, L is a characteristic size of the continental plate block being split.

Judging by the seismic waves' advance rate in the subcrustal lithosphere ($V_p \approx 8.1$ km/s, $V_s \approx 4.6$ km/s) and $E \approx 1.8 \cdot 10^{12}$ dyne/cm^2, rock's tensile strength may be determined based on the earthquake focal zone's magnitude and area. Usually σ_0 is equal to a few units per 10^7 dyne/cm^2 [105]. For massive lithospheric rocks, the strength may be somewhat greater, on the order of $\sigma_0 \approx 10^8$ dyne/cm^2. Assuming now $L \approx 2 \cdot 10^8$ cm, we find that the maximum lithospheric plate opening ΔL may have reached a few dozen or even a hundred meters.

Sometimes, continental plate extension situation might have occurred even at continental collision as this had happened nearly 400 MYa at the collision of the Canadian-Greenland platform with the Baltic shield and the Barents Sea platform at the closing of the Pra-Atlantic Ocean Yapetuis (see below). A consequence of this event had been extension fractures having had emerged then in the lithospheric block of the Karelian-Kola region and the Archangel Province. It is very difficult to estimate theoretically the maximum fracture size in such situations as they had substantially depended on geodynamic regime and geometry of the colliding plates.

However, due to a finite viscosity of the melt, its lower density and limited volume of a kimberlite magmatism focus, the maximum fracture width at the stages of magma eruption had never been reached. Instead, some equilibrium width $\Delta\tilde{L}$ had been established which had been defined by the equilibrium between extension stresses working on the fracture walls, viscous friction and buoyancy forces in the melts rising in the channel. At rising of a magma melt much lighter than its enclosing lithospheric rocks, the fracture's upward advance might have been accompanied by its "slamming" (total closing) from below under the influence of lithostatic pressure. That is a reason to expect that kimberlite dykes at great depths (in the subsurface lithosphere) might also have been pinching out leaving after themselves only narrow traces of the former magma-withdrawing channels.

Therefore, because of density difference between lithospheric rocks and kimberlite melts ($\Delta\rho \approx 0.5$ g/cm^3), the latter should have been squeezed out

of the lower part of a fracture and invaded the continental crust (Fig. 15.1) under a great excessive pressure

$$\Delta p \approx \Delta h \cdot \Delta p \cdot g, \tag{15.2}$$

where Δh is fracture's depths interval in the lithosphere filled up with melts; Δρ is the lithosphere and kimberlite magma density difference, $g \approx 10^3$ cm/s^2 is the gravity acceleration.

Obviously, such mechanism of melts squeezing on Earth's surface might have operated only at $\Delta p > 10^8$ dyne/cm^2. For this, satisfaction of the following inequality Δh > 2 km had been necessary (Fig. 15.1), which appeared to have been a quite real condition. Should the kimberlite melts have been rising from the base of the continental lithosphere in an open channel in the entire interval of its thickness, then the excess pressure underneath the continental crust must have been reaching 10^{10} dyne/cm^2 which is approximately hundredfold of the lithospheric rocks' tensile strength. For this reason, the opening of a magma-withdrawing fracture under the influence of tensile lithospheric stresses, most likely, must have been occurring only at the expense of hydraulic fracturing effect of the overlying rocks. This could have happened under excess pressure Δ*p* action in the column of a rising magma as shown in Fig. 15.1., i.e., in a case when the height of the magma

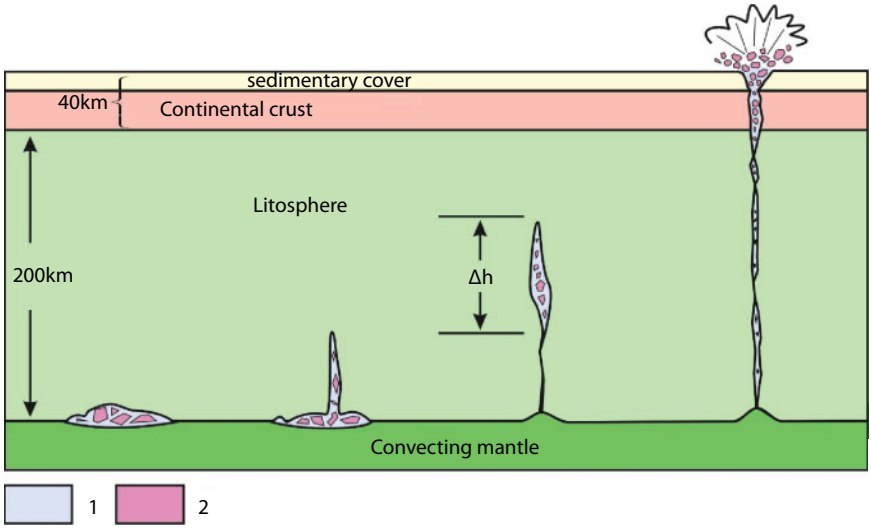

Fig. 15.1 Formation mechanism of the kimberlite magmatism magma-withdrawing cannels. 1. The kimberlite composition magma, 2. Depth rock xenoliths and diamond xenocrysts.

column's open portion had exceeded two kilometers. At that, the initial fracture evolution might have occurred only from below and on condition that tensile tectonic stresses operating at the base of the lithosphere had exceeded the same rock tensile strength of 10^8 dyne/cm^2.

The magma-withdrawing channel formation process had been developing as rapidly as allowed by viscosity of the fracture filling magma. Average liquid laminar flow rate in a flat channel (a dyke) is defined by a simple expression which is a solution of the Navier-Stokes equation

$$\bar{U} = \frac{(\Delta L)^2}{12\eta}\Delta\rho g, \tag{15.3}$$

where η is liquid's (melt's) dynamic viscosity. It must be noted that the formula (15.3) determines only the upper limit of the magma rise velocity in the lithospheric fracture. The real velocity must have been much lower because of a turbulent vorticity of the rising magma flow.

The minimal rate of the kimberlite magma rise apparently may be determined from the velocity ϑ of heavy xenoliths immersion in a viscous liquid of the magma flow. From the Stokes' formula, this rate is equal to

$$u = \frac{r^2\Delta\rho g}{3\eta}, \tag{15.4}$$

where r is radius of a spherical shape xenolith. The emergence of the flow vorticity is determined by the critical value of Reynold's number R_e > 2,300 [225]

$$R_e = \rho\bar{U}\Delta L/\eta. \tag{15.5}$$

Most hardly determinable parameters in Eqs. (15.3)–(15.5) are the kimberlite melt viscosity η and the width ΔL of the magma-withdrawing channel in the lithospheric plate. Kimberlite melts rising from the lower lithospheric levels where the medium temperature had been substantially over the kimberlite magma melting temperature (see Fig. 12.2) had turned out overheated approximately by 400–500°C. Besides, the kimberlite magma saturation with volatiles (H_2O and CO_2) had even greater decreased its viscosity. So, it is reasonable to assume that the kimberlite melt viscosity must have been much lower than the viscosity of liquid basalt lavas. As the

Hawaiian volcanos' basalts at 1,200°C have viscosity on the order of $5 \cdot 10^2$ П [401], it is reasonable to take the viscosity of the fluid-saturated kimberlite melts at $\eta \leq 10^2$ П.

Assuming now in Eq. (15.4) for the eclogite composition xenoliths $r \approx$ 10 cm, $\Delta\rho \approx 0.7$ g/cm^3 and kimberlite melt viscosity $\eta \leq 10^2$ П, we determine $u \approx 2.3$ m/s.

For the delivery of depth xenoliths, for instance, eclogite nodules, on Earth's surface from a 200 km depth, it is necessary that the conditions $\bar{U} >> u$ and $\Delta L >> 2r$ had been satisfied. If we assume, under the second condition, $\Delta\bar{L} \approx 2$ m then from Eq. (15.3) we find $\bar{U} \approx 160$ m/s, i.e., $\bar{U} >> u$ indeed.

The magma flow turbulization under these conditions, judging by Eq. (15.5), would have begun already at the velocity $\bar{U}_{cr} > 4$ m/s. The real rate of the kimberlite melt rise must have been within the range $4 < \bar{U} < 160$ m/s. Most likely, this rate had been close to a value $\bar{U} \approx 50$ m/s. At such kimberlite magma rise velocity (around 180 km/h), it should have crossed the entire lithosphere from the depth of about 200–220 km in just 1–1.5 hours.

After estimating the kimberlite magma rise velocity, we would like to point out again that only due to its high values ($\bar{U} >> u$), the high-density xenoliths of eclogite and lherzolite-garnet composition might have been brought up on the surface. A high velocity of this magma rise may be an explanation why the diamonds metastable at low pressure and high temperature, still had been able quickly enough to "leapfrog" through the hot graphitization zone, which was dangerous for them, and be preserved in the kimberlite rapidly cooling down after the rise.

The lamproite magma viscosity, due to lack of the carbonatite components in its melts, must have been substantially higher. If we assume for them $\eta \approx 10^3$ П, then at the same channel width $\Delta\bar{L} \approx 2$ m and $\bar{U} \approx 16$ m/s, the critical velocity of magma flow turbulization would have risen to $\bar{U}_{cr} \approx 41$ m/s. It follows thence that the lamproite melts had been rising as laminar flows without a notable flow turbulization and had crossed the distance from the base of the lithosphere to Earth's surface in 3.5–4 hours. Without turbulence, large depth xenoliths might not have been brought out on the surface because during the travel time they had lagged behind in their advance by a few kilometers and had remained on deeper horizons. Whereas the diamonds, due to their smaller size, same as small xenoliths, had been brought out by viscous lamproite melts without substantial losses. A testimony to it, in particular, is the fact that a lamproite diatreme Argyle in West Australia is the world's largest primary diamond deposit [402]. However, because of a slower rise velocity and longer diamond residence time within a hot zone of their metastable state, most

diamond crystals bear a stigma of corrosion caverns, dissolution and surficial graphite sprinkling [2].

As soon as a rising kimberlite magma had reached a level at which the pressure of fluid phase released from the melt had become equal to lithostatic pressure of the overlying rocks, an explosion would have occurred, and through the formed channel, the kimberlite magma, together with enclosing rock fragments and depth xenoliths, would have been thrown on the surface as a magma breccia typical of kimberlites. Along with depth xenoliths, the kimberlite magma had carried out the noble diamonds thereby closing another branch of carbon turnover in the nature.

As previously mentioned in Chapter 12, in a case of kimberlite and their affine magma invasion of an Archaean age crystalline basement, they had formed not typical diatremes but peculiar spider-like shaped dyke bodies. Therefore, at the release of these magmas into the continental crust's near-surface horizons, not only lithostatic pressure levelling must have occurred but also the density levelling of the magma and the enclosing medium. It is natural to expect that in case of kimberlite and their affine magma invasion of the sediment cover, the parameters listed above would have been satisfied much more often than in its absence.

In most cases, kimberlites through diatremes had broken through on Earth's surface from the depth of 2–3 km. Analyzing this pattern, J. Dawson [48] noted that exactly at such depth (i.e., under pressure of about 0.8 kbar) water and CO_2 solubility in the kimberlite magma drastically declines. As a result, these fluids had begun releasing from the melt in abundance, had caused its frothing (boiling) and eventually exploding. The adiabatic expansion of fluids released from the magma had caused a sharp cooling of explosion products (the magma breccias). The blowup rate of volcanism products had sharply increased reaching near the surface (in kimberlite diatremes) 400 m/s [1].

The amount of kimberlite magma generated in the former plate subduction zones had been naturally limited by the volume of pullet into them Early Proterozoic "heavy" deposits. So, after the kimberlites or their affine rocks breakthrough on Earth's surface, the kimberlite magmatism had been exhausted. The magma in the supply channel had crystallized welding again earlier temporarily separated continental plate fragments. Due to that, the plate's tensile strength had sharply risen again on the account of a new "switching in" of the plastic mechanism of lithosphere deformations with its exceptionally high extension viscosity. The rate of deformations themselves had equally sharply slowed down. Should have the geodynamic environment on Earth changed again at that time and the subject continental plate had gotten again under a quiescent tectonic environment or

in the area of a compression force operation, the unity of plate would have been preserved and a chain of diamond-bearing kimberlite diatremes on its surface would have remained as an inarticulate testimony to an unsuccessful attempt on the formation of a young ocean.

Accurate determination of the geological time of kimberlite and other deep melts' invasion of the continental crust is quite difficult. Unfortunately, radiological dating techniques produced rather ambiguous and inaccurate results [403]. Geological techniques are more accurate but also imprecise. That is why today we may identify only a "crude" periodicity of kimberlite volcanism manifestations. With this in mind, we tried to restore the periods and historical sequence in depth magmatism manifestations based on the data included in the publications by ([3, 24, 127, 402] and many others).

It is suggested that the first kimberlite volcanism had shown up in Middle Proterozoic of the Western, Central and Southern Africa at first impulses of a split in the Stille's supercontinent Megagea about 1,800–1,700 MYa. That is when, for instance, one of the richest diamond diatremes, Premier (RSA) and a number of diatremes in the West and Central Africa, Canada and West Greenland had formed. The second impulse of kimberlite volcanism had occurred around 1 BYa, at the split of the third in Earth's history supercontinent Mesogea (Rodinia). At that time, for instance, diatremes National in RSA, Madgavan in India and Argyle in West Australia had formed. It is possible, of course, that Argyle diatreme had emerged somewhat earlier, at the formation time of the supercontinent Mesogea. Mesogea disintegration had been occurring in a few stages. First, around 800–750 MYa, this supercontinent had fallen apart into Laurasia and Gondwana. Then, about 650 MYa, Gondwana had disintegrated into the eastern and western continents. The Venice diatreme in RSA and River Ranch diatreme in Zimbabwe, perhaps, had been also connected with this process. Laurasia splits had happened at the same time [127] and had continued even in Middle Paleozoic. In particular, the Vilyuy paleo-rift on the Siberian platform had been started in Devonian same as a cutoff from it of the Kolyma massif with the formation of the East Siberian paleo-ocean. The main phase of kimberlite-formation on the Siberian Platform had belonged exactly with this time period [127, 402].

However, most kimberlite diatremes in the world had formed at the Wegenerian Pangea split around 200–80 MYa. The kimberlite magmatism association with the processes of a young ocean formation had manifested itself especially clearly at the total plate tear-off as this had been observed in Middle and Late Mesozoic at Gondwana split [404]. Examples of this are numerous kimberlite manifestations in South Africa and Canada or lamproite magmatism in Australia. This type of magmatism had been

clearly associated in time with the Pangea split and the formation start of the South Atlantics, the Indian and Southern Oceans. In space, they had also gravitated to peripheral portions of continents washed now by the young oceans formed exactly due to such splits of the ancient supercontinent Pangea unified in the past. Thus, the main impulse of kimberlite magmatism in South Africa had occurred at the formation start of the South Atlantic and of the Indian Ocean. Late Mesozoic formations in RSA include kimberlite diatremes Wesselton, Dutoitspan, De Beers, Kimberly, etc. Some diatremes in Tanzania, Botswana and the Democratic Republic of the Congo also belong with the same group of young kimberlite magmatism manifestations.

In Yakutia, the young kimberlite magmatism epoch had coincided with the emergence of the Triassic trap formations (about 200 MYa) associated with the Wegenerian Pangea split and disintegration of the Siberian platform. Somewhat younger kimberlites of Middle Jurassic and Cretaceous also corresponding in time with Pangea split and formation of the North Atlantic are known in Slave Province (Eastern Canada, north of the Great Lakes). In Australia, the main impulse of the lamproite magmatism had been associated with the moment of this continent's breakaway from the Antarctic and the start of its northward drift in Oligocene-Miocene.

Except the depth magmatism manifestations in the environment of the continental crust extension, also known are the cases of kimberlite and their affine magmas invasions in the environment of continental plates' asymmetric compression. A graphic example of such a situation is tectonic activation of the Baltic shield's northern areas. It had occurred in Devonian, about 390–370 MYa at closing of the Paleo-Atlantic Ocean Iapetus and northern areas of the Paleo-Uralian Ocean in Carboniferous, around 340–320 MYa. In both cases, the frontal areas of adjacent plates colliding with the Baltic shield had been like giant wedges not only compressing the lithosphere of this shield but also spreading aside its side areas (Fig. 16.7). At the intersection of so formed strike-slip faults had to have emerged "gaping" channels – natural deep magma release ways (if, of course, such channels had emerged above the foci of their melts). Importantly, the entire alkali-ultramafic, carbonatite, melilitite and kimberlite magmatism on the Kola Peninsula and Archangel Province, as is known, age-wise had belonged exactly with these Middle Paleozoic tectonic events. This is in complete agreement with the mentioned formation schematics of the Baltic Shield deformations.

16

The Forecast Criteria of Diamond Magmatism Localization Zones and the Evolution of Some Diamond-Bearing Provinces

As we saw in the previous chapters, the melts of diamond-bearing kimberlites and their affine depth rocks had been formed at the expense of pulling in "heavy" ferruginous Early Proterozoic deposits to great depths (up to 200-250 km) underneath the ancient continents, their melting and magmatic differentiation. Only after the emergence of tensile stress in the continental lithosphere might these melts have erupted blisteringly on Earth's surface.

The described mechanism of kimberlite formation in plate subduction zones shines light on cause and effect ties of this process, defining that the kimberlites are undoubtedly depth rocks but emerged from the exogenous matter. The affine to kimberlites are the formations of the alkali-ultramafic series, melilitites, lamproites and carbonatites. Their main distinction is in that all these rocks are magmatic series well differentiated in density whereas kimberlites are mixes of the densest magnesium-silicate melts of lamproite composition with calcium carbonatites. Besides, magmas forming alkali-ultramafic intrusions of Khibin type and sodium carbonatites, had been usually begotten at substantially shallower depths than the melts of lamproites, calcium carbonatites and kimberlites.

Besides, it is possible that in some cases, magmas might have emerged close in composition to the subject rock series in the crustal conditions like, for instance, at basalt melt invasion of the continental crust medium stages made of water-containing sedimentary-carbonate sequences. Melting of such sediment rocks on contact with hot basalts might have resulted in emergence of silicate-carbonate magmas compositionally close to them. Possibly, that had been the way, for instance, for the emergence of sienites (miaskites) in the Ilmen Mountains in Urals.

N. O. Sorokhtin (ed.) The Origins of Natural Diamonds, (443–475) © 2019 Scrivener Publishing LLC

The reviewed kimberlite and their affine alkali-ultramafic and carbonatite rock formation mechanism as well as the distribution nature of iron ore accumulation epochs displayed in Fig. 11.9 allow to phrase in a general form forecast criteria for the search of appropriate rocks on Earth's surface subsequent upon the model:

1. The diamond-bearing bed-rocks, kimberlites and lamproites, as well as their affine rocks had been formed mostly on the Archaean continental crust; although in some cases they might have invaded the Proterozoic crust but must never be found on young (Phanerozoic) platforms and even more so, on the ocean floor.
2. Diamond-bearing kimberlite and lamproite diatremes, as well as their affine carbonatite and alkali-ultramafic intrusions, are mostly positioned above plate subduction zones of Svecofennian (Karelian) age that had been functioning about 2.0-1.8 BYa although sometimes might have emerged above the younger Grenvillian plate subduction zones.
3. Appropriately to the formation depth of a rock series under consideration and a plate subduction zone dip steepness (see Figs. 3.1 and 12.1), the closest to the front of a former plate subduction zone (100 to 200–300 km from its front) are positioned alkali-ultramafic intrusions and (sodium) carbonatites. Then (at a distance of 200 to 400 km) follows the zone of calcium carbonatites and melilitites and sometimes non-diamond-bearing kimberlites. The diamond-bearing kimberlite and lamproite diatremes are positioned farther than other similar formations, approximately at a distance of 300 to 600–650 km from the front of Early Proterozoic plate subduction zone.

An additional forecast criterion for the search of the subvolcanic complexes under consideration may be the presence in the suture zones on contact with an Archaean crustal block of Early Proterozoic iron ore formations (if such ones had been preserved) and especially if it is known that these formations are submerging underneath it. Inasmuch as heavy iron ore deposits, having gotten in the gap between plates, had played there the role of a lubricant, the Early Proterozoic plate subduction zones into which such deposits indeed had been pulled, had always remained practically amagmatic, without any manifestations of the calcareous-alkali volcanism.

The cited criteria define only a conceptual possibility of finding in a given region the kimberlite, alkali-ultramafic or carbonatite complexes. However, the realization of this possibility, as follows from the withdrawal mechanism of depth melts on the surface, had depended on the emergence in the past geological epochs of tectonic regimes of lithosphere expansion underneath a given region. That is why, if from independent geological data is known that the region under study during some period of time (after Early Proterozoic event of plate collision) had experienced tensile deformations, the probability for the formation of a rock series under consideration sharply increases. Examples are the richest diamond-bearing provinces in Canada, South Africa, Brazil, India, Australia and Siberia, as well as the north of the Baltic shield. Indeed, the initiation of all these diamond-bearing provinces had developed underneath the Archaean crust and close to the Early Proterozoic collision zones of ancient cratons that had occurred in the formation epoch of Stille's Megagea at the time of the Eburnean or Svecofennian (Karelian) epoch of tectono-magmatic diastrophism. Whereas the final stage of the formation of these provinces (connected with delivery on the surface of depth melts) had occurred at the split and deformation times of ancient supercontinents (Megagea, Mesogea and Pangea). However, the main impulse of the kimberlite and alkali-ultramafic magmatism had occurred at the disintegration time of the Paleozoic supercontinent, Wegenerian Pangea.

Beside the already identified world diamond-bearing provinces, in the context of the mechanism under consideration of depth melt formation and the emergence of diamond-bearing rocks, no less potential provinces are the Baltic shield, Russian platform with the Voronezh shield and the Ukrainian shield.

16.1 Some Formation Examples of World Diamond-Bearing Provinces

We will now consider the extent to which the positions of the kimberlite and lamproite diatremes in the world's best-known diamond-bearing provinces correspond with the search criteria of the crustal diamond-bearing rocks listed above. We will start with the classic example of South Africa.

The kimberlites in the South African Republic are found within a huge territory of the Kaapvaal Archaean craton between the Early Proterozoic fold belt Limpopo in the north and Early Paleozoic Cape mobile belt in the south. Diamond-bearing is also Zimbabwe craton (Fig. 16.1) adjacent in the north to Limpopo belt. Both Archaean cratons had been separated in

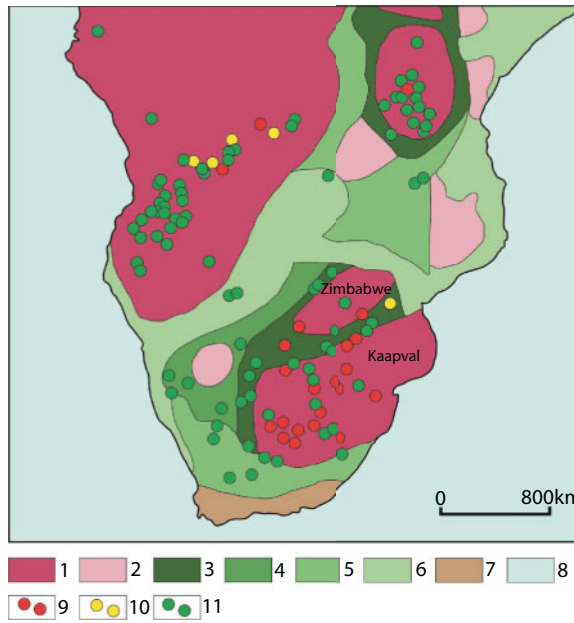

Fig. 16.1 Schematic location map of alkali-ultramafic and kimberlite diatremes in the territory of South Africa [405]: 1. Archaean cratons; 2. Paleo-Proterozoic continental massifs; 3-7. Fold belts: 3. Paleo-Proterozoic, 4. Paleo-Meso-Proterozoic, 5. Meso-Proterozoic, 6. Neo-Proterozoic, 7. Neo-Proterozoic– Paleozoic; 8. Atlantic and Indian Oceans; 9. Diatremes of diamond-bearing kimberlites; 10. Placer diamond deposits; 11. Diatremes of non-diamond-bearing kimberlites and alkali-ultramafic rocks.

Early Proterozoic and apparently had been positioned at a substantial distance from each other. At the end of Early Proterozoic (about 2.0 BYa) they had merged and formed a fold belt Limpopo and a unified proto-platform Kalahari. Herewith, the mobile belt marginal zones had obducted both cratons, Kapvaal and Zimbabwe [127]. The latter circumstance suggests that the subduction of the oceanic plates had been simultaneously occurring underneath both cratons (underneath the Kapvaal to a greater extent and underneath Zimbabwe). Besides, the Archaean age of the Limpopo fold belt in the central zone indicates that at collision of the stated cratons, between them had been squeezed also a small terrane with more ancient crust. After the formation of a united proto-platform Kalahari, Magongi and Case mobile belts had been squeezed to it from the west. They had been evolving, same as Limpopo, in the time interval 2.0–1.7 BYa [127]. A similar situation had developed also in the vicinity of other diamond provinces in Africa. Such provinces are bordered everywhere or are even

surrounded by Early Proterozoic fold belts that had been developing at formation of the supercontinent Megagea about 2.0–1.8 BYa.

The major mass of diamond-bearing kimberlites in North America is positioned on the Archaean cratons Slave and Superior separated from each other by the Trans-Hudson Svecofennian age fold belt emerged about 1.9–1.8 BYa at Megagea formation (Fig. 16.2). After the appraisal operations in the 1990s, it was determined that the Slave craton may become one of the richest world diamond-bearing provinces [402]. As seen in Fig. 16.2, some

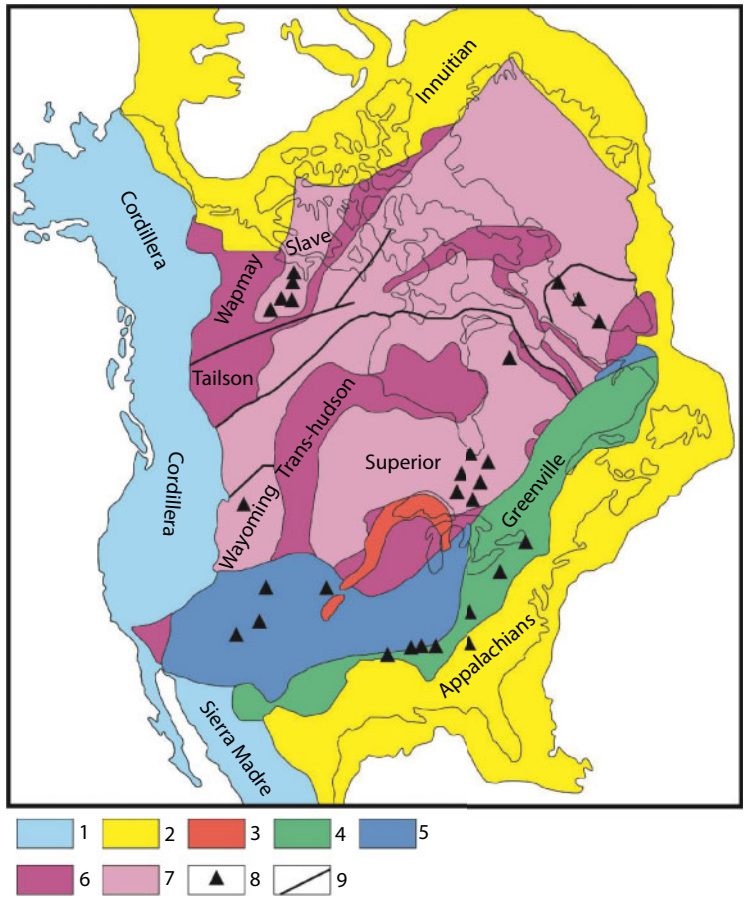

Fig. 16.2 Schematic map of age subdivision of the North American basement. The map shows kimberlite bodies after J. Dawson [1] and for the Slave craton, based on the data in publication [402]. 1. Mesozoic-Quaternary orogens; 2. Paleozoic orogens and passive continental margins; 3. 1.1 Ba continental rift; 4. 1.3-1.0 BYa orogens, 5. 1.8-1.6 BYa orogens; 6. 2.3-1.8 BYa orogens; 7, Archean cratons; 8. Kimberlite diatremes; 9. Faults.

kimberlite bodies in North America are positioned not on the Archaean but on the Proterozoic crust. Apparently, the emergence of these kimberlites had been associated either with Riphaean iron accumulation impulses in Fig. 11.9 or with that the North American Proterozoic formations in the past had been obducted over the Archaean crust.

A similar situation is observed in West Australia. As described in a fundamental monograph by A. Jakes, J. Louis and C. Smith [2], "basic structural positions of the kimberlite and lamproite intrusions in West Australia are defined by their location within the Early Proterozoic mobile zones at the boundaries of Archaean nuclei although these zones may be overlain by the Phanerozoic sediment cover" (Fig. 16.3). Here, however, a fact should be kept in mind that underneath the Kimberly depression filled up with Riphaean sediments is suggested the existence of an Archaean block surrounded

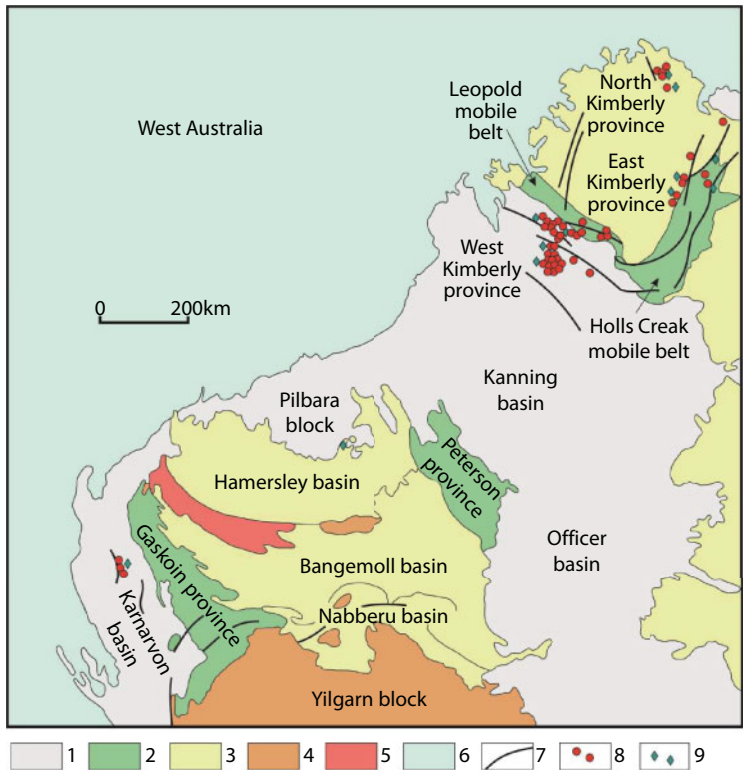

Fig. 16.3 Major tectonic structures in West Australia and the positions of kimberlite and lamproite provinces [2]: 1. Regions overlain by Phanerozoic sediment complexes; 2. Proterozoic fold belts; 3. Proterozoic basins; 4. Archaean cratons; 5. Ashberton trough; 6. Indian Ocean; 7. Large faults; 8. Lamproite and kimberlite intrusions; 9. Diamond deposits.

from south and east by Early Proterozoic folded systems, respectively, King-Leopold and Halls-Creek. Herewith, the age of final deformations (cratonisation) of this entire area of the West Australia is estimated at 1,850–1,890 MYa [127]. Thence, a conclusion may be made that, as in North America, most kimberlite and lamproite intrusions in West Australia had emerged on the Archaean crust and the appropriate depth melts underneath it had emerged at the time of Early Archaean plate subduction episode homochronous with the Svecofennian orogenesis of the Baltic shield.

We will now examine one more classical example: the Yakut diamond-bearing province positioned in the eastern part of Siberia. Basement of the Siberian platform is exposed on the surface in two large shields, in the north the Anabar and in the southwest, the Aldan. Diamond-bearing are mostly the Anabar megablock and, in part, the Aldan shield (Fig. 16.4). The Central part of the Aldan megablock is composed of granite-greenstone rocks dominated by Late Archaean formations aged about

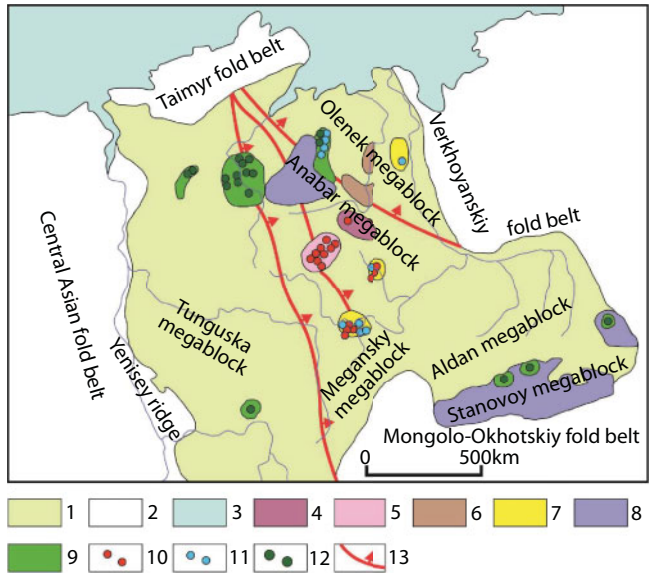

Fig. 16.4 Tectonic схема of the Siberian craton: 1. Siberian platform (Archaean age); 2. Paleozoic and Mesozoic overthrust belts fringing the Siberia craton; 3. Arctic ocean; 4-9. Areas of the kimberlite and its affine magmatism; 4. Early Paleozoic age, 5. Late Paleozoic age, 6. Unsubdivided Paleozoic age, 7. Early Mesozoic age, 8. Undifferentiated Paleozoic and Mesozoic age, 9. Areals of alkali-ultramafic and carbonatite magmatism; 10-11. Diamond deposits, 10. Bedrock, 11. Placer; 12. Largest diatremes of alkali-ultramafic and carbonatite composition; 13. Suggested plate subduction zones along the Baikal-Taymyr suture and eastern blocks of the Anabar shield (author's interpretation).

2.75 BY, although Middle Archaean are also encountered. Three blocks are identified in the Anabar massif composition. They are separated by fold belts aged about 1.9–1.8 BY. Along them occurs the subduction of the western blocks underneath the eastern. The age of the western (Magan) and central (Daldyn or Central Anabar) blocks is 3.2 BY. Juncture of the western (Tungus) megablock with the other parts of the Siberian platform, apparently, had occurred in the second half of Early Proterozoic about 1.9–1.8 BYa, inasmuch as exactly with this time had corresponded the epoch of platform cratonisation whereas in Early Riphaean (i.e., during the destruction of Megagea supercontinent) had already begun the aulacogen stage in the Siberian platform evolution.

It is hard to judge the basement age of the western (Tunguska) megablock as it is overlain by a thick sequence of the platform cover. However, the exposure in the Yenisei Range (in the west) and in the southwest of the Archaean rocks megablock, in our view, indicates Archaean time of its formation. Based on geophysical data, the Baikal-Taymyr suture belt is a plate subduction zone along which the Tunguska megablock is subducted under the Anabar one. In this case, the kimberlite emergence of Mirny to Daldyn and Upper Muna fields, as well as Mesozoic diatremes abutting the Anabar shield (see Fig. 16.4) may be explained by pulling in ferruginous deposits of Early Proterozoic Central-Siberian paleo-ocean under the Megan and Anabar Archaean megablocks. In all these cases, the distance between the front of the subduction zone of the Baikal-Taymyr suture zone and these kimberlite development fields is exactly 400–500 km. Still, the eastern kimberlite development fields, apparently, are tied with the Magan block subduction underneath the eastern Khapchan block.

Thus, on the Siberian platform, as in South Africa, we see a classical example of the kimberlite rocks formation at the expense of pulling-in Early Proterozoic pelagic (ferruginous) deposits underneath the Archaean cratons.

16.2 Geodynamical Evolution of the Western Part of the Russian Arctic and its Diamond-Bearing

The most important task in forecasting alkali-ultramafic and diamond-bearing magmatism localization zones is the identification of Early Proterozoic suture structures which mark the former plate subduction zones of the oceanic crust underneath the Archaean cratons. Then it is necessary to determine their dip direction.

The internal structure of the Baltic shield mostly had been formed by the Sveco-Karelian tectogenesis about 1.9–1.8 BYa. It had welded together individual blocks and shields of Archaean age. Presently, the Baltic shield includes two different in age and structure Earth's crust areas, the Archaean Karel-Kola (in the east of the Baltic shield) and the Early Proterozoic or Svecofennian in the west of the shield. Similar to the present-day shield limits had been formed in Caledonian time when in its northwestern part had formed a mighty fold belt of the Caledonides overlying the Archaean and Proterozoic formations as a result of closing the Proto-Atlantic Ocean Iapetus. The southeastern part of the shield is dipping at a low angle underneath the Riphaean-Paleozoic cover sediments of the Russian plate's north part. The northern and northeastern boundary is running along Murmansk coast and is restricted by a system of Karpinsky faults where a sharp stepwise plunge of the crystalline basement underneath the Timanides and the Barents Sea platform is observed.

The Kola Peninsula and Karelian continental blocks with adjacent from the east territory of Archangel area had been formed in Late Archaean in the interval of 3.5-2.7 BYa (Isotopic... 1989). At the end Archaean, about 2.7–2.6 BYa, their juncture had occurred along the Belomorid fold belt as a result of global Kenoran diastrophism that had merged all previously separate Archaean shields in a single supercontinent Monogea. In the first 100 MY of Monogea's existence, this entire part of the Baltic shield had been evolving in a platform regime. However, the invasion of stratified basite-hyperbasite composition intrusion in the Archaean crust in the 2.49–2.39 BYa interval [406] had marked first expansion impulses of the Archaean crust and initiation of paleo-rifts and paleo-oceans and had formed Early Proterozoic greenstone belts. Within the Karel-Kola lithospheric plate, greenstone belts of this age are grouped in two areas of their development. One is localized within the Kola Peninsula and is represented by Pechenga – Imandra-Varzug and Vetrenny [Windy] greenstone belts [194]. Its material fill corresponds with riftogenic and proto-ophiolite formations [407, 408]. Individual fragments of this belt are separated by transform type faults. Also, in the first half of Early Proterozoic, about 2.4–2.3 BYa, had occurred the splits of its entire territory and in the Archaean granite-gneiss crust had begun invading stratified peridotite-pyroxenite and gabbro-norite intrusions. The evolution of this process had resulted in the emergence within the Kola-Karelian plate of a whole number of riftogenic structures with northwest stretching long axes [407, 408]. In some of them, the expansion had caused a total breaking of the continental crust, the emergence of oceanic basins and the formation of oceanic type crust. It is important to keep this in mind as in the issue of the diamond-bearing rock emergence, the width of emerged oceanic depression

is of a major significance inasmuch as kimberlite melts might have emerged only at a plunge of the oceanic crust to a depth equal to average thickness of the continental lithosphere, i.e., up to 200–250 km. However, such a process, considering the dip angle of the plate subduction zones, might have been occurring only at closing of the ocean at least 800–1,000 km-wide, or even 1,500–2,000 km. A number of authors are developing a concept of large-scale displacements of moving apart crustal blocks [407] and, appropriately, of the development of wide oceanic basins within the Karel-Kola region.

The Early Proterozoic Earth's tectonic activity had been noticeably weaker than the Archaean one but still had exceeded the present-day one at least three-fold. Besides, taking into consideration the then existing asymmetry in the convecting mantle composition (in the mantle of that time, fragments of Earth's primordial matter had still remained), it may be expected that Megagea supercontinent (1.9–1.8 BY), most likely, had formed in the opposite hemisphere relative to Monogea (~2.6 BY). It follows thence that intercontinental oceanic basins in Early Proterozoic had been sufficiently wide and in the Karel-Kola region under consideration it might have been a series of three or four oceans with the total width of up to a few thousand kilometers.

During the time interval 2.0–1.8 BYa, the geodynamical environment on the Baltic shield had been replaced by the regime of a ubiquitous compression. The result had been the continental crust consolidation and formation of its general tectonic plan. The closing of Early Proterozoic oceanic basins positioned in the present-day coordinates southwest of Belomorides had been accompanied by a large-scale absorption of the oceanic crust in the plate subduction zones southwest of Kola Archaean lithospheric plate (Fig. 16.5). As a result of happened after this collision of earlier separated (in the beginning of Early Proterozoic) Archaean microcontinents and terranes, had occurred the consolidation of the Karel-Kola megablock and the Svecofennian area.

The Svecofennian folded area occupies the central part of the Baltic shield and borders in the northeast with the Karelian granite-greenstone area. The formation model of this territory was proposed by A. Hiltanen [409] and Gaal [410]. Under this model, the Svecofennian area had been formed in Early Proterozoic at the expense of evolution of the island arc system in a wide ocean that had existed then between the Karel-Kola Archaean craton and the Archaean cratons of other regions. At the end of Early Proterozoic, about 2 BYa, the Svecofennian ocean had begun closing. As a result, all inter-arc basins had closed and the oceanic crust had subducted underneath the Karel-Kola craton having formed a multistage suture system.

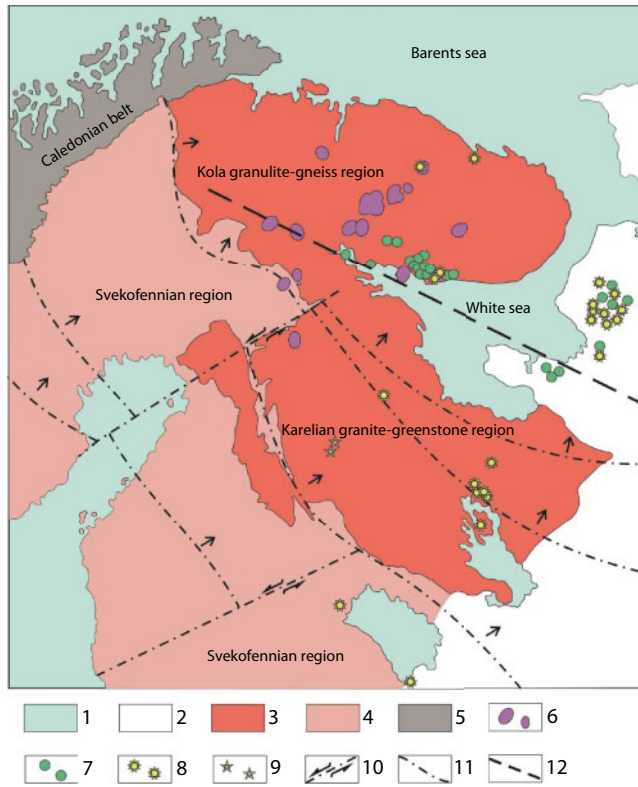

Fig. 16.5 Geological scheme of the eastern Baltic shield: 1. Hydrosphere; 2. Sediment cover of the Russian platform; 3. Continental-crustal Archaean associations; 4. Early Proterozoic (Svecofennian) sedimentary-volcanogenic and intrusive complexes; 5. Caledonian allochthonous nappes; 6. Alkali-ultramafic intrusives; 7. Diatremes of picrite and melilitite composition; 8. Kimberlites; 9. Lamproites; 10. Transform type faults; 11 Plate subduction - zones and oceanic plate subduction directions (arrows) of Early Proterozoic (1.9–1.8 BYa); 12. Paleozoic Kandalaksha-Dvina rift system axis.

The Svecofennian folded area is a complex system of volcanogenic-sedimentary complexes broken through by synorogenic gabbro-tonalite and gabbro-granodiorite series batholiths. Here and there, they form vast Earth's crust areas, merging and making independent geostructural elements. The age of the plutonic formations fluctuates within 2.2–1.9 BY. Synchronous with the plutonic magmatism had been volcanic manifestations of the entire rock spectrum from basalt-andesite to dacite-rhyolite composition. Geochemistry of these rocks is a testimony of this complex belonging to island arc formations [411]. Effusives alternate with deposits whose amount increases to the periphery of volcanic belts [410]. All these

data allow to consider the described volcano-plutonic Svecofennian associations as magmatic complexes of ancient island arcs whose collision had resulted in the formation of the region's continental crust. These associations are broadly developed and sometimes are broken through with granitoids, and someplace enrobe some terranes of the Archaean continental crust. Among the island arc series are sometimes found fragments of the oceanic type crust with typical features of ophiolite complexes. The intrusive and volcanogenic part of the ophiolite section is composed of tholeiite series ultrabasites and basites which take the main volume of such belts. The sedimentary part is albitized clay deposits, pelites, carbonates, conglomerates, siliceous associations and graphite-sulfide crystalline schists. Numerous are interbeds of ferruginous quartzites. In the volcanic sections of greenstone belts, the basalt parts have the structure of pillow lavas. The geochemical features of ophiolite complexes in the Svecofennides identified some their distinctions in some elements. For instance, the more ancient of them (2.4–2.2 BY) are significantly enriched in Fe and Mg.

Specifics of spatial position, internal structure and age of volcanogenic-sedimentary complex formation suggest the presence in the Karel-Kola megablock and in the Svecofennian area of at least four or five paleo-subduction zones dipping northeast (Fig. 16.5). The first one is cutting the Karel-Kola Archaean continental plate in southeastern direction south of the White Sea fold belt. The Berlomoride formation had occurred in Late Archaean (2.9–2.8 BYa). However, at the end Early Proterozoic, the belt had undergone intense tectonic reworking due to the collision of the Kola and Karelian continental blocks. The White Sea belt is a typical granulite-gneiss collision belt of the nappe structure [206]. Farther northeast it most likely dives underneath the Kola granulite-gneiss craton. We identified the second subduction zone based on indirect indications. It also is cutting the Karel-Kola megablock south of the first zone and dipping northeast. At last, the third, best expressed plate subduction zone fringes the Karel-Kola Archaean megablock from the southwest and is marked by a change of the age of the rock features from Archaean in the northeast to Early Proterozoic in the southwest. Besides, northeast of this zone, the formation age of continental margin complexes varies in the 2.4–2.2 BY range whereas southwestward the island arc complex youngs to 2.1–1.9 BY. The fourth zone of the suggested plate paleo-subduction is not as certainly identified. However, it may be drawn on the change boundary of the proto-oceanic and island arc associations material fill. On the other hand, the fourth and fifth zones are quite certainly recorded by geophysical data in the seismic project "Babel" in the Gulf of Bothnia [412]. The geophysical data also indicate a plunge of the paleo-oceanic plate underneath the Karel-Kola Archaean megablock.

It is important to note that the Archaean continental lithospheric plate thickness by end Early Proterozoic had already reached about 200–250 km. Therefore, at dip angles of the subducted oceanic lithosphere at 20-25°, the horizontal distance between this plate subduction front and the kimberlite melt generation zone at depth of about 250 km underneath the Archaean craton might have been 300 to 600–650 km.

An interesting feature of most of Archaean continents active margins in Early Proterozoic is their practically totally amagmatic nature [201]. The remarkable feature makes it more difficult to use a uniformitarian approach to the identification of plate subduction zones. The reason is that the time period 2.0–1.8 BY had been a period of the most intense accumulation on the ocean floor of jaspilite type iron ore deposits in Earth's history, as has already mentioned above more than once. Having gotten in the plate subduction zones, they had served a lubricant sharply decreasing the plate friction temperature below the andesite magma generation temperature. Herewith they had substantially heavied the oceanic plate allowing its subduction underneath the Archaean continent.

The final closing of Svecofennian oceans had occurred about 1.9–1.8 BYa. Since then and to our days the Karel-Kola megablock of the Archaean crust and attached to it Early Proterozoic Svecofennian structures had only the platform evolution regimes of the continental crust.

In the evolution process of the East-European Platform, its northern and northwestern (in modern-day bearings) ends, beginning in Paleo-Proterozoic, had periodically experienced processes of split and collision with the North American lithospheric plate [127]. This is supported, in particular, by comparability of the structure-material complexes of the Svecofennides on the Baltic shield and the Ketilides of south Greenland and Canada. They had formed about 1.9-1.8 BYa at the closing time of the Svecofennian paleo-ocean at the formation of Megagea supercontinent (1.9-1.8 BYa). Later, in the Peri-Timan area and in the Kandalaksha-Dvin basin, about 1,350-1,050 MYa, had been occurring basement subsidence and the accumulation of continental clastic deposits with an admixture of volcanites [127]. At the same time, in the northeast of the Russian plate had been forming shelf and slope sediment complexes of a passive continental margin known today as Timan-Varanger belt of the Baikalides [413]. Data of these processes agree with factual material about disintegration of Megagea supercontinent (about 1.7 BYa) which had been continuing up to Late Riphaean (for about 1,000 MYa) when the next in Earth's history supercontinent Mesogea (Rodinia) had been formed [17]. At that time, in the northwestern peripheral zone of the Eastern European platform the Dalsland folded area had been forming which is the extension of the Grenvillian belt of Canada and Greenland

marking the closing zone of Paleo-Iapetus ocean (not to be confused with Iapetus ocean that had formed later).

A relatively quiescent tectonic environment in the eastern and north-eastern East-European Platform within a very long time period (more than 800 MY, 1,350 through 535 MYa) indicates a possible accumulation of huge sedimentary sequences on the shelf, slope and at the foot of the continent. In that epoch, the continent had continuously migrated from the subequatorial zone (about 1,0 BYa) where it had been at the moment of Mesogea formation, into the Circum-Arctic area (800-650 MYa) and back (about 550 MY) [17, 18, 414, 415] (Figs. 9.4-9.7).

In Vendean (600-535 MYa), processes of its peneplanation had caused the formation of a continental clastic deposit complex with traces of tillites in the northwest and nearshore marine formations in the north, in the area of Varanger Peninsula [204, 416] (Fig. 16.6). At the same time period had

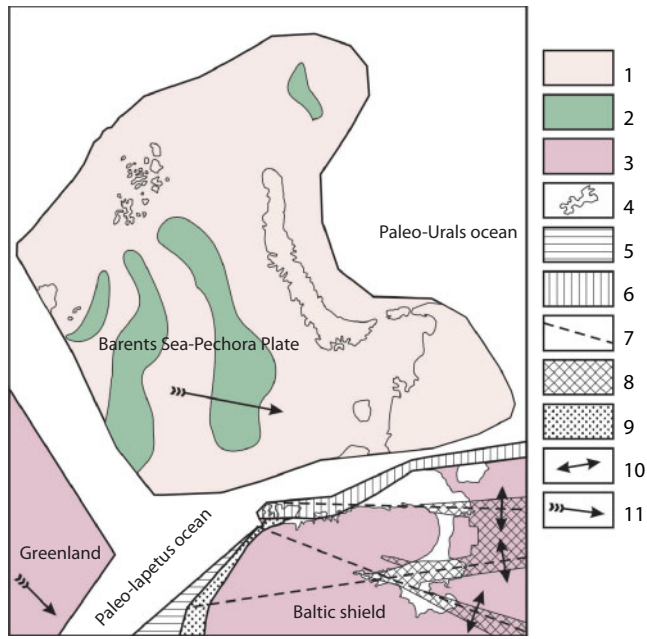

Fig. 16.6 Paleo-geodynamical reconstruction of the East-European platform northern part and the adjacent Arctic basin in Middle Riphaean – Vendean (1,350-540 MYa). 1. Folded formation of Middle-Upper Riphaean in the Dalsland area (1,200-900 MYa), 2. Middle-Upper Riphaean and Vendean sediment complexes on the shelf and continental slope of the passive margin in the northeastern part of the Russian plate and the Baltic shield (1,350-620 MYa), 3. Baltic shield's major lineaments, 4. Upper Riphaean riftogenic formations, 5. Vendean continental clastic deposits (650-570 MYa), 6. Outline of the present-day shoreline, 7. Vectors of the stress fields in the continental lithosphere, 8. Generalized lithospheric plates' displacement directions.

been continuing the accumulation of a shelf and continental-slope sedimentary complex on the north and northeastern passive margin of the Russian plate. Dalsland orogenesis in the west had caused the formation of a number of regularly positioned in space graben-like systems in its northeastern areas. Herewith the tectonic condition of their formation had borne a clearly reflected nature which is supported by their practically total amagmaticity. Only on the northern end of the Kola Peninsula and on the Sredniy and Rybachiy islands were found rare dolerite bodies and dykes attributed to this time period.

Currently, the Riphaean formations of the northern and northeastern passive margin (in the present-day bearings) of the Russian plate are exposed on Varanger Peninsula of Northern Norway, on Sredny ["Medium"], Rybachy ["Angler's"] Peninsulas and Kildin Island (north end of the Kola Peninsula), as well as on the Kanin Nos Peninsula and Timan salient of the Archangel area. In geological publications, these formations are identified as Timan-Varanger system of the Baikalides [417, 418] and present a monoclinal bedding of Middle, Upper Riphaean and Vendean weakly metamorphosed sediment complexes, tectonically reverse-faulted and sometimes thrusted over the Archaean and Lower Proterozoic formations of the Russian plate's Baltic shield [419]. According to the seismic data, the monocline surface is dipping at a low angle (2-5°, then 5-10°) toward the South Barents Depression [418, 420].

Middle Riphaean sediment complexes are composed of gray-colored polymictic conglobreccias, conglomerates and gravelites with siltstone and psammite interbeds. The alternation of dark-colored argillites, siltstones, polymictic psammites and conglomerates with lenses and concretions of carbonate rocks is observed in the upper part of the section. The Upper Riphaean and Vendean formations are the alternating versicolor quartz, oligomictic and arkose psammites, siltstones, pelites and dolomites. In the section are encountered interbeds of polymictic conglobreccias with phosphorite and carbonate concretions' fragments. Secondary transformations correspond with the stage of deep catagenesis – initial metamorphism (metagenesis) [421]. The geodynamical accumulation conditions of the listed complexes correspond with a single lateral series of shelf, continental-slope and continental-foot formations [413]. Phosphorites and carbonate concretions in the section indicate the existence at that time of epi-continental marine conditions in the northeastern part of the lithospheric plate and the presence of upwelling zones.

In Late Vendean - Early Cambrian, about 570-510 MYa, the merger had occurred of the northern and northeastern end of the ancient Russian plate with the Grenvillian age North Kara-Barents-Pechora plate which

subsequently had been separated into the Barents Sea (Svalbard), North Kara and Pechora plates [127, 422]. Thus, northwest of it had still existed Iapetus Ocean formed after the disintegration of Mesogea (Rodinia) supercontinent. The accretion process of the East-European platform in this its part had been running without folding and magmatism manifestations. The merger of the two continents had been occurring along zones of a tangential slippage similar to displacement of lithospheric blocks along a transform fault (Fig. 16.6).

The collision process of the two plates had resulted in the reverse-faulting and in some places overthrusting of Middle and Upper Riphaean and Vendean shelf and continental slope sediment complexes on the East-European Platform margin and the formation in the area of Sredniy and Rybachiy Peninsulas of large dextral slip-strike and reverse fault-overthrust structures. At this, A.P. Simonov with coauthors [418] noted that the processes of the Timan-Varanger suture zone formation had been associated with a sharp thickness decrease of the section in the northwestern (Kola-Kanin) segment and its multiple increase in the southeastern (Timan) direction. It should be added to this that in the section are missing Lower Riphaean formations present only in the southeastern part of the Timan-Varanger suture zone [127].

Apparently, the described facts should have been connected with the dextral-strike-slip juncture of two lithospheric plates at which their separating oceanic basin had been closed without the subduction intake of its major part. Thus, the youngest fragments of the shelf and continental-slope formations of the East-European platform had been reverse-faulted over the plate edge partially cut-off, displaced and unloaded in the southeastern direction. The older Lower Riphaean complexes composing lower levels of the slope and foot of the continental passive margin most likely had been buried in the base of the formed suture zone. These processes had resulted in an increased manifestation of folding and metamorphism up to the greenstone facies within the Kanin and Timan parts of the section, as well as in the manifestation of a contrasting magmatism of granitoid and granodiorite up to gabbro-dolerite in the southwest. Even further south (in the Cis-Ural region), this zone passes in a convergent structure. An evidence of it is a complex reached by drilling of island arc type magmatic rocks on its eastern end [127].

Basement of the North Kara-Barents-Pechora plate is exposed within the northeastern land of Spitzbergen, north part of Novaya Zemlya and on Taymyr Peninsula. It is penetrated by wells on the islands of Franz Joseph Land and within the Pechora plate. The section is represented by gneisses and crystalline schists (biotite and two-mica), coaliferous and graphite-containing, chlorite-sericite schists, quartzites, marbles, dolomites, calciphyres and conglomerates poly-folded and metamorphosed in conditions of epidote-amphibolite facies of metamorphism. These complexes had

been pierced by the Riphaean and Vendean granites. The basement age is 1.55 – 1.3 BY [127, 310, 423]. This lithospheric plate as a nonuniformly structured basement which is expressed in the conjugation of continental (granite) and sub-oceanic types. It should be kept in mind that its western part had been formed and upbuilt in the epoch of the Caledonian phase of folding and is reflecting the conditions of Iapetus Ocean closing.

Somewhat later the closing of the Paleo-Urals Ocean in the east had occurred. As at the closing of the Iapetus Ocean, the formation of the Uralian folded system had been accompanied by a multistage and non-uniform approach and subduction of the ancient East European Platform underneath the active margin of the West Siberian plate. This had caused the formation of a complex configuration collision structure in the period of Late Devonian through Early Carboniferous (about 350 MY) in the south and through Early Triassic (about 265 MY) in the north [417]. On the north end of the forming folded system, the North Kara plate passive margin had been thrown over the Siberian craton thereby having formed the Taymyr folded system and the Yenissei-Khatanga foredeep. The total closing of the Paleo-Urals Ocean had been marked by the evolution of post-collision granites with the age 264 MY [423]. As a result of this, between the East European Platform and West Siberian Plate had been formed an orogen structure. This structure has vari-directional, sometimes arcuate, up to oxygonally oriented folded zones, sometimes with transform faults. An example is the folded system of the Polar Urals, Pay-Khoy, Novaya Zmlya and Taymyr Peninsula (Fig. 16.7).

The closing of the north part of the Paleo-Urals Ocean had caused a practically simultaneous collision of three continental lithospheric plates with a heterochronous basement. Based on a pattern that in Phanerozoic an older lithospheric plate had always subducted under a younger one of the same type, at the collision of two oceanic or two continental plates the ancient one had always subducted underneath the young one. Therefore, with its basement age of 1.55 – 1.3 BY, the Barents Sea - Pechora plate had subducted by its southern part underneath a younger West Siberia one and had obducted in the north over the ancient Siberia platform.

As a termination result of the Caledonian and Hercynian tectogenesis stages, a single supercontinent Pangea had been formed. In its northern part had been combined by collision lithospheric plates of the North American, East European and Siberian ancient cratons. Between them, had been squeezed young lithospheric plates with a Grenvillian basement to which may be attributed the West Siberian and North Kara-Barents Sea-Pechora young platforms (Fig. 9.8). Apparently, at that very time had also been mostly formed a large Amerasian oceanic depression. A major part

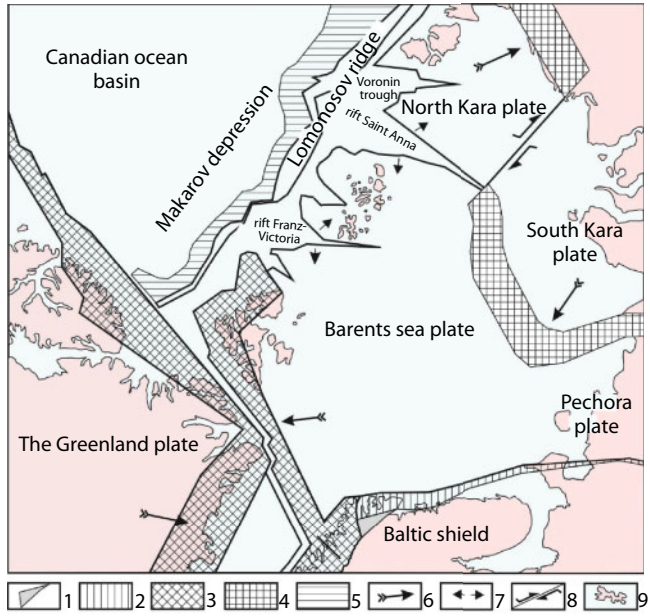

Fig. 16.7 Paleo-geodynamical reconstruction of northern part of the East European platform and West Siberian plate and the adjacent Arctic basin in Paleozoic and Early Mesozoic (650-241 MY). 1. Vendean continental clastic deposits (650-570 MY), 2. Middle-Upper Riphaean and Vendean passive marginal shelf and continental slope sedimentary complexes in the northeastern part of the Baltic shield and Russian plate, 3. Folded formations of North Atlantic Caledonides in Early Ordovician - Late Devonian (505-362 MY), 4. Folded formations of the Polar Urals, Novaya Zemlya and Taymyr Peninsula in Early Permian - Early Triassic (290-241 MY), 5. Passive continental margin, 6. Generalized direction of lithospheric plate movement, 7. Stress field vectors in the continental lithosphere, 8. Transform fault, 9. Present-day shoreline outline.

in it is occupied by the Canada kettle. In Jurassic and Cretaceous, within its limits had possibly still continued the ill-defined axial spreading which, however, had later stopped [127, 424].

The closing process of Iapetus Paleo-ocean may be restored from the present-day outlines of the continental plates in the northern part of the Atlantic Ocean and from banded magnetic anomalies as well as from the structural nature of Caledonian allochthone slab in the northern part of the Baltic shield marking the ancient merger zone. Thus, a wedge-like shape of the eastern part of the Greenland lithospheric plate at the collision with the European plate must have resulted in the emergence of a series of tensile stresses in the north of the Baltic shield along the line North Norway – Kola Peninsula – Archangel area, i.e., northwest - southeast (Figs. 16.7 and 16.8).

Similarly, at closing of the Carboniferous-Triassic Paleo-Urals Ocean and at the collision of the West Siberian Epi-Paleozoic platform with the East European platform apparently had occurred emergence of a tensile stress zone along the line Novaya Zemlya – Nokuyev Island – city of Kandalaksha – Strait of Bothnia and Novaya Zemlya – White Sea Throat – Lakes Onega and Ladoga (Fig. 16.8). At this, the Kara plate salient marked with a geniculate bend of the Novaya Zemlya structures had invaded like a wedge in the Barents Sea young platform.

The events occurred in the Baltic shield framework might not have but actively affected its internal physical state. As a result, in the shield's eastern part had been formed almost orthogonal system of northwestern and northeastern – to meridional branch direction faults (Fig. 16.8). The manifestation nature of these deformations had predetermined the emergence of one more fault system formed as a result of the decomposition

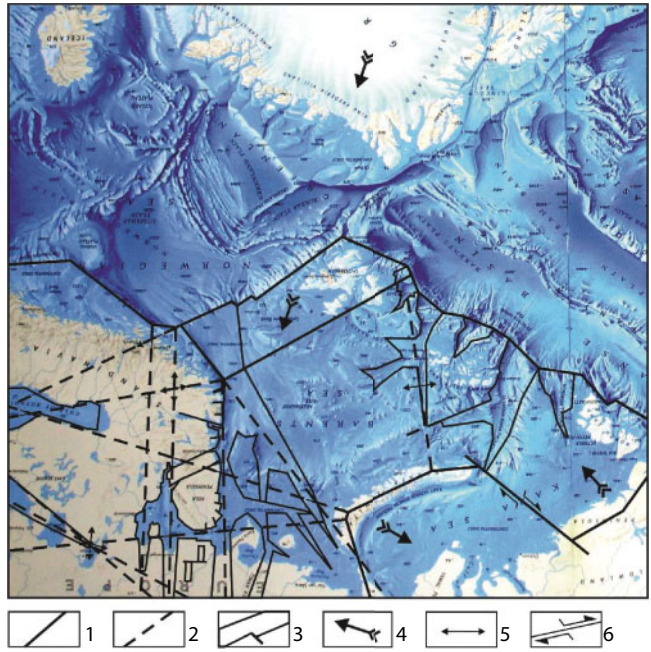

Fig. 16.8 A reconstruction of faults on the ancient East European, young West Siberian and ancient Siberian platforms in Paleozoic – Early Mesozoic (650-241 MY). 1. The lithospheric plate boundaries along which had been occurring closing and collision of the Paleo Oceans, 2. Major lineament formed in the continental lithospheric plate, 3. Rifts, 4. Generalized direction of the lithospheric plate movement, 5. Stress field vectors in the continental lithosphere, 6. Transform fault.

of forces. The formation of sub-longitudinal – sub-latitudinal orthogonal system in the described time period had been of a secondary nature and had been implemented without any substantial displacement along faults. The unavoidable emergence of tensile stresses in the eastern Baltic shield had caused formation of a whole number of riftogenic structures. Within the Kola Peninsula and its framework are identified the White Sea (Kandalaksha-Dvina) and Norway-Mezen rift systems enveloping it from north and south and the marking faults of a northwestern strike. As a result of closing the Paleo-Urals Ocean and forming of a regular fault system in the East European platform lithosphere, slightly later had been formed a rift system of southwestern strike marked by the White Sea Throat aquatorium and extended to Lake Ladoga and farther on in the Baltic Sea. Due to this, east of the White Sea had occurred a combination of the two northwesterly rift systems and a transformation of the structure-material ensemble of the Mezen syneclise.

The Kandalaksha-Dvina (White Sea) rift system extends from the Kola Peninsula to the Timan. Its length is about 900 km and width 50-270 km [425]. In its northwestern part, the Kandalaksha rift gradually pinches out and in the Tersk shore area, the northwesterly directed Yermakov graben branches off of it [426]. The Barents Sea rift system is observed from Laxefjord and Tanafjord on the north coast of Norway along the Murmansk coast of the Kola Peninsula and farther on southwest. Its total length is about 1,500 km and width up to 200 km. In the area of Norway north coast this rift system pinches out and has the appearance of a dextral strike-slip fault.

The Mezen syneclise within which the Archangel diamond-bearing province is developed, had been formed as a result of Baicalian and then Caledonian-Hercynian stage manifestation of geodynamic activity. It had been initiated at the edge of the Russian plate as a result of its merger in Riphaean with the Barents Sea - Pechora lithospheric plate and had been a typical foredeep on the Archaean basement. Somewhat later, the formation of the Kandalaksha-Dvina (White Sea) Riphaean aulacogen had occurred as a reflection of the Dalsland folding phase in the west of the Baltic shield. Even later, structures of the Caledonian and Hercynian tectogenesis phases had superposed over the Mezen syneclise structures which undoubtedly had made the internal structure of the region more complex (Fig. 16.9).

The Mezen syneclise basement is of an Archaean or Early Proterozoic age. It is composed of intensely dislocated and variously metamorphosed (ultra-metamorphosed) sediment-volcanogenic and volcanogenic complexes as well as of base and acidic intrusions which combine into heterochronic tectonic complexes.

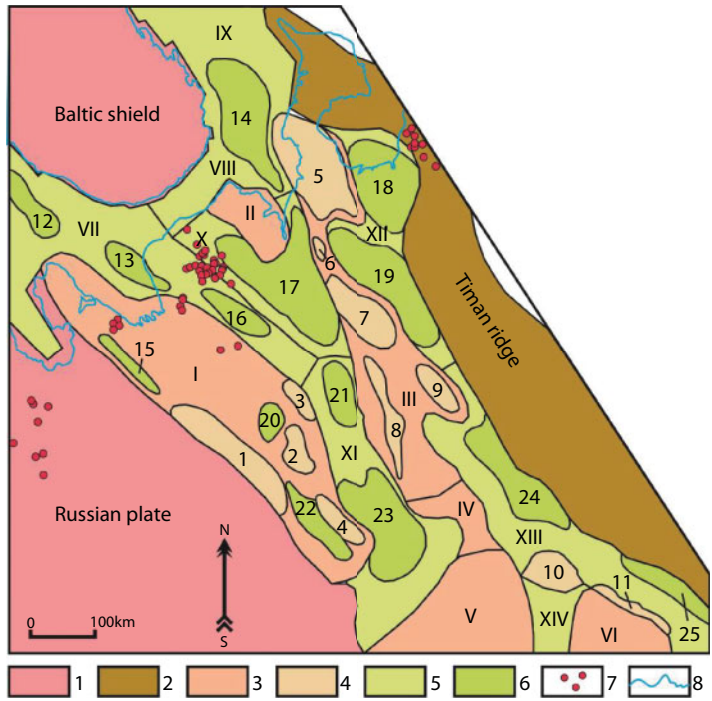

Fig. 16.9 Tectonic structure of the Mezen syneclise basement (after N.A.Malyshev [428], modified and amended). 1-2. Structure in the framework of the Mezen syneclise; 3-4. Basement highs within the syneclise: I-VI. First order, 1-11. Second order; I. North Dvina monocline and Archangel Arch; II. Nessk-Tylug high; III. Mezen mega-swell; IV. Yertym saddle; V. Sysol Arch; VI. Komi-Permyak Arch; 1. Middle Dvina Swell; 2. Yulsl High; 3. Karpogor Swell; 4. Uftyug High; 5. Tylug High; 6. Lower Pez High; 7. Tsenogor High; 8. Vashkin Swell; 9. Koslan Swell; 10. Storozhev High; 11. Prub Swell; 5-6. Basement troughs within the syneclise: VII-XIV. First order, 12-25. Second order; VII. Kandalaksha-Keretsk trough; VIII. White Sea Throat Trough; IX. White Sea Funnel Trough; X. White Sea-Leshukon Trough; XI. Pinezh Trough; XII. Peshsk-Safonov Trough; XIII. Vychegda Trough; XIV. Kirov-Kazhim Trough; 12- Kandalaksha depression; 13- West Keretsk Depression; 14. Prikanin Depression; 15. Onega Depression; 16. Kerets Depression; 17. Leshukon Depression; 18. Pesh Kettle; 19. Safonov Depression; 20. Poksheng Depression; 21. Middle Pinezh Depression; 22. Toem Depression; 23. Upper Pinezh Kettle; 24. Vishera Depression; 25. North Kerltmen Depression; 7. Alkali-ultramafic and kimberlite diatremes; 8. Shoreline.

The lower part of the platform cover is mostly clastic Upper Proterozoic complex combining marine, near shore-marine and continental rocks and subdivided in two structural stages, lower (Middle Riphaean) and upper (Upper Riphaean). Up the section is the Upper Proterozoic-Phanerozoic complex subdivided in two structural stages, lower (Upper Proterozoic)

and upper (Phanerozoic). The lower structural stage is composed of Upper Vendean sediments and has areal development over the entire territory of the syneclise. The upper, Phanerozoic structural stage is subdivided in three substages, lower (Silurian-Devonian), middle (Carboniferous-Lower Permian) and upper (Upper Permian - Cenozoic) [427].

Based on the data by D.A. Kuzmin 427], the lower part of the platform cover had been formed synchronously with intense tectonic processes and establishment of the Norway-Mezen system of Riphaean aulacogens (Fig. 16.9).

The Mezen basin basement is a system of isolated linear graben-like inter-craton troughs (Paleo-rift zones) - Kandalaksha-Kerets, Prikanin-Leshukon and Pinezh bounded by horst-like highs and northwest striking pericratonic troughs: Peshsk-Safonov and Vychegda (Fig. 16.9). West to east, structure zones of alternating relative highs and lows are identified there: North Odvin, Keretsk-Leshukon-Pinezh, Mezen-Vishera, Peshsk-Safonov-Vychegda and West Timan. The latter is a fold-overthrust structure zone bounded by the West Timan and Central Timan reverse faults - overthrusts [429]. Riphaean rocks in this zone are distinct from the homochronous formations of the Vychegda and Peshsk-Safonov troughs of the Mezen syneclise only in a higher extent of dislocations.

Analysis of depressions, troughs and highs' distribution system within Mezen basin reveals surprising pattern in their positions. Thus, a long series of depressions gravitating to the Timan range apparently are foredeep structures whereas the other are separated from them by a system of highs and reflect pinch-out conditions of the Phanerozoic rift systems (Fig. 16.9).

Tectonic evolution of the Mezen basin may be subdivided into three stages. At early stage, the Russian platform continental margin had subsided as a result of its merger with the Barents Sea-Pechora plate and then separated by the Norway-Mezen aulacogen system formed in Riphaean. In Devonian and Permian-Triassic had occurred the formation of Kandalaksha-Dvina (White Sea) and Norway-Mezen system of rift superposed on the Riphaean grabens, as well as of the White Sea Throat rift. That had complicated formation processes of the platform type syneclise. As a result of this had been formed the Mezen heterogenic sedimentary basin composed of structure-material (litho-dynamic) rock complexes corresponding with paleo-basins belonging to various tectono-sedimentary types. Dominating in the section of the Mezen syneclise is the Riphaean complex overlain by Upper Vendean and Phanerozoic formations playing a subordinated role.

The alkali-ultramafic and kimberlite composition diatremes invading the Mezen syneclise basement had become a component part of a large magmatic province of this region.

Processes of the Caledonian-Hercynian activation on the Baltic shield had led to the invasion of a number of magmatic complexes formed on the shoulders of these structures, in rift evolution zones as well as in the intersection nodes of the largest lineaments (Fig. 16.10). Due to this, within the Baltic shield and the northern Russian plate had been formed a Paleozoic age alkali-ultramafic, melilitite and kimberlite magmatic province.

In particular, in the central part of the Kola Peninsula is encountered a complex of nepheline sienites and alkali-ultramafic central type intrusions (Fig. 16.5). Two age intervals of this magmatism manifestation are identified. Early intrusive bodies, diatremes and dykes had invaded during the period 480-400 MYa and formed an extended in northwestern direction zone along the Kandalaksha Bay shore and farther, including the Kovdor Massif [426]. Later magmatism manifestations had the age 400-320 MY and are associated with northeastern and northern strike faults [426, 430].

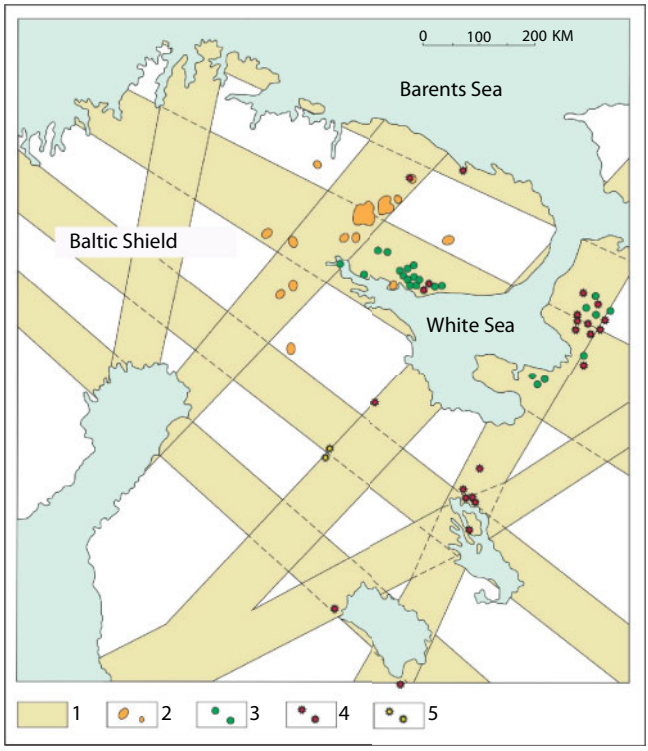

Fig. 16.10 Schematic display of tectonics and distribution of Paleozoic base composition intrusive massifs and diatremes in the NE part of the Baltic shield. 1. Linear concentration zones of Paleozoic age depth tectonic faults, 2. Intrusions of alkali-ultramafic composition, 3. Melilitite diatremes, 4. Kimberlite diatremes, 5. Lamproite diatremes.

The identified pattern supports our earlier conclusions of a poly-stadial manifestation of the structure-forming processes in the region and the magmatism associated with them [58, 194].

On the north coast of the White Sea Kandalaksha Bay is mapped a dolerite complex of sub-longitudinal and northeastern strike with the composition of oceanic basalts. Also there, on both its coasts are found lamprophyre dykes of northeastern strike, picrite, melilitites and kimberlite diatremes. In the area of Lake Onega is identified an evolution field of diamond-bearing kimberlite diatremes and in Kostomukshin area, lamproite diatremes (Fig. 16.10). In Archangel area, in the evolution zone of the Norway-Mezen rift system is identified a large Zimneberezhnoye melilitite and kimberlite field. In the Barents and Kara Seas aquatoria, based on geological-geophysical data, are identified several stages of sub-alkali magmatism. It is represented by base composition sills and dykes of Late Permian-Early Triassic and Jurassic-Cretaceous age localized within the East Barents and South Kara Depressions and their framework. On Franz Joseph Land and on Spitzbergen is found younger, Cenozoic magmatism. It is expressed in a northwesterly striking complex of base composition subparallel dykes and covering volcanites as well as dolerites and dolerite-basalt sills. They had invaded the Upper Triassic sediments and, most likely, marked the processes of opening the Arctic Ocean in Eocene.

According to E.V. Shipilov [313], typical of the Barents-Kara region in Phanerozoic are manifestations of several stages in a base composition dyke (sill) magmatism. The first one belongs with the Late or Post-Riphaean stage and is developed within the Barents Sea coast of the Baltic shield and the Novaya Zemlya folded zone. The next, Silurian stage had manifested in the interval of 434-400 MY. Later, Late Devonian-Early Carboniferous magmatism had developed (360-330 MY), then Late Permian-Early Triassic (257-228 MY) and Late Jurassic-Early Cretaceous (159-131 MY). The magmatic activity had ended with Paleogene-Quaternary formations (60-25 and ~1 MY).

As mentioned above, the first magmatism stage had been tied with closing in Late Proterozoic of the Paleo-Iapetus Ocean. The second and third stages had been associated with closing of Iapetus Ocean and poly-stadial formation of the North Atlantic Caledonides folded system and the fourth and fifth characterize closing of the Paleo-Urals Ocean and the completion of the Hercynian tectogenesis stage. The latest magmatics had been associated with opening in Cenozoic of the Arctic Ocean. Their composition most often corresponds with normal alkalinity basalts. An exception is the Late Permian-Early Triassic and Late Jurassic – Early Cretaceous magmatism periods. They, in our view, record the processes of completing the Hercynian folding active stage and removal of the tectonic stress at the post-collision evolution

stage of the Barents – Kara region. This had led to a large-scale invasion of sub-alkali series dyke and sill complex in the framework of the Polar Urals – Novaya Zemlya - Taymyr Peninsula collision zone. Besides, in Cenozoic had occurred opening of the modern Arctic Ocean which also had affected the nature of dyke magmatism manifestation in the continental shelf edge zone.

In 1997 the author conducted a study in the east of the Kola Peninsula (the area of rivers Pyalitsa, Pulonga, Babya and Sosnovka) on the White Sea Throat coast. The study identified a great number of melilitite and kimberlite composition dykes in the crystalline foundation of Archaean basement. It has already been mentioned above that these dyke formations have in part a peculiar shape of "spider-like" bodies with isometric matter separation in the center and four to six rays of diverging dykes. The central body diameter is 2 to 8 meters, the length of apophyses is 30 – 80 and even 100 meters. The dyke bodies cut through the Archaean crystalline basement, they are not metamorphosed and partially have a natural appearance of cooling fractures formed at magma crystallization in near-surface conditions. Possibly, these bodies had been supply channels for the eroded diatremes which enables a forecast of diamond-bearing placer formation in the White Sea sediment cover [58, 431, 432]. On the other hand, if these dyke-like diatremes had invaded originally crystalline basement and not the sediment cover, they might not have formed structures natural for diatremes.

The eastern part of the White Sea basin (including the Throat) is coincident with a large node of intersecting depth faults whose kinematic has the extension nature (Fig. 16.8). Exactly for this reason in the adjacent areas is developed an intense magmatism of their formation age. Continuous isostatic heaving of the northeastern part of the Baltic shield throughout the duration of Paleozoic-Cenozoic time and bringing on the surface of deep crust levels must have unavoidably caused the formation of rich placers in the bottom deposits of a semi-closed basin aquatorium which the White Sea is.

Extremely important in this connection is an issue of reevaluating the parameters of placer diamond-bearing in the White Sea basin and its littoral part. For almost 20 years after the discovery of diamond-bearing diatremes in Archangel kimberlite province, diamond exploration was conducted in the territory of continental part of the Murmansk Province and North Karelia [433, 434].

The Tersk coast kimberlites have been discovered in 1986 at drilling of the "diatreme type" local magnetic anomalies. According to M.M. Kalinkin and I.V. Polyakov [434], the Yermakov kimberlite field includes 60 explosive objects, among them two diamond-bearing kimberlite diatremes. All other diatremes and explosion dykes are composed of melilitites and ultramafic foidites. In a vertical cross-section, diatremes are steeply-dipping vents with eroded upper crater parts. 131 diamonds have been identified in two technical

samples from the "Yermakovskaya-7" diatreme. Small specimens (0.1-0.2 mm) are dominant. The diamonds larger than 0.5 mm are rare. However, there are fragments which indicates breaking of larger grains. The diamonds are of octahedral configuration, colorless, with a blue-light blue luminescence. In one technical sample from the diatreme "Yermakovskaya-20" were found five diamond grains of up to 0.4 mm in size.

Lithofacies studies of loose sediments in the littoral zone and in the White Sea Throat aquatorium resulted in composing a lithological facies scheme of this region (Fig. 16.11). The derived data testify a wide development areal of coarse-grained deposits (gravels, pebbles and cobbles) with which are as a rule associated diamond-bearing placers. The major clastic material delivery source apparently should have been abrasion of the shores and the continental runoff. In favor of the former way is a broad development of abrasion terraces along the White Sea Throat Tersk Coast, and the specific of the destruction mechanism had been in washing out from the near-shore zone practically the entire material coming from the shore abrasion.

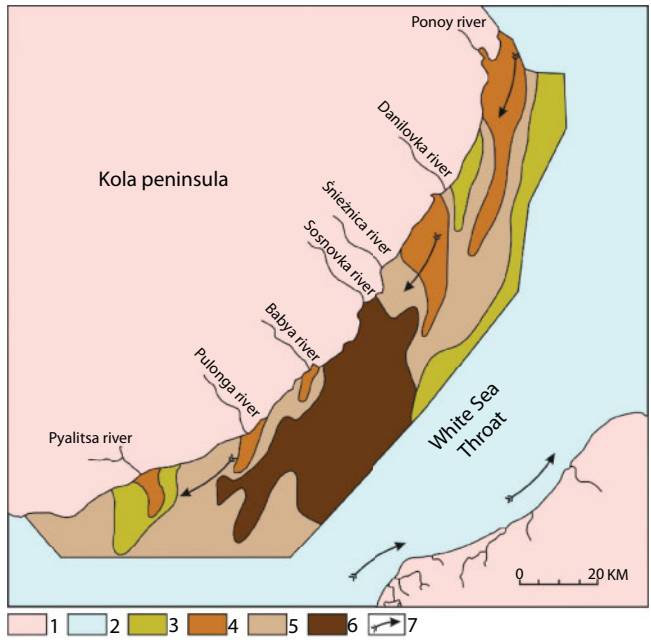

Fig. 16.11 Schematic lithofacies distribution in the White Sea Throat aquatorium. After [432]. 1. Continental dry land; 2. Marine basin aquatorium outside the detailed study area; 3-6. Detailed lithofacies study area; 3. Small- and medium-grained polymictic sands, 4. Coarse-grained polymictic sands, 5. Mixtite deposits (sand+gravel+pebbles), 6. Cobble-pebble deposits; 7. Direction of the bottom currents.

Continental runoff had also substantially affected the formation of clastic deposit sequence at the expense of eroding the crystalline basement surface in the northeastern part of the Baltic shield and bringing the erosion products in the White Sea basin. The reason is that the present-day Kola region rivers have the nature of mountain streams and therefore are able to transport coarse-grained material. Besides, very common in the region is the process of destruction and subsequent transport of moraine deposits.

A poor sorting and an angular nature of the clastic material in the White Sea basin littoral zone as well as a rather monotonous petrographic composition of pebbles and cobbles (mostly gneiss, granite-gneiss, amphibolites, granites and arcose psammites) indicate a close distance to bedrock sources runoff material.

The White Sea is distinct in a rather complex water-exchange system whose substantial mechanism is the continental runoff. An excess of a low-density desalted water comes from the closed White Sea area in the Barents Sea basin whereto is directed a permanent compensation marine current [435]. From the Barents Sea through the White Sea Depression Throat is coming the opposite flow of heavy normal-salinity oceanic water. Exactly this flow is controlling the dynamics of runaway sedimentary material on the bottom of the aquatorium's Tersk portion. This conclusion is supported by the sand facies distribution within the study area, exactly by the displacement of deltaic detrital cones to the southwest.

Analysis of the clastic deposits transport and accumulation process in the region showed that the northeastern part of the Baltic shield is the generation area of a whole number of placer economic minerals, whereas the White Sea basin is a natural concentration point and simultaneously the gravity separator.

The diamond exploration conducted by the author with colleagues in the White Sea Throat aquatoria showed that in coarse-grained clastic deposits are encountered satellite minerals and individual grains of this mineral.

The samples obtained by dragging the bottom deposits have been separated into fractions and subsequently studied by lithologic, petrographic and mineralogic methods. A total of 130 samples have been collected. The 0.5-1.0 mm fraction has been studied in all of them. Its composition is mostly rock-forming minerals, mostly dark-colored minerals: amphibole, pyroxene and epidote. Their share is often 100% of the heavy fraction. The second and third places belong to kyanite and sillimanite. The reason is a broad development at a small distance from the Tersk coast (30-100 km northwest of it) of Keiv series kyanite schists spatially concentrated in the basin of most full-water Kola Peninsula river, the Pona. The source of garnet (almandine and andradite) and especially of the staurolite are kyanite and staurolite-garnet-kyanite schists of the Keiv tundra. The garnet areal is much broader inasmuch as garnet as a rock-forming

mineral is present in many metamorphic rocks in the entire region. The elevated biotite content gravitates to the area of the Pona deltaic sands. Sometimes are encountered the perovskite, apatite, ilmenite and sphen.

The finer-grained fraction (0.25-0.5 mm) is also dominated by rock-forming dark-colored minerals: amphibole, pyroxene and epidote, however, a relative fraction is increased of the garnet (up to 30%), sphen (up to 30%), staurolite (up to 10%), perovskite and biotite.

The diamond companion minerals we discovered are garnets, chrome-diopside and moissanites. They are encountered mostly in classes 0.5-1.0 and 0.25-0.5 mm as whole crystals or their fragments. Grain rounding is low. One sample included chrome-pyrope typical of kimberlites and diamond inclusions [432].

The garnets are mostly calcium pyrope-almandines encountered in kimberlites, garnet lherzolites, garnet olivine websterites and eclogites. The grain shape is angular, uneven which is an evidence of the closeness to the provenance area. In the Yermakov kimberlite field, such garnets are discovered in explosion melilitites and ultramafic foidites [433]. In view of low pyrope contents in the diamond-bearing kimberlites of the Kola-Archangel province, even its single finds are of a practical interest. In chrome-containing diopsides are encountered olivine and native iron inclusions which is a possible indication of their crystallization at significant depths. In marine deposits was numerously found another diamond companion, the moissonite (SiC). The moissonite finds coincide in space with finds of chrome-containing diopsides and magnesial garnets which indicates their genetic connection. A single diamond crystal, 0.5-0.7 mm in size, was found. It had a few well-formed facets. The crystal is semi-transparent, of a dray hue. The crystal shape is close to cuboctahedron.

Thus, in process of the mineralogical studies, both direct (finds of a diamond and of chrome-pyropes) and indirect (finds of pyrope-almandines, chrome containing diopsides, olivines and moissanites) indications of the placer diamond-bearing in the northeastern part of the Baltic shield have been identified.

16.3 The Zoning of Alkali-Ultramafic and Kimberlite Magmatism Localization Areas in the Northeastern Part of the Baltic Shield

Spatial patterns in the localization of the described magmatic complexes are in a strict correlation of their placement in the region. Alkali-ultramafic and carbonatite intrusions are positioned mostly in the central part of the

Kola Peninsula and Northern Karelia. They practically do not interfere with the picrite and melilitite magmatism manifestation zone that spatially gravitates to Tersk coast of the Kola Peninsula (Fig. 16.5). East of them, in the Archangel Province, a zone is positioned of exceptionally kimberlite magmatism also having strict limitations in space (Fig. 16.9). The found correlation between the spatial placement of different in composition and the way of bringing on the ground surface of magmatic complexes indicate a change in magma formation depth increasing along the Kandalaksha-Dvina rift system northwest to southeast. Most likely, the latter rift system at a sharp angle opened up magmatic chambers buried in the Proterozoic age paleo-subduction zone (Fig. 16.5).

It may be recalled that, based on J. Dawson data [1], the begetting depth of alkali-ultramafic magmas varies between 80 and 100 km, whereas kimberlite magmas form at depths of 150–180 km to 200–220 km. Earlier, describing the formation mechanisms of alkali-ultramafic and kimberlite magmas, we emphasized a direct tie between their begetting depth and the distance to the front of Early Proterozoic plate subduction zone. That is exactly why mutual position of these zones and Caledonian-Hercynian rift formations is of an utmost importance for forecasting localization areas of the kimberlite magmatism.

The subduction of oceanic plates at closing time of the Svecofennian Ocean had been occurring approximately northeastwardly underneath the Karel-Kola Archaean megablock. The imaginary extension of these zones' dipping plains enables a depth evaluation of the absorbed surface depending on the distance from the front of a former plate subduction zone. A zone of paleo-subduction fringing the Karel-Kola Archaean region from the west was chosen as an example (Fig. 16.12). However, for estimating the penetration depth of the crust matter in this zone it was necessary to know the angle of the oceanic lithospheric plate plunging underneath the continental one in Early Proterozoic. This is a quite complex problem, theoretically not uniquely solvable. As a first approximation, an empiric rule may be used: the higher the lithospheric plate subduction rate, the flatter is the subduction zone. For instance, the Pacific plate is being subducted underneath the Mariana island arc at a rate of about $u_l \approx 4$ cm/year at a dip angle of the Wadati Benioff zone $\beta \approx 70°$ and steeper. Underneath the Kuril arc $u_l \approx 7–9$ cm/year, $\beta \approx 45°$. The South American plate Nazca is being subducted underneath the Andes at a rate of about $u_l \approx 15$ cm/year, and β angle declines to 30°.

In Early Proterozoic, average movement rate of lithospheric plates had been approximate 5-6 times faster than it is today and had reached 25-30 cm/year [18]. That is why it should be expected that at that remote epoch the minimal dip angles of plate subduction zones had been about 20°

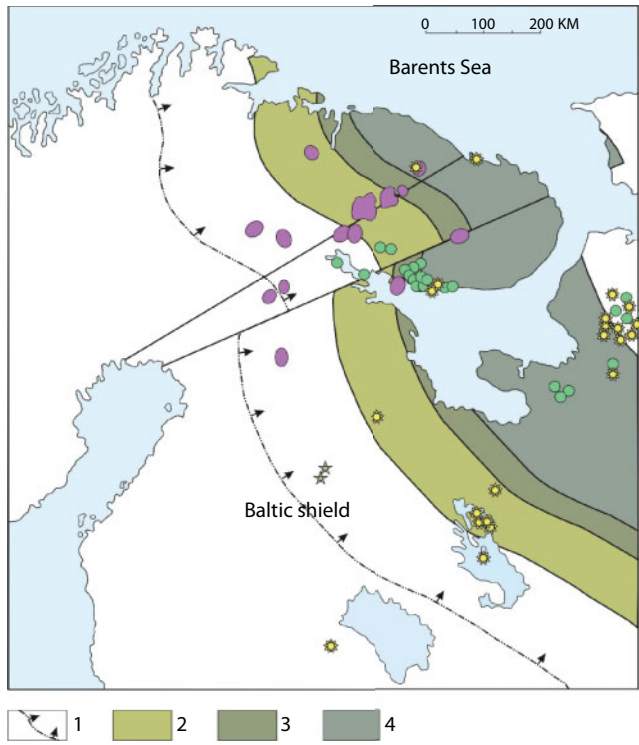

Fig. 16.12 Example of projecting on the ground surface of buried melt localization zone relative the selected subduction zones. 1. Paleo-subduction zone relative which projecting is done; 2. Area of buried alkali-ultramafic magmas' balanced existence; 3. Same for the diatremes of picrite, melilitite and carbonatite composition; 4. Same for the kimberlite and lamproite diatremes.

although might have existed steeper dips of these zones. If, however, a position of a lithospheric plate subduction zone front and the exposure of alkali-ultramafic intrusions or kimberlite diatremes are known, the dip angle of a plate paleo-subduction zone may be determined at a much higher accuracy.

In case of en echelon position of the Early Proterozoic plate subduction zones, as it is observed in the Karel-Kola craton, a spatial superposition of the complexes of alkali-ultramafic, transitional-depth carbonatite, melilitite and even kimberlite magmatism is obviously possible. For instance, the melilitite composition diatremes on the Tersk coast of the Kandalaksha Bay are positioned together with weakly diamond bearing kimberlite diatremes. A similar picture is observed in the Archangel Province where the Zolotitsky and Kepinsky field kimberlites are adjacent with olivine and olivine-phlogopite melilitites of the Verkhotin and Izhmorero fields. An empirical

estimate showed that dip angle of the Early Proterozoic plate subduction zone had been almost 23°. This is the ideal agreement with the present-day data of suture zones' dip angle.

If we now assume that maximum thickness of the continental lithosphere at the formation moment of depth melts had reached 250 km, then maximum distance to the ancient plate subduction zone at which a manifestation of the diamond-bearing magmatism still may be expected, is $L_{max} \approx 650–700$ km (see Fig. 16.12). Minimum formation depth of diamond-bearing melts is defined by the intersection of the present-day continental geotherm T_l with the temperature boundary of the graphite-diamond phase transition $T_{\gamma\alpha}$ (see Fig. 12.2). In our case, the point $T_l = T_{\gamma\alpha}$ correspond with a depth of 130 km. Therefore, a minimal distance from the suture zone to the band of a possible diamond-bearing magmatism manifestation is equal approximately to 400 km.

The manifestation belt of explosive melilitite and no-diamond kimberlite magmatism must be positioned closer to the paleo-subduction zones. The maximum distance in this belt is coincident with the internal boundary of the diamond-bearing magmatism manifestation area. Whereas the internal boundary of the explosive magmatism belt is defined by the minimum existence depth of the melt capable to "breakthrough" on the ground surface without magma crystallization at intermedium near-surface levels. According to the estimates in Fig. 12.2, this depth is approximately 115 km. Based on this, we find that the minimal distance from the subject suture zone to the explosive magmatism belt is approximately 320 km (Fig. 16.12).

Even closer to the front of a former plate subduction zone is positioned the belt of intrusive alkali-ultramafic magmatism. Its minimal distance from the suture zone is defined by a minimal existence depth of melts in the continental lithosphere, i.e., the intersection depth of T_{lk} geotherm with the pelagic deposits melting temperature curve $T_l = T_{ss}$ (see Fig. 12.2). This depth if approximately 70 km, wherefrom we find that the internal boundary of the intrusive magmatism belt is apart from the front of a former plate subduction zone by 190 km (Fig. 16.12).

Should the paleo subduction zone we selected as an example have been the only one, then theoretically there should have been no depth magmatism manifestations closer than this distance. However, they are observed. Three explanations of this phenomenon are possible.

First, it is not impossible that the rise of depth magmas to the surface at the lithosphere expansion had been occurring not only through the vertical fractures as shown in Fig. 15.1 but also along an inclined surface of the plate subduction zone itself, even more so that it is simultaneously a weakness zone of the lithosphere. If this is so indeed then alkali-ultramafic

magma intrusions might have invaded the continental crust at any distance from the suture zone within a wide band of 0 to 320 km.

Second, such intrusions might have emerged at the expense of depth melts penetration from the second and third row subduction zones in the rear of the selected paleo-subduction zone (Fig. 16.5). On the one hand, this explains the magmatism manifestation outside the limit of modeled areas, and on the other hand, it explains the finds of vari-depth formations at a close distance from each other. Indeed, at formation of en echelon subduction zones formed partially at the merger of a number of island arcs emerges a multi-stage vertical system of diverse composition magmatic reservoirs as shown in Fig. 3.1.

Third, there is a possibility that a paleo-subduction zone exists unidentified by us because of a poor knowledge of the territory or as a result of its being overlain by a thick sediment cover.

The proposed zoning technique of a possible manifestation of the depth magmatism defines only a conceptual possibility of finding this or that depth rock complex in the study territory. However, their actual discovery becomes possible only in those cases when all aforementioned necessary factors form a unified system.

In conclusion, we would like to do a very interesting, important and sufficiently substantiated forecast of the discovery of new, not yet known manifestations of diamond-bearing kimberlite magmatism in the study region.

The case is that the ore-controlling system of Paleozoic rifts had been initiated on an earlier large Riphaean age aulacogen of a similar strike developed in the White Sea and Mezen syneclise. In the northwest of this aulacogen, there had been no magmatism because a fissure in the Baltic shield continental lithosphere had not occurred. However, the aulacogen has a clearly expressed wedge-like structure. This suggests the presence of a substantial pull-apart at its southeastern end. This is, in particular, indicated by a small-block key-type structure of the Mezen syneclise. If the formation of a Riphaean aulacogen in it had reached the stage of a complete lithospheric fracturing, it is possible to expect there a broad manifestation of kimberlite magmatism of that time.

Today, the Mezen syneclise is overlain by thick (2.0-2.5 km) deposits of the Paleozoic – Cenozoic age. Therefore, if magmatism had taken place in Riphaean, the kimberlites had invaded the sediment cover of that time and then had been buried by the subsequent deposition processes. At that, the Riphaean magmatism impulse would have to have been broader and included a greater number of diamond-rich kimberlite magma than the Paleozoic one. The case is that the hottest, therefore, the richest in ore matter magmas erupt first whereas for the second impulse may remain

only residual melts. An example is the Premier diatreme in RSA with the formation in Proterozoic. Exactly in this diatreme have been discovered world largest diamonds the Cullinan (3,106.75 carats) and the De Beers (428.5 carats). A later, Mesozoic magmatism impulse in that region have not caused the formation of diatremes equally rich with large diamonds, although their quality is at least that high.

Thus, the present-day outlook of the Archangel diamond-bearing province may be substantially amended by a hidden at depth of 2-2.5 km development field of richer diamond-bearing kimberlite diatremes. Hopefully, the discovery time has not ended yet!

Conclusions

Developing Earth's global evolution concept helped clarify the physical nature of major endogenous processes controlling the geologic evolution of our planet and establishing cause and effect interconnections between them and geological phenomena observed on Earth's surface. Within this context, issues of the emergence and formation of economic mineral deposits obtained a totally new ring. In particular, it was shown that the accumulation in Earth's crust of endogenous trace and ore economic minerals had occurred only with an active participation of exogenous factors in this process and by way of numerous reprocessing of the crust matter itself. The origin of diamonds, clearly depth minerals, is no exception. Their nature is also interesting in that this enigmatic mineral is a microcosm of the entire geological history of our planet commencing with the formation of Archaean cratons, Earth's core separation and transition associated with it, from Archaean geodynamics to the regime of lithospheric plate tectonics. Within the same train of events is the evolution of the oceans in Early Proterozoic that had caused the accumulation of unique iron ore deposits of the same age. The logical succession had ended in occurring in Proterozoic and Phanerozoic continental splits opening the path for depth diamond-bearing melts to Earth's surface.

That is exactly why it was possible to resolve an apparent contradiction between a great melt-out depth of kimberlite magmas (around 200–250 km) and the results of mantle rocks' experimental melting showing that the mantle melts simply might not have emerged and existed deeper than 80–85 km in the juvenile mantle (outside of plate subduction zones). Besides, a natural explanation was found for another major contradiction between the mantle position of diamond-bearing melts and clearly lithophilic composition of the rocks emerging from them, the rocks saturated on top of everything with alien for the mantle volatile elements. For the same reason passed out the need in a difficult explanation of the emergence in a uniform mafic mantle of contrasting lithophilic nonuniformities with which was conventionally associated the origins of diamond-bearing rocks.

N. O. Sorokhtin (ed.) The Origins of Natural Diamonds, (477–482) © 2019 Scrivener Publishing LLC

All the above relates not only to the kimberlites and lamproites but also to their affine depth rocks of the carbonatite and alkali-ultramafic series. Under the model developed on the basis of new ideas, diamond-bearing kimberlites, lamproites and their affine rocks had emerged at the expense of pulling "heavy" (ferruginous) Early Proterozoic oceanic deposits to great depths (up to 200-250 km) through ancient subduction zones underneath the Archaean shields. Lithospheric plate temperature at such depths reaches 1,400–1,500°C (the mantle rocks' melting temperature at these depths is around 1,700–1,800°C) and significantly exceeds the melting temperature of water-saturated deposits (approximately 600–700°C). This being said, the kimberlite magmas had emerged by means of melting carbonate-rich deposits of Earth's tropical belt whereas the lamproite magmas had formed due to melting of the silica- and potassium-rich clayey deposits of the boreal and circumpolar Earth's climatic zones.

The deposits pulled in to great depths through the subduction zones had unavoidably melted and differentiated through melts' liquation. The heavy ferruginous fraction had been submerging into the mantle whereas a lighter carbonate-silicate matrix had been preserved for a long time in the lithosphere's lower part as depth magma foci. The diamonds proper had been forming through carbon reduction in an exothermal reaction of interacting carbon dioxide gas with methane and simple organic hydrocarbons pulled in to great depths along with ferruginous deposits. In turn, carbon dioxide gas had been released due to temperature dissociation of carbonates in the environment of emerged in subsequent geological epochs extension tectonic conditions of the ancient shields. So formed depth magmas together with diamond crystals had been blisteringly erupted on Earth's surface, forming there the diatremes of diamond-bearing rocks.

Under the model we propose, the depth melt formation moment had been rigidly restricted to the second half of Early Paleozoic. The reason had been that in Archaean conditions for generation of the subject-type magmas had not yet existed: a very high Earth's tectonic activity and very high heat flows had not then permitted the continental lithospheric plate thickness increase over 60–80 km (combined with the continental crust). Subduction zones at that time had not existed at all (instead, there had been crowding and piling-up zones of comparatively thin substantially basaltic composition oceanic lithospheric slabs).

After the Earth's core separation at the end Archaean and to the beginning of Early Proterozoic, Earth's tectonic activity had sharply declined. As a result, first subduction zones had emerged, and the Archaean continental plate thickness had been rapidly increasing and reaching already by the end Early Proterozoic its maximum value (on the order of 250 km). This had

created an environment for a possible formation of depth (diamond-bearing) melts. However, this opportunity had been implemented only after heavy jaspilite-type iron ore deposits had been accumulating on the ocean floor.

We know from Earth's geological history that most outstanding iron ore accumulation epoch when giant iron deposits had been formed (Hamersly, Krivoy Rog, Kursk Magnetic Anomaly, Lake Superior, Karskapay and many other deposits), had lasted a relatively short time approximately between 2,200 and 1,900 MYa (Goldich, 1975). These deposits concentrate more than 90% of the planet's total iron reserves. That epoch had ended with a most powerful phase of the Svecofennian orogeny (1.9-1.8 BYa). At that time, most Early Proterozoic intercontinental oceans had closed and had again formed a single supercontinent, Stille's Megagea. Exactly these events should have caused the submersion of heavy pelagic deposits deep underneath of the Archaean continents.

The very accumulation of such heavy ferruginous deposits on the bottom of Early Proterozoic oceans had been a result of preservation in the Precambrian mantle of the (metallic) iron that had finally vanished from it only by the Proterozoic/Phanerozoic timeline. (Our estimate of the metallic iron contents in Earth's primordial matter is about 13%). Besides, exactly at that time (around 2.2 BYa), the growing ocean surface had risen over average mid-oceanic ridge crests stand level. As a result, mantle's free iron in Earth's rift zones had come in contact with carbon dioxide saturated oceanic water that had oxidized it to a soluble iron bicarbonate and spread it in the entire World ocean's water layer. The iron had been further oxidized in the near-surface environment by cyanobacteria, microalgae and photodissociation oxygen to the insoluble trivalent form, thereby gradually forming renowned Early Proterozoic iron ore deposits.

The proposed diamond-bearing rocks and diamonds' formation model appears convincingly substantiated in the context of geological, geochemical and physical knowledge. Within its context it was possible to justify from a unified position most specific features and sometimes even subtle details of the diamond-bearing and their affine rocks including the diamonds themselves and mineral inclusions in them. Thus, under this model the kimberlites are indeed depth rocks, having emerged, however, from carbonate-rich pelagic deposits of Earth's tropical belt. Hereunder, the lamproites had emerged from shaly deposits of Earth's boreal and circumpolar zones. It follows herefrom that carbon, phosphorus, nitrogen, most lithophilic elements (Li, B, F, Cl, K, Ti, Rb, Sr, Y, Zr, Nb, Cs, Ba, Ta, Pb, Th, U), water and other fluids in diamond-bearing rocks are not of a mantle but of the primary depositional, i.e., exogenous origins. This is also supported by

rare-earth elements high concentrations and spectra. Potassium/sodium, thorium/uranium ratios, hydrogen, oxygen, sulfur and strontium isotopes in the kimberlites and lamproites as well as gas-liquid inclusions in the diamonds (H_2O; H_2; CH_4; CO_2; CO; N_2; Ar; C_2H_4 and even ethyl alcohol C_2H_5OH) and carbon isotope ratio shifts in crystals clearly support a biogenic origin.

The eclogite xenoliths found in the kimberlites also carry similar evidences of a primary near-surface origin. Despite the clearly depth associations of minerals in them, their bulk composition nicely matches oceanic tholeiite basalts melted out only at shallow depths (no deeper than 35 km) under the oceanic rift zones. Combined together, these facts, in our view, are a convincing evidence of a relatively near-surface formation of the entire complex of the subject rocks, their subsequent submersion to great depths and a blistering new rise to the surface (at the rate on the order of 30-50 m/s).

Accepting the presented kimberlite, lamproite and their affine carbonatite and alkali-ultramafic complexes' formation mechanism, it is possible to word, in a most general form, forecast criteria at exploring for these quite exotic rocks. Thus, all these rocks may be encountered only on Archaean or, as a last resort, on Early Proterozoic continental shields but must never form on younger Riphaean and Phanerozoic platforms and, even more so, on the ocean floor. On the Archaean crust, diamond-bearing diatremes must always be positioned in the obducting (autochthonous) flank of the Svecofennian plate subduction zones approximately at a distance of 400 to 600 km from their appropriate suture zones on Earth's surface. Alkali-ultramafic intrusions and subvolcanic bodies as shallower formations must be encountered at somewhat shorter distances from those suture zones (200 to 400 km).

The quoted criteria define only a conceptual opportunity of discovering diamond-bearing and alkali-ultramafic complexes. However, the implementation of such opportunity is possible only in an environment of continental lithospheric plates' extension and split. So, if it is known based on independent geological data that the Archaean or Early Proterozoic crust in a study area had experienced extensions and splits in Phanerozoic, the probability of finding in this territory of looked-for rocks sharply increases. An example is the analysis of a possible diamond-bearing of the Kola Peninsula and northeastern Baltic Shield regions reviewed in our work.

Studying the diamond formation issue, one has to remember that this process is a component part of the carbon crust-mantle cycle. This process is the formation of this element under one geodynamic environment and its transport by the mantle convection flows under another environment.

Thus, it is subjected to a multistage transformation from a chemogenic state in the biogenic and back, to the immersion in the mantle and removal from it on the surface through rift zones. This phenomenon is closely tied with carbon crust-atmospheric cycle as its primary supplier is carbon dioxide gas and its transformation products (carbides, carbonates, hydrocarbons, organic matter). Together, they form the global carbon cycle in nature.

At depths exceeding 250-300 km, carbon again converts in the graphite phase and, getting in the metal carbide stability area forms various compounds with them. Most likely, metal carbide minerals are more common in the upper mantle than on the surface. Perhaps, that is exactly these carbides are carbon transporters from under subduction zones into riftogenesis areas.

In rift zones, a broad spectrum of hydrocarbon gas manifestation is observed from methane (CH_4) and ethane (C_2H_6) to propane (C_3H_8) and butane (C_4H_{10}). In and of themselves, complex hydrocarbons in a free state become unstable under high PT environment and tend to decompose into simpler compounds, up to methane (CH_4). Which means that there are no and may not be these compounds in the mantle. So, how do they form and where do they come from? The answer is simple; their generation occurs under the near-surface low temperature medium environments (below 400°C) existing in rift zones due to the decomposition of metal carbides at the expense of metal carbide decomposition.

The data included in the monograph suggest that the notion of global carbon cycle first proposed by the Academician A.E. Fersman in the 1920s should be expanded with the inclusion of the mantle carbon transfer from subduction zones in rift systems. Therefore, the traditional branch of carbon crust-mantle cycle should be amended with addition of the crust-mantle component.

Analysis of the Baltic shield geodynamic evolution performed in this book as well as an interpretation of the available geological data from the perspective of the lithospheric plate tectonics showed that the continental crust's Karel-Kola megablock is fringed in the southwest by a few plunging under it Svecofennian (around 1,900 MYa) oceanic crust subduction zones. Besides, on the Kola Peninsula, in Sweden and Finland are long-known exposures of alkali-ultramafic and carbonatite intrusions, i.e., kimberlite affine rocks. The melilitite- and kimberlite-like bodies have been discovered on the Kola Peninsula and in the adjacent Archangel Province, diamond-bearing kimberlite diatremes. Therefore, the subject area had been subjected in the past to extension impulses resulting in manifestations of the typical depth magmatism. The conducted analysis indicated that the extensions and splits of the Karel-Kola megablock had been connected with continental collisions at the closure of the Paleo-Atlantic Ocean Iapetus

about 400 MYa and of the Paleo-Urals Ocean about 320 MYa. All of this is a testimony to a quite probable diamond bearing on the northeastern Baltic Shield and the northern Russian Platform and suggests setting up there scientifically substantiated and purposeful exploration for search of these valuable mineral. Moreover, the entirety of geological data supported by theoretical concepts quoted in the book enables a suggestion that the northeastern Baltic Shield, including the Kola-Karel megablock of the Archaean crust, the northeastern areas of Sweden and Finland as well as adjacent to the Timanides northeastern part of the Russian Platform may be one of the world's richest diamond-bearing provinces.

The other examples of applying new techniques to the diamond exploration might have served the already-known richest diamond-bearing provinces in Brazil, South Africa, India and Australia, whose formation indeed had begun in early Proterozoic.

References

1. Dawson, J.B., *Kimberlites and Their Xenoliths*, Springer-Verlag, Heidelberg, 1980.
2. Jakes, A., Louis, J., Smith, K., *Kimberlites and lamproites of the Western Auistralia*, Mir, Moscow, 1989, 430 p.
3. Ilupin, I.P., Vaganov, Prokopchuk, *Kimberlites. Reference Book*, Nedra, Moscow, 1990, 248 pp.
4. Bogatikov, O.A., Ryabchikov, I.D., Kononova, V.A., *Lamproites*, p. 302, Nauka, Moscow, 1991.
5. Kostyuk, V.P., *Mineralogy and issues of Siberian alkali igneous rock genesis*, Nauka, Novosibirsk, 1974, 247 p.
6. Borodin, L.S., Lapin, A.V., Pyatenko, I.K., *Petrology and geochemistry of alkaline-ultramafic rock and kimberlite dykes*, Nauka, Moscow, 1976, 244 p.
7. Serensen, H. (Ed.), *Alkali rocks*, Mir, Moscow, 1976, 400 p.
8. Tattle, O. and Gittince, J. (Eds.), *Carbonatites*, Mir, Moscow, 1969, 486 p.
9. Samoylov, V.S., *Carbonatite (facies and foirmation environments)*, Nauka, Moscow, 1977, 202 p.
10. Kuleshov, V.N., *Isotope Composition and Origin of the Depth Carbonates*, Nauka, Moscow, 1986, 126 pp.
11. Sorokhtin, O.G., *Tectonics of the Lithospheric Plates and the Origins of the Diamondiferous Kimberlites. General and Regional Geology*, VIEMS, Moscow, 1985, 47 pp.
12. Sorokhtin, N.O., Lobkovsky, L.I., Semiletov, I.P., Carbon depth cycle and the formation of abiogenous hydrocarbons. Proc. Of Tomsk Polytechnical University. *Georesour. Eng.*, 329, 8, 156–173, 2018.
13. Sorokhtin, N.O., Lobkovsky, L.I., Kozlpov, N.E., Subduction zone ore-genesis patterns. *Oceanology*, 58, 1, 118–128, 2018b.
14. Muramatsu, Y., Geochemical investigations of kimberlites from the Kimberley area, South Africa. *Geochem. J.*, 17, 2, 71–86, 1983.
15. Sorokhtin, O.G., *Global Evolution of Earth*, Nauka, Moscow, 1974, 184 pp.
16. Sclater, J.G., Jaupart, C., Galson, D., The heat flow through oceanic and continental crust and the heat loss of the Earth. *Rev. Geophys. Space Phys.*, 18, 269–311, 1980.
17. Sorokhtin, O.G. and Ushakov, S.A., *Global Evolution of Earth*, MGU Publishers, Moscow, 1991, 446 pp.

N. O. Sorokhtin (ed.) The Origins of Natural Diamonds, (483–507) © 2019 Scrivener Publishing LLC

18. Sorokhtin, O.G. and Ushakov, S.A., *Evolution of Earth*, MGU Publishers, Moscow, 2002, 560 pp.
19. Sorokhtin, O.G., Chilingarian, G.V., Sorokhtin, N.O., *Evolution of Earth and its climate*, vol. 10, Elsevier Science. Developments in Earth and Environmental Sciences, New York, 2011, 763 pp.
20. Melton, C.E. and Giardini, A.A., The composition and significance of gas released from natural diamonds from Africa and Brazil. *Am. Miner.*, 59, 7, 8775–782, 1974.
21. Melton, C.E. and Giardini, A.A., Experimental results and theoretical interpretation of gaseous inclusions found in Arkansas natural diamonds. *Am. Miner.*, 60, 5, 6413–417, 1975.
22. Kostylkeva-Labuntsova, U.U., Borutsky, B.E., Sokololva, M.N., Shlyukova, Z.V. *et al.*, *Mineralogy of the Khibin massif*, vol. 1, Nauka, Moscow, 1978, 228 p.
23. Sobolev, N.V., *Depth inclusions in kimberlites and the upper mantle composition issue*, Nauka, Novosibirsk, 1974, 264 p.
24. Trofimov, V.S., *Geology of Natural Diamond Deposits*, Nedra, Moscow, 1980, 304 pp.
25. Vladimirov, B.M., Solovyeva, L.V., Kiselev, A.I., Yegorov, K.N. *et al.*, Kimberlites and kimberlite-like rocks, in: *Kimberlite – An Ultramafic Formation of Ancient Platforms*, pp. 190–264, Novosibirsk, Nauka, 1990.
26. Groves, D.I., Ho, S.E., Rock, N.M.S., Barley, M.E., Muggeridge, M.T., Archean cratons, diamond and platinum: Evidence for couple long-lived crust-mantle systems. *Geology*, 15, 9, 801–805, 1987.
27. Lisitsin, A.P., *Geology of the Ocean (Oceanology, Geophysics of the Ocean)* Nauka, Moscow, 1980, 464 pp.
28. Sobolev, V.S., Formation conditions of diamond deposits. *Geol. Geophys.*, 1, 7–22, 1960.
29. Green, D.H. and Ringwood, A.E., Origin of the calcalkalaine igneous rock suite. *Earth Planet. Sci. Lett.*, 1, 307–316, 1966.
30. Green, D.H. and Ringwood, A.E., An experimental investigation of the gabbro to eclogite transition and its petrological applications. *Geochim. Cosmochim. Acta*, 31, 767–833, 1976.
31. Reid, A.M., Brown, R.W., Dawson, J.B., Whitfield, G.G., Siebert, J.C., Garnet and pyroxene compositions in some diamondiferous eclogites. *Contrib. Miner. Petrol.*, 58, 203–220, 1976.
32. Perchuk, L.L., Upgrading of the double-pyroxene geo-thermometer for depth peridotites. *Proc. AH USSR*, 233, 3, 456–459, 1977a.
33. Perchuk, L.L., Pyroxene barometer and "pyroxene geotherms". *Proc. AH USSR*, 233, 6, 1196–1199, 1977b.
34. Ringwood, A.E. and Major, A., The system Mg2SiO4-Fe2SiO4 at high pressures and temperatures. *Phys. Earth Planet. Int.*, 4, 89–108, 1970.
35. Boyd, F.R., A pyroxene geotherm. *Geochim. Cosmochim. Acta*, 27, 2533–2546, 1973.

36. Mercier, J.C.C. and Carter, N.L., Pyroxene geotherms. *J. Geophys. Res.*, 80, 3349–3362, 1975.
37. Kaminsky, F.V., *Diamond-bearing of non-kimberlite igneous rocks*, Nedra, Moscow, 1984, 173 p.
38. Kennedy, C.S. and Kennedy, G.C., The equilibrium boundary between graphite and diamond. *J. Geophys. Res.*, 81, 2476–2470, 1976.
39. Sobolev, N.V., Parageneses of the diamonds and the issues of the depth mineral formation. *Notes of All-Union Mineralogical Soc.*, 4, CXII, 389–397, 1983.
40. Takahashi, I., Melting of dry peridotite KLB-1 up to 14 Gpa: Implications on the origin of peridotitic mantle. *J. Geophys. Res.*, 91, 899367–9382, 1986.
41. Harte, B., Rock nomenclature with particular relation to deformation and recrystallization textures in olivine-bearing xenoliths. *J. Geol.*, 85, 279–288, 1977.
42. Frank, F.C., Diamonds and deep fluids in the mantle, in: *The Application of Modern Physics to Earth and Planetary Interiors*, S.R. Runcorn (Ed.), pp. 247–250, J.Wiley, New York, 1969.
43. Swart, P.K., Pillinger, C.T., Milledge, H.J., Seal, M., Carbon isotopic variation within individual diamonds. *Nature*, 303, 793–795, 1983.
44. Wyllie, P.J., Kimberlite magmas from the system peridotite - CO_2-H_2O, in: *Kimberlites, Diatremes and Diamonds: Their Geology, Petrology and Geochemistry*, F.R. Boyd and H.O.A. Meyer (Eds.), pp. 319–329, AGU, Wash, 1979.
45. Harris, P.G., Zone refining and the origin of potassic basalts. *Geochim Cosmochim. Acta*, 12, 3, 195–208, 1957.
46. Harris, P.G. and Middlemost, E.A.K., The evolution of kimberlites. *Lithos*, 3, 77–88, 1969.
47. O'Hara, M.J. and Yoder, H.S., Formation and fractionation of basic magmas at high pressures. *Scott. J. Geol.*, 3, 67–117, 1967.
48. Dawson, J.B., Advances in kimberlite geology. *Earth Sci. Rev.*, 7, 187–214, 1971.
49. Orlov, Y.L., *Mineralogy of the diamond*, Nauka, Moscow, 1984, 264 p.
50. Ringwood, A.E., *Composition and petrology of the Earth's mantle*, Nedra, Moscow, 1981, 584 p.
51. Sobolev, V.S. and Sobolev, N.V., New evidences of the Earth crust eclogite rocks subsidence to great depths. *Proc. AN USSR*, 250, 3683–685, 1980.
52. Galimov, E.M., Issues of the carbon geochemistry. *Geochemistry*, 2, 258–278, 1988a.
53. Galimov, E.M., On the ocean's emergence and evolution based on the data of $^{18}O/^{16}O$ ratio variations in Earth's sedimentary shell in geologic time. *Proc. AN USSR*, 299, 4977–981, 1988b.
54. Eldrdge, C.S., Compston, W., Williams, I.S. *et al.*, Isotope evidence for the involvement of recycled sediments in diamond formation. *IBID*, 353, 649–653, 1991.

55. Sorokhtin, O.G., Mitrofanov, F.P., Sorokhtin, N.O., *Origin of Diamonds and Potential of Diamond Bearing of the Eastern Baltic Shield*, p. 144, KNC RAN, Apatity, 1996.
56. Monin, A.S. and Sorokhtin, O.G., On the deposits suck-in to great depths under the continents. *Proc. AN USSR*, 286, 3583–586, 1986.
57. Sorokhtin, O.G., Structure of the continental lithospheric plates and the origins of kimberlites, in: *Issues of Theoretical Geodynamics and the Tectonics of the Lithospheric Plates*, A.S. Monin (Ed.), pp. 161–168, Oceanology Institute of AN USSR, Moscow, 1981b.
58. Sorokhtin, O.G., Mitrofanov, F.P., Sorokhtin, N.O., *Global Evolution of Earth and Origin of Diamonds*, Nauka, Moscow, 2004, 269 pp.
59. Bogatikov, O.A. (Ed.), *Archangel diamond-bearing province (geology, petrology, geochemistry and mineralogy)*, Publishers MGU, Moscow, 2000, 552 p.
60. Levin, B.Y., *The origin of Earth and the planets*, Nauka, Moscow, 1964, 116 p.
61. Safronov, V.S., *Evolution of the pre-planetary cloud and the formation of Earth and planets*, Nauka, Moscow, 1969, 244 p.
62. Cameron, A.G.W., The origin and evolution of the solar system. *Sci. Am.*, 233, 32–41, 1972.
63. Cameron, A.G.W., Accumulation processes in the primitive solar nebula. *Icarus*, 18, 407–450, 1973.
64. Ruskol, E.L., *On the Origins of Moon*, Nauka, Moscow, 1975, 188 pp.
65. Voytkevich, G.V., *Fundamentals of the Earth's Origin Theory*, Nedra, Moscow, 1979, 135 pp.
66. Alfven, H. and Arrhenius, G., *Evolution of the Solar System*, Scientific and Technical Information Office National Aeronautics and Space Administration, Washington, DC, 1976.
67. Vityazev, A.V., Pechernikova, G.V., Safonov, V.S., *Earth's Group Planets: Origin and Early Evolution*, Nauka, Moscow, 1990, 296 pp.
68. Schmidt, O.Y., New theory of the Earth's origins. *Nature*, 7, 6–16, 1946.
69. Kaufmann, W. J., III., *Planets and Moons*, W. H. Freeman and Company, San Francisco, 1982, 216 pp.
70. Fisher, D.E., *The Birth of the Earth*, Columbia University Press, New York, 1987.
71. Schmidt, O.Y., *Four Lectures on the Theory of the Earth's Origins*, AN USSR Publishers, Moscow, 1948, 76 pp.
72. Voitkevich, G.V., Kokin, A.V., Miroshnikov, A.E., Prokhorov, V.G., *Reference book of geochemistry*, Nedra, Moscow, 1990, 480 p.
73. Ronov, A.B. and Yaroshevsky, A.A., *Chemical Composition of the Earth's Crust and of Her Shells. Tectonosphere of Earth*, pp. 376–402, Nedra, Moscow, 1978.
74. Dmitriyev, L.V., *Mid-Oceanic Ridge Bedrock Geochemistry and Petrology*, Abstract of PhD thesis, GEOCHI, Moscow, 1973, 45 pp.
75. Ringwood, A.E., *The Chemical Composition and Origin of the Earth. Advances in Earth Sciences*, pp. 276–356, MIT Press, Cambridge, 1966.

76. Urey, H.C. and Craig, H., The composition of the stone meteorites and the origin of meteorites. *Geochim. Cosmochim. Acta*, 4, 36–82, 1953.
77. Mason, B., *Basics of Geochemistry*, Moscow, Nedra, 1971, 312 p.
78. Tozer, D.C., Thermal history of the Earth. 1: The formation of the core. *Geophys. J. R. Astron Soc.*, 9, 95–112, 1965.
79. Oversby, V.M. and Ringwood, A.E., Time of formation of the Earth's core. *Nature*, 234, 463–465, 1971.
80. Jacobs, J.A., *The Earth's Core*, Academic Press, New York, 1975.
81. Runcorn, S.K., Convection currents in the Earth's mantle. *Nature*, 195, 1248–1249, 1962.
82. Runcorn, S.K., Changes in the convection pattern in the Earth's mantle and continental drift: Evidence for a cold origin of the Earth. *Phil. Trans. Roy. Soc. Ser. A*, 258, 228–251, 1965.
83. Elsasser, W.M., *Early History of the Earth. Earth Science and Meteoritics*, pp. 1–30, North-Holland, Amsterdam, 1963.
84. Murbat, S., Boundary conditions of the Archaean crust evolution based on the age and isotope data, in: *Early history of Earth*, pp. 356–366, Mir, Moscow, 1980.
85. Taylor, S.P. and McLennan, S.M., *The Continental Crust: Its Composition and Evolution*, Blackwell Scientific, Oxford, 1985.
86. Wilde, S.A., Vailey, J.W., Peck, W.H., Graham, C.M., Evidence from detrital zircons for the existence of continental crust and oceans on the Earth 4.4 BY ago. *Nature*, 409, 175–178, 2001.
87. Tolstikhin, I.L., *Isotopic Geochemistry of Helium, Argon and Rare Gases*, Nauka, Leningrad, 1986, 200 pp.
88. Ozima, M. and Podosek, F.A., *Noble Gas Geochemistry*, Cambridge University Press, Cambridge, London, New York, Melbourne, Sydney, 1983.
89. Azbel, I.Y. and Tolstikhin, I.N., *Radiogenic Isotopes and Evolution of the Earth's Mantle, Crust and Atmosphere*, Geol. Inst. AN USSR, Apatity, 1988, 140 pp.
90. Sorokhtin, O.G. and Ushakov, S.A., *Origin of Moon and Its Effect on the Global Evolution of Earth*, MGU Publishers, Moscow, 1989b, 111 pp.
91. Sorokhtin, O.G., *Life of Earth. "Regular and Chaotic Dynamics"*, Institute of computer studies, Moscow-Izhevsk, 2007, 452 pp.
92. Ringwood, A.E., *Origins of Earth and Moon*, Nedra, Moscow, 1982, 175 p.
93. Monin, A.S. and Sorokhtin, O.G., Earth's evolution at volumetric differentiation in her depths. *Proc. AN USSR*, 263, 3572–575, 1982a.
94. Sorokhtin, O.G., Early stages in the evolution of the Earth-Moon system. *Izv. Sect. Earth Sci. RAEN*, 2, 141–153, 1999.
95. Safronov, V.S. and Vityazev, A.V., *Origins of the Solar System. Results of Science and Technology, Astronomy*, vol. 4, G. Rives (Ed.), pp. 5–93, VINITI, Moscow, 1983.
96. Sorokhtin, O.G. and Ushakov, S.A., *Process of the Earth's Core Separation. Life of the Earth, Evolution of Earth and the Planets*, pp. 6–34, Izd. MGU, Moscow, 1990.

97. Sorokhtin, O.G. and Sorokhtin, N.O., Earth's core separation is the main planetary process controlling geologic evolution of Earth. *Izv. Sect. Earth Sci. RAEN*, 13, 99–116, 2005.
98. Sorokhtin, O.G., *Origins of Moon and the Initial Stages of the Earth Evolution Life of Earth*, pp. 5–24, MGU Publishers, Moscow, 1988.
99. Glukhovsky, M.Z., Moralev, V.M., Kuzmin, M.I., Hot belt of the early Earth and its evolution. *Geotectonics*, 5, 3–15, 1994.
100. Sorokhtin, O.G. and Ushakov, S.A., On three stages in the tectonic evolution of Earth. *Proc. AN USSR*, 307, 177–83, 1989a.
101. Sorokhtin, O.G. and Ushakov, S.A., *Nature of Earth's tectonic activity. Results of Science and Technology. Series Physics of Earth*, vol. 12, p. 292, VINITI, Moscow, 1993.
102. Khain, V.E. and Bozhko, N.A., *Historical geotectonics, Precambrian*, Nedra, Moscow, 1988, 382 pp.
103. Vinogradov, A.P. and Yaroshevsky, A.A., On physical conditions of zonal melting in Earth's shells. *Geochemistry*, 7, 779–790, 1965.
104. Vinogradov, A.P. and Yaroshevsky, A.A., Dynamics of the zonal melting and some geochemical consequences. *Geochemistry*, 12, 79–93, 1967.
105. Magnitsky, V.A., *Internal Structure and Physics of the Earth*, Nedra, Moscow, 1965, 379 pp.
106. Naimark, L.M., On possible gravity differentiation mechanism in a medium which separates at heating. *Proc. AN USSR*, 276, 4846–850, 1984a.
107. Naimark, L.M., Zonal melting as a gravity differentiation mechanism. *Proc. AN USSR*, 278, 3580–584, 1984b.
108. Kovalenko, V.I. *et al.*, General patterns of the magmatism evolution in Earth's history, in: *Magmatic Rocks', Magmatism Evolution in the Earth's History*, vol. 6, O.A. Bogatikov (Ed.), pp. 332–348, Nauka, Moscow, 1987.
109. Zharkov, V.N., *Internal Structure of Earth and Planets*, Nauka, Moscow, 1983, 415 pp.
110. Monin, A.S. and Sorokhtin, O.G., On the volumetric gravity differentiation of Earth. *Proc. AN USSR*, 259, 51076–1079, 1981.
111. Kirkinsky, V.A., Decomposition of solid solutions, in: *Experiment in Mineralogy and Petrography*, Nauka, Moscow, 1975, 1735 pp.
112. Sorokhtin, O.G., Chilingar, G.V., Sorokhtin, N.O., *Theory of Earth development (the origin, evolution and a tragic future)*, Institute for computer studies, Moscow-Izhevsk, 2010, 751 p.
113. Sorokhtin, O.G., Possible physicochemical processes of Earth's core formation. *Proc. AH USSR.*, 198, 6, 1327–1330, 1971.
114. Ohtani, E., Ringwood, A., Hibberson, W., Composition of the core II. Effect of high pressure on solubility of FeO in molten iron. *Earth Planet. Sci. Lett.*, 71, 194–103, 1984.
115. Teng, T., Attenuation of body waves and the Q structure of the mantle. *J. Geophys. Res.*, 73, 62195–2208, 1968.

116. Zharkov, V.N. *et al.*, Test distribution of the Q (t) dissipative function in the Earth's shell. *Izv. AN USSR Phys. Earth*, 12, 3–12, 1974.
117. Berzon, I.S., Kogan, S.D., Pasechnik, I.P., On a possibility of constructing a thin-layer model of the shell to core transition area. *Proc. AN USSR*, 178, 186–89, 1968.
118. Berzon, I.S. and Pasechnik, I.P., Dynamic parameters of the PcP wave in a case of a thin-layer model of the mantle to core transition area. *Izv. AN USSR. Phys. Earth*, 6, 21–33, 1972.
119. Carslow, G. and Yeager, D., *Heat-Conductivity of Solid Bodies*, Nauka, Moscow, 1964.
120. Sorokhtin, O.G., Tectonics of the lithospheric plates and the nature of global transgressions, in: *Issues of Paleohydrology*, M.V. Astaykin (Ed.), pp. 59–69, Moscow, Nauka, 1976.
121. Morelli, A. and Dziewonski, A., Topography of the core—Mantle boundary and lateral homogeneity of the liquid core. *Nature*, 325, 6106678–683, 1987.
122. Keondzhyan, V.P. and Monin, A.S., Gravity differentiation model of the planetary subsurface. *Proc. AN USSR*, 220, 4825–828, 1975.
123. Keondzhyan, V.P. and Monin, A.S., Calculation of the planetary subsurface evolution. *Izv. AN USSR. Phys. Earth*, 4, 3–13, 1976.
124. Hale, C.J., Palaemagnetic data suggest link between Archaean-Proterozoic boundary and inner-core nucleation. *Nature*, 329, 6136233–236, 1987.
125. O'Neil, J., Carlson, R.W., Francis, D., Stevenson, R.K., Neodymium-142 evidence for Haden Mafic Crust. *Nature*, 321, 1828–1831, 2008.
126. Khain, V.E., Particulars of the Earth's crust evolution in Early Precambrian—Real and fictitious, in: *Issues of the Early Precambrian Geology*, pp. 5–12, Nauka, Leningrad, 1977.
127. Khain, V.E., *Tectonics of the Continents and Oceans*, Nauchny Mir, Moscow, 2001, 606 pp.
128. Tera, F. and Wasserburg, G.J., U-Th-Pb systematics on lunar rocks and inferences evolution and the age of the Moon, in: *Proceedings of the Fifth Lunar Science Conference*, vol. 2, pp. 1571–1599, Elsevier, Cambridge, MA, 1974.
129. Tera, F. and Wasserburg, G.J., The evolution end History of mare basalts as inferred from U-Th-Pb systematic. *Lunar Sci.*, VI, 807–809, 1975.
130. Tera, F., Papanastassion, D.A., Wasserburg, G.J., Isotopic evidence for a terminal lunar cataclysm. *Earth Planet. Sci. Lett.*, 22, 1–21, 1974.
131. Jessberger, E.K., Huneke, I.C., Podosek, F.A., Wasserburg, G.J., High resolution argon analysis of neutron-irradiated Appollo 16 rocks and separated minerals. *Proc. Fifth Lunar Sci. Conf.*, 2, 1419–1449, 1974.
132. Holmes, A., An estimate of the age of the Earth. *Nature*, 157, 680–684, 1946.
133. Fore, G., *The fundamentals of isotopic geology*, Moscow, Mir, 1989, 590 p.
134. Stacey, J.S. and Kramers, J.D., Approximation of terrestrial lead isotope evolution by a two-stage model. *Earth Planet. Sci. Lett.*, 26, 207–221, 1975.

135. Naimark, L.M. and Sorokhtin, O.G., *Density Distribution in Earth's Model with a Lherzolite*, pp. 28–41, USSR Institute Oceanology Moscow, 1977a.
136. Naimark, L.M. and Sorokhtin, O.G., *Energy of Earth's Gravity Differentiation. Tectonics of the Lithospheric Plates*, pp. 42–56, USSR Institute of Oceanology, Moscow, 1977b.
137. Birch, F., Differentiation of the Mantle. *Geol. Soc. Am. Bull.*, 69, 4483–486, 1958.
138. Tilton, G.B. and Read, G.W., Radioactive heat production in eclogites and some ultramafic rocks, in: *Earth Science and Meteoritics*, J. Geiss and E.D. Goldberg (Eds.), pp. 31–43, In North-Holland Publishing Company, Amsterdam, 1963.
139. Lyubimova, E.A., *Thermics of Earth and Moon*, Nauka, Moscow, 1968, 280 pp.
140. Gast, P.W., The chemical composition of the Earth, the Moon and chondritic meteorites, in: *The Nature of the Solid Earth*, E.C. Robertson (Ed.), pp. 19–40, McGraw-Hill, New York, 1972.
141. Peive, A.V., Oceanic crust of the geologic past. *Geotectonics*, 4, 5–23, 1969.
142. Peive, A.V., Knipper, N.A., Shtreys, A.A. *et al.*, Ocean and the geosynclinal process. *Proc. AN USSR*, 196, 3657–659, 1971.
143. Coleman, R.G., Petrological and geophysical nature of serpentinites. *Geol. Soc. Am. Bull.*, 82, 4897–918, 1971a.
144. Coleman, R.G., Plate tectonic emplacement of upper mantle peridotites along continental edges. *J. Geophys. Res.*, 76, 51212–1222, 1971b.
145. Dewey, J. and Bird, J., Plate tectonics and geosynclines. *Tectonophysics*, 10, 5, 6625–638, 1970a.
146. Dewey, J. and Bird, J., Mountain belts and the new global tectonics. *J. Geophys. Res.*, 75, 142625–2647, 1970b.
147. Physical properties of rocks and of economic deposits (Petrophysics), *Reference Book of Geophysicists*, Nedra, Moscow, 1976, 527 pp.
148. Sclater, J., Parsons, B., Laupart, C., Oceans and continents: Similarities and differences in the mechanism of heat transport. *J. Geophys. Res.*, 86, 11535–11552, 1981.
149. Taylor, S.R., Trace element abundances and the chondritic Earth model. *Geochim. Cosmochim. Acta*, 28, 1989–1998, 1964.
150. Turcotte, D.L. and Schubert, J., *Geodynamics*, vol. 1 and 2, Mir, Moscow, 1985, 374 pp., 730 pp.
151. Gast, P.W., Upper mantle chemistry and evolution of the Earth's crust, in: *The History of the Earth's Crust*, R.A. Phinney (Ed.), pp. 15–27, Princeton University Press, Princeton, USA, 1968.
152. Hurley, P.M., Absolute abundance and distribution of Rb, K and Sr in the Earth. *Geochim. Cosmochim. Acta*, 323, 273–284, 1968.
153. Sorokhtin, O.G., Contents of radioactive elements in Earth and the radiogenic energy, in: *Tectonics of the Lithospheric Plates (Sources of the Tectonic Processes Energy and the Plate Dynamics)*, A.S. Monin (Ed.), pp. 7–27, IOAN, Moscow, 1977.

154. Vinogradov, A.P., Average contents of chemical elements in major types of Earth's crust igneous rocks. *Geochemistry*, 7, 188, 1962.
155. Taylor, S.R., Chemical evidence for lunar melting and differentiation. *Nature*, 245, 203–205, 1973.
156. Pariysky, N.N., On the effects of Earth's tides on centenarian slowdown of Earth's revolution. *Astron. J.*, 37, 543–555, 1960.
157. McDonald, G.J.F., Tidal friction, in: *The Tides and Resonances in the Solar System*, pp. 9–96, Mir, Moscow, 1975.
158. Sorokhtin, O.G., Correlation of the mid-oceanic ridge topography with the lithospheric plate spreading rate. *Proc. AN USSR*, 208, 6, 1338–1341, 1973a.
159. Sorokhtin, O.G., Possible formation mechanism of the regional overthrusts and geosynclinal folding. *Izv. AN USSR. Phys. Earth*, 7, 55–67, 1973b.
160. Ushakov, S.A. and Fedynsky, V.V., Riftogenesis as a mechanism of control over the Earth's heat loss. *Proc. AN USSR*, 209, 51182–1185, 1973.
161. Gorodnitsky, A.M. and Sorokhtin, O.G., Map of the calculated values of heat flow through the ocean floor, in: *Issues of Theoretical Geodynamics and Lithospheric Plate Tectonics*, O.G. Sorokhtin (Ed.), pp. 122–128, USSR Institute of Oceanology, Moscow, 1981.
162. Anderson, R.N. and Hobart, V.A., The relation between heat flow, sediment thickness and age in the Eastern Pacific. *J. Geophys. Res.*, 81, 2968–2989, 1976.
163. Lister, C.R.B., On the thermal balance of a midocean rise. *Geophys. J. Roy. Astron. Soc.*, 26, 516–520, 1972.
164. Edmond, L.M., Measures, C., McDuff, R.E. *et al.*, Ridge crest hydrothermal activity and the balances of the major and minor elements in the ocean: The Galapagos data. *Earth Planet. Sci. Lett.*, 46, 1–18, 1979.
165. Francheteau, J., Needham, H.D., Chourone, P., Juteau, T. *et al.*, Massive deep-sea sulfide ore deposits discovered on the East Pacific Rise. *Nature*, 277, 523–528, 1979.
166. Hekinian, R., Rosendahl, B.R., Cronan, D.S. *et al.*, Hydrothermal deposits and associated basement rocks from the Galapagos spreading center. *Oceanol. Acta*, 1, 3473–482, 1978.
167. Hekinian, R., Francheteau, J., Renard, V., Ballard, R.D. *et al.*, Intense hydrothermal activity at the rise axis of the East Pacific Rise near 13 N: Submersible witnesses the growth of sulfide chimney. *Mar. Geophys. Res.*, 6, 11–14, 1983.
168. Sorokhtin, O.G., Oceanic riftogenesis and the expanding Earth hypothesis, in: *The Continental and Oceanic Riftogenesis*, pp. 121–136, Nauka, Moscow, 1985b.
169. Artyushkov, E.V., Gravity convection in Earth's depth. *Izv. AN USSR. Phys. Earth*, 9, 3–18, 1968.
170. Artyushkov, E.V., Earth's matter density differentiation and the associated phenomena. *Izv. AN USSR. Phys. Earth*, 5, 18–30, 1970.
171. Sorokhtin, O.G., Differentiation of the Earth's matter and the evolution of tectonic processes. *Izv. AN USSR. Phys. Earth*, 7, 55–66, 1972.
172. Monin, A.S., *History of Earth*, Leningrad, Nauka, 1977, 228 pp.

173. Monin, A.S., *Hydrodynamics of the Atmosphere, Ocean and Earth's Depths*, Gidrometeoiz- dat, Moscow, 1999, 524 pp.
174. Green, D.H. and Ringwood, A.E., The genesis of basaltic magmas. *Contrib. Miner. Petrol.*, 15, 103–190, 1967.
175. Sorokhtin, N.O., *Evolution of the Continental Lithosphere in Early Precambrian (on the Example of the Eastern Baltic Shield)*, PhD thesis, MGU, Moscow, 2001a, 368 pp.
176. Sorokhtin, O.G., Greenhouse effect: Myth and reality. *Herald RAEN*, 1, 18–21, 2001b.
177. Kuskov, O.L. and Fabrichnaya, O.B., Phase relations in the system FeO-MgO-SiO_2 at the transition zone—Lower mantle boundary. *Geochemistry*, 2, 266–278, 1990.
178. Ringwood, A.E., *Composition and Petrology of the Earth's Mantle*, McGraw-Hill, New York, 1975.
179. Forsyth, D. and Uyeda, S., On the relative importance of the driving forces of plate motion. *Geophys. J. Roy. Astron. Soc.*, 43, 163–200, 1975.
180. Fisher, O., *Physics of the Earth Crust*, 2nd ed., Macmillan, London, 1889.
181. Duffield, W.A., A naturally occurring model of global plate tectonics. *J. Geophys. Res.*, 7, 2543–2555, 1972.
182. Holmes, A., Radioactivity and Earth movements. *Geol. Soc. Glasgow Trans.*, 18, 559–606, 1928.
183. Chandrasekhar, S., *Hydrodynamic and Hydro- magnetic Stability*, p. 198, Oxford University Press, Oxford, England, Chap. VI, 1961.
184. Richter, F.M., Dynamical models of see-floor spreading. *Rev. Geophys. Space Phys.*, 11, 223–287, 1973.
185. McKenzie, D. and Richter, F., Convection currents in the Earth's mantle. *Sci. Am.*, 235, 572–89, 1976.
186. Trubitsin, V.P. and Rykov, V.V., *Mantle Convection with Floating Continents. Issues of Global Geodynamics*, pp. 7–28, GEOC, Moscow, 2000.
187. Zharkov, V.N. and Trubitsin, V.P., *Physics of the Planetary Subsurface*, Nauka, Moscow, 1980, 448 p.
188. Ranelli, G. and Fischer, B., Diffusion creep, dislocation creep, and mantle rheology. *Phys. Earth Planet. Int.*, 34, 77–84, 1984.
189. Glukhovsky, M.Z., *Geologic Evolution of Basements of the Ancient Platforms (Nuclear Concept)*, Nauka, Moscow, 1990, 215 pp.
190. Condie, K.C., *Archean Greenstone Belts*, Elsevier, Amsterdam, 1981.
191. Monin, A.S., Seidov, D.G., Sorokhtin, O.G., Sorokhtin, Y.O., Numerical experiments with forms of the mantle convection. *Proc. AN USSR*, 295, 51080–1083, 1987a.
192. Monin, A.S., Seidov, D.G., Sorokhtin, O.G., Sorokhtin, Y.O., Numerical modeling of the mantle convection. *Proc. AN USSR*, 295, 158–63, 1987b.
193. Monin, A.S., *Theoretical Fundamentals of Geophysical Hydrodynamics*, Leningrad, Gidrometeoizdat, 1988, 424 pp.

194. Kozlov, N.E., Sorokhtin, N.O. *et al.*, *Archaean Geology of the Baltic Shield*, Nauka, Sankt-Peterburg, 2006, 329 pp.
195. Sorokhtin, N.O., Theoretical aspects of the Early Precambrian geodynamics on the example of the continental crust formation in the NW White Sea region, in: *Geologic Mapping of Early Precambrian complexes*, N.V. Mezhelovsky (Ed.), pp. 438–498, Moscow, 1994.
196. Wit, M.J., Roering, C., Hart, R.J., Armstrong, R.A., de Ronde, C.E.J., Green, R.W.E., Tredoux, M., Peberdy, E., Hart, R.A., Formation of an Archaean Continent. *Nature*, 357, 553–562, 1992.
197. Wit, M.J., On Archean granites, greenstones, cratons and tectonics: Does evidence demand a verdict? *Precambrian Res.*, 91, 181–226, 1998.
198. Sorokhtin, N.O. and Sorokhtin, O.G., Continent stand level and possible nature of the Early Proterozoic glaciation. *Proc. RAN*, 354, 2234–237, 1997.
199. Moralev, V.M. and Glukhovsky, M.Z., Partial melting of meta-basites and the evolution of the Pre-cambrian lithosphere. *Proc. AN USSR*, 284, 2427–431, 1985.
200. Glikson, A., Stratigraphy and evolution of primary and secondary greenstone complexes; data for the shields of the southern hemisphere, in: *Early History of Earth*, pp. 264–285, Mir, Moscow, 1980.
201. Borukayev, C.B., *The Structure of Precambrian and the Plate Tectonics*, Nauka, Novosibirsk, 1985, 190 pp.
202. Frolova, T.I. and Burikova, I.A., Andesite volcanism in the Earth's history. Herald MGU. *Geology*, 4, 3–17, 1992.
203. Veizer, J., Evolution ratio, $^{87}Sr/^{86}Sr$ in marine water, in: *The Early History of the Earth*, B.F. Windley (Ed.), pp. 363–373, Wiley, New York, 1976.
204. Chumakov, N.M., *Precambrian Tillites and Tilloids*, Nauka, Moscow, 1978, 2006-published by GEOS in Russia. 202 pp.
205. Lisitsin, A.P., Avalanche deposition, ocean level changes, hiatuses and the pelagic deposition as the global patterns, in: *Paleo-Oceanology*, vol. 3, E.A. Kozlovsky (Ed.), pp. 3–21, Nauka, Moscow, 1984.
206. Sorokhtin, N.O., Dual-layer model of the continental crust formation in Archaean, in: *Abstracts of Reports at the International Conference "New Ideas in Earth Sciences"*, vol. 1, pp. 136–137, Moscow State University, 1997.
207. Tikhonov, A.N. and Samarinsky, A.A., *Equations of Mathematical Physics*, Nauka, Moscow, 1966, 724c.
208. Zharikov, V.A., *Fundamentals of Physicochemical Petrology*, MGU Publishers, Moscow, 1976, 420 pp.
209. Smirnov, Y.B., *Heat Field of the USSR Territory (Explanatory Note to the Heat Flow and Depth Temperature Maps 1:10, 000, 000)*, GUGK, Moscow, 1980, 150 pp.
210. Lehmann, I., Velocities of longitudinal waves in the upper part of the Earth's mantle. *Ann. Geophys.*, 15, 93–118, 1959.
211. Parker, R.L. and Oldenburg, D.W., Thermal model of Ocean Ridges. *Nat. Phys. Sci.*, 242, 122137–139, 1973.

212. Clarke, P. (Ed.), *Reference Book of Rocks' Physical Constants*, Mir, Moscow, 1969, 544 pp.
213. Yoshii, T., Regionality of group velocities of Rayleigh waves in the Pacific and thickening of the plate. *Earth Planet. Sci. Lett.*, 25, 3305–312, 1975.
214. Vogt, P.R., Volcano height and plate thickness. *Earth Planet. Sci. Lett.*, 23, 3, 1974.
215. Gorodnitsky, A.M., Thickness of the oceanic lithosphere and maximum height of the underwater volcanoes, in: *Tectonics of the Lithospheric Plates*, A.S. Monin (Ed.), pp. 24–32, USSR Institute of Oceanology, Moscow, 1977.
216. Vening Meinesz, F.A., *GravityExpedition at Sea 4*, Neth. Geol. Comm, Delft, 1948.
217. Vening Meinesz, F.A., Plastic buckling of the Earth's crust: The origin of geosynclines, in: *Crust of the Earth (A Symposium)*, vol. 62, A. Poldervaart (Ed.), pp. 319–330, Geological Society of America, New York, 1955, Spec. Papers.
218. Wadati, K., On the activity of deep-focus earthquakes in the Japan Island and neighborhood. *Geophys. Mag.*, 8, 305–326, 1935.
219. Benioff, H., Seismic evidence for crustal structure and tectonic activity. *Geol. Soc. Am. Spec. Paper*, 62, 67–74, 1955a.
220. Benioff, H., Seismic evidence for crustal structure and tectonic activity. *Geol. Soc. Am. Spec. Paper*, 62, 61–74, 1955b.
221. Zavaritsky, A.N., *Introduction to the Petrochemistry of Igneous Rocks*, 2nd ed, AN USSR Publishers, Moscow, Leningrad, 1950, 400 pp.
222. Lobkovsky, L.I. and Sorokhtin, O.G., *Plastic Deformations of the Oceanic Lithosphere in the Plate Subduction Zones. Tectonics of the Lithospheric Plates*, pp. 22–52, Oceanology Institute, AN USSR, Moscow, 1976.
223. Shemenda, A.I., Similarity criteria at mechanical modeling of tectonic processes. *Geol. Geophys.*, 10, 10–19, 1983.
224. Sorokhtin, O.G., *Geodynamics (Oceanology, Geophysics of the Ocean, Vol. 2)*, Nauka, Moscow, 1979b, 416 pp.
225. Schlichting, H., *Grenzschicht-Theorie*, Verlag G. Braun, Karlsruhe, 1974, 712 pp.
226. Lobkovsky, L.I., *Geodynamics of the Spreading and Subduction Zones and the Double-Staged Plate Tectonics*, Nauka, Moscow, 1988, 251 pp.
227. Lobkovsky, L.I. and Sorokhtin, O.G., Tectonics of the lithospheric plates and the origin of the tsunami earthquakes. *Proc. AN USSR*, 251, 51092–1095, 1980.
228. Lobkovsky, L.I., Catastrophic earthquake and tsunami 12. 26.2004 in the northern Sunda island arch, Indian Ocean: Geodynamic analysis and analogy with the central Kuril Islands. *Science*, 5, 253–61, 2005.
229. Garkalenko, I.A. and Ushakov, S.A., Earth's crust of the Kuril Region. *Soviet Geol.*, 11, 46–59, 1978.
230. Bijy-Duval, B., Moore, J.C., Bergen, J. *et al.*, Leg 78 A, Eastern Caribbean sea. *JOIDES J.*, VII, 221, 1981.
231. Bondarenko, B.A., Garkalenko, I.A., Zhuravlev, A.V. *et al.*, New data on the structure of deep crust in the Kuril-Kamchatka trough. *Proc. AN USSR*, 234, 135–137, 1977.

232. Sorokhtin, O.G. and Lobkovsky, L.I., A mechanism of pulling-in the oceanic deposits into the oceanic plate subduction zones. *Izv. AN USSR. Phys. Earth*, 5, 3–10, 1976.
233. Borukayev, C.B. *et al.*, *Precambrian of the Continents. Major Features of Tectonics*, Nauka, Novosibirsk, 1977, 264 pp.
234. Kratz, O.K. *et al.*, *Evolution Stages and Types in the Precambrian Crust of the Ancient Shields*, Nauka, Leningrad, 1981, 164 pp.
235. Khain, V.E., Issues of the Early Precambrian Tectonics. Herald MGU, Series 4. *Geology*, 4, 13–24, 2000.
236. Anatolyeva, A.I., *Main Evolution Boundaries of the Red-Bed Formations*, Nauka, Novosibirsk USSR, 1978, 190 pp.
237. Stille, H., *Geotectonic subdivision of Earth's history. Selected works*, Mir, Moscow, 1964, 888 p.
238. Zonenshain, L.P. *et al.*, *Global Tectonics, Magmatism and Metallogeny*, p. 231, Nedra, Moscow, 1977.
239. Piper, J.D.F., Paleomagnetic evidence for a Proterozoic supercontinent. *Phil. Trans. Roy. Soc. Lond.*, 280A, 469–490, 1976.
240. Chumakov, N.M., Early-Paleozoic glaciation and Biospheric events of Late Ordovician, in: *Proc. GIN, 580: Cause-and-Effect Associations and Factors of Global Changes in Phanerozoic*, pp. 25–41, GEOC, Moscow, 2006.
241. Wegener, A., Die Entstehung der Kontinente. *Geol. Rundsch.*, 3, 4276–292, 1912.
242. Smith, A.G. and Brieden, J.C., *Mesozoic and Cenozoic Paleocontinental Maps*, Cambridge University Press, London, New York, Melbourn, 1977, 63 pp.
243. Sorokhtin, O.G. (Ed.), *Geodynamics (oceanology, geophysics of the ocean)*, vol. 2, Nauka, Moscow, 1979, 416 p.
244. Yoder, H.S., Jr., *Generation of Basaltic Magma*, National Academy of Sciences, Washington, DC, 1976.
245. Pugin, V.A. and Khitarov, N.I., *Experimental Petrology of the Depth Magmatism*, Nauka, Moscow, 1978, 175 pp.
246. Lisitsin, A.P. *et al.*, *Hydrothermal Formations in the Oceanic Rift Zones*, Nauka, Moscow, 1990, 256 pp.
247. Rona, P., *Hydrothermal Mineralization of Spreading Areas in the Oceans*, Mir, Moscow, 1986, 160 pp.
248. Bogdanov, Yu. A., Lisitsin, A.P., Sagalevich, A.M., Gurvich, E.G., *Hydrothermal Ore Genesis of the Ocean Floor*, Nauka, Moscow, 2006, 527 pp.
249. Menard, G.U., *Geology of the Pacific Ocean Floor*, Mir, Moscow, 1966, 273 pp.
250. Pitman, W.C. and Heys, J.D., Upper cretaceons spreading rates and the great transgression. *Geol. Soc. Am. Abstr.*, 5, 72344–2357, 1973.
251. Turcotte, D. and Burke, K., Global sea-level changes and the thermal structure of the Earth. *Earth Planet. Sci. Lett.*, 41, 341–346, 1978.
252. Joly, J., *The surface history of Earth*, Dublin Soc, 1929.
253. Belousov, V.V., *Fundamentals of Geotectonics*, Gosgeoltekhizdat, Moscow, 1954, 607 pp.

254. Vail, P.R., Mitchum, R.M., Sr., Thompson, S., Seismic stratigraphy and global changes in sea level, part 4: Global cycles of relative changes in sea level. *Am. Assoc. Petrol. Geol. Memoir*, 26, 83–97, 1976.
255. Robertson, J.O., Chilingar, G.V., Sorokhtin, O.G., Sorokhtin, N.O., Long, W., *The Evolution of Earth's Climate*, Scrivener Publishing Wiley, Hoboken, 2018, 302 p.
256. Watanabe, S., Mishima, K., Matsuo, S., Isotopic ratios of carbonaceous materials incorporated in olivine crystals from the Hualalai volcano Hawaii. An approach to mantle carbon. *Geochim. J.*, 17, 295–104, 1983.
257. Sakai, H., Marais, D., Ueda, A., Moore, J., Concentrations and isotope ratios of carbon, nitrogen and sulfur in ocean-floor basalts. *Geochim. Cosmochim. Acta*, 48, 122433–2441, 1984.
258. Exley, R.A., Mattey, D.P., Clague, D.A., Pillinger, C.T., Carbon isotope systematic of a mantle "hotspot": A comparison of Loihi Seamount and MORB glasses. *Earth Planet. Sci. Lett.*, 78, 189–199, 1986.
259. Sorokhtin, N.O., Climate of Early Precambrian and the nature of the Huron glaciation. *Herald MGU*, 5, 125–42, 2002.
260. Schopf, T., *Paleoceanography*, Harvard University Press, Cambridge, MA, 1980, 312 pp.
261. Makkaveyev, P.M. and Sorokhtin, O.G., Experience in the reconstruction of the carbonate balance in the ancient ocean. *Oceanology*, 45, 3374–380, 2005.
262. Lisitsin, A.P. and Vinogradov, M.E., Global patterns of life distribution in the oceans and their reflection in the composition of the ocean-floor deposits. The formation and distribution of biogenic deposits. *Izv. AN USSR. Geol.*, 4, 5–24, 1982.
263. Romankevich, E.A., *Geochemistry of organic matter in the ocean*, Nauka, Moscow, 1977, 256 p.
264. Romankevich, E.A., *Geochemistry of Organic Matter in the Ocean*, Springer-Verlag, Moscow, 1984, 33 pp.
265. Ronov, A.B., *Stratisphere or the Sedimentary Shell of Earth*, Nauka, Moscow, 1993, 144 pp.
266. Chumakov, N.M., Dynamics and possible causes of climatic changes in Late Mesozoic, in: *Climate in the Epochs of Major Biospheric Changes*, pp. 149–157, Nauka, Moscow, 2004b.
267. Sorokhtin, O.G., Causes of changes in the Earth's global climate. *Ecol. Ind. Russ.*, 4, 35–40, 2008.
268. Radzig, A.A. and Smirnov, B.M., *Reference book of the atomic and molecular physics*, Mir, Moscow, 1980, 240 p.
269. Walker, J.C.G., *Evolution of the Atmosphere*, Macmillan Publishing Company, New York, 1977, 318 pp.
270. Walker, J.C.G., Stability of atmospherics oxygen. *Am. J. Sci.*, 274, 193–214, 1974.
271. Salop, L.I., *General Stratigraphic Scale of Precambrian*, Nedra, Leningrad, 1973, 310 pp.

272. Fryer, B.J., Rare Earth evidence in iron-formations for changing Precambrian oxidation states. *Geochim. Cosmochim. Acta*, 41, 361–367, 1977.
273. Sorokhtin, O.G., Lein, A. Yu., Balanyuk, I.E., Thermodynamics of the oceanic hydrothermal systems and the abiogenic generation of methane. *Oceanology*, 41, 6898–909, 2001.
274. Schidlowski, M., Application of stable carbon isotopes to early biochemical evolution on Earth. *Ann. Rev. Earth Planet. Sci.*, 15, 47–72, 1987.
275. Semikhatov, M.A., Raaben, M.E., Sergeyev, V.N., Veis, A.F., Artemova, O.B., Biotic events and a positive isotopic anomaly of the carbonate carbon 2.3-2.06 BY ago. *Stratigr. Geol. Correl.*, 2, 3–27, 1999.
276. Dmitriyev, L.V. *et al.*, Hydrogen and methane formation in serpentinization of the oceanic hyper- basites and the origin of oil. *Russ. Earth Sci. Mag.*, 1, 11–16, 2000.
277. Galimov, E.M., *Phenomenon of Life: Between Equilibrium and Linearity. ORIGINS and Principles of the Evolution*, Editorial URSS, Moscow, 2001, 256 pp.
278. Dmitriyevsky, A.N. and Balanyuk, I.E., *Gas hydrates of seas and oceans are hydrocarbon source of the future*, OOO IRC Gazprom, Moscow, 2009, 416 p.
279. Lein, A.Y. *et al.*, Geochemical features of gasbearing (CH_4) deposits of a subwater mud volcano in the Norwegian Sea. *Geochemistry*, 3, 230–249, 1998.
280. Lein, A.Y. and Sagalevich, A.M., Smokers of the Rainboe Field as area of a large-scale abiogenic methane synthesis. *Nature*, 8, 44–53, 2000.
281. Perisypkin, V.I., Lein, A.Y., Bogdanov, Y.A., Bortnikov, N.S., Lipids in hydrothermal formations in the area of 14°45'N and 29°N of the Mid-Atlantic Ridge. *Oceanology*, 38, 5, 1998.
282. Dobretsov, N.L. and Kirdyashkin, A.G., Evaluations of the global processes of the matter exchange between Earth's shells: A comparison of real geological and theoretical data. *Geol. Geophys.*, 39, 9, 1269–1279, 1998.
283. Zharikov, V.A., *Selected Proc. In 2 volumes*, vol. 1, Nauka, Moscow, 2011, 422 p.
284. Kontorovich, A.E., *Essays on the naftido-genesis theory: Selected articles*, Publishers SO RAN, "Geo" affiliate, Novosibirsk, 2004, 545 p.
285. Korzhinsky, D.S., *A theory of the metasomatic zoning*, Moscow, Nauka, 1982, 104 p.
286. Marakushev, A.A., Paneyakh, N.A., Rusinov, V.L. *et al.*, Petrological model of giant ore deposit formation. *GRM*, 40, 3, 236–255, 1998.
287. Marakushev, A.A., Paneyakh, N.A., Marakushev, S.A., *Sulfide ore formation and its hydrocarbon specialization*, GEOS, Moscow, 2014, 184 p.
288. Rundquist, D.V., Theoretical metallogeny: Status and ways of evolution, *Geology of Ore Deposits*. 32, 6, 89–100, 1990.
289. Rundquist, D.V. (Ed.), *Metallogeny of Early Precambrian geodynamic environments series*, Geokart, Moscow, 1999, 399 p.
290. Smirnov, V.I., *Metallogeny. Selected Proc*, Nauka, Moscow, 1993, 175 p.

291. Starostin, V.I., Major geologo-metallogenic periods in Earth evolution. Harbinger MGU. Ser. 4. *Geology*, 4, 19–27, 1996.
292. Starostin, V.I. and Sokolov, B.A., Fluid-dynamic conditions for the formation of metallogenic provinces and petroleum basins. *Proc. Sect. Earth Sci. RAEN*, 1, 12–22, 1998.
293. Starostin, V.I. and Sorokhtin, O.G., Evolution of Earth and metallogeny. *Izv. SNZ RAEN*, 8, 64–76, 2002.
294. Tvarchelidze, G.A., *Earth's crust metallogeny*, vol. 160 p, Nedra, Moscow, 1985, 160 p.
295. Khanchuk, A.I. and Ivanov, V.V., Meso-Cenozoic geodynamic environments and gold mineralization in the Russian Far East. *Geol. Geophys.*, 40, 11, 1635–1645, 1999.
296. Khanchuk, A.I. (Ed.), *Geodynamics, magmatism and metallogeny of the eastern Russia. Books 1 and 2*, DalNauka, Vladivostok, 2006, 527 p.
297. Shcheglov, A.D., Nedra, Leningrad, 1987, 231 p.
298. Gurvich, E.G., *Metal bearing deposits of the word ocean*, Moscow, Nauchny, Mir, 1998, 340 p.
299. Balanyuk, I.E. and Dongaryan, L.S., Role of hydrothermal methane in the formation of gas- hydrate accumulations. *Geol. Geophys. Dev. Fields*, 3, 22–28, 1994.
300. Savelyeva, G.N., Bortnikov, N.S., Bayanova, T.B. *et al.*, Isotope Sm-Nd, Rb-Sr systems, captured He and hydrocarbon gases as melt fluid regime source markers at the formation of Mid-Atlantic ridge crust in the area of 5–6° N. *Geochemistry*, 8, 803–817, 2008a.
301. Savelyeva, G.N., Sobolev, A.V., Batanova, V.G., Suslov, P.V., Brugmann, H., Structure of melt flow channels in the mantle. *Geotectonics*, 6, 25–45, 2008b.
302. Savelyeva, G.N., Batanova, V.G., Bystretskikh, A.V., Ipatyeva, I.S., Mineral associations of chromite ores in ophiolites as melt transport markers through mantle peridotites. Bull. of Moscow nature explorers society. *Sect. Geol.*, 84, 1, 44–57, 2009.
303. Sobolev, R.N., Starostin, V.I., Pelymsky, G.A., Tin deposits types and their distribution in space and time. Harbinger MGU. Ser. 4. *Geology*, 1, 30–39, 2000.
304. Sobolev, R.N., Pelymsky, G.A., Starostin, V.I., Molybdenum mineralization evolution in Earth's history. *Bull. MOIP. Geol. Section*, 72, 5, 65–71, 1997.
305. Antipin, V.S. and Makrygina, V.A., *Geochemistry of endogenous processes*, IGU Publishers, Irkutsk, 2006, 130 p.
306. Yardley, B.W.D., Rochelle, C.A., Barnicoat, A.C., Lloyd, G.E., Oscillatory zoning in metamorphic minerals: An indicator of infiltration metasomatism. *Mineral. Mag.*, 55, 357–365, 1991.
307. Smirnov, S.Z., Kulik, N.A., Litasov, Y.D., Vishnevsky, A.V., Strakhovenko, V.D., INGG SO RAS, Novosibirsk, 2014, 77 p.
308. Hoefs, J., *Stable isotope geochemistry*, Springer, 2009, 285 p.

309. Kontar, E.S., *Geologo-industrial types of copper, zinc, lead deposits in the Urals (geological conditions of placement, formation history, potential)*, UGGU, Yekaterinburg, 2013, 199 p.
310. Wasserman, B.Y., Exploration maturity of hydrocarbon resources in Timan-Pechora petroleum province as of the beginning of начало XXI century. *Geol. Oil Gas*, 2, 10–16, 2001.
311. Klubov, B.A. and Korago, E.A., On the nature of liquid bitumens in the northern Novaya Zemlya. *Proc. AN USSR*, 315, 4, 925–928, 1990.
312. Fedorovsky, Y.F., *Petroleum potential of carbonate Upper-Middle Paleozoic sediments in the Barents Sea Russian shelf*, Abstract of PhD thesis, VNIIGAZ, Moscow, 2007, 27 p.
313. Shipilov, E.V., On base magmatism periodicity on the West Arctic Eurasia margin In Phanerozoic. *Harbinger MGTU*, 1, 3, 97–104, 1998.
314. Shipilov, E.V., Late-Mesozoic magmatism and Cenozoic tectonic deformations on the Barents Sea continental margin: The influence on hydrocarbon potential distribution. *Geotectonics*, 1, 60–85, 2015.
315. Sorokhtin, O.G., Issues of oil generation within the plate subduction zones, in: *Oceanology, Geophysics of the Ocean, Vol. 2, Geodynamics*, O.G. Sorokhtin (Ed.), pp. 377–383, Nauka, Moscow, 1979a.
316. Smirnov, V.I., Periodicity of ore formation in the geologic history, in: *Metallogeny and Ore Deposits*, pp. 3–10, Nauka, Moscow, 1984.
317. Voitkevich, G.V. and Lebedko, G.I., *Commercial deposits and Precambrian metallogeny*, Nedra, Moscow, 1975, 231 p.
318. Smirnov, V.I., *Geology of commercial deposits*, Nedra, Moscow, 1982, 669 p.
319. Tugarinov, A.I. and Voitkevich, G.V., *Precambrian geochronology of the continents*, Nedra, Moscow, 1970, 434 p.
320. Slobodkin, A.I. *et al.*, Magnetite formation by thermophilic micro-organisms. *Proc. RAN*, 345, 5, 694–697, 1995.
321. Hollend, H.D., *The Chemical Evolution of the Atmosphere and Oceans*, Princeton University Press, Princeton, NJ, 1984.
322. Bykhover, N.A., *World Mineral Resource Distribution by the Ore-Formation Epochs*, Nedra, Moscow, 1984, 576 pp.
323. Sobolev, N.V., Kharkiv, A.D., Pokhilenko, N.P., Kimberlites, lamproites and the issue of the upper mantle composition. *Geol. Geophys.*, 7, 18–28, 1987.
324. Frololva, T.I., Rudnik, G.B., Kashintsev, G.L., Some general patterns of magmatism in the oceans and the issues of magmatic rock origin, in: *Oceanology, Oceanic Geology, Sediment Formation and Magmatism of the Ocean*, pp. 69–87, Nauka, Moscow, 1979.
325. Kashintsev, G.L., *Oceanic depth rocks*, Moscow, Nauka, 1991, 279 p.
326. Baturin, G.N., *Phosphorites on the ocean floor*, Nauka, Moscow, 1978, 231 p.
327. Kholmiakov, A.P. and Franzesson, E.V., Apatite composition from kimberlites of the Yakut diamond-bearing province and the distribution of rare-earth elements in it. *Geol. Geophys.*, 2, 121–125, 1978.

328. Allsopp, H.L., Nicholaysen, L.O., Hahn-Weinheimer, P., Rb/K ratios and Sr-isotopic compositions of minerals in eclogitic and peridotitic rock. *Earth Planet. Sci. Lett.*, 5, 231–244, 1969.
329. Manton, W.J. and Tatsumoto, M., Some Pb and Sr isotopic measurements in eclogites from the Roberts Victor Mine, South Africa. *Earth Planet. Sci. Lett.*, 10, 217–222, 1971.
330. Dawson, J.B. and Hawthorne, J.B., Magmatic sedimentation and carbonatitic differentiation in kimberlite sills at Benfontein, South Africa. *J. Geol. Soc. (London, U.K.)*, 129, 61–85, 1973.
331. Lisitsin, A.P., *Processes of the Oceanic Sedimentation*, Nauka, Moscow, 1978, 392 pp.
332. Boyd, F.R. and Finnerty, A.A., Conditions of origin of natural diamonds of peridotite affinity. *J. Geophys. Res. Solid Earth*, 85, 6911–6918, 1980.
333. Perchuk, L.L., Yapaskurt, V.O., Okay, F., Comparative petrology of diamond-bearing metamorphic complexes. *Petrology*, 3, 3, 267–309, 1995.
334. Kvasnitsa, V.N., Zinchuk, N.N., Koptil, V.I., *Typomorphism of diamond micro-crystals*, Nedra, Moscow, 1999, 224 p.
335. Marakushev, A.A., Diamond mineral associations and diamond-bearing magma formation issues. *Essays Physicochem. Petrol.*, 13, 5–53, 1985.
336. Marakushev, A.A., Pertsev, N.N., Zotov, I.A. *et al.*, Some petrological aspects of diamond genesisa. *Geology of Ore Deposits*, Moscow. 37, 2, 105–121, 1995.
337. Simakov, S.K., Diamond formation and recrystallizing in the upper mantle condition. *Proc. AN USSR*, 301, 4, 951–954, 1988.
338. Garanin, V.K., Kudryavtseva, G.P., Marfunin, A.S., Mikhaylichenko, O.A., *Inclusions in diamonds and diamond-bearing rocks*, Publishers MGU, Moscow, 1991, 240 p.
339. Karrer, P., *Lehrbuch der organichen Chemie*, Georg Thieme Verlag, Stuttgart, 1959.
340. Sorokhtin, O.G., Possible physicochemical processes of the Earth's core formation. *Proc. AN USSR*, 198, 61327–1330, 1981a.
341. Naumov, G.B., Ryzhchenko, B.N., Khodakovsky, I.L., *Reference book of thermodynamic values (for geologists)*, Atomizdat, Moscow, 1971, 240 p.
342. Haggerty, S.E., Toft, P.B., Tompkins, L.A., Diamonds in graphitic schists. *Trans. Am. Geophys. Union, EOS*, 62, 17, 416, 1981.
343. Sabatier, P., *Catalysis on organic chemistry*, Leningrad, Gochemtechizdat, 1932, 124 p.
344. Betekhtin, A.G., *Mineralogy*, Gosizdat of Geologic Literature, Moscow, 1950, 957 pp.
345. Lazarenko, E.K., *Course of Mineralogy*, Higher Education Publishers, Moscow, 1971, 608 pp.
346. Giardini, A.A. and Tydings, J.E., Diamond synthesis: Observations on the mechanism of formation. *Am. Mineral.*, 47, 1393–1421, 1962.

347. Uspensky, V.A., Carbon balance in the biosphere and the issue of carbon distribution in Earth's crust, in: *Ministry of Oil Industry*, Gostoptekhizdat. Leningrad affiliate, VNIGRI. Leningrad, 1956, 101 p.
348. Burkov, V.D., Krapivin, V.F., Shalaev, V.S., Balanced model of carbon global biochemical turnover. Vol. 9, Forest Bulletin, Moscow, 2012, 86–94 pp.
349. Romankevich, E.A. and Vetrov, A.A., Carbon mass in Earth hydrosphere. *Geochemistry*, 6, 483–509, 2013.
350. Krapivin, V.F., Shalayev, V.S., Burkov, V.D., *Modeling of carbon and methane global cycles*, vol. 1, pp. 170–176, Forest Harbinger, Moscow, 2015.
351. Galimov, E.M., *Geochemistry of carbon stable isotopes*, Nedra, Moscow, 1968, 226 p.
352. Dobretsov, N.L. and Shatsky, A.F., Carbon depth cycle and depth geodynamics: A role of the core and carbonatite melts in the lower mantle. *Geol. Geophys.*, 53, 11, 1455–147, 2012.
353. Dobretsov, N.L., Kulakov, I.Yu., Litasov, K.D., Kukarina, E.V., Significance of geology, experimental petrology and seismic tomography for a complex evaluation of the subduction processes. *Geol. Geophys.*, 56, 1–2, 21–55, 2015.
354. Sobolev, N.V., Dobretsov, N.L., Otani, E., Taylor, L.A., Shertl, H.-P., Palyanov, Y.N., Litasov, K.D., Issues of crystallo-genesis and carbon depth cycle. *Geol. Geophys.*, 56, 1–2, 5–20, 2015.
355. Cooper, B.S., Coleman, S.H., Barnard, P.C., Butterworth, J.S., Paleotemperatures in the northern North Sea Basin. *Petrol. Cont. Shelf North-West Europe Geology*, 1, 487–492, 1975.
356. Cruse, A.M. and Seewald, J.S., Chemistry of low-molecular weight hydrothermal fluids from Middle Valley, Northen Juan de Fuca Ridge. *Geochim. Cosmochim. Acta*, 70, 2079–2092, 2006.
357. Karrer, P., *A course of organic chemistry*, Goskhimizdat, Moscow, 1962, 1216 p.
358. Kenney, J.F., Kutcherov, V.A., Bendeliani, N.A., Alekseev, V.A., The evolution of multicomponent system at high pressures: VI. The thermodynamic stability of the hydrogen–carbon system: The genesis of hydrocarbons and the origin of petroleum. *Proc. Natl. Acad. Sci. U.S.A.*, 99, 10976–10981, 2002.
359. Kutcherov, V.A., Bendeliani, N.A., Alekseev, V.A., Kenney, J.F., Synthesis of hydrocarbons from minerals at pressures up to 5 GPa. *Doklady Phys. Chem.*, 387, 328–330, 2002.
360. Kosolapova, T.Y., *Carbides*, Publ. "Metallurgy", Moscow, 1968, 300 p.
361. Lisitsin, A.P., *World ocean hydrothermal systems – delivery of endogenous matter, hydrothermal systems and sedimentary formations of Atlantic mid-oceanic ridges*, pp. 147–245, Nauka, Moscow, 1993.
362. Bogdanov, Y.A., Lein, A.Y., Lisitsin, A.P., *Polymetallic ores in rifts of the mid-Atlantic ridge (15 – 40N.): Mineralogy, geochemistry, genesis*, GEOS, Moscow, 2015, 256 p.

363. Proskurowski, G., Lilley, M.D., Seewald, J.S., Früh-Green, G.L., Olson, E.J., Lupton, J.E., Sylva, S.P., Kelley, D.S., Abiogenic hydrocarbon production at Lost City hydrothermal field. *Science*, 319, 604–607, 2008.
364. Sapart, C.J., Shakhova, N., Semiletov, I., Jansen, J., Szidat, S., Kosmach, D., Dudarev, O., van der Veen, C., Egger, M., Sergienko, V., Salyuk, A., Tumskoy, V., Tison, J.L., Rockmann, T., The origin of methane in the East Siberian Arctic Shelf unraveled with triple isotope analysis. *Biogeosciences*, 14, 9, 2283–2292, 2017.
365. Shakhova, N., Semiletov, I., Sergienko, V., Lobkovsky, L., Yusupov, V., Salyuk, A., Salomatin, A., Chernykh, D., Kosmach, D., Panteleev, G., Nicolsky, D., Samarkin, V., Joye, S., Charkin, A., Dudarev, O., Meluzov, A., Gustafsson, Ö., The East Siberian Arctic Shelf: Towards further assessment of permafrost-related methane fluxes and role of sea ice. *Phil. Trans. R. Soc. A*, 373, 20140451, 2015. (Philosophical Transactions of the Royal Society A).
366. Shakhova, N., Semiletov, I., Gustafsson, O., Sergienko, V., Lobkovsky, L., Dudarev, O., Tumskoy, V., Grigoriev, M., Mazurov, A., Salyuk, A., Ananiev, R., Koshurnikov, A., Kosmach, D., Charkin, A., Dmitrevsky, N., Karnaukh, V., Gunar, A., Meluzov, A., Chernykh, D., Current rates and mechanisms of subsea permafrost degradation in the East Siberian Arctic Shelf. *Nat. Commun.*, 8, 15872, 2017, doi: 10.1038/ncomms15872.
367. Galimov, E.M., $^{13}C/^{12}C$ of the diamonds. A vertical zoning of diamond-formation in the lithosphere, in: *Proc. 27-th International Geology Congress, Reports, Vol. 11, Section C 11. Geochemistry and Cosmochemistry*, pp. 110–123, Nauka, Moscow, 1984.
368. Sobolev, N.V., Galimov, E.M., Ivanovskaya, I.M., Yefgimova, E.S., Isotope composition of carbon in diamonds containing crystalline incluisions. *Proc. AN USSR*, 249, 6, 1217–1220, 1979.
369. Millendge, H.J., Mendelssohn, M.J., Seal, M., Rouse, J.E., Swart, P.K., Pillinger, C.T., Carbon isotopic variation in spectral type II diamonds. *Nature*, 303, 791–792, 1983.
370. Gritsik, V.V. and Dyakova, A.G., On the isotope composition of roundish diamonds, in: *Abstracts of the 10th All-Union Symp. on stable isotopes in geochemistry*, p. 238, Nauka, Moscow, 1984.
371. Mattey, D., Lowry, D., Macpherson, C., Oxygen-isotope composition of mantle peridotite Earth. *Planet Sci. Lett.*, 128, 231–241, 1994.
372. Kovalsky, V.V., Nikishov, K.N., Yegorov, O.S., *Kimberlite and carbonatite formations on the east and southeast slopes of the Anabar anteclize*, Nauka, Moscow, 1969, 288 p.
373. Franzesson, E.V. and Kaminsky, F.V., Carbonado as a diamond variery of non-kimberlite origin. *Proc. AN USSR*, 219, 1, 124–133, 1974.
374. Sidorenko, S.A. and Sidorenko, A.V., Organic matter in Precambrian sedimentary-metamorphic rocks. *Proc. Geol. Inst. AH USSR*, 277, 1975. 140 p.

375. Sorokhtin, O.G., *Formation of Diamondiferous Kimberlites and the Affined Rocks from a Standpoint of the Lithospheric Plate Tectonics. Geodynamic Analysis and the Patterns of Formation and Distribution of Economic Deposits*, pp. 92–107, Nedra, Leningrad, 1987.
376. Hoefs, J., *Geochemistry of stable isotopews*, Moscow, Mir, 1983, 200 p.
377. Galimov, E.M., Prokhorov, V.S., Fedoseyev, D.V., Varnin, V.P., Heterogenous isotope effects in carbon at diamond and graphite synthesis from gas. *Geochemistry*, 3, 416–424, 1973.
378. Kroopnick, P., Weiss, R.F., Graig, H., Total CO_2, $^{13}{}_{18}C$ and dissolved oxygen - ^{18}O at Geosecs II in the North Atlantic. *Earth Planet. Sci. Lett.*, 16, 103, 1972.
379. Kaminsky, F.V. and Sobolev, N.V., On the variations in carbon isotope composition within diamond crystals. *Proc. AN USSR*, 286, 6, 1436–1439, 1985.
380. Sheppard, S.M.F. and Dawson, J.B., $^{13}C/^{12}C$ and D/H isotope variations in "Primary" igneous carbonatites. *Fortschr. Mineral.*, 9, 747–763, 1973.
381. Maltsev, K.A. and Galimov, E.M., Hydrogen isotope composition in diamonds. *Proc. AN USSR*, 308, 6, 1451–1453, 1989.
382. Veizer, J. and Hoefs, J., The nature of O^{18}/O^{16} and C^{13}/C^{12} secular trends in sedimentary carbonate rocks. *Geochim. Cosmochim. Acta*, 40, 1387–1395, 1976.
383. Perry, E.C., Jr. and Tan, F.C., Significance of oxygen and carbon isotope variations in early pre-cambrian cherts and carbonate rocks of southern Africa. *Geol. Soc. Am. Bull.*, 83, 647–664, 1972.
384. Knauth, L.P. and Epstein, S., Hydrogen and oxygen isotope ratios *in silica* from the Deep Sea Drilling Project. *Earth Planet. Sci. Lett.*, 25, 1–10, 1975.
385. Knauth, L.P. and Epstein, S., Hydrogen and oxygen isotope ratios in modular and bedded cherts. *Geochim. Cosmochim. Acta*, 40, 1095–1108, 1976.
386. Allsopp, H.L. and Barrett, D.R., *Rb-Sr age determinations on south Africa kimberlite pipes*, vol. 9, pp. 605–617, Phys. and Chemistry of the Earth. Pergam. Press, Oxford, 1975.
387. Faure, G., *Principles of Isotope Geology*, 2nd ed., John Wiley & Sons, New York, 1977.
388. Smith, C.B., Pb, Sr and Nd isotopic evidence for sources of Southern African Cretaceous kimberlites. *Nature*, 304, 5921, 51–54, 1983.
389. McCulloch, M.T., Jaques, A.L., Nelson, D.R., Lewis, J.D., Nd and Sr isotopes in kimberlites and lamproites from Western Australia: An enriched mantle origin. *Nature*, 302, 5907, 400–403, 1983.
390. Sobotovich, E.V., Bortnitsky, B.N., Tson, O.V., Kononenko, L.V., *Reference book of isotopic geochemistry*, Energizdat, Moscow, 1982, 240 p.
391. Balashov, Y.A., *Geochemistry of rare-earth elements*, Nauka, Moscow, 1976, 267 p.
392. Heskin, L.A., Frey, F.A., Schmitt, R.A., Smith, R.H., Meteoritic, solar and terrestrial rare-earth distribution. *Phys. Chem. Earth.*, 7, 167–321, 1966.
393. Ukhanov, A.V., Ryabchikov, I.D., Kharkiv, A.D., *Lithospheric mantle in the Yakut kimberlite province*, Nauka, Moscow, 1988, 284 p.

394. Faure, G., *Principles of Isotope Geology*, Second Edition, J.Wiley & Sons, New York, 1987.
395. Krotkov, V.V., Kudryavtseva, G.P., Bogatikov, O.A. *et al.*, *New technologies in diamond deposits exploration*, GEOS, Moscow, 2001, 310 p.
396. Beard, A.D., Downes, H., Hegner, E. *et al.*, Mineralogy and geochemistry of Devonian ultramafic minor intrusions of the Southern Kola Peninsula Russia: Implications for the petrogenesis of kimberlites and melilitites. *Contrib. Miner. Petrol.*, 130, 288–303, 1998.
397. O'Brien, H.E. and Tyni, M., Mineralogy and geochemistry of kimberlites and related rocks from Finland, in: *Proc. VII Int. Kimberlites Conf*, vol. 2, pp. 625–636, 1999.
398. Artyushkov, E.V. and Sobolev, S.V., Mechanisms of kimberlite magma rise from depth. *Proc. AN USSR*, 236, 3692–695, 1977.
399. Anderson, O.L., The role of fracture dynamics in kimberlite pipe formations, in: *Kimberlites, Diatremes and Diamonds: Their Geology, Petrology and Geochemistry*, F.R. Boyd and H.O.P. Meyer (Eds.), American Geophysical Union, Washington, pp. 344–353, 1979.
400. Artyushkov, E.V. and Sobolev, S.V., Physics of kimberlite magmatism, in: *Kimberlites I: Kimberlites and Related Rocks*, pp. 309–322, Elsevier, Amsterdam, 1984.
401. Lebedev, E.B. and Khitarov, N.I., *Physical properties of magma melts*, Nauka, Moscow, 1979, 200 p.
402. Kharkiv, A.D., Zinchuk, N.N., Kryuchkov, A.I., *Bedrock Diamond Deposits of the World*, Nedra, Moscow, 1998, 555 pp.
403. Milashov, V.A., *Kimberlites and the depth geology*, Nauka, Leniongrad, 1990, 167 p.
404. Williams, H.R. and Williams, R.A., Kimberlites and plate tectonics in West Africa. *Nature*, 270, 507–508, 1977.
405. Ustinov, V.N., Golubev, Y.K., Zagayuny, A.K., Kukuy, I.M., Mikoev, I.I., Lobkova, L.P., Antonov, S.A., Konkin, V.D., Potential diamond-bearing analysis of the African province and the development of Russian Federation mineral-raw materials base abroad. *Homeland Geol.*, 6, 52–66, 2017.
406. Bayanova, T.B. *et al.*, The gabbro-norites age of the lower laminated horizon (Reef) in the Fedorov-Pansk massif (Kola Peninsula). *Proc. RAN*, 337, 1, 95–97, 1994.
407. Minz, M.V., Paleogeodynamic reconstructions of Early Precambrian on the most ancient (eastern and northeastern) part of the Baltic Shield, in: *Geodynamics and Deep Structure in the Soviet Part of the Baltic Shield*, F.P. Mitrofanov (Ed.), pp. 34–49, KNC RAN, Apatity, 1992.
408. Smolkin, V.F., *Petrology and ore genesis of komatiite and picrite associations on the NE Baltic shield*, Abstract of a doctorate thesis, St. Petersburg, 1992, 42 p.
409. Hiltanen, A., Generation of potassium-poor magmas in the northern Sierra Nevada and the Svecofenian in Finland. *J. Res. U.S. Geol. Surv.*, 3, 631–656, 1975.

410. Gaal, G., Proterozoic tectonic evolution and late Svecokarelian plate deformation of the central Baltic Shield. *Geol. Rundsch.*, 71, 1, 158–169, 1982.
411. Pharaon, T.C. and Pearce, J.A., Geochemical evidence for the geotectonic setting of Early Proterozoic metavolcanic sequences in Lapland. *Precambrian Res.*, 25, 283–308, 1984.
412. Babel Working Group, Integrated seismic studies of the Baltic Shield using data in the Gulf of Bothnia region. *Geophys. J. Int.*, 112, 3, 305–343, 1993.
413. Negrutsa, V.Z., Basalayev, A.A., Chikirev, I.V., *The Barents Sea phosphorite basin*, Publishers KNC RAN, Apatity, 1993, 119 p.
414. Vernikovsky, V.A. and Vernikovskaya, A.E., Central Taimyr accretionary belt (Arctic Asia): Meso–Neoproterozoic tectonic evolution and Rodinia breakup. *Prec. Res.*, 110, 127–141, 2001.
415. Vernikovsky, V.A., Metelkin, D.V., Vernikovskaya, A.E., Matushkin, N.Yu., Lobkovsky, L.I., Shipilov, E.V., *Early stages of evolution of the arctic margins (NeoproterozoicPaleozoic) and plate reconstructions. Origins of Northeastern Russia: Paleomagnetism, Geology, and Tectonics. ICAM-VI. Abstracts*, Fairbanks, Alaska, CD, 2011.
416. Raaben, M.E., Lubtsov, V.V., Predovsky, A.A., *Correlation of stromatolitic formations of northern Norway (Finnmark) and northwestern Russia (Kildin Island and Kanin Peninsula)*, pp. 233–246, Nor. Geol. Unders. Spesial Publ. Trondheim, Finland, 1995.
417. Milanovsky, E.E., *Geology of Russia and of the near abroad (Northern Eurasia)*, Publishers MGU, Moscow, 1996, 448 p.
418. Simovov, A.P., Guberman, D.M., Yakovlev, Y.N., Snetko, P.P., Mitrofanov, F.P., Lyubtsov, V.V., Predovsky, A.A., Pripachkin, V.A., Riphaean oil on Rybachy Peninsula: A myth or a key to a conceptually new direction in petroleum exploration on the Barents Sea shelf? *Harbinger MGTU*, 1, 2, 121–140, 1998.
419. Sharov, N.V. (Ed.), *Seismogeological model of Northern European Lithosphere: Lapland-Pechenga Area*, Publ. KNC RAN, Apatity, 1997, 225 p.
420. Zamozhnyaya, N.G. *et al.*, Region-zonal aeismic surveys MOV-?GT on Rybacy Peninsula complexed with high-precision gravimetry for studying geological structure and petroleum potential of the Riphaean sediments. Moscow, Fund library of Murmansk Geological Committee, Apatity, Moscow, 2001.
421. Chikirev, I.V., *Upper Precambrian phosphorite-containing sediments of the Kola Peninsula*, Abstract of PhD thesis, MGU, Moscow, 1995, 18 p.
422. Sorokhtin, N.O., Chilingar, G.V., Kozlov, N.E., Shin, S., Geodynamic evolution of oil and gas basins in the European part of the Eurasian Arctic Shelf. *Energy Sources Part A*, 34, 22, 2092–2103, 2012.
423. *The explanatory memo to the Barents Sea and northern European Russia tectonic map, 1:2,500,000*, ILOVM RAN, Moscow, 1996, 94 p.
424. Lobkovgsky, L.I., Shipilov, E.V., Kononov, M.V., Geodynamic model of the upper mantle convection and Arctic lithosphere transformations in Mesozoic and Cenozoic. *Phys. Earth*, 6, 1–19, 2013.

425. Dobrynina, M.I., Riftogenesis in geological history of the Precambrian of the northern Russian plate, in: *Depth Structure and Geodynamics of the Crystalline Shields in the European USSR*, pp. 71–78, Publ. KNC RAN, Apatity, 1992.
426. Vetrin, V.R. and Kalinkin, M.M., *Reconstruction of inter-crustal and crust-mantle magmatism and metensomatosis processes (based on a study of depth inclusions)*, Publishers KNC RAN, Apatity, 1992, 108 p.
427. Kuzmin, D.A., Geologo-geochemical prerequisites of petroleum potential in Upper Proterozoic sediments of the Mezen besin, PhD thesis in geological-mineralogical sciences, 2006, 245 p.
428. Malyshev, N.A., *Tectonics, evolution and petroleum occurrences ai sedimentary basins of Russia European north*, UrO RAN, Yekaterinburg, 2002, 270 p.
429. Pimenov, B.A. and Malyshev, N.A., Resource estimation and the direction of geological exploration for oil and gas in the Mezen sedimentary basin, Geology of combustible fossil minerals of the Russia European north, in: *Proc. Institute of Geology*, vol. 85, pp. 26–40, Komi NC UrO RAN, Syktyvkar, 1995.
430. Dudkin, O.B., Minakov, F.M. *et al.*, *Khibin carbonatites*, Publ. KPh AN USSR, Apatity, 1984, 96 p.
431. Sorokhtin, N.O., Gavrilenko, B.V., Polyakov, N.V., Geologo-genetic model of base rock and placid diamond-bearing as applied to NW Russia. *Report abstracts at an international conference "New ideas in Earth's sciences"*, Moscow, vol. 2, pp. 87–89, 1997.
432. Gavrilenko, B.V., Mitrofanov, F.P., Zozulya, D.R., Chikirev, I.V., Sorokhtin, N.O., Kalachev, V.Y., Basalayeva, B.I., Potential of a placer diamond-bearing in Kola region. *Harbinger MGTU*, 3, 2, 86–96, 2000. Murmansk.
433. Polyakov, I.V. and Kalinkin, M.M., Diamonds and satellite minerals in kimberlites and loose deposits of the Kola Peninsula Tersk coast. *ZVMO*, 1, 96–101, 1993.
434. Polyakov, I.V., *Potential of diamond-bearing in the North Karelia. Issues of gold-bearing and diamond-bearing in the northern European part*, pp. 81–87, KNC RAN, Petrozavodsk, 1997.
435. Timonov, V.V., Schematic general water circulation in the White Sea basin and the origin of its depth water. *Proc. State Oceanogr. Inst.*, 1, 13, 118–131, 1947.
436. *Essays of the comparative planetology*, Nauka, Moscow, 1981, 327 p.
437. Forest Harbinger, 86–93, 2012.
438. Galimov, E.M., $^{13}C/^{12}C$ ratio in diamonds. Vertical zoning of diamond formation in the lithosphere, in: *Proceedings of 27th International Geologic Congress, Vol. 11, Section C 11. Geochemistry and Cosmochemistry*, pp. 110–123, Nauka, Moscow, 1984.
439. Garrels, R.M. and Mackenzie, F.T., *Evolution of Sedimentary Rocks*, W.W. Norton, New York, 1971.
440. Goldich, S.S., The age of Precambrian striated iron ore formations, in: *Precambrian Iron Ore Formations of the World*, pp. 286–297, Mir, Moscow, 1975.

441. *Isotope geochronology of the Precambrian*, Nauka, Leningrad, 1989, 160 p.
442. Joder, G.S. and Tilly, K.E., *Origins of basalt magmas*, Mir, Moscow, 1965, 248 p.
443. Kalinkin, M.M. and Polyakov, I.V., *Kimberlites and their affine rocks on the Tersk Coast of the Kola Peninsula. Issues of gold-bearing and diamond-bearing in the north of the European Russia*, pp. 117–123, Karelian Scientific Center RAN, Petrozavodsk, 1997.
444. Kaminsky, F.V., *Diamond Bearing of NonKimberlite Igneous Rocks*, Nedra, Moscow, 1984, 173 pp.
445. Kirkinsky, V.A., Decomposition of solid, in: *Experiment in Mineralogy and Petrography*, pp. 90–96, Nauka, Moscow, 1975.
446. MacDonald, G.J.F., Tidal friction. *Rev. Geophys.*, 2, 467–541, 1964a.
447. MacDonald, G.J.F., Tidal friction. *Rev. Geophys.*, 2, 3467–541, 1964b.
448. Mantle Composition and Oxide-Iron Core, *Tectonics of the Lithospheric Plates*, pp. 28–41, USSR Institute of Oceanology, Moscow, 2012.
449. Ringwood, A.E. and Major, A., The system Mg2SiO4—Fe2SiO4 at high pressures and temperatures. *Phys. Earth Planet. Int.*, 3, 89–108, 1970.
450. Safronov, V.S., *Evolution of the Preplanetary Cloud and the Formation of Earth and Planets*, Nauka, Moscow, 1969, 244 pp.
451. Shipilov, E.V., On the periodicity of basic magmatism manifestations within Eurasian Western Artic margin in Phanerozoic. *Harbinger MGTU*, 1, 3, 97–104, 1998.
452. Simakov, S.K., Evaluation of thermodynamic effect of redox conditions on the formation of critical diamond and graphite embryos in the process of methyane condensation at low pressure. *Mag. Phys. Chem.*, 69, 2, 346–347, 1995.
453. Weizer, Ya., Evolution of 87Sr/86Sr in sea water in geologic history and its importance as indicator of the Earth's crust evolution, in: *Early History of Earth*, pp. 565–575, Moscow, Mir, 1980.
454. Kushev, V. G., Baltic and Ukraine Shields in the general structure of the East-European basement as a system of meso- and mini-plates, in: *Depth Structure and Geodynamics of the Crystalline Shields in the European USSR*, O. A. Bogatikova (Ed.), pp. 85–94. Nauka, KNC AN USSR, Apatity (Russia), 1992.
455. Janke E., Emde F., Lesh F., *Special functions, formulae, diagrams, tables*. Moscow, Naula, 1968, 344 p.

Index

N. O. Sorokhtin (ed.) The Origins of Natural Diamonds, (509–512) © 2019 Scrivener Publishing LLC